

Simulation models to support Intensive Care Unit decision-making in pandemic and non-pandemic times



Daniel García de Vicuña Bilbao

Department of Statistics, Computer Science and Mathematics

Public University of Navarre

Advisor: Prof. Fermín Mallor Giménez

December 2021

*To my parents,
my siblings,
my family,
my friends,
and
Maite.*

Acknowledgements

I would like to acknowledge all the people who have helped me during this journey, especially Maite, and all my family and friends.

First, I would like to express my sincere gratitude to my advisor, Prof. Fermin Mallor for his unvaluable continuous support, help, and guidance since I started in the research field developing my Master Thesis until the final stage of this dissertation.

I also wish to thank

- Laida Esparza, an experienced physician at the Intensive Care Unit (ICU), who has been my travel companion in the analysis of the ICU management problems. She has helped me to understand the work carried out by physicians in the ICU and then to keep the mathematical models developed in this thesis connected with reality and therefore, making the results useful to improve the management of the ICU.
- the *Department of Statistics, Computer Science and Mathematics* of the Public University of Navarre, in particular to Dr. Cristina Azcárate for her unconditional support.
- all my colleagues at my department at the Public University of Navarre, especially Dr. Marta Cildo, with whom I shared many unforgettable hours.
- Dr Pedro Mateo, from the University of Zaragoza, who initiated and accompanied me into the Java programming language world.
- Prof. Ana Póvoa, Dr. Daniel Santos, Mariana, Edgar, and all my colleagues at the Instituto Superior Técnico at the University of Lisbon for their infinity hospitality during my research stay that made the experience wonderful.
- Juan María Guergue and Juan Pedro Tirapu, Heads of service of the ICU of the Navarre Hospital Compound, for facilitating my access to the ICU and collaborating with the development and validation of the ICU simulation models.
- René Peña, software engineer responsible for the implementation of Metavision® software (iMDsoft, Tel Aviv, Israel) and the development of a communication interface capable of integrating iMDsoft's Healthcare Management System with the rest of the applications of the Navarre Health Service, as well as extending the

functionalities of the management system itself. Thanks to this system, a lot of data has been collected from real ICU patients.

- Isabel Rodrigo, who works at the *Servicio de Apoyo a la Gestión Clínica y la Subdirección de Procesos de Hospitalización y Urgentes, del Complejo Hospitalario de Navarra*, infinite source of real management problems arising in the Navarre Hospital Compound.
- Sergio Santana, responsible for patient data management in Navarre, for providing us with all the information on COVID-19 patients and helping in the improvement and validation of the simulation model. Also for discussing with us the functionalities of the COVIDSIM programme developed for the prediction of hospital resources during the pandemic.
- Carlos Miguel Artundo, General Director of Health of the Government of Navarre, for his support and authorization to access the data and resources necessary for the development of this research. He has followed up on the information and results obtained during the pandemic.
- Juan Carlos Oliva, Director of Healthcare Innovation in La Rioja, for his interest in the implementation of the COVIDSIM software at the San Pedro hospital.
- Alberto Lafuente, Manager of the Health Service of La Rioja, who was informed of the results and saw how useful it would be to have these predictions in the hospital service of La Rioja.
- Ángel Moreno and Beatriz Martínez, responsible for patient data management in La Rioja.
- all the people in the CCAES group led by Fernando Simón, and in particular to Susana Monge, for their follow-up of the reports provided on a daily basis during the pandemic.
- Navarre Hospital Compound, García Orcoyen Hospital, and Reina Sofia Hospital in Navarre; Guipúzcoa Polyclinic in the Basque Country; and San Pedro Hospital in La Rioja for their collaboration in the research carried out in this thesis, both in providing patient data for analysis and for its interest in participating in the use of the interactive ICU simulator.
- all the people who have tested and used the ICU simulator, especially the ICU practitioners for lending their time to this study. We have successfully collected a large number of simulations to compare the different ways of managing the ICU.
- the Public University of Navarre for its Ph.D. grant that allowed me to enter the exceptional world of research.
- the ORAHS community and their experienced professors and researchers for their stimulating atmosphere which encourages fellowship and intellectual communication.

Abstract

The aim of this thesis is the construction of simulation models to analyse and improve patient admission and inpatient discharge decisions in an Intensive Care Unit (ICU). These decisions are especially relevant in situations of high ICU occupancy because they can lead to the early discharge of an admitted patient or the redirection of a newcomer. Exceptional circumstances, such as the global COVID-19 pandemic that broke out in 2019, increase the need for ICU beds, making this type of study even more relevant. The development of two interactive simulators has enabled us to understand and support ICU decision-making, both in and out of pandemics.

The first part of this thesis describes the development of the first ICU Management Flight Simulator, which enables the analysis of physician decision-making in relation to patient admission and discharge issues, while also serving as a useful learning-training tool. The developed Discrete Event Simulation (DES) model mimics real ICU admission and discharge processes, and recreates patients' health status from real clinical data instead of using a single length of stay (LoS) value. This flexible tool, which enables the recreation of ICUs with different characteristics (numbers of beds, patient arrival types, congestion levels...), has been used and validated by ICU physicians and nurses in four hospitals. Preliminary results reveal variability in the decision-making of physicians faced with the dilemma of the last bed, an issue which is addressed in broad terms, paying attention not only to the allocation of the last available ICU bed, but also to the evolving decision-making process surrounding patient admission and discharge as ICU occupancy increases. The simulator is freely available on the internet to be used by anyone interested (<https://icusimulator.unavarra.es>); only the username (ICU-simulator) and the password (ICU_S1mulat0r*) are required in order to access it. The sequence of decisions made by the simulator users constitute a new type of data for which new distance measures were developed to enable the characterization and clustering of users based on their ICU management approach.

The second part of this thesis presents a DES model to support decision-making for the short-term planning of hospital resource needs, especially ICU beds, to cope with outbreaks, such as the COVID-19 pandemic. Given its purpose as a short-term forecasting tool, the simulation model requires an accurate representation of the current system state and high fidelity in mimicking the system dynamics from that state. The two main components of the simulation model are the stochastic modelling of patient admission and patient flow processes. The patient

arrival process is modelled using a Gompertz growth model, which enables representation of the exponential growth in patient arrivals caused by the initial spread of the virus, followed by a period during which the arrival rate peaks before gradually declining until the wave subsides. An empirical study showed that the Gompertz model provides a better fit to pandemic-related data (positive cases and hospitalization numbers) and is superior in prediction capacity to other sigmoid models based on Richards, Logistic, and Stannard functions. We also propose a new parameterization of the Gompertz growth model to facilitate the creation of patient arrival scenarios in a pandemic simulation. A methodology is proposed for the simulation of future patient arrivals. Patient flow modelling considers different pathways and dynamic LoS estimation in several healthcare stages using patient-level data. We propose an estimation method based on an Expectation-Maximisation algorithm using data from all patients admitted to the hospital to date. Different pandemic waves are simulated in order to compare the performance of this method with that of two other statistical estimators that work only with complete data. Results collected to measure the accuracy of the parameter estimates and their influence when forecasting healthcare resource needs for pandemic patients reveal the superior performance of the new estimation method. We report on the application of the simulation model in two Autonomous Regions of Spain (Navarre and La Rioja) during the two COVID-19 waves experienced in 2020. The simulation model was employed on a daily basis to inform the regional logistic health care planning team, who programmed the ward and ICU beds based on the resulting predictions.

Contents

Acknowledgements	v
Abstract	vii
Contents	ix
List of Figures	xv
List of Tables	xxv
1 Introduction	1
1.1 Contextualization.....	1
1.2 Research objectives	3
1.3 Thesis structure.....	4
2 Background	7
2.1 Intensive Care Units	7
2.1.1 ICU definition	7
2.1.2 ICU bed management.....	9
2.2 The COVID-19 pandemic	10
Part I Analysis of Intensive Care Unit bed management using an interactive simulator	13
3 The dilemma of the last bed	15
3.1 Introduction	15
3.2 The problems inherent in the shortage of ICU beds.....	16
3.2.1 Triage of patients admitted to the ICU.....	16
3.2.2 Triage of patients for possible ICU admission.....	17
3.2.3 Referral to other centres	18
3.2.4 Cancellation of scheduled surgeries	18
3.2.5 Stress in medical staff due to work overload	19

3.3	An illustrative example of the dilemma of the last bed.....	19
3.4	Conclusions	23
4	Management Flight Simulator of an Intensive Care Unit.....	25
4.1	Literature review.....	26
4.1.1	Simulation in ICU	26
4.1.2	The use of management flight simulators	27
4.2	Modelling an ICU.....	30
4.2.1	Modelling the patient flow and admission/discharge decisions.....	30
4.2.2	The discrete event simulation model.....	32
4.2.3	Sampling initial scenarios from the steady state	36
4.3	The ICU management flight simulator.....	38
4.3.1	Main features of the simulator	38
4.3.2	Setting up the ICU characteristics.....	39
4.3.3	Interface.....	41
4.3.4	Information recorded.....	42
4.4	Discussion and conclusions	43
5	Methodologies for the analysis of decision-making in the ICU	45
5.1	Descriptive study	46
5.1.1	Simulator users profiles.....	46
5.1.2	User qualitative assessment of the simulator	47
5.2	Decision-making analysis by using global performance measures.....	48
5.2.1	Definition of global management indicators.....	48
5.2.2	Dissimilarity analysis in the ICU decision-making.....	51
5.2.3	Clustering and 2D representation of management decision-making	55
5.3	Analysis of decision-making conditioned by the ICU pressure level	57
5.3.1	Defining the ICU pressure level.....	57
5.3.2	Decision-making analysis in a collectively managed ICU.....	62
5.3.3	Distance between observations by aggregating neighbouring components...	64
5.4	Analysis of ICU management over time	67
5.5	Analysis of patient-level decisions	71
5.6	Discussion and future work	75

Part II Hospital preparedness during epidemics: the use of simulation to better support the Health Services managers.....	77
6 Forecasting the needs of ward and ICU beds in the COVID-19 pandemic.....	79
6.1 The use of simulation models in hospital management.....	80
6.2 Modelling the patient arrival pattern with the Gompertz model	82
6.2.1 Population growth models.....	82
6.2.2 Simulation of the patient arrival pattern.....	85
6.2.3 New parametrization of the Gompertz growth model.....	86
6.3 Modelling the patient flow	88
6.3.1 Hospital patient pathway	88
6.3.2 Stochastic modelling of hospital LoS.....	89
6.4 The discrete event simulation model	90
6.4.1 Entities, state variables, and events	91
6.4.2 Starting the simulation run	93
6.4.3 Simulation output	94
6.5 Estimation of parameters and probability distributions.....	97
6.5.1 The online estimation problem.....	97
6.5.2 Data and taxonomy of patients.....	98
6.5.3 Maximum likelihood estimation at the end of the pandemic wave.....	100
6.5.4 The Expectation-Maximization algorithm for parameter estimation during the pandemic wave.....	100
6.6 Importance of a good dynamic parameter estimation	103
6.6.1 Experimental design.....	104
6.6.2 Parameter estimation accuracy.....	105
6.6.3 Impact on the simulation output: bed occupancy prediction accuracy	106
6.7 Conclusions	107
7 Practical application of methodologies to support hospital management	111
7.1 Implementation of the methodology in a simulation software	111
7.2 Application example in Navarre and La Rioja	112
7.2.1 Incidence of COVID-19 disease during 2020 and 2021	113
7.2.2 Stochastic modelling of hospitalizations and lengths of stay.....	114
7.2.3 Ward and ICU bed occupancy forecasts	117

7.2.4	Tips for the use of the DES model in practice	119
7.3	Use as a support for decision making in hospital management.....	120
7.3.1	Chronological overview of the use of the simulation model in practice.....	120
7.3.2	Additional simulation model functionalities	123
7.4	Conclusions	124
Conclusions		127
8	Conclusion	129
8.1	General conclusions.....	129
8.2	Thesis contributions.....	131
8.3	Future work and research	133
8.4	Final remarks	134
References and appendices.....		137
References		139
A	List of acronyms and their definitions	151
B	Information of the example of the dilemma of the last bed	155
B.1	Real patients' description	155
B.2	All combinations of the example of the dilemma of the last bed	156
C	Set of patient variables included in the ICU management flight simulator	161
C.1	Patient information data.....	161
C.2	Patient's clinical data	163
D	ICU simulator user guide	169
D.1	Access to the simulator.....	169
D.2	Defining the characteristics of user and the simulation scenario	171
D.3	Starting the simulation.....	173
D.4	Bed management in the ICU	176
D.5	Conflictive situations during the simulation.....	180
D.6	Saving and loading simulations.....	182
D.7	Help menu and exit the simulator.....	184
E	ICU management flight simulator results	189
E.1	Reviews about the ICU simulator.....	189
E.2	Global performance results.....	190

E.3	Global results considering the ICU pressure level	192
E.4	Temporal evolution of the number of manageable beds	198
F	Aggregation of neighbouring components in distance calculation.....	203
F.1	Analysis of the Euclidean-Aggregate distance expression.....	203
F.2	Number of aggregations considered according to their size.....	206
G	Using PG models to represent the evolution of the COVID-19 pandemic	211
G.1	Statistical analysis to elucidate the suitability of PG models	211
G.2	Positive cases predictions for the following 5, 10, and 15 days, at 25%, 40%, and 65% of total cases detected	223
H	COVIDSIM software user guide	249
H.1	Starting the software	249
H.2	Modelling pandemic spread.....	250
H.3	Modelling of patient stays in hospital.....	258
H.4	Pandemic simulation.....	267
H.5	Analysis of the system saturation risk	271
H.6	Extension to flu.....	273
H.7	Input data file.....	276

List of Figures

Figure 4.1. Representation of the dynamics of an ICU through the change of the bed's state. The two types of patients are distinguished (scheduled and emergency ones) and also the direct entry to the ICU from a delayed one.....	31
Figure 4.2. Diagram of both emergency and scheduled patients' arrivals.....	35
Figure 4.3. ICU simulation model.	36
Figure 4.4. Real ICU data screen of Metavision® software.	39
Figure 4.5. Configuration screen of the simulation scenario.	40
Figure 4.6. ICU simulator's main screen.	41
Figure 4.7. Information of patient's clinical data, mimicking real screens of Metavision®.	42
Figure 5.1. Main results of the questionnaire about the ICU simulator.....	48
Figure 5.2. Dendrogram obtained from the distances between the 18 ICU physicians presented in Table 5.8.	56
Figure 5.3. 2D representation obtained from the distances between the 18 ICU physicians presented in Table 5.8. The 3 clusters obtained with the dendrogram are visualized.	57
Figure 5.4. Probability of diverting emergency patients by each group conditioned by ICU pressure levels $PgD Lk$	61
Figure 5.5. Probability of cancelling scheduled surgeries by each group conditioned by ICU pressure levels $PgC Lk$	61
Figure 5.6. Probability of shortening stays by each group conditioned by ICU pressure levels $PgS Lk$	62
Figure 5.7. Probability of being in each ICU pressure level $PgLk$	62
Figure 5.8. Graph showing the trajectory of the number of manageable beds of two different physicians (physicians 7 and 10).	68
Figure 5.9. Graph showing the trajectory of the number of manageable beds of two similar physicians according to their global results (physicians 1 and 12).....	68

Figure 5.10. Graph showing the trajectories of the number of manageable beds of 18 ICU physicians, 14 ICU nurses, 4 ICU nurse technicians, and 6 residents.	69
Figure 5.11. Graph showing the trajectory of the number of manageable beds of the two most similar physicians to each other according to their dynamic distance (physicians 6 and 14). 70	
Figure 5.12. Graph showing the trajectory of the number of manageable beds of the two most different physicians to each other according to their dynamic distance (physicians 7 and 16).	71
Figure 6.1. The simulation procedure for the patient arrival pattern. Steps 2-4 are replicated as often as necessary for the different patient arrival and hospitalization sequences to be simulated.	86
Figure 6.2. Nine Gompertz curves generated by fixing the three parameters of Equation (6.13). In the first row of the graphs, the parameter A is varied ($A = 2000, 20000, \text{ and } 100000$). As A increases, the horizontal upper asymptote of the curve increases. In the second row, the value of $T_{0.1}$, which controls the duration of the wave, is modified ($T_{0.1} = 30, 60, \text{ and } 75$). Finally, in the third row, the parameter D is modified ($A = 10, 30, \text{ and } 50$), which allows to move the Gompertz curve on the x-axis.	88
Figure 6.3. Representation of COVID-19 patient flow in the health system.	89
Figure 6.4. Flow diagram of the health system simulation model. Two types of events are considered, external arrivals and ward or ICU end of stays.	92
Figure 6.5. Simulation output for ICU bed demand for the following days. The left-hand side shows four different trajectories starting from the SSP; the 3 lines on the right-hand side correspond to the 5 th , 50 th , and 95 th percentiles.	95
Figure 6.6. Saturation risk curves associated with hospital ward bed numbers between 200 and 300.	96
Figure 6.7. Parameters and probability distributions for modelling Ward-to-ICU transition (left) and ICU-to-Ward transition (right).	97
Figure 6.8. Diagram of the state of a patient at time t	99
Figure 6.9. Estimation of parameters pWI and θZ over time (the horizontal axes represent the time during the pandemic) with the 3 methods ($I, I-5, \text{ and } EM$) and the real values. Results are shown for different values of parameter A of the Gompertz curve (2000, 20000, and 100000).	105
Figure 6.10. Prediction of ICU bed occupancy on the 20th, 25th, and 30th days of the pandemic with the 3 methods ($I, I-5, \text{ and } EM$) compared to prediction with actual parameters.	107
Figure 7.1. Daily recorded hospitalizations in Navarre and La Rioja from early March 2020 to mid-December 2020.	114

Figure 7.2. Daily recorded hospitalizations in Navarre and La Rioja from early March 2020 to mid-December 2021.	114
Figure 7.3. Cumulative hospitalizations in La Rioja from March 3 to June 9, 2020, and different curve fits obtained from the Gompertz growth model.	115
Figure 7.4. Six different curve fits obtained from the Gompertz growth model compared with the daily hospitalization series for La Rioja from March 3 to June 30, 2020.	115
Figure 7.5. Probability plots of the fits of the ward and ICU LoS distributions during the first wave of the pandemic in Navarre.	116
Figure 7.6. The prediction made on March 21, 2020 for bed occupancy in the hospitals of Navarre and the real occupancy levels. The area shaded yellow highlights the ability of the simulator to obtain accurate 10-day occupancy forecasts.	117
Figure 7.7. The prediction made on March 16, 2020 for bed occupancy in the ICUs of Navarre and the real occupancy levels. The area shaded yellow highlights the ability of the simulator to obtain accurate 15-day occupancy forecasts.	118
Figure 7.8. Comparison between the predictions made on different days (2020/03/26, 2020/03/29, 2020/04/01, and 2020/04/04) for the number of hospitalization and ICU beds occupied in Navarre and the real occupancies.	118
Figure 7.9. Comparison between the predictions made in Navarre at different moments of the second wave (2020/09/20, 2020/10/27, and 2020/11/13) for the number of beds occupied in both hospital and ICU, and real occupancies.	119
Figure 7.10. Daily flow of data, information and reports.	121
Figure 7.11. Comparison between 7-day forecasts made in Navarre at different times of the fourth wave (between March 2021 and June 2021) for the number of occupied hospital beds and actual occupancies.	122
Figure 7.12. Sources of arrival in the ICU in times of pandemic. In addition to the two usual sources (emergencies and operating rooms), patients infected, in this case, by COVID-19, are added.	123
Figure D.1. Login screen of the ICU simulator.	169
Figure D.2. Initial screen of the ICU simulator in English.	170
Figure D.3. Initial screen of the ICU simulator in Spanish.	170
Figure D.4. ICU simulator registration screen.	171
Figure D.5. ICU simulator initial screen after registration.	172
Figure D.6. User configuration screen.	172
Figure D.7. Configuration screen of the simulation scenario.	173
Figure D.8. Information window of the ICU to be simulated.	173

Figure D.9. Simulation help window.	174
Figure D.10. Main screen of the simulator before starting the simulation.	174
Figure D.11. Window indicating the initialization of the ICU.	175
Figure D.12. Main screen of the ICU simulator at the beginning of the simulation.....	175
Figure D.13. Representation of the dynamics of an ICU through the change of the bed's state. The two types of patients are distinguished (scheduled and emergency ones) and also the direct entry to the ICU from a delayed one.....	176
Figure D.14. Window with information about the patient that is on bed 14 and buttons to access the patient's medical history and patient data.	177
Figure D.15. Medical history of the patient that is on bed 14.....	177
Figure D.16. Information of clinical data of the patient that is on bed 14, mimicking real screens of Metavision®.	178
Figure D.17. The window for discharging the patient that is on bed 14.....	179
Figure D.18. The window for managing the surgeries.	179
Figure D.19. The window for admitting or diverting emergency patients.	180
Figure D.20. The situation when an emergency patient arrives at the ICU with all beds occupied. Only two patients are stabilized while the rest are in severe condition.....	181
Figure D.21. The situation in which the admitted emergency patient has to wait for the bed of the discharged patient to be freed up.	181
Figure D.22. The situation when two surgeries have to be managed but only one can be confirmed due to lack of ICU beds.	182
Figure D.23. The situation where the only stabilised patient in the ICU has to be discharged because one of the two surgeries scheduled for that day has been confirmed.....	182
Figure D.24. Option to save the simulation with the simulator.	183
Figure D.25. Saving the simulation with the ending ".properties".	183
Figure D.26. Window for loading saved simulations.	184
Figure D.27. The window to restart the simulation from the beginning. Unsaved progress is lost.....	184
Figure D.28. Help menu with information about the ICU simulator.....	185
Figure D.29. Help menu with information about the scenarios that can be created with the simulator.	186
Figure D.30. Help menu with information about the types of simulation the user can access to.	186

Figure D.31. Help menu with information about the information collected with the simulator.	187
Figure D.32. Help tab about different aspects of the simulation.	187
Figure D.33. The window to exit the simulation. Unsaved progress is lost.	188
Figure D.34. The window for logging out and disconnecting from the ICU simulator.....	188
Figure E.1. Conditional probabilities recorded by 18 ICU physicians.	194
Figure E.2. Conditional probabilities recorded by 14 ICU nurses.....	195
Figure E.3. Conditional probabilities recorded by 4 ICU nurse technicians.	195
Figure E.4. Conditional probabilities recorded by 6 residents.....	196
Figure E.5. Conditional probabilities recorded by 6 medical students.	196
Figure E.6. Conditional probabilities recorded by 11 OM-OR researchers.....	197
Figure E.7. Conditional probabilities recorded by 11 engineers.....	197
Figure E.8. Conditional probabilities recorded by 12 other users not included in former groups.....	198
Figure E.9. Graph showing the trajectory of the mean number of manageable beds of 18 ICU physicians.....	198
Figure E.10. Graph showing the trajectory of the mean number of manageable beds of 14 ICU nurses.	199
Figure E.11. Graph showing the trajectory of the mean number of manageable beds of 4 ICU nurse technicians.....	199
Figure E.12. Graph showing the trajectory of the mean number of manageable beds of 6 residents.	199
Figure E.13. Graph showing the trajectory of the mean number of manageable beds of 6 medical students.....	200
Figure E.14. Graph showing the trajectory of the mean number of manageable beds of 11 OM-OR researchers.	200
Figure E.15. Graph showing the trajectory of the mean number of manageable beds of 11 engineers.	200
Figure E.16. Graph showing the trajectory of the mean number of manageable beds of by12 other users not included in former groups.	201
Figure F.1. Diagram of the aggregations included in term $S1$ of the Euclidean-Aggregate distance between two observations. For each iteration k , all possible aggregations of size $s =$ k are formed and the Euclidean distance between them is calculated.....	204

Figure F.2. Diagram of the aggregations included in term S_2 of the Euclidean-Aggregate distance between two observations. For each iteration k , the aggregations of size $s = k$ at the edges are included and the Euclidean distance between them is calculated.....	205
Figure F.3. Number of times each aggregation of $s = 1$ is considered in both S_1 and S_2 .	207
Figure F.4. Number of times each aggregation of $s = 2$ is considered in both S_1 and S_2 .	208
Figure F.5. Number of times each aggregation of $s = 3$ is considered in both S_1 and S_2 .	208
Figure F.6. Number of times each aggregation of size s is considered in both S_1 and S_2 .	209
Figure F.7. Number of times each aggregation of $s = Q - 2$, $s = Q - 1$, and $s = Q$ is considered in both S_1 and S_2	210
Figure G.1. Cumulative positive cases in USA and fits obtained from the four PG models.	213
Figure G.2. Cumulative positive cases in Brazil and fits obtained from the four PG models.	213
Figure G.3. Cumulative positive cases in Russia and fits obtained from the four PG models.	214
Figure G.4. Cumulative positive cases in India and fits obtained from the four PG models.	214
Figure G.5. Cumulative positive cases in UK and fits obtained from the four PG models.	215
Figure G.6. Cumulative positive cases in Spain and fits obtained from the four PG models.	215
Figure G.7. Cumulative positive cases in Italy and fits obtained from the four PG models.	216
Figure G.8. Cumulative positive cases in Peru and fits obtained from the four PG models.	216
Figure G.9. Cumulative positive cases in Iran and fits obtained from the four PG models.	217
Figure G.10. Cumulative positive cases in Germany and fits obtained from the four PG models.	217
Figure G.11. Cumulative positive cases in Turkey and fits obtained from the four PG models.	218
Figure G.12. Cumulative positive cases in Chile and fits obtained from the four PG models.	218
Figure G.13. Cumulative positive cases in France and fits obtained from the four PG models.	219

Figure G.14. Cumulative positive cases in Mexico and fits obtained from the four PG models.	219
Figure G.15. Cumulative positive cases in Pakistan and fits obtained from the four PG models.	220
Figure G.16. Cumulative positive cases in Saudi Arabia and fits obtained from the four PG models.	220
Figure G.17. Cumulative positive cases in Canada and fits obtained from the four PG models.	221
Figure G.18. Cumulative positive cases in Bangladesh and fits obtained from the four PG models.	221
Figure G.19. Cumulative positive cases in China and fits obtained from the four PG models.	222
Figure G.20. Cumulative positive cases in Qatar and fits obtained from the four PG models.	222
Figure G.21. Cumulative positive cases predictions for the following days at 25% (left), 40% (centre), and 65% (right) of total cases detected in USA using the four PG models.	228
Figure G.22. Cumulative positive cases predictions for the following days at 25% (left), 40% (centre), and 65% (right) of total cases detected in Brazil using the four PG models.	229
Figure G.23. Cumulative positive cases predictions for the following days at 25% (left), 40% (centre), and 65% (right) of total cases detected in Russia using the four PG models.	230
Figure G.24. Cumulative positive cases predictions for the following days at 25% (left), 40% (centre), and 65% (right) of total cases detected in India using the four PG models.	231
Figure G.25. Cumulative positive cases predictions for the following days at 25% (left), 40% (centre), and 65% (right) of total cases detected in UK using the four PG models.	232
Figure G.26. Cumulative positive cases predictions for the following days at 25% (left), 40% (centre), and 65% (right) of total cases detected in Spain using the four PG models.	233
Figure G.27. Cumulative positive cases predictions for the following days at 25% (left), 40% (centre), and 65% (right) of total cases detected in Italy using the four PG models.	234
Figure G.28. Cumulative positive cases predictions for the following days at 25% (left), 40% (centre), and 65% (right) of total cases detected in Peru using four PG models.	235
Figure G.29. Cumulative positive cases predictions for the following days at 25% (left), 40% (centre), and 65% (right) of total cases detected in Iran using the four PG models.	236
Figure G.30. Cumulative positive cases predictions for the following days at 25% (left), 40% (centre), and 65% (right) of total cases detected in Germany using the four PG models.	237
Figure G.31. Cumulative positive cases predictions for the following days at 25% (left), 40% (centre), and 65% (right) of total cases detected in Turkey using the four PG models.	238

Figure G.32. Cumulative positive cases predictions for the following days at 25% (left), 40% (centre), and 65% (right) of total cases detected in Chile using the four PG models.....	239
Figure G.33. Cumulative positive cases predictions for the following days at 25% (left), 40% (centre), and 65% (right) of total cases detected in France using the four PG models.....	240
Figure G.34. Cumulative positive cases predictions for the following days at 25% (left), 40% (centre), and 65% (right) of total cases detected in Mexico using four PG models.	241
Figure G.35. Cumulative positive cases predictions for the following days at 25% (left), 40% (centre), and 65% (right) of total cases detected in Pakistan using the four PG models.	242
Figure G.36. Cumulative positive cases predictions for the following days at 25% (left), 40% (centre), and 65% (right) of total cases detected in Saudi Arabia using the four PG models.	243
Figure G.37. Cumulative positive cases predictions for the following days at 25% (left), 40% (centre), and 65% (right) of total cases detected in Canada using the four PG models.....	244
Figure G.38. Cumulative positive cases predictions for the following days at 25% (left), 40% (centre), and 65% (right) of total cases detected in Bangladesh using the four PG models. .	245
Figure G.39. Cumulative positive cases predictions for the following days at 25% (left), 40% (centre), and 65% (right) of total cases detected in China using the four PG models.	246
Figure G.40. Cumulative positive cases predictions for the following days at 25% (left), 40% (centre), and 65% (right) of total cases detected in Qatar using the four PG models.....	247
Figure H.1. Start window of the COVIDSIM software.	249
Figure H.2. Modelling pandemic spread.....	250
Figure H.3. Estimation of the parameters of the Gompertz curve, both manually and using a data file.....	251
Figure H.4. Window to search the data file.	252
Figure H.5. Fields to be filled in for the display of the fitting curve.	253
Figure H.6. Fields needed to obtain the fit of the Gompertz curve to the historical data. ..	254
Figure H.7. Gompertz curve fit to historical data, represented by the black dots from 2020-08-01 to 2020-10-05.	254
Figure H.8. Fitting of the Gompertz curve to daily data.	255
Figure H.9. Linearization of the fitted Gompertz curve.	256
Figure H.10. Fit obtained by manually modifying the total number of cases at the end of the pandemic (700).	257
Figure H.11. Customized pandemic curve obtained after fitting the total number of admissions (1,000), the duration of the pandemic (90 days), and the number of cases on a selected day (300 on 2020-10-01).....	258

Figure H.12. Modelling of patient stays in the hospital.....	259
Figure H.13. Patient flow diagram through the hospital.....	259
Figure H.14. Fields related to the cut-off age of patients and the stays file.	260
Figure H.15. Female patients tab for the fields related to the cut-off age and the stays file.	260
Figure H.16. Branching probabilities.....	261
Figure H.17. Probability distributions of hospital stays.....	261
Figure H.18. Parameter fitting using the data file.....	263
Figure H.19. Density function and quality of fit to a Weibull distribution for LoS in hospital for patients over 65 years old who do not require ICU.....	263
Figure H.20. Density function and quality of fit to a Lognormal distribution for LoS in hospital for patients over 65 years old who do not require ICU.....	263
Figure H.21. Parameter fitting using a data file in which there is insufficient data for the LoS in the hospital of patients over 65 years old discharged from the ICU.....	264
Figure H.22. Manually entered modifications with respect to the default values.	265
Figure H.23. Manually entered parameters of LoS distributions, before recalculating missing values.	266
Figure H.24. Manually entered LoS distributions parameters recalculated for missing or incorrect ones.	266
Figure H.25. Pandemic simulation.....	267
Figure H.26. Pandemic simulation progress with historical data date from 2020-08-01, simulation horizon to 2020-12-31, simulation seed of 123,456, and 1,000 replications.....	268
Figure H.27. Simulation results for hospital beds.....	269
Figure H.28. Simulation results for ICU beds.	269
Figure H.29. Generated trajectories in the ICU, from among the 1000 simulations run by the software.....	270
Figure H.30. Window used to save the simulation results in files.....	270
Figure H.31. Analysis of the system saturation risk.	271
Figure H.32. Results obtained of system saturation risk for the hospital and ICU analysed up to 2020-11-15.....	272
Figure H.33. Window used to save the results of the saturation risk in the files.....	272
Figure H.34. Cumulative and daily data for patients admitted to the hospital with flu in the 2017-18 season in La Rioja.....	273

Figure H.35. Cumulative and daily data for patients admitted to the hospital with flu in the 2018-19 season in La Rioja.....	274
Figure H.36. Weekly incidence of the flu. Sentinel Flu Surveillance System in Spain. Seasons 2014-15 to 2018-19, Spain.....	274
Figure H.37. Tab where the graphs of admissions and bed occupancy are obtained for the two diseases aggregated and individually.....	276
Figure H.38. Tab showing the hospital and ICU saturation risk analysis taking into account both diseases.	276
Figure H.39. Excel file format of patient stay data.	277
Figure H.40. Excel file format of daily case data.	277

List of Tables

Table 3.1. Patients to manage in the example of the dilemma of the last bed.	20
Table 3.2. Selected decisions based on clinics in the example of the dilemma of the last bed. The last column includes the number of practitioners out of 90 that would make each decision in a real ICU.	21
Table 3.3. Decisions made by the 90 professionals separated by type of employment in the ICU.	22
Table 5.1. Comparison of simulation global results recorded by 18 ICU physicians. Users faced a 24-bed ICU, which was initialized with 23 patients in different health statuses. Over three weeks, 34 emergency patients and 23 scheduled patients arrived at the ICU. Each physician has a different number of total discharges (dTi). Bold values represent the highest (red) and lowest (green) values.	51
Table 5.2. Global mean results of all users of the simulator divided by different groups. Bold values represent the highest and lowest values.	51
Table 5.3. Variance-covariance matrix obtained from the observations of all users of the ICU simulator.	52
Table 5.4. Correlation matrix obtained from the observations of all users of the ICU simulator.	53
Table 5.5. Variance-covariance matrix obtained from the observations of the 18 ICU physicians who have used the simulator.	53
Table 5.6. Correlation matrix obtained from the observations of the 18 ICU physicians who have used the simulator.	53
Table 5.7. Euclidean distances between the 18 ICU physicians who have used the simulator.	54
Table 5.8. Mahalanobis distances between the 18 ICU physicians who have used the simulator.	54
Table 5.9. Ratio between the normalized Mahalanobis and Euclidean distances ($\delta M \delta E$) of the 18 ICU physicians who have used the simulator.	55

Table 5.10. Comparison of simulation global results recorded by 18 ICU physicians considering the ICU pressure level.	60
Table 5.11. Global mean results of all users of the simulator considering the ICU pressure level.	60
Table 5.12. Decision-making results of 18 ICU physicians in a collectively managed ICU. The probabilities of diverting patients, $PiD Lg$, cancelling surgeries $PiC Lg$, and shortening stays, $PiS Lg$, are shown. Bold values represent the highest (red) and lowest (green) values.	64
Table 5.13. Dynamic distances between the 18 ICU physicians who have used the simulator. Bold values represent the five lowest distances (green) and the five highest distances (red). 70	
Table 5.14. Contingency table representing at time td the coincidences and discrepancies of two users i and j in patient admission decisions.	73
Table 7.1. The parameters fitted to different populations at different moments during the pandemic, sorted by region (Navarre and La Rioja), wave, and gender, showing ward and ICU lengths of stay distributions and ICU admission probabilities.	116
Table A.1. List of acronyms and their definitions used in this thesis, sorted alphabetically.	151
Table B.1. All 57 possible combinations of the example of the dilemma of the last bed... 156	
Table C.1. Unified principal diagnosis.	161
Table C.2. Type of discharge.	162
Table C.3. Type of infection.	165
Table C.4. Germs.	166
Table C.5. Antibiotics.	167
Table E.1. Simulation global results recorded by 14 ICU nurses.	190
Table E.2. Simulation global results recorded by 4 ICU nurse technicians.	190
Table E.3. Simulation global results recorded by 6 residents.	190
Table E.4. Simulation global results recorded by 6 medical students.	191
Table E.5. Simulation global results recorded by 11 OM-OR researchers.	191
Table E.6. Simulation global results recorded by 11 engineers.	191
Table E.7. Simulation global results recorded by 12 other users not included in former groups.	191
Table E.8. Information about the specific tables and figures for each group.	192
Table E.9. Simulation global results recorded by 14 ICU nurses considering the ICU pressure level.	192

Table E.10. Simulation global results recorded by 4 ICU nurse technicians considering the ICU pressure level.....	193
Table E.11. Simulation global results recorded by 6 residents considering the ICU pressure level.....	193
Table E.12. Simulation global results recorded by 6 medical students considering the ICU pressure level.	193
Table E.13. Simulation global results recorded by 11 OM-OR researchers considering the ICU pressure level.....	193
Table E.14. Simulation global results recorded by 11 engineers considering the ICU pressure level.....	193
Table E.15. Simulation global results recorded by 12 other users not included in former groups considering the ICU pressure level.	194
Table F.1. Final amount of each aggregation of size s included in the expressions $S1$ and $S2$	206
Table G.1. The 20 most-affected countries by COVID-19 until June 15, 2020. The last four columns show the MAE calculated for the fit with each of the applied models.	212
Table G.2. List of figures with graphs of cumulative positive cases in each country, fitted with each of the four PG models.....	212
Table G.3. The number of countries in which each model is equal or better than the others in terms of predicting new positive cases for the next 5, 10, and 15 days.....	223
Table G.4. MAE calculated for the fit of each model at 25% of total cases detected in each country.	224
Table G.5. Normalized MAEs obtained for each prediction and model at 25% of total cases detected in each country.....	224
Table G.6. MAE calculated for the fit of each model at 40% of total cases detected in each country.	225
Table G.7. Normalized MAEs obtained for each prediction and model at 40% of total cases detected in each country.....	225
Table G.8. MAE calculated for the fit of each model at 65% of total cases detected in each country.	226
Table G.9. Normalized MAEs obtained for each prediction and model at 65% of total cases detected in each country.....	226
Table G.10. List of figures with predictions for the following days at 25%, 40%, and 65% of total cases detected in each country using each of the four PG models.	227

1 Introduction

This thesis includes the study and development of simulation models and simulators for studying, understanding, and supporting decision-making in Intensive Care Units (ICUs) in pandemic and non-pandemic times. These decisions are especially relevant in high occupancy situations because they can lead to an admitted patient being discharged earlier than planned or to a new patient being denied admission. Therefore, these simulators need to generate an ICU environment similar to what a physician might find in real life where he or she needs to consult the monitoring screens of admitted patients to decide which have to be discharged.

The research group q-UPHS (www.unavarra.es/quphs) of the Department of Statistics, Computer Science and Mathematics at the Public University of Navarre has been collaborating for more than 10 years with the Navarre Hospital Compound's ICU medical staff. This makes it possible to bring together two different views on the ICU bed management problem and thus consider both the clinical and technical aspects of ICU operations. The medical knowledge provided by the ICU staff has been fundamental to provide the necessary background for the models and methodology developed in this thesis.

The rest of this chapter is organized as follows. Section 1.1 begins with a contextualization of this research, specifically concerning ICUs and the global COVID-19 pandemic. The research objectives of this thesis are indicated in Section 1.2. Finally, Section 1.3 concludes with an overview of the chapters and appendices.

1.1 Contextualization

ICUs are essential for the care of patients combining high levels of severity with reasonable expectations of substantial recovery. Factors such as the advent of multiple organ support systems or the population ageing process have led to an increase both in the number of patients being admitted, and increased demand expectations.

However, the cost of an ICU bed is much higher than that of a standard hospital bed, due to the high tech equipment that is required and, above all, the large number of professionals needed to staff these Units. For this reason, ICU bed management is a double-edged problem. On the one hand, there is the costliness of the service, due mainly to the high fixed costs of the beds (regardless of the occupancy level), which means that the economic aim is to maximise ICU bed occupancy to avoid under-utilisation. On the other hand, there is the high risk to public health from a potential bed shortage, such that, clinically speaking, high occupancy is something to be avoided.

On a daily basis, ICU medical staff have to balance the demand for beds with the capacity of the service. The stochastic nature of both patient arrivals and ICU length of stay (LoS) inevitably creates a periodic need to shorten some patients' stay in order to cope with high occupancy. However, early discharge carries the risk of possible readmission in the future, while the denial of intensive care to patients who need it, whether due to a bed shortage or for any other reason, is associated with a poorer prognosis. In these cases, physicians opt to cancel scheduled surgeries preventing the admission of emergency patients arriving at the ICU.

Therefore, early discharge decisions are up to the individual criterion of the physician in charge, who has to balance the expected outcome for the discharged patient against the potential benefit of ICU treatment for the one newly admitted. In other words, these decisions are based both on the clinical evaluation of the patients already admitted, and the perceived risk to a patient in transit who might derive more benefit from intensive care than one of the patients already admitted. This risk perception has a subjective component that leads to different patient discharge decisions.

In addition to the above high-pressure scenario due to bed shortage, other factors impact on patient discharge. One is physicians varying in their assessments of the stability of the patient for transfer to another unit (an issue usually discussed among the medical staff during daily clinical sessions). Meanwhile, non-clinical factors also come into play, such as the availability of beds in the unit to which the patient is to be referred, or the day of the week on which the decision is being made. Analysing this variability is a necessary step in assessing the effectiveness and efficiency of the health service provided and thus determining its quality. Variability is not necessarily and not always negative, but it can lead to inefficiencies in the quality of care. Therefore, its causes need to be analysed in order to improve patient care quality and standardise criteria.

Variability in clinical practice can occur for one or a combination of different reasons: lack of standardised clinical criteria in certain processes, change in clinical criteria or recommendations, differences in the experience of physicians, increase in the rate of admissions (increase in scheduled surgery, epidemics...), increase in the level of occupancy, etc. Through simulation, it is possible to control some of the contributing factors of this

variability, and thus enable the analysis of others that are either more subjective or impossible to control.

ICU healthcare practitioners frequently confront ethical dilemmas. In situations of ICU saturation, physicians must decide which patient is allocated the last available bed. They assess which patient stands to benefit most from ICU care and analyse the consequences of the three bed control actions (BCA) available to ICU managers: shortening the stay of admitted patients, cancelling scheduled surgeries, and diverting emergency patients to another facility. These are daily decisions in ICUs but they become more problematic in exceptional circumstances, such as the global pandemic caused by a novel virus from the coronavirus family that appeared in central China in December 2019 (COVID-19), and remains prevalent at the time of writing this thesis.

In this context, shortage of beds is no longer an individual problem but a collective one. Bed allocation is managed collectively, and can involve the cancellation of all surgical operations, which are not imminently life-saving, or stricter triage criteria in ICUs based on the patient's condition and chances of recovery. Thus, over and above expected bed occupancy requirements, there is a need for forecasting tools to predict hospital and ICU admissions of COVID-19 patients several days ahead. With this information, healthcare managers can better plan hospital resources such as ward and ICU beds for these patients, and medical staff to care for them.

1.2 Research objectives

The overall aim of this thesis is the development and application of data analysis and computational simulation techniques and methods to contribute to improving the understanding of medical decision-making, in general, and in particular as it affects ICU triage.

Decision-making in the field of healthcare presents greater difficulty since it is not guided by purely economic criteria and/or reliability standards, but is mainly motivated by the health status of the patients, which sometimes raises ethical concerns, such as deciding how to allocate scarce resources (beds, in the ICU case) among different patients requiring them. The aim with this thesis is to develop a more accurate simulator than is currently available for reproducing ICU conditions, that is, a virtual environment that ICU physicians can accept as offering a true reflection of a real ICU, and with which they can interact.

Performing a comparative analysis of the physician decisions on the admission and discharge of ICU patients helps to investigate all this. Retrospective statistical analysis of ICU administrative records can prove very difficult. Not only is every decision-making scenario unique; there is not always a record of the circumstances surrounding the decision or the physician responsible for making it. However, simulation techniques enable the reproduction

of scenarios and the control of all factors influencing the dynamics and decision making in complex systems.

Within the general objective set out above, we can highlight the following specific objectives, which will apply to any ICU:

1. **Development of an interactive simulator** capable of creating a virtual environment in which the operation of an ICU is represented. This includes the collection of information on decision-making through simulator use by medical staff and the design of scenarios likely to generate disparity in medical decision-making.
2. **Quantitative analysis of medical decisions**, by seeking patterns in ICU decision-making, using mathematical modelling to learn how decisions are made, and developing new metrics to enable the comparison of decision-making sequences across different circumstances.
3. **Development of a mathematical methodology for real-time prediction** of hospital and ICU admissions and occupancy levels several days ahead during the COVID-19 pandemic. Development of a methodology for simulating the health system in its transitory phase and improved statistical estimators capable of capturing all data on patients who are still hospitalized.
4. **Validation of the methodology in a real context** by supporting healthcare authorities during the pandemic with daily forecast reports to help them to respond quickly and effectively in managing and planning public health resources.

In summary, this thesis, based on a multidisciplinary research framework for the analysis of real problems, aims to contribute to academic advances in the solution of these problems, while making a real impact in the improvement of ICUs.

1.3 Thesis structure

This thesis is structured in two main parts, each addressing a different research topic. After two initial chapters, the two parts are presented separately, each with its own chapters. The last chapter presents the overall conclusions and possibilities for future research. The thesis ends with the list of references used and eight appendices are also attached.

Chapter 1 presents the research setting and describes the general and specific aims of the thesis.

Chapter 2 describes the background to each part of this thesis, beginning with aspects such as the definition of ICUs and the management problems they entail, and proceeding with a chronological account of the global pandemic produced by COVID-19.

Part I of this thesis, which includes Chapters 3, 4, and 5, is dedicated to developing an interactive simulator mimicking actual ICU conditions. Also included is a proposal for a methodology to analyse decision-making in the ICU.

Chapter 3 deals with one of the great ethical dilemmas arising in healthcare, namely, the last bed dilemma. The problems associated with bed shortages are described, and an example with real patients illustrates the different views of ICU professionals regarding admission and discharge decisions in conflicting situations.

Chapter 4 presents the development of the first ICU Management Flight Simulator (MFS), which enables analysis of ICU management and decision-making processes, by presenting scenarios that cause discrepancies between ICU practitioners. It can also be used as a learning-training tool.

Chapter 5 defines statistical methods for the analysis of a new type of data, i.e., decision-making sequences as influenced by contextual factors. Proposals for clustering methods aimed at identifying different ICU management strategies are also provided.

Part II, which contains Chapters 6 and 7, addresses the issue of hospital preparedness during epidemics, focusing on the development of simulation models to better support Health Service managers.

Chapter 6 presents a Discrete Event Simulation (DES) decision-making support model for short-term hospital resource planning, especially in relation to ICU beds, to cope with outbreaks, such as the COVID-19 pandemic.

Chapter 7 describes the use of the simulation model by two Autonomous Regions in Spain (Navarre and La Rioja) during the two waves of the pandemic that struck Spain in 2020. The simulation model was used on a daily basis to inform healthcare managers in both regions about the number of predicted COVID-19 admissions and provide several-days-ahead bed occupancy forecasts both for wards and ICUs.

Chapter 8 summarises the conclusions drawn from previous sections, discusses research limitations and points to possible future extensions to this work. The contributions of this thesis are also highlighted in this chapter and some final remarks are presented.

Appendix A provides an alphabetical list of the 63 acronyms used in this thesis, with their definitions. In order to preserve the independence of the different parts of this thesis, acronyms are defined separately in each part the first time they appear.

Appendix B gives the clinical description of the six real patients considered in the example used to illustrate the last bed dilemma in Section 3.3 and a table with the 57 possible combinations of the proposed dilemma.

Appendix C presents the set of patient variables included in the MFS to represent patients' clinical evolution. 275 clinical variables are collected in addition to general patient data.

Appendix D contains the ICU simulator user guide. The DES model used in its development is explained in Chapter 4. This interactive simulator has been used to capture users' decisions when faced with ICU bed allocation problems.

Appendix E shows the results obtained with the MSF of the ICU. Firstly, the reviews of some users of the simulator are presented, followed by the global performance results, the global results considering the ICU pressure level, and the temporal evolution of the number of manageable beds. Tables and graphs are used to visualize the results.

Appendix F explains the aggregation of neighbouring components in distance calculation introduced in Section 5.3.3. The mathematical expression of the proposed Euclidean-Aggregate distance is discussed and the number of aggregations considered according to their size is indicated. Tables with generic and particularized expressions at certain sizes are included.

Appendix G gives a graphic representation of the evolution of the COVID-19 pandemic using Population Growth (PG) models. Through a statistical analysis of the 20 most-affected countries until June 15, 2020, the suitability of different PG models is elucidated (Logistic, Gompertz, Richards, and Stannard). The predictive capacity of each PG model at different phases of the pandemic and with different time horizons is also studied. Tables and graphs are included to illustrate the results obtained.

Appendix H contains a user's guide to the COVIDSIM software, the pandemic resource simulator, which integrates the simulation model developed in Chapter 6. This guide explains all the features of the software and the steps for its use. The data used in the guide were provided by the main hospital of La Rioja (San Pedro Hospital).

2 Background

This chapter describes the motivational background to each part of the thesis. Section 2.1 provides a description and extended definition of ICUs and an indication of the undesirable consequences of bed shortages. This section is related to the simulator developed in Part I to study decision-making in the ICU. Secondly, Section 2.2 describes the evolution and impact of the COVID-19 pandemic worldwide, including the social, economic, and healthcare consequences. Some of the new and emerging challenges involved in managing this outbreak are mentioned in this section and further explained in Part II, which presents the simulation model developed to predict hospital occupancy of COVID-19 patients.

2.1 Intensive Care Units

There is a large amount of medical literature relating to ICUs. As these Units are one of a hospital's most expensive and complex resources, most of the research deals with patient admission and discharge policies. This subsection begins with a conceptual description of an ICU, followed by an account of the associated management problems.

2.1.1 ICU definition

ICUs are special sections of the hospital for providing intensive medical care and are therefore fundamental for high severity patients and those likely to recover under complex monitoring. These Units have emerged with the development of technology for creating multiple organ support systems. However, although the purpose of ICUs is well defined, it is less clear which patients should benefit from this highly specialised care, especially in contexts of scarce resources. In an attempt to clarify this issue, the Working Group on Quality Improvement (WGQI) of the European Society of Intensive Care Medicine (ESICM) established in 2011 (Valentin et al. 2011) a set of criteria to determine which patients might benefit from admission to an ICU:

- Patients requiring monitoring and treatment because one or more vital functions are threatened by an acute (or an acute on chronic) disease (e.g., sepsis, myocardial infarction, gastrointestinal haemorrhage) or by the sequelae of surgical or other intensive treatment (e.g., percutaneous interventions) leading to life-threatening conditions.
- Patients with failure in one vital function (cardiovascular, respiratory, renal, metabolic, or cerebral) but with a reasonable chance of meaningful functional recovery. As a rule, patients known to be in the terminal stage of an untreatable disease are not admitted. Sometimes patients in need of palliative care requiring intensive care measures may be considered.
- Patients with brain death or in whom brain death is expected to occur and in whom organ donation is considered may be admitted.

From a normative point of view, in Spain, the “Real Decreto 1277/2003”, which establishes the general rules for the approval of health centres, services and facilities, defines Intensive Medicine as “a healthcare Unit in which an intensive medical specialist is responsible for providing accurate, continuous and immediate health care to patients with pathophysiological alterations that have reached a level of severity representing a current or potential threat to their life but still have potential for recovery”. In 2010, the Ministry of Health and Social Policy of Spain issued a report on ICUs (Palanca et al. 2011), proposing a definition of ICU as “an organisation of health professionals offering multidisciplinary assistance in a specific hospital ward satisfying the necessary functional, structural and organisational requirements to guarantee the conditions of safety, quality and efficiency needed to assist patients who, while having potential for recovery, require full or basic respiratory support along with dual or multiple organ support, and any complex patient with multi-organ failure. The ICU can also care for patients requiring a lower level of care”. Thus, both from the care and regulatory perspective, there is a need for clarity with respect to the characteristics of patients eligible for admission to ICU (high severity, complex monitoring, and reasonable expectations of recovery).

Despite these efforts to define ICU admission eligibility characteristics, in practice, few hospitals use admission criteria (Barnato et al. 2007). This is partly because they are usually very general and susceptible to subjective interpretation. In addition, concepts such as “reasonable chance of recovery”, “expected prognosis”, and “quality of life after discharge” have not been fully defined for all the pathologies that motivate ICU admission, and are therefore used differently among physicians. Furthermore, there is no precise definition of what is covered by the term “ICU bed”. In some regions it is related to the severity of the disease and the possibility of sustaining the various organic dysfunctions, while, in others, it is based on the intensity of the allocated medical and nursing support (Murthy and Wunsch 2012). Globally speaking, however, the ICU bed is where the patient satisfying ICU admission criteria is treated.

2.1.2 ICU bed management

It is the lack of a strict admission protocol and the subjective component in the decision-making process that motivate the research on patient admission and discharge policies in the medical literature. Several studies show that when there is a shortage of beds in the ICU, both admission and discharge are subject to triage processes (Shmueli et al. 2003; Dobson et al. 2010; Anderson et al. 2011). Costa et al. (2003) observe changes in ICU management policy as bed occupancy rises, such that physicians try to limit admissions or resort to early discharge for patients whose condition permits it. Ridge et al. (1998) report early discharge and transfer to a less ICU of more fully recovered patients as a typical solution when there is a bed shortage in the ICU. In general, a high ICU bed occupancy level increases the number of rejected admission requests and the severity threshold for admission, while shortening patients' LoS (Sinuff et al. 2004; Walter et al. 2008). The main objective is often to free up ICU beds (Capuzzo et al. 2010; Kramer et al. 2012; Robert et al. 2012; Sprung et al. 2012; Marmor et al. 2013). Other consequences of an excessive bed occupancy rate are scheduled surgery cancellations and interhospital patient transfers. Therefore the patient discharge process is influenced not only by patient health factors but also by environmental and organisational issues (Lin et al. 2009).

Another factor influencing ICU bed management is the cost per bed, which is much higher than for a standard hospital bed, due to the high-tech equipment, and, more especially, the large number of staff required to run these Units. According to Halpern and Pastores (2015), ICU costs per day in 2010 amounted to \$4,300 in the US, while the total annual cost of critical care medicine amounted to \$108 billion. In a previous study, Halpern and Pastores (2010) estimated that critical care accounted for 13.4% of total hospital costs, 4.1% of the national health budget, and 0.66% of the gross domestic product. In highly developed European healthcare systems, the mean actual cost per ICU patient was estimated at €17,000 in Greece (Geitona et al. 2010), whereas the calculated average cost per ICU patient was €1,200 per day in Germany, Italy, the Netherlands, and the United Kingdom (Tan et al. 2012). Lefrant et al. (2015) estimated the daily cost of ICU stays on a sample of 23 ICUs in French National Hospitals as €1,425 (95% CI = €1,323 to €1,526). Mahomed and Mahomed (2018) conducted a study of intensive care services at a central hospital in the South African public sector, including a retrospective cost analysis for the 2015/16 financial year across two ICUs, a 10-bed trauma ICU and an 18-bed combined neurosurgical / medical / general surgical ICU. The estimated cost per patient day in the combined ICU was 58% higher than in the trauma ICU (ZAR26,954 v. ZAR17,021 or the equivalent of €1,642 v. €1,037).

Therefore, the efficient use of these resources in ICU management and, by extension, general hospital management is essential. According to the latest guidelines of the Society of Critical Care Medicine (SCCM) for ICU admission, discharge, and triage (Nates et al. 2016), more research is needed on all aspects of critical care rationing to address current deficiencies. Furthermore, the bed occupancy rate is highly variable and rather unpredictable, since it

depends both on programmed factors, such as surgery requiring post-operative referral to the ICU, and random factors such as emergency admissions. This implies that too strong a focus on high occupancy, to avoid wasting costly resources, can mean that there is no free bed for a newcomer requiring it.

Most ICU costs are fixed (irrespective of the occupancy level); thus, from an economic point of view, it is preferable for an ICU to maintain high bed occupancy and thus avoid the underuse of an extremely costly service (Halpern and Pastores 2010). However, bed shortages trigger the undesirable consequences listed previously: cancellation of scheduled surgeries, delayed or refused admissions to the ICU, and early or inadequate discharges of patients to free up beds, all of which are associated with poorer prognosis (Chalfin et al. 2007; Cardoso et al. 2011) and a higher risk of mortality (Young et al. 2003; Iapichino et al. 2004; Bing-Hua 2014). Thus, from a clinical point of view, high occupancies will be avoided.

2.2 The COVID-19 pandemic

The coronavirus disease 2019 (COVID-19) pandemic is a crisis caused by severe acute respiratory syndrome coronavirus 2 (SARS-CoV-2). The first outbreak was detected in the city of Wuhan, Hubei Province, China, in early December 2019, and it soon spread to the rest of Hubei and all the country's remaining provinces. Within mainland China, the epidemic was largely under control by mid to late March 2020, having generated more than 81,000 cases (cumulative incidence on March 20, 2020). This was primarily due to intensive quarantine and social distancing (SD) measures (Novel 2020; Wang et al. 2020). These measures included, among others, isolation of detected cases, tracing and management of close contacts, and closure of potential zoonotic sources of SARS-CoV-2. There were also strict traffic restrictions and quarantine of entire provinces, including suspension of public transport, closures of airports, railway stations and inner-city highways. Mass gathering events were also cancelled; and various other measures were introduced to reduce transmission of infection.

Despite unprecedented national control measures, COVID-19 was not completely contained and the disease reached other countries. By January 31, 2020, the number of confirmed cases reached 9,776 worldwide with a death toll of 213, and the World Health Organization (WHO) recognised the epidemic as a Public Health Emergency of International Concern (PHEIC) (WHO 2020a). By February 9, 2020, the global death toll had risen to 811, surpassing the total death toll of the 2003 SARS epidemic, and the confirmed cases continued to climb globally. On March 11, 2020, the WHO finally declared the outbreak a pandemic (WHO 2020b). The effects of the COVID-19 pandemic have rapidly spilled over from the healthcare sector into the international trade, tourism, travel, energy, and finance sectors, causing severe economic and social repercussions (Lenzen et al. 2020). Although other worldwide public health emergencies, such as the swine flu pandemic of 2009, have been brought under control in the

past (Ferguson et al. 2005; Longini et al. 2005; Nsoesie et al. 2012, 2014), the socio-economic repercussions of the COVID-19 pandemic are of a magnitude unparalleled in recent history.

In healthcare terms, the COVID-19 pandemic poses a major global threat to human health. Since the outbreak in China, more than 270 million confirmed cases, and more than five million deaths from COVID-19 infection (up to the end of December 2021 <https://coronavirus.jhu.edu/map.html>) have been recorded. Regular updates on the COVID-19 outbreak are available on the websites of the [European Centre for Disease Prevention and Control \(ECDC\)](#), the [European Commission \(EC\)](#), and the [WHO](#). This outbreak has brought changes in health care delivery, and in hospital systems stretched by the sudden increase in demand. The treatment of COVID-19 patients requires dedicated resources, material, and personnel. The pandemic has had a particularly intense impact on ICUs, which require highly specialised personnel and costly technical equipment. Accurate planning requires accurate prediction of resource needs. In addition, hospitalised COVID-19 patients need to be isolated from other types, making advance preparation of wards necessary. Therefore, the management of both ICU and ward beds for COVID-19 patients benefits from accurate short-term demand forecasting. Other resource needs, such as personnel requirements, can be calculated from bed demand numbers. Usually, the hospitalisation bed is still widely used as a hospital (ICU) management parameter both at the strategic and operational levels.

The number of hospitalised COVID-19 patients needs to be forecast in order to determine the allocation of resources to COVID-19 and non-COVID-19 patients. The health status of a COVID-19 patient can change rapidly and unexpectedly (Murk et al. 2020). As a result, it is not possible to accurately forecast the resource needs of COVID-19 patients many days in advance (Ioannidis et al. 2020). With COVID-19 patient data becoming increasingly available, it is possible to predict the infection rate a few days in advance (Wu et al. 2020), and also the LoS (Ebinger et al. 2021). Predictions of the number of hospitalized COVID-19 based on regression methods can be found, for example, in (Manca et al. 2020; Farcomeni et al. 2021; Goic et al. 2021). Methods for estimating LoS for patients with COVID-19 infection in the UK using both a nationally collected dataset and local data from a large inner city hospital are proposed in (Vekaria et al. 2021).

Hospitals are complex systems evolving in a stochastic environment with a level of uncertainty which intensifies during pandemics due to lack of knowledge about the spread of the disease and its consequences for those infected. In this unsettled context, simulation emerges as a suitable tool of analysis, since it is able to reproduce both the complexity of the system and the variability and uncertainty of the environment, as well as being eligible for use in combination with other analytical techniques. The literature contains numerous bibliographical references relating to the use of simulation models for decision making in the healthcare context (Salleh et al. 2017). Most applications use simulation to support strategic decisions, usually for resource sizing, scheduling or management. All these cases require the design of a simulation model to reproduce stationary state healthcare system performance and

evaluate resource levels, patient flow management policies, and the long-term decision making process. The recommendations obtained from the simulation analysis are intended for a pre-determined implementation period.

However, a simulation model designed to enable tactical decisions for the provision of specialist health resources during the current outbreak needs to focus on the transition period if it is to generate a short-term projection of the current state of the hospital. To achieve this goal, the simulation model must account for non-stationary and non-periodic patient input to the hospital, the evolution in the recovery of patients currently admitted to the hospital, variation in patients' hospital LoS patterns and censored data. Tools for real-time forecasting of COVID-19 ward and ICU bed occupancy, such as the data-driven model developed by Baas et al. (2021), enable hospitals to make informed decisions about whether or not to admit additional COVID-19 patients into their ward or ICU.

Part I

**Analysis of Intensive
Care Unit bed
management using an
interactive simulator**

3 The dilemma of the last bed

Faced with a full Intensive Care Unit (ICU), physicians need to decide between diverting a new patient in need of critical care to another facility or freeing up a bed by prematurely discharging an already admitted patient. This dilemma is discussed extensively in the medical literature, where the influencing factors are identified, the patient discharge process is described and the consequences for patient health are analysed.

This chapter is organized as follows. We first begin with an introduction in Section 3.1 describing the dilemma of the last bed and including some literature focused on this problem. The problems inherent in the shortage of beds are shown in Section 3.2, in terms of triage of patients admitted to the ICU or for possible ICU admission, referral to other centres, cancellation of surgeries and stress in medical staff. Section 3.3 describes an illustrative example of the last bed dilemma, showing the differences in decision-making by ICU professionals in this specific situation with real patients. Finally, Section 3.4 ends the chapter with some conclusions.

3.1 Introduction

Teres (1993) posed as one of the great ethical dilemmas a situation that he described as the ritual of the last bed. This situation occurs when the occupancy of the ICU is at the limit, and the physicians must decide on the admission of a new patient. The increase in the ICU occupancy rate and access block rates are leading to complete or even overwhelmed ICUs (Duke et al. 2009; Hall 2013). The average occupancy rate of ICUs in the US is 90% (Pronovost et al. 2004), where it is reported that 90% of ICUs cannot provide beds when required (Green 2002). In this chapter we consider a broad definition of the dilemma of the last bed, as it is discussed in (Azcarate et al. 2020); it is not only how to assign the last available bed but how is the physician decision making respect to the admission and discharge of patients as the ICU is getting full. Physicians have to assess the benefits that receive patients already at the ICU and confront them with the benefits that could receive future patients coming from scheduled

surgeries and other potential emergency patients. Clearly, no physician wants neither to divert an emergency patient nor cancel a surgery nor to discharge in advance a patient, but these decisions may be inevitable in high bed-occupancy situations.

The discharge decision problem has been addressed by developing optimization models trying to minimize the number of rejected admissions and the LoS shortened for patients in the ICU (Mallor et al. 2015, 2016). They formulate a stochastic optimization problem that is solved by using a simulation-based optimization methodology. The solutions determine the service rates at which the queue model representing the ICU should work to achieve the goals and they are interpreted as probabilities of discharging patients in advance, which are dependent on the bed-occupancy level. These models provide normative policies that can be classified into three types (Mallor et al. 2015): aggressive, equitable, and cautious.

Mathematical models usually propose “aggressive” discharge policies, that is, no actions are taken until there are no free beds and one of them must be released to admit a new incoming patient. Nevertheless, physicians consider another more “cautious” policy, which is more representative of the decision-making that occurs in practice. They claim that early discharge of patients is more frequent as more beds are occupied, but these decisions are made before the ICU is complete. In situations of high occupancy, they advance the discharge of a patient in time in order to anticipate future emergency and scheduled patients’ arrivals. In this way, physicians avoid extreme occupancies in which patients are discharged at unconventional hours, which increases mortality if the discharge occurs at night (Azevedo et al. 2015). Mallor et al. (2016) propose a queuing model with LoS dependent on occupancy level. However, in this model, the exchange between a patient who is discharged and another who enters is considered instantaneous.

3.2 The problems inherent in the shortage of ICU beds

The ICU bed is a very costly resource, as it is exposed in Section 2.1.2. So low occupancy means under-utilization of an excessively expensive service since most of the costs do not depend on the degree of bed occupancy (Carrasco et al. 2006). However, occupancy is highly variable and unpredictable, as it depends on both programmed factors, such as surgery requiring post-operative referral to the ICU, and random factors such as urgent patient admissions. This implies that some management policies focus on high occupancy to avoid wasting an expensive resource. And in certain circumstances, the problem of a lack of a bed for a patient who requires it arises. In the following subsections, the problems related to bed shortages are described.

3.2.1 Triage of patients admitted to the ICU

One of the procedures, when a bed is urgently required, is the triage of admitted patients. That

patient with better clinical status is transferred to another area of the hospital with less care, in order to free up a bed. Since ICU discharge management is complicated, this triage process occurs not in situations of imminent need, but in situations of high occupation, when new admissions are planned.

Patients can be early discharged if the physician who treats them and is responsible for assigning discharges, has the conviction that there are guarantees to attend them properly in another ward of less assistance. Thus other patients of greater severity can benefit from admission to the ICU (Ouanes et al. 2012). The consequences of these discharges have been evaluated concerning one or several markers of the evolution of patients who suffer from them: hospital mortality, readmission to the ICU and hospital length stay (Kramer et al. 2013).

Most of the published papers in this regard find a relationship between early discharges and an unfavourable result for the patient. However, some studies on this subject do not find a relationship between non-scheduled discharge and mortality (Singer et al. 1983; Strauss et al. 1986), perhaps because their mortality rates are lower than in the rest of the papers and the impact of early discharge on it would also be lower. In turn, (Campbell et al. 2008) determine that non-scheduled discharges at night are not related to a higher admission rate or higher mortality.

3.2.2 Triage of patients for possible ICU admission

Another consequence of high bed occupancy levels in an ICU is the triage of patients susceptible to admission. This fact has been analysed by medical literature from two points of view. On the one hand, some studies focus on the increase of admitted patients' severity when the availability of beds is low, and on the other hand, some papers analyse the consequences of patients who in situations of greater availability of resources would have been admitted to the ICU.

Regarding the first point of view, Sinuff et al. (2004) conclude that, in situations of high occupancy, admitted patients are more severe, reducing the number of patients admitted for monitoring. Authors propose the possibility of Intermediate Care Units for patients who require monitoring and minor care to those provided in the ICU. In this way, the use of ICU beds would be rationalized.

Regarding the second point of view, Robert et al. (2012) conduct a study on patients whose admission to the ICU was initially denied. The study is conducted in 10 ICUs in France, during two 45-day periods. The admission to the ICU is denied due to lack of beds, either initially or permanently, to 193 out of 1,332 patients. It is observed that mortality is higher among patients who are not admitted or those who have a delayed admission, compared to those who are admitted in the first instance.

The European Society of Intensive Care Medicine's (ESICM) ethics section establishes principles on which decisions should be made (Sprung et al. 2013), in order to help in the triage process (both of patients already admitted and of patients that are susceptible to be admitted). These principles are based on the consensus of 37 professionals related to Critical Medicine, getting an agreement of at least 80% of the participants for each of the discussed points. However, despite these recommendations and the implications of triage, there are hardly any scales that facilitate these decisions (Sprung et al. 2012).

3.2.3 Referral to other centres

When there is a shortage of beds in the ICU, it is necessary to divert patients to another nearby centre where there are available beds and patients can be admitted there. The referral of patients involves two types of problems. The first one is the risk inherent in the referral itself, and the second one is the delay in the adequate care of patients caused by the time they remain outside the hospital.

On the first problem, Ligtenberg et al. (2005) analyse in Netherlands the risks associated with the inter-hospital transport of 100 consecutive patients. They observe that adverse effects occurred in 34% of these referrals, of which 30% were due to technical problems. There are no published papers that study the relationship between the result of the diverted patient and the medical staff and equipment used in such referral. For instance, in Navarre, these transports of critical patients are carried out by specific personnel for this task that is highly qualified. So, it is assumed that the risks associated with the referral are low.

However, more important than the implicit risk of the referral is the delay that this may cause to the appropriate treatment of patients. There are pathologies such as acute myocardial infarction (AMI), sepsis, or cerebral stroke, in which early treatment is very necessary. (Chalfin et al. 2007), after analysing 50,322 patients who required admission to the ICU, conclude that those whose admission is delayed more than 6 hours present greater hospital length of stay (LoS) and higher mortality in ICU and hospital. In addition to this, other studies recognize an increase in mortality when admission to the ICU is delayed (Combes et al. 2005).

3.2.4 Cancellation of scheduled surgeries

Another response to the lack of ICU beds consists of cancelling the scheduled activity, usually highly complex surgeries. Although this seems the most feasible and intuitive solution, it faces two important problems. On the one hand, the possibility that patients worsen their health status or even die while they are on the waiting list and, on the other hand, the administrative pressure to meet response deadlines (Colmenero 2011).

Scheduled patients who have been cancelled have a priority position on the waiting list, but both they and other patients in subsequent positions on the list have an additional risk of health

deterioration. For instance, Sobolev et al. (2013) analyse the evolution of 12,030 patients awaiting surgery for coronary revascularization, of whom 104 die and 382 have to undergo emergency surgery.

3.2.5 Stress in medical staff due to work overload

The work overload, the unavailability of beds, which results in a rapid exchange of patients, and situations in which patient triage is necessary are factors that have been associated with a higher level of stress among medical personnel of the ICU (Embriaco et al. 2007; Verdon et al. 2008; Halpern et al. 2013).

Different studies associate this stress with medical errors. Valentin et al. (2009) conduct an extensive study in 113 Units of 27 countries about errors made in parenteral drug administration. They report 74.5 error events per 100 patients per day (95% confidence interval 69.5 to 79.4). Most of these errors are due to medication omissions or supplies at the wrong time, although 0.9% of the patients studied die or experienced permanent harm because of these errors. In 32% of all errors, Unit staff admits workload, stress, or fatigue as a contributing factor.

In conclusion, given a standard situation in which the medical staff is under stress, work overload and bed shortages represent an additional stress factor. In these situations, medical errors are more frequent, resulting in worse results for patients admitted to the ICU.

3.3 An illustrative example of the dilemma of the last bed







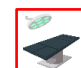
The problem of the last bed is not just a theoretical concept, but it occurs many times at hospitals: whenever several patients need treatment at the ICU at the same time, but there are no available beds for everyone. A specific situation is presented below, with real patients, to illustrate better this problem. The chosen scenario is a real situation that ICU physicians usually face.

An ICU with only 4 beds is assumed, and 3 of them are occupied by three patients who have different diseases and ages, which are not totally recovered. In the first bed, there is a 56-years old patient (Peter) who has a brain infection due to a virus. In the second bed, a 73-years old cardiac surgery patient (Phil) is allocated. In the third bed, there is a 63-years old patient (Cate) with a lung infection due to a bacterium.

ICU physicians, during the clinical morning session, must discuss whether these patients continue to be treated in the ICU or are early discharged. At that moment, physicians are informed about an ambulance that is coming to the ICU with another patient (Harvey, 28), who has suffered a traffic accident and he has head trauma. Besides this, two scheduled surgeries

need admission for the ICU that day. The first one is to treat a patient (Anne, 37) with a brain tumour, and the second one is for a patient (Paul, 52) who has suffered a heart attack. So, in this situation, not only discharge decisions have to be made, but physicians also must decide whether the incoming patient is accepted or diverted to another hospital, and which surgery is confirmed or cancelled. In summary, what physicians have to decide is which patients must be treated in these four beds. Table 3.1 shows all the relevant information of patients that must be managed at that moment (detailed clinical information of these patients is provided in Appendix B.1).

Table 3.1. Patients to manage in the example of the dilemma of the last bed.

Location	Patient	Age	Principal diagnostic	Icon
Bed 1	Peter	56	Acute viral meningoencephalitis due to Herpes Simplex Virus I	
Bed 2	Phil	78	Postoperative control of aortic valve replacement cardiac surgery	
Bed 3	Cate	63	Severe community-acquired pneumonia due to Streptococcus pneumoniae	
Bed 4	-	-	-	
Ambulance	Harvey	28	Polytrauma with severe traumatic brain injury secondary to a car accident	
Waiting for Operating Room 1	Anne	37	Postoperative course of glioblastoma multiforme	
Waiting for Operating Room 2	Paul	52	Postoperative cardiac surgery for coronary artery bypass grafting	

Over this situation, an ICU physician can differentiate 21 reasonable decisions based on clinic, as it is shown in Table 3.2 (if all combinations were considered, the possibilities would rise to 57, which are provided in Appendix B.2, but many of them are unlikely in a real context, as discharging all inpatients and admitting no new patient). For example, decision number 2 consists of admitting only the emergency patient that is coming in the ambulance, and both surgeries are cancelled. In addition, no inpatient is early discharged with this election. However, decision number 12 is based on confirming both surgeries. Now, the incoming patient is diverted to another hospital, because only one inpatient has been early discharged (bed 2). Decisions number 15, 19, and 20 consist of admitting one out of the three patients requiring admission (emergency patient and both scheduled surgeries) and assigning one early discharge (bed 2). With these elections, physicians would reserve a free bed for future emergency patients considered in more severe conditions. Therefore, it is clear that in order to manage these situations, physicians can (1) refer patients to other hospitals, (2) cancel scheduled surgeries, and (3) shorten the inpatients' LoS.

Table 3.2. Selected decisions based on clinics in the example of the dilemma of the last bed. The last column includes the number of practitioners out of 90 that would make each decision in a real ICU.

Decision	ICU occupancy	Deviations/Cancellations	Early discharges	Practitioners
1			-	-
2			-	7
3			-	-
4			-	-
5				-
6				1
7				29
8				26
9				1
10				1
12				4
15				6
19				1
20				1
24				-
26		-		1
28		-		10
29				-
30				-
33				1
34				1

This situation was presented to 90 different practitioners working in the ICU (31 physicians, 40 nurses, 18 nurse technicians, and 1 resident). As it is exposed in Table 3.2, they made different decisions to manage the situation. Slightly more than 60% of the practitioners (55 out of 90) decided to admit the emergency patient and one of the surgeries, discharging the patient located in bed 2 (decisions number 7 and 8). 3 more people opted for the same decision although they discharged a different patient (decisions number 6, 9, and 10). A group of 15 individuals confirmed the two scheduled surgeries, with the difference that 11 of them also admitted the emergency patient (decisions number 26 and 28) and the other 4 diverted him (decision number 12). There were also a total of 10 people who reserved a free bed for future admissions. 8 of these persons admitted one out of the three patients requiring admission (decisions number 15, 19, and 20) while the other 2 cancelled only one scheduled surgery (decisions number 33 and 34). Finally, 7 practitioners decided not to discharge any patient and to admit only the emergency patient (decision number 2). Table 3.3 shows the decisions made in this situation by all professionals separated by type of employment.

Table 3.3. Decisions made by the 90 professionals separated by type of employment in the ICU.

Decision	Physician	Nurse	Nurse tech	Resident
2	3	2	2	0
6	0	1	0	0
7	6	16	7	0
8	14	11	1	0
9	0	1	0	0
10	0	1	0	0
12	3	1	0	0
15	3	1	2	0
19	0	1	0	0
20	0	0	1	0
26	1	0	0	0
28	1	4	4	1
33	0	0	1	0
34	0	1	0	0
Total	31	40	18	1

The differences in decision-making observed in Table 3.2 and Table 3.3 motivate us to develop statistical methods for their analysis in the future. The definition of distances to compare the results would allow the graphical representation of each of the decisions. By applying clustering methods, it would be possible to identify the most similar decisions to each other and characterised them in order to determine the type of strategy followed in each case.

3.4 Conclusions

The medical literature reviewed in this chapter highlights the existing ICU saturation problem and its patient health implications, and describes the triage of current ICU patients. The dilemma of the last bed is a real and relevant, continuously occurring problem in the ICU and its importance multiplies in a time of pandemic. States of saturation must be included in mathematical models intended for use in the analysis and improvement of hospital management. These situations are worth studying both from the clinical and the quantitative point of view and cannot be ignored in any mathematical model that is intended for decision-making analysis.

Early patient discharge has become an ICU management tool. With it, physicians try to balance the percentage of admission refusals due to a full ICU and the degree of LoS reduction for patients already admitted. The patient discharge process, as described in the literature, can take several hours, because it involves physicians from other units and the patient's family. These factors are important in guarding against the instantaneous substitution of one patient with another in an ICU bed.

However, most of the mathematical models found in the literature treat ICU patient transfer as an instantaneous event. These models neglect the entire discharge process, despite their focus on obtaining an accurate representation of the stochasticity of the patient arrival process and patient LoS. This is no minor issue, as it implies a misrepresentation of the discharge decisions made prior to the arrival of a newcomer needing the bed that would be freed up by discharging some inpatient. None of the queuing theory models or other stochastic models in the mathematical literature include this anticipatory process. Thus, the management policies examined in the mathematical models consider only the triage of the last bed, while ignoring the pressure on physicians working close to full capacity. Existing ICU simulation models with these characteristics are reviewed in more detail in Chapter 4. Any model of ICU physician discharge decisions must include the bed requirements of planned elective surgery arrivals, which requires that early discharge decisions be made prior to full occupancy.

Regarding the example of the dilemma of the last bed given in Section 3.3, we can note that the responses to this simple realistic example reveal variability in decision making relating to patient admission and discharge and motivate the need to create a tool to facilitate the analysis of such decisions. The tool presented in Chapter 4 not only generates scenarios of the type described, it represents the evolving ICU system over time by implementing the decisions suggested by the users. In this way, users are able to observe the consequences of their decisions and learn by doing. The success of the interactive simulator stems from its ability to recreate this environment by mimicking real ICU dynamics and including all the information required to support the decision making.

4 Management Flight Simulator of an Intensive Care Unit

This chapter presents a computational tool useful for the analysis of the decisions made by physicians related to the admission and discharge of patients in an ICU. The analysis of patient-admission and inpatient-discharge decisions can be done safely in virtual environments that reproduce with high fidelity the characteristics and dynamics of an ICU. In this chapter, a Management Flight Simulator (MFS) that mimics a real ICU is presented. The main features that distinguish this simulator from others are the simulation of the patients' stay by evolving their health status (instead of using a single LoS value) and the recreation of real discharge and admission processes. Both elements are determinant for creating credible virtual scenarios allowing the users the management of the ICU as they would do in a real ICU, that is, with the same information and environment.

The simulator records all the admission/discharge decisions made by users. The analysis of the recorded data about cancelled surgeries, early discharged inpatients, admissions delayed, diverted patients, etc. can be used to characterize bed management policies implemented by users. Furthermore, differences among users can be detected and quantified as well as the identification of scenarios in which decisions differ the most. These controversial scenarios are of special interest for physicians because they support the discussion to elaborate consensus protocols for triage decisions in the hospital that can help to reduce variability in medical practice. Therefore, the purpose of the developed MSF is double: firstly, to characterize how physicians made decisions and to assess the variability among physicians in making such decisions; secondly, providing a training tool for the management of ICUs.

This chapter is organized as follows. In Section 4.1 related literature is reviewed about the use of simulation models in ICUs, as well as the use of MFS. The mathematical modelling of the ICU dynamics and its implementation in a DES is presented in Section 4.2. Section 4.3 focuses on the simulator itself, detailing different features of this tool such as the definition of

virtual ICUs, the initialization process, the interface, and the recorded data. Finally, this chapter closes with a discussion and the conclusions in Section 4.4.

4.1 Literature review

In this section, we review relevant literature related to the use of simulation models in ICUs, as well as the use of MFS (flight/virtual/serious game simulators) in general and in health care services in particular.

4.1.1 Simulation in ICU

Simulation is a very suitable tool to study stochastic and complex systems such as hospitals and, in particular, ICUs. Since Fetter and Thompson (1965) published a paper about the simulation of various subsystems of a hospital, simulation models for decision-making in healthcare context have been developed in order to study problems related to patient flow bed-planning, waiting list management, health service design, medical staff scheduling, operating theatre management, etc. Bibliography about reviews of these simulation models can be found in (Fone et al. 2003; Brailsford et al. 2009; Günal and Pidd 2010; Katsaliaki and Mustafee 2011; Rais and Vianaa 2011; Mielczarek and Uziako-Mydlikowska 2012; Zhang et al. 2018).

With regard to the ICUs, sizing and management problems have been studied through simulation models. Bai et al. (2018) review Operations Research (OR) methods used in ICU management, which include simulation. The medical literature uses simulation to propose mathematical solutions to ICU capacity problems in (Costa et al. 2003; Nguyen et al. 2003; McManus et al. 2004; Shahani et al. 2008; Pearson et al. 2012; Zhu et al. 2012; Steins and Walther 2013) and the need to optimize surgery admissions and the distribution of beds (Kolker 2009; Troy and Rosenberg 2009; Yang et al. 2013).

Mathematical studies also include simulation models for analysing ICU capacity problems (Ridge et al. 1998; Masterson et al. 2004; Litvak et al. 2008) and ICU admission and discharge processes (Kim et al. 1999). Furthermore, Kim et al. (2000) compare bed allocation rules using bi-objective optimization and Griffiths et al. (2013) propose a bed management optimization making a distinction between emergency and scheduled surgery patients. Other studies analyse changes in the patient-flow circuit with the use of intermediate care wards (Marmor et al. 2013; Rodrigues et al. 2018). Griffiths et al. (2005), given a current bed occupancy, present a simulation model to adjust staffing; and Steins and Walther (2013) assess bed occupancy and patient transfers to other ICU facilities in view of a shortage of resources. All these models have the ultimate goal of minimizing the rejection of patients arriving at the ICU while maintaining a manageable occupancy level.

There are also some studies (Ridge et al. 1998) in which early discharge is suggested as a bed management tool, but they are not explicitly modelled. In order to obtain valid simulation models, it is necessary to include the process of physicians' patient-discharge decision-making (Barado et al. 2012; Mallor and Azcárate 2014). These authors embedded the simulation model in an optimization framework in order to mimic the physicians' decisions through the calibration of patient discharge parametric rules. Azcárate et al. (2012) perform a sensitivity analysis of the effects of such discharge decisions on ICU rejection rates and LoS of patients. They implemented their discharge decision models in a simulation framework with no time-consuming discharge processes. Mallor et al. (2015) assess by simulation modelling the optimal discharge strategies obtained in (Mallor et al. 2016).

The literature reviewed shows that some researches can propose mathematical solutions to problems associated with ICU capacity and bed management. However, as far as we know, there are no papers that provide an analysis of how physicians' decisions are really made in ICUs.

4.1.2 The use of management flight simulators

MFS, also known in the literature as virtual simulations, can be used both as a learning-training tool and for research (Lamé and Simmons 2018). For research, this kind of simulators enables to analyse key processes, detect biases, and recreate decision-making processes, testing theories about them. As a learning-training tool, these MFS have a close connection with serious games, which are not only intended to entertain but are also used for pedagogical purposes (Sawyer and Rejeski 2002). According to Zyda (2005), a serious game is "a mental contest, played with a computer in accordance with specific rules, that uses entertainment to further government or corporate training, education, health, public policy, and strategic communication objectives." Long before the term "serious game" began to be used, some games were already developed with a purpose other than entertainment.

An example of this is The Beer Game (or the Beer Distribution Game), which was developed in the 1960s at the Massachusetts Institute of Technology's (MIT) Sloan School of Management. Since Sterman (1989a, 1992) popularized this simulation game, one of the most popular games used in logistics management and production management class, many applications have appeared in which The Beer Game has been utilized in order to research the behaviour of participants (Snider et al. 2010; Jin 2015; Alfieri and Zotteri 2017). In other cases, the original game has been modified to investigate new approaches (Goodwin and Franklin 1994; D'Atri et al. 2009; Sarkar and Chaki 2012).

In addition to The Beer Game, there are more management games in the economic context in which researchers analyse the behaviour of a group of people, as well as the participants learn from the experience (Joseph 1965; Dolbear, Jr. et al. 1968; Sterman 1989b; van Miltenburg 1989; Lengwiler 2004; Borrajo et al. 2010; Pozo-Barajas et al. 2013). Besides, the

use of this type of simulations as a learning tool is usual in other contexts such as politics (Sawyer and Rejeski 2002; Kahn and Perez 2009) and environmental care (Moxnes and Saisel 2009; Worm et al. 2010; Bathke et al. 2019; Kim et al. 2019). All these applications focus on management learning for general situations, and new concepts acquired by participants can be applied at any time in the real processes. Furthermore, there are other types of simulators, designed for specific situations as defence, aviation, and construction, where decision-making processes are crucial for specific situations. Virtual Reality (VR) simulators are developed here to include a real description of the environment.

In defence area, Chung and Huda (1999) developed a simulator to better respond to bomb threats; Wahl et al. (2020) present a simulator-based training of professional maritime deck officers so as to improve critical operations at sea; and Goldberg and Knerr (1997) and Saastamoinen et al. (2019) use training simulators for army and marine cadets respectively. VR simulators are also useful to train firefighters as it is proved in (Cha et al. 2012).

In aviation, apart from traditional flight simulators used to capture flight skills, new types of simulators are arising. Koglbauer (2015) designed a simulator training for students to improve the estimation of collision parameters; Kraemer et al. (2019) analyse the behaviour of four different pilots during the take-off after managing a flight simulator developed by Aeronautics Institute of Technology (ITA) and Embraer. Furthermore, Valentino et al. (2017) designed a VR flight simulator that simulates the environment of a real flight. This simulator is able to provide stronger sensations than traditional flight simulators.

In terms of construction applications, both types of simulators have been found. On the one hand, Sherif and Mekkawi (2010) present in their work an Excavation Game, a computer-aided-learning tool that focuses on improving students' decision-making skills in the aspects of excavation and related activities. On the other hand, VR training systems are presented in (Oliveira et al. 2007; Vahdatikhaki et al. 2019) for industrial training.

Although no articles have been found in which these methods are used in healthcare to learn about the complexity of the ICU management, many healthcare applications have been developed in which virtual simulation has a relevant role in order to teach students at universities and especially to learn from the experience of using (Lane et al. 2001). Most of these are traditional simulations, and they use patient care manikins or play-role patients. Sherwood and Francis (2018) made a systematic review of the effect of this kind of mannequins in terms of learning for nursing, midwifery, and allied healthcare practitioners. Other types of works, not as popular as previous ones, are those which develop VR simulators or implement a decision-making process in management games. Sauré and Puterman (2014) developed an easy to use teaching game to learn how to manage patients appointment scheduling, whereas Vliegen and Zonderland (2017) designed a classroom game to introduce Operations Management (OM) in healthcare.

VR simulators developed in the healthcare context intend to transfer skills, as they do in other contexts Brown et al. (2012) designed and developed a virtual world for teaching and training Intensive Care nurses in the approach and method for shift handover. VR simulators are also used in urological training, replacing traditional training approaches (Aggarwal and Adhikary 2017). But, where this tool is commonly used in healthcare is at operating rooms, with the objective not only for the learning of beginning surgeons but also as a training to reduce the operating time. Jain et al. (2019) developed a VR surgical simulator that facilitates trainees for functional endoscopic sinus surgery. The positive effect of these kinds of simulators is also demonstrated in (Seymour et al. 2002; Fried et al. 2010; Lopez-Beauchamp et al. 2020).

Management games in healthcare, mainly known as hospital management games, gained importance because of the increment of health care costs due to expensive technology, ageing of the population, and the increasing number of demanding patients. This type of games first appeared during the 1970s and Kraus et al. (2010) made an extensive review of different hospital management games. These games simulate situations of the real world modelling complex decision-making processes, which are influenced by the external hospital environment. In the review, the authors distinguish functional games that are applied to specific hospital departments and general games, which focus on the main function of the hospital. As a functional game, Hans and Nieberg (2007) developed the "Operating Room Manager Game" illustrating operating room management, whereas Rauner et al. (2008) designed an internet-based management game ("COREMAIN") to illustrate the economic and organizational decision-making process in a hospital.

We also found other examples of game-based simulators in the healthcare area not related to hospital management. Brown et al. (1997) designed an educational videogame to improve self-care among young people with diabetes. Grunewald et al. (2003) developed an interactive Web-based training program for radiology, which offers radiographic anatomy cases and exercises, with the possibility of selecting different levels of difficulty. The "HealthBound" model and game was developed to help people think widely about health reform options and discover for themselves a promising solution (Homer et al. 2007; Milstein and Hirsch 2009; Milstein et al. 2010, 2011). Katsaliaki et al. (2014) developed a game that simulates the supply chain of donor blood units to patients based on a real case study.

Finally, some studies have been revised that focus on the decision-making processes in resource management. Rodríguez et al. (2010) present a decision support system to help humanitarian NGOs better manage resources during a natural disaster response. Rauner et al. (2016) developed a policy management game to provide a learning-training tool for mass casualty incidents. Bean et al. (2019) programmed a patient flow simulator with which professionals and students can learn important concepts of patient flow and healthcare management.

Reviewing the literature about MFS we realized that those works that focus on management issues, then they are driven by theoretical concepts and models fail to reproduce with high fidelity characteristics of real situations. In these models, many assumptions are made in order to simplify them for the user and to avoid misunderstandings. By contrast, VR simulators, which transfer skills to the user, are very realistic, but then they do not present management-related features in broad contexts. Just as flight simulators in the aviation sector generate in pilots exactly the same autonomic responses when faced up with an emergency, whether this is real or simulated, medical simulations must generate autonomic, cognitive and behavioural responses in participants equal to those observed around medical tasks in the real world (Streufert et al. 2001). Fidelity is very important if we want to recreate participant's experience with total realism. In this chapter, we present an ICU simulator that combines, for the first time, these two different approaches (management decision processes are implemented in a real simulation environment).

4.2 Modelling an ICU

In this section, the mathematical modelling of the ICU dynamics is presented. In the first subsection, the modelling of the patient flow is exposed, explaining the discharge and admission process, discharge decision times, and the patient's health status. The second subsection focuses on the implementation of these features in a Discrete Event Simulation (DES) model, and the third subsection describes how to sample initial scenarios from the steady state.

4.2.1 Modelling the patient flow and admission/discharge decisions

An ICU can be mathematically modelled into the framework of queuing models. The queue model representation of the ICU considers that the servers are ICU beds, the clients are the patients that arrive randomly for emergency patients or according to a known schedule for those coming from elective surgeries, there is no waiting room and the queue discipline is "first come, first served". The service is individually provided with duration modelled by a probability distribution. This description leads to a queuing model $G/G/c/c$, where c is the number of the beds in the ICU.

Nevertheless, this model fails in modelling the dependence between patient LoS and the congestion level, allows for admissions and discharges at any time, the diversion of patients can occur only at full occupancy and the servers (beds) can switch instantaneously from one patient to the next one. In addition, the queueing model does not represent the real admission and discharge processes. These drawbacks preclude the use of this basic queue model to build the simulation model. Therefore, we extend the mathematical modelling of the ICU to represent more accurately both discharge and admission processes and to reproduce the patient's health

status while their stay in the ICU. The purpose of the mathematical modelling is to be implemented in an interactive simulator allowing the users to make informed decisions in a virtual environment as physicians do in real practice.

Discharge and admission process

Both the discharge and the admission of a patient are complex and not automatic processes. The discharge process needs the coordination of the ICU medical staff with their counterpart in the destination ward. Moreover, the necessary time to free up the bed depends on its necessity. In cases of imminent patient admission, the process speeds up and the discharging process could take around one hour, for example. However, when there is no urgency, the entire discharge process with peace could last from three to four hours.

The admission of the patient is virtually instantaneous when a patient arrives at the ICU and there is a totally cleaned and disinfected bed. When an admitted patient arrives at a full ICU and no recently freed up bed is ready yet, the patient is temporarily located in a special room where he or she can temporarily be treated.

The flow diagram in Figure 4.1 shows the admission and the discharge processes as they are considered in the simulation model. On the left side, the emergency and scheduled patients' arrivals are represented. Medical staff must decide whether to reject or admit them to the ICU. Scheduled patients first occupy a bed in the operating theater area (dark blue icon). Admitted patients occupy a free bed (white icon) in the ICU, when they are available, when not, the patient is placed in a bed in the above-mentioned special room (light blue icon). The right side represents the ICU where the beds can be in 7 different occupancy states: an occupied bed by a patient that is in the process of being discharged (dark grey icon); a bed occupied by a deceased patient (brown icon); bed under cleaning process (light grey icon); available bed (white icon); and occupied beds by patients in severe, stabilized and recovered health status (red, orange and green icons, respectively).

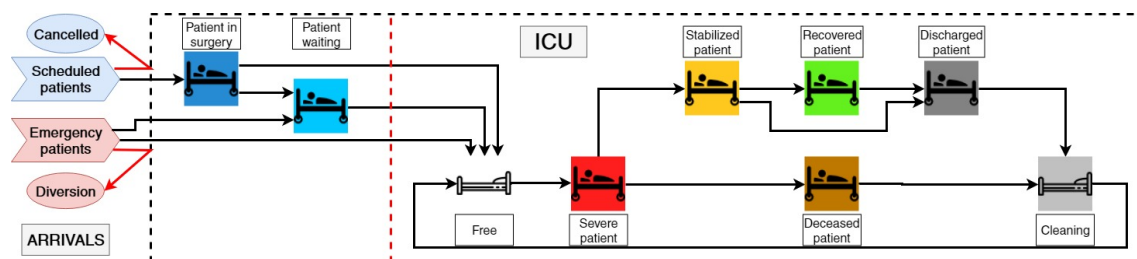


Figure 4.1. Representation of the dynamics of an ICU through the change of the bed's state. The two types of patients are distinguished (scheduled and emergency ones) and also the direct entry to the ICU from a delayed one.

Discharge decision times

Patient discharge decisions normally occur only at a few scheduled times of the day. These moments are denominated clinical sessions and depending on the ICU they can take place once,

twice, or even three times a day (morning, afternoon, and evening). During clinical sessions, physicians analyse the inpatients' clinical conditions and decide which ones are going to be discharged. They also propose possible patients who would be discharged if an emergency patient had to be admitted and there were no beds available. At the same time, in the morning clinical session, physicians manage the surgeries of that day, by either confirming or cancelling them.

Therefore, the patient cannot be discharged at any time, as it is implemented in classic queueing models. Essentially, the discharge decision process is periodic and throughout the day no more patients are discharged, except in the following case. When an emergency patient arrives at ICU, physicians decide on his or her admission, which in the case of admission in a situation of full ICU implies the discharge decision of an inpatient (the arriving patient is temporarily located in the special room).

The simulator reproduces the dynamics of the ICU and stops at such decision times waiting for the discharge and/or admission decisions of the user. The simulator continues simulating the ICU assuming the decisions made.

Patient's health status

Queueing models represent the LoS of a patient as a certain random variable with a probability distribution fitted usually by using historical data. Therefore, a sampled time from this probability distribution determines the event in which the patient is automatically discharged. However, the implementation of this approach in the simulator would not allow the users to make the discharge/admission decisions clinically grounded and informed. They should rely on probability properties of the probability distribution as for example the expected remaining time, as it is the case of many simulation models (see discussion in Azcarate et al. 2020).

To overcome this strong drawback, we model the health status of a patient by using 275 health indicators (medical and nursing reports included), all recorded by the software Metavision® software (iMDsoft, Tel Aviv, Israel), which is a dedicated software to monitor the health of admitted patients of ICU. These variables (described in Appendix C.2) give an extended and realistic description of the evolution of the patient health status. They provide enough information to assess the health condition of a patient in order to decide whether the patient is stable enough to be transferred to a lower level of care. These health indicators include neurological, hemodynamic, respiratory parameters among others such as provenance and principal diagnosis. All of them are presented to the user of the simulator mimicking the way in which their information systems do.

4.2.2 The discrete event simulation model

The proposed DES model is designed to incorporate the characteristics of a real ICU described in Section 4.2.1. A DES model is defined by the set of state variables, which provide at any

time a complete description of the simulated system, and the set of events, which modify through time the value of these state variables. We propose three different kinds of state variables to describe the ICU at any time, and a set of events grouped into four different categories.

State variables

The first set of variables is composed of three variables, $X = (X_1, X_2, X_3)$, which describe the number of patients in the ICU (X_1), the number of patients that are waiting in the special room to be admitted (X_2), and the number of patients coming from surgery already accepted but not admitted to the ICU yet (X_3). Observe that the number of total patients admitted (N) in the ICU at time t is the sum of these three state variables ($N = X_1 + X_2 + X_3$).

The second category describes the health status of patients and it is composed of 275 state variables per each inpatient, $Y_{hi}, h = 1, \dots, 275; i = 1, \dots, X_1$. These variables can be continuous as the temperature ($^{\circ}\text{C}$) or the systolic blood pressure (mmHg), discrete as the heart rate (rpm), binary as being intubated (yes or no), or qualitative as those describing prognosis of physicians and nurses. During the simulation, these variables change in order to recreate the health status evolution of each patient. Therefore, they are considered important indicators to differentiate which patients can be discharged.

Finally, the third group of state variables describes the bed occupancy state. Each one is associated with an ICU bed, $Z_j, j = 1, \dots, c$. They are qualitative variables that can take the following values:

- *Free*: the bed is completely available for the admission of a patient.
- *With a deceased patient*: there is a patient who has just died and is waiting for discharge.
- *With a severe patient*: there is a very serious patient who cannot be discharged under no circumstances.
- *With a stabilized patient*: there is a stabilized patient who could be considered eligible to be discharged under circumstances of high occupancy pressure.
- *With a recovered patient*: there is a patient who has recovered and is ready to be discharged.
- *With a discharged patient*: there is a patient who is waiting for transfer to a lower level of care. A discharge decision has already been made.
- *Cleaning*: the bed is undergoing cleaning tasks to condition it for the admission of a new patient.

Therefore, the vector (X, Y, Z) describes at any time t the situation of the ICU (the number of patients admitted in the ICU, the number of patients waiting for an imminent admission, the health description of each one of these patients, and each bed occupancy state).

Events

There are four different types of events modifying through time the value of state variables.

The first set of events E_A are associated with the patient's arrival times classified in emergency and scheduled patients. The probability that a patient is of the emergency type is p_E , and of the scheduled type is p_S ($p_E + p_S = 1$). On the one hand, emergency patients' arrivals occur 24/7, which are modelled by using a Poisson Process (PP) with arrival rate λ_E . These patients are classified into illness groups whose percentages define the type of ICU that is being modelled. In our model we consider 6 different groups (E_1 : urgent surgery, E_2 : polytrauma, E_3 : patient hospitalized in Medical Service, E_4 : patient hospitalized in Surgical Service, E_5 : emergency/observation patient, and E_6 : patient admitted for organ donation/others) and probabilities $p_{E_i}, i = 1, \dots, 6$ of belonging to each illness group, which determine the mix of emergency patients ($\sum_{i=1}^6 p_{E_i} = p_E$). When an emergency patient arrives at time t_i , the next arrival occurs at time t_{i+1} obtained from the equation (4.1). Aside from assigning the arrival time, the type of emergency patient who arrives is selected. The patient will belong to the type E_i with a probability of p_{E_i}/p_E .

$$t_{i+1} = t_i - \frac{1}{\lambda_E} \ln u_i ; \text{with } u_i \sim U(0,1) \quad (4.1)$$

On the other hand, once per week, the number of scheduled surgeries for each day of next week is simulated. It is assumed an average number of scheduled surgeries of λ_S per week. We distinguish patients that recover from standard surgery procedure, S_1 , with probability p_{S_1} , which can be in the ICU for an expected short stay, and patients that can be for an expected long stay due to a complicated surgery or critical condition of them, S_2 , with probability p_{S_2} ($p_{S_1} + p_{S_2} = p_S$). During the first clinical session in the morning scheduled patients are presented to physicians. Those patients who are admitted arrive at ICU when the surgery is finished (this time is previously defined for each scheduled patient). Under the assumption of the number of scheduled surgeries each working day is uniformly distributed throughout the week, and no surgeries are scheduled on weekends, the expected number of surgeries in each labour day is $\lambda_{S^*} = \lambda_S/5$, and the expected number of arrivals for each type of scheduled patients is $\lambda_{S^*_i} = \lambda_{S^*} p_{S_i}/p_S$. From these expected values, we simulate the number of arrivals of each type of patient S_i as $\lfloor \lambda_{S^*_i} \rfloor$ patients with probability $\lfloor \lambda_{S^*_i} \rfloor + 1 - \lambda_{S^*_i}$, and $\lfloor \lambda_{S^*_i} \rfloor + 1$ with probability $\lambda_{S^*_i} - \lfloor \lambda_{S^*_i} \rfloor$ (where $\lfloor \cdot \rfloor$ denotes the integer part of the number). These simulated arrivals represent the number of surgeries that the decision-maker must confirm or cancel. When the surgeries are confirmed, those patients are the ones who finally enter the ICU. The diagram of the two types of patients' arrivals is shown in Figure 4.2.

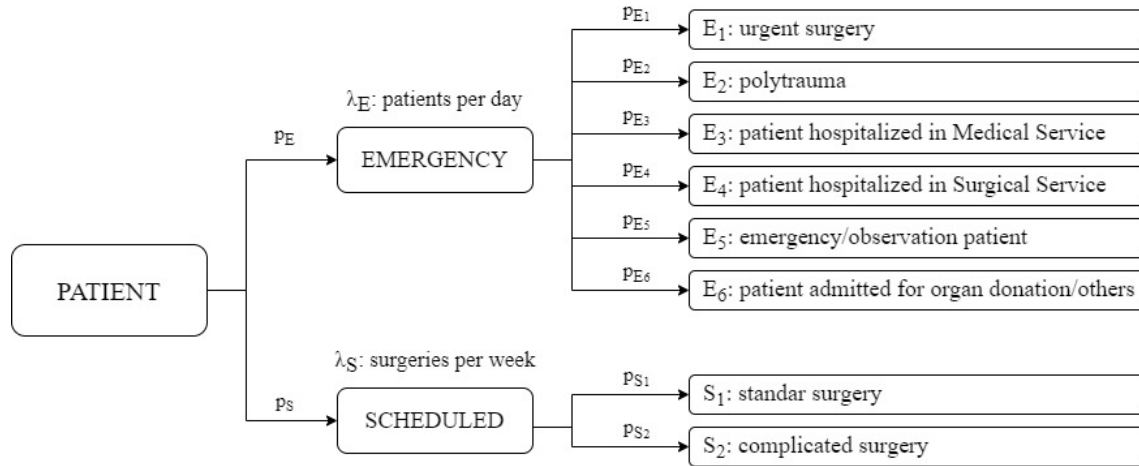


Figure 4.2. Diagram of both emergency and scheduled patients' arrivals.

The second set of events E_B produces changes in the value of the patient's clinical variables. The sequence of these events describes the health status of each patient described by 275 clinical variables recorded by the Metavision® software. Some of these variables, such as health indicators (the temperature, the heart rate, etc.), change their status every hour. Others related to Analytics, Gasometry, or physicians' reports, change their status every day.

The third category of events E_C is associated with discharge/admission decision-making. These events stop the simulation when there is a clinical session programmed, and discharge and admission decisions must be made by the user in order to continue. Observe that these decisions also appear when an emergency patient arrives at the ICU.

Finally, the last events E_D modify the beds' condition. Some of the previous events can trigger the change of an ICU bed's state. Changes in patient clinical variables can generate that the patient transits to a stabilized health or a recovery condition and then his/her bed does too. The bed's status also changes after the user's admission or discharge decisions. In the first case, when a patient is admitted, the bed's status change from *free* to *with a severe patient* (see Figure 4.1). In the second case, if a patient is discharged, his or her bed associated changes to *with discharged patient*. However, two transitions are independent of the other events and must be simulated. On the one hand, once a patient has been discharged, the departure time of the ICU is simulated depending on whether the bed is urgently required or not. Also, in deceased patients, the transfer time may depend on whether the organs are to be previously removed for donation. On the other hand, when a patient leaves the ICU, a bed cleaning time is simulated until the bed is free again. Figure 4.3 outlines the simulation model of the ICU.

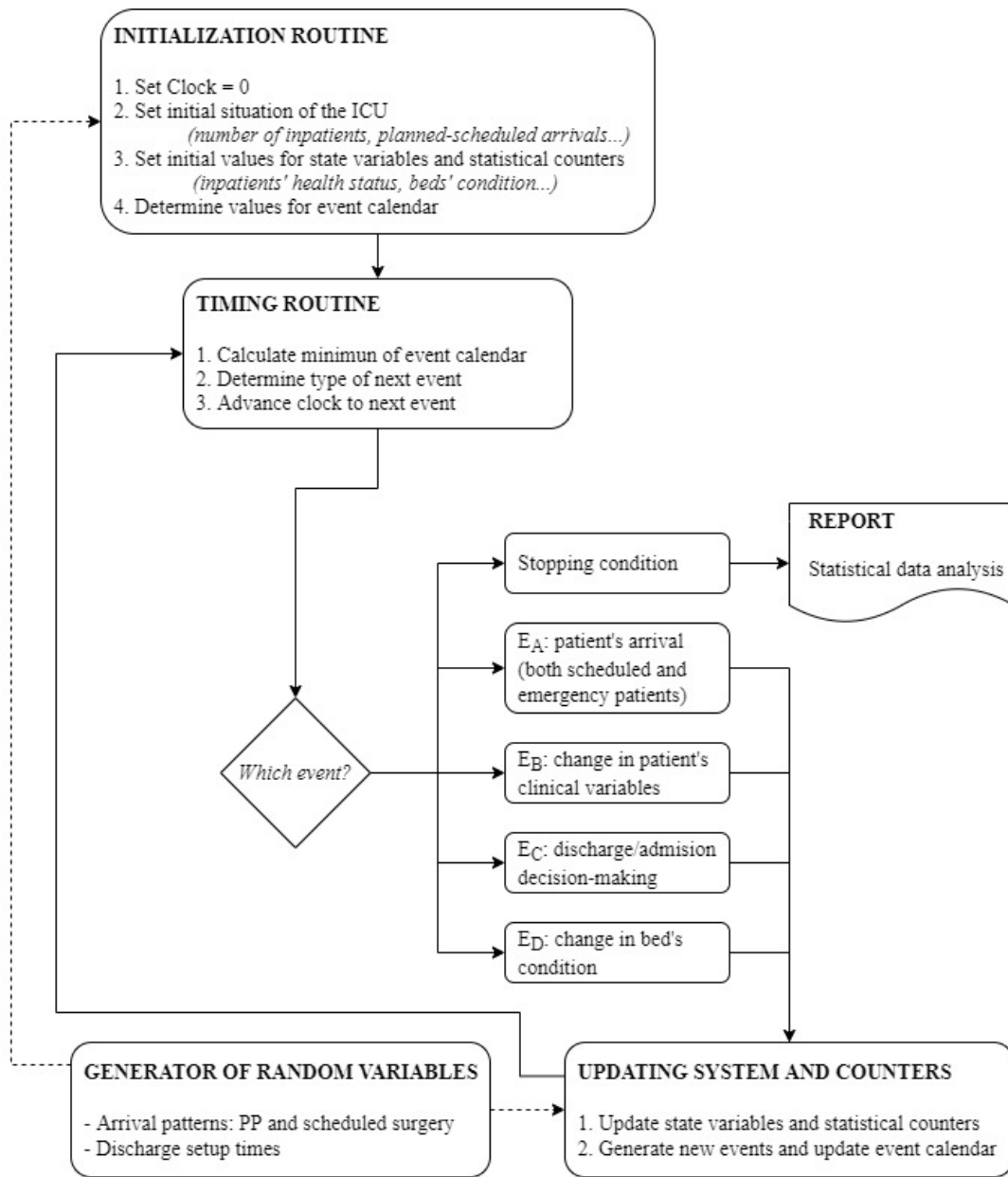


Figure 4.3. ICU simulation model.

4.2.3 Sampling initial scenarios from the steady state

The simulation starts at time zero by creating an initial scenario representative of the ICU stationary state, which means to assign value to all state variables and simulate the time for the first event of each type. The ICU is defined by the user through a set of parameters, as we expose in Section 4.3.2. The parameters necessary to generate the ICU scenario at time zero are the number c of ICU beds, the probabilities p_i that define the mix of patients, and the *traffic intensity* ρ .

The *traffic intensity* is the ratio of the arrival rate λ to the departure rate μ , where λ is the number of arrivals per day and μ the number of departures per day. The *traffic intensity* is a measure of the congestion of the system. It is used to determine the patient arrival processes (for both emergency and scheduled patients) and the number of occupied beds at time zero.

Determining patient arrival rates

The total arrival rate is calculated as $\lambda = \rho\mu$. The departure rate μ_b of one bed is estimated from the expected days in ICU of each category of patient, $LoS(E_i), i = 1, \dots, 6$, and $LoS(S_i), i = 1, 2$:

$$\frac{1}{\mu_b} = \sum_{i=1}^6 p_{E_i} E(LoS(E_i)) + \sum_{i=1}^2 p_{S_i} E(LoS(S_i)) \quad (4.2)$$

where $E(LoS(E_i))$ is estimated from historical data and the probabilities of each patient group are set by the simulator user to define the mix of patients.

Therefore, the total ICU departure rate is $\mu = c\mu_b$, and $\lambda = \rho\mu$. Then, the arrival rate is calculated for each category of patients as $\lambda_E = p_E\lambda$ and $\lambda_S = 7p_S\lambda$ and the first arrival of patients can be simulated as it is explained in Section 4.2.2 (observe that λ_S refers to arrivals per week).

Number of occupied beds at time zero

It is determined from the expected value ρc in the stationary state (assuming no early discharge is assigned, and no patient is diverted). To get an integer value for the number of occupied beds the lower or the upper integer is selected at random: $[\rho c]$ occupied beds with probability $[\rho c] + 1 - \rho c$, and $[\rho c] + 1$ with probability $\rho c - [\rho c]$. When the congestion rate ρ is greater or equal to 1, then the number of occupied beds at the beginning is c .

Simulating the type of patient that occupies each bed at time zero

The probability θ_i that a patient of a certain group of patients $P_i \in \{E_1, \dots, E_6, S_1, S_2\}$ occupies a bed is calculated as the expected time that a bed is occupied for that group of patients; that is, $\theta_i = \lambda_i LoS(P_i) / \sum_j \lambda_j LoS(P_j)$, where $\lambda_i = \lambda_{E_i} = \frac{p_{E_i}}{p_E} \lambda_E$ is the arrival rate for emergency patients of type E_i , and $\lambda_i = \lambda_{S_i} = \frac{p_{S_i}}{p_S} \lambda_S / 7$ is the arrival rate for scheduled patients of type S_i .

Sampling the patient that occupies a bed at time zero

Once the type of patients P_i is assigned to occupy a bed, a specific patient j is selected at random from the set of patients (see Section 4.3.2) according to a probability φ_{ij} which is proportional to the LoS, that is, $\varphi_{ij} = t_{ij} / \sum_k t_{ik}$, where t_{ik} is the LoS of the k th patient of type P_i .

Assigning values to the health status state variables Y_{hj} , $h = 1, \dots, 275$

Once the patient j th of type P_i is selected to occupy a bed, the LoS already consumed at time zero is considered uniformly distributed in his/her total LoS t_{ij} . Therefore, the health status of the patient is described by the state variables recorded at time ut_{ij} of the LoS of that patient, where $u \sim U(0,1)$.

4.3 The ICU management flight simulator

This section focuses on describing the MFS developed, detailing its main features, such as the definition of virtual ICUs, the interface, and the information recorded.

4.3.1 Main features of the simulator

The main purpose of this simulator is to mimic a real ICU, providing an extended and realistic description of the evolution of each patient and recreating real discharge and admission processes. To fulfil these characteristics, the simulator has to generate a familiar environment that is almost indistinguishable from that of the ICU physicians when consulting the monitoring screens of admitted patients' data. To achieve this level of similarity, the simulator presents the following features:

- The simulator generates emergency and elective patients' arrivals according to real arrivals patterns to the ICU.
- For each patient, the simulator shows enough clinical information to make decisions about discharge. Specifically, information about the patient's antecedents, principal diagnostic, and system monitoring values are displayed (as we mentioned in Section 4.2.1 and described in Appendix C.2). Information about scheduled surgeries for the following days is also shown in a calendar. The information displayed for each simulated patient corresponds to real patients, which have been completely anonymized.
- The visualization of each patient's data mimics the screen of Metavision® software presented in Figure 4.4, which is used in a real ICU.
- The simulator moves the time forward generating the events described in Section 4.2.2 and evolving the health of status of each admitted patient (vital signs, analytical parameters, life support measures, medications, etc.). When a decision-making type of event occurs, the simulation stops and waits for the user's instructions about possible patient discharges or admissions. The simulator updates the status of the ICU according to these decisions and it moves the time forward until the next decision-making event.

- The randomness of the simulation is controlled by the initial seed of the random generator and the use of the common random numbers technique. Therefore, the simulator can run the same scenario (identical sequence of patient arrivals and with the same typology) so that it can be evaluated by different users.
- This simulator allows the definition of different ICUs by setting a set of parameters (see Section 4.3.2). Therefore, the simulator has enough flexibility to define numerous ICUs with different characteristics.
- The simulator collects all decisions made by the users.

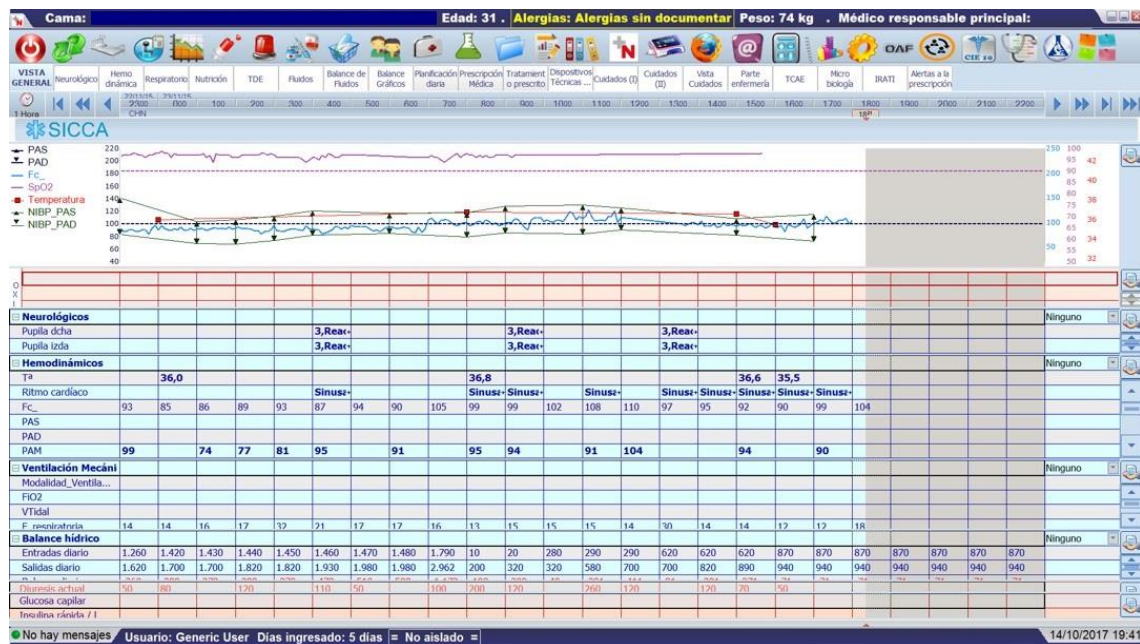


Figure 4.4. Real ICU data screen of Metavision® software.

To facilitate the medical staff using the simulator, it must be easily accessible, and also from different locations. Therefore, the simulator is freely available on the internet to be used by any interested user (<https://icusimulador.unavarra.es>); only the username (ICU-simulator) and the password (ICU_S1mulat0r*) are required in order to access it.

4.3.2 Setting up the ICU characteristics

The simulator is adaptable enough to create different ICUs according to its number of beds, the percentage of different types of patients, the congestion level, and the discharge/admission decision process. We can modify all these parameters as it is shown in Figure 4.5. Furthermore, it is possible to save all created scenarios and open them later. Thus, everyone faces the same situations and at the same moments during the simulation.

The size of the ICU is defined by the number of beds. The mix of patients is established by assigning a percentage for emergency and scheduled patients as we mentioned in Section 4.2.2.

It would be necessary to select the appropriate percentages for each type of patient and fill in the ones that are not included with zeros. Patients' health status is simulated using 200 clinical reports of 200 real patients treated in the ICU of Hospital Compound of Navarre, who have been completely anonymized. 112 out of the total are emergency patients, and they are distributed among the 6 categories mentioned in Section 4.2.2. The rest, 82 scheduled patients, are distinguished by their expected stay (short or long).

The screenshot shows a configuration window titled "CONFIGURATION SCREEN OF SIMULATION SCENARIO". It is organized into several panels:

- Emergency patient admissions:** 58%. Sub-categories include Urgent Surgery (9%), PTM (9%), Patient hospitalized in Medical Service (16%), Patient hospitalized in Surgical Service (7%), Emergency/Observation Patient (16%), and Donation/Others (1%).
- Scheduled admissions:** 42%. Sub-categories include Standard stay (26%) and Extended stay (16%).
- Number of beds:** 20.
- Type of hospital:** Tertiary.
- ICU initialization:** Automatic (with a Generate button).
- Congestion level:** Extreme.
- Start day of simulation:** Wednesday.
- Duration of simulation in days:** 10.
- Days of the arrival record:** 20.
- Blocking beds from hospital:** NO.
- RandomSeed:** 2908833429088334.
- TYPES OF DISCHARGE:**
 - Regular programming sessions of discharges:** Morning Session (08:00), Afternoon Session (15:00), Night Session (22:00).
 - Schedule of discharges by high occupation:** 10:00 to 18:00.
 - Schedule of discharges by saturation of the ICU:** 00:00 to 24:00.

At the bottom right, there are three buttons: "Start", "Save settings", and "Exit".

Figure 4.5. Configuration screen of the simulation scenario.

Three congestions levels are considered (*high*, *very high*, and *extreme*), which refers to the value of the *traffic intensity* ($\rho = \lambda/\mu$). The *high* congestion determines a *traffic intensity* $\rho = 0.85$ and the *very high* congestion a value of $\rho = 0.95$. The *extreme* level ($\rho > 1$) causes many situations in which the dilemma of the last bed occurs. This level has been selected to evaluate which decisions users make in each of those situations. Other complementary parameters that can be modified are the day of the week on which the simulation begins and the number of days that the simulation lasts.

Finally, on the lower-left side of Figure 4.5, the discharge/admission decision process is defined. It is possible to configure different timetables of clinical sessions, as well as those moments in which physicians can assign a discharge. For example, the schedules in Figure 4.5, indicate that every day there is a clinical session at 8 a.m., in which it is assessed which patients are discharged and which surgeries are confirmed. Also, between 10 a.m. and 6 p.m., it is possible to discharge patients in situations of high occupation, to free up beds for future patients. The last defined schedule indicates that at any time it is possible to admit an incoming patient, even if there are no free beds in the ICU, as long as there is the possibility of assigning a discharge.

4.3.3 Interface

The user must interact with the simulator in order to manage the ICU. At decision times, those patients who are occupying the ICU are presented to the user and he or she must make discharge decisions by using all data provided by the ICU information technologies. This information is based on the health status of the inpatients, the occupancy level, and the forecasted scheduled patients.

The ICU simulator's main screen is shown in Figure 4.6. In the lower part, there is a history of the number of emergency patient arrivals for the last days (left) and a panel with the scheduled surgeries of the following days (right). In the upper-right part, events related to the change of health of patients appear, as well as information about admissions and discharges. On the top left side, the occupancy of the ICU is shown in a panel that represents the beds with a color code. Clicking on a patient, all the clinical history to date is shown (the evolution of the 275 variables describing the health status as well as the medical and nursery reports). In fact, the health status is reported on a different screen of the simulator that mimics and provides the same information that is displayed and recorded by the dedicated software Metavision® (see Figure 4.7). Thus, the simulator creates a totally realistic and credible ICU environment. Users will be able to access the values of these variables in the case of all stabilized and recovered patients. The volume of information provided is simplified by preventing the consultation of the data of those patients who finally die and those who remain in serious conditions since the data of the patients that clearly cannot be discharged is meaningless.

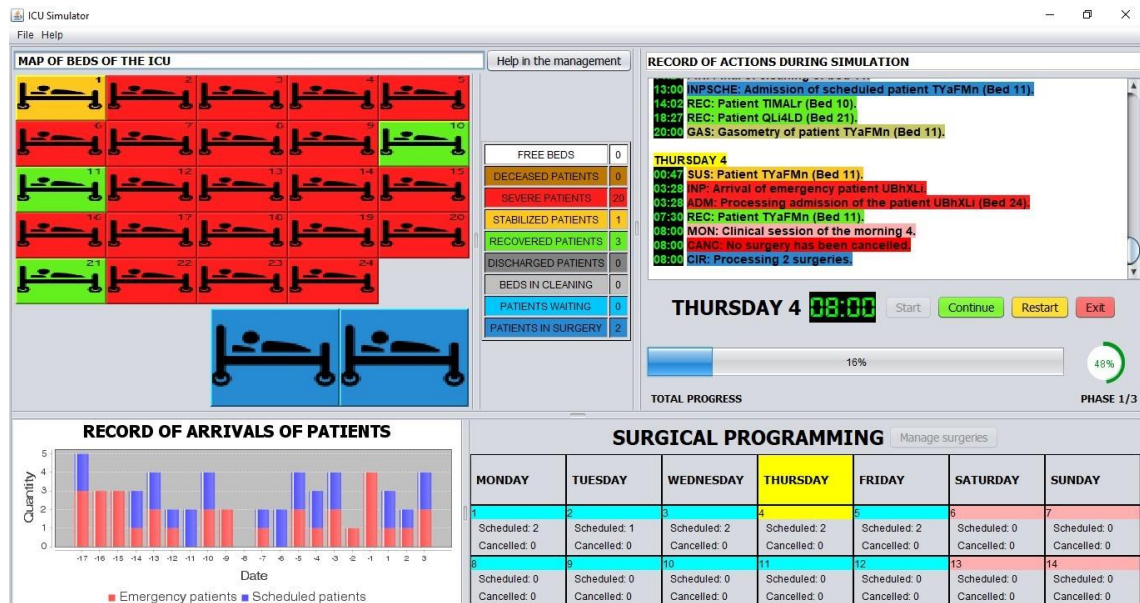


Figure 4.6. ICU simulator's main screen.

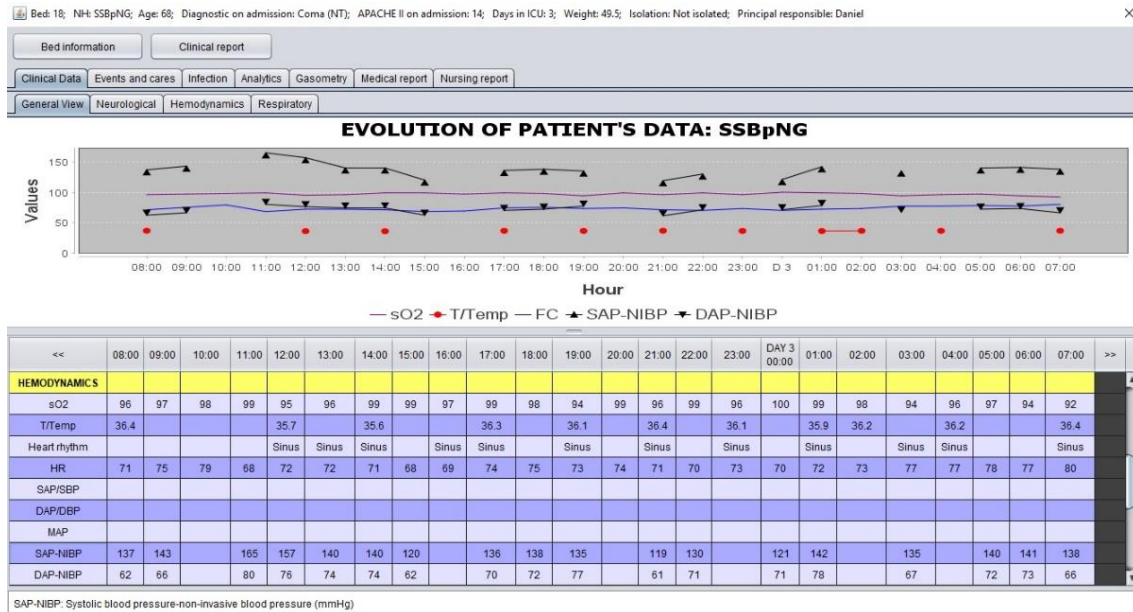


Figure 4.7. Information of patient's clinical data, mimicking real screens of Metavision®.

As we said previously, we have collected variables of 200 real patients of an ICU. The objective of the simulator is to collect information on how each user manages an ICU in which the congestion level is *extreme*. It is not intended to assess the user's medical knowledge. Consequently, some ICU physicians collaborating in the development of the simulator, to shorten the time to assess the clinical status of all inpatients, analysed the medical records of all patients to define three states along their stay, which help the user to make decisions. On the one hand, we consider in severe conditions to be discharge a patient who has just been admitted in the ICU (red color in Figure 4.1). On the other hand, patients who has finished their LoS are considered totally recovered and they should be discharged (green color in Figure 4.1). Finally, an intermediate state is established for each patient (orange color in Figure 4.1), which indicates the moment from which the patient is sufficiently stabilized to be discharged, although risks to his/her health are assumed.

4.3.4 Information recorded

When simulation finishes, all decisions and general results (number of patients admitted, number of surgeries cancelled, number of early discharges...) are recorded. Given that a well-done simulation run could last many minutes, this simulator allows the user to save the simulation and finishing it later.

Two documents are automatically sent to each user after a simulation is completed. The first one records general information regarding the number of emergency patients diverted, the number of surgeries that have been cancelled, the number of discharges assigned in an early way as well as the average time of shortened LoS in hours. The second document shows the evolution of the number of occupied beds along the simulation. It also has information about

those specific moments in which emergency patients are admitted or diverted, and the same for scheduled patients.

The simulator, in addition to sending those two types of documents, also generates files that record all the information associated with the individual decisions of the users. The decisions consist of determining at what moment the user has decided to discharge each patient and if patients who need care in the ICU are admitted or diverted, both emergency and scheduled. These files, which can also be opened by the simulator, allow reproducing step by step one simulation that is already finished. As we already mentioned the simulator controls the randomness, so we can reproduce two different simulations in order to compare bed management with each other.

4.4 Discussion and conclusions

In ICU management and, by extension, in hospital management in general, it is essential to use all resources efficiently. The transfer of a patient to an area of less care should be carried out when he or she is stable enough, and the assessment should be fully based on clinical judgement. Clinicians are aware of the risks involved in discharging a patient in advance to be able to admit another when the ICU is full, however, these decisions depend not only on the patient's health status but also on organizational and teamwork issues (Lin et al. 2009).

According to the Society of Critical Care Medicine (SCCM) guidelines for ICU admission, discharge, and triage (Nates et al. 2016), more research is needed on all aspects of critical care rationing to address current deficiencies. This chapter contributes to this research by developing, for the first time, an MFS of an ICU that reproduces the necessary operational processes to handle the patient flow and interacts with the user by presenting the same patient clinical information and in the same way as the ICU information technologies do in real ICUs. Specifically, the simulator allows representing the information related to the uncertain, complex, and dynamic features of the ICU and their patients' admission and discharge processes. The purpose of this simulator is to design a decision tool that collects informed decisions of the user to help in the analysis of the decision-making variability to reduce it. The simulator is able to present conflicting scenarios, that is, scenarios that generate discrepancies among physicians.

The MFS is flexible to recreating any type of ICU, defined by its size, mix of patients, congestion level, etc. It is also possible to introduce bed-blocking from wards, although it has not been considered so far in the simulations performed by physicians. In situations of blockage, the patient cannot be discharged whether the user wants it or not. Therefore, we avoid these forced situations to collect the decisions that the user freely make. The simulator has been used and validated by ICU physicians and nurses of the three hospitals of the public network

of the Spanish Autonomous Community of Navarre (Pamplona, Tudela, and Estella) and of a private one of concerted management of Guipúzcoa.

The study conducted by de Freitas (2006) demonstrated that these types of simulators have a learning function. Other more recent researches also show that the use of MFS has a positive effect on the learning of participants (Elsawah et al. 2017; Pennock et al. 2018). Based on this, we also propose this ICU simulator as a learning tool from two different points of view.

On the one hand, both medical and nursing students could use this simulator at universities in order to learn how ICUs are managed. When students run the simulation, they will take part in the decision-making process of the ICU for the first time, but in a safe environment, in which their decision will not have bad consequences for patients. Apart from this, students can compare their own results with those that are supposed to be the best, that is, decisions about patients of simulations performed by experienced ICU physicians. They can also watch step by step how the simulation has been performed. The success of using this type of tools can be seen in (Grunewald et al. 2003).

On the other hand, physicians who work in the ICU not only could use the simulator in order to improve their knowledge of bed management individually, but they could also learn in a collective way. Comparing all results of the decision-making process generated by simulations performed by many physicians of the same ICU, it would be possible to identify which situations cause the greatest disparity among them. These scenarios could be labelled as conflicting scenarios because the decisions that physicians make when managing these situations differ. In addition, it would be possible to detect which patients are complicated to treat, because there are no unified decisions about them (decision about admission, time to discharge...).

5 Methodologies for the analysis of decision-making in the ICU

This chapter shows the results obtained with the *ICU simulator* presented in Chapter 4, and also different metrics are studied and proposed to compare management decisions. The objective is to develop new methodologies that, based on the data collected by the simulator, allow us to detect discrepancies between users in ICU decision-making. Some tables and figures are shown as an illustration of the methodology developed here, but the large number of graphs that may result from applying this methodology is not included. Discussions about them are beyond the scope of this chapter.

Before showing the results and metrics, a descriptive study on the use of the simulator is carried out in Section 5.1. This analysis consists of describing the experiment carried out by the users, specifying the type of users who have used the simulator, and showing a qualitative assessment of the *ICU Simulator* by users. The results of these experiments are used to illustrate the methodology developed in the next sections to analyse ICU management decisions. Then four types of measures are proposed for the analysis of the user decision-making. During the simulation, users can manage the ICU through three bed control actions (BCA): admitting or diverting emergency patients, confirming or cancelling surgeries, and discharging ICU patients. Our first approach in Section 5.2 consists of determining global indicators that quantify each of the management actions. This section includes dissimilarity and statistical analysis to compare and graphically represent decision-making.

The use of the three BCA to manage ICU occupancy depends on the number of beds available in the ICU. With our second approach, in Section 5.3 we calculate new indicators that account for the ICU pressure level. In Section 5.4 we analyse how decision-making evolves over time. Specifically, for each user, we define the trajectory of available beds over time, which is the direct effect of the three BCA discussed above. In our last approach, we consider the management at the patient level in Section 5.5, that is, we analyse users' decisions about individual patients. Users with very similar results in the previous measures may have

discrepancies in the patients to whom the decisions are applied. In these cases, the differences in decisions are due to the clinical characteristics of the patients only. Finally, this chapter closes with a discussion and some comments about the future work in Section 5.6.

5.1 Descriptive study

The main objective of MSF of the ICU described in Chapter 4 is to propose conflicting situations in the ICU in order to collect and compare how different users manage such situations. With this premise, we try to better understand how ICUs are managed and use this learning to develop more accurate mathematical models of the ICU. The ultimate goal is to apply the knowledge acquired to improve the management of a real ICU. This simulator allows analysing decisions about the discharge of patients in an ICU, through an interactive simulation with the user. These decisions are especially relevant in situations of high occupation, because they can lead to the anticipation of the discharge of a patient or to the rejection for ICU admission. The simulator can generate an environment similar to what a physician could find in the ICU so that he or she can consult the monitoring screens of the admitted patients on which the discharge decision has to be made.

In our study, all users managed a 24-bed ICU with an *extreme* congestion level (see Section 4.3.2), which was initialized on Monday with 23 patients in different health statuses. Over three weeks, 34 emergency patients and 23 scheduled patients arrived at the ICU. The ICU blocking discharge from wards was not included and during the simulation, there were regular programming sessions of discharges in the morning at 8 a.m. Every user runs the simulator with the same stochastic environment, that is, the patients have the same clinical profile and arrive at the same time. However, the total number of discharges by each user is different because it is influenced by the number of patients admitted to the ICU.

5.1.1 Simulator users profiles

Participants from different professional backgrounds have used the simulator. Since 20th May 2019, more than 100 people have registered to use the simulator, of which 82 have completed the simulation to the end to analyse and compare their results. The vast majority of them was from Navarre (64), but there have also been responses from professionals from other parts of Spain such as the Basque Country (8), La Rioja (2), Catalonia (2), and Aragon (1), and even from Lisbon (5).

Among the participants, we can find *Physicians* (18), *Nurses* (14), *Nurse technicians* (4), *Residents* (6), *Medical students* (6), *Operation Management and/or Operational Research (OM-OR) researchers* (11), *Engineers* (11) and *Others* (12). About 50% of the users have work experience in the ICU. On the one hand, it is not only interesting to study the differences between ICU professionals (*Physicians, Nurses, and Nurse technicians*), but also to incorporate

profiles, such as *OM-OR researchers* or *Engineers*, where resource management is also important. On the other hand, some users who have acquired theoretical knowledge of patient care in ICUs, without having the opportunity to have worked in these Units, such as *Residents* or *Medical students*, can provide other types of results. Finally, the *Others* group includes users who are not considered in any of the previous groups.

5.1.2 User qualitative assessment of the simulator

From the beginning, stakeholders were involved in the development of the simulator, providing feedback on how to implement all the features of a real ICU. Months before the final development, a pilot test of the program was presented at the ICU of the Navarre Hospital Compound, to the Head of Service and several physicians and nurses of the ICU. Thanks to their feedback, an enhanced version of the simulator was presented to professionals in this and other ICUs to collect information from users who may have a different way of managing the ICU.

The program's interface is easy to use, and this is exposed by some users in their feedback after finishing the simulation. Appendix E.1 contains the reviews of 18 users. Furthermore, a questionnaire is provided at the end of the simulation. The users had to respond to four questions using a five-point agree/disagree scale (Likert scale survey). The following questions were used to gather this data:

- Q1: “Did you find that the interactive simulator reflects in a real way how to manage the patients of an ICU?”
- Q2: “To what extent do you agree that the simulator allows you to analyse the decision-making regarding the management of beds in your ICU?”
- Q3: “To what extent do you agree that the simulator can be used as a better learning tool on the management of ICU beds compared to traditional methods such as reports or slide presentations?”
- Q4: “Do you think that the simulator can help you better understand the management of beds in your unit and apply measures to improve it?”

Figure 5.1 shows the main results of the evaluation, which includes all the participants mentioned in Section 5.1.1. The strongly agree and agree scores together have shown a more than 85% satisfaction from the users of the simulator in all questions. Almost all participants agree with the accuracy with which the simulator represents a real ICU (Q1, only 2.38% disagree), and the vast majority find useful this simulator in order to learn on the management of ICU beds (Q3, 66.67% strongly agree).

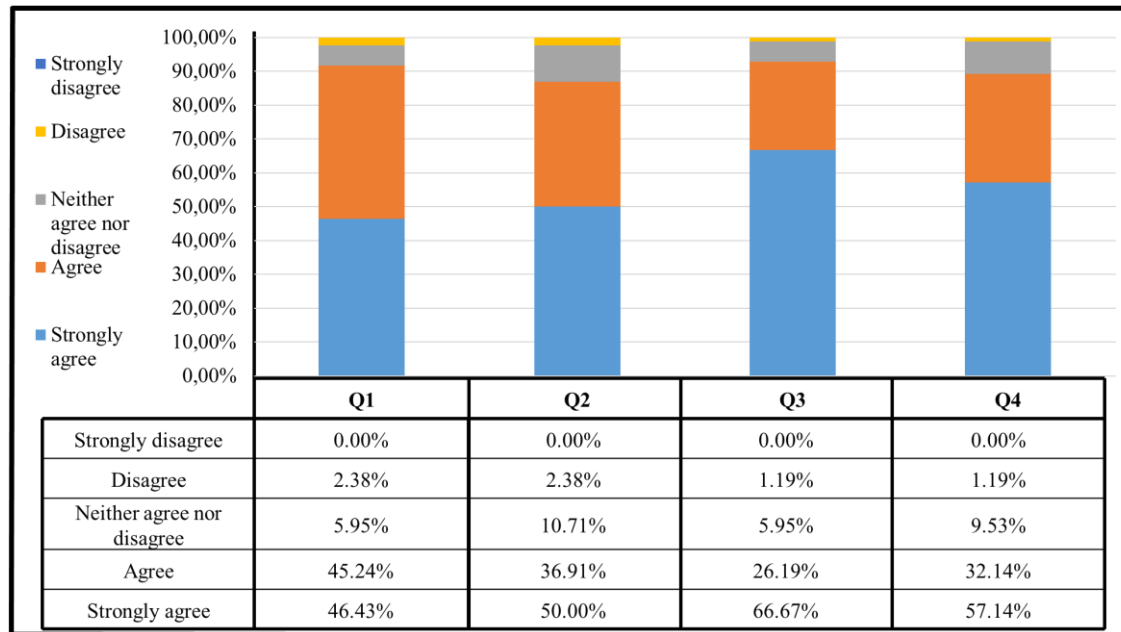


Figure 5.1. Main results of the questionnaire about the ICU simulator.

In general, both *Physicians* and *Nurses* find it more feasible the fact that the simulator allows them to understand the management of ICU beds (Q4) rather than being able to use it to analyse the decisions made there (Q2). These responses reflect the fact that although it is possible to understand how an ICU is managed using the simulator, it is not obvious to carry out an analysis of the decisions made in the ICU in order to draw general conclusions about decision-making. This supports the fact that deeper statistical-mathematical analyses are required, which are carried out in the following sections. Completing the analysis, for each question (Q1-Q4) a chi-square test of homogeneity has been conducted to determine whether frequency counts are distributed identically across different groups. In all cases, the test does not reject the hypothesis that the distribution of responses is the same in each type of participant ($p > 0.05$).

5.2 Decision-making analysis by using global performance measures

5.2.1 Definition of global management indicators

During the simulation, the user performs three BCA to manage ICU occupancy: diverting emergency patients (D), cancelling scheduled surgeries (C), and shortening the stay of patients already admitted (S). In this section, we compare the management carried out by decision-makers by measuring the number of times each of the BCA is used to control de occupancy.

We define the *manageable beds* as the number of beds that the user keeps available to be assigned to a new patient in a short time if necessary. The number of manageable beds at time t in the ICU is defined as the number of those beds in any state but occupied *with a severe patient*, minus the number of patients already accepted but not yet occupying an ICU bed. (state variables X_2 and X_3 defined in Section 4.2.2). When a user keeps a low number of manageable beds, then he or she is assuming risks of having to divert emergency patients or cancelling surgeries. And the opposite, having a large number of manageable beds in the ICU can avoid the diversion of emergency patients and cancellation of some surgeries but would require the discharge in advance of some patients or the cancelation of some surgeries not considered as very urgent. The following variables and parameters are defined for the analysis:

- e_{Di} : number of emergency patients diverted by user i .
- e_T : total number of emergency patients arrived at the ICU.
- s_{Ci} : number of scheduled surgeries cancelled by user i .
- s_T : total number of scheduled surgeries in the ICU.
- d_{Si} : number of stays shortened by user i .
- d_{Ti} : total number of patients discharged by user i .
- T : total time of the simulation in hours.
- $m_i(t)$: number of manageable beds in the ICU of user i at time t .
- $\bar{m}_i = \int_0^T m_i(t) dt / T$: mean manageable beds in the ICU of user i .
- n_B : total ICU beds.

The following global indicators are defined for each user i based on these actions: $P_i(D)$ is the proportion of emergency patients diverted by user i to another ICU, $P_i(C)$ is the proportion of scheduled surgeries cancelled by user i , and $P_i(S)$ is the proportion of stays shortened by user i . These ratios allow us to assess the intensity with which each user performs each type of action. In addition, we define $P_i(M)$ as the proportion of manageable beds in the ICU on average during the simulation of user i . The calculation of these four ratios are shown in equation (5.1). These ratios can be interpreted as probabilities, since $P_i(D)$, for example, can be interpreted as the probability that a patient is diverted by user i . The same can be deduced for $P_i(C)$ and $P_i(S)$ with cancelled surgeries and shortened stays respectively. Similarly, $P_i(M)$ indicates the probability that a bed is available (manageable) at any time during the simulation.

$$P_i(D) = \frac{e_{Di}}{e_T}, \quad P_i(C) = \frac{s_{Ci}}{s_T}, \quad P_i(S) = \frac{d_{Si}}{d_{Ti}}, \quad P_i(M) = \frac{\bar{m}_i}{n_B} \quad (5.1)$$

Since users belong to different groups, it is possible to perform an aggregate calculation of the global management indicators in order to compare the results between types of users. Let us define G as the number of different groups using the simulator and N_g as the number of users in group g . The variables and ratios for each group g are calculated according to equations (5.2) and (5.3) respectively.

$$e_{Dg} = \frac{\sum_i e_{Di}}{N_g}, \quad s_{Cg} = \frac{\sum_i s_{Ci}}{N_g}, \quad d_{Sg} = \frac{\sum_i d_{Si}}{N_g}, \quad d_{Tg} = \frac{\sum_i d_{Ti}}{N_g}, \quad (5.2)$$

$$\bar{m}_g = \frac{\sum_i \bar{m}_i}{N_g}$$

$$P_g(D) = \frac{e_{Dg}}{e_T}, \quad P_g(C) = \frac{s_{Cg}}{s_T}, \quad P_g(S) = \frac{d_{Sg}}{d_{Tg}}, \quad P_g(M) = \frac{\bar{m}_g}{n_B} \quad (5.3)$$

Methodology application

Table 5.1 summarizes results recorded by *Physicians*. They performed the simulation under exactly the same ICU scenario, as it is mentioned in Section 5.1. The differences in the indicator values suggest that *Physicians* make decisions quite differently. Some of them cancelled few surgeries but following two different strategies: there are those who decide not to assign early discharges and not admit emergency patients (e.g., physician 7) and others decide to admit more patients assigning early discharges (e.g., physician 11). By contrast, several physicians decided to cancel more surgeries in order to admit more emergency patients (e.g., physician 4). Finally, some physicians try to maximize the number of patients admitted to the ICU (e.g., physician 16). Concerning the mean manageable beds in the ICU (\bar{m}_i), in all cases, the values are between 2 and 5. It can be observed that, in general, high values of d_{Si} correspond to low values of \bar{m}_i , and vice versa. Although there are cases where, on the one hand, similar values in variables e_{Di} , s_{Ci} , and d_{Si} correspond to different values of \bar{m}_i (e.g. physicians 1 and 12), and on the other hand, different values in these variables correspond to similar values of \bar{m}_i (e.g. physicians 13 and 17).

A chi-square test of homogeneity has been conducted to compare these ratios among physicians. Results indicate that there are significant differences in the ratio of cancelling surgeries and shortening stays ($p < 0.01$), but no significant differences are found ($p > 0.1$) in the ratio of emergency patients diverted. Table 5.2 presents the aggregated results for each type of user. Here, the main differences observed are in variables e_{Dg} and s_{Cg} . *Nurse technicians*, *Nurses*, and *Physicians* stand out for diverting more emergency patients and for cancelling fewer scheduled surgeries. In addition, it can be seen that *Nurse technicians* and *Nurses* shorten stays the least and maintain the highest value of mean manageable beds. The overall results for each user individually, and separated by group, are collected in Appendix E.2.

Table 5.1. Comparison of simulation global results recorded by 18 ICU physicians. Users faced a 24-bed ICU, which was initialized with 23 patients in different health statuses. Over three weeks, 34 emergency patients and 23 scheduled patients arrived at the ICU. Each physician has a different number of total discharges (d_{Ti}). Bold values represent the highest (red) and lowest (green) values.

Physician	e_{Di}	$P_i(D)$	s_{Ci}	$P_i(C)$	d_{Si} (d_{Ti})	$P_i(S)$	\bar{m}_i	$P_i(M)$
Phy_1	13	0.3824	2	0.0870	4 (34)	0.1176	4.64	0.1933
Phy_2	9	0.2647	6	0.2609	14 (33)	0.4242	3.06	0.1277
Phy_3	9	0.2647	8	0.3478	14 (30)	0.4667	3.06	0.1277
Phy_4	6	0.1765	7	0.3043	18 (34)	0.5294	3.00	0.1250
Phy_5	7	0.2059	6	0.2609	11 (33)	0.3333	2.95	0.1231
Phy_6	6	0.1765	4	0.1739	21 (38)	0.5526	2.98	0.1240
Phy_7	16	0.4706	0	0.0000	0 (34)	0.0000	4.88	0.2033
Phy_8	11	0.3235	3	0.1304	7 (35)	0.2000	4.06	0.1690
Phy_9	7	0.2059	5	0.2174	16 (34)	0.4706	2.81	0.1172
Phy_10	7	0.2059	3	0.1304	27 (39)	0.6923	2.57	0.1071
Phy_11	9	0.2647	0	0.0000	23 (41)	0.5610	3.31	0.1378
Phy_12	13	0.3824	3	0.1304	5 (32)	0.1563	3.67	0.1528
Phy_13	12	0.3529	5	0.2174	8 (33)	0.2424	3.56	0.1484
Phy_14	10	0.2941	1	0.0435	10 (35)	0.2857	3.15	0.1313
Phy_15	10	0.2941	1	0.0435	21 (35)	0.6000	3.01	0.1253
Phy_16	4	0.1176	4	0.1739	21 (37)	0.5676	2.45	0.1022
Phy_17	10	0.2941	1	0.0435	24 (38)	0.6316	3.51	0.1463
Phy_18	11	0.3235	2	0.0870	13 (35)	0.3714	4.23	0.1764

Table 5.2. Global mean results of all users of the simulator divided by different groups. Bold values represent the highest and lowest values.

Group	N_g	e_{Dg}	$P_g(D)$	s_{Cg}	$P_g(C)$	d_{Sg} (d_{Tg})	$P_g(S)$	\bar{m}_g	$P_g(M)$
Physicians	18	9.44	0.2778	3.39	0.1473	14.28 (35.00)	0.4079	3.38	0.1410
Nurses	14	10.64	0.3130	3.50	0.1522	10.36 (34.29)	0.3021	4.25	0.1772
Nurse techs	4	13.75	0.4044	1.25	0.0543	10.75 (36.00)	0.2986	4.70	0.1958
Residents	6	5.50	0.1618	5.17	0.2246	18.33 (35.50)	0.5164	2.99	0.1244
Medical students	6	4.67	0.1373	5.17	0.2246	15.00 (36.33)	0.4128	3.59	0.1494
OM-OR researchers	11	6.64	0.1952	4.00	0.1739	19.00 (35.55)	0.5345	2.80	0.1168
Engineers	11	5.73	0.1684	3.82	0.1660	17.27 (36.64)	0.4715	3.06	0.1274
Others	12	8.17	0.2402	3.33	0.1449	12.50 (36.25)	0.3448	3.73	0.1554

5.2.2 Dissimilarity analysis in the ICU decision-making

The decision-making of a user i is described by a vector of four components: $P_i(D)$, $P_i(C)$, $P_i(S)$, and $P_i(M)$. The dissimilarity between the decision-making of two users is calculated by using a distance measure between vectors. Many methods of calculating the distance between vectors can be found in the literature when different variables have been measured for each observation (Anderberg 1973; Deza and Deza 2016). In this application, we propose the use of the Euclidean distance (note that the Pythagorean theorem in a Cartesian coordinate system in Euclidean space can be interpreted as a distance formula [Tabak 2014]) and the Mahalanobis distance (Mahalanobis 1936).

Let us denote $u'_i = (u_{i1}, \dots, u_{iP})$ and $u'_j = (u_{j1}, \dots, u_{jP})$ the observations of two objects or individuals resulting from measuring P variables U_1, \dots, U_P on them. Euclidean distance (δ_E) and Mahalanobis distance (δ_M) are defined in equation (5.4) and (5.5) respectively.

$$\delta_E(u_i, u_j) = \sqrt{\sum_{k=1}^P (u_{ik} - u_{jk})^2} = \sqrt{(u_i - u_j)'(u_i - u_j)} \quad (5.4)$$

$$\delta_M(u_i, u_j) = \sqrt{(u_i - u_j)' \Sigma_U^{-1} (u_i - u_j)} \quad (5.5)$$

where Σ_U is the variance-covariance matrix of U .

Using (5.4) or (5.5) we can calculate the distance between two observations, with $u'_i = [P_i(D), P_i(C), P_i(S), P_i(M)]$. On the one hand, the Euclidean distance is not invariant to changes in the scale of the variables and it does not take into account the correlation structure between variables. In this situation, all values of the variables belong to the interval $[0,1]$, although there is some correlation between them and their variances are different. On the other hand, the Mahalanobis distance is invariant to non-singular linear transformations of the variables and takes into account the correlations between them. For example, the distance does not increase simply by increasing the number of observed variables, but it will only increase when the new variables are not redundant concerning the information provided by the previous ones. However, as the variance-covariance matrix is included in its calculation, with each new observation, the distances will be altered somewhat. Both distances could be validly used in this context. The difference between the two distances is greater when the Σ_U matrix differs from the $\sigma^2 I$ matrix, where σ^2 represents the common value of the variance of the variables and I is the identity matrix.

Methodology application

On the one hand, Table 5.3 shows the variance-covariance matrix calculated from the observations of all users. The differences observed in the main diagonal of this matrix imply that different results will be obtained in the calculation of the distance depending on the way they are calculated (Euclidean or Mahalanobis distance). On the other hand, Table 5.4 shows the correlation matrix obtained from the observations of all users.

Table 5.3. Variance-covariance matrix obtained from the observations of all users of the ICU simulator.

	$P(D)$	$P(C)$	$P(S)$	$P(M)$
$P(D)$	0.0176	-0.0086	-0.0172	0.0049
$P(C)$	-0.0086	0.0118	0.0055	-0.0012
$P(S)$	-0.0172	0.0055	0.0383	-0.0072
$P(M)$	0.0049	-0.0012	-0.0072	0.0025

Table 5.4. Correlation matrix obtained from the observations of all users of the ICU simulator.

	$P(D)$	$P(C)$	$P(S)$	$P(M)$
$P(D)$	1	-0.5968	-0.6636	0.7381
$P(C)$	-0.5968	1	0.2600	-0.2177
$P(S)$	-0.6636	0.2600	1	-0.7352
$P(M)$	0.7381	-0.2177	-0.7352	1

We can observe that the action of diverting emergency patients (D) is opposite to the actions of cancelling scheduled surgeries (C) and shortening inpatients' stays (S), as they are negatively correlated. Moreover, the more emergency patients are diverted, the higher the proportion of manageable beds is in the ICU. From this correlation matrix it can also be interpreted that in order to maintain a higher number of available manageable beds, the strategy followed is to divert emergency patients, without the need to cancel surgeries or shorten stays. Finally, a high proportion of shortened stays leads to a lower number of manageable beds and a lower proportion of diversions. Table 5.5 and Table 5.6 show the variance-covariance matrix and the correlation matrix calculated from the observations of *Physicians* respectively. We can note that the correlation within the same group is stronger than taking into account all users.

Table 5.5. Variance-covariance matrix obtained from the observations of the 18 ICU physicians who have used the simulator.

	$P(D)$	$P(C)$	$P(S)$	$P(M)$
$P(D)$	0.0073	-0.0043	-0.0127	0.0021
$P(C)$	-0.0043	0.0103	0.0030	-0.0013
$P(S)$	-0.0127	0.0030	0.0370	-0.0041
$P(M)$	0.0021	-0.0013	-0.0041	0.0008

Table 5.6. Correlation matrix obtained from the observations of the 18 ICU physicians who have used the simulator.

	$P(D)$	$P(C)$	$P(S)$	$P(M)$
$P(D)$	1.0000	-0.4911	-0.7739	0.8769
$P(C)$	-0.4911	1.0000	0.1561	-0.4637
$P(S)$	-0.7739	0.1561	1.0000	-0.7807
$P(M)$	0.8769	-0.4637	-0.7807	1.0000

As an example of the methodology application, Table 5.7 and Table 5.8 show the Euclidean and Mahalanobis distances between *Physicians* respectively. In each table, the five lowest distances are marked in bold green and the five highest distances in bold red. As the distance

between physicians depends on the method used, the minimum and maximum distances correspond to different pairs of physicians. To observe how different the Euclidean distances are from Mahalanobis distances, we normalise the values obtained in each method between zero and one and calculate the ratio of the normalized distances (δ_M/δ_E). Table 5.9 shows the ratios obtained (we define the indeterminate form $0/0 = 1$), where the five smaller values are marked in bold green and the five larger ones in bold red. Values that are less than 1 indicate that the Euclidean distance is larger while those greater than 1 indicate that the Mahalanobis distance is larger. Excluding distances that are zero, it is observed that the Mahalanobis distance is larger in 66% of the values. With this result, it is demonstrated that the distances obtained with each method are certainly different. And in view of the strong correlation between the observed variables, it would seem more appropriate to use the Mahalanobis distance in this case.

Table 5.7. Euclidean distances between the 18 ICU physicians who have used the simulator.

	1	2	3	4	5	6	7	8	9	10	11	12	13	14	15	16	17	18
1	0.000	0.377	0.456	0.514	0.336	0.494	0.171	0.113	0.423	0.609	0.470	0.071	0.188	0.204	0.497	0.537	0.525	0.261
2	0.377	0.000	0.097	0.144	0.108	0.178	0.544	0.269	0.087	0.305	0.295	0.321	0.208	0.259	0.281	0.224	0.302	0.197
3	0.456	0.097	0.000	0.117	0.170	0.213	0.622	0.351	0.144	0.319	0.361	0.398	0.275	0.355	0.334	0.250	0.348	0.288
4	0.514	0.144	0.117	0.000	0.203	0.132	0.682	0.403	0.109	0.241	0.319	0.461	0.349	0.376	0.295	0.150	0.305	0.311
5	0.336	0.108	0.170	0.203	0.000	0.238	0.506	0.225	0.144	0.382	0.351	0.284	0.180	0.240	0.355	0.266	0.380	0.220
6	0.494	0.178	0.213	0.132	0.238	0.000	0.655	0.387	0.098	0.150	0.196	0.450	0.360	0.320	0.182	0.064	0.194	0.254
7	0.171	0.544	0.622	0.682	0.506	0.655	0.000	0.283	0.588	0.759	0.601	0.228	0.351	0.346	0.632	0.698	0.660	0.410
8	0.113	0.269	0.351	0.403	0.225	0.387	0.283	0.000	0.312	0.510	0.390	0.075	0.103	0.131	0.413	0.429	0.442	0.177
9	0.423	0.087	0.144	0.109	0.144	0.098	0.588	0.312	0.000	0.238	0.244	0.373	0.273	0.269	0.234	0.139	0.255	0.210
10	0.609	0.305	0.319	0.241	0.382	0.150	0.759	0.510	0.238	0.000	0.197	0.566	0.483	0.426	0.156	0.159	0.143	0.351
11	0.470	0.295	0.361	0.319	0.351	0.196	0.601	0.390	0.244	0.197	0.000	0.441	0.396	0.280	0.067	0.231	0.088	0.220
12	0.071	0.321	0.398	0.461	0.284	0.450	0.228	0.075	0.373	0.566	0.441	0.000	0.126	0.180	0.462	0.494	0.491	0.228
13	0.188	0.208	0.275	0.349	0.180	0.360	0.351	0.103	0.273	0.483	0.396	0.126	0.000	0.189	0.403	0.406	0.430	0.188
14	0.204	0.259	0.355	0.376	0.240	0.320	0.346	0.131	0.269	0.426	0.280	0.180	0.189	0.000	0.314	0.358	0.346	0.110
15	0.497	0.281	0.334	0.295	0.355	0.182	0.632	0.413	0.234	0.156	0.067	0.462	0.403	0.314	0.000	0.223	0.038	0.240
16	0.537	0.224	0.250	0.150	0.266	0.064	0.698	0.429	0.139	0.159	0.231	0.494	0.406	0.358	0.223	0.000	0.233	0.306
17	0.525	0.302	0.348	0.305	0.380	0.194	0.660	0.442	0.255	0.143	0.088	0.491	0.430	0.346	0.038	0.233	0.000	0.267
18	0.261	0.197	0.288	0.311	0.220	0.254	0.410	0.177	0.210	0.351	0.220	0.228	0.188	0.110	0.240	0.306	0.267	0.000

Table 5.8. Mahalanobis distances between the 18 ICU physicians who have used the simulator.

	1	2	3	4	5	6	7	8	9	10	11	12	13	14	15	16	17	18
1	0.000	2.526	3.550	2.718	2.017	2.268	0.998	0.584	2.055	3.053	2.839	1.651	2.253	1.420	2.809	2.393	3.181	1.610
2	2.526	0.000	1.152	1.090	1.244	2.200	3.173	2.055	1.094	2.501	3.603	1.816	1.050	2.699	2.782	2.509	3.328	2.539
3	3.550	1.152	0.000	1.667	2.174	3.146	4.176	3.124	2.167	3.274	4.576	2.719	1.709	3.846	3.653	3.507	4.106	3.512
4	2.718	1.090	1.667	0.000	1.541	1.628	3.578	2.247	1.015	2.098	3.272	2.610	2.035	2.919	2.629	1.998	2.949	2.278
5	2.017	1.244	2.174	1.541	0.000	2.140	2.703	1.460	1.079	2.905	3.602	1.518	1.336	2.134	3.136	2.147	3.686	2.519
6	2.268	2.200	3.146	1.628	2.140	0.000	3.079	1.929	1.224	1.187	1.747	2.845	2.849	2.075	1.559	0.701	1.793	1.212
7	0.998	3.173	4.176	3.578	2.703	3.079	0.000	1.414	2.814	3.687	3.268	1.773	2.650	1.588	3.260	3.143	3.710	2.323
8	0.584	2.055	3.124	2.247	1.460	1.929	1.414	0.000	1.528	2.762	2.806	1.385	1.882	1.261	2.645	2.016	3.098	1.589
9	2.055	1.094	2.167	1.015	1.079	1.224	2.814	1.528	0.000	1.830	2.721	1.919	1.726	1.943	2.136	1.425	2.674	1.811
10	3.053	2.501	3.274	2.098	2.905	1.187	3.687	2.762	1.830	0.000	1.638	3.340	3.244	2.663	0.848	1.618	1.165	1.753
11	2.839	3.603	4.576	3.272	3.602	1.747	3.268	2.806	2.721	1.638	0.000	3.722	4.033	2.375	1.217	1.900	1.103	1.534
12	1.651	1.816	2.719	2.610	1.518	2.845	1.773	1.385	1.919	3.340	3.722	0.000	1.045	1.831	3.190	2.938	3.859	2.653
13	2.253	1.050	1.709	2.035	1.336	2.849	2.650	1.882	1.726	3.244	4.033	1.045	0.000	2.581	3.295	3.074	3.911	2.860
14	1.420	2.699	3.846	2.919	2.134	2.075	1.588	1.261	1.943	2.663	2.375	1.831	2.581	0.000	2.362	1.898	2.977	1.891
15	2.809	2.782	3.653	2.629	3.136	1.559	3.260	2.645	2.136	0.848	1.217	3.190	3.295	2.362	0.000	1.937	0.898	1.549
16	2.393	2.509	3.507	1.998	2.147	0.701	3.143	2.016	1.425	1.618	1.900	2.938	3.074	1.898	1.937	0.000	2.254	1.660
17	3.181	3.328	4.106	2.949	3.686	1.793	3.710	3.098	2.674	1.165	1.103	3.859	3.911	2.977	0.898	2.254	0.000	1.642
18	1.610	2.539	3.512	2.278	2.519	1.212	2.323	1.589	1.811	1.753	1.534	2.653	2.860	1.891	1.549	1.660	1.642	0.000

Table 5.9. Ratio between the normalized Mahalanobis and Euclidean distances (δ_M/δ_E) of the 18 ICU physicians who have used the simulator.

	1	2	3	4	5	6	7	8	9	10	11	12	13	14	15	16	17	18
1	1.000	1.110	1.291	0.877	0.996	0.761	0.967	0.858	0.806	0.831	1.001	3.865	1.983	1.152	0.937	0.739	1.004	1.023
2	1.110	1.000	1.974	1.255	1.904	2.045	0.967	1.266	2.080	1.362	2.027	0.937	0.838	1.725	1.641	1.854	1.825	2.135
3	1.291	1.974	1.000	2.369	2.124	2.447	1.113	1.474	2.503	1.699	2.104	1.134	1.031	1.795	1.816	2.322	1.957	2.022
4	0.877	1.255	2.369	1.000	1.259	2.037	0.869	0.925	1.540	1.445	1.702	0.938	0.968	1.287	1.479	2.211	1.605	1.216
5	0.996	1.904	2.124	1.259	1.000	1.493	0.886	1.075	1.242	1.260	1.699	0.888	1.231	1.477	1.464	1.339	1.608	1.899
6	0.761	2.045	2.447	2.037	1.493	1.000	0.780	0.826	2.080	1.311	1.480	1.049	1.311	1.076	1.421	1.803	1.534	0.790
7	0.967	0.967	1.113	0.869	0.886	0.780	1.000	0.830	0.793	0.806	0.901	1.292	1.254	0.760	0.856	0.747	0.933	0.940
8	0.858	1.266	1.474	0.925	1.075	0.826	0.830	1.000	0.812	0.898	1.194	3.058	3.024	1.594	1.063	0.780	1.163	1.488
9	0.806	2.080	2.503	1.540	1.242	2.080	0.793	0.812	1.000	1.273	1.853	0.854	1.047	1.197	1.512	1.701	1.742	1.428
10	0.831	1.362	1.699	1.445	1.260	1.311	0.806	0.898	1.273	1.000	1.381	0.978	1.114	1.037	0.904	1.688	1.347	0.827
11	1.001	2.027	2.104	1.702	1.699	1.480	0.901	1.194	1.853	1.381	1.000	1.398	1.690	1.405	3.030	1.366	2.070	1.156
12	3.865	0.937	1.134	0.938	0.888	1.049	1.292	3.058	0.854	0.978	1.398	1.000	1.375	1.682	1.146	0.987	1.303	1.925
13	1.983	0.838	1.031	0.968	1.231	1.311	1.254	3.024	1.047	1.114	1.690	1.375	1.000	2.260	1.357	1.255	1.507	2.524
14	1.152	1.725	1.795	1.287	1.477	1.076	0.760	1.594	1.197	1.037	1.405	1.682	2.260	1.000	1.246	0.878	1.426	2.846
15	0.937	1.641	1.816	1.479	1.464	1.421	0.856	1.063	1.512	0.904	3.030	1.146	1.357	1.246	1.000	1.440	3.924	1.070
16	0.739	1.854	2.322	2.211	1.339	1.803	0.747	0.780	1.701	1.688	1.366	0.987	1.255	0.878	1.440	1.000	1.605	0.898
17	1.004	1.825	1.957	1.605	1.608	1.534	0.933	1.163	1.742	1.347	2.070	1.303	1.507	1.426	3.924	1.605	1.000	1.020
18	1.023	2.135	2.022	1.216	1.899	0.790	0.940	1.488	1.428	0.827	1.156	1.925	2.524	2.846	1.070	0.898	1.020	1.000

5.2.3 Clustering and 2D representation of management decision-making

Using the distance matrix, clustering techniques can be applied to obtain homogeneous groups of users in terms of ICU management. The Agglomerative Hierarchical Clustering (AHC) algorithm is an important and well-established technique in statistics and machine learning (Müllner 2011) to build a cluster tree (a dendrogram) to represent data, where each cluster links to two or more successor clusters. From a distance matrix, the groups are nested and organised as a tree, which ideally ends up as a meaningful classification scheme. There are functions implemented in free software that perform AHC, for instance, the *linkage()* function in the *cluster* package of SciPy in Python.

There are also statistical techniques such as Multidimensional Scaling (MDS) that allow the graphical representation of multidimensional data. MDS is used to transform the measured distances between pairs of a set of n objects or individuals into a configuration of n mapped points in an abstract Cartesian space (Mead 1992). Given a distance matrix with the distances between each pair of objects in a set, and a chosen number of dimensions, N , an MDS algorithm places each object into N -dimensional space (a lower-dimensional representation) such that the distances between objects are preserved as well as possible. For $N = 1, 2$, and 3 , the resulting points can be visualized in a scatter plot (Borg and Groenen 2005). Objects that are more similar (or have shorter distances) are closer together on the graph than objects that are less similar (or have longer distances). As well as interpreting dissimilarities as distances on a graph, MDS can also serve as a dimension reduction technique for high-dimensional data (Buja et al. 2008). Again, we can find functions implemented in free software that perform MDS, for instance, the *MDS()* function in the *manifold* module of Scikit-learn in Python.

Methodology application

As an illustration of this methodology Figure 5.2 shows the dendrogram obtained from the

distance matrix presented in Table 5.8. Ward variance minimization algorithm (Ward 1963) is used here for calculating the distance between the newly formed cluster. The dendrogram shows three differentiated clusters, two of them with 7 physicians each and the third with 4.

The 2D scatter plot of the distance matrix presented in Table 5.8 is shown in Figure 5.3. The SMACOF (Scaling by MAjorizing a COmplicated Function) algorithm for metric MDS has been used. It minimizes an objective function (the stress) using a majorization technique. Stress majorization, also known as the Guttman Transform (Guttman 1968), guarantees a monotone convergence of stress, and is more powerful than traditional techniques such as gradient descent. With this 2D representation it is possible to visualize the three clusters obtained with the dendrogram.

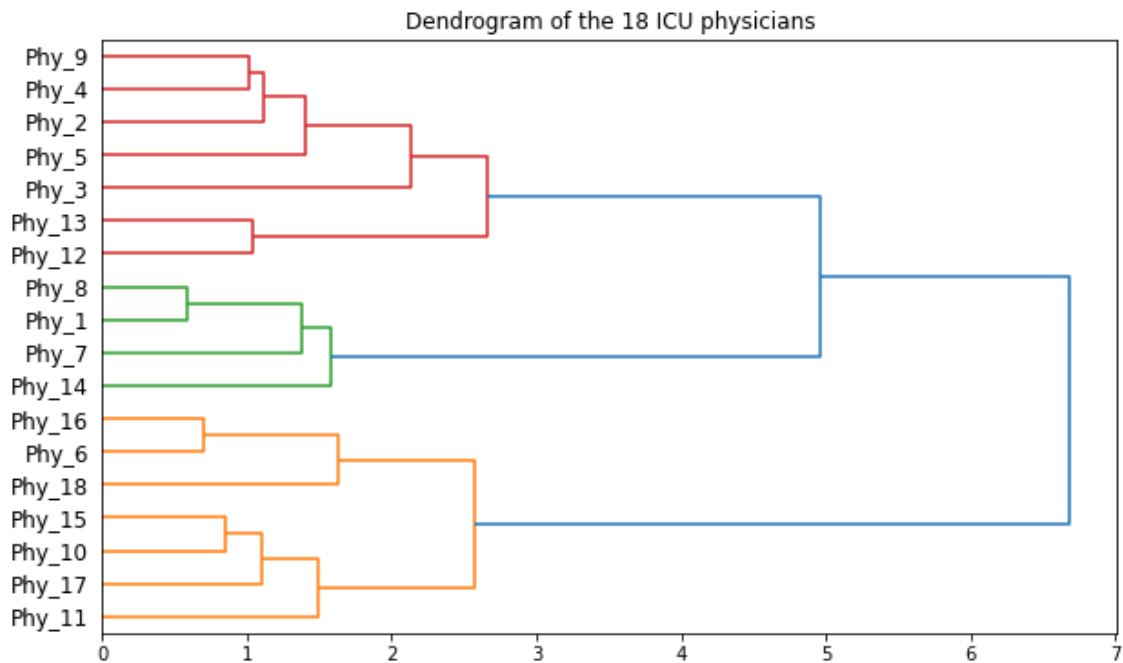


Figure 5.2. Dendrogram obtained from the distances between the 18 ICU physicians presented in Table 5.8.

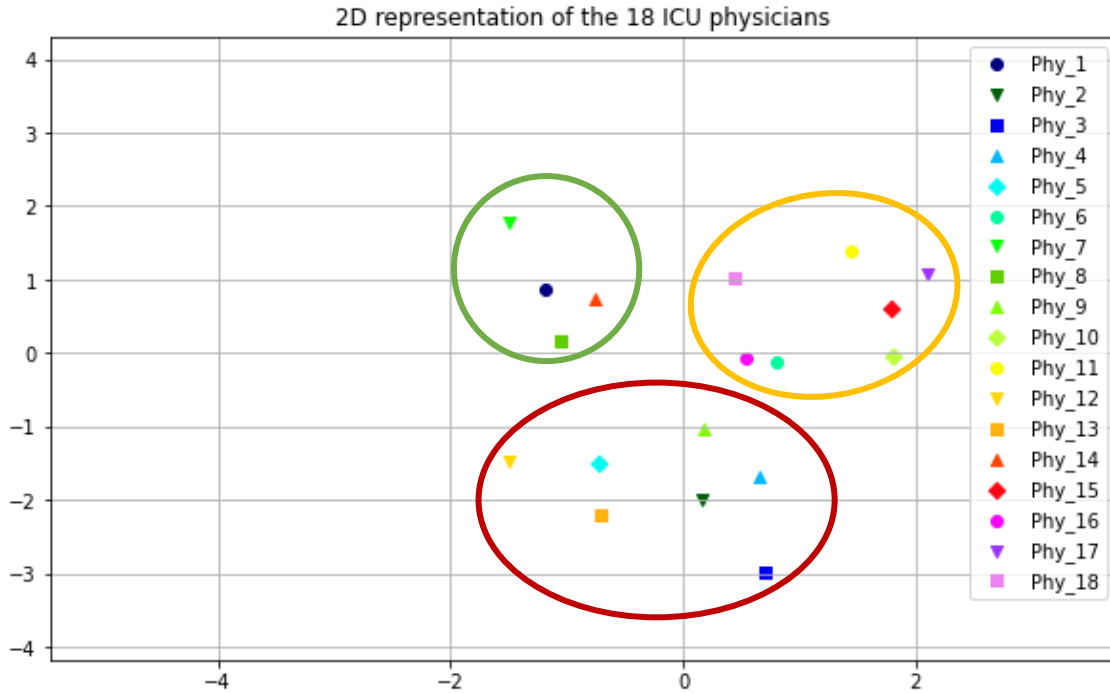


Figure 5.3. 2D representation obtained from the distances between the 18 ICU physicians presented in Table 5.8. The 3 clusters obtained with the dendrogram are visualized.

5.3 Analysis of decision-making conditioned by the ICU pressure level

The results obtained and analysed in the Section 5.2 provide an overview of the performance of each user. It allows us to quantify each of the BCA used to manage the ICU. In this section, we extend our analysis considering that the use of the three BCA may depend on the level of pressure of the ICU. In the management of a real ICU, the same decisions are not made when the level of pressure is high or when bed occupancy is “under control”.

5.3.1 Defining the ICU pressure level

The ICU pressure level depends on the number of manageable beds (defined in Section 5.2.1). Medical decisions in the ICU are not only based on the current occupancy or the clinical condition of the current patients in the ICU, but also on the next known admissions. Let us denote N_D as the total number of decision-making instants. Decision times t_d , with $d = 1, \dots, N_D$, are fixed for all users. They coincide with the arrival times of emergency patients and with the general clinical sessions when the discharge of patients already admitted is assessed and decisions are made on the confirmation or cancellation of the scheduled surgeries for that day. At such times t_d , we define the concept of *pressure level* as the proportion of occupied

ICU beds resulting from admitting all known incoming patients and discounting the number of manageable beds at time t_d . The ICU pressure level $p_i(t_d)$ is used to analyse the application of the three BCA in a disaggregated manner. Its expression is shown in equation (5.6):

$$p_i(t_d) = \frac{n_B + n_{Si}(t_d) + n_{Ei}(t_d) - m_i(t_d)}{n_B} \quad d = 1, \dots, N_D \quad (5.6)$$

where,

- $p_i(t_d)$ is the ICU pressure level at time t_d of user i .
- n_B : total ICU beds.
- $n_{Si}(t_d)$ is the number of scheduled surgeries in the next 24 hours known at time t_d by user i .
- $n_{Ei}(t_d)$ is the number of emergency patients arriving at time t_d and for whom an admission decision has to be made by user i .
- $m_i(t_d)$ is the number of manageable beds in the ICU at time t_d of user i .

The ICU pressure level, defined for the decision instants t_d , may be less than or greater than unity. We consider five pressure levels with cut-off points suggested by ICU physicians. From lowest to highest ICU pressure level, each pressure level L_k is defined as follows:

- L_1 : moderate level, with $p_i(t_d) < 0.8$.
- L_2 : high level, with $p_i(t_d) \in [0.8, 0.9)$.
- L_3 : very high level, with $p_i(t_d) \in [0.9, 1)$.
- L_4 : extreme level, with $p_i(t_d) \in [1, 1.05)$.
- L_5 : saturation level, with $p_i(t_d) \geq 1.05$.

The ratios $P_i(D)$, $P_i(C)$, and $P_i(S)$ can be interpreted as probabilities (see Section 5.2.1), so we can also express the conditional probabilities on the pressure level. In equation (5.7) we calculate ratios depending on each pressure level k . The probability of diverting emergency patients conditional on pressure level L_k , $P_i(D|L_k)$, is obtained by dividing the number of emergency patients diverted at level L_k , $e_{Di}(L_k)$, by the total number of emergency patients who arrived at level L_k , $e_{Ti}(L_k)$. Similarly, the probability of cancelling scheduled surgeries conditional on pressure level L_k , $P_i(C|L_k)$, is obtained by dividing the number of scheduled surgeries cancelled at level L_k , $s_{Ci}(L_k)$, by the total number of scheduled surgeries at level L_k , $s_{Ti}(L_k)$. Finally, the probability of shortening stays conditional on pressure level L_k , $P_i(S|L_k)$, is obtained by dividing the number of stays shortened at level L_k , $d_{Si}(L_k)$, by the total number of patients discharged at level L_k , $d_{Ti}(L_k)$.

$$P_i(D|L_k) = \frac{e_{Di}(L_k)}{e_{Ti}(L_k)}, \quad P_i(C|L_k) = \frac{s_{Ci}(L_k)}{s_{Ti}(L_k)}, \quad P_i(S|L_k) = \frac{d_{Si}(L_k)}{d_{Ti}(L_k)} \quad (5.7)$$

Observe that $e_{Ti}(L_k)$ and $s_{Ti}(L_k)$ vary between users because each decision-making creates a different distribution of the ICU pressure levels. However, $\sum_k e_{Ti}(L_k) = e_T$ and $\sum_k s_{Ti}(L_k) = s_T$ for every user i .

In addition to detecting different ways of managing the ICU due to the disaggregated probabilities, these results may allow ICU practitioners to answer the following questions:

- In the face of extreme situations, which is prioritised more, the cancellation of scheduled surgeries or the diversion of emergency patients?
- Which BCA is more predominant among physicians?
- Do these BCA depend on bed occupancy?
- Can strategies be deduced to achieve a specific occupancy level?

Individual results can be aggregated by group of users g according to equation (5.8). To compare these values, we recommend the use of graphical representations of the results for a better appreciation.

$$P_g(D|L_k) = \frac{\sum_i e_{Di}(L_k)}{\sum_i e_{Ti}(L_k)}, \quad P_g(C|L_k) = \frac{\sum_i s_{Ci}(L_k)}{\sum_i s_{Ti}(L_k)}, \quad (5.8)$$

$$P_g(S|L_k) = \frac{\sum_i d_{Si}(L_k)}{\sum_i d_{Ti}(L_k)}$$

Another interesting issue derived from the above analyses is the probability of being in each pressure level L_k by each user i , $P_i(L_k)$. For each decision time t_d , the number of times the ICU pressure level belongs to the level L_k is counted and the result is divided by the total number of decisions (N_D), as it is shown in equation (5.9). The same probabilities can be obtained for each group g , $P_g(L_k)$, using the expression shown in equation (5.10).

$$P_i(L_k) = \frac{\sum_{d=1}^{N_D} 1_{\{p_i(t_d) \in L_k\}}}{N_D} \quad (5.9)$$

$$P_g(L_k) = \frac{\sum_{i=1}^{N_g} \sum_{d=1}^{N_D} 1_{\{p_i(t_d) \in L_k\}}}{N_g N_D} = \frac{\sum_{i=1}^{N_g} P_i(L_k)}{N_g} \quad (5.10)$$

Methodology application

Table 5.10 summarizes results recorded by *Physicians*, but now considering the ICU pressure level (the results of the rest of the users individually and separated by group are collected in Appendix E.3). We can observe that some physicians avoid managing the ICU at certain pressure levels, such as physicians 1, 7, 11, 12, 13, 17 and 18 who have avoided the pressure level L_5 in all three BCA, corresponding to the saturation level of the ICU.

Table 5.10. Comparison of simulation global results recorded by 18 ICU physicians considering the ICU pressure level.

Physician	$P_i(D)$					$P_i(C)$					$P_i(S)$				
	L_1	L_2	L_3	L_4	L_5	L_1	L_2	L_3	L_4	L_5	L_1	L_2	L_3	L_4	L_5
Phy_1	0.167	0.222	0.500	0.667	-	0.000	0.077	0.143	-	-	0.000	0.083	0.429	-	-
Phy_2	-	0.143	0.231	0.333	0.500	0.000	0.000	0.111	0.833	-	0.000	0.462	0.444	0.600	1.000
Phy_3	-	0.167	0.267	0.250	1.000	0.000	0.200	0.333	0.667	-	0.000	0.556	0.600	0.600	-
Phy_4	0.333	0.000	0.125	0.222	0.250	0.000	0.000	0.182	0.600	1.000	0.250	0.400	0.600	0.750	1.000
Phy_5	-	0.167	0.067	0.364	0.500	0.000	0.125	0.300	0.500	-	0.000	0.091	0.500	0.571	1.000
Phy_6	-	0.000	0.167	0.200	0.500	0.000	0.000	0.000	0.667	-	0.000	0.500	0.625	0.833	-
Phy_7	0.000	0.385	0.636	0.800	-	0.000	0.000	0.000	-	-	0.000	0.000	0.000	-	-
Phy_8	0.000	0.167	0.400	0.500	0.000	0.000	0.000	0.250	0.500	-	0.000	0.100	0.333	0.667	1.000
Phy_9	-	0.000	0.176	0.250	1.000	0.000	0.000	0.000	0.833	-	0.000	0.455	0.533	0.600	-
Phy_10	0.000	0.000	0.231	0.182	0.333	0.000	0.000	0.000	0.143	1.000	0.571	0.667	0.722	0.667	1.000
Phy_11	-	0.000	0.263	0.444	-	0.000	0.000	0.000	0.000	-	0.000	0.688	0.579	0.500	-
Phy_12	0.000	0.571	0.267	0.500	-	0.000	0.000	0.100	0.500	-	0.000	0.000	0.429	0.400	-
Phy_13	0.333	0.333	0.385	0.333	-	0.000	0.000	0.200	0.750	-	0.000	0.091	0.300	0.800	-
Phy_14	-	0.200	0.176	0.500	0.500	0.000	0.000	0.000	0.333	-	0.000	0.000	0.333	0.800	1.000
Phy_15	0.000	0.000	0.364	0.357	0.500	0.000	0.000	0.000	0.143	-	0.000	0.667	0.714	0.750	-
Phy_16	-	0.000	0.063	0.143	0.500	0.000	0.000	0.000	0.500	-	0.000	0.500	0.667	0.625	1.000
Phy_17	0.000	0.000	0.200	0.636	-	0.000	0.000	0.000	0.500	-	0.333	0.556	0.900	0.750	-
Phy_18	0.200	0.143	0.375	0.500	-	0.000	0.000	0.091	0.500	-	0.154	0.250	0.583	1.000	-

Table 5.11 presents the aggregated results for each group g , calculated according to equation (5.8). The conditional probabilities of diverted emergency patients, cancelled surgeries and shortened stays, for each group, are shown in Figure 5.4, Figure 5.5, and Figure 5.6 respectively. These three figures show that the probabilities increase as the level of pressure increases, which is logical. The greatest differences are observed in the probability of diverting emergency patients (see Figure 5.4). *Physicians, Nurses, and Nurse technicians* (users with ICU experience) divert more patients than the other groups with pressure levels L_1 , L_2 , L_3 , and L_4 . For better visualization, the graphs of these conditional probabilities separated by groups can be found in Appendix E.3.

Table 5.11. Global mean results of all users of the simulator considering the ICU pressure level.

Group (N_g)	$P_g(D)$					$P_g(C)$					$P_g(S)$				
	L_1	L_2	L_3	L_4	L_5	L_1	L_2	L_3	L_4	L_5	L_1	L_2	L_3	L_4	L_5
Physicians (18)	0.129	0.179	0.262	0.363	0.440	0.000	0.028	0.090	0.514	1.000	0.072	0.358	0.547	0.675	1.000
Nurses (14)	0.333	0.239	0.311	0.356	0.667	0.000	0.054	0.161	0.591	1.000	0.081	0.350	0.405	0.610	1.000
Nurse techs (4)	0.286	0.429	0.425	0.400	0.500	0.000	0.000	0.050	0.200	1.000	0.136	0.343	0.452	0.600	1.000
Residents (6)	0.000	0.029	0.130	0.190	0.571	0.000	0.028	0.141	0.577	1.000	0.087	0.434	0.550	0.788	1.000
Medical students (6)	0.000	0.020	0.108	0.209	0.889	0.000	0.104	0.245	0.500	1.000	0.026	0.373	0.519	0.688	1.000
OM-OR researchers (11)	0.000	0.034	0.132	0.214	0.649	0.067	0.045	0.044	0.371	1.000	0.082	0.468	0.611	0.678	1.000
Engineers (11)	0.000	0.045	0.085	0.246	0.783	0.000	0.062	0.088	0.415	1.000	0.038	0.462	0.485	0.727	1.000
Others (12)	0.302	0.239	0.144	0.207	0.710	0.120	0.026	0.026	0.317	1.000	0.000	0.258	0.478	0.639	1.000

These graphs illustrate that decisions depend on the level of pressure. Differences can also be found between the different user groups. Figure 5.7 show the probabilities of each group of being in each ICU pressure level L_k . It is observed that *Nurses* and *Nurse technicians* show a tendency towards lower levels of pressure.

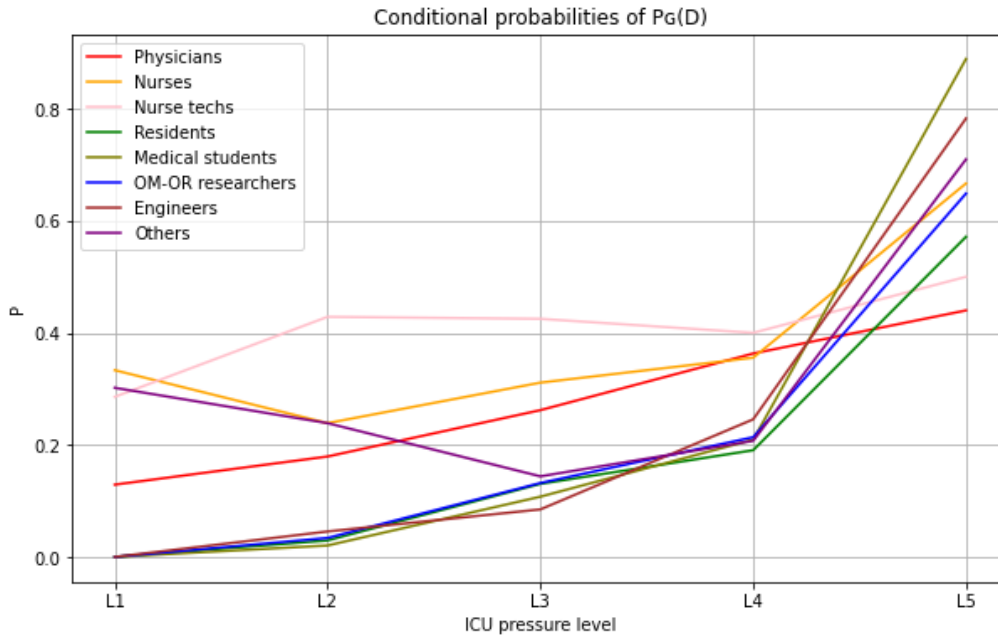


Figure 5.4. Probability of diverting emergency patients by each group conditioned by ICU pressure levels $P_g(D|L_k)$.

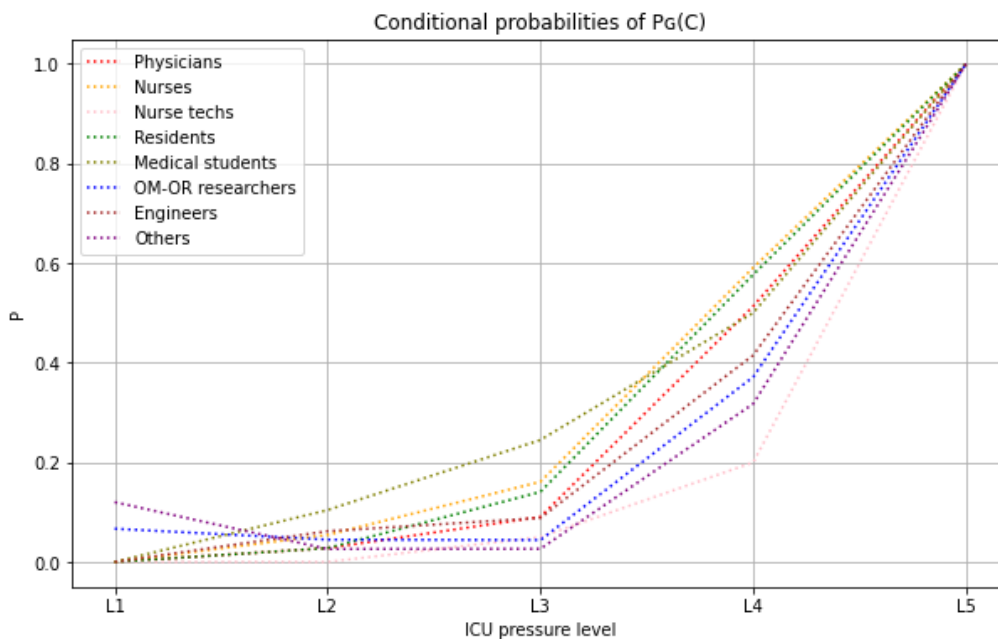


Figure 5.5. Probability of cancelling scheduled surgeries by each group conditioned by ICU pressure levels $P_g(C|L_k)$.

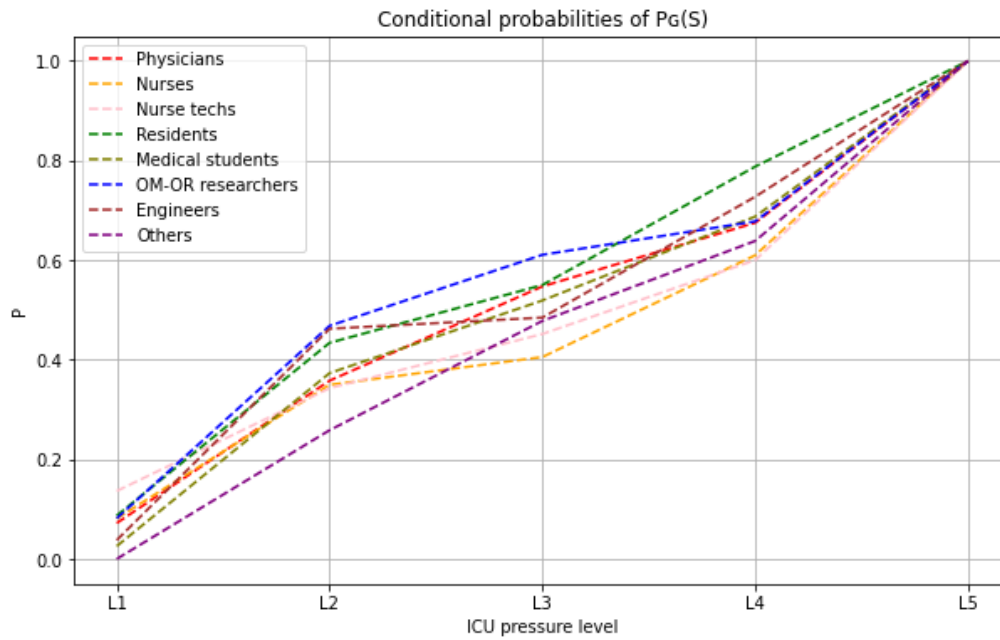


Figure 5.6. Probability of shortening stays by each group conditioned by ICU pressure levels $P_g(S|L_k)$.

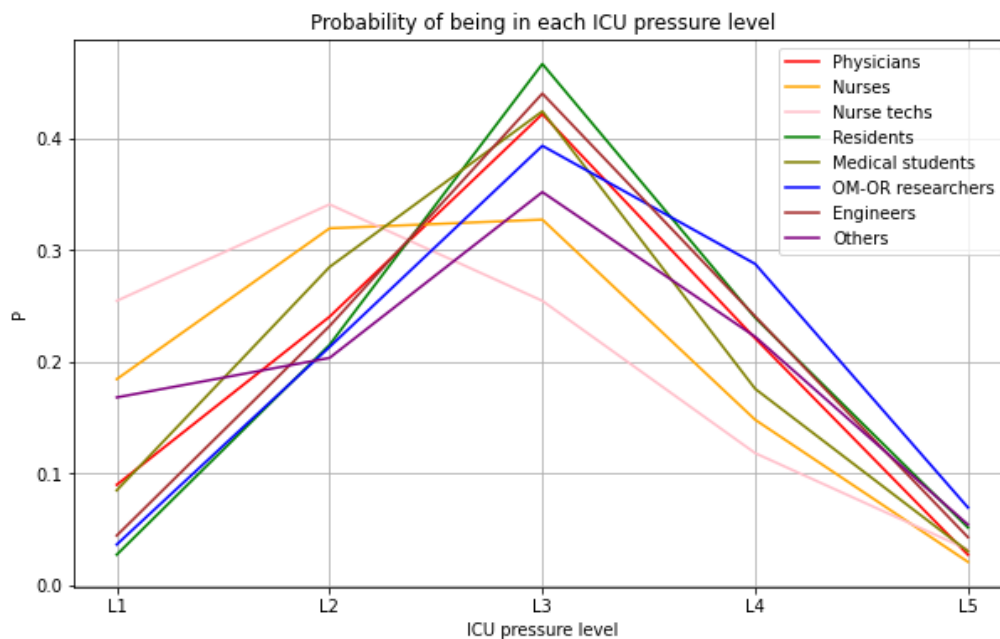


Figure 5.7. Probability of being in each ICU pressure level $P_g(L_k)$.

5.3.2 Decision-making analysis in a collectively managed ICU

A real ICU is managed by a group of physicians, and the ICU pressure levels are the result of the combination of decisions made by all individuals in the group. In this section we calculate for each user the probability of doing each of the BCA, diverting emergency patients (D),

cancelling scheduled surgeries (C), and shortening inpatients' stays (S), conditioned on the probability distribution of the ICU pressure levels (L_g) resulting from the combined decisions of the group to which he or she belongs. The probability distribution of the ICU pressure levels of group g is $P_g(L_k)$.

The conditional probabilities of diverting emergency patients, $P_i(D|L_g)$, cancelling scheduled surgeries, $P_i(C|L_g)$, and shortening patient stay, $P_i(S|L_g)$, are calculated for each user i as shown in equation (5.11).

$$\begin{aligned} P_i(D|L_g) &= \sum_k P_i(D|L_k)P_g(L_k), & P_i(C|L_g) &= \sum_k P_i(C|L_k)P_g(L_k), \\ P_i(S|L_g) &= \sum_k P_i(S|L_k)P_g(L_k) \end{aligned} \quad (5.11)$$

Note that some conditional probabilities like $P_i(D|L_k)$, $P_i(C|L_k)$, or $P_i(S|L_k)$ may not have been calculated. In these cases, $P_g(D|L_k)$, $P_g(C|L_k)$, or $P_g(S|L_k)$ corresponding to the user's group g is used instead. In addition, for users in the same group g , the probabilities of being in each pressure level L_k by that group, $P_g(L_k)$, $P_g(L_k)$, and $P_g(L_k)$, are used.

Methodology application

Table 5.12 shows the probabilities of diverting emergency patients (D), cancelling scheduled surgeries (C), and shortening inpatients' stays (S) of *Physicians* in an ICU managed by all of them. Comparing these results with those presented in Table 5.1, it can be seen that there are, on the one hand, physicians who maintain similar values in both approaches (e.g. physicians 2, 3 and 9), and on the other hand, physicians whose initial values have been considerably modified (e.g. physicians 1, 7 and 10). An increase in the initial values indicates that the user has made decisions with pressure levels lower than those of his/her group (e.g. physician 1 and 7), while a decrease in the initial values indicates that the user has made decisions with pressure levels higher than those of his/her group (e.g. physicians 10 and 16).

With these results, the next steps would be to apply the methods introduced in Section 5.2.2 and Section 5.2.3 (dissimilarity analysis, AHC, and MDS). New dendrograms and 2D scatter plots of the distance matrix would be obtained, which could be analysed and compared with existing ones (such as those in Figure 5.2 and Figure 5.3) representing distances between users.

Table 5.12. Decision-making results of 18 ICU physicians in a collectively managed ICU. The probabilities of diverting patients, $P_i(D|L_g)$, cancelling surgeries $P_i(C|L_g)$, and shortening stays, $P_i(S|L_g)$, are shown. Bold values represent the highest (red) and lowest (green) values.

Physician	$P_i(D L_g)$	$P_i(C L_g)$	$P_i(S L_g)$
Phy_1	0.4385	0.2193	0.3771
Phy_2	0.2305	0.2581	0.4581
Phy_3	0.2465	0.3631	0.5463
Phy_4	0.1385	0.2364	0.5645
Phy_5	0.1737	0.2942	0.3861
Phy_6	0.1396	0.1744	0.5950
Phy_7	0.5495	0.1406	0.1763
Phy_8	0.3192	0.2431	0.3391
Phy_9	0.1684	0.2112	0.4939
Phy_10	0.1466	0.0587	0.6906
Phy_11	0.2327	0.0271	0.5470
Phy_12	0.3722	0.1798	0.2963
Phy_13	0.3579	0.2772	0.3523
Phy_14	0.2581	0.1008	0.3445
Phy_15	0.2459	0.0587	0.6543
Phy_16	0.0831	0.1376	0.5666
Phy_17	0.2369	0.1376	0.7359
Phy_18	0.3329	0.1760	0.5680

5.3.3 Distance between observations by aggregating neighbouring components

The calculation of the Euclidean or Mahalanobis distance between two observations (see section 5.2.2) consists of measuring the differences component by component and the summands involved in the definition of these distances could be permuted. That is, keeping the same values, any permutation of the components as long as the relative distances are maintained gives the same result, with Euclidean distance, Mahalanobis distance, and in general with all distance definitions that are defined component by component. In this section, we propose an extension of the Euclidean distance in which, in addition to taking into account the component-by-component differences in the vector of observations, we take into account the differences between the sums of consecutive components of the vectors. We denote these sums as aggregations of neighbouring components, which can be of different sizes (a size of 3 means that three consecutive components are added together).

We define this distance as the Euclidean-Aggregate distance (δ_{EA}), which will allow us to calculate the dissimilarities from a novel point of view in which both the value and the position of all the components of the vector of observations will be relevant in the result. For illustrative purposes, an example is shown below in which the use of the classical Euclidean distance has weaknesses when used in specific contexts, which justifies the development of this Euclidean-Aggregate distance.

Let's assume that we compare ICU management by analysing the emergency patients diverted at different pressure levels by the user. Let denote $\vec{e}_{Di} = [e_{Di}(L_1), e_{Di}(L_2), e_{Di}(L_3), e_{Di}(L_4), e_{Di}(L_5)]$ the vector of emergency patients diverted at each level k of user i . We consider three different users with the following proposed vectors: $\vec{e}_{D1} = [1, 2, 1, 1, 1]$, $\vec{e}_{D2} = [1, 1, 2, 1, 1]$, and $\vec{e}_{D3} = [1, 1, 1, 1, 2]$. Applying the Euclidean distance calculation expression in equation (5.4), we obtain the following values for the distance between observations: $\delta_E(\vec{e}_{D1}, \vec{e}_{D2}) = \sqrt{2}$, $\delta_E(\vec{e}_{D1}, \vec{e}_{D3}) = \sqrt{2}$, and $\delta_E(\vec{e}_{D2}, \vec{e}_{D3}) = \sqrt{2}$. These results do not reflect the fact that the managements of users 1 and 2 are more similar to each other than with respect to user 3. Although in this example all three users diverted the same number of emergency patients in total ($e_{D1} = e_{D2} = e_{D3} = 6$), users 1 and 2 diverted the same number of emergency patients at similar pressure levels. (3 patients at levels L_2 and L_3). Applying the Euclidean-Aggregate distance defined in the following paragraphs, the results have the following relationship: $\delta_E(\vec{e}_{D1}, \vec{e}_{D2}) < \delta_E(\vec{e}_{D2}, \vec{e}_{D3}) < \delta_E(\vec{e}_{D1}, \vec{e}_{D3})$.

Let us denote $v_i = (v_{i1}, \dots, v_{iQ})$ and $v_j = (v_{j1}, \dots, v_{jQ})$ the observations of two objects or individuals resulting from measuring one variable V that can be disaggregated into Q ordered categories V_1, \dots, V_Q , which can be temporal or spatial values, defined levels or established sequences. Two weight vectors are also defined here, $\omega = (\omega_1, \dots, \omega_Q)$ and $\alpha = (\alpha_1, \dots, \alpha_Q)$ with $\sum_{s=1}^Q \omega_s = \sum_{k=1}^Q \alpha_k = 1$. ω_s is the weight assigned to the differences between the observed variables grouped into a set of size s . α_k is the weight assigned to each category or level k separately. The expression of δ_{EA}^2 , when $Q > 1$, is shown in equation (5.12). Note that when $Q = 1$ then $\delta_{EA}^2(v_i, v_j) = (v_i - v_j)^2$.

$$\begin{aligned} \delta_{EA}^2(v_i, v_j) = & \sum_{k=1}^Q \sum_{l=1}^{Q-k+1} \left[\omega_k \left(\sum_{m=l}^{l+k-1} \alpha_m v_{im} - \sum_{m=l}^{l+k-1} \alpha_m v_{jm} \right)^2 \right] \\ & + \sum_{k=1}^{Q-1} \left\{ (Q-k-1) \omega_k \left[\left(\sum_{m=1}^k \alpha_m v_{im} - \sum_{m=1}^k \alpha_m v_{jm} \right)^2 \right. \right. \\ & \left. \left. + \left(\sum_{m=Q-k+1}^Q \alpha_m v_{im} - \sum_{m=Q-k+1}^Q \alpha_m v_{jm} \right)^2 \right] \right\} \end{aligned} \quad (5.12)$$

ω_s is expected to decrease as the size of the group considered increases ($\omega_s \geq \omega_{s+1}$). With α_k , we can give more importance to some categories individually. For example, we could give more weight to differences observed in more demanding or important categories. In this case, as we are observing only one variable, the Euclidean-Aggregate distance $\delta_{EA}(v_i, v_j) = \sqrt{\delta_{EA}^2(v_i, v_j)}$. However, in the general case where R variables are observed, we can apply

equation (5.12) for each variable r obtaining $\delta_{EA_r}^2$. Then, the Euclidean-Aggregate distance would be calculated according to equation (5.13). Additional information on the aggregation of the neighbouring components in the calculation of this distance, as well as the results of the distances $\delta_{EA}(\vec{e}_{D1}, \vec{e}_{D2})$, $\delta_{EA}(\vec{e}_{D1}, \vec{e}_{D3})$, and $\delta_{EA}(\vec{e}_{D2}, \vec{e}_{D3})$ of the example proposed before can be found in Appendix F.

$$\delta_{EA}(v_i, v_j) = \sqrt{\sum_{r=1}^R \delta_{EA_r}^2(v_i, v_j)} \quad (5.13)$$

Applying this methodology, we can calculate the Euclidean-Aggregate distance between two observations. In this context, we propose 3 variables ($R = 3$) whose values are ordered in 5-component vectors ($Q = 5$): $e_D = [e_D(L_1), e_D(L_2), e_D(L_3), e_D(L_4), e_D(L_5)]$, $s_C = [s_C(L_1), s_C(L_2), s_C(L_3), s_C(L_4), s_C(L_5)]$, and $d_S = [d_S(L_1), d_S(L_2), d_S(L_3), d_S(L_4), d_S(L_5)]$. The diversion of emergency patients, the cancellation of elective surgeries, and the shortening of stays are conditioned by the level of pressure observed when making each decision. In cases where the scales of the variables included are very different from each other, a normalization could be carried out. However, this normalization depends on each observation and is strongly influenced by outliers. In this context, the variables proposed for the calculation of the Euclidean-Aggregate distance are considered to be of the same scale, so that normalization would not be necessary. Regarding the two weight vectors, a first approach would be to consider all their components equal ($\alpha_k = \omega_s = 1/Q$). But these values can be discussed with ICU practitioners to decide whether to assign more weight to high-pressure levels or to aggregations of neighbouring components of smaller sizes. Even for each variable r , these values can be different. Once all the Euclidean-Aggregate distances between each pair of users are calculated, it is possible to obtain the distance matrix and, from it, representing the appropriate dendrograms and 2D scatter plots.

Demonstration that the Euclidean-Aggregate distance is a metric.

The Euclidean-Aggregate distance can be expressed as a generalization of the Euclidean distance. We can rewrite equation (5.12) as follows:

$$\delta_{EA}^2(x, y) = \sum_{k=1}^Q \sum_{l=1}^{Q-k+1} (x_{kl} - y_{kl})^2 + \sum_{k=1}^{Q-1} (x_{k1} - y_{k1})^2 + \sum_{k=1}^{Q-1} (x_{k2} - y_{k2})^2 \quad (5.14)$$

where,

- $x_{kl} = \sqrt{\omega_k} \sum_{m=l}^{l+k-1} \alpha_m v_{im}$.
- $y_{kl} = \sqrt{\omega_k} \sum_{m=l}^{l+k-1} \alpha_m v_{jm}$.

- $x_{k1} = \sqrt{(Q - k - 1)\omega_k} \sum_{m=1}^k \alpha_m v_{im}$.
- $y_{k1} = \sqrt{(Q - k - 1)\omega_k} \sum_{m=1}^k \alpha_m v_{jm}$.
- $x_{k2} = \sqrt{(Q - k - 1)\omega_k} \sum_{m=Q-k+1}^Q \alpha_m v_{im}$.
- $y_{k2} = \sqrt{(Q - k - 1)\omega_k} \sum_{m=Q-k+1}^Q \alpha_m v_{jm}$.

Grouping all the summations and generalising the indices, the Euclidean-Aggregate distance can be formulated as shown in equation (5.15). Note that $x = (x_1, \dots, x_n)$ and $y = (y_1, \dots, y_n)$ belong to \mathbb{R}^n .

$$\delta_{EA}(x, y) = \sqrt{\sum_{i=1}^n (x_i - y_i)^2} \quad (5.15)$$

Equation (5.15) is the definition of Euclidean distance between x and y vectors (see equation (5.4)). The Euclidean distance is a metric, so it is demonstrated that the Euclidean-Aggregate distance is also a metric.

5.4 Analysis of ICU management over time

There is still the possibility that the decisions made by two users may be different even if they have similarities in the global use of BCA (results shown in Section 5.2 and Section 5.3). Time is a variable that has not been taken into account so far in the analysis of the results. Assuming that the purpose of using the BCA is to keep a certain number of beds available for future patients, we propose to track over time the number of manageable beds to describe, with trajectories, the dynamic management of the ICU beds. That is, we compare the functions $m_i(t)$.

Figure 5.8 shows the trajectories $m_i(t)$ of two different physicians. The physician number 7 prefers more control over the ICU and reserves at least 3 manageable beds most of the time in order not to cancel any surgeries. However, physician number 10, works on a lower level of manageability, which means that more new patients are admitted, with the risk of running out of manageable beds at certain times. This representation is consistent with the results shown in Table 5.1. By contrast, Figure 5.9 shows the trajectories of two physicians who were not so different according to Table 5.1 (physicians 1 and 12). It is observed that the evolution they have followed is quite different. Accordingly, global results do not fully describe how users manage the ICU, and it is necessary to analyse their evolution. Likewise, the evolution of mean manageable beds for each type of user can be represented. Figure 5.10 shows the trajectories obtained by *Physicians*, *Nurses*, *Nurse technicians*, and *Residents*. It can be seen that *Nurse technicians* and *Nurses* reserve on average more manageable beds than *Physicians* and

Residents during their management of the ICU. In particular, *Residents* present the lowest mean manageable beds and they are the only ones with no ICU experience among these four groups. Each of the trajectories for each type of user is listed individually in Appendix E.4.

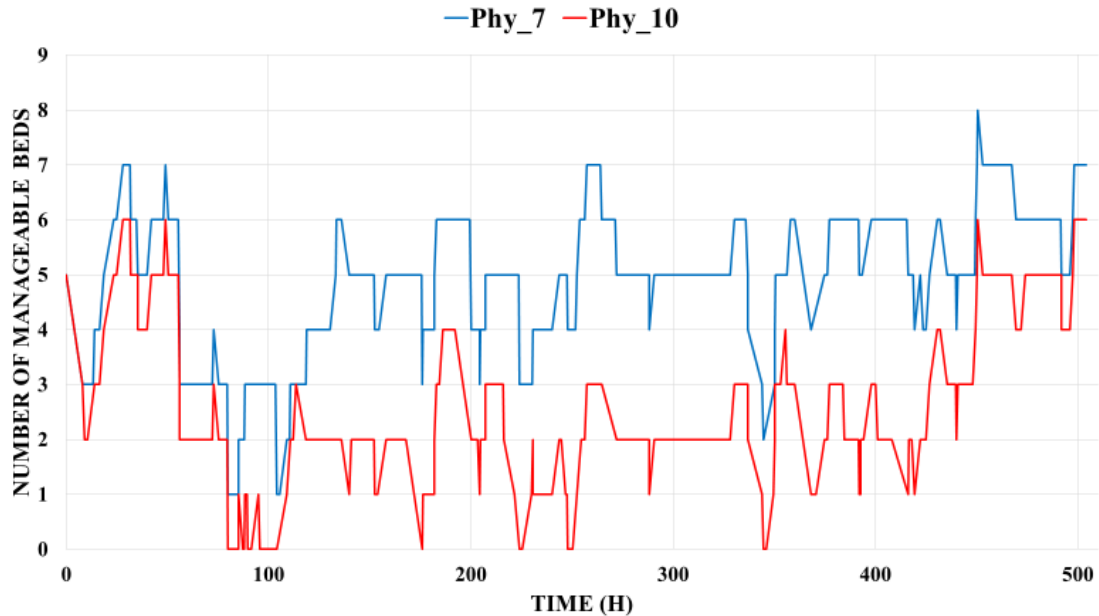


Figure 5.8. Graph showing the trajectory of the number of manageable beds of two different physicians (physicians 7 and 10).

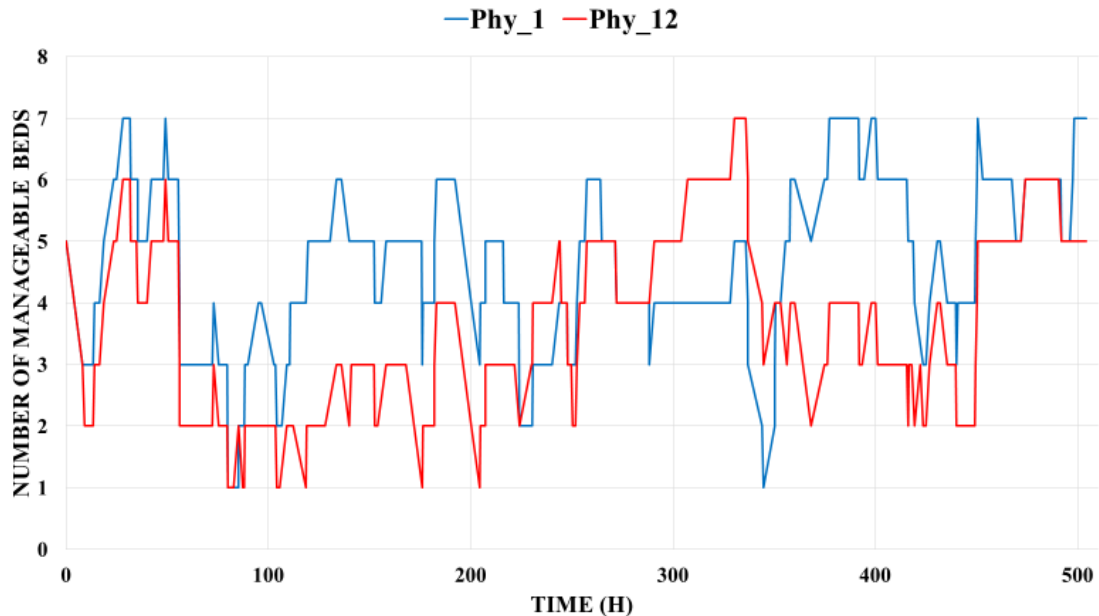


Figure 5.9. Graph showing the trajectory of the number of manageable beds of two similar physicians according to their global results (physicians 1 and 12).

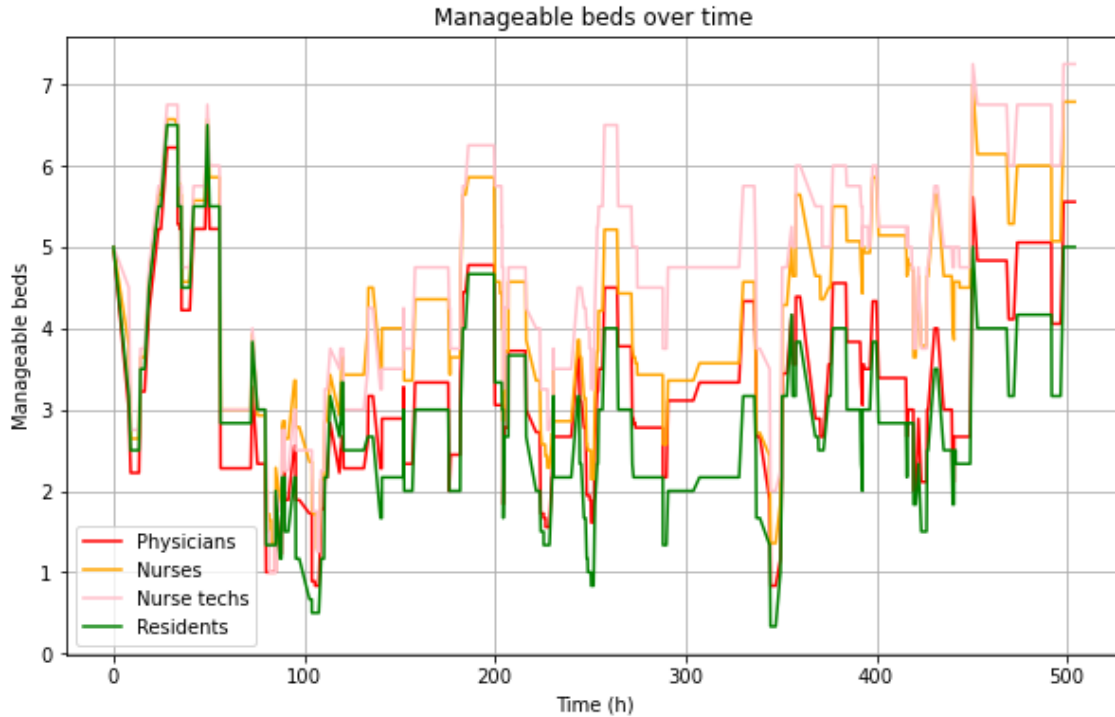


Figure 5.10. Graph showing the trajectories of the number of manageable beds of 18 ICU physicians, 14 ICU nurses, 4 ICU nurse technicians, and 6 residents.

These trajectories $m_i(t)$ can be compared by the distance between them. For this purpose, the area between two curves is calculated. The expression of this dynamic measure of distance (δ_D) is shown in equation (5.16):

$$\delta_D(m_i(t), m_j(t)) = \frac{1}{n_B T} \int_0^T |m_i(t) - m_j(t)| dt \quad (5.16)$$

where,

- n_B : total ICU beds.
- T : total time of the simulation in hours.
- $m_i(t)$: number of manageable beds in the ICU of user i at time t .

This calculation allows us to obtain the distances between all users and groups.

Methodology application

Table 5.13, for example, shows the dynamic distances between the 18 ICU physicians who have used the simulator. With this information, it is possible to unequivocally detect the pair of physicians who are most or least similar in terms of the management of the ICU manageable beds. Specifically, Figure 5.11 shows the two most similar physicians to each other in this

matter, while Figure 5.12 shows the two most different physicians. Further comparisons can be made here by means of representations such as dendrograms and 2D scatter plots.

Table 5.13. Dynamic distances between the 18 ICU physicians who have used the simulator. Bold values represent the five lowest distances (green) and the five highest distances (red).

	1	2	3	4	5	6	7	8	9	10	11	12	13	14	15	16	17	18
1	0.000	0.068	0.066	0.068	0.071	0.069	0.022	0.039	0.078	0.086	0.060	0.060	0.047	0.062	0.068	0.091	0.048	0.051
2	0.068	0.000	0.019	0.026	0.027	0.021	0.076	0.046	0.018	0.031	0.038	0.030	0.026	0.028	0.029	0.028	0.035	0.053
3	0.066	0.019	0.000	0.029	0.028	0.021	0.076	0.043	0.031	0.029	0.038	0.040	0.034	0.029	0.026	0.033	0.030	0.060
4	0.068	0.026	0.029	0.000	0.034	0.026	0.078	0.048	0.026	0.021	0.049	0.037	0.028	0.033	0.023	0.035	0.038	0.059
5	0.071	0.027	0.028	0.034	0.000	0.021	0.080	0.047	0.028	0.040	0.045	0.048	0.043	0.030	0.029	0.025	0.033	0.072
6	0.069	0.021	0.021	0.026	0.021	0.000	0.079	0.046	0.022	0.027	0.031	0.035	0.033	0.013	0.024	0.025	0.025	0.057
7	0.022	0.076	0.076	0.078	0.080	0.079	0.000	0.042	0.086	0.096	0.070	0.058	0.056	0.072	0.078	0.101	0.058	0.044
8	0.039	0.046	0.043	0.048	0.047	0.046	0.042	0.000	0.058	0.063	0.059	0.051	0.037	0.048	0.045	0.068	0.037	0.067
9	0.078	0.018	0.031	0.026	0.028	0.022	0.086	0.058	0.000	0.033	0.040	0.038	0.038	0.031	0.033	0.016	0.041	0.059
10	0.086	0.031	0.029	0.021	0.040	0.027	0.096	0.063	0.033	0.000	0.046	0.050	0.041	0.030	0.019	0.028	0.039	0.069
11	0.060	0.038	0.038	0.049	0.045	0.031	0.070	0.059	0.040	0.046	0.000	0.053	0.051	0.034	0.050	0.045	0.042	0.051
12	0.060	0.030	0.040	0.037	0.048	0.035	0.058	0.051	0.038	0.050	0.053	0.000	0.023	0.039	0.041	0.052	0.043	0.030
13	0.047	0.026	0.034	0.028	0.043	0.033	0.056	0.037	0.038	0.041	0.051	0.023	0.000	0.036	0.031	0.047	0.030	0.047
14	0.062	0.028	0.029	0.033	0.030	0.013	0.072	0.048	0.031	0.030	0.034	0.039	0.036	0.000	0.022	0.035	0.015	0.053
15	0.068	0.029	0.026	0.023	0.029	0.024	0.078	0.045	0.033	0.019	0.050	0.041	0.031	0.022	0.000	0.037	0.021	0.065
16	0.091	0.028	0.033	0.035	0.025	0.025	0.101	0.068	0.016	0.028	0.045	0.052	0.047	0.035	0.037	0.000	0.049	0.074
17	0.048	0.035	0.030	0.038	0.033	0.025	0.058	0.037	0.041	0.039	0.042	0.043	0.030	0.015	0.021	0.049	0.000	0.052
18	0.051	0.053	0.060	0.059	0.072	0.057	0.044	0.067	0.059	0.069	0.051	0.030	0.047	0.053	0.065	0.074	0.052	0.000

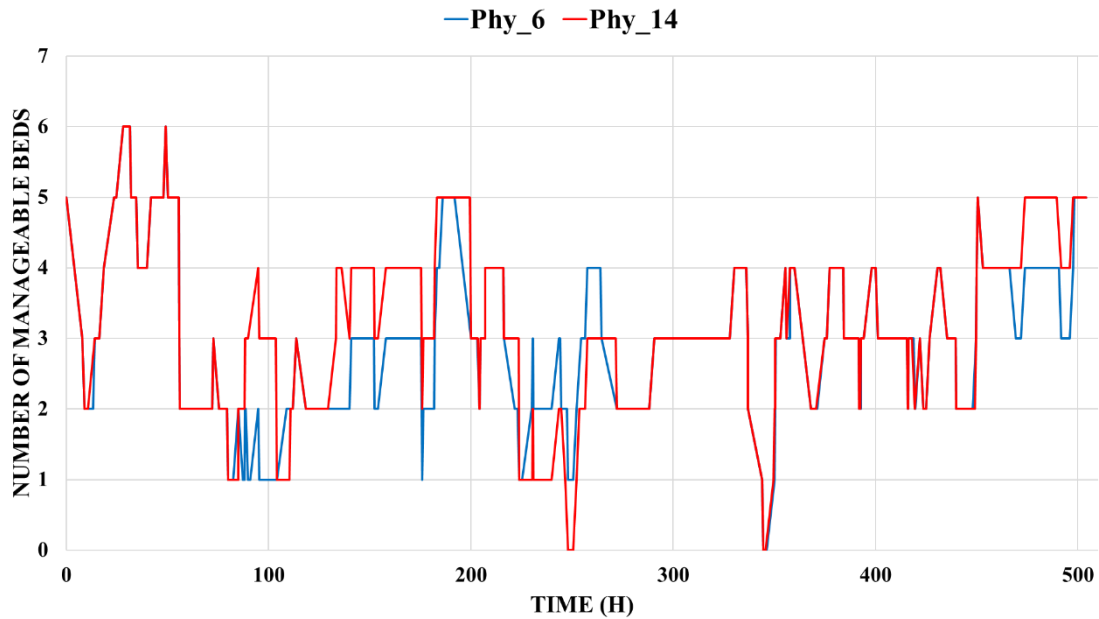


Figure 5.11. Graph showing the trajectory of the number of manageable beds of the two most similar physicians to each other according to their dynamic distance (physicians 6 and 14).

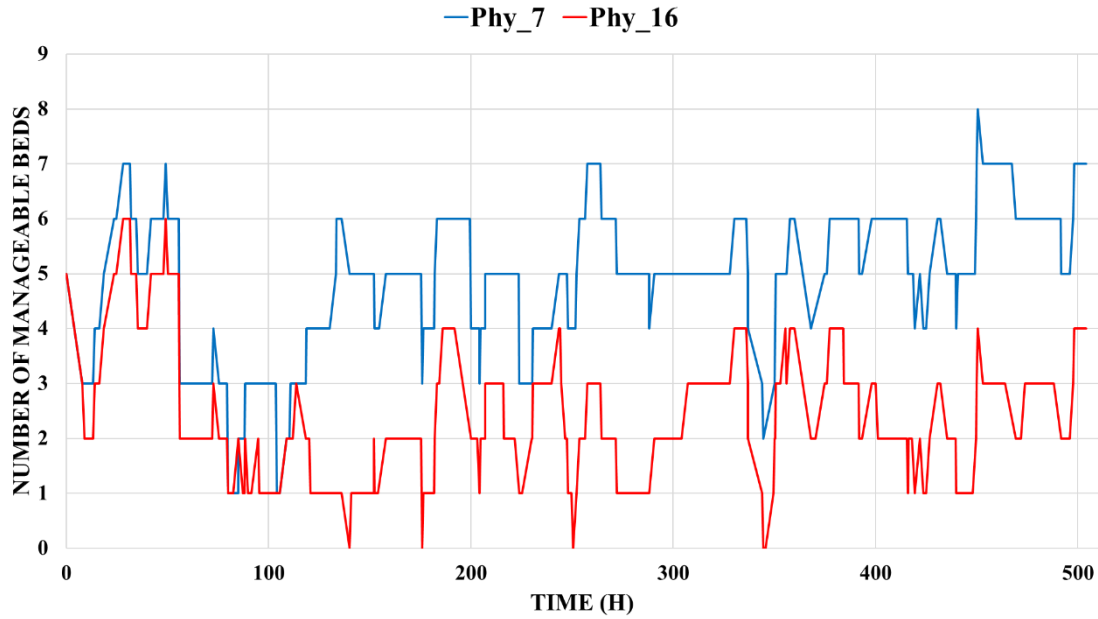


Figure 5.12. Graph showing the trajectory of the number of manageable beds of the two most different physicians to each other according to their dynamic distance (physicians 7 and 16).

5.5 Analysis of patient-level decisions

In this section, we propose an analysis of the ICU management through the decisions made by each user on each of the ICU patients. So we need a mathematical representation of the decisions to disaggregate and analyse them at the patient level.

Let us denote N_p as the total number of patients observed in the simulation by the user. The occupancy of the ICU changes or may change at decision times t_d $d = 1, \dots, N_D$, where N_D is the total number of decision-making instants (see Section 5.3.1). We define the *time slot* (τ_d) as the period between two consecutive decision times ($\tau_d = t_{d+1} - t_d$ and $\tau_{N_D} = T - t_{N_D}$). Let Γ_i be the binary matrix $N_D \times N_p$ of occupancy, which for each user i is defined as:

$$\gamma_{idl} = \begin{cases} 1 & \text{if patient } l \text{ is admitted during } \tau_d & d = 1, \dots, N_D \\ 0 & \text{otherwise} & l = 1, \dots, N_p \end{cases} \quad (5.17)$$

This matrix mathematically represents the medical decisions in the ICU. The following two examples attempt to clarify the definition of the occupancy matrix Γ_i . In the case that the scheduled surgery of patient l is confirmed at time t_d , then $\gamma_{idl} = 1$ even if the patient is not physically in the ICU until the surgery is completed. In the case that a patient l is discharged at time t_d , then $\gamma_{idl} = 0$ even if the patient does not leave the ICU immediately. Therefore, each row d of the matrix Γ_i ($\gamma_{id\cdot}$), represents the patients virtually admitted to the ICU at time t_d , that is, the patients that the user has decided to remain in the ICU or those who will be

admitted to the ICU. The information associated with the initial occupancy of the ICU is stored in the binary vector p as shown in equation (5.18), which is the same for all users.

$$p_l = \begin{cases} 1 & \text{if patient } l \text{ is initially admitted in the ICU} \\ 0 & \text{otherwise} \end{cases} \quad l = 1, \dots, N_P \quad (5.18)$$

The occupancy matrix Γ_i , together with the vector p , allows the simulation performed by any user to be reproduced from the initial instant. All medical patient-level decisions are stored sequentially. The difference between the management of the ICU of two users i and j will be measured as a distance between their respective binary matrices Γ_i and Γ_j . Numerous binary similarity and distance measures have been proposed in different fields to compare binary feature vectors. Choi et al. (2010) have collected 76 binary similarity and distance measures used over the last century. Here, our binary feature vector is each row $\gamma_{id\bullet} = (\gamma_{id1}, \dots, \gamma_{idN_P})$ of matrix Γ_i , which represents for each user i the virtual occupancy of the ICU at time t_d as mentioned above. To measure the distance or similarity between user i and user j , with occupancy matrixes Γ_i and Γ_j respectively, we define the following variables that will be used later:

- a_{ija} : the number of times that each patient l is admitted by both user i and user j at time t_d , see equation (5.19).
- b_{ija} : the number of times that each patient l is only admitted by the user i at time t_d , see equation (5.20).
- c_{ija} : the number of times that each patient l is only admitted by the user j at time t_d , see equation (5.21).
- d_{ija} : the number of times that each patient l is admitted neither by user i nor by user j at time t_d , see equation (5.22).

$$a_{ija} = \sum_{l=1}^{N_P} (\gamma_{idal} \cdot \gamma_{jdl}) \quad (5.19)$$

$$b_{ija} = \sum_{l=1}^{N_P} [\gamma_{idal} \cdot (1 - \gamma_{jdl})] \quad (5.20)$$

$$c_{ija} = \sum_{l=1}^{N_P} [(1 - \gamma_{idal}) \cdot \gamma_{jdl}] \quad (5.21)$$

$$d_{ijd} = \sum_{l=1}^{N_P} [(1 - \gamma_{idl})(1 - \gamma_{jdl})] \quad (5.22)$$

These variables can be expressed in a 2x2 contingency table (see Table 5.14) where a_{ijd} is the number of patients where the values of γ_{idl} and γ_{jdl} are both 1 (or admitted), meaning ‘admission matches’, b_{ijd} is the number of patients where the value of γ_{idl} and γ_{jdl} is (0,1), meaning ‘ i admission mismatches’, c_{ijd} is the number of patients where the value of γ_{idl} and γ_{jdl} is (1,0), meaning ‘ j admission mismatches’, and d_{ijd} is the number of patients where both γ_{idl} and γ_{jdl} are 0 (or not admitted), meaning ‘non-admission matches’. The diagonal sum $a_{ijd} + d_{ijd}$ represents the total number of matches between $\gamma_{id\bullet}$ and $\gamma_{jd\bullet}$, the other diagonal sum $b_{ijd} + c_{ijd}$ represents the total number of mismatches between $\gamma_{id\bullet}$ and $\gamma_{jd\bullet}$. The total sum of the 2x2 table, $a_{ijd} + b_{ijd} + c_{ijd} + d_{ijd}$ is always equal to N_P .

Table 5.14. Contingency table representing at time t_d the coincidences and discrepancies of two users i and j in patient admission decisions.

$\gamma_{idl} \backslash \gamma_{jdl}$	1	0	Sum
1	a_{ijd}	b_{ijd}	$a_{ijd} + b_{ijd}$
0	c_{ijd}	d_{ijd}	$c_{ijd} + d_{ijd}$
Sum	$a_{ijd} + c_{ijd}$	$b_{ijd} + d_{ijd}$	$a_{ijd} + b_{ijd} + c_{ijd} + d_{ijd} = N_P$

Using these variables, we want to measure both the differences between decisions on patient admissions and the differences on the virtual occupancy that each user maintains during the simulation in the ICU. None of the binary similarity and distance measures reported in the literature captures the two aspects we want to measure. For example, the *Jaccard* similarity measure (S_{jd}), shown in equation (5.23) (Jaccard 1901), is very useful for measuring the degree of similarity between decisions made. Or the *Hamming* distance measure (D_{Hd}), shown in equation (5.24) (Hamming 1950), can be used to detect different decisions among users.

$$S_{jd}(\gamma_{id\bullet}, \gamma_{jd\bullet}) = \frac{a_{ijd}}{a_{ijd} + b_{ijd} + c_{ijd}} \quad (5.23)$$

$$D_{Hd}(\gamma_{id\bullet}, \gamma_{jd\bullet}) = b_{ijd} + c_{ijd} \quad (5.24)$$

However, these measures do not reflect in the results when two users have maintained similar occupancy levels. To illustrate this in a very simple way, let us assume that there are only two patients to decide on their admission at time t_d . We define the following decision vectors: $\gamma_{1d\bullet} = (1, 1)$, $\gamma_{2d\bullet} = (0, 0)$, $\gamma_{3d\bullet} = (1, 0)$, and $\gamma_{4d\bullet} = (0, 1)$. Comparing user 1 with user 2, and user 3 with user 4, we obtain the following variables: $a_{12d} = 0$, $b_{12d} = 2$, $c_{12d} = 0$, $d_{12d} = 0$, $a_{34d} = 0$, $b_{34d} = 1$, $c_{34d} = 1$, and $d_{34d} = 0$. According to equations (5.23) and (5.24), $S_{jd}(\gamma_{1d\bullet}, \gamma_{2d\bullet}) = S_{jd}(\gamma_{3d\bullet}, \gamma_{4d\bullet}) = 0$ and $D_{Hd}(\gamma_{1d\bullet}, \gamma_{2d\bullet}) = D_{Hd}(\gamma_{3d\bullet}, \gamma_{4d\bullet}) = 2$. Although it is true that between users 1 and 2, and between users 3 and 4 the two decisions have been different, the management of users 3 and 4 is more similar due to the fact that the occupancy of the ICU is the same. This fact is not reflected with these types of distances.

Note that $a_{ijd} + c_{ijd}$ and $a_{ijd} + b_{ijd}$ represent the virtual occupancy at time t_d of user i and user j respectively. Therefore, the difference in absolute value between virtual occupancies of users i and j is given by: $|[a_{ijd} + c_{ijd}] - [a_{ijd} + b_{ijd}]| = |c_{ijd} - b_{ijd}| = |b_{ijd} - c_{ijd}|$. So we propose to include this expression, together with the two Hamming distance terms, in the calculation of the distance at the patient-level and dividing the result by the number of observed patients to normalize. Equation (5.25) shows the Extended Weighted Normalized Hamming distance (D_{EWNHd}), where β is the weight assigned to the difference in virtual occupancy and $1 - \beta$ is the weight assigned to the difference in admission decisions ($0 \leq \beta \leq 1$).

$$\begin{aligned} D_{EWNHd}(\gamma_{id\bullet}, \gamma_{jd\bullet}) &= \frac{\beta |b_{ijd} - c_{ijd}| + (1 - \beta)(b_{ijd} + c_{ijd})}{a_{ijd} + b_{ijd} + c_{ijd} + d_{ijd}} \\ &= \frac{\beta |b_{ijd} - c_{ijd}| + (1 - \beta)(b_{ijd} + c_{ijd})}{N_p} \end{aligned} \quad (5.25)$$

The proposed distance D_{EWNHd} allows comparing the decision-making of two users at time t_d taking into account the virtual occupancy. Now, with $\beta = 0.5$ we obtain that $D_{EWNHd}(\gamma_{1d\bullet}, \gamma_{2d\bullet}) = 1$ and $D_{EWNHd}(\gamma_{3d\bullet}, \gamma_{4d\bullet}) = 0.5$ which is consistent with the user's managements. Extending the calculation for all decisions times, we obtain the distance δ_{EWNH} that measures the observed differences between all users' decisions in the simulation. Equation (5.26) shows the calculation of δ_p , in which time is indirectly taken into account. Differences in patient decisions persist over time and are directly proportional to the duration of the corresponding *time slot* τ_d . The result is then divided by the total time T of the simulation to normalise.

$$\begin{aligned}
\delta_{EWNH}(\Gamma_i, \Gamma_j) &= \frac{1}{T} \sum_{d=1}^{N_D} \tau_d \frac{\beta |b_{ijd} - c_{ijd}| + (1 - \beta)(b_{ijd} + c_{ijd})}{N_p} \\
&= \frac{1}{T} \sum_{d=1}^{N_D} \tau_d D_{EWNHd}(\gamma_{id\bullet}, \gamma_{jd\bullet})
\end{aligned} \tag{5.26}$$

As in the previous sections, once the distances at the patient-level between all users are calculated, the distance matrix can be obtained. The analysis would then continue by representing these distances with dendrograms and 2D scatter plots.

Deceased patients during the simulation

The decrease of a patient is not considered as one of the BCA that the user uses to manage the ICU, as it is not part of the decision-making. Therefore, the times in which patients decrease are not included in the decision-making times t_d . However, when a patient decreases, the bed occupancy decreases, and this has to be taken into account in the calculation of the distance at the patient-level.

Let us consider a patient l who decreases at time $t_p \in (t_d, t_{d+1})$ during the simulation of the user i . Then $\gamma_{idl} = 1$ and $\gamma_{i(d+1)l} = 0$, but the change in value from 1 to 0 occurs at time t_p and not at time t_{d+1} . Therefore, the summand with index d in equation (5.26) has to be separated into 2, a first one calculating the differences over the period from t_d to t_p and a second one for the period from t_p to t_{d+1} . Equation (5.27) shows the summation term d to be substituted into equation (5.26) when in only one of the simulations of user i or user j the patient l decreases between time t_d to t_{d+1} . If in that period the patient l decreases in the simulations of both users, the expression in equation (5.26) is still valid.

$$\begin{aligned}
&(t_p - t_d) \frac{\beta |b_{ijd} - c_{ijd}| + (1 - \beta)(b_{ijd} + c_{ijd})}{N_p} \\
&+ (t_{d+1} - t_p) \frac{\beta |b_{ijd} - c_{ijd} + \varepsilon| + (1 - \beta)(b_{ijd} + c_{ijd} - 1)}{N_p}
\end{aligned} \tag{5.27}$$

where $\varepsilon = -1$ if the patient l only decreases in the simulation of user i and $\varepsilon = 1$ if the patient l only decreases in the simulation of user j . Note that if patient l does not decrease in the simulation of user i , it means that he or she has not been admitted in the ICU (because decreases are predetermined), so $\gamma_{idl} = \gamma_{i(d+1)l} = 0$ in that case.

5.6 Discussion and future work

In this chapter, we develop new methodologies enabling us to compare the way an ICU is

managed. To supplement the global evaluation criteria such as the number of diverted emergency patients, cancelled surgeries, and shortened stays, we define new metrics to measure the use of these BCA conditional to the ICU pressure level. We also propose distance measures that take into account ICU bed management dynamics and patient-level decisions.

This is possible thanks to an interactive tool such as a MFS of an ICU (see Chapter 4), which has been used by different user profiles. This *ICU simulator* saves all the decisions of each user and the situations in which they are taken. It is also important to highlight the participation of the ICU practitioners in this type of initiative, since their results enable us to develop appropriate methodology to reflect their different ways of managing the ICU and show how they vary.

The developed methodology can be extended in future research. It might be very interesting, for example, to compare the decisions made by a single user of the ICU simulator on separate occasions. This would make it possible to check whether, by using the simulator, the user is able to improve the outcomes of his or her decisions. Also, by detecting discrepancies in their own decisions, users can identify situations in which a decision was taken without full conviction, examine the details and reach a definitive decision.

Other lines of research that remain open are the detection of dilemma-inducing scenarios and patients. In other words, detecting which situations in the ICU lead to greater discrepancy between medical decisions or which patients generate a greater variety of opinion, in terms of their admission, for example. However, it must be taken into account that, from the first discrepancy between two users, the scenarios that result in each case are different, and the decisions made are not exactly the same.

Finally, the next objective is to obtain and implement practical conclusions in reality. In collaboration with the hospital, we can gather further results and conduct a more comprehensive study with more data. A more detailed clustering analysis will enable us to deduce which kind of ICU management patterns will potentially lead to discussions at the clinical level. Mallor et al. (2016) identify different management policies (aggressive, equitable, and cautious) in a normative analysis of decision-making using stochastic optimization methods. Physicians' behaviour could be classified according to these or similar policy categories. In summary, our purpose is to use the simulator to collect ICU management data enabling us to test theories about physicians' decision-making, analyse triage processes, and detect biases and patterns.

Part II

**Hospital preparedness
during epidemics: the
use of simulation to
better support the
Health Services
managers**

6 Forecasting the needs of ward and ICU beds in the COVID-19 pandemic

This chapter presents a Discrete Event Simulation (DES) model combining dynamic forecasting to predict (simulate) new patient arrivals and the reproduction of patient flow patterns and designed to address all the issues just raised. The simulation process yields future resource-use scenarios to inform the health authorities of future needs and give them time to plan. Therefore, the main feature of the simulation model presented here is its capacity to reproduce the evolution of the health system from its current state, in a non-stationary and changing environment, thus providing a useful forecasting tool.

The main contribution of this chapter is our proposal for a new simulation framework enabling short-term (from days to a few weeks) prediction of critical resource needs for the care of COVID-19 patients. The simulation framework can be adapted for application in potential future outbreaks.

This chapter is organized as follows. Section 6.1 offers a review of related literature dealing with the use of quantitative methods for the prediction and efficient management of health care system requirements. Section 6.2 studies the adequacy of Population Growth (PG) models to predict the spread trend of a pandemic. The modelling of patient flow through the hospital is presented in Section 6.3. The structure of the DES model and the methodology used to set up the simulation are included in Section 6.4. In Section 6.5 we propose a new estimator that, based on an Expectation-Maximization (EM) algorithm, estimates the branching probabilities using information from patients who do not yet know which path they will follow, as well as the parameters of the length of stay (LoS) probability distributions. The estimation method is based on the maximum likelihood method and uses exact and censored data. The new estimators are tested in Section 6.6 by simulating pandemic scenarios and compared with other estimators that make use of complete information only. Finally, Section 6.7 ends the chapter with the conclusions of this work.

6.1 The use of simulation models in hospital management

Simulation is one of the most suitable analytical tools for the analysis of complex systems, such as healthcare systems, as reflected in numerous specialist articles describing the use of simulation models for decision-making in the healthcare context. DES has been used to model and analyse all aspects of logistics management in healthcare, particularly the improvement of patient flow management, bed-planning, waiting list management, health service design, medical staff scheduling, etc. For reviews of the use of simulation models in healthcare, see Brailsford et al. (2009), Günal and Pidd (2010), Katsaliaki and Mustafee (2011), and Mielczarek and Uziako-Mydlikowska (2012). These simulation models usually focus on studying the stationary state of the health system to support strategic decisions for resource sizing or management policy design purposes.

The ultimate goal of these models is to match resource availability with demand in order to provide high-quality patient care while maintaining adequate human and technological resource provision. Some of the problems analysed in this framework are patient flow (Shahani et al. 2008; Kolker 2009), bed planning (Ridge et al. 1998; Zhu et al. 2012; Rodrigues et al. 2018), health service design (Mallor et al. 2016), and medical staff scheduling (Erhard et al. 2018), among others. Despite reports in the medical literature of discrepancies between assumptions in mathematical simulation models and the behaviour of real healthcare systems (Azcarate et al. 2020), there is no doubt about the usefulness of simulation models for the analysis of relevant problems in complex healthcare systems.

However, simulation not only helps to ensure the highest quality healthcare in terms of staff and facilities, it also improves the delivery of best practice. Since the pandemic began, all national governments and the World Health Organization (WHO) have extensively used simulation modelling to identify the best strategies for reducing the impact of COVID-19. Currie et al. (2020) identify challenges from this disease and discuss how simulation modelling can help decision-makers to make the best informed decisions.

The accuracy of a simulation model for the prediction of resource needs during a pandemic is dependent upon the design of an accurate model to forecast patient arrivals at the health facility. Most infectious disease prediction methods rely on differential equation models based on population dynamics (Grassly and Fraser 2008; Brauer and Castillo-Chavez 2012). These mathematical models are essential for understanding the course of the epidemic and planning effective control strategies (Anderson and May 1991; Diekmann and Heesterbeek 2000; Hethcote 2000). One of the most widely used models of human-to-human transmission is the SIR model (Kermack and McKendrick 1927). Members of the population are sorted into different status categories: S (Susceptible), I (Infected), and R (Remove). The portion of population in each state is calculated over time by estimating the rate of transition from one state to another. With more complex model specifications, it is possible to recreate the spread of a specific epidemic. Extensions of the classical SIR model (Anastassopoulou et al. 2020;

Giordano et al. 2020; Lin et al. 2020; Zhou et al. 2020; Casella 2021), as well as stochastic transmission models (Hellewell et al. 2020; Kucharski et al. 2020) have indeed been developed for the COVID-19 pandemic. However, such models are complicated and need strong assumptions and simplifications, because they are based on a set of differential equations with initial conditions and a number of adaptive parameters (Xia et al. 2009; Li et al. 2014; Magal et al. 2016; Li and Zhang 2017). Reliable values of those parameters only become available at the end of the pandemic and they depend on non-pharmaceutical interventions dictated by political decisions. There is also a need for other mathematical models that can be adapted to daily pandemic data.

PG models provide a simpler alternative for modelling the number of cumulative positive cases, hospitalizations and other pandemic variables. Growth curves are used in a wide range of research areas, such as fishery research (Oliveira Zardin et al. 2019; Oribe-Pérez et al. 2020), biology (Sun et al. 2020), or other infectious disease outbreaks (Horimoto et al. 1997; Roberts and Saha 1999; Viboud et al. 2016; Ghazvini et al. 2019). Specifically, Logistic, Gompertz, Rosenzweig, and Richards models have been used to model the spread of outbreaks such as A/H1N1 and Ebola in (Liu et al. 2015). The COVID-19 research has produced several papers describing the development of a growth model to predict new cases in countries such as China (Shen 2020), India (Malavika et al. 2021), Spain (Sánchez-Villegas and Daponte Codina 2020), and other European countries (Cássaro and Pires 2020). These mathematical models present a set of mathematical equations including adaptive parameters that can be determined numerically based on available real data (Panovska-Griffiths 2020). The model can be used daily (by updating the number of positive cases) and automatically adapted to individual parameter trends.

If all the mathematical models mentioned in the previous paragraphs could be fitted to real data, it would be possible to obtain an accurate prediction of what might happen in the future (e.g., emergency planning, resource allocation) (He et al. 2020; Poston et al. 2020; Steinberg et al. 2020). This is very important; especially for typically scarce hospital resources, such as Intensive Care Unit (ICU) beds. Manca et al. (2020) present and discuss a few regression models built on historical ICU admissions and patient death data during the COVID-19 pandemic. They are capable of reproducing the bed occupancy curve using regression models with great potential for decision-making and emergency planning in future pandemics.

In recent decades, moreover, healthcare simulation models using advanced technology have become a new experience-based learning support (Almagooshi 2015; Persson 2017) enabling healthcare professionals to acquire new cognitive, technical, and behavioural skills. Before working in real-world patient treatment scenarios, both professionals and students can benefit from this experience-based form of learning in a risk-free decision-making environment (Palominos et al. 2019). Simulation models of the type presented in this chapter also enable training in the management of health care services during emergencies. When resources are in short supply, one of the most critical decisions is how to allocate them to patients, especially

when they can mean the difference between survival and death, as is the case with ICU patients. This triage becomes even more difficult during pandemics, when resources are stretched even further. Different ICU triage protocols for use in pandemics have been suggested in Cheung et al. (2012), Christian et al. (2014), and Zhang et al. (2020). Forecasting bed demands is essential to avoid ethical dilemmas (Azcarate et al. 2020; Garcia-Vicuña et al. 2020b). According to Utley et al. (2011), “the impact of triage is dependent on the level of demand and on the scale of achievable differences between included and excluded groups in terms of anticipated LoS and critical care survival”. A simulation model can improve critical resource planning during a pandemic; and can be used as an off-line learning tool to test new triage protocols, which are not always as effective as might be desired, and other hard-to-anticipate factors must be considered.

6.2 Modelling the patient arrival pattern with the Gompertz model

In this section, we discuss the adequacy of PG models for case prediction purposes. First, we perform a statistical comparison of four different models for their suitability. We then describe the use of the Gompertz PG model to simulate daily hospitalization series.

6.2.1 Population growth models

The simulation model needs to generate the daily patient arrivals to the hospital(s), which is a non-stationary process highly dependent on the number of positive (active) cases in the population. A compartmentalized epidemiological model, such as the SEIR model, enables analysis of the spread of the disease throughout a population. It models transition dynamics between four different states of a population: susceptible (S), exposed (E), infective (I), and recovered (R). The model depends on epidemiological parameters such as the infection rate (the number of people that an infective person infects per day), the disease latent time (the lag between contact with an infected person and the appearance of symptoms), the recovery rate, and the death rate. The basic SEIR model has been extended to categories such as the protected (P) and the quarantined people (Q) (Godio et al. 2020) and other case detection and symptom statuses, up to a total of eight or more compartments (Giordano et al. 2020). Stochastic transmission models have also been considered (Kucharski et al. 2020). All these extensions add details to the model but also more complexity, which does not necessarily mean greater forecasting reliability, since it increases the number of model parameters to be estimated (Roda et al. 2020). Roda et al. (2020) demonstrate a linkage between the transmission rate and the case-infection ratio, resulting in a continuum of best-fit parameter values. These can produce significantly different predictions for the epidemic: the hallmark of a non-identifiability problem. These difficulties motivated us to consider parametrically parsimonious models, such

as the PG type, which are able to generate curves of the shapes generally associated with pandemic variables (positive (active) cases, hospitalizations, deaths): monotonic, humped, and S-shaped. Rypdal and Rypdal (2020) found that PG models are obtained from the SIR model by making reasonable assumptions about the SIR parameter trends over time.

Examples of growth models found in the literature include the Gompertz (Gompertz 1825), the Richards (Richards 1959), the Stannard (Stannard et al. 1985), and the Logistic model (Ricker 1979). They all start with exponential growth but each has a specific, gradually decreasing growth rate. All produce S-shaped curves describing the evolution of pandemic variables departing from one or a few initial cases, growing initially at an exponential rate before reaching a plateau, and then decreasing to zero when the pandemic expires. The equations describing the number of cases in population y , at time x , take the following form:

$$\text{Gompertz:} \quad y(x) = a \cdot \exp[-\exp(b - cx)] \quad (6.1)$$

$$\text{Logistic:} \quad y(x) = \frac{a}{[1 + \exp(b - cx)]} \quad (6.2)$$

$$\text{Richards:} \quad y(x) = a\{1 + v \cdot \exp[k(\tau - x)]\}^{(-1/v)} \quad (6.3)$$

$$\text{Stannard:} \quad y(x) = a \left\{ 1 + \exp \left[-\frac{(l + kx)}{p} \right] \right\}^{(-p)} \quad (6.4)$$

We carried out two statistical analyses to elucidate the adequacy of PG models for representing and predicting the evolution of the pandemic caused by the SARS-CoV-2 virus. The first analysis evaluates the capacity of the four PG models to fit complete sets of real positive case data registered in the 20 most-affected countries during the first wave of the pandemic (as recorded in [Worldometer](#) on June 15, 2020). The results included in Appendix G.1 show that, measuring the fit quality by the Mean Absolute Errors (MAE), the Gompertz, Richards, and Stannard models have similar goodness of fit; and with all three outperforming the Logistic model. These results are consistent with Rypdal and Rypdal (2020) who found that the COVID-19 related death rate curves of most countries are well described by the Gompertz growth model. The cumulative positive case, hospitalization and death curves have similar shapes because they are all scaled by the factor s , and translated by the factor t .

$$y_h(x) = s_h y_l(x - t_h) \quad (6.5)$$

$$y_d(x) = s_d y_l(x - t_d) \quad (6.6)$$

where y_l , y_h , y_d are the cumulative series of positive cases, hospitalizations and deaths, respectively; s_h , s_d are the scaling factors for hospitalizations and deaths, respectively, and t_h , t_d are the time lags between infection and hospitalization, and infection and death, respectively.

The second statistical analysis is designed to test the short-medium term predictive capacity of the PG models. For each of the 20 countries used in the first statistical analysis, the data up to the day on which cases exceed 25%, 40%, and 65% of the total cases registered at the end of the pandemic wave are used to predict the cases for the following successive 5, 10 and 15 day horizons. Thus, nine prediction exercises are performed for each country and each PG model. The prediction of the fitted curves for the next 5, 10, and 15 days is assessed by calculating the MAE. The results included in Appendix G.2 show that the Gompertz model surpasses the predictive capacity of the other PG models, outperforming them in all nine cases, and being equalled by the Richards and Stannard models in only four.

Our statistical analysis supports the use of the Gompertz for modelling series of cumulative hospitalizations. The parameters of the original equation of this model, presented above, are more suited to mathematical than biological interpretation, like most equations describing sigmoidal growth curves. Therefore, before using it in our modelling, some transformation will aid interpretation of the curve. Zwietering et al. (1990) rewrite the Gompertz growth model as shown in equation (6.7).

$$G(t) = A \exp\left(-\exp\left(\frac{Ke}{A}(D-t) + 1\right)\right) \quad (6.7)$$

where,

- $e = \exp(1)$
- $G(t)$ is the cumulative number of hospitalizations up to time t .
- A is a growth model parameter corresponding to the total number of hospitalizations at the end of the outbreak. It is the upper asymptote of the curve.
- K is the absolute growth rate of the curve at its inflection point.
- D , known as the lag time, is the time at which $G(t) = A \exp(-e)$, which means that it always occurs at the same percentage (6.6%) of the upper asymptote. This value is less intuitive than either of the others.

Suppose we are at pandemic day $n + 1$ and have recorded and denoted by $h(t)$, $t = -n, \dots, -1$ the number of hospitalizations at day t and by $H(t)$ the cumulative number of hospitalizations $H(t) = \sum_{i=-n}^t h(i)$, $t = -n, \dots, -1$. Using these data, the Gompertz growth model parameters $p = (A, K, D)$ are estimated by minimizing the sum of the squared errors (SSE). The estimated parameter vector is denoted by $\hat{p} = (\hat{A}, \hat{K}, \hat{D})$ and the Gompertz model by $G_{\hat{p}}(t)$. The values of $G_{\hat{p}}(t)$ are used to predict the expected number of hospitalizations for the current and following days, $t = 1, \dots, T$, as required by the simulation methodology described in the following subsection.

6.2.2 Simulation of the patient arrival pattern

Once the curve $G_{\hat{p}}(t)$ is fitted to the hospitalization data $H(t)$, $t = -n, \dots, -1$ of a certain region up to the present day, it is used to predict and simulate the number of new hospitalizations for each of the following days $t = 1 \dots, T$. The function argument t is continuous and we will assume that $t = 0$ represents both the end of the last day of recorded hospitalizations and the start of the current day. Therefore, $t = 1$ is the time at which the current day ends.

The simulation procedure is summarized in the following four steps:

1. **Fit the Gompertz curve** to cumulative hospitalization data series (e.g. by using the least squares method). Record the estimated parameter vector $\hat{\mathbf{p}} = (\hat{A}, \hat{K}, \hat{D})$ and its covariance matrix $\Sigma_{\hat{\mathbf{p}}}$.
2. **Simulate a parameter vector** $\mathbf{p} = (A, K, D)$ from the Multivariate Normal distribution $N(\hat{\mathbf{p}}, \Sigma_{\hat{\mathbf{p}}})$.
3. **Calculate the expected number of arrivals** $N(t)$ for day t , $t = 1, \dots, T$, where $t = 1$ represents the current day (start of the simulation) and T is the simulation horizon. Use the Gompertz curve $G_p(t)$ with parameters \mathbf{p} to calculate $E(N(t)) = G_p(t) - G_p(t - 1)$.
4. **Simulate the number of hospitalizations**, for each day t , $t = 1, \dots, T$, in the future, as observations from a Poisson distribution with mean $\lambda(t) = E(N(t))$:

$$P(N(t) = k) = \frac{e^{-(\lambda(t))}(\lambda(t))^k}{k!} \quad t = 1, \dots, T \quad (6.8)$$

5. **Repeat steps 2-4** as many times as necessary for the different hospitalization sequences to be simulated.

This simulation procedure takes into account both variability due to uncertainty in the estimation of the Gompertz parameters and variability in hospital arrival numbers around the mean. Figure 6.1 illustrates the four steps. The upper-left hand corner of the graph shows the Gompertz model (green curve) fitted to the available data (black dots); the point estimator $\hat{\mathbf{p}}$ and the covariance matrix $\Sigma_{\hat{\mathbf{p}}}$ are used in the second step to sample a parameter vector \mathbf{p} . The upper-right hand corner of the graph shows the Gompertz curves associated with parameter vectors \mathbf{p} in a tolerance region obtained from the multivariate normal distribution (Dong and Mathew 2015), using equation (6.9).

$$R = \{\mathbf{p} \mid (\mathbf{p} - \hat{\mathbf{p}})' \Sigma_{\hat{\mathbf{p}}}^{-1} (\mathbf{p} - \hat{\mathbf{p}}) \leq \chi_3^2(q)\} \quad (6.9)$$

where $\chi_3^2(q)$ denotes the q th percentile of a chi-square distribution with $df = 3$. Clearly, R is the central $100q\%$ region of the multivariate normal distribution $N(\hat{\mathbf{p}}, \Sigma_{\hat{\mathbf{p}}})$.

Each parameter vector \mathbf{p} in the region R is associated with a Gompertz curve $G_p(t)$ (shown in the lower left hand corner of Figure 6.1) compatible with the observed data (and different from $G_{\hat{\mathbf{p}}}(t)$). This Gompertz curve $G_p(t)$ provides the expected number of hospitalizations among simulated arrivals generated by sampling from a Poisson distribution. A sequence of trajectories with the simulated number of hospitalizations for future days $t = 1, \dots, T$ (shown in the lower right hand corner of Figure 6.1) is obtained by replicating the sampling of a vector \mathbf{p} , the calculation of the expected number of future arrivals $\lambda(t)$, $t = 1, \dots, T$, from the Gompertz curve $G_p(t)$, and the simulation of simulated arrivals $N(t)$, $t = 1, \dots, T$, from the Poisson distribution. The Gompertz curve is refitted after every new observation and the simulation of future arrivals is carried out again following steps 1 to 5.

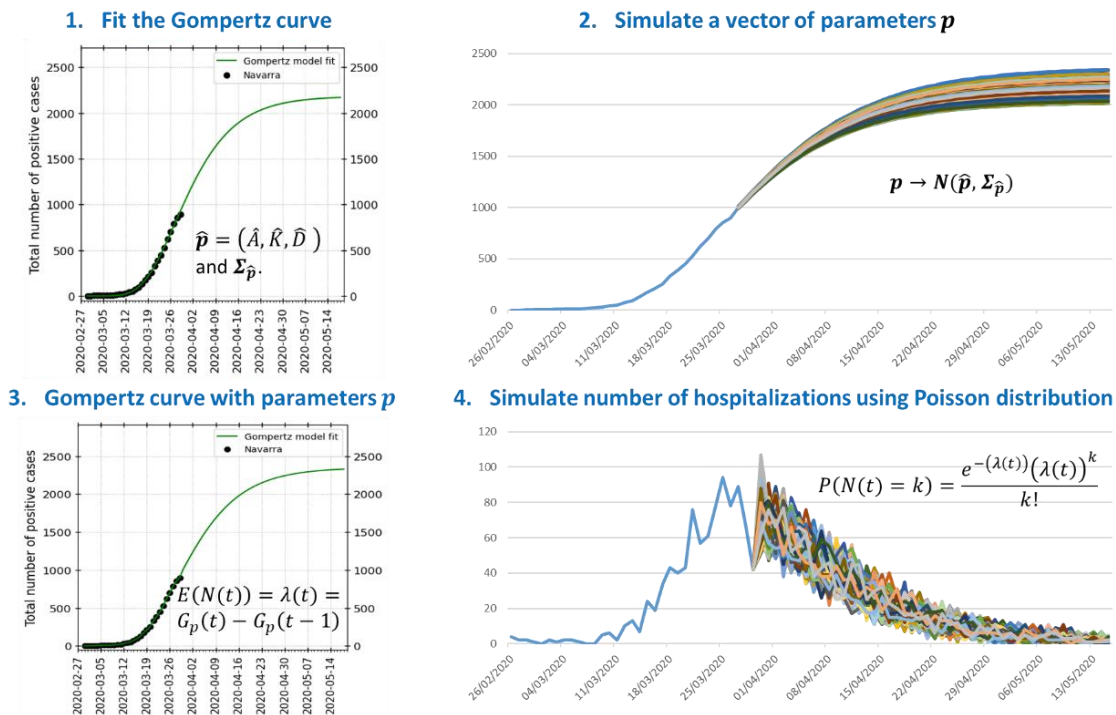


Figure 6.1. The simulation procedure for the patient arrival pattern. Steps 2-4 are replicated as often as necessary for the different patient arrival and hospitalization sequences to be simulated.

6.2.3 New parametrization of the Gompertz growth model

In this subsection, we introduce a new parameterization easier to interpret and to use for creating pandemic scenarios over which running hospital offline simulation models. The new parameterization depends on three parameters that reflect the size, the temporal spread, and the temporal location of the pandemic.

The original equation of the Gompertz model, proposed in (Gompertz 1825), was rewritten in (Zwietering et al. 1990) to ease the biological interpretation of its parameter, see equation (6.7) shown in the Section 6.2.2. In the context of a pandemic mathematical modelling, parameter A has a clear meaning: the total number of infected persons or the total number of hospitalized patients at the end of the pandemic wave, when the Gompertz curve is used to model the series of new positive cases or the hospitalization process, respectively. However, the parameter K has no intuitive meaning, and health managers may have difficulties in assigning a value to it in order to create an “artificial” pandemic. To overcome this difficulty we propose to replace the parameter K by other parameter linked with the duration of the pandemic wave. The new parameterization is obtained from equation (6.7) by calculating the percentile t_p ($G(t_p) = pA$) as $t_p = G^{-1}(pA)$:

$$t_p = D - \frac{A}{Ke} [\ln(-\ln(p)) - 1] \quad (6.10)$$

Let us denote by T_{p_1, p_2} the elapsed time between percentiles t_{p_1} and t_{p_2} .

$$T_{p_1, p_2} = t_{p_2} - t_{p_1} = \frac{[-\ln(-\ln(p_2)) + \ln(-\ln(p_1))] A}{e} = \frac{C_{p_1, p_2} A}{e} \frac{1}{K} \quad (6.11)$$

Where, C_{p_1, p_2} is a constant that depends on proportions p_1 and p_2 . Then, the parameter K is equal to $K = C_{p_1, p_2} A / (e T_{p_1, p_2})$, and substituting in equation (6.7), we obtain:

$$G(t) = A \exp \left(-\exp \left(\frac{C_{p_1, p_2}}{T_{p_1, p_2}} (D - t) + 1 \right) \right) \quad (6.12)$$

To simplify this expression, we consider the length of the interval time associated to the central proportion α of cases, that is, proportions p_1 and p_2 are defined as $p_1 = \alpha/2$ and $p_2 = 1 - \alpha/2$ to get the constant $C_{p_1, p_2} = C_\alpha$ and the parameter $T_{p_1, p_2} = T_\alpha$. With $\alpha = 0.1$, we obtain $C_\alpha \cong 4.0674$ and the Gompertz curve is:

$$G(t) = A \exp \left(-\exp \left(\frac{4.0674}{T_{0.1}} (D - t) + 1 \right) \right) \quad (6.13)$$

This new parameterization determines the Gompertz curve by setting the total number of cumulative cases at the end of the outbreak, the duration of the wave, and the time at which 6.6% of the total cases are reached. Therefore, giving values to parameters A , $T_{0.1}$, and D , from equation (6.13), custom curves can be obtained in order to recreate an outbreak. Figure 6.2 shows nine different scenarios generated from the combination of the three parameters. In each row of graphs, two of the three parameters are held constant. Parameter A is modified in the first row, $T_{0.1}$ in the second one, and D in the third one. Note that the parameter D affects only the displacement of the curve on the t -axis. Therefore, only two parameters need to be manipulated to modify the shape.

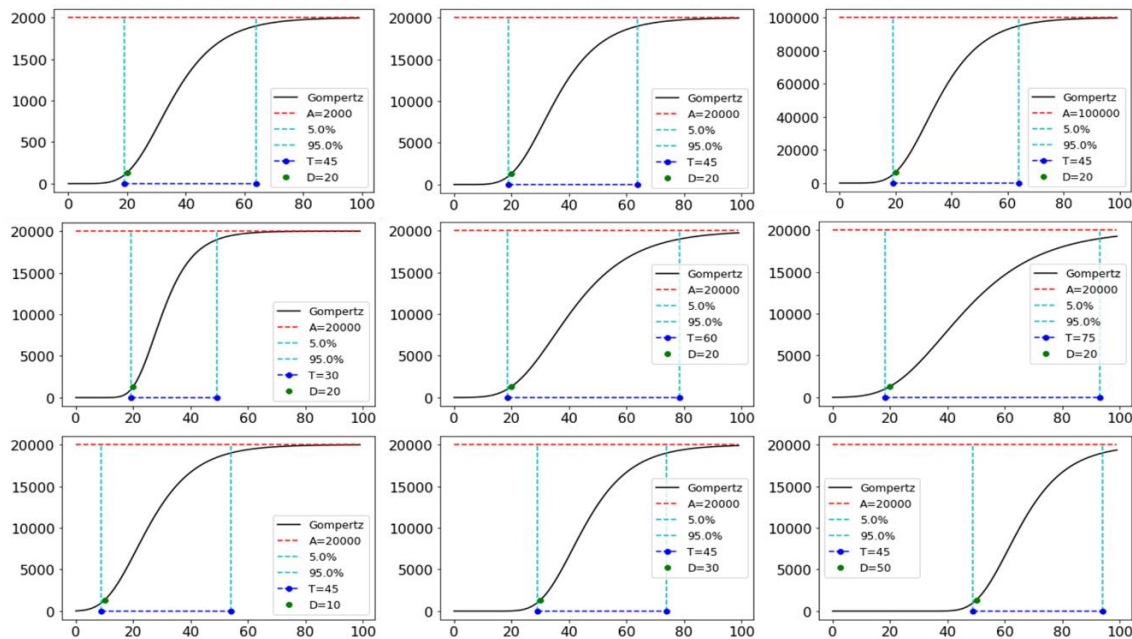


Figure 6.2. Nine Gompertz curves generated by fixing the three parameters of Equation (6.13). In the first row of the graphs, the parameter A is varied ($A = 2000, 20000,$ and 100000). As A increases, the horizontal upper asymptote of the curve increases. In the second row, the value of $T_{0,1}$, which controls the duration of the wave, is modified ($T_{0,1} = 30, 60,$ and 75). Finally, in the third row, the parameter D is modified ($A = 10, 30,$ and 50), which allows to move the Gompertz curve on the x -axis.

6.3 Modelling the patient flow

This subsection focuses on modelling patient flow through the health system. First, we describe the possible patient pathways through the hospital, and then explain how the LoS of each patient is modelled.

6.3.1 Hospital patient pathway

COVID-19 patients can access the health system in a variety of ways: following diagnosis with COVID-19 in a primary healthcare facility, hospital emergency department, or nursing home; or after undergoing a SARS-CoV-2 test control (such as a *Polymerase chain reaction (PCR)* test), etc. Depending on the severity of his/her condition, the person is admitted to the health care system as a COVID-19 patient, either in a hospital ward or directly in the ICU.

The COVID-19 patient pathway through the hospital is the same as for other hospital patients, but, due to the highly contagious nature of the virus, COVID-19 patients require dedicated resources and cannot be mixed with other patients. Figure 6.3 shows the patient flow through the health system, highlighting the transitions between the hospital ward and the ICU (the variables and the probabilities that appear are defined in Section 6.3.2). Patients can be

admitted either to the ICU or first to a hospital ward with potential transfer to the ICU if their condition deteriorates. Discharge from a ward can follow either death or a health improvement. Patient transfers from the ICU to a hospital ward occur after a health improvement.

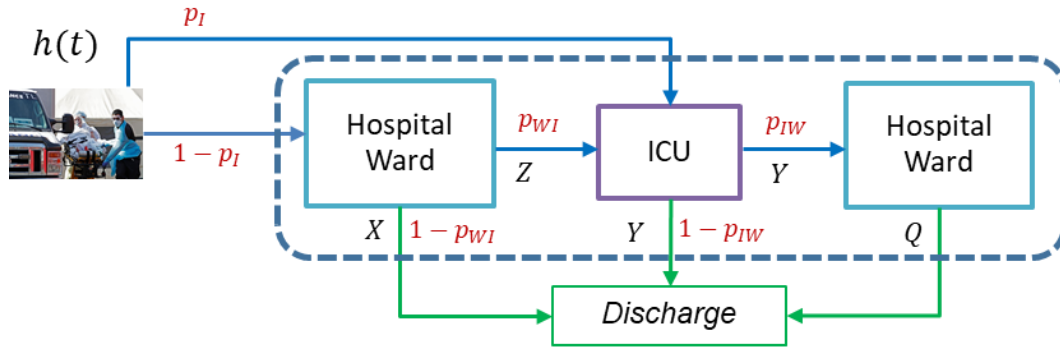


Figure 6.3. Representation of COVID-19 patient flow in the health system.

6.3.2 Stochastic modelling of hospital LoS

The following variables are used to model LoS in the hospital:

- X , the LoS in the hospital ward of a patient not needing ICU.
- Y , the LoS of a patient in the ICU.
- Z , time spent by a patient in the hospital ward before transfer to the ICU (applies only to patients transferred to the ICU from the hospital ward).
- Q , the LoS of a patient in the hospital ward after being discharged from the ICU.

The following probabilities determine the patient-pathway through the healthcare facilities:

- p_I , the probability of direct admission to ICU upon arrival.
- p_{WI} , the probability of a patient initially admitted to a ward requiring transfer to ICU.
- p_{IW} , the probability of patient transfer from ICU to a ward. Then, $1 - p_{IW}$ is the probability of death in the ICU.

Then, the probability of ICU requirement is $p_I + (1 - p_I)p_{WI}$.

As the pandemic progresses and more COVID-19 patients need hospitalization, the new data collected from these patients can be used to update the probability distribution parameters estimates and patient pathway probabilities. Given that only a small percentage of ward admissions and an even smaller percentage of ICU admissions have been discharged after a few weeks from the start of the outbreak, the associated information on most of them is partly unknown, that is, they constitute censored data. For example, a patient admitted to the ICU 10 days ago provides an ICU LoS datum y such that $y > 10$.

This motivates us to perform daily updates of the distribution parameters and probabilities by adding the fresh data, thereby enlarging the sample size, reducing the degree of censorship bias and ultimately obtaining more accurate parameter estimates. The parameter estimation is done by the maximum likelihood method. For example, for the estimation of θ_Y , the parameter vector of the distribution function of variable Y is performed by maximizing the following likelihood function:

$$L_Y(\theta_Y | y(t)) = \prod_{i=1}^{n_Y} f_{\theta_Y}(y_i) \prod_{i=1}^{n_{Y^*}} (1 - F_{\theta_Y}(y_i^*)) \rightarrow \theta_Y = \arg \max_{\theta_Y} L_Y(\theta_Y | y(t)) \quad (6.14)$$

where,

- $\{y_i, i = 1, \dots, n_Y\}$ is the set of exact value observations, that is, those corresponding to the LoS of patients now discharged from the ICU, and $f_{\theta_Y}(y_i)$ is the density function.
- $\{y_i^*, i = 1, \dots, n_{Y^*}\}$ is the set of censored values, that is, those corresponding to the LoS of patients remaining in the ICU at the time of the statistical analysis, and $F_{\theta_Y}(y_i)$ is the cumulative distribution function.

The use of probability plots and statistics as Anderson-Darling facilitates identification of the parametric probability distribution family that best fits the data. The parameters of the selected probability distribution family are estimated by the maximum likelihood method. Weibull and Lognormal distribution families have proved to be good probability models for LoS variables, as will be shown in Chapter 7.

At the beginning of a new pandemic, there is insufficient understanding of the disease and possibly no known effective treatment, as was the case with the COVID-19 outbreak. As medical and biological research progresses, the discovery of new drugs and therapeutic protocols improves patient care and alters lengths of stay in hospital wards or ICUs. This observation reinforces the need to gather every possible new piece of patient admission and discharge data for use in updating estimated distribution parameters and branching probabilities.

6.4 The discrete event simulation model

In this section, we present the mathematical modelling of hospital dynamics using a DES model. We pay attention to starting the simulation from the current state of the health system, which is one of the distinguishing features of this application of healthcare system simulation modelling.

6.4.1 Entities, state variables, and events

DES models create moving entities that are transformed by several processes until they exit the modelling system. In the health care system that concerns us, the entities are the COVID-19 patients and the processes are the health care received in the hospital ward and/or ICU. The system is described by a set of state variables, which provide at any time a complete representation of the simulated system, and the set of events, which modify the value of the state variables. The simulation model represents patient flow through the different hospitalization routes; that is, the area enclosed by dashed lines in Figure 6.3. In this subsection, we present two types of healthcare system state variables and the set of events separated into two categories.

We consider two distinct types of state variables: global and patient-level. The two global variables, $B(t) = (B_W(t), B_I(t))$, describe bed occupancy by COVID-19 patients in hospital wards and the ICU, respectively, at any time t . Total COVID-19 hospitalizations at time t , $N(t)$, is given by the sum of these two state variables, $N(t) = B_W(t) + B_I(t)$.

Each patient i admitted to hospital has two associated state variables. The patient-level state variable $S_i(t)$, which records the condition of patient i at time t , can take one of three values: W_1 , when patient i is admitted to a ward without a previous stay in ICU; I , when patient i is admitted to ICU; and W_2 , when patient i is in a ward after transferral from ICU. The patient-level state variable $R_i(t)$ records the time at which patient i enters state $S_i(t)$.

Two different types of events can affect the values of the state variables. They have been classified by the nature of the variation in $B(t)$: an increase or decrease in $N(t)$, or a variation in $B_W(t)$ and $B_I(t)$ not affecting their sum. The first set of events E_A are associated with patient arrival times. This group includes only external arrivals, i.e., positive cases detected outside the hospital that require hospitalization. These events are generated by the simulation methodology described in Section 6.2.2, and each arrival is classified as an ICU arrival or a ward arrival with probabilities p_I and $1 - p_I$, respectively. The last type of patients are also subdivided into two groups, those who will require ICU admission after some time on the ward (with probability p_{WI}) and those who will not (with probability $1 - p_{WI}$).

The second category includes the events E_B leading to a patient's end of a stay in the ICU or the ward, and altering the value of their patient-level state variables, and also either $B_W(t)$, or $B_I(t)$ or both. As stated in Section 6.3, there are several events of this type:

- E_{BZ} events dictating end of ward stay prior transfer to ICU, which are generated by sampling from the variable Z . The variable $B_W(t)$ decreases by one unit and $B_I(t)$ increases by one.
- E_{BX} events signalling end of ward stays with no need for ICU transfer, which are generated by sampling from the variable X . The variable $B_W(t)$ decreases by one unit.

- E_{BQ} events associated with end of ward stay for a patient transferred from ICU, and generated by sampling from the variable Q . The variable $B_W(t)$ decreases by one unit.
- E_{BY} events associated with end of ICU stay and generated by sampling from the variable Y . The variable $B_I(t)$ decreases by one unit. The patient is transferred to a ward with probability p_{IW} , and $B_W(t)$ increases by one unit.

The event calendar vector at time t has $B_W(t) + B_I(t) + 1$ positions. One includes the time of the next patient arrival (associated with event E_A), $B_W(t)$ positions, one for each ward patient, containing their hospital discharge times (associated with events E_{BX} or E_{BQ}) or ICU transfer times (associated with event E_{BZ}), and $B_I(t)$ positions, one for each ICU patient, storing the discharge time from ICU.

Figure 6.4 outlines the DES model of the health system.

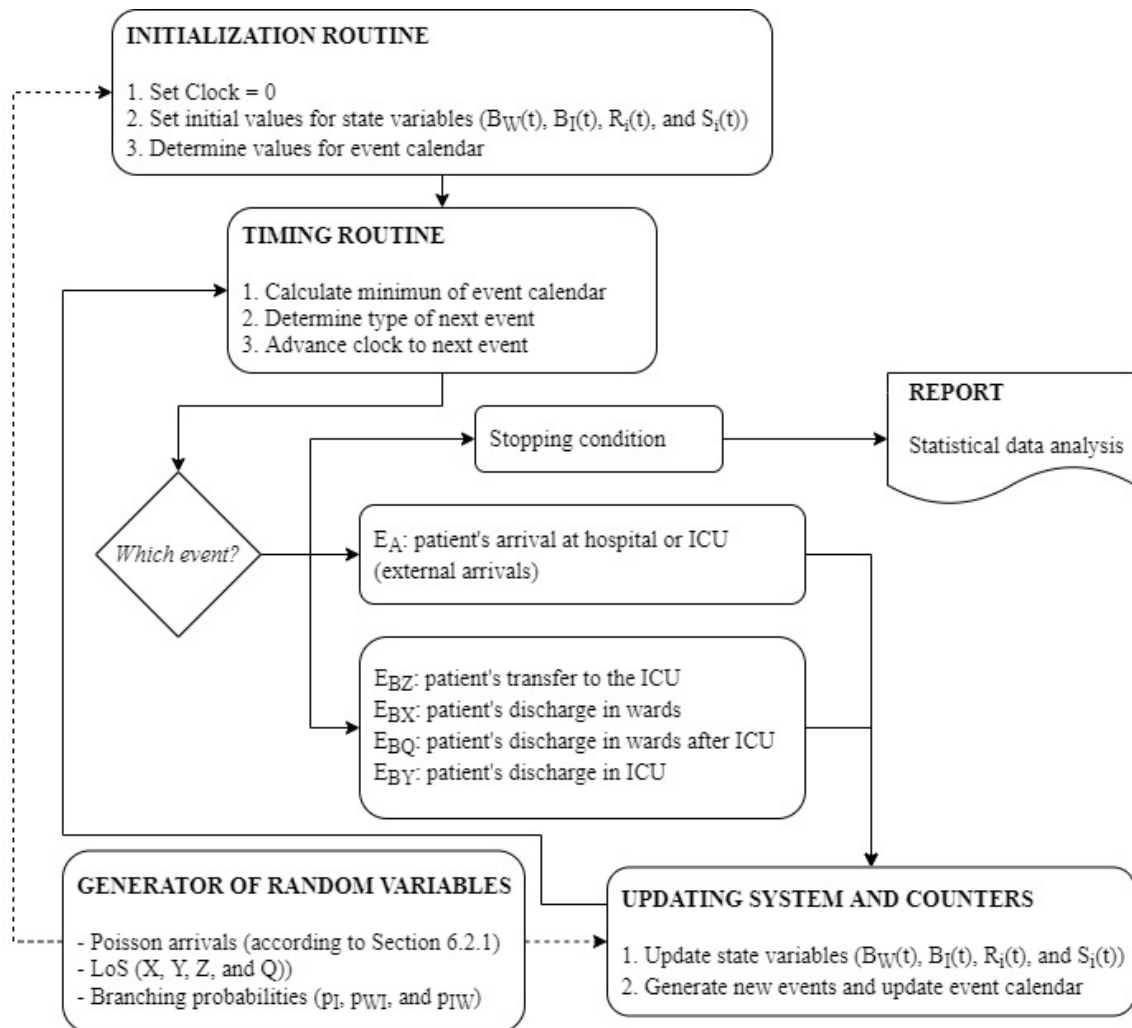


Figure 6.4. Flow diagram of the health system simulation model. Two types of events are considered, external arrivals and ward or ICU end of stays.

6.4.2 Starting the simulation run

The purpose of the simulation model is to predict short-term resource needs, with precision strongly depending on the model's accuracy both in representing the initial state of the healthcare system and the initial resource utilization rate. This last aspect of mathematical modelling is usually not very important when the aim of the simulation is to investigate the long-term behaviour of a system in its stationary state, which is usually independent of its initial state. However, when the simulation is used as a predictive tactical decision-making support tool, the initial state of the simulation model and the initial dynamics of the system are the main determining factors of the state of the healthcare system in the near future.

The simulation clock is set to zero at the time of the last update of the Electronic Health Record (EHR)-file, which we assume to have taken place at the end of the k th day of the pandemic. The simulation model begins to simulate future changes from day $(k + 1)$ th, using the information collected during the first k days of the pandemic, taking hospitalizations at the end of the k th day as the initial state. The point of transition from the past to the future occurs at the beginning of the simulation run, for which the event calendar must be initialized (Law 2014). The simulation of event type E_A , a new patient arrival, was explained in Section 6.2.2. We will now explain how to simulate type E_B events for patients currently admitted, that is, at time zero in the simulation model. The value of the state variables, number of ward patients, $B_W(0)$, and number of ICU patients, $B_I(0)$, as well as times $R_i(0)$ in the current state $S_i(0)$ for each patient i , can be calculated from the EHR-file, which records admission, discharge, and ward/ICU transfer dates for each patient. This set of state variables defines the initial state of the healthcare system simulation model.

The discharge time of each ICU patient i is calculated by sampling from the random variable Y conditioned to a stay longer than $r_i = (k + 1 - R_i(0))$, the number of days already spent in the ICU. Let y_i be a value sampled from the conditional distribution $Y|Y > r_i$, then the value $y_i - r_i$ is the simulated ICU discharge date for patient i , which is assigned to the position E_{BI} of the event calendar vector associated with patient i .

A patient admitted to a ward for r_i days can ultimately be discharged from the hospital or transferred to ICU. The probability of ICU transfer for a patient hospitalized for r_i days, denoted by $p_{ICU|r_i}$, is calculated with Bayes theorem:

$$\begin{aligned}
 p_{ICU|r_i} &= P(B|r_i \text{ days in ward}) = \frac{P(Z > r_i|B) P(B)}{P(r_i \text{ days in ward})} \\
 &= \frac{P(Z > r_i|B) P(B)}{P(Z > r_i|B) P(B) + P(X > r_i|C) P(C)} \\
 &= \frac{(1 - F_{\theta_Z}(r_i)) p_{WI}}{(1 - F_{\theta_Z}(r_i)) p_{WI} + (1 - F_{\theta_X}(r_i)) (1 - p_{WI})}
 \end{aligned} \tag{6.15}$$

where,

- B is the event of a ward patient requiring ICU transfer.
- C is the event of a ward patient not requiring ICU transfer.
- $F_{\theta_Z}(r_i)$ is the cumulative distribution function of variable Z .
- $F_{\theta_X}(r_i)$ is the cumulative distribution function of variable X .

A hospital trajectory is simulated for each patient i already admitted to a hospital ward. The first step of the simulation concerns the decision as to whether the patient will be admitted to the ICU (with probability p_{ICU/r_i}) or not (with probability $1 - p_{ICU/r_i}$). Time to ICU transfer is then simulated by sampling from the conditional distribution $Z|Z > r_i$, and assigning the value $z_i - r_i$ to the event E_{BZ} . If the patient i does not require ICU care, the hospital discharge event E_{BX} will occur at time $x_i - r_i$, where x_i is sampled from the conditional distribution $X|X > r_i$.

Similarly, for each ward patient i previously discharged from the ICU, the time of discharge from the hospital is simulated by sampling a value q_i from the conditional variable $Q|Q > r_i$. The value $q_i - r_i$ is the simulated discharge time and is assigned to position E_{BQ} of the event calendar vector associated with patient i .

Once discharge times and transfer times between ward and ICU have been simulated for each hospitalized patient, and recorded in the event calendar (together with the arrival time of the next COVID-19 patient) the DES model is ready to advance the simulation clock from time zero to the minimum of the times recorded in the event calendar. The state variables and calendar events are then updated accordingly and the main loop of Figure 6.4 is repeated until the simulation run is complete.

The fitted Gompertz curve forecasts daily patient arrivals, which can be uniformly distributed over the following 24 hours or according to a non-stationary pattern when, for example, arrivals drop significantly overnight.

6.4.3 Simulation output

The DES model works by generating patient arrivals, discharges, and transfers causing variations in ward and ICU occupancy levels, which are recorded by statistical counters. The simulation model includes two sources of randomness: the number of patient arrivals (hospital and ICU), and patients' LoS. Therefore, each time the DES model is run departing from the current situation of the healthcare system (generating randomness based on a different seed) the ward and ICU bed requirements differ. Figure 6.4 in Section 6.4.1 shows one iteration of the simulation, with which different trajectories can be obtained with each replication of that routine. Thus, the simulation model is run many times (thousands) to get a statistical distribution of the number of ward and ICU beds needed each day.

The DES simulator generates percentile data, which are stored in an Excel file. The 5th percentile (P5), 50th percentile (P50), and 95th percentile (P95) are plotted on a graph as confidence bands for future resource needs. Figure 6.5 shows an example of these graphic outputs. The green line represents the real occupancy trend and the black dot indicates the Simulation Starting Point (SSP), that is, the moment from which the hospital system dynamics are simulated. The left-hand side shows four different possible ICU bed demand trajectories (T1, T2, T3, and T4), while the right-hand side shows the confidence bands.

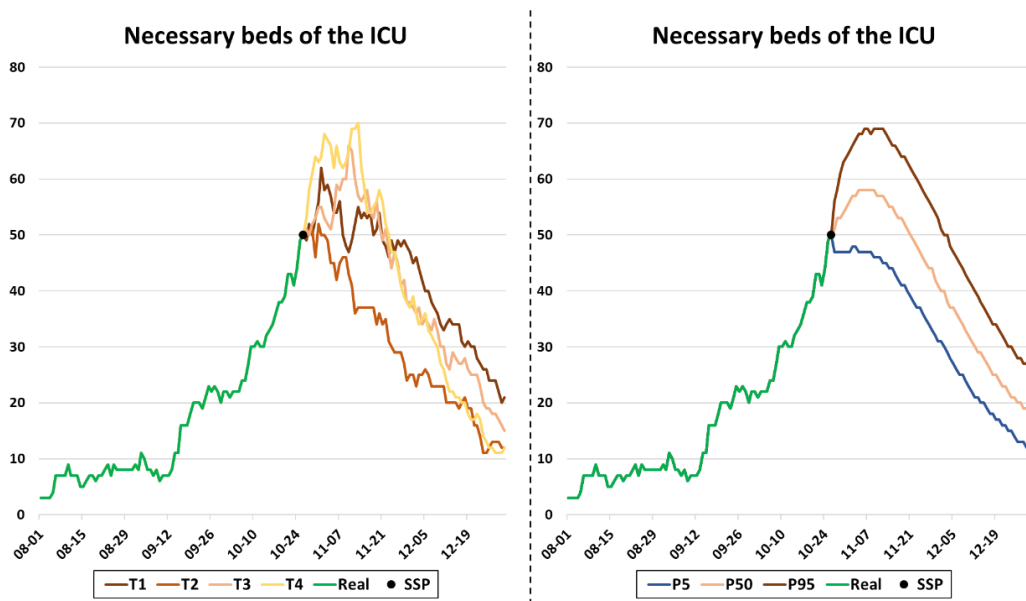


Figure 6.5. Simulation output for ICU bed demand for the following days. The left-hand side shows four different trajectories starting from the SSP; the 3 lines on the right-hand side correspond to the 5th, 50th, and 95th percentiles.

ICU and hospital wards saturation risk

During the pandemic, it is critical for physicians to have enough beds available to treat all COVID-19 patients arriving at the hospital system, both in the hospital wards and in the ICU. A very important aspect for managers when coping with resource-scarce situations is the measure related to saturation of these. With the results obtained in the simulation, it is possible to determine a measure of the risk of ICU and hospital wards saturation over the following days of the pandemic.

Let us denote $r_b(t)$ as the risk of system saturation at time t when b beds are considered available for COVID-19 patients. This risk, which can be particularized for both hospital ward and ICU beds, is obtained for each day t as the percentage of times the number of beds observed on that day in the simulation replications exceeds the number of available beds b considered. Equation (6.16) show the expression to calculate the ICU and hospital wards saturation risk $r_b(t)$.

$$r_b(t) = \frac{\sum_{i=1}^{N_R} 1_{\{\beta_i(t) > b\}}}{N_R} \times 100 \tag{6.16}$$

where,

- N_R is the number of simulation replications.
- $\beta_i(t)$ is the number of beds occupied with COVID-19 patients at time t of replication i .

This risk can be studied for different numbers of beds, and curves such as those shown in Figure 6.6 can be obtained. In this example, the blue line at the top of the graph corresponds to the risk associated with a number of beds $b = 200$. It can be seen that between October 15 and November 1, 2020, the risk of saturation is 100%, that is, in the simulations, in all replications, the number of beds occupied by COVID-19 patients observed has always been greater than 200 between these dates. With the green line, we can interpret that from October 8 onwards, having more than 220 beds occupied by COVID-19 patients presents a risk of more than 60%. The higher the number of beds associated with the risk, the lower the risk values. The shape of these risk curves is given by the shape of the bed occupancy curves in the simulations.

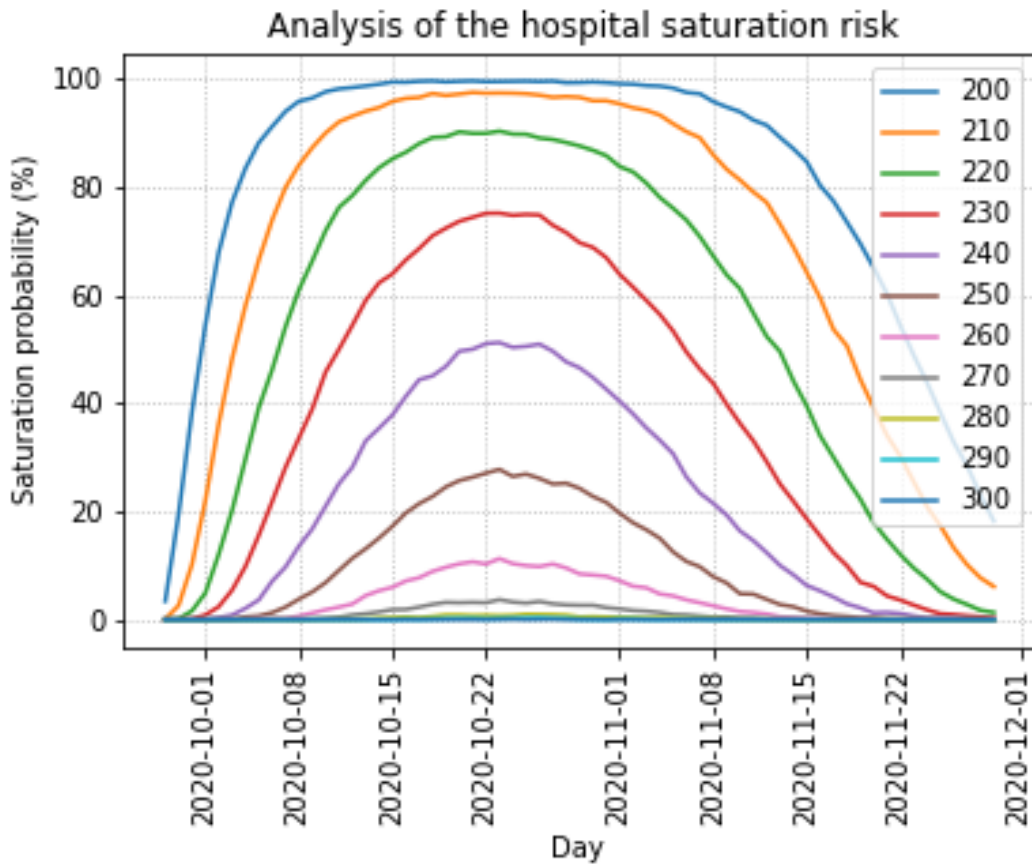


Figure 6.6. Saturation risk curves associated with hospital ward bed numbers between 200 and 300.

6.5 Estimation of parameters and probability distributions

In this section, we deal with the problem of getting reliable estimations of all the parameters that define the trajectory and LoS of patients in the hospital facilities. These parameters cannot be calibrated in advance by using historical data because each pandemic wave may have different characteristics, affecting different population groups with different intensity, and even change during the pandemic wave. However, during the first days, and even weeks, of the pandemic, few complete data are available since a significant proportion of patients are still admitted to the hospital. For this reason, it is essential to develop estimation methods that also take into account data coming from the patients of the current pandemic wave, even if this information is incomplete.

6.5.1 The online estimation problem

We consider the problem of estimating the parameters associated with the pathway and LoS of patients hospitalized during a pandemic. This is a non-stationary situation, in which hospitalization parameters may vary between different waves, between different places, and evolve during the pandemic. We propose to estimate them by using all data collected during the pandemic wave in which the simulation model is being applied, that is, from the time the first infected patient was admitted until the present time. However, the use of data associated with patients still hospitalized is a complex task, not only because of censorship but it is also unknown which event will be observed in the future and then from which variable is observed the value. Specifically, it is unknown whether a patient who has been hospitalized for some time will be finally admitted to the ICU or not, so it is unknown whether the observed value of the stay is a censored data for the variable Z , “time until admission to the ICU”, or for the variable X , “time to hospital discharge”.

In this section, we propose an estimation method for the probability distributions of these variables, as well as the probability of admission to the ICU from the ward, p_{WI} , that uses the information of all patients admitted currently at the hospital (Figure 6.7, left). The same estimation methodology can be applied, to the estimation of the probability distributions of Y , “LoS in the ICU before being transfer to hospital ward”, and D , “LoS in the ICU until death”, and p_{IW} , the probability of discharge to hospital ward (Figure 6.7, right).



Figure 6.7. Parameters and probability distributions for modelling Ward-to-ICU transition (left) and ICU-to-Ward transition (right).

6.5.2 Data and taxonomy of patients

Hospital EHR systems provide information at the patient level that allows knowing the pathway of all patients admitted at the hospital and their current location, ward or ICU, in the case they are still admitted. Pathway and current location result from the times at hospital admission and discharge (t_{HA} and t_{HD} , respectively) and the times of ICU admission and discharge (t_{IA} and t_{ID} , respectively).

Therefore, for each patient i admitted to the hospital until time t , we assume to know vector $u_i(t)$ that contains these four times ($u_i(t) = [t_{HA_i}, t_{HD_i}, t_{IA_i}, t_{ID_i}]$). At time t , not all four times have been observed or are exactly known for all patients. For example, for an already discharged patient i from the hospital ward that did not need care in the ICU, the two components of vector $u_i(t)$ related with the ICU are not observed and are left “empty” (we denote by the symbol \emptyset this situation): $u_i(t) = [t_{HA_i}, t_{HD_i}, \emptyset, \emptyset]$. For an admitted patient at the ICU at time t , it is known that both discharge times, from ICU and from hospital, will certainly happen but in a future time. This situation is denoted by $u_j(t) = [t_{HA_j}, t, t_{IA_i}, t]$, and then $t - t_{IA_i}$ is a censored time for the LoS of this patient in the ICU. In turn, a patient j with $u_j(t) = [t_{HA_j}, t, \emptyset, \emptyset]$ indicates that he or she is still admitted to the hospital, and his/her LoS is censored by the value $t - t_{HA_j}$ and that so far the patient has not required admission into the ICU but it is not known if the admission will happen or not.

According to the values observed for the vector $u_i(t)$, 10 different types of patient states can be distinguished at time t . In the taxonomy of the type of patient, we use the letter H to refer to the hospital ward and the letter I to the ICU. The sequence of letters corresponds to the trajectory in the hospital facilities. The asterisk symbol (*) indicates that the patient is still admitted into the facility indicated by the preceding letter, and therefore provides censored data.

- H : Patients with a full stay in the hospital ward who have not needed ICU ($[t_{HA}, t_{HD}, \emptyset, \emptyset]$).
- H^* : Patients with an incomplete stay in the hospital ward who have not needed ICU ($[t_{HA}, t, \emptyset, \emptyset]$). They do not have a discharge date and may or may not be admitted to the ICU.
- HI^* : Patients with an incomplete stay in the ICU transferred from the hospital ward ($[t_{HA}, t, t_{IA}, t], t_{HA} < t_{IA}$).
- HI : Patients died in the ICU after being transferred from the hospital ward ($[t_{HA}, t_{HD}, t_{IA}, t_{ID}], t_{HA} < t_{IA}, t_{HD} = t_{ID}$).
- HIH^* : Patients with a full stay in the ICU after being transferred from the hospital ward. They are still admitted to the hospital ward after leaving the ICU ($[t_{HA}, t, t_{IA}, t_{ID}], t_{HA} < t_{IA}$).

- *HIH*: Patients with a full stay in the ICU after being transferred from the hospital ward. They have been discharged from the hospital ward after leaving the ICU ($[t_{HA}, t_{HD}, t_{IA}, t_{ID}], t_{HA} < t_{IA}, t_{HD} > t_{ID}$).
- *I**: Patients admitted directly to the ICU with an incomplete stay ($[t_{HA}, t, t_{IA}, t], t_{HA} = t_{IA}$).
- *I*: Patients admitted directly to the ICU who die there ($[t_{HA}, t_{HD}, t_{IA}, t_{ID}], t_{HA} = t_{IA}, t_{HD} = t_{ID}$).
- *IH**: Patients admitted directly to the ICU with a full stay. They are still admitted to the hospital ward after leaving the ICU ($[t_{HA}, t, t_{IA}, t_{ID}], t_{HA} = t_{IA}$).
- *IH*: Patients admitted directly to the ICU with a full stay. They have been discharged from the hospital ward after leaving the ICU ($[t_{HA}, t_{HD}, t_{IA}, t_{ID}], t_{HA} = t_{IA}, t_{HD} > t_{ID}$).

The diagram shown in Figure 6.8 helps to better understand the different types of patients defined in the previous points.

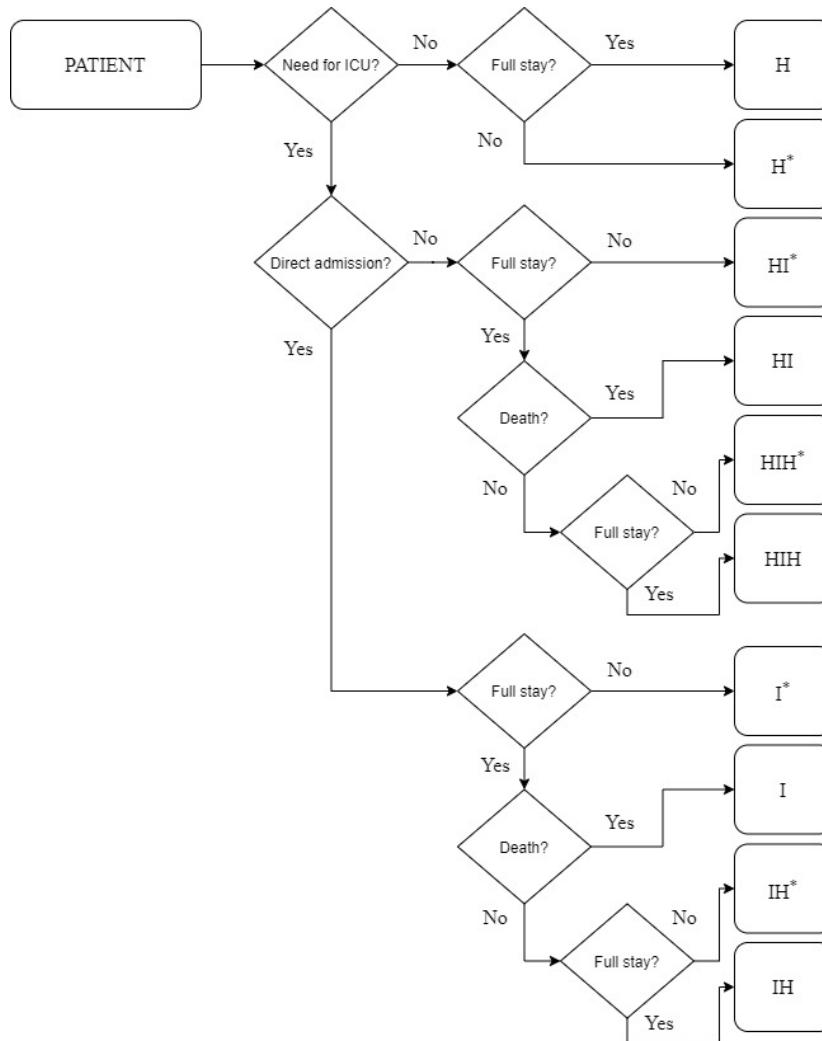


Figure 6.8. Diagram of the state of a patient at time t .

6.5.3 Maximum likelihood estimation at the end of the pandemic wave

First, we address the problem of estimating the parameters and probability distributions involved in the patient transition Ward-to-ICU when, for each patient admitted to the hospital, the values of the vector $u_i(t)$ are fully known. Therefore, the pandemic wave is over and all patients have been discharged from the hospital (classified in the types H , HI , HIH , I and IH).

For the rest of this section we denote:

- $n_G(t)$ as the number of patients of type G (generic) at time t . To simplify the notation, and when there is no confusion, we will use n_G instead of $n_G(t)$.
- $x(t) = (x_1(t), \dots, x_i(t), \dots, x_{n_X(t)}(t))$ the realization of the variable X , with $x_i(t) = t_{HD_i} - t_{HA_i}$.
- $z(t) = (z_1(t), \dots, z_i(t), \dots, z_{n_Z(t)}(t))$ the realization of the variable Z , with $z_i(t) = t_{IA_i} - t_{HA_i}$.
- θ_V as the vector of parameters of the distribution function of variable V .
- $\hat{\theta}_V$ as the estimation of the vector of parameters θ_V .
- $L_V(\theta_V|v(t))$: is the likelihood function of sample $v(t)$ used to estimate θ_V .

The estimation of the probability distribution parameters of the LoS variables X and Z is done by the maximum likelihood method.

$$L_X(\theta_X|x(t)) = \prod_{i=1}^{n_X} f_{\theta_X}(x_i) \rightarrow \hat{\theta}_X = \arg \max_{\theta_X} L_X(\theta_X|x(t)) \quad (6.17)$$

$$L_Z(\theta_Z|z(t)) = \prod_{i=1}^{n_Z} f_{\theta_Z}(z_i) \rightarrow \hat{\theta}_Z = \arg \max_{\theta_Z} L_Z(\theta_Z|z(t)) \quad (6.18)$$

Where $f_{\theta_X}(x_i)$ and $f_{\theta_Z}(z_i)$ are the density functions of variables X and Z , respectively, and $n_X(t) = n_H(t)$ and $n_Z(t) = n_{HI}(t) + n_{HIH}(t)$ are the sizes of the samples for variables X and Z .

The probability p_{WI} is estimated by the observed ratio of patients that are admitted to ICU from wards:

$$\hat{p}_{WI} = \frac{n_{HI} + n_{HIH}}{n_{HI} + n_{HI} + n_{HIH}} \quad (6.19)$$

6.5.4 The Expectation-Maximization algorithm for parameter estimation during the pandemic wave

In this subsection, we develop an algorithm to estimate the probability p_{WI} , and the parameters of the probability distributions of variables X and Z at any time t during the development of

the epidemic wave, making use of the information of all patients that have been admitted so far at the hospital. Let us consider the variable vector $W = (S, \delta)$ with S the time spent in hospital by a patient until discharge or until admission in the ICU and δ the indicator of whether the patient is admitted to the ICU or not.

$$\delta_i = \begin{cases} 1 & \text{if patient } i \text{ is admitted in the ICU} \\ 0 & \text{if patient } i \text{ is not admitted in the ICU} \end{cases} \quad (6.20)$$

Variable X , the time spent in hospital by a patient that is discharged from hospital with no admission in the ICU, verifies that $X \equiv S|\delta = 0$, and Z , the time spent in hospital by a patient before his/her admission in the ICU is $Z \equiv S|\delta = 1$. At the end of the pandemic the value of δ_i is observed for each patient i admitted to the hospital. However, at a time t , when the pandemic is not over, the value of δ_i is not known for patients already admitted at the hospital ward that have not been admitted in the ICU.

Specifically, for each patient i of type H ($t_{HD_i} < t$) or types HI, HIH, HI^*, HIH^* ($t_{IA_i} < t$) the value of the indicator variable δ_i has been observed, and the vector $w_i = (s_i, \delta_i)$ provides an observation for variable X in case $\delta_i = 0$ ($x_i = s_i$), or for Z in case $\delta_i = 1$ ($z_i = s_i$). However, for each patient i of type H^* (with $t_{HA_i} < t$, $t_{HD_i} > t$ and $t_{IA_i} > t$ or \emptyset) the variable δ_i has not been observed at time t , and then $t - t_{HA_i}$ is a censored time that is not known to which variable corresponds, X or Z .

Suppose that at time t of the pandemic there are $n(t)$ patients that have been admitted at a hospital ward. We denote as $w(t) = (w_1(t), \dots, w_i(t), \dots, w_{n(t)}(t))$ the realization of the variable W in these $n(t)$ patients. The vector $w(t)$ can be divided in two parts $w(t) = (w_F(t), w_I(t))$: $w_F(t)$, contains the observations of patients for which the value of δ_i has been observed, and $w_I(t)$ contains the observations of those patients with unknown value for δ_i . We have developed an iterative procedure, based on the EM algorithm, to estimate the distribution functions of variables X and Z and the probability p_{WI} . First, an initial estimation of the parameters is carried out by only using the fully-known data (those observations with known value for δ_i). In the main iteration, the estimated parameters are used to update the probability of being admitted to the ICU for each one of the patients admitted in the ward. These updated probabilities are used to calculate a new likelihood function for the parameters, which is maximized to obtain a new estimation of the probability distribution parameters. These two steps (updating ICU admission probabilities and getting and maximizing new likelihood function) are repeated until stopping criteria are met. We use the following additional notation:

- $\hat{\theta}_X^{(k)}$: is the estimation of vector θ_X in the k -th iteration of the algorithm.
- $\hat{\theta}_Z^{(k)}$: is the estimation of vector θ_Z in the k -th iteration of the algorithm.
- $\hat{F}_{\theta_X}^{(k)}(x) = F_{\theta_X}(x; \hat{\theta}_X^{(k)})$: is the distribution function of X with parameters $\hat{\theta}_X^{(k)}$.
- $\hat{F}_{\theta_Z}^{(k)}(x) = F_{\theta_Z}(x; \hat{\theta}_Z^{(k)})$: is the distribution function of Z with parameters $\hat{\theta}_Z^{(k)}$.

- $\hat{P}_{WI}^{(k)}$: is the estimation of the probability P_{WI} in the k -th iteration of the algorithm.
- $n_F(t)$: number of patients with full information at time t (the size of vector $w_F(t)$).
- $n_I(t)$: number of patients with incomplete information at time t (the size of vector $w_I(t)$).

To simplify the notation, and when there is no confusion, we will use n_F and n_I , instead of $n_F(t)$ and $n_I(t)$, respectively.

Steps of the algorithm

1. Initialization.

$k = 0$. Estimate the parameters θ_X , θ_Z and the probability P_{WI} by using the data in the vector $w_F(t)$:

$$\hat{P}_{WI}^{(0)} = \frac{1}{n_F} \sum_{i=1}^{n_F} 1_{\{\delta_i=1\}} \quad (6.21)$$

$$L_X^{(0)}(\theta_X|w_F(t)) = \prod_{i=1}^{n_F} f_{\theta_X}(s_i) (1 - \delta_i) \rightarrow \hat{\theta}_X^{(0)} = \arg \max_{\theta_X} L_X^{(0)}(\theta_X|w_F(t)) \quad (6.22)$$

$$L_Z^{(0)}(\theta_Z|w_F(t)) = \prod_{i=1}^{n_F} f_{\theta_Z}(s_i) \delta_i \rightarrow \hat{\theta}_Z^{(0)} = \arg \max_{\theta_Z} L_Z^{(0)}(\theta_Z|w_F(t)) \quad (6.23)$$

2. Repeat until the stop criteria is met.

Iteration $k + 1$. From the k -th iteration, $k \geq 0$, we know the estimations $\hat{\theta}_X^{(k)}$, $\hat{\theta}_Z^{(k)}$, and $\hat{P}_{WI}^{(k)}$; of the parameters θ_X , θ_Z , and the probability P_{WI} . The iteration is divided into two steps: in the first one the calculation of the expected value of the indicator function δ_i in each patient with incomplete data is carried out, which allows estimating the probability of admission in the ICU, P_{WI} , and the expectation of the likelihood function when all data, complete and incomplete, are considered. The second step estimates θ_X and θ_Z by maximizing the likelihood functions estimated in the previous step.

2.1. Expectation.

For each patient i , the probability of being admitted to the ICU is updated as the posterior probability given the time already spent at the ward:

$$\begin{aligned} \hat{P}_i^{(k+1)} &\equiv \hat{P}^{(k+1)}(\delta_i = 1 | \hat{P}_{WI}^{(k)}, \hat{\theta}_X^{(k)}, \hat{\theta}_Z^{(k)}) \\ &= \frac{(1 - \hat{F}_{\theta_Z}^{(k)}(s_i)) \hat{P}_{WI}^{(k)}}{(1 - \hat{F}_{\theta_Z}^{(k)}(s_i)) \hat{P}_{WI}^{(k)} + (1 - \hat{F}_{\theta_X}^{(k)}(s_i)) (1 - \hat{P}_{WI}^{(k)})} \end{aligned} \quad (6.24)$$

The updated probabilities of being admitted in ICU for each patient of type H^* allows to update the unconditional probability of admission in the ICU

$$\begin{aligned}\hat{P}_{WI}^{(k+1)} &= E[\delta = 1 \mid \hat{P}_{WI}^{(k)}, \hat{\theta}_X^{(k)}, \hat{\theta}_Z^{(k)}] = \frac{1}{n(t)} \sum_{i=1}^{n(t)} E[1_{\{\delta_i=1\}}] \\ &= \frac{1}{n(t)} \left(\sum_{i=1}^{n_F} 1_{\{\delta_i=1\}} + \sum_{i=1}^{n_I} \hat{P}_i^{(k+1)} \right)\end{aligned}\quad (6.25)$$

and, the likelihood functions of the sample as expected functions:

$$\begin{aligned}L_X^{(k+1)}(\theta_X | w(t)) &= E[L_X(\theta_X | w(t))] \\ &= \prod_{i=1}^{n_F} f_{\theta_X}^{(k)}(s_i) (1 - \delta_i) \prod_{i=1}^{n_I} (1 - F_{\theta_X}^{(k)}(s_i)) (1 - \hat{P}_i^{(k+1)})\end{aligned}\quad (6.26)$$

$$\begin{aligned}L_Z^{(k+1)}(\theta_Z | w(t)) &= E[L_Z(\theta_Z | w(t))] \\ &= \prod_{i=1}^{n_F} f_{\theta_Z}^{(k)}(s_i) \delta_i \prod_{i=1}^{n_I} (1 - F_{\theta_Z}^{(k)}(s_i)) \hat{P}_i^{(k+1)}\end{aligned}\quad (6.27)$$

2.2. Maximization.

The likelihood functions are maximized to find the estimation of the parameters.

$$\hat{\theta}_X^{(k+1)} = \arg \max_{\theta_X} (L_X^{(k+1)}(\theta_X | w(t))) \quad (6.28)$$

$$\hat{\theta}_Z^{(k+1)} = \arg \max_{\theta_Z} (L_Z^{(k+1)}(\theta_Z | w(t))) \quad (6.29)$$

3. Stop criteria.

Repeat Step 2 until the sequence of values of the likelihood function or the values of the estimated parameters converges:

$$\left| L_X^{(k+1)}(\hat{\theta}_X | w(t)) - L_X^{(k)}(\hat{\theta}_X | w(t)) \right| \leq \varepsilon_1 \quad (6.30)$$

$$\left| \hat{\theta}_X^{(k+1)} - \hat{\theta}_X^{(k)} \right| \leq \varepsilon_2 \quad (6.31)$$

6.6 Importance of a good dynamic parameter estimation

In this section, we compare, by simulating different pandemic waves, the performance of the EM estimator with other two statistical estimators that use only complete data. We measure the accuracy in the parameters estimation and their influence in the forecasting of necessary resources to provide healthcare to pandemic patients.

6.6.1 Experimental design

A simulation experiment has been designed to validate the estimation method developed in Section 6.5 (named EM method) and its impact on the quality of the predictions made on the necessary resources, specifically, about the necessary ICU beds. The simulation of a pandemic wave requires the simulation of the patient arrival process, which is carried out using the Gompertz model exposed in equation (6.13), and the generation of a trajectory in the hospital for each patient, which is carried out according to the flow of patients shown in Figure 6.3.

Specifically, generated pandemic waves mimic those observed in reality (Garcia-Vicuña et al. 2021) with the parameters for the arrival and hospitalization processes described below. Each pandemic wave simulation generates data over time that is used to test the performance of the proposed estimation method EM and its comparison with the other two estimation methods. The results about the estimation accuracy are shown in Section 6.6.2 and the impact on the precision of the predictions in Section 6.6.3.

Gompertz model parameters. Patient arrivals are generated according to the accumulated curve described by equation (6.13) with parameters $A = 2,000; 20,000; \text{ and } 100,000$, $T_{0.1} = 60$, and $D = 18$. That is, a pandemic wave that spreads 60 days (to account for the 90% central cases) and varying sizes, from 2,000 (corresponding to a small region) to 100,000 (corresponding to a medium-size country). Daily admissions are determined by the difference between the value of the Gompertz curve in two consecutive days, rounded to the nearest integer number.

Patient hospital path. Probability distributions for the LoS are assumed to be Weibull ($W(\alpha, \beta)$, where α is the scale parameter and β the shape parameter): LoS in the hospital ward of a patient not needing ICU (variable X) $W(10.74, 1.25)$, the time spent by a patient in the hospital ward before transfer to the ICU (variable Z) $W(5.06, 0.98)$. In addition, the LoS of a patient in the ICU $W(18.91, 1.15)$, and the LoS of a patient in the hospital ward after being discharged from the ICU $W(12.90, 1.4)$.

The probability of a patient initially admitted to a ward requiring transfer to ICU (p_{WI}) (0.073). Moreover, the probability of direct admission to ICU upon arrival (0.021), and the probability of patient transfer from ICU to hospital ward (0.75).

Estimation methods. Three parameter estimation methods are compared. In the first one (method I), the probability p_{WI} is estimated by the ratio of patients that were admitted at the ICU divided by patients admitted at a hospital ward, to date. Therefore times at the hospital of patients of type H^* are considered censored times for variable X . The second method is similar to the first one, but only patients that were admitted more than 5 days before are considered for the estimation calculations (method $I-5$). This avoids overestimating the number of patients

who will not require ICU in the future. Finally, the third method is the one developed in Section 6.5.4 (method *EM*).

6.6.2 Parameter estimation accuracy

This subsection assesses the accuracy in the estimation of the probability p_{WI} and the scale and shape parameters of the Weibull distribution of variables X and Z as the pandemic progresses. The simulation model recreates the patients' arrival and their stay at the hospital according to the parameters and probability distributions fixed in Section 6.6.1. After simulating one day of the pandemic, the three estimation methods are applied to estimate the probability parameters and distributions. The results of these estimations are shown in Figure 6.9. Therefore, the differences in the estimations produced by the three methods are assigned to the differences in their prediction capability and not to the randomness of the simulation because it is controlled and the same for each method.

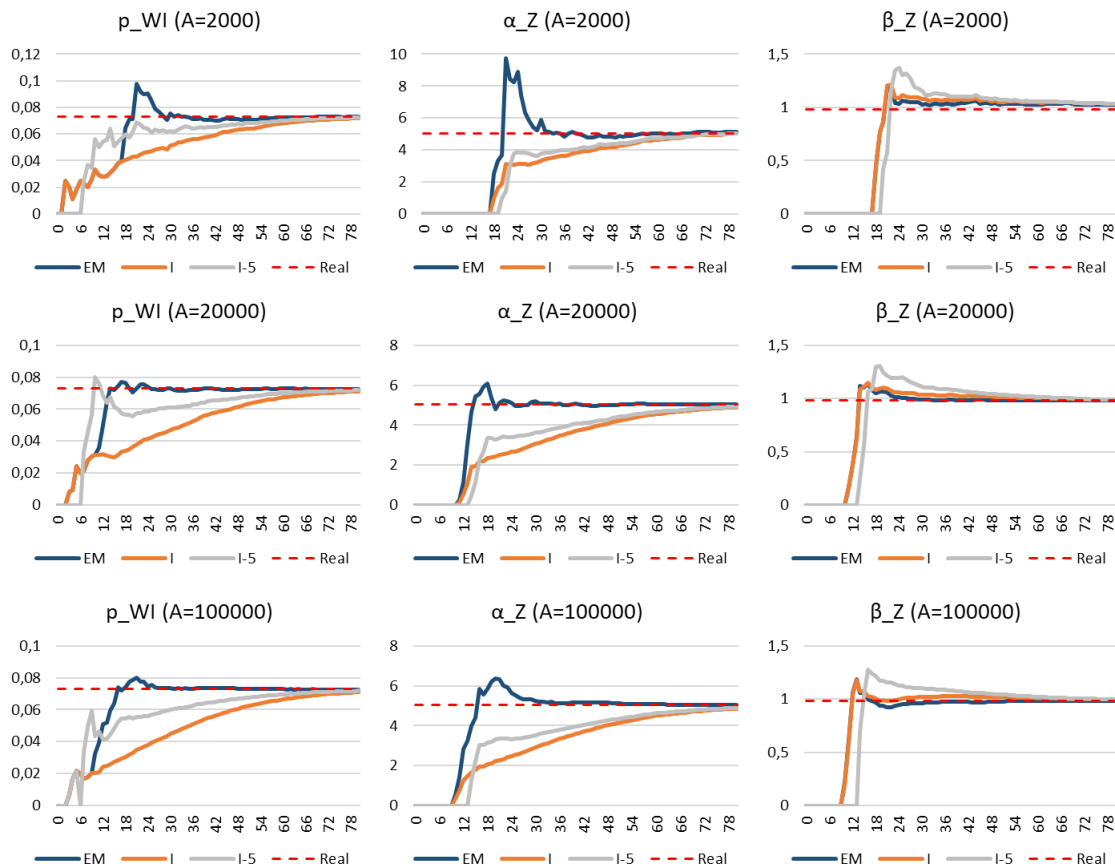


Figure 6.9. Estimation of parameters p_{WI} and θ_Z over time (the horizontal axes represent the time during the pandemic) with the 3 methods (*I*, *I-5*, and *EM*) and the real values. Results are shown for different values of parameter A of the Gompertz curve (2000, 20000, and 100000).

Figure 6.9 shows the evolution of the estimation of parameters p_{WI} and θ_Z over time ($\hat{\theta}_X$ values show small differences among different methods). Each pandemic scenario is simulated 10 times and the results show the estimation averages over the 10 runs. The x -axis represents the pandemic days when the estimations are made, and the y -axis represents the value of the parameter being estimated. The red dashed line marks the real value of the parameter. The three methods provide results that converge to the true value of the estimated parameter. However, the method *EM* has a fast convergence in all simulated cases, which turns to be important when the simulation model is used as a prediction tool for the resources needed in the future, as we expose in the next subsection.

6.6.3 Impact on the simulation output: bed occupancy prediction accuracy

The objective of the simulation model is to predict the future bed occupancy level during the course of the pandemic wave. The predictions of the simulation model are obtained by the statistical analysis of the output of many simulation model runs. In this subsection, we evaluate the quality of the predictions made with the simulation model with each of the three estimation methods. For each estimation method, predictions are obtained at different times of the pandemic evolution by simulating patient pathways and LoS by using the respective estimated branching probabilities and probability distribution parameters. The results obtained from each method are compared with those obtained by simulating using the true value of the parameters and probabilities.

Once the prediction day is set, many simulations are run with each method and the predictions obtained are compared with those made from the actual parameters. Figure 6.10 shows nine predictions of ICU bed occupancy made with all methods from 3 different days (20th, 25th, and 30th). Note that these days are quite far away from the peak occupancy. The green line in each graph represents the evolution of the simulated pandemic up to the SSP, which is represented by a black dot. For each prediction, the 5th percentile (P5) and the 95th percentile (P95) are plotted. As the pandemic progresses, the predictions of occupation become closer to reality. But in all cases, the *EM* method is the closest.

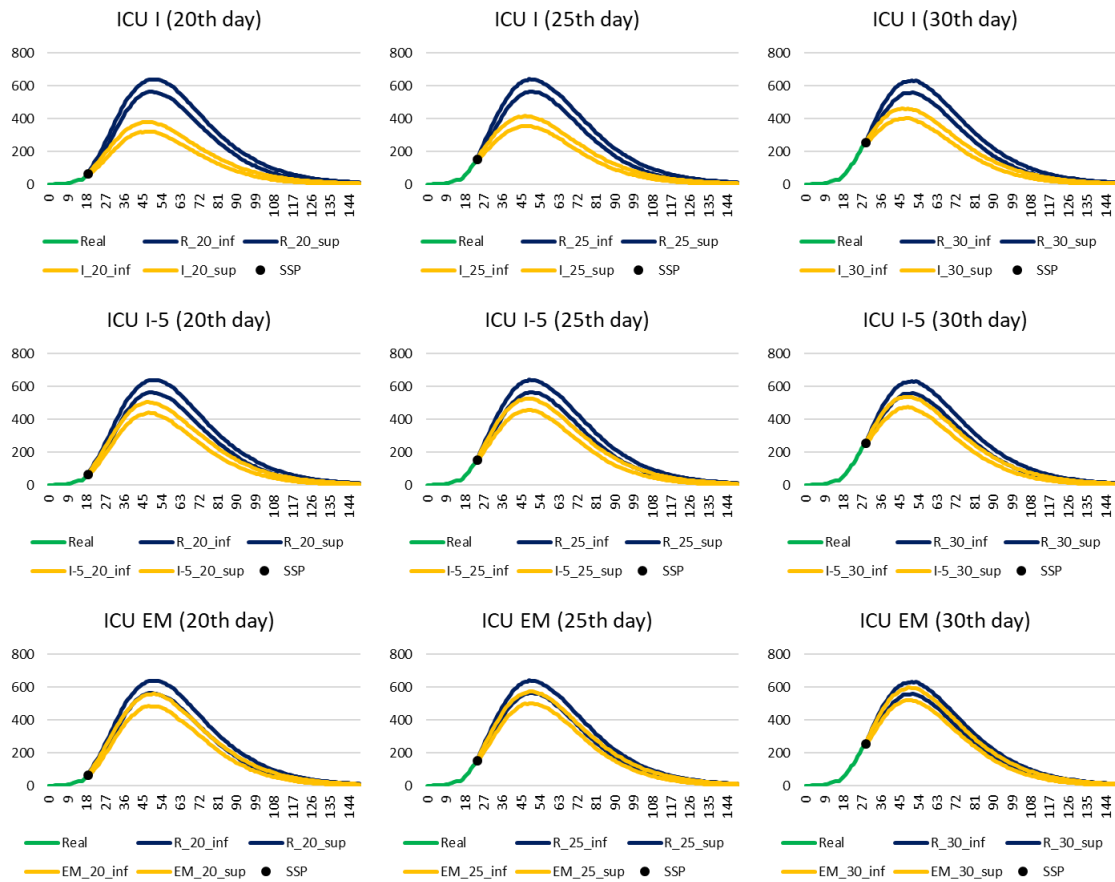


Figure 6.10. Prediction of ICU bed occupancy on the 20th, 25th, and 30th days of the pandemic with the 3 methods (*I*, *I-5*, and *EM*) compared to prediction with actual parameters.

6.7 Conclusions

Healthcare systems are overburdened as high demand for healthcare services from COVID-19 patients places strains on ICU capacity and creates excessive workloads for healthcare professionals. Accurate predictions of patient care resource needs are essential to advanced resource planning which can ease pressure on the system and relieve stress among hospital staff. Accurate predictions optimize response times and thus help to save lives.

Under normal circumstances, managers cope with demand surges through resource contingency plans based on predictions made about one week in advance. In this chapter, we have developed a DES model to predict hospital resource needs, particularly in terms of ward and ICU beds. The simulation model is fed with new hospitalization predictions generated by a PG model. The Gompertz growth model was selected following an analysis of the fit and forecasting properties of four PG models: Logistic, Richards, Stannard, and Gompertz. Forecasting improvements could be achieved using an ensemble of these models, but such an exercise is beyond the scope of this chapter and remains for future research. Forecasting

accuracy can be improved by including other factors affecting resource consumption, such as age and the Adjusted Morbidity Group (AMG), in LoS stochastic models.

The structural simplicity of the simulation model makes it appropriate for general use, i.e., it can be adapted to estimate bed needs in any geographic area. The growth model requires only three parameter estimates, which can be obtained directly from the observed data. Easy online parameter estimation is one of the advantages of this model over other complex models, such as the SIR type.

It is worth mentioning the strength of simulation models in this context of uncertainty, that is, their capability to run what-if scenarios enabling decision-makers to explore the consequences of different policy choices, such as the spatial allocation and quantity of additional healthcare resources required by COVID-19 patients in a context of uncertain demand. The simulation model is data-driven, patient arrivals and lengths of stay can be estimated from data, but it also has the flexibility of allowing the use of simulation from user-determined input to explore additional scenarios.

A distinct technical/methodological feature of the simulation model is its focus on the transition period of the health system rather than the stationary state as is usual in simulation studies or on transition periods following regeneration points. This simulated transition period is unique, given that the outbreak has no regeneration points. Therefore, accurate representation of the initial health system status is paramount. The simulation of remaining LoS per hospitalization has shown to be a key point to the smooth projection of health system dynamics and the process of linking them (and mixing them) with the new dynamics obtained from simulated new patient arrivals and lengths of stay. However, the simulation of the remaining LoS depends on the amount of information known about hospitalized patients. In this chapter, we have considered patient-level information (exact admission and discharge dates). In cases where only aggregated hospital-level information is available, that is, daily numbers of admissions and discharges, an estimated admission date per patient at time zero of the simulation is required.

The method we have developed based on an EM algorithm is suitable for the online estimation of hospital simulation-model input parameters. This method allows the use of the data provided by all patients admitted so far. This characteristic is a big advantage when only a small ratio of patients have been discharged and can provide full information about their hospital pathway and LoS. Simulation tests have shown a better performance than other estimation methods that use only complete information. Poor estimation of the parameters and probabilities leads to poorer estimations of the output variables of interest as the number of beds necessary to attend to all pandemic coming patients.

The estimation method has been applied to the estimation of the admission probability to the ICU from the ward and to the parameters of the probability distributions of variables LoS in the hospital ward and the time to admission to the ICU. The same stochastic situation occurs

for the admitted patients to the ICU, since it is unknown whether at the end of their stay they will be transferred back to the ward, due to improved health, or will leave the ICU due to death. The application of the estimation method to this case allows estimating the probability of recovery, and the parameters of the probability distributions of the time until transfer to the ward and the time until death.

Note that, in addition to the probabilities and parameters set forth above, it is only necessary to estimate the probability of direct admission to the ICU and the LoS in the ward after transfer from the ICU to complete the estimation of all the variables and parameters that describe the randomness of the pathways and LoS of patients through the hospital, as it is described in Figure 6.3. The probability of direct admission to the ICU is estimated by means of the observed proportion, which obviously uses the information of all the patients admitted so far. The probability distribution parameters of the LoS in the hospital ward after ICU can be estimated by maximum likelihood: those patients already discharged provide an exact value, while those who are still hospitalized provide a censored value.

The simulation model can be extended to include non-COVID-19 ICU and ward bed utilization. This extension would enable the creation of hospital scenarios on which to test the effects of decisions involving other hospital areas, such as a reduction in elective surgeries to free more beds for COVID-19 patients during epidemic waves. The ultimate purpose is to create a learning tool, as we did in the Part I of this thesis, by developing an interactive simulation model to enable the inclusion of patients from all types of pathways (ordinary and non-ordinary, such as pandemic patients), where bed management decisions are made by the program user.

7 Practical application of methodologies to support hospital management

This chapter reports a successful real application of simulation the simulation methodology exposed in Chapter 6 to support the decision-making of hospital logistic managers in broad regions of Spain. The results of the simulation model were used on a daily basis during the successive waves of the pandemic (from March 2020 to December 2021) by local governments of two Spanish regions and by the Spanish Ministry of Health as a health resources planning instrument. In addition, the simplicity of this simulation model and the lack of local assumptions about the COVID-19 behaviour make it usable in other countries and regions.

This chapter is organized as follows. First, in Section 7.1, we briefly introduce the implementation of the methodology developed in Chapter 6 in simulation software. Results of the application in the Autonomous Regions of Navarre and La Rioja (Spain) during pandemic waves in 2020 are included in Section 7.2. Section 7.3 includes a chronological account of the practical application of the simulation model and outlines the usefulness of these models in non-acute phases of the pandemic to aid decision-making during the phase of return to the normal operation of the health services or as a management learning tool. Finally, in Section 7.4, we conclude with lessons learned from all collaborations and some conclusions of this work.

7.1 Implementation of the methodology in a simulation software

The methodology presented in Chapter 6 was implemented in software using the Python programming language. It takes input from a data file containing a record of six variables including sex and age of patient and four dates representing the hospital and ICU admission and discharge times for each patient admitted to the hospital so far. Dates of events that do not

occur or have not yet been observed are left blank, such as the date of admission to ICU or the dates of discharge from both ward and ICU. These four dates enable estimation of all the LoS probability distributions and branching probabilities. The additional age and sex data enable segmentation of the patient population. The functionalities and manner of use of the software evolved through time and from one pandemic wave to another.

Initially (from March 2020 to June 2020), the simulation model was computationally implemented on its own, such that a daily manual statistical analysis was required to fit probability distributions. Throughout this period, the predictions and reports were drawn up by the research group and sent to the hospital's COVID-19 logistics manager. Only one regional government, specifically that of Navarre, used the results of our simulation model during this period.

After discussions with the hospital managers of Navarre, improvements were implemented in the software such as the computational implementation of the dynamic estimation of the probability distributions of hospital stay. Later, the assessment of a measure of the hospital saturation risk emerged, so the results were extended to include this measure. The statistical analysis was automatized and integrated in the software during the summer of 2020. In addition, the user interface, output analysis and automatic reports generation were also implemented.

Then, from October 2020 and throughout the second pandemic wave, the analyses were performed by local government health administration personnel (Govts. of Navarre and La Rioja), under the supervision of the research group. From December 2020, and throughout the third, fourth, and fifth waves, the health administration analysts worked almost autonomously. During the last period (January to June, 2021) the research group also assisted the Spanish Health Ministry by providing predictions for each of the 17 Autonomous Communities in Spain.

As a result of all these collaborations, the simulation software COVIDSIM was developed. This simulator, which allows the predictions of necessary beds in both hospital wards and ICUs during a pandemic, integrates all the parts developed in Chapter 6. In Appendix H, the COVIDSIM software user guide is provided. It explains how the software works and the steps that the user has to take to obtain an adequate prediction.

7.2 Application example in Navarre and La Rioja

The COVIDSIM software introduced in Section 7.1 has been used by the Governments of the Spanish Autonomous Regions of Navarre and La Rioja to support bed planning in their hospitals during the pandemic waves experienced in 2020 and 2021. We briefly describe how the virus has affected these two regions globally, then explain the stochastic modelling of the

hospitalized patients and their pathway through the hospital, and then present the predictions obtained by the DES model at different times and the deviations of these predictions from the real values. We conclude this section with some observations and tips for the practical use of this forecasting tool.

7.2.1 Incidence of COVID-19 disease during 2020 and 2021

Navarre and La Rioja are two Regions of northern Spain with populations of about 650,000 and 350,000, respectively, more than half concentrated around the capitals (Pamplona and Logroño). With this population distribution, Navarre Health Services have a main hospital in Pamplona, with a bed capacity of more than 1,000, and two secondary hospitals in two of the most populated cities (Estella and Tudela) bringing total bed capacity to 1,466 ward beds and 45 ICU beds. La Rioja has a main hospital in Logroño with 630 hospital beds and 21 ICU beds and a secondary 80-bed hospital in Calahorra. Both regions have the possibility of increasing bed numbers if necessary.

Navarre and La Rioja figure among the five Spanish autonomous regions with the highest cumulative COVID-19 rates during the first both waves of the pandemic, according to data collected by the [Governments of Navarre](#) and [La Rioja](#). Daily numbers of new admissions have important implications for hospital management teams. Figure 7.1 shows hospital admission statistics for both regions from early March 2020 to mid-December 2020. Two waves can be appreciated each with its own characteristics. The first is shorter but steeper, while the second is more prolonged. By December 16, 2020, 4,228 COVID-19 patients had been admitted to hospitals in Navarre (6.5 per 1,000) and 2,235 COVID-19 patients in La Rioja (6.4 per 1,000). A more extended series of hospitalized patients in Navarre and La Rioja between March 2020 and December 2021 can be seen in Figure 7.2. A total of 6 waves can be distinguished, with different characteristics between them in terms of magnitude and duration. In total, between February 26, 2020, and December 19, 2021, 7,213 COVID-19 patients were admitted to the hospital in Navarra and 3,712 in La Rioja.

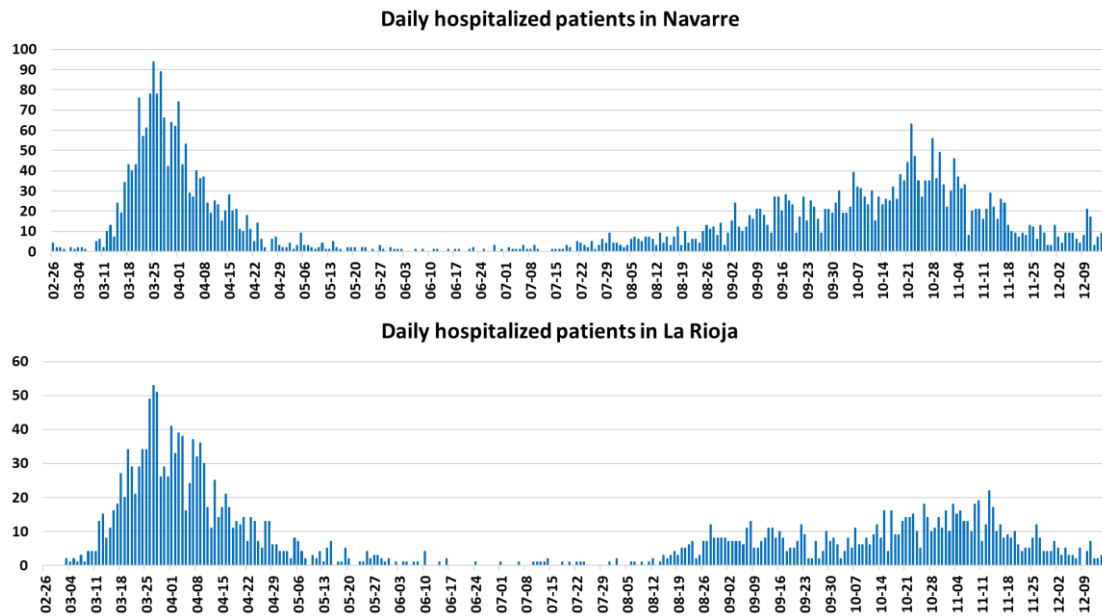


Figure 7.1. Daily recorded hospitalizations in Navarre and La Rioja from early March 2020 to mid-December 2020.

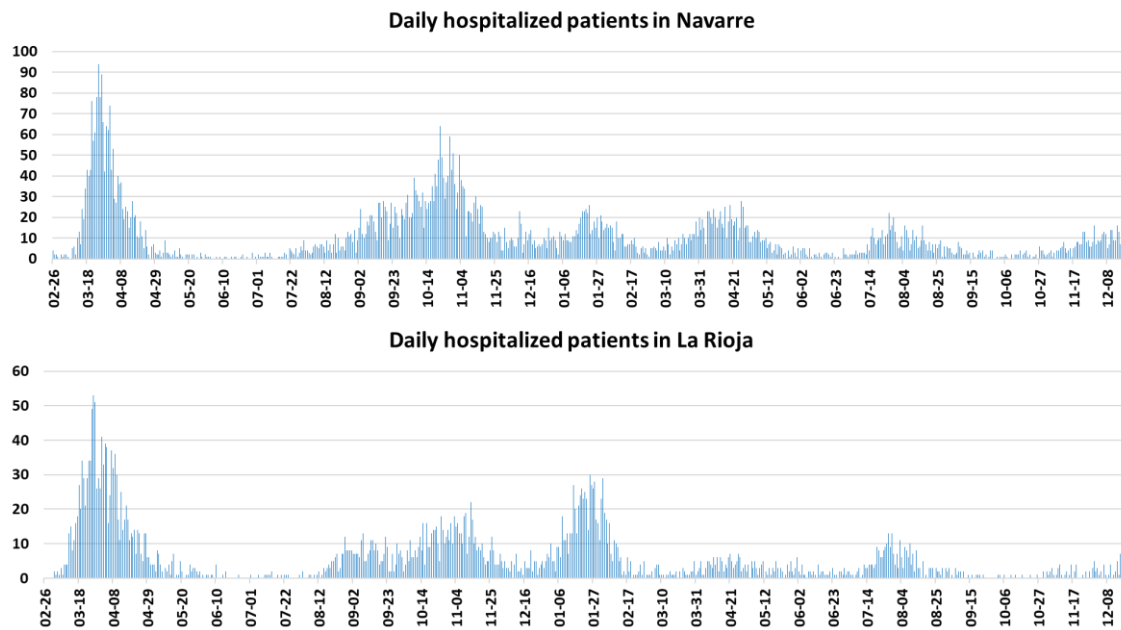


Figure 7.2. Daily recorded hospitalizations in Navarre and La Rioja from early March 2020 to mid-December 2021.

7.2.2 Stochastic modelling of hospitalizations and lengths of stay

As the pandemic spreads, the data load increases, making it possible to improve the accuracy of the statistical estimations. Since March 16, 2020, the arrival pattern is calculated from the hospital admission series. Figure 7.3 shows different results after fitting the Gompertz growth

model to cumulative hospitalizations in La Rioja during the first wave. As the pandemic progresses and more data becomes available, the Gompertz curve fit usually improves. However, due to the wide variability of the real data, minor fit deviations, such as that of March 31, 2020, are possible. Separate curve fits are shown in Figure 7.4, along with the real daily hospitalization series. These graphs show the wide variability of the data.

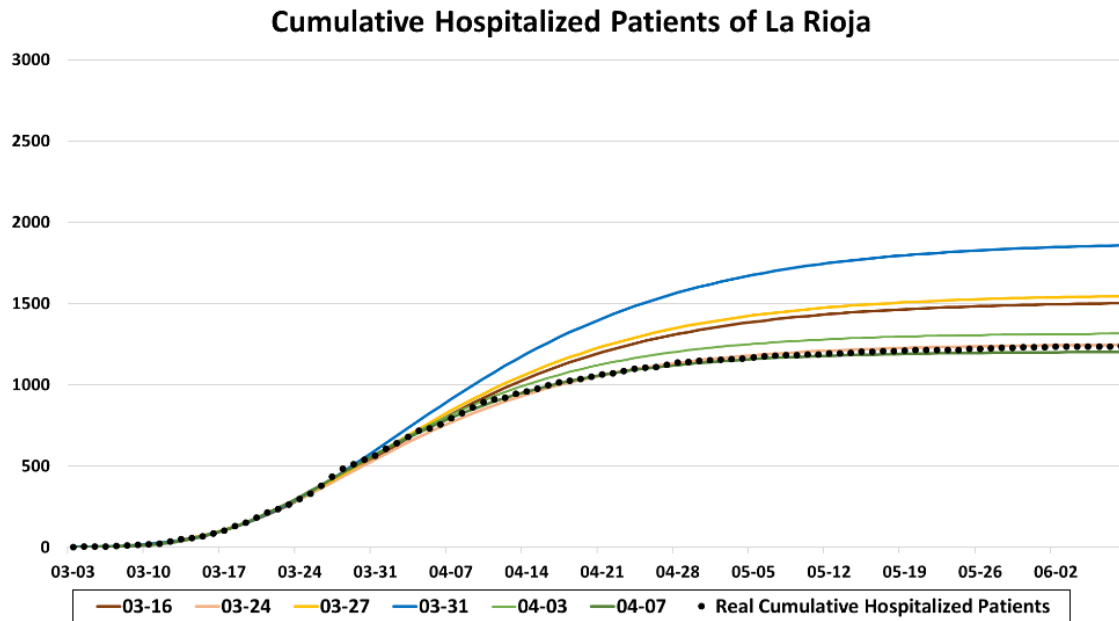


Figure 7.3. Cumulative hospitalizations in La Rioja from March 3 to June 9, 2020, and different curve fits obtained from the Gompertz growth model.

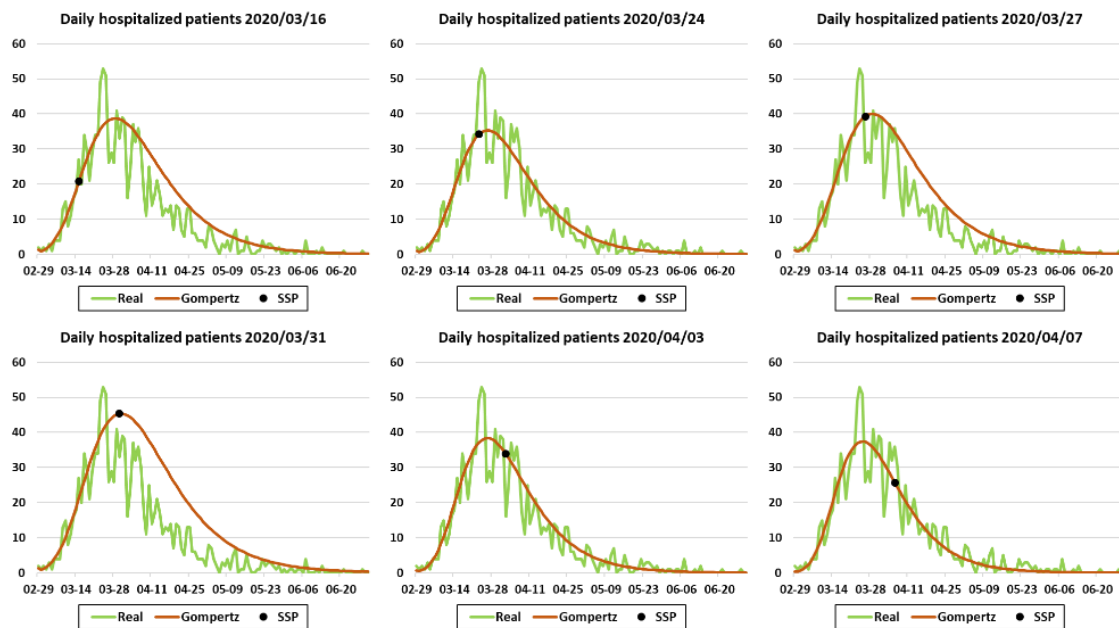


Figure 7.4. Six different curve fits obtained from the Gompertz growth model compared with the daily hospitalization series for La Rioja from March 3 to June 30, 2020.

Both ward and ICU lengths of stay are estimated daily, as explained in Section 6.3. Ward lengths of stay (X) fit reasonably well to a lognormal distribution ($LN(\mu, \sigma)$), whilst the Weibull ($W(\alpha, \beta)$) distribution is found to provide a better fit for ICU LoS (Y). During the pandemic, each time the data was analyzed, the distribution parameters were reset for the simulation. Table 7.1 lists the probability distributions that best fit the lengths of stay in the two waves for Navarre (Na) and La Rioja (Ri), sorted by gender, male (M) and female (F). N stands for the number of patients analysed. Differences can be observed between regions, waves, and genders, especially in ICU lengths of stay and the percentages of ICU admissions. Figure 7.5 shows two probability plots obtained from the fits of the ward and ICU LoS distributions (regardless of gender) during the first wave of the pandemic in Navarre.

Table 7.1. The parameters fitted to different populations at different moments during the pandemic, sorted by region (Navarre and La Rioja), wave, and gender, showing ward and ICU lengths of stay distributions and ICU admission probabilities.

Region	Wave	Gender	N	X (days)	\bar{X} (days)	Y (days)	\bar{Y} (days)	p_I	p_{WI}	p_{IW}
Na	1 st	M	929	LN (2.220; 0.845)	13.148	W (30.191; 1.184)	28.501	0.026	0.074	0.682
Na	1 st	F	807	LN (2.131; 0.819)	11.781	W (18.304; 1.055)	17.919	0.011	0.040	0.683
Na	2 nd	M	1,313	LN (2.021; 0.792)	10.325	LN (2.550; 1.075)	22.815	0.021	0.095	0.678
Na	2 nd	F	1,189	LN (1.970; 0.834)	10.151	LN (2.427; 0.876)	16.613	0.020	0.049	0.859
Ri	1 st	M	662	LN (1.882; 0.875)	9.630	W (14.385; 1.028)	14.226	0.039	0.063	0.455
Ri	1 st	F	583	LN (1.843; 0.779)	8.555	W (14.196; 1.038)	13.986	0.012	0.031	0.480
Ri	2 nd	M	559	LN (1.965; 0.774)	9.625	W (25.719; 1.166)	24.381	0.081	0.115	0.769
Ri	2 nd	F	450	LN (1.874; 0.805)	9.002	W (14.283; 1.184)	13.483	0.044	0.035	0.800

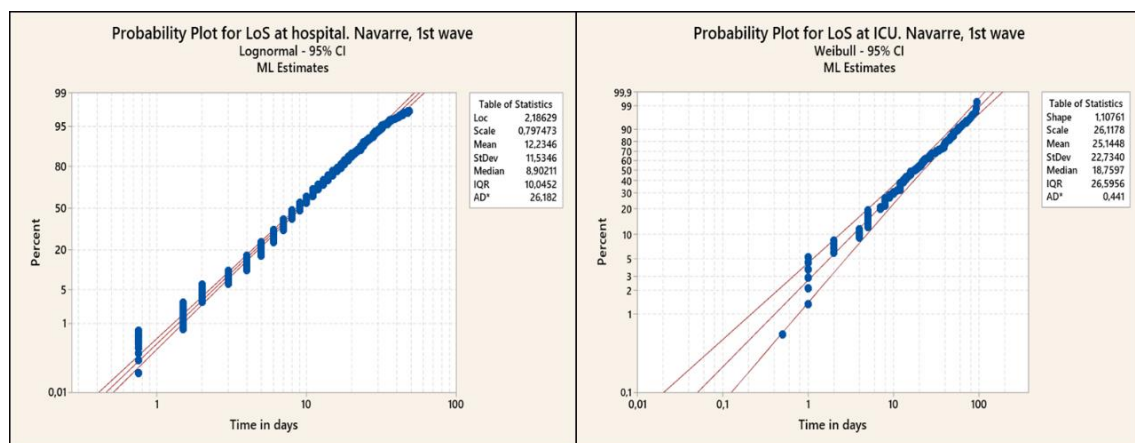


Figure 7.5. Probability plots of the fits of the ward and ICU LoS distributions during the first wave of the pandemic in Navarre.

7.2.3 Ward and ICU bed occupancy forecasts

Figure 7.6 shows the bed occupancy forecasts for the hospitals of Navarre based on the March 21, 2020 simulation for the following days. Note that the most important predictions for the medical staff are for the short-medium term (yellow-colored area in Figure 7.6), and there is a close match between the simulated and the real data, plotted in green. Besides, in Figure 7.7 we present the bed occupancy forecasts for the ICUs of Navarre based on the March 16, 2020 simulation for the following days. The simulator's ability to obtain accurate 10-day and 15-day forecasts, even in the early stages of the pandemic, is demonstrated here.

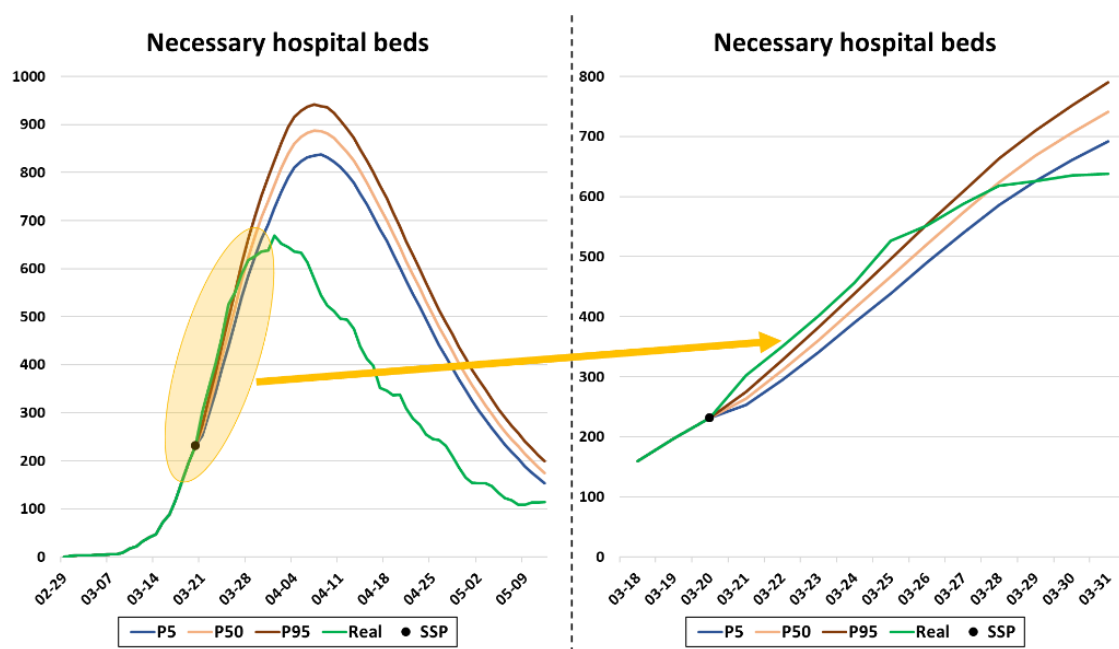


Figure 7.6. The prediction made on March 21, 2020 for bed occupancy in the hospitals of Navarre and the real occupancy levels. The area shaded yellow highlights the ability of the simulator to obtain accurate 10-day occupancy forecasts.

Figure 7.8 shows 4 simulations carried out on March 26 and 29 and April 1 and 4, 2020, comparing the results with the real evolution of the first pandemic wave in Navarre. It is observed that as the days go by, the results are more accurate because more information is available. More ward and ICU bed occupancy predictions at different moments of the second wave in Navarre, in comparison with real occupancy can be seen in Figure 7.9. Three dates have been selected to show the data trend pattern. The first is September 20, 2020, when the occupation began to increase significantly. The second is October 27, 2020, some days before the peak in ward and ICU bed occupancy. The last is November 13, 2020, when peak occupancy had passed and a downward trend had begun. All these results were derived from the 2,000 simulation runs conducted for each date.

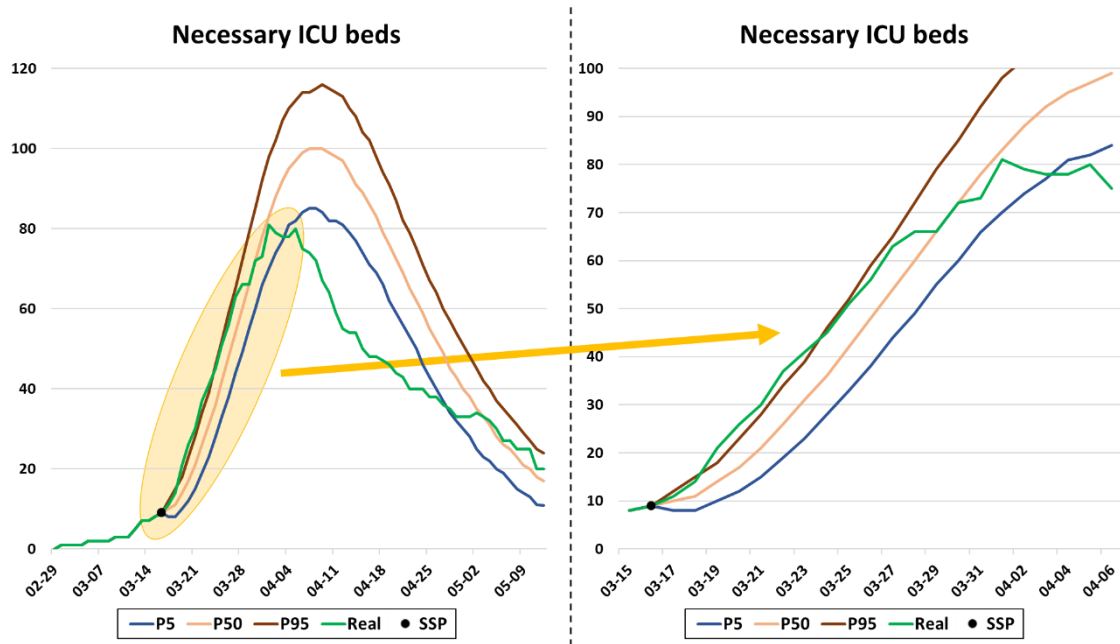


Figure 7.7. The prediction made on March 16, 2020 for bed occupancy in the ICUs of Navarre and the real occupancy levels. The area shaded yellow highlights the ability of the simulator to obtain accurate 15-day occupancy forecasts.

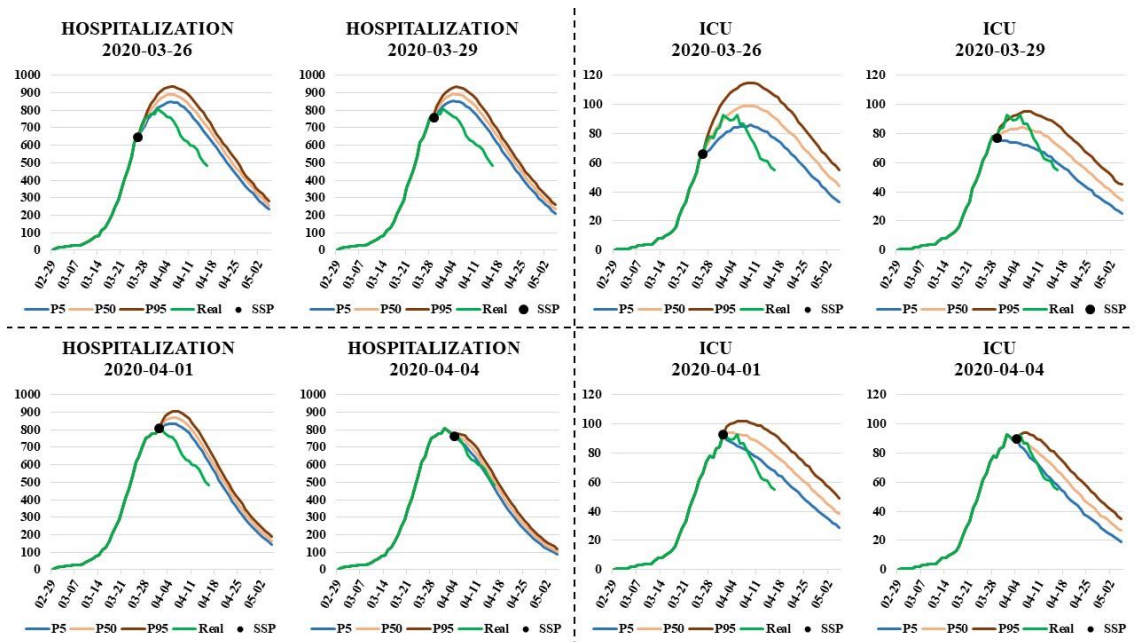


Figure 7.8. Comparison between the predictions made on different days (2020/03/26, 2020/03/29, 2020/04/01, and 2020/04/04) for the number of hospitalization and ICU beds occupied in Navarre and the real occupancies.

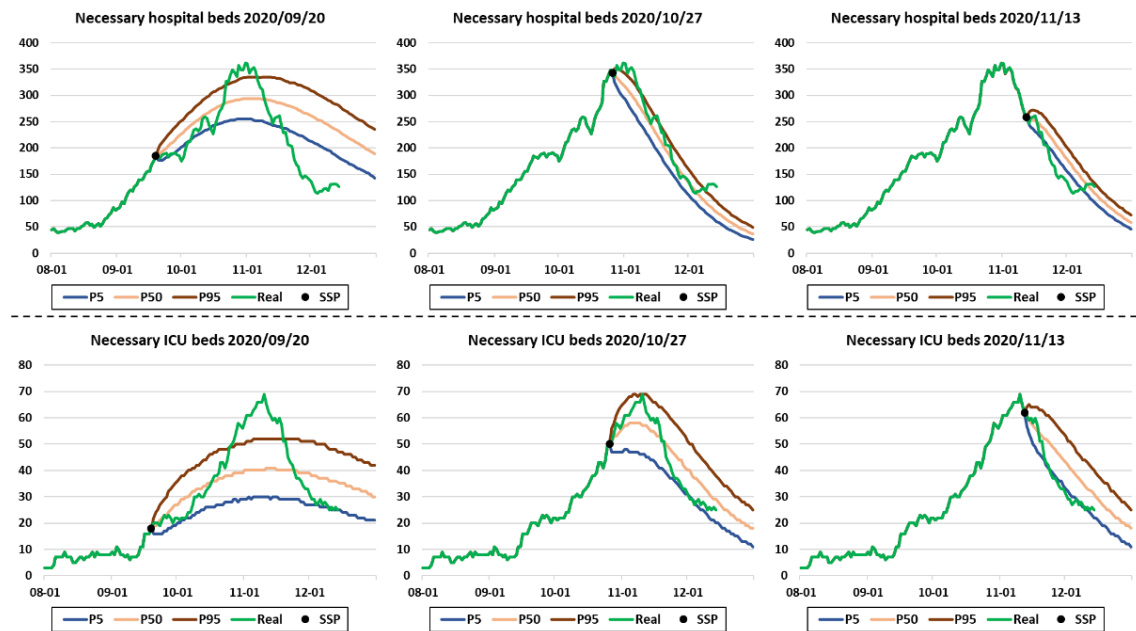


Figure 7.9. Comparison between the predictions made in Navarre at different moments of the second wave (2020/09/20, 2020/10/27, and 2020/11/13) for the number of beds occupied in both hospital and ICU, and real occupancies.

7.2.4 Tips for the use of the DES model in practice

All results shown in the previous subsections were obtained by fitting the growth model and probability distributions to the available data at the prediction times. However, during the first stages of an outbreak, when patient hospitalization data are scant, it could be hard to achieve accurate Gompertz model parameters and LoS probability distribution estimates to feed the simulation model. The beginning of an outbreak is usually marked by exponential growth in the data, potentially leading to a very high upper asymptote from the Gompertz model, which, in practical terms, could be considered as infinity (e.g. several orders of magnitude greater than the total population of the region). Taking this estimation as a simulation input, bed demand rises exponentially to figures much higher than the entire regional population. This is not a realistic estimation even in the worst case scenario of the entire population being infected. Nevertheless, in this case, the estimation would be valid for as many days as the exponential growth holds, and, as more data is collected, the accuracy of the upper asymptote estimate increases.

However, to avoid unlimited exponential growth, and improve the accuracy of the estimates at the beginning of a new pandemic wave, we recommend conducting a mixed estimation of the Gompertz parameters, combining an estimate based on expert opinion for one parameter with statistical fit estimates for the other two. Specifically, experts are able to estimate total hospitalizations based on the population incidence rate scaled by a hospitalization factor. For example, at the beginning of the first wave of the pandemic, Navarre Health Administration

professionals guessed that 1% of the population would catch the virus (based on flu incidence), and 40% of the cases would require hospitalization (estimating from initial data). Using values ranging around these estimates, we could run the simulation model to obtain possible hospitalization scenarios throughout the entire wave. These predictions overestimated total hospitalizations by the end of the first wave by only 30%. At the beginning of the second wave, the initial predicted maximum can be the value observed in the first wave or a percentage of it. However, as soon as enough data are available for an accurate parameter estimation, the simulation model should be completely data-driven.

A similar problem arises when estimating the parameters of the LoS probability distributions at the onset of a new wave. When insufficient data prevents the statistical estimation of all parameters, the simulation model has to be flexible enough to allow manual parameter input. We recommend the use of the triangular distribution to represent the LoS for different hospital status levels. The triangular distribution family is a popular choice for the estimation of task completion times because it embodies the idea of the ‘three-point estimation’ where subjective judgment is used to estimate a minimum, a ‘best guess’, and a maximum value of the variable of interest (Law 2014). Experts can rely on values reported for the countries first affected by the pandemic (for example the cases of China and Italy are described in Grasselli et al. (2020); Guan et al. (2020); Young et al. (2020); and Zhou et al. (2020)). For the second and successive waves, the probability distributions estimated at the end of previous waves can be used initially. For example, during the first days of the outbreak, Navarre Health Administration experts fixed the minimum, maximum, and most probable total LoS as 10, 18, and 13 days respectively.

7.3 Use as a support for decision making in hospital management

7.3.1 Chronological overview of the use of the simulation model in practice

The simulation model and its computational implementation have been a successful application of operational research, as the predictions provided were used in decision-making on the planning of resources needed to care for COVID-19 patients, mainly hospital and ICU beds. Those responsible for hospital logistics wanted to know the needs within a time horizon of one week, which was enough time for the preparation and deployment of field hospitals and the adaptation of other facilities to receive patients. Therefore, although the errors in the predictions could increase considerably as the time horizon is extended, they were reasonable for time horizons of up to one week. Thus, the simulator provides objective values on which to base decisions, thus avoiding arbitrariness in resource planning.

The use of the simulator for short-term prediction requires knowledge of the exact state of the hospital system at the time the simulation is started. With this information, in addition to

defining the initial state of the simulation model, the estimates of the parameters of the probability distributions and the branching probabilities that determine the flow of patients are readjusted. At the beginning of March 2020, the Government of Navarre prepared an information collection structure capable of providing complete information every morning at 9:00 a.m. that describes the state of the hospital system in the entire Autonomous Community one hour earlier, at 8:00 a.m. This information system involves the Department of Health Systems and Technologies of the Government of Navarre, in charge of storing, organising, and replicating health information (represented as operational systems in Figure 7.10), and the Data Management Unit of the Navarre Hospital Compound, in charge of processing the information received from the Government of Navarre and preparing the hospitalization data file on a daily basis. This unit, in addition to preparing the data files, also prepares reports, which integrate our forecasts, which are sent to the hospital management, the Health Counselling, and the political decision-makers of the Autonomous Community.

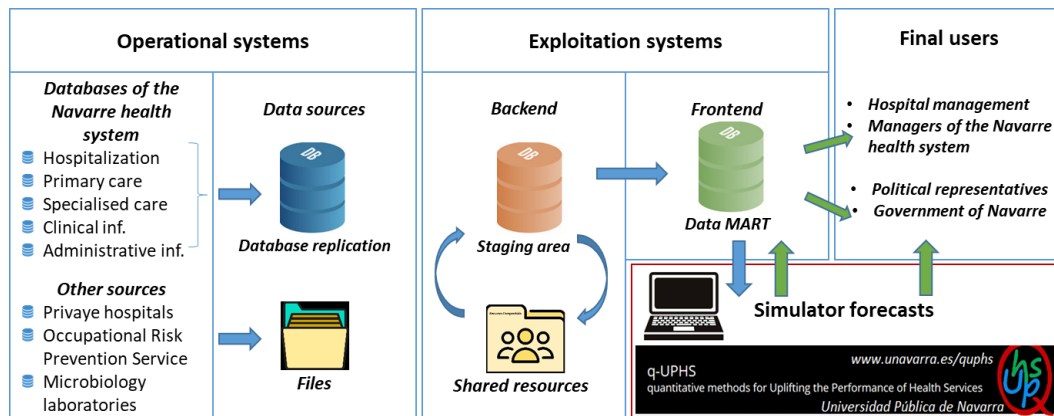


Figure 7.10. Daily flow of data, information and reports.

This collaboration started on March 12, 2020, when the management of the Navarre Hospital Compound contacted the q-UPHS research group asking about the possibility of forecasting the necessary resources. The first model was based on the simulation model of *Part I Analysis of Intensive Care Unit bed management using an interactive simulator*. This model was adapted and used for the initial analysis, but in the first stage of development, it required manual statistical analysis of the data file for fitting distributions, as well as launching the simulations, extracting results, and writing reports manually.

On March 16, 2020, we presented the first prototype of the simulator to those responsible for hospital management and Health Counselling, who approved the tool and agreed to provide the necessary data for its implementation. On the same day, the first forecasts were made using triangular distributions and parameter estimates based on values published in the literature. Numerous scenarios were run to see in which scenarios the existing capacities were sufficient and in which situations additional resources had to be prepared and in what quantity. In the daily reports generated for the government of Navarre, these scenarios were evaluated, expressly indicating the maximum number of beds to be occupied, as well as the day on which

this occurred. In the hospital, the maximum bed occupancy occurred on April 1, 2020, with 669 beds, while in the ICU the maximum of 81 beds lasted from April 1 to April 5, 2020. After the first peak of the pandemic, the research group provided support through a surveillance system for early detection of outbreaks (the development of this is not part of this research). In addition, during the first pandemic wave of 2020, we acknowledged that dynamic estimation of the parameters of probability distributions acquires great importance. Therefore, these dynamic estimates were improved by proposing new estimators.

At the end of the first wave of COVID-19 in June 2020, hospital system managers were satisfied with the results and found it to be a very useful tool. In addition, there was some media coverage, which made the methodology known to other governments such as La Rioja's, which became interested in using it in future pandemic waves. The scaling up necessary to serve several communities motivated the use of some procedures in the computational improvement, automating parts, so as to avoid manual statistical analysis, the launching of simulations, and the collection of results or the elaboration of reports. With the new computer application (the COVIDSIM software), hospital managers in Navarre and La Rioja gained the autonomy to make their own predictions, under the supervision of the research team. The new software was used in both Navarre and La Rioja from the second wave onwards. Figure 17 shows a graph with the 7-day occupancy predictions that the Navarre hospital managers obtained autonomously during the fourth pandemic wave (between March 2021 and June 2021) and the real curve of occupied beds in the hospital.

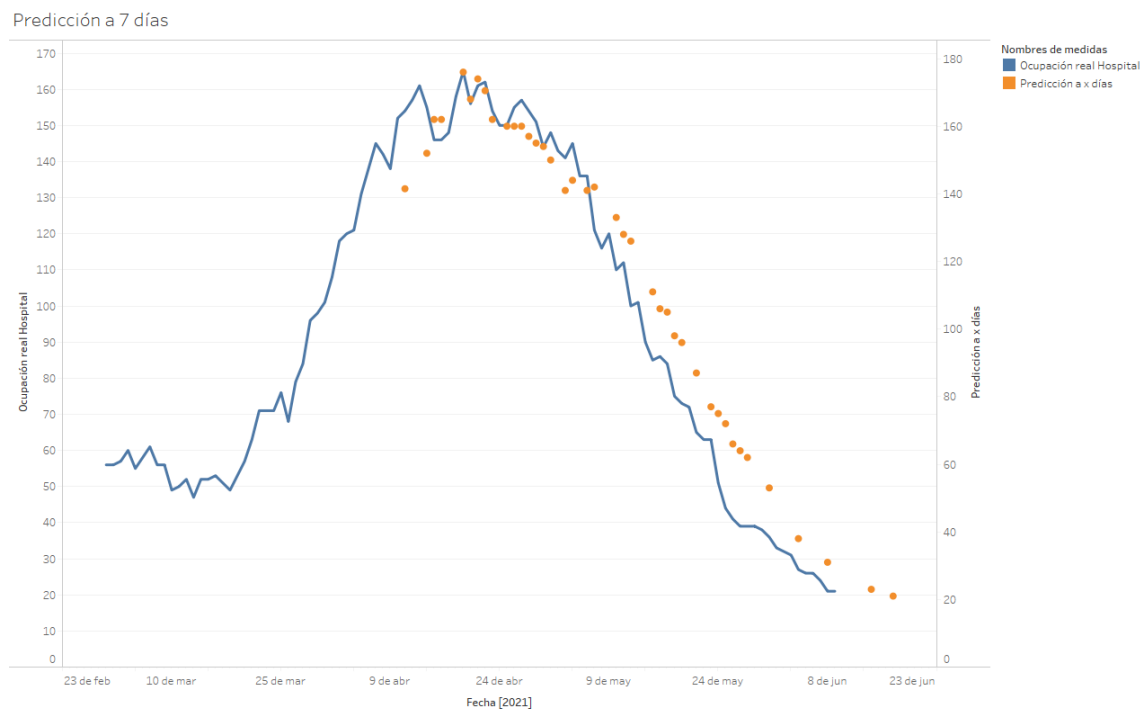


Figure 7.11. Comparison between 7-day forecasts made in Navarre at different times of the fourth wave (between March 2021 and June 2021) for the number of occupied hospital beds and actual occupancies.

In November 2020, the Health Alerts and Emergency Coordination Centre (CCAES) heard about the existence of our software and requested our collaboration to prepare individualized reports for each of the Spanish autonomous communities. It was applied during the third and fourth pandemic waves (between January and June 2021). Some autonomous communities, such as Castile and León and the Balearic Islands, requested a disaggregation by provinces and islands to facilitate management. In order to collaborate with the Ministry of Spain, we were allowed to access all centrally available data sources, which include the information system on hospital capacity (CMC) and other databases, receiving direct notification from public and private hospitals on admitted and discharged patients, active beds, and beds occupied by COVID-19 patients. All databases were updated daily and have national coverage.

7.3.2 Additional simulation model functionalities

The COVID-19 pandemic has required the use of all available resources in hospital services, leading to the cancellation of the usual activity of many departments and services. Thus, the activity in operating rooms, except for very urgent cases, was cancelled in order to free up beds in the ICUs. The incorporation of the usual sources of patients to an ICU into the simulation model allows it to be used to schedule the activity of the manageable sources, and its impact on future occupancy can be predicted. In times of pandemic, patients requiring intensive care can be classified into COVID-19 patients, patients from scheduled surgeries, and emergency patients (see Figure 7.12).

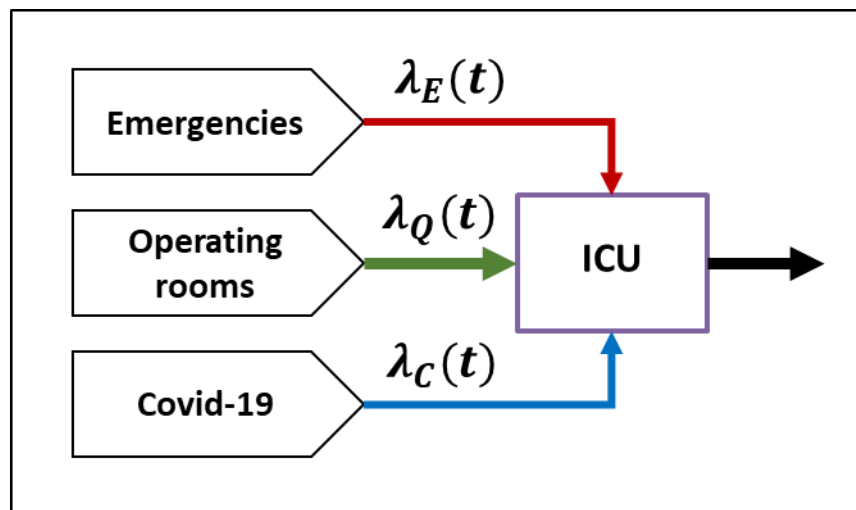


Figure 7.12. Sources of arrival in the ICU in times of pandemic. In addition to the two usual sources (emergencies and operating rooms), patients infected, in this case, by COVID-19, are added.

Typically, emergencies follow a stable random pattern, well described by a Poisson Process (PP), which in the pandemic period has decreased its arrival rate due to lockdown and a decrease in the activity. In periods of pandemic remission, the arrivals of COVID-19 patients progressively decreases, freeing resources for the reactivation of surgical activity. The

determination of optimal operating room schedules in these transition periods can be done using the simulation model in combination with heuristic optimisation techniques, to solve problems that seek to maximise the ICU bed resource, subject to probabilities of rejection/diversion of patients below a certain risk threshold and that address the priorities of patients waiting on the waiting lists of the different specialties. Similarly, this simulation model can be used for the gradual suspension of activity in operating rooms during subsequent outbreaks of the pandemic.

In general, the situation described raises the problem of the distribution and allocation of scarce healthcare resources among a wide range of patients. The pandemic may lead to changes in admission and discharge protocols for other types of patients who may be indirectly affected by the new disease. The confrontation of medical staff with the allocation of scarce resources is not new to this pandemic (Azcarate et al. 2020), although it has overemphasized the problem. Simulation models can be used to assess the effects of changes in medical care for other patients, both individually and collectively in terms of increased waiting lists (Wood 2020).

On the other hand, the simulation model can also be used in offline mode, in other words, outside the pandemic period as a learning tool for the management of resources by those responsible for health logistics. The simulation model is capable of recreating different pandemic scenarios, providing the necessary resources in each one, and comparing them with those available or programmed. It also makes it possible to test the influence of different ways of managing the hospitalization of patients (hospital, home, nursing homes, etc.).

7.4 Conclusions

After 21 months' cooperation with health authorities, we have reached the conclusion that the success of this operations-research support system for decision-makers in difficult pandemic times is due to the following factors:

- Multidisciplinary teamwork and a background of cooperation with health managers. The research group q-UPHS (www.unavarra.es/quphs) has been cooperating for more than 10 years in the solving of real problems surrounding health service improvements. Problem analysis is always addressed through multidisciplinary teamwork involving academics (engineers and mathematicians) and health service personnel (managers, medical staff, and computer scientists).
- A request for assistance from the health administration. At the beginning of the pandemic, health managers raised the need for a short- and medium-term bed-demand forecasting method to improve their bed management system. Medical space and equipment (including staff) planning is based on 10-bed modules. Prior knowledge of bed needs therefore facilitates resource planning.

- Rapid response. Five days after the original request, the group presented the simulation model and the initial results (predictions) for validation by the region's hospital and healthcare logistics managers.
- Joint development of the model. Decision-makers were involved in the development of the model and maintained continuous communication with the research team.
- Continuous improvement of the computer application. Suggestions made by health managers and a user-friendly software interface were implemented to free users gradually from the need for supervision by the research team.
- Joint monitoring of the results. Quality assessment and critical analysis of the predictions were performed jointly by the research team and health managers.

Thus, the simulation paradigm presented in this chapter is suitable for the realistic representation of health service processes, which makes it more credible and easier to understand by the managers who will have to rely on the results in their decision-making. From March 2020 until the moment of writing this thesis (end of December 2021), the simulation model has been used daily to predict hospital resource needs in the Spanish regions of Navarre and La Rioja, and all other Spanish Communities from January, 2021.

Conclusions

8 Conclusion

This thesis presents a research project using quantitative data analysis to enable the study and the comparison of decisions made by Intensive Care Unit (ICU) physicians. This opens up a future line of research based on the mathematical modelling of an ICU including the decisions made by medical staff. The outcome is the development of a learning tool for ICU resource management that was subsequently adapted for use as a prediction tool during the global COVID-19 pandemic, which created a surge in demand for hospital and ICU beds. During the pandemic, hospital beds, ICU beds, and healthcare staff are essential, not only to achieve optimal public health resource planning to assist all COVID-19 patients, but also to minimize the impact of the pandemic on other public health services (such as scheduled surgeries and medical consultations).

The rest of this chapter is organised as follows. The general conclusions of this thesis are explained in Section 8.1. The main contributions are summarised in Section 8.2. Section 8.3 indicates possible future extensions of this work. Both parts of this thesis leave issues to be addressed in future research. This chapter ends with Section 8.4, which contains some final remarks and a report of the scientific publications and conference presentations that have resulted from this work.

8.1 General conclusions

The research conducted for this thesis contributes to **improving the understanding of decision-making processes for ICU admission and discharge in high-occupancy periods**. The ICU work environment is one of intense stress due both to the critical state of the patients, whose chances of survival depend upon the medical staff's clinical decisions, and also to the uncertainty of future patient admission requirements. The need to hold resources in reserve to deal with unplanned or unexpected admissions can impact upon clinical decisions involving either admitted patients or expected arrivals, especially at times of high occupancy. Despite the crucial importance of this problem and the potential patient-health repercussions of the

eventual decisions, there is no protocol to guide professionals when faced with such challenges. Protocol design entails the added complication of a setting marked by a conflicting combination of patients already admitted and potential arrivals, making the ICU environment one of infinite casuistry, where the historical comparison of clinical decisions becomes impossible.

Against this background, the simulator proposed in this thesis becomes a valuable alternative for understanding the patient admission and discharge decisions of ICU professionals. It is to this end that the research work has focused primarily on creating a simulator with the capacity to faithfully reproduce the decision-making environment faced by ICU physicians. A key factor in achieving this is the simulation of ICU patient length of stay (LoS) using real (duly anonymised) clinical cases described by over 250 variables and physician and nurse reports. It is superior in this respect to the simplified approach used in the mathematical models developed to date, which describe hospital stays in terms of the number of days spent in hospital, and, at best, a small set of variables including gender, age, type of pathology or reason for admission. The information is presented as it is on the screens of the clinical record software (Metavision®) used in the ICU of the Navarre Hospital Compound. Moreover, the simulator creates a historical decision-making record, which can be understood as the raw datum describing the user's decision-making process. The challenge to be addressed in this thesis is the statistical analysis of this new data source with proposed metrics and statistical methodology for comparing physicians' decision-making processes. The preliminary results indeed show that there is variability across ICU professionals' decision-making processes, and differences between and within professional groups (physicians, nurses, residents, etc.).

Successive waves of the COVID-19 epidemic have triggered a surge in the number of patients requiring hospitalisation and intensive care which has rapidly exhausted the supply of acute and ICU beds. Hospitals have had to increase their capacity to deal with the surge in demand from these patients, while trying as far as possible to minimise the impact on the quality of attention given to other types of patients. This has called for flexible management strategies to ensure quality care for all patients needing it, while also maintaining some elective surgery. One way in which a hospital can increase its capacity for the implementation of management policies adapted to exceptional circumstances is by means of informed decision making based on the analysis of available data and accurate future demand forecasts.

The research carried out in the second part of the thesis contributes towards **obtaining short term demand forecasts both for acute and ICU beds, to cover the needs of COVID patients**, with a proposed forecasting method based on a combination of epidemiological statistical models and simulation techniques. This method uses known real-time data, the COVID-19 patient hospitalisation record, and a mechanistic simulation model that can be easily understood by the decision makers. The conceptual simplicity of the model belies its potential for addressing the methodological challenges raised in this thesis: from the dynamic parameter estimation of probabilistic models with incomplete data, to transitory state simulation of the hospital system, and future patient volume forecasting using a growth curve

model. Its conceptual simplicity, rigorous methodology and data accessibility have enabled its practical implementation as a decision-making support for hospital logistics managers.

The pandemic has thrown a spotlight on many areas of research where Operations Research (OR) models can provide solutions. It has also served to accelerate processes of change in patient care, such as telemedicine and home care. These changes, together with an ageing population and the threat of the re-emergence of this or similar viruses, will define public health in the 21st century and are a clarion call for researchers to prepare our models to support the development of sustainable and efficient health services and to be better prepared for the next health crisis.

8.2 Thesis contributions

Part I of this thesis consists of the development of simulation models and methodology for the analysis of ICU bed management. This includes the first ICU Management Flight Simulator (MFS), which enables analysis of the decision-making process and how it is managed, as well as providing a useful learning-training tool. This interactive simulator is based on a Discrete Event Simulation (DES) model that mimics real ICU admission and discharge processes. We recreate patients' health status using real clinical data recorded with Metavision® software, instead of using a single LoS value. The status of real patients is monitored with 275 health indicators, to give an extended and realistic description of their evolution, with possible improvement or deterioration. Thus, the first objective of this thesis, the "*Development of an interactive simulator capable of creating a virtual environment in which the operation of an ICU is represented...*" is fulfilled. We have designed a flexible tool which enables the recreation of ICUs with different characteristics (numbers of beds, patient arrival types, congestion levels...) and which begins the simulation with a scenario that is representative of the stationary state of an ICU.

Furthermore, we have developed statistical methods to analyse a new type of data in this context, patient admission and discharge decision-making sequences considering ICU status at each point of time. Preliminary results of global performance measures reveal variability among physicians' decision-making when faced with the dilemma of the last bed. The ICU pressure level is an important factor when analysing decision-making. Results based on this parameter reveal differences in management approaches across different user profiles (ICU nurses and ICU physicians, for example). One contribution in this respect is the development of a new metric to compare decisions according to the ICU pressure level, which consists of an extension of the Euclidean distance, which we have defined as the Euclidean-Aggregate distance. We have also defined a proper distance to compare decisions at patient level, the Extended Weighted Normalised Hamming distance between two binary vectors. It is mathematically expressed taking into account both the sum and the absolute difference of the non-common values, which, in this context, refer to the difference between patients and

between bed occupancy, respectively. Thus, the research described here fulfils the second specific objective, *“Quantitative analysis of medical decisions, by seeking patterns in ICU decision-making, using mathematical modelling to learn how decisions are made...”*.

Part II of this thesis consists of the development of simulation models and methodologies to predict both hospital and ICU admissions and bed occupancy several days ahead. The COVID-19 pandemic prompted the development of these models and their use in real-time. We had the opportunity to use them during the pandemic with daily updated data from the hospital. Thus, the model and methodology were validated by the Health Services managers. Specifically, we have developed a method to simulate COVID-19 patient arrival times based on Population Growth (PG) models. These are better suited for the prediction of hospitalization (and positive cases) series than other mathematical alternatives such as SIR-type models, which require detailed knowledge of the spread of the disease throughout the population and the estimation of many parameters. PG models produce S-shape curves able to represent the evolution of pandemic variables, such as positive cases and hospitalisations, from beginning to end of the outbreak. A statistical analysis of the accuracy of four different PG models in simulating and forecasting the spread of the pandemic has been carried out. We represent the current state of the health system based on a set of state variables and a dynamic statistical analysis of patient flow which enables the accurate simulation of the bed occupancy rate in the following days. We have developed methodological improvements in the estimation of hospital LoS and the probability of ICU admission. We have proposed a new estimator based on the Expectation-Maximization (EM) technique, which uses information on all patients admitted to the hospital and improves the results obtained with traditional estimators that do not use all the available information. We have combined all these elements in a DES model that is flexible enough to recreate scenarios based on stochastic models fitted to data (data-driven prediction), scenarios defined by expert judgement, and a mixture of both. Thus, we have satisfactorily fulfilled the third objective of this thesis, the *“Development of a mathematical tool for real-time prediction of hospital and ICU admissions and occupancy of these units in the following days during the pandemic caused by COVID-19...”*.

Finally, in practical terms, this thesis also reports the validation of the developed methodology by means of a successful real-world application of the simulation model to support a decision-making process of crucial importance to the health of patients in two Autonomous Regions of Spain (Navarre and La Rioja). Healthcare authorities in these two regions received, daily throughout all the pandemic waves, results predicting hospital and ICU admissions and occupancy for the following days. With this information, we helped them to act quickly and effectively. In addition, our model was used from the third pandemic wave, which started in December 2020, by Health Alert and Emergency Coordination Centre (CCAES), associated with the Spanish Ministry of Health. Some Spanish autonomous communities, such as Castile and León and the Balearic Islands, requested a disaggregation analysis by provinces and islands to facilitate the management of hospital resources. With these reports, we accomplish the fourth objective of the thesis, the *“Validation of the methodology*

in a real context by supporting healthcare authorities during the pandemic with daily forecast reports to help them to respond quickly and effectively in managing and planning public health resources”.

8.3 Future work and research

This thesis analyses problems of various kinds, some of which require further analysis and research. As far as Part I is concerned, we plan to continue studying the properties of the metrics proposed in Chapter 5 in greater depth, and to propose new metrics for comparing decision-making sequences between two physicians. An exhaustive analysis of all the results obtained with the ICU simulator is also required for the identification of different ICU management profiles. The observed ICU management behaviour can be compared with strategies formulated in optimization models in order to detect patterns. The objective would be to include physician decision-making in ICU simulation models to achieve a closer fit to real-life ICU decision-making processes. The computational implementation of these models will enable the development of methods for the analysis of medical staff workload and resource utilization.

A better understanding of physicians' decision-making processes will help to the correct choice of action in complex management situations, such as periods of high occupancy in which it is necessary to decide between the early discharge of an admitted patient or the redirection of others arriving at ICU. With the help of the ICU simulator, it will be possible to detect, study, and recreate difficult-choice scenarios, for discussion by professionals with a view to developing consensual action protocols. In addition, the implications of medical decisions in bed management on patients' health must be assessed, such as the health risk for patients when LoS is reduced for reasons of high ICU occupancy and other variables, such as the number of planned surgical admissions.

With respect to Part II of this thesis, some aspects remain to be analysed. On the one hand, the modelling of COVID-19 patient arrival can be improved by using combined methods to increase prediction efficiency. This requires assessing the sensitivity of different methods to the addition of new data and incorporating the results into the model. We would also like to compare the EM method used to estimate the pandemic wave parameters with other non-parametric methods. Through pandemic simulation, we will be able to conclude which method provides more accurate estimates with earlier convergences and whether it is more appropriate to develop an algorithm combining both methods.

A further aim would be to create an interactive simulator for use in healthcare resource management during a pandemic, to enable the user, based on predictions, to decide the amount of resources, in terms of ward and ICU beds and medical staff, to be allocated for the care of infected patients in the following days, bearing in mind that other health services, such as scheduled surgical operations, may be affected as a result. In addition, the tool would also

enable measurement of the impact of the decisions on other units of the hospital, and could be used as a training tool in manager performance comparisons and the evaluation of learning from repeated use.

8.4 Final remarks

The original plan for this thesis was modified due to the global COVID-19 pandemic. The initial objectives were those associated with Part I, however, the outbreak of the virus in China in December 2019 and in Spain in March 2020 prevented the dissemination of the simulator and the collection of usage data. This pandemic has provided a research opportunity for the development of new methodologies and the practical application of the developed simulation models. At the request of the Navarre healthcare services, we adapted our models to collaborate in the COVID-19 healthcare crisis and support the healthcare authorities with short-term predictions. Therefore, the first line of research relating to the analysis of admission and discharge decisions was adapted to include both aspects of our research in this thesis.

I would also like to emphasise that this thesis, involving direct contact with real clinical problems, was possible thanks to the efforts of the ICU Management at the Navarre Hospital Compound and the generous and kind collaboration of the ICU physicians and nurses. We would also like to highlight the work of the data analysis and hospital logistics management teams at the Navarre Hospital Compound during the pandemic, at whose request we provided data analysis support.

This thesis was only possible thanks to the support of the General Directorate of Health Services of Navarre, by whom we were authorised to access the data of the Regional Ministry of Health of the Government of Navarre, which was indispensable for the completion of this thesis. Similarly, access to all the data from La Rioja was provided by the Rioja Salud Foundation. The Spanish Ministry of Health also allowed us daily access to the Information system on hospital capacity (CMC) and other databases, to enable the national level analyses and predictions. All these entities were aware of the information and our daily forecast results, when making hospital logistics decisions and also political decisions such as lockdown and social distancing (SD) measures to cut the spread of the virus.

This work has resulted in the publication of two scientific papers in international indexed journals (Garcia-Vicuña et al. 2020b, 2021). One disclosure paper has also been published nationally (Garcia-Vicuña et al. 2020a), and another on the academic website The Conversation (Garcia-Vicuña and Mallor 2021), a network of not-for-profit media outlets publishing news stories and research reports online, with accompanying expert opinion and analysis. Specifically, the latter has had some media repercussions, with 13 re-publications in other media, having also generated over 2,600 reads in the following countries: Spain, Colombia, Peru, the United States, Chile, Mexico, Argentina, France, the United Kingdom, and Ecuador.

Furthermore, this thesis has been presented at 11 international conferences (Winter Simulation Conference, Operational Research Applied to Health Services, European Conference on Operational Research, European Society of Intensive Care Medicine LIVES, INFORMS Healthcare Conference, and New Bridges Between Mathematics and Data Science) and 5 national conferences (SEMICYUC National Congress). Our work has also had an impact on some Spanish hospitals, presentations having been made in five hospitals, three in Navarre (Navarre Hospital Compound, García Orcoyen Hospital, and Reina Sofia Hospital), one in the Basque Country (Guipúzcoa Polyclinic), and one in La Rioja (San Pedro Hospital).

References and appendices

References

- Aggarwal, G., and S.D. Adhikary. 2017. "Simulators in the urological training armamentarium: A boon or a bane?". *Arab J Urol* 15(2):166–169.
- Alfieri, A., and G. Zotteri. 2017. "Inventory theory and the Beer Game". *Int J Logist Res Appl* 20(4):381–404.
- Almagooshi, S. 2015. "Simulation Modelling in Healthcare: Challenges and Trends". *Procedia Manuf* 3:301–307.
- Anastassopoulou, C., L. Russo, A. Tsakris, and C. Siettos. 2020. "Data-based analysis, modelling and forecasting of the COVID-19 outbreak". *PLoS One* 15(3):e0230405.
- Anderberg, M.R. 1973. "Cluster Analysis for Applications". New York: Academic Press
- Anderson, D., C. Price, B. Golden, W. Jank, and E. Wasil. 2011. "Examining the discharge practices of surgeons at a large medical center". *Health Care Manag Sci* 14(4):338–347.
- Anderson, R.M., and R.M. May. 1991. "Infectious diseases of humans: dynamics and control". Oxford University Press, New York
- Azcarate, C., L. Esparza, and F. Mallor. 2020. "The problem of the last bed: Contextualization and a new simulation framework for analyzing physician decisions". *Omega* 96:102120.
- Azcárate, C., F. Mallor, and J. Barado. 2012. "Calibration of a decision-making process in a simulation model by a bicriteria optimization problem". In: Proceedings of the 2012 Winter Simulation Conference. Berlin, Germany, pp 782–791
- Azevedo, L.C., I.A. De Souza, D.A. Zygun, H.T. Stelfox, and S.M. Bagshaw. 2015. "Association between Nighttime Discharge from the Intensive Care Unit and Hospital Mortality: A Multi-Center Retrospective Cohort Study". *BMC Health Serv Res* 15(1):378.
- Baas, S., S. Dijkstra, A. Braaksma, P. van Rooij, F.J. Snijders, L. Tiemessen, et al. 2021. "Real-time forecasting of COVID-19 bed occupancy in wards and intensive care units". *Health Care Manag Sci* 24:402–419.
- Bai, J., A. Fügner, J. Schoenfelder, and J.O. Brunner. 2018. "Operations research in intensive care unit management: a literature review". *Health Care Manag Sci* 21(1):1–24.
- Barado, J., J.M. Guergué, L. Esparza, C. Azcárate, F. Mallor, and S. Ochoa. 2012. "A mathematical model for simulating daily bed occupancy in an intensive care unit". *Crit Care Med* 40(4):1098–1104.
- Barnato, A.E., J.M. Kahn, G.D. Rubenfeld, K. McCauley, D. Fontaine, J.J. Frassica, et al. 2007. "Prioritizing the organization and management of intensive care services in the United States: The PrOMIS Conference". *Crit Care Med* 35(4):1003–1011.
- Bathke, D.J., T. Haigh, T. Bernadt, N. Wall, H. Hill, and A. Carson. 2019. "Using Serious Games to Facilitate Collaborative Water Management Planning Under Climate Extremes". *J Contemp Water Res Educ* 167(1):50–67.
- Bean, D.M., P. Taylor, and R.J.B. Dobson. 2019. "A patient flow simulator for healthcare management education". *BMJ Simul Technol Enhanc Learn* 5(1):46–48.

- Bing-Hua, Y.U. 2014. "Delayed admission to intensive care unit for critically surgical patients is associated with increased mortality". *Am J Surg* 208(2):268–274.
- Borg, I., and P.J.F. Groenen. 2005. "Modern Multidimensional Scaling: Theory and Applications". 2nd ed. New York: Springer
- Borrajo, F., Y. Bueno, I. de Pablo, B. Santos, F. Fernández, J. García, et al. 2010. "SIMBA: A simulator for business education and research". *Decis Support Syst* 48(3):498–506.
- Brailsford, S.C., P.R. Harper, B. Patel, and M. Pitt. 2009. "An analysis of the academic literature on simulation and modelling in health care". *J Simul* 3(3):130–140.
- Brauer, F., and C. Castillo-Chavez. 2012. "Mathematical models in population biology and epidemiology, 2nd edn.". Springer, New York
- Brown, R., R. Rasmussen, I. Baldwin, and P. Wyeth. 2012. "Design and implementation of a virtual world training simulation of ICU first hour handover processes". *Aust Crit Care* 25(3):178–187.
- Brown, S.J., D.A. Lieberman, B.A. Gemeny, Y.C. Fan, D.M. Wilson, and D.J. Pasta. 1997. "Educational video game for juvenile diabetes: Results of a controlled trial". *Med Informatics* 22(1):77–89.
- Buja, A., D.F. Swayne, M.L. Littman, N. Dean, H. Hofmann, and L. Chen. 2008. "Data Visualization With Multidimensional Scaling". *J Comput Graph Stat* 17(2):444–472.
- Campbell, A.J., J.A. Cook, G. Adey, and B.H. Cuthbertson. 2008. "Predicting death and readmission after intensive care discharge". *Br J Anaesth* 100(5):656–662.
- Capuzzo, M., R.P. Moreno, and R. Alvisi. 2010. "Admission and discharge of critically ill patients". *Curr Opin Crit Care* 16(5):499–504.
- Cardoso, L.T., C.M. Grion, T. Matsuo, E.H. Anami, I.A. Kauss, L. Seko, et al. 2011. "Impact of delayed admission to intensive care units on mortality of critically ill patients: a cohort study". *Crit Care* 15(1):R28.
- Carrasco, G., À. Pallarés, and L. Cabré. 2006. "Costes de la calidad en medicina intensiva. Guía para gestores clínicos". *Med Intensiva* 30(4):167–179.
- Casella, F. 2021. "Can the COVID-19 epidemic be controlled on the basis of daily test reports?". *IEEE Control Syst Lett* 5(3):1079–1084.
- Cássaro, F.A.M., and L.F. Pires. 2020. "Can we predict the occurrence of COVID-19 cases? Considerations using a simple model of growth". *Sci Total Environ* 728:138834.
- Cha, M., S. Han, J. Lee, and B. Choi. 2012. "A virtual reality based fire training simulator integrated with fire dynamics data". *Fire Saf J* 50:12–24.
- Chalfin, D.B., S. Trzeciak, A. Likourezos, B.M. Baumann, R.P. Dellinger, and DELAY-ED Study Group. 2007. "Impact of delayed transfer of critically ill patients from the emergency department to the intensive care unit". *Crit Care Med* 35(6):1477–1483.
- Cheung, W.K., J. Myburgh, I.M. Seppelt, M.J. Parr, N. Blackwell, S. DeMonte, et al. 2012. "A multicentre evaluation of two intensive care unit triage protocols for use in an influenza pandemic". *Med J Aust* 197(3):178–181.
- Choi, S.-S., S.-H. Cha, and C.C. Tappert. 2010. "A Survey of Binary Similarity and Distance Measures". *J Syst Cybern Informatics* 8:43–48.
- Christian, M.D., C.L. Sprung, M.A. King, J.R. Dichter, N. Kissoon, A. V Devereaux, et al. 2014. "Triage: Care of the critically ill and injured during pandemics and disasters: CHEST consensus statement". *Chest* 146(4 Suppl):e61S-e74S.
- Chung, C.A., and A. Huda. 1999. "An interactive multimedia training simulator for responding to bomb threats". *Simulation* 72(2):68–77.
- Colmenero, M. 2011. "El ritual de la falta de camas". *Med Intensiva* 35(3):139–142.
- Combes, A., C.E. Luyt, J.L. Trouillet, J. Chastre, and C. Gibert. 2005. "Adverse effect on a referral intensive care unit's performance of accepting patients transferred from another intensive care unit". *Crit Care Med* 33(4):705–710.

- Costa, A.X., S.A. Ridley, A.K. Shahani, P.R. Harper, V. De Senna, and M.S. Nielsen. 2003. "Mathematical modelling and simulation for planning critical care capacity". *Anaesthesia* 58(4):320–327.
- Currie, C.S.M., J.W. Fowler, K. Kotiadis, T. Monks, B.S. Onggo, D.A. Robertson, et al. 2020. "How simulation modelling can help reduce the impact of COVID-19". *J Simul* 14(2):83–97.
- D'Atri, A., P. Spagnoletti, A. Banzato, C. Bonelli, E. D'Atri, V. Traversi, et al. 2009. "From supply chains to supply networks: The Beer Game evolution". *IFAC Proc Vol* 42(4):1316–1321.
- de Freitas, S.I. 2006. "Using games and simulations for supporting learning". *Learn Media Technol* 31(4):343–358.
- Deza, M.M., and E. Deza. 2016. "Encyclopedia of distances". 4th ed. Berlin: Springer
- Diekmann, O., and J.A.P. Heesterbeek. 2000. "Mathematical epidemiology of infectious diseases: model building, analysis and interpretation". John Wiley, Chichester
- Dobson, G., H.H. Lee, and E. Pinker. 2010. "A Model of ICU Bumping". *Oper Res* 58(6):1564–1576.
- Dolbear, Jr., F.T., R. Attiyeh, and W.C. Brainard. 1968. "A Simulation Policy Game for Teaching Macroeconomics". *Am Econ Rev* 58(2):458–468.
- Dong, X., and T. Mathew. 2015. "Central tolerance regions and reference regions for multivariate normal populations". *J Multivar Anal* 134:50–60.
- Duke, G.J., M.D. Buist, D. Pilcher, C.D. Scheinkestel, J.D. Santamaria, G.A. Gutteridge, et al. 2009. "Interventions to circumvent intensive care access block: A retrospective 2-year study across metropolitan Melbourne". *Med J Aust* 190(7):375–378.
- Ebinger, J., M. Wells, D. Ouyang, T. Davis, N. Kaufman, S. Cheng, et al. 2021. "A Machine Learning Algorithm Predicts Duration of hospitalization in COVID-19 patients". *Intell Med* 5:100035.
- Elsawah, S., A. McLucas, and J. Mazanov. 2017. "An empirical investigation into the learning effects of management flight simulators: A mental models approach". *Eur J Oper Res* 259(1):262–272.
- Embriaco, N., L. Papazian, N. Kentish-Barnes, F. Pochard, and E. Azoulay. 2007. "Burnout syndrome among critical care healthcare workers". *Curr Opin Crit Care* 13(5):482–488.
- Erhard, M., J. Schoenfelder, A. Fügener, and J.O. Brunner. 2018. "State of the art in physician scheduling". *Eur J Oper Res* 265(1):1–18.
- European Centre for Disease Prevention and Control (ECDC). COVID-19 2020. <https://www.ecdc.europa.eu/en/novel-coronavirus-china>. Accessed 30 Jul 2020
- European Commission (EC). COVID-19. https://ec.europa.eu/health/coronavirus_en. Accessed 30 Jul 2020
- Farcomeni, A., A. Maruotti, F. Divino, G. Jona-Lasinio, and G. Lovison. 2021. "An ensemble approach to short-term forecast of COVID-19 intensive care occupancy in Italian regions". *Biometrical J* 63(3):503–513.
- Ferguson, N.M., D.A.T. Cummings, S. Cauchemez, C. Fraser, S. Riley, A. Meeyai, et al. 2005. "Strategies for containing an emerging influenza pandemic in Southeast Asia". *Nature* 437:209–214.
- Fetter, R.B., and J.D. Thompson. 1965. "The Simulation of Hospital Systems". *Oper Res* 13(5):689–711.
- Fone, D., S. Hollinghurst, M. Temple, A. Round, N. Lester, A. Weightman, et al. 2003. "Systematic review of the use and value of computer simulation modelling in population health and health care delivery". *J Public Health Med* 25(4):325–335.
- Fried, M.P., B. Sadoughi, M.J. Gibber, J.B. Jacobs, R.A. Lebowitz, D.A. Ross, et al. 2010. "From virtual reality to the operating room: The endoscopic sinus surgery simulator experiment". *Otolaryngol - Head Neck Surg* 142(2):202–207.
- García-Vicuña, D., M. Cildoz, M. Gastón-Romeo, C. Azcarate, F. Mallor, and L. Esparza. 2020a. "Operations research helps public health services managers planning resources in the COVID-19 crisis". *Bol Estad e Invest Oper* 36(2):127–151.
- García-Vicuña, D., L. Esparza, and F. Mallor. 2020b. "Safely learning intensive care unit management by using a management flight simulator". *Oper Res Heal Care* 27:100274.
- García-Vicuña, D., L. Esparza, and F. Mallor. 2021. "Hospital preparedness during epidemics using simulation:

- the case of COVID-19". *Cent Eur J Oper Res*. DOI: 10.1007/s10100-021-00779-w
- García-Vicuña, D., and F. Mallor. 2021. "Un modelo para predecir cuántas camas UCI harán falta durante cada oleada". <https://theconversation.com/un-modelo-para-predecir-cuantas-camas-uci-haran-falta-durante-cada-oleada-158101>. Accessed 15 Dec 2021
- Geitona, M., L. Androutsou, and D. Theodoratou. 2010. "Cost estimation of patients admitted to the intensive care unit: A case study of the Teaching University Hospital of Thessaly". *J Med Econ* 13(2):179–184.
- Ghazvini, K., S. Mansouri, M. Shakeri, M. Youssefi, M. Derakhshan, and M. Keikha. 2019. "Prediction of Tuberculosis Using a Logistic Regression Model". *Rev Cinical Med* 6(3):108–112.
- Giordano, G., F. Blanchini, R. Bruno, P. Colaneri, A. Di Filippo, A. Di Matteo, et al. 2020. "Modelling the COVID-19 epidemic and implementation of population-wide interventions in Italy". *Nat Med* 26:855–860.
- Godio, A., F. Pace, and A. Vergnano. 2020. "SEIR modeling of the Italian epidemic of SARS-CoV-2 using computational swarm intelligence". *Int J Environ Res Public Health* 17(10):3535.
- Goic, M., M.S. Bozanic-Leal, M. Badal, and L.J. Basso. 2021. "COVID-19: Short-term forecast of ICU beds in times of crisis". *PLoS One* 16(1):e0245272.
- Goldberg, S.L., and B.W. Knerr. 1997. "Collective training in virtual environments: Exploring performance requirements for dismounted soldier simulation". In: Siedel RJ, Chatelier PR (eds) *Virtual reality, training's future?: Perspectives on virtual reality and related emerging technologies*. New York: Plenum, pp 41–51
- Gompertz, B. 1825. "On the nature of the function expressive of the law of human mortality, and on a new mode of determining the value of life contingencies". *Philos Trans R Soc London B Biol Sci* 182:513–585.
- Goodwin, J.S., and S.G. Franklin. 1994. "The Beer Distribution Game: Using Simulation to Teach Systems Thinking". *J Manag Dev* 13(8):7–15.
- Government of Navarre. <https://gobiernoabierto.navarra.es>. Accessed 30 Jul 2020
- Grasselli, G., A. Pesenti, and M. Cecconi. 2020. "Critical care utilization for the COVID-19 outbreak in Lombardy, Italy: early experience and forecast during an emergency response". *JAMA* 323(16):1545–1546.
- Grassly, N.C., and C. Fraser. 2008. "Mathematical models of infectious disease transmission". *Nat Rev Microbiol* 6(6):477–487.
- Green, L. V. 2002. "How many hospital beds?". *Inquiry* 39(4):400–412.
- Griffiths, J.D., V. Knight, and I. Komenda. 2013. "Bed management in a Critical Care Unit". *IMA J Manag Math* 24(2):137–153.
- Griffiths, J.D., N. Price-Lloyd, M. Smithies, and J.E. Williams. 2005. "Modelling the requirement for supplementary nurses in an intensive care unit". *J Oper Res Soc* 56(2):126–133.
- Grunewald, M., R.A. Heckemann, H. Gebhard, M. Lell, and W.A. Bautz. 2003. "COMPARE radiology: creating an interactive Web-based training program for radiology with multimedia authoring software". *Acad Radiol* 10(5):543–553.
- Guan, W., Z. Ni, Y. Hu, W. Liang, C. Ou, J. He, et al. 2020. "Clinical characteristics of coronavirus disease 2019 in China". *N Engl J Med* 382:1708–1720.
- Günal, M.M., and M. Pidd. 2010. "Discrete event simulation for performance modelling in health care: A review of the literature". *J Simul* 4(1):42–51.
- Guttman, L. 1968. "A general nonmetric technique for finding the smallest coordinate space for a configuration of points". *Psychometrika* 33:469–506.
- Hall, R. 2013. *Patient Flow: Reducing Delay in Healthcare Delivery*. 2nd ed. New York: Springer
- Halpern, N.A., and S.M. Pastores. 2015. "Critical care medicine beds, use, occupancy, and costs in the United States: A methodological review". *Crit Care Med* 43(11):2452–2459.
- Halpern, N.A., and S.M. Pastores. 2010. "Critical care medicine in the United States 2000-2005: An analysis of bed numbers, occupancy rates, payer mix, and costs". *Crit Care Med* 38(1):65–71.
- Halpern, N.A., S.M. Pastores, J.M. Oropello, and V. Kvetan. 2013. "Critical care medicine in the united states: Addressing the intensivists shortage and image of the specialty". *Crit Care Med* 41(12):2754–2761.

- Hamming, R.W. 1950. "Error detecting and error correcting codes". *Bell Syst Tech J* 29(2):147–160.
- Hans, E.W., and T. Nieberg. 2007. "Operating Room Manager Game". *INFORMS Trans Educ* 8(1):25–36.
- He, H., C. Hu, N. Xiong, C. Liu, and X. Huang. 2020. "How to transform a general hospital into an "infectious disease hospital" during the epidemic of COVID-19". *Crit Care* 24:145.
- Hellewell, J., S. Abbott, A. Gimma, N.I. Bosse, C.I. Jarvis, T.W. Russell, et al. 2020. "Feasibility of controlling COVID-19 outbreaks by isolation of cases and contacts". *Lancet Glob Heal* 8(4):e488–e496.
- Hethcote, H.W. 2000. "The mathematics of infectious diseases". *SIAM Rev* 42(4):599–653.
- Homer, J., G. Hirsch, and B. Milstein. 2007. "Chronic illness in a complex health economy: the perils and promises of downstream and upstream reforms". *Syst Dyn Rev banner* 23(2–3):313–343.
- Horimoto, K., I. Hofuku, and K. Oshima. 1997. "Population dynamics of HIV positive by application of a locally modified Gompertz curve: A case study for Japan". *Nonlinear Anal Theory, Methods Appl* 30(2):985–993.
- Iapichino, G., L. Gattinoni, D. Radrizzani, B. Simini, G. Bertolini, L. Ferla, et al. 2004. "Volume of activity and occupancy rate in intensive care units. Association with mortality". *Intensive Care Med* 30(2):290–297.
- Ioannidis, J.P.A., S. Cripps, and M.A. Tanner. 2020. "Forecasting for COVID-19 has failed". *Int J Forecast*. DOI: 10.1016/j.ijforecast.2020.08.004
- Jaccard, P. 1901. "Étude comparative de la distribution florale dans une portion des Alpes et du Jura". *Bull la Soc Vaudoise des Sci Nat* 37(142):547–579.
- Jain, S., S. Lee, S.R. Barber, E.H. Chang, and Y.J. Son. 2019. "Virtual reality based hybrid simulation for functional endoscopic sinus surgery". *IIEE Trans Healthc Syst Eng*. DOI: 10.1080/24725579.2019.1692263
- Jin, H.W. 2015. "Analysis of student behavior in the beer game". *Inf* 18(6):2275–2282.
- Joseph, M.L. 1965. "Role Playing in Teaching Economics". *Am Econ Rev* 55(1–2):556–565.
- Kahn, M.A., and K.M. Perez. 2009. "The game of politics simulation: An exploratory study". *J Polit Sci Educ* 5(4):332–349.
- Katsaliaki, K., and N. Mustafee. 2011. "Applications of simulation within the healthcare context". *J Oper Res Soc* 62(8):1431–1451.
- Katsaliaki, K., N. Mustafee, and S. Kumar. 2014. "A game-based approach towards facilitating decision making for perishable products: An example of blood supply chain". *Expert Syst Appl* 41(9):4043–4059.
- Kermack, W.O., and A.G. McKendrick. 1927. "A contribution to the mathematical theory of epidemics". *Proc R Soc Lond A* 115(772):700–721.
- Kim, R., J. Kim, I. Lee, U. Yeo, and S. Lee. 2019. "Development of a VR simulator for educating CFD-computed internal environment of piglet house". *Biosyst Eng* 188:243–264.
- Kim, S.C., I. Horowitz, K.K. Young, and T.A. Buckley. 1999. "Analysis of capacity management of the intensive care unit in a hospital". *Eur J Oper Res* 115(1):36–46.
- Kim, S.C., I. Horowitz, K.K. Young, and T.A. Buckley. 2000. "Flexible bed allocation and performance in the intensive care unit". *J Oper Manag* 18(4):427–443.
- Koglbauer, I. 2015. "Simulator Training Improves the Estimation of Collision Parameters and the Performance of Student Pilots". *Procedia - Soc Behav Sci* 209:261–267.
- Kolker, A. 2009. "Process modeling of ICU patient flow: Effect of daily load leveling of elective surgeries on ICU diversion". *J Med Syst* 33(1):27–40.
- Kraemer, A.D., E. Villani, and D.H. Arjoni. 2019. "Aircraft FDI and human factors analysis of a take-off manoeuvre using SIVOR flight simulator". *IFAC-PapersOnLine* 51(34):184–189.
- Kramer, A.A., T.L. Higgins, and J.E. Zimmerman. 2012. "Intensive care unit readmissions in U.S. hospitals: Patient characteristics, risk factors, and outcomes". *Crit Care Med* 40(1):3–10.
- Kramer, A.A., T.L. Higgins, and J.E. Zimmerman. 2013. "The association between ICU readmission rate and patient outcomes". *Crit Care Med* 41(1):24–33.
- Kraus, M., M.S. Rauner, and S. Schwarz. 2010. "Hospital management games: A taxonomy and extensive

- review". *Cent Eur J Oper Res* 18(4):567–591.
- Kucharski, A.J., T.W. Russell, C. Diamond, Y. Liu, J. Edmunds, S. Funk, et al. 2020. "Early dynamics of transmission and control of COVID-19: a mathematical modelling study". *Lancet Infect Dis* 20(5):553–558.
- Lamé, G., and R.K. Simmons. 2018. "From behavioural simulation to computer models : how simulation can be used to improve healthcare management and policy". *BMJ Simul Technol Enhanc Learn* :Published Online First: 20 October 2018.
- Lane, J.L., S. Slavin, and A. Ziv. 2001. "Simulation in medical education: A review". *Simul Gaming* 32(3):297–314.
- Law, A.M. 2014. "Simulation modeling and analysis, 5th edn.". McGraw-Hill, New York
- Lefrant, J.Y., B. Garrigues, C. Pribil, I. Bardoulat, F. Courtial, F. Maurel, et al. 2015. "The daily cost of ICU patients: A micro-costing study in 23 French Intensive Care Units". *Anaesth Crit Care Pain Med* 34(3):151–157.
- Lengwiler, Y. 2004. "A monetary policy simulation game". *J Econ Educ* 35(2):175–183.
- Lenzen, M., M. Li, A. Malik, F. Pomponi, Y.-Y. Sun, T. Wiedmann, et al. 2020. "Global socio-economic losses and environmental gains from the Coronavirus pandemic". *PLoS One* 15(7):e0235654.
- Li, C.H., C.C. Tsai, and S.Y. Yang. 2014. "Analysis of epidemic spreading of an SIRS model in complex heterogeneous networks". *Commun Nonlinear Sci Numer Simul* 19(4):1042–1054.
- Li, G.H., and Y.X. Zhang. 2017. "Dynamic behaviors of a modified SIR model in epidemic diseases using nonlinear incidence and recovery rates". *PLoS One* 12(4):e0175789.
- Ligtenberg, J.J.M., L.G. Arnold, Y. Stienstra, T.S. van der Werf, J.H.J.M. Meertens, J.E. Tulleken, et al. 2005. "Quality of interhospital transport of critically ill patients: a prospective audit.". *Crit Care* 9(4):446–451.
- Lin, F., W. Chaboyer, and M. Wallis. 2009. "A literature review of organisational, individual and teamwork factors contributing to the ICU discharge process". *Aust Crit Care* 22(1):29–43.
- Lin, Q., S. Zhao, D. Gao, Y. Lou, S. Yang, S.S. Musa, et al. 2020. "A conceptual model for the coronavirus disease 2019 (COVID-19) outbreak in Wuhan, China with individual reaction and governmental action". *Int J Infect Dis* 93:211–216.
- Litvak, N., M. van Rijsbergen, R.J. Boucherie, and M. van Houdenhoven. 2008. "Managing the overflow of intensive care patients". *Eur J Oper Res* 185(3):998–1010.
- Liu, W., S. Tang, and Y. Xiao. 2015. "Model Selection and Evaluation Based on Emerging Infectious Disease Data Sets including A/H1N1 and Ebola". *Comput Math Methods Med* 2015:207105.
- Longini, I.M., A. Nizam, S. Xu, K. Ungchusak, W. Hanshaoworakul, D.A.T. Cummings, et al. 2005. "Containing pandemic influenza at the source". *Science (80-)* 309(5737):1083–1087.
- Lopez-Beauchamp, C., G.A. Singh, S.Y. Shin, and M.T. Magone. 2020. "Surgical simulator training reduces operative times in resident surgeons learning phacoemulsification cataract surgery". *Am J Ophthalmol Case Reports* 17:100576.
- Magal, P., O. Seydi, and G. Webb. 2016. "Final size of an epidemic for a two-group SIR model". *SIAM J Appl Math* 76(5):2042–2059.
- Mahalanobis, P.C. 1936. "On the Generalised Distance in Statistics". In: Proceedings of the National Institute of Sciences of India. pp 49–55
- Mahomed, S., and O.H. Mahomed. 2018. "Cost of intensive care services at a central hospital in South Africa". *South African Med J* 109(1):35–39.
- Malavika, B., S. Marimuthu, M. Joy, A. Nadaraj, E. Sam, and L. Jeyaseelan. 2021. "Forecasting COVID-19 epidemic in India and high incidence states using SIR and logistic growth models". *Clin Epidemiol Glob Heal* 9:26–33.
- Mallor, F., and C. Azcárate. 2014. "Combining optimization with simulation to obtain credible models for intensive care units". *Ann Oper Res* 221(1):255–271.
- Mallor, F., C. Azcárate, and J. Barado. 2015. "Optimal control of ICU patient discharge: from theory to

- implementation". *Health Care Manag Sci* 18(3):234–250.
- Mallor, F., C. Azcárate, and J. Barado. 2016. "Control problems and management policies in health systems: application to intensive care units". *Flex Serv Manuf J* 28(1–2):62–89.
- Manca, D., D. Caldiroli, and E. Storti. 2020. "A simplified math approach to predict ICU beds and mortality rate for hospital emergency planning under Covid-19 pandemic". *Comput Chem Eng* 140:106945.
- Marmor, Y.N., T.R. Rohleder, D.J. Cook, T.R. Huschka, and J.E. Thompson. 2013. "Recovery bed planning in cardiovascular surgery: a simulation case study". *Health Care Manag Sci* 16(4):314–327.
- Masterson, B.J., T.G. Mihara, G. Miller, S.C. Randolph, M.E. Forkner, and A.L. Crouter. 2004. "Using models and data to support optimization of the military health system: A case study in an intensive care unit". *Health Care Manag Sci* 7(3):217–224.
- McManus, M.L., M.C. Long, A. Cooper, and E. Litvak. 2004. "Queuing Theory Accurately Models the Need for Critical Care Resources". *Anesthesiology* 100(5):1271–1276.
- Mead, A. 1992. "Review of the Development of Multidimensional Scaling Methods". *J R Stat Soc Ser D (The Stat* 41(1):27–39.
- Mielczarek, B., and J. Uziako-Mydlikowska. 2012. "Application of computer simulation modeling in the health care sector: A survey". *Simulation* 88(2):197–216.
- Milstein, B., and G. Hirsch. 2009. "The HealthBound Policy Simulation Game: An Adventure in US Health Reform". In: Proceedings of the 27th International Conference of the System Dynamics Society. Albuquerque, NM
- Milstein, B., J. Homer, P. Briss, D. Burton, and T. Pechacek. 2011. "Why behavioral and environmental interventions are needed to improve health at lower cost". *Health Aff* 30(5):823–832.
- Milstein, B., J. Homer, and G. Hirsch. 2010. "Analyzing national health reform strategies with a dynamic simulation model". *Am J Public Health* 100(5):811–819.
- Moxnes, E., and A.K. SAYSSEL. 2009. "Misperceptions of global climate change: Information policies". *Clim Change* 93(1):15–37.
- Müllner, D. 2011. "Modern hierarchical, agglomerative clustering algorithms". arXiv:1109.2378.
- Murk, J.L., R. van de Biggelaar, J. Stohr, J. Verweij, A. Buiting, S. Wittens, et al. 2020. "De eerste honderd opgenomen COVID-19-patiënten in het Elisabeth-Tweesteden Ziekenhuis [The first 100 COVID-19 patients admitted to the Elisabeth-Tweesteden Hospital, Tilburg, The Netherlands]". *Ned Tijdschr Geneesk* 164:D5002.
- Murthy, S., and H. Wunsch. 2012. "Clinical review: International comparisons in critical care - lessons learned". *Crit Care* 16(2):218.
- Nates, J.L., M. Nunnally, R. Kleinpell, S. Blosser, J. Goldner, B. Birriel, et al. 2016. "ICU admission, discharge, and triage guidelines: A framework to enhance clinical operations, development of institutional policies, and further research"
- Nguyen, J.M., P. Six, R. Parisot, D. Antonioli, F. Nicolas, and P. Lombrail. 2003. "A universal method for determining intensive care unit bed requirements". *Intensive Care Med* 29(5):849–852.
- Novel, C.P.E.R.E. 2020. "The epidemiological characteristics of an outbreak of 2019 novel coronavirus diseases (COVID-19) in China". *Zhonghua Liu Xing Bing Xue Za Zhi* 41(2):145–151.
- Nsoesie, E.O., R.J. Beckman, and M. V. Marathe. 2012. "Sensitivity analysis of an individual-based model for simulation of influenza epidemics". *PLoS One* 7(10):e45414.
- Nsoesie, E.O., J.S. Brownstein, N. Ramakrishnan, and M. V. Marathe. 2014. "A systematic review of studies on forecasting the dynamics of influenza outbreaks". *Influenza Other Respi Viruses* 8(3):309–316.
- Oliveira, D.M., S.C. Cao, X.F. Hermida, and F.M. Rodríguez. 2007. "Virtual reality system for industrial training". In: Proceedings of 2007 IEEE International Symposium on Industrial Electronics. Vigo, Spain, pp 1715–1720
- Oliveira Zardin, A.M. da S., C.A.L. de Oliveira, S.N. de Oliveira, G.M. Yoshida, D.T. de Albuquerque, C.M. de

- Campos, et al. 2019. "Growth curves by Gompertz nonlinear regression model for male and female Nile tilapias from different genetic groups". *Aquaculture* 511:734243.
- Oribe-Pérez, I.A., I. Velázquez-Abunader, and G.R. Poot-López. 2020. "Age and multi-model growth estimation of white grunt, *Haemulon plumieri*, in the southern Gulf of Mexico from otolith macrostructure analysis". *Reg Stud Mar Sci* 34:101069.
- Ouanes, I., C. Schwebel, A. Français, C. Bruel, F. Philippart, A. Vesin, et al. 2012. "A model to predict short-term death or readmission after intensive care unit discharge". *J Crit Care* 27(4):422.e1-422.e9.
- Palanca, I., A. Esteban de la Torre, J. Elola, J.L. Bernal, and J.L. Paniagua. 2011. "Plan de Calidad del Sistema Nacional de Salud. Unidades de Cuidados Intensivos. Estándares y recomendaciones". <https://www.msbs.gob.es/organizacion/sns/planCalidadSNS/docs/UCI.pdf>
- Palominos, E., T. Levett-Jones, T. Power, and R. Martinez-Maldonado. 2019. "Healthcare students' perceptions and experiences of making errors in simulation: An integrative review". *Nurse Educ Today* 77:32–39.
- Panovska-Griffiths, J. 2020. "Can mathematical modelling solve the current Covid-19 crisis?". *BMC Public Health* 20:551.
- Pearson, G.A., F. Reynolds, and J. Stickley. 2012. "Calculating the need for intensive care beds". *Arch Dis Child* 97(11):943–946.
- Pennock, M.J., Z. Yu, K.B. Hirschman, K. Pepe, M. V Pauly, M.D. Naylor, et al. 2018. "Developing a Policy Flight Simulator to Facilitate the Adoption of an Evidence-Based Intervention". *IEEE J Transl Eng Heal Med* 6:1–12.
- Persson, J. 2017. "A review of the design and development processes of simulation for training in healthcare – A technology-centered versus a human-centered perspective". *Appl Ergon* 58:314–326.
- Petzoldt, T. 2019. growthrates: Estimate Growth Rates from Experimental Data. R package version 0.8.1. <https://cran.r-project.org/package=growthrates>
- Poston, J.T., B.K. Patel, and A.M. Davis. 2020. "Management of critically ill adults with COVID-19". *JAMA - J Am Med Assoc* 323(18):1839–1841.
- Pozo-Barajas, R., M.D.P. Pablo-Romero, and R. Caballero. 2013. "Evaluating a computer-based simulator program to teach the principles of macroeconomic equilibria". *Comput Educ* 69:71–84.
- Pronovost, P.J., D.M. Needham, H. Waters, C.M. Birkmeyer, J.R. Calinawan, J.D. Birkmeyer, et al. 2004. "Intensive care unit physician staffing: Financial modeling of the Leapfrog standard". *Crit Care Med* 32(6):1247–1253.
- Python Software Foundation. Python Language Reference, version 3.7.3. <http://www.python.org>
- Rais, A., and A. Viana. 2011. "Operations research in healthcare: A survey". *Int Trans Oper Res* 18(1):1–31.
- Rauner, M.S., M. Kraus, and S. Schwarz. 2008. "Competition under different reimbursement systems: The concept of an internet-based hospital management game". *Eur J Oper Res* 185(3):948–963.
- Rauner, M.S., H. Niessner, U. Leopold-Wildburger, N. Peric, and T. Herdlicka. 2016. "A policy management game for mass casualty incidents: an experimental study". *Flex Serv Manuf J* 28(1–2):336–365.
- Richards, F.J. 1959. "A flexible growth function for empirical use". *J Exp Bot* 10(2):290–301.
- Ricker, W.E. 1979. "Growth rates and models". *Fish Physiol* 8:677–743.
- Ridge, J.C., S.K. Jones, M.S. Nielsen, and A.K. Shahani. 1998. "Capacity planning for intensive care units". *Eur J Oper Res* 105(2):346–355.
- Robert, R., J. Reignier, C. Tournoux-Facon, T. Boulain, O. Lesieur, V. Gissot, et al. 2012. "Refusal of intensive care unit admission due to a full unit: Impact on mortality". *Am J Respir Crit Care Med* 185(10):1081–1087.
- Roberts, M.G., and A.K. Saha. 1999. "The asymptotic behaviour of a logistic epidemic model with stochastic disease transmission". *Appl Math Lett* 12(1):37–41.
- Roda, W.C., M.B. Varughese, D. Han, and M.Y. Li. 2020. "Why is it difficult to accurately predict the COVID-19 epidemic?". *Infect Dis Model* 5:271–281.

- Rodrigues, F., G.S. Zaric, and D.A. Stanford. 2018. "Discrete event simulation model for planning Level 2 "step-down" bed needs using NEMS". *Oper Res Heal Care* 17:42–54.
- Rodríguez, J.T., B. Vitoriano, and J. Montero. 2010. "A natural-disaster management DSS for Humanitarian Non-Governmental Organisations". *Knowledge-Based Syst* 23(1):17–22.
- Rypdal, K., and M. Rypdal. 2020. "A parsimonious description and cross-country analysis of COVID-19 epidemic curves". *Int J Environ Res Public Health* 17(18):6487.
- Saastamoinen, K., A. Rissanen, and R. Linnervuo. 2019. "Usage of simulators to boost marine corps learning". *Procedia Comput Sci* 159:1011–1018.
- Salleh, S., P. Thokala, A. Brennan, R. Hughes, and A. Booth. 2017. "Simulation modelling in healthcare: An umbrella review of systematic literature reviews". *Pharmacoeconomics* 35:937–949.
- Sánchez-Villegas, P., and A. Daponte Codina. 2020. "Modelos predictivos de la epidemia de COVID-19 en España con curvas de Gompertz". *Gac Sanit*. DOI: 10.1016/j.gaceta.2020.05.005
- Sarkar, B.B., and N. Chaki. 2012. "A Distributed Retail Beer Game for Decision Support System". *Procedia - Soc Behav Sci* 65:278–284.
- Sauré, A., and M.L. Puterman. 2014. "The Appointment Scheduling Game Antoine". *INFORMS Trans Educ* 14(2):73–85.
- Sawyer, B., and D. Rejeski. 2002. "Serious Games: Improving Public Policy through Gamebased Learning and Simulation". Woodrow Wilson Int Cent Sch
- Seymour, N.E., A.G. Gallagher, S.A. Roman, M.K. O'Brien, V.K. Bansal, D.K. Andersen, et al. 2002. "Virtual reality training improves operating room performance: results of a randomized, double-blinded study". *Ann Surg* 236(4):458–464.
- Shahani, A.K., S.A. Ridley, and M.S. Nielsen. 2008. "Modelling patient flows as an aid to decision making for critical care capacities and organisation". *Anaesthesia* 63(10):1074–1080.
- Shen, C.Y. 2020. "Logistic growth modelling of COVID-19 proliferation in China and its international implications". *Int J Infect Dis* 96:582–589.
- Sherif, A., and H. Mekki. 2010. "Excavation game: Computer-aided-learning tool for teaching construction engineering decision making". *J Prof Issues Eng Educ Pract* 136(4):188–196.
- Sherwood, R.J., and G. Francis. 2018. "The effect of mannequin fidelity on the achievement of learning outcomes for nursing, midwifery and allied healthcare practitioners: Systematic review and meta-analysis". *Nurse Educ Today* 69:81–94.
- Shmueli, A., C.L. Sprung, and E.H. Kaplan. 2003. "Optimizing admissions to an intensive care unit". *Health Care Manag Sci* 6(3):131–136.
- Singer, D.E., P.L. Carr, A.G. Mulley, and G.E. Thibault. 1983. "Rationing intensive care - Physician responses to a resource shortage". *N Engl J Med* 309(19):1155–1160.
- Sinuff, T., K. Kahnemouli, D.J. Cook, J.M. Luce, and M.M. Levy. 2004. "Rationing critical care beds: A systematic review". *Crit Care Med* 32(7):1588–1597.
- Snider, B., J. Balakrishnan, and G.J.C. da Silveira. 2010. "Running "The Beer Game" for Large Classes Details of Approach". In: Proceedings of Decision Sciences Institute (DSI) Forty-First Annual Meeting. San Diego, CA, pp 3251–3258
- Sobolev, B.G., G. Fradet, L. Kuramoto, and B. Rogula. 2013. "The occurrence of adverse events in relation to time after registration for coronary artery bypass surgery: A population-based observational study". *J Cardiothorac Surg* 8:74.
- Sprung, C.L., M. Baras, G. Iapichino, J. Kesecioglu, A. Lippert, C. Hargreaves, et al. 2012. "The Eldicus prospective, observational study of triage decision making in European intensive care units: Part I-European Intensive Care Admission Triage Scores". *Crit Care Med* 40(1):125–131.
- Sprung, C.L., M. Danis, G. Iapichino, A. Artigas, J. Kesecioglu, R. Moreno, et al. 2013. "Triage of intensive care patients: Identifying agreement and controversy". *Intensive Care Med* 39(11):1916–1924.

- Stannard, C.J., A.P. Williams, and P.A. Gibbs. 1985. "Temperature/growth relationships for psychrotrophic food-spoilage bacteria". *Food Microbiol* 2(2):115–122.
- Steinberg, E., A. Balakrishna, J. Habboushe, A. Shawl, and J. Lee. 2020. "Calculated decisions: COVID-19 calculators during extreme resource-limited situations". *Emerg Med Pract* 22(5):CD1–CD5.
- Steins, K., and S.M. Walther. 2013. "A generic simulation model for planning critical care resource requirements". *Anaesthesia* 68(11):1148–1155.
- Sterman, J.D. 1989a. "Modeling Managerial Behavior: Misperceptions of Feedback in a Dynamic Decision Making Experiment". *Manage Sci* 35(3):321–339.
- Sterman, J.D. 1992. "Teaching Takes Off: Flight Simulators for Management Education". *OR/MS Today* :40–44.
- Sterman, J.D. 1989b. "Misperceptions of Feedback in Dynamic Decision Making". *Organ Behav Hum Decis Process* 43(3):301–335.
- Strauss, M.J., J.P. LoGerfo, J.A. Yeltatzie, N. Temkin, and L.D. Hudson. 1986. "Rationing of intensive care unit services. An everyday occurrence". *J Am Med Assoc* 255(9):1143–1146.
- Streufert, S., U. Satish, and P. Barach. 2001. "Improving medical care : The use of simulation technology". *Simul Gaming* 32(2):164–174.
- Sun, K., J.S. Ren, T. Bai, J. Zhang, Q. Liu, W. Wu, et al. 2020. "A dynamic growth model of *Ulva prolifera*: Application in quantifying the biomass of green tides in the Yellow Sea, China". *Ecol Modell* 428:109072.
- Tabak, J. 2014. "Geometry: The Language of Space and Form". New York: Infobase Publishing
- Tan, S.S., J. Bakker, M.E. Hoogendoorn, A. Kapila, J. Martin, A. Pezzi, et al. 2012. "Direct cost analysis of intensive care unit stay in four European countries: Applying a standardized costing methodology". *Value Heal* 15(1):81–86.
- Teres, D. 1993. "Civilian triage in the intensive care unit the ritual of the last bed". *Crit Care Med* 21(4):598–606.
- Troy, P.M., and L. Rosenberg. 2009. "Using simulation to determine the need for ICU beds for surgery patients". *Surgery* 146(4):608–620.
- Utley, M., C. Pagel, M.J. Peters, A. Petros, and P. Lister. 2011. "Does triage to critical care during a pandemic necessarily result in more survivors?". *Crit Care Med* 39(1):179–183.
- Vahdatikhaki, F., K. El Ammari, A.K. Langroodi, S. Miller, A. Hammad, and A. Doree. 2019. "Beyond data visualization: A context-realistic construction equipment training simulators". *Autom Constr* 106:102853.
- Valentin, A., M. Capuzzo, B. Guidet, R. Moreno, B. Metnitz, P. Bauer, et al. 2009. "Errors in administration of parenteral drugs in intensive care units: Multinational prospective study". *BMJ* 338:b814.
- Valentin, A., P. Ferdinande, and ESICM Working Group on Quality Improvement. 2011. "Recommendations on basic requirements for intensive care units: structural and organizational aspects". *Intensive Care Med* 37(10):1575–1587.
- Valentino, K., K. Christian, and E. Joelianito. 2017. "Virtual reality flight simulator". *Internetworking Indones J* 9(1):21–25.
- van Miltenburg, H. 1989. "Simulation Game Economic Policy". In: Proceedings of the 5th Congress of the European Association for Research and Development in Higher Education (EARDHE) and the Dutch Association for Research and Development in Higher Education (CRWO). pp 521–524
- Vekaria, B., C. Overton, A. Wiśniowski, S. Ahmad, A. Aparicio-Castro, J. Curran-Sebastian, et al. 2021. "Hospital length of stay for COVID-19 patients: Data-driven methods for forward planning". *BMC Infect Dis* 21:700.
- Verdon, M., P. Merlani, T. Perneger, and B. Ricou. 2008. "Burnout in a surgical ICU team". *Intensive Care Med* 34(1):152–156.
- Viboud, C., L. Simonsen, and G. Chowell. 2016. "A generalized-growth model to characterize the early ascending phase of infectious disease outbreaks". *Epidemics* 15:27–37.
- Vliegen, I.M.H., and M.E. Zonderland. 2017. "Game—The BedGame—A Classroom Game Based on Real Healthcare Challenges". *INFORMS Trans Educ* 17(3):128–133.
- Wahl, A., T. Kongsvik, and S. Antonsen. 2020. "Balancing Safety I and Safety II: Learning to manage

- performance variability at sea using simulator-based training". *Reliab Eng Syst Saf* 195:106698.
- Walter, K.L., M. Siegler, and J.B. Hall. 2008. "How decisions are made to admit patients to medical intensive care units (MICUs): A survey of MICU directors at academic medical centers across the United States". *Crit Care Med* 36(2):414–420.
- Wang, C., P.W. Horby, F.G. Hayden, and G.F. Gao. 2020. "A novel coronavirus outbreak of global health concern". *Lancet* 395(10223):470–473.
- Ward, J.H. 1963. "Hierarchical Grouping to Optimize an Objective Function". *J Am Stat Assoc* 58(301):236–244.
- WHO. 2020a. "Statement on the second meeting of the International Health Regulations (2005) Emergency Committee regarding the outbreak of novel coronavirus (2019-nCoV)". [https://www.who.int/news/item/30-01-2020-statement-on-the-second-meeting-of-the-international-health-regulations-\(2005\)-emergency-committee-regarding-the-outbreak-of-novel-coronavirus-\(2019-ncov\)](https://www.who.int/news/item/30-01-2020-statement-on-the-second-meeting-of-the-international-health-regulations-(2005)-emergency-committee-regarding-the-outbreak-of-novel-coronavirus-(2019-ncov)). Accessed 15 Dec 2021
- WHO. 2020b. "WHO Director-General's opening remarks at the media briefing on COVID-19 - 11 March 2020". <https://www.who.int/director-general/speeches/detail/who-director-general-s-opening-remarks-at-the-media-briefing-on-covid-19---11-march-2020>. Accessed 15 Dec 2021
- Wood, R.M. 2020. "Modelling the impact of COVID-19 on elective waiting times.pdf". *J Simul*. DOI: 10.1080/17477778.2020.1764876
- World Health Organization (WHO). Coronavirus disease (COVID-19) outbreak. <https://www.who.int/emergencies/diseases/novel-coronavirus-2019>. Accessed 30 Jul 2020
- Worldometer - real time world statistics. <https://www.worldometers.info/coronavirus/>. Accessed 15 Jun 2020
- Worm, G.I.M., A.W.C. van der Helm, T. Lapikas, K.M. van Schagen, and L.C. Rietveld. 2010. "Integration of models, data management, interfaces and training support in a drinking water treatment plant simulator". *Environ Model Softw* 25(5):677–683.
- Wu, K., D. Darcet, Q. Wang, and D. Sornette. 2020. "Generalized logistic growth modeling of the COVID-19 outbreak: comparing the dynamics in the 29 provinces in China and in the rest of the world". *Nonlinear Dyn* 101:1561–1581.
- Xia, C.Y., S.W. Sun, Z.X. Liu, Z.Q. Chen, and Z.Z. Yuan. 2009. "Epidemics of sirs model with nonuniform transmission on scale-free networks". *Int J Mod Phys B* 23(9):2203–2213.
- Yang, M., M.J. Fry, J. Raikhelkar, C. Chin, A. Anyanwu, J. Brand, et al. 2013. "A model to create an efficient and equitable admission policy for patients arriving to the cardiothoracic ICU". *Crit Care Med* 41(2):414–422.
- Young, B.E., S.W.X. Ong, S. Kalimuddin, J.G. Low, S.Y. Tan, J. Loh, et al. 2020. "Epidemiologic features and clinical course of patients infected with SARS-CoV-2 in Singapore". *JAMA* 323(15):1488–1494.
- Young, M.P., V.J. Gooder, K. McBride, B. James, and E.S. Fisher. 2003. "Inpatient transfers to the intensive care unit: delays are associated with increased mortality and morbidity". *J Gen Intern Med* 18(2):77–83.
- Zhang, C., T. Grandits, K.P. Härenstam, J.B. Hauge, and S. Meijer. 2018. "Correction to: A systematic literature review of simulation models for non-technical skill training in healthcare logistics". *Adv Simul* 3:15.
- Zhang, J., L. Zhou, Y. Yang, W. Peng, W. Wang, and X. Chen. 2020. "Therapeutic and triage strategies for 2019 novel coronavirus disease in fever clinics". *Lancet Respir Med* 8(3):E11–E12.
- Zhou, F., T. Yu, R. Du, G. Fan, Y. Liu, Z. Liu, et al. 2020. "Clinical course and risk factors for mortality of adult inpatients with COVID-19 in Wuhan, China: a retrospective cohort study". *Lancet* 395(10229):1054–1062.
- Zhu, Z., B.H. Hen, and K.L. Teow. 2012. "Estimating ICU bed capacity using discrete event simulation". *Int J Health Care Qual Assur* 25(2):134–144.
- Zwietering, M.H., I. Jongenburger, F.M. Rombouts, and K. van 't Riet. 1990. "Modeling of the bacterial growth curve". *Appl Environ Microbiol* 56(6):1875–1881.
- Zyda, M. 2005. "From Visual to Virtual Reality to Games". *IEEE Comput Soc* 38(9):25–32.

A List of acronyms and their definitions

Table A.1 provides the list of acronyms and their definitions used in this thesis, sorted alphabetically. In total, 63 acronyms have been used.

Table A.1. List of acronyms and their definitions used in this thesis, sorted alphabetically.

Acronym	Definition
AES	Atrial extrasystoles
AF	Atrial fibrillation
AFL	Atrial flutter
AHC	Agglomerative Hierarchical Clustering
ALT	Alanine transferase
AMG	Adjusted Morbidity Group
AMI	Acute myocardial infarction
aPTT	Activated partial thromboplastin time
ARDS	Acute respiratory distress syndrome
AST	Aspartate transferase
AV	Atrioventricular
BCA	Bed control actions
CCAES	Health Alert and Emergency Coordination Centre
CK-MB	Creatine kinase myocardial band
CMC	Information system on hospital capacity
COPD	Chronic obstructive pulmonary disease
CT	Computed tomography
cTnI	Troponin I
DES	Discrete Event Simulation
EC	European Commission
ECDC	European Centre for Disease Prevention and Control
EM	Expectation-Maximization

EN	Enteral nutrition
ESICM	European Society of Intensive Care Medicine
GGT	Gamma-glutamyl transpeptidase
IABP	Intra-aortic balloon pump
ICP	Intracranial pressure
ICU	Intensive Care Unit
INR	International normalized ratio
ITA	Aeronautics Institute of Technology
LoS	Length of stay
MAE	Mean Absolute Errors
MDS	Multidimensional Scaling
MFS	Management Flight Simulator
MIT	Massachusetts Institute of Technology
NEMS	Nine equivalents of nursing manpower use score
non-VAP	Non ventilator-associated pneumonia
non-VAT	Non-ventilator-associated tracheobronchitis
OM	Operations Management
OR	Operations Research
PACs	Premature atrial contractions
PCR	Polymerase chain reaction
PG	Population Growth
PHEIC	Public Health Emergency of International Concern
PM	Pacemaker
PN	Parenteral nutrition
PP	Poisson Process
PtiO ₂	The partial pressure of O ₂ in brain tissue
PVCs	Premature ventricular contractions
SCCM	Society of Critical Care Medicine
SD	Social distancing
SSE	Sum of the squared errors
SMACOF	Scaling by MAjorizing a COMplicated Function
SSP	Simulation Starting Point
SVES	Supraventricular extrasystole
SVT	Supraventricular tachycardia
VAP	Ventilator-associated pneumonia
VAT	Ventilator-associated tracheobronchitis
VES	Ventricular extrasystole
VR	Virtual Reality

VT	Ventricular tachycardia
WHO	World Health Organization
WGQI	Working Group on Quality Improvement

B Information of the example of the dilemma of the last bed

B.1 Real patients' description

Peter, 56 years old. Admitted for acute viral meningoencephalitis due to Herpes Simplex Virus I.

- Intubated and connected to mechanical ventilation.
- Neuromonitoring of intracranial pressure (ICP) control by first level measurements.
- In treatment with intravenous acyclovir.
- He requires norepinephrine in continuous infusion at 0.3 $\mu\text{g}/\text{Kg}/\text{min}$.

Phil, 78 years old. Admitted for postoperative control of aortic valve replacement cardiac surgery.

- Hemodynamically stable without requiring vasopressors and with low doses of dobutamine at 2 $\mu\text{g}/\text{Kg}/\text{min}$.
- Chest tube with a rate of drainage less than 100 mL/d.
- Acute kidney injury without oliguric and creatinine and urea levels of 1.8 mg/dL and 80 mg/dL, respectively.

Cate, 63 years old. Admitted for severe community-acquired pneumonia due to Streptococcus pneumoniae.

- Situation of severe acute respiratory distress syndrome (ARDS) requiring respiratory support with veno-venous extracorporeal membrane oxygenation and ultra-protective mechanical ventilation.
- In treatment with meropenem and linezolid.
- With continuous extrarenal depuration techniques.

Harvey, 28 years old. Polytrauma with severe traumatic brain injury secondary to a high-energy car accident after leaving the roadway.

- Intubated and connected to mechanical ventilation.
- Fitted with rigid cervical collar and pelvic stabilization device.
- Hemodynamic instability, with worsened hypotension (blood pressure, 80/50 mmHg) and persistent bradycardia (heart rate, 105 beats/min).
- An inadequate response to fluid resuscitation during transfer by mobile ICU.

Anne, 37 years old. Postoperative course of glioblastoma multiforme.


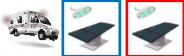

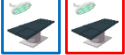
- Clinic of headache difficult to control with usual analgesics, nausea-vomiting and progressive left hemiparesis for two days.
- In the emergency room, he suffered a partial motor epileptic seizure, secondarily generalized.
- Cranial computed tomography (CT) scan showed right frontoparietal glioblastoma multiforme with significant perilesional edema and incipient data of transtentorial herniation.

Paul, 52 years old. Postoperative cardiac surgery for coronary artery bypass grafting.

- Admitted for acute coronary syndrome with ST-segment elevation.
- Cardiac catheterization with left main coronary artery and three-vessels disease.
- Echocardiography with severe ventricular dysfunction and segmental alterations, with extensive anterior hypokinesia.
- Hemodynamic support with intra-aortic balloon pump (IABP) and solinitrin perfusion for refractory postinfarction angina.

B.2 All combinations of the example of the dilemma of the last bed

Table B.1. All 57 possible combinations of the example of the dilemma of the last bed.

Decision	ICU occupancy	Deviations/Cancellations	Early discharges
1			-
2			-

3				-
4				-
5				
6				
7				
8				
9				
10				
11				
12				
13				
14				
15				
16				
17				
18				
19				
20				
21				
22				
23				
24				
25				

26		-	
27		-	
28		-	
29			
30			
31			
32			
33			
34			
35			
36			
37			
38			
39			
40			
41			
42			
43			
44			
45			
46			
47			
48			

49			
50		-	
51			
52			
53			
54			
55			
56			
57			

C Set of patient variables included in the ICU management flight simulator

C.1 Patient information data

Patient data

Coded ICU number, coded Medical Record number, age, gender, weight, LoS, ICU admission time, ICU discharge time, principal diagnosis (see Table C.1), provenance, and type of discharge (see Table C.2).

Table C.1. Unified principal diagnosis.

Code	Principal diagnostic
1	Cardiac surgery postoperative
2	Neurosurgery postoperative
3	Vascular surgery postoperative
4	Thoracic surgery postoperative
5	General surgery postoperative
6	Other postoperative
7	Acute respiratory failure
8	Chronic obstructive pulmonary disease (COPD)
9	Pneumonia
10	Pulmonary embolism
11	Acute respiratory distress syndrome (ARDS)
12	Heart failure
13	Acute myocardial infarction (AMI)
14	Stroke
15	Other neurological disorders

16	Renal insufficiency
17	Acute pancreatitis
18	Other digestive disorders
19	Polytrauma
20	Intoxication
21	Septic shock
22	Hemorrhagic shock
23	Cardiorespiratory arrest
24	Other
99	Donation

Table C.2. Type of discharge.

Code	Reason for discharge
0	Planned discharge
1	Suspension of discharge on clinical grounds
2	Suspension of discharge due to lack of ward beds
3	Suspension of discharge on other criteria
6	Unplanned discharge after morning physician's assessment
7	Unplanned discharge due to shortage of beds
8	Exitus/donation
9	Other

Personal background

Comorbidities as recorded in the APACHE II score, liver diseases (y/n), dyspnoea or unstable angina (New York Heart Association Class IV) (y/n), respiratory background (y/n), chronic kidney dialysis (y/n), and immunocompromised (y/n)

Type of patient

Emergency patient (E):

- Urgent surgery (E_1).
- Polytrauma (E_2).
- Patient hospitalized in Medical Service (E_3).
- Patient hospitalized in Surgical Service (E_4).
- Emergency/observation patient (E_5). Polytrauma patients (E_2) and those undergoing emergency surgery from the Emergency Department (E_1) are excluded from this group.

- Patients admitted for organ donation and others not included in previous groups (E_6).

Scheduled patients (S):

- Patients that recover from standard surgery procedure, which can be in the ICU for an expected short stay (S_1).
- Patients that can be for an expected long stay due to a complicated surgery or critical condition of them (S_2).

C.2 Patient's clinical data

Neurological parameters (10)

Both pupil size in millimetres (1-8 mm) and reactivity (unreactive-sluggish-reactive-undetermined), Glasgow Coma Scale (Glasgow-Motor response, Glasgow-Eye response, and Glasgow-Verbal response), external ventricular drain (ml), and RASS scale (-5: unarousable sedation, -4: deep sedation, -3: moderate sedation, -3: moderate sedation, -2: light sedation, -1: drowsy, 0: alert and calm, 1: restless, 2: agitated, 3: very agitated, or 4: combative).

Hemodynamic parameters (17)

Oxygen saturation (%), the temperature in degrees Celsius ($^{\circ}\text{C}$), type of heart rhythm (sinus rhythm, junctional rhythm, atrial fibrillation [AF], atrial flutter [AFL], supraventricular tachycardia [SVT], ventricular tachycardia [VT], atrioventricular [AV] block [1st, 2nd, and 3rd degree], Premature ventricular contractions [PVCs], atrial extrasystoles [AES], ventricular extrasystole [VES], supraventricular extrasystole [SVES], premature atrial contractions [PACs], and pacemaker [PM]), heart rate (rpm), systolic blood pressure (mmHg), diastolic blood pressure (mmHg) (invasive are non-invasive), mean arterial blood pressure (mmHg), systolic blood pressure-non-invasive blood pressure (mmHg), diastolic blood pressure-non-invasive blood pressure (mmHg), pacemaker rhythm (y/n), type of pacemaker (temporary epicardial or permanent bicameral), pacemaker operating modes (ventricular (VVI) or atrioventricular (DDD), pacing rate (rpm), pacing capture threshold (mA), cardiac output-Vigileo, cardiac index-Vigileo, and stroke volume-Vigileo.

Respiratory parameters (14)

Spontaneous breathing trials (L/minute), tracheotomy (y/n), fenestrated cannula/speaking valve (y/n), tracheostomy cap (y/n), conventional mechanical ventilation (y/n), noninvasive positive pressure ventilation (y/n), reservoir mask (y/n), Venturi mask (y/n), nasal cannula (L/minute), inspired gas flow with high-flow nasal cannula oxygen therapy (L/minute), fraction of inspired oxygen with high-flow nasal cannula oxygen therapy (%), fraction of inspired oxygen (%), extrinsic positive end-expiratory pressure (cmH₂O), and respiratory rate (rpm).

Kidney parameters (2)

Continuous renal replacement therapies (y/n) and intermittent hemodialysis (y/n).

Fluid balances (2)

Diuresis (mL) and chest drainage (mL).

Medication (123)

Plasmalyte (mL/h), propofol 2% (mg/Kg/h), midazolam 50 mg ($\mu\text{g}/\text{Kg}/\text{h}$), remifentanyl / ultiva ($\mu\text{g}/\text{Kg}/\text{min}$), morphic chloride (mg/h), intravenous fentanyl ($\mu\text{g}/\text{Kg}/\text{h}$), cisatracurium ($\mu\text{g}/\text{Kg}/\text{min}$), dexmedetomidine / dexdor ($\mu\text{g}/\text{Kg}/\text{min}$), norepinephrine ($\mu\text{g}/\text{Kg}/\text{min}$), dobutamine ($\mu\text{g}/\text{Kg}/\text{min}$), dopamine ($\mu\text{g}/\text{Kg}/\text{min}$), levosimendan ($\mu\text{g}/\text{Kg}/\text{min}$), epinephrine ($\mu\text{g}/\text{Kg}/\text{min}$), urapidil (mg/h), nimodipine (mg/h), nitroglycerin ($\mu\text{g}/\text{min}$), labetalol (mg/min), nitroprusside ($\mu\text{g}/\text{Kg}/\text{min}$), clevidipine (mg/h), amiodarone (mg/h), furosemide 250 mg (mg/min), regular insulin (IU/h), enteral nutrition (EN) - water (mL/h), EN - gastrointestinal mucosal disruption / GI protein (mL/h), EN - surgery (mL/h), EN - hyperproteic diabetes (mL/h), EN - normo-protein diabetes (mL/h), EN - standar (mL/h), EN - standard with fibre (mL/h), EN - metabolic stress (mL/h), EN - metabolic stress / Perative (mL/h), EN - hypercaloric (mL/h), EN - hypercaloric with fibre (mL/h), EN - hypercaloric with fibre / Jevity (mL/h), EN - hyperproteic (mL/h), EN - hyperproteic with fibre (mL/h), EN - liver failure (mL/h), EN - kidney failure (mL/h), EN - respiratory failure / Oxepa (mL/h), EN - oncology (mL/h), EN - peptidic (mL/h), EN - hyperproteic hypercaloric peptidic (mL/h), EN - hyperproteic peptidic with glutamine (mL/h), parenteral nutrition (PN) - moderate liver disease 1,800 mL (mL/h), PN - hypercaloric 2,000 mL (mL/h), PN - hypercaloric 2,500 mL (mL/h), PN - hypercaloric 3,000 mL (mL/h), PN - hyperproteic hypercaloric 2,200 mL (mL/h), PN - hyperproteic hypercaloric 2,600 mL (mL/h), PN - hyperproteic hypercaloric 3,000 mL (mL/h), PN - hypocaloric 2,000 mL (mL/h), PN - hypocaloric 2,500 mL (mL/h), PN - hypocaloric 3,000 mL (mL/h), PN - individualized (mL/h), PN - isoplasmal (mL/h), PN - normocaloric 2,000 mL (mL/h), PN - normocaloric 2,500 mL (mL/h), PN - normocaloric 3,000 mL (mL/h), PN - normocaloric with glutamine 2,000 mL (mL/h), PN - hyperproteic normocaloric 2,000 mL (mL/h), PN - hyperproteic normocaloric 2,500 mL (mL/h), PN - hyperproteic normocaloric 3,000 mL (mL/h), PN - hyperproteic normocaloric with glutamine 2,000 mL (mL/h), PN - pancreatitis 2,375 mL (mL/h), albendazole oral (y/n), amikacin (y/n), amoxicilin-clavulanic (y/n), ampicilin (y/n), azithromycin (y/n), aztreonam (y/n), cefazolin (y/n), cefepime (y/n), cefotaxime (y/n), ceftazidime (y/n), ceftriaxone (y/n), intravenous ciprofloxacin (y/n), oral ciprofloxacin (y/n), clarithromycin (y/n), clindamycin (y/n), cloxacilin (y/n), intravenous colistin (y/n), nebulized colistin (y/n), intravenous trimethoprim-sulfamethoxazole / TMP-SMX (y/n), oral trimethoprim-sulfamethoxazole / TMP-SMX (y/n), daptomycin (y/n), doxycycline (y/n), intravenous doxycycline (y/n), oral doxycycline (y/n), ertapenem (y/n), gentamicin (y/n), imipenem (y/n), intravenous isoniazid (y/n), oral isoniazid (y/n), intravenous levofloxacin (y/n), oral levofloxacin (y/n), linezolid (y/n), meropenem (y/n), metronidazole (y/n), moxifloxacin (y/n), penicillin G sodium (y/n), piperacillin-tazobactam (y/n), rifampicin

(y/n), teicoplanin (y/n), tigecycline (y/n), tobramycin (y/n), vancomycin (y/n), oral vancomycin (y/n), lipid complex amphotericin B (y/n), liposomal amphotericin B (y/n), anidulafungin (y/n), caspofungin (y/n), intravenous fluconazole (y/n), oral fluconazole (y/n), micafungin (y/n), intravenous voriconazole (y/n), oral voriconazole (y/n), intravenous acyclovir (y/n), oral acyclovir (y/n), ganciclovir (y/n), oral suspension oseltamivir (y/n), oral oseltamivir (y/n), nebulized ribavirina (y/n), and oral ribavirina (y/n).

Events and care (54)

Percutaneous tracheostomy (y/n), cardiopulmonary resuscitation (y/n), defibrillation (y/n), electrical cardioversion (y/n), pharmacologic cardioversion (y/n), transcutaneous pacing (y/n), pericardiocentesis (y/n), pulmonary embolectomy (y/n), vena cava filters (y/n), coronary catheterization (y/n), open surgical tracheostomy (y/n), indwelling pleural catheter (y/n), indwelling pleural catheter (ICU) (y/n), thoracentesis (y/n), bronchoscopy (y/n), bronchoalveolar lavage (y/n), plasmapheresis (y/n), therapeutic hypothermia (y/n), the partial pressure of O₂ in brain tissue (PtiO₂) (y/n), intraparenchymal intracranial pressure (ICP) monitoring catheters (y/n), external ventricular drain (y/n), lumbar puncture (y/n), decompressive craniectomy (y/n), endovascular techniques (y/n), thrombolytic therapy in acute ischemic stroke (y/n), surgical intervention in a patient admitted to the ICU (y/n), surgical reintervention in a patient admitted to the ICU (y/n), percutaneous imaging-guided catheter drainage of abdominal collections (y/n), intra-abdominal pressure (y/n), neuroendovascular techniques (y/n), neuroendovascular techniques II (y/n), gastroscopy (y/n), colonoscopy (y/n), endoscopic sclerosis of esophagogastric varices (y/n), paracentesis (y/n), gastrostomy tube (y/n), transjugular intrahepatic portosystemic shunt (y/n), sengstaken-blakemore tube (y/n), fibrinolytic (thrombolytic) therapy (y/n), immunoglobulin (y/n), unplanned decannulation (y/n), unplanned extubation (y/n), accidental central venous catheter removal (y/n), accidental removal of a drain (y/n), accidental arterial catheter removal (y/n), accidental removal of a urinary catheter (y/n), accidental removal of a nasogastric tube (y/n), fall in ICU (y/n), medication errors (y/n), drainage obstruction (y/n), obstruction of a tracheostomy tube (y/n), physical restraints (y/n), sitting position (y/n), and sitting position using a hoist (y/n).

Infections (5)

Type of infection (see Table C.3), origin (community-acquired infection, intra-ICU, extra-ICU, or other hospitals), inflammatory response (non sepsis, sepsis, severe sepsis, or septic shock), germs (see Table C.4), and antibiotics (see Table C.5).

Table C.3. Type of infection.

#	Type of infection
1	Acalculous cholecystitis
2	Bacteremia of unknown origin
3	Bacteremia secondary to respiratory infection

4	Bacteremia secondary to respiratory infection
5	Bloodstream infection of abdominal origin
6	Bloodstream infections secondary to central nervous systems
7	Bloodstream infections secondary to soft tissue infection
8	Bloodstream infections secondary to urinary tract infection
9	Catheter-related bloodstream infections
10	Central nervous system infection
11	Deep infection of surgical incision
12	Deep infection of surgical wound
13	Infection of unknown origin
14	Intra-abdominal infection
15	Non ventilator-associated pneumonia (non-VAP)
16	Non-surgical infection of digestive system
17	Non-ventilator-associated tracheobronchitis (non-VAT)
18	Organ-space surgical site infections
19	Primary peritonitis
20	Skin and soft tissue infection
21	Urethral catheter-related urinary tract infection
22	Urinary tract infection not related to urethral catheter
23	Ventilator-associated pneumonia (VAP)
24	Ventilator-associated tracheobronchitis (VAT)
25	Other

Table C.4. Germs.

#	Germ
1	Acinetobacter Baumanii
2	Candida albicans
3	Citrobacter freundii
4	Citrobacter spp
5	Clostridium difficile
6	Enterobacter aerogenes
7	Enterobacter cloacae
8	Enterococcus faecalis
9	Enterococcus faecium
10	Escherichia coli
11	Haemophilus influenzae
12	HIV 1

13	Klebsiella oxytoca
14	Klebsiella pneumoniae
15	Klebsiella spp
16	Moraxella catarrhalis
17	Morganella morganii
18	Neisseria spp
19	Proteus mirabilis
20	Pseudomonas aeruginosa
21	Salmonella spp
22	Serratia marcescens
23	Staphylococcus aureus
24	Staphylococcus epidermidis
25	Streptococcus pneumoniae
26	Streptococcus salivarius
27	Streptococcus viridans group
28	Zoster-varicella
29	Other

Table C.5. Antibiotics.

#	Antibiotic
1	Acyclovir
2	Amikacin
3	Amoxicilin-clavulanic
4	Ampicilin
5	Anidulafungin
6	Aztreonam
7	Caspofungin
8	Cefazolin
9	Cefepime
10	Cefotaxime
11	Ceftazidime
12	Ceftriaxone
13	Ciprofloxacin
14	Cloxacilin
15	Colistin
16	Cotrimoxazole
17	Daptomycin

18	Fluconazole
19	Gentamicin
20	Levofloxacin
21	Linezolid
22	Meropenem
23	Metronidazole
24	Oseltamivir
25	Piperacillin-tazobactam
26	Rifampicin
27	Tigecycline
28	Vancomycin
29	Voriconazole
30	Other

Analytics (37)

Hemoglobin (g/dL), hematocrit (%), leukocytes ($\times 10^9/L$), neutrophils (%), Lymphocytes (%), monocytes (%), eosinophils (%), basophils (%), band neutrophils (%), platelets ($\times 10^9/L$), prothrombin time (s), prothrombin activity (%), international normalized ratio (INR), activated partial thromboplastin time (aPTT) (s), glucose (mg/dL), urea (mg/dL), creatinine (mg/dL), glomerular filtration ($ml/min/1.73m^2$), protein (g/dL), albumin (g/dL), bilirubin (mg/dL), aspartate transferase (AST) (IU/L), alanine transferase (ALT) (IU/L), gamma-glutamyl transpeptidase (GGT) (IU/L), alkaline phosphatase (IU/L), lactate dehydrogenase (IU/L), troponin I (cTnI) (pg/mL), creatine kinase (IU/L), creatine kinase myocardial band (CK-MB), alpha-amylase (IU/L), lactate (mmol/L), sodium (mmol/L), potassium (mmol/L), chlorine (mmol/L), calcium (II) (mg/dL), procalcitonin (ng/mL), and C-reactive protein (mg/dL).

Gasometry (7)

pH, pCO_2 (mmHg), pO_2 (mmHg), lactate (mmol/L), saturation (%), HCO_3 (mmol/L), and base excess (mmol/L).

Reports (4)

Admission, medical, nursing, and clinical reports. The nursing reports include the nine equivalents of nursing manpower use score (NEMS) and the therapeutic intervention scoring system-28 (TISS-28).

D ICU simulator user guide

This is a user guide to the ICU simulator, an online interactive simulator to study patients admission and inpatients discharge decisions in situations of high occupancy in the ICU. This guide explains all the parts and steps necessary for its use, as well as showing the different possibilities offered by the software. The data used in this guide have been provided by Navarre Hospital Compound using Metavision® software.

D.1 Access to the simulator

The ICU simulator is freely available on the internet to be used by any interested user (<https://icusimulator.unavarra.es>). Figure D.1 shows the login screen for the simulator. Only the username (**ICU-simulator**) and the password (**ICU_S1mulat0r***) are required in order to access it.



The image shows a login screen for the ICU simulator. At the top, there is the 'upna' logo in red, with the text 'Universidad Pública de Navarra' and 'Nafarroako Unibertsitate Publikoa' below it. The title 'SIMULADOR UCI' is centered in bold black text. Below the title are two input fields: the first is labeled 'Usuario' and the second is labeled 'Contraseña'. At the bottom, there is a dark grey button with the text 'Iniciar Sesión' in white.

Figure D.1. Login screen of the ICU simulator.

The username and password are the same for all users. Pressing the "Iniciar Sesión" button the user starts with several initial screens before the start of the simulation. The first screen of the simulator can be seen in Figure D.2. This screen presents the ICU simulator. Initially the selected language is English but it can be changed to Spanish (see Figure D.3).

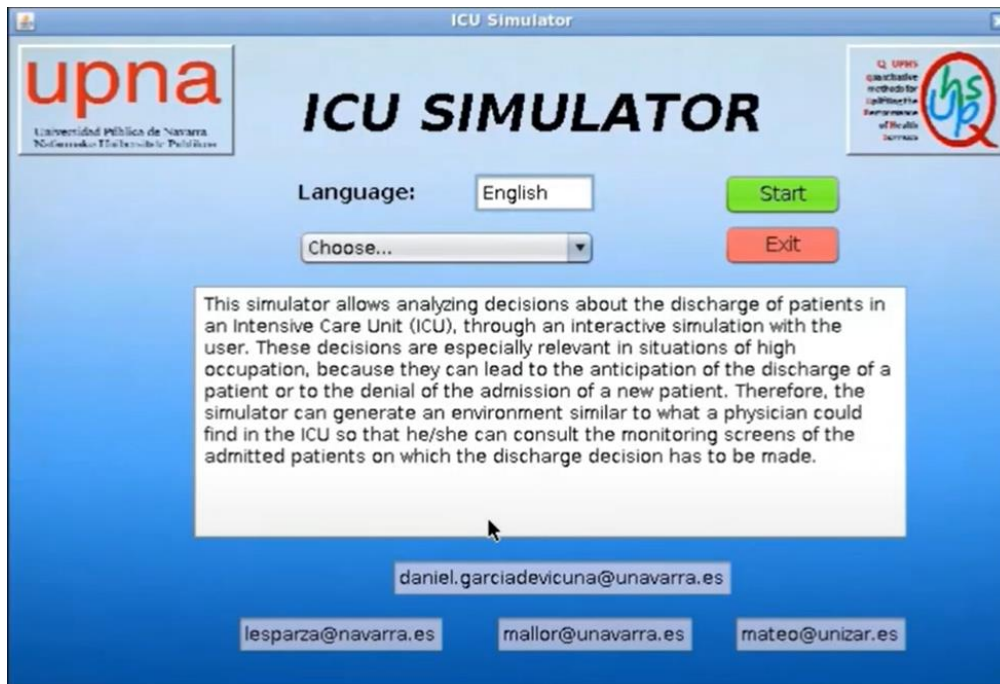


Figure D.2. Initial screen of the ICU simulator in English.

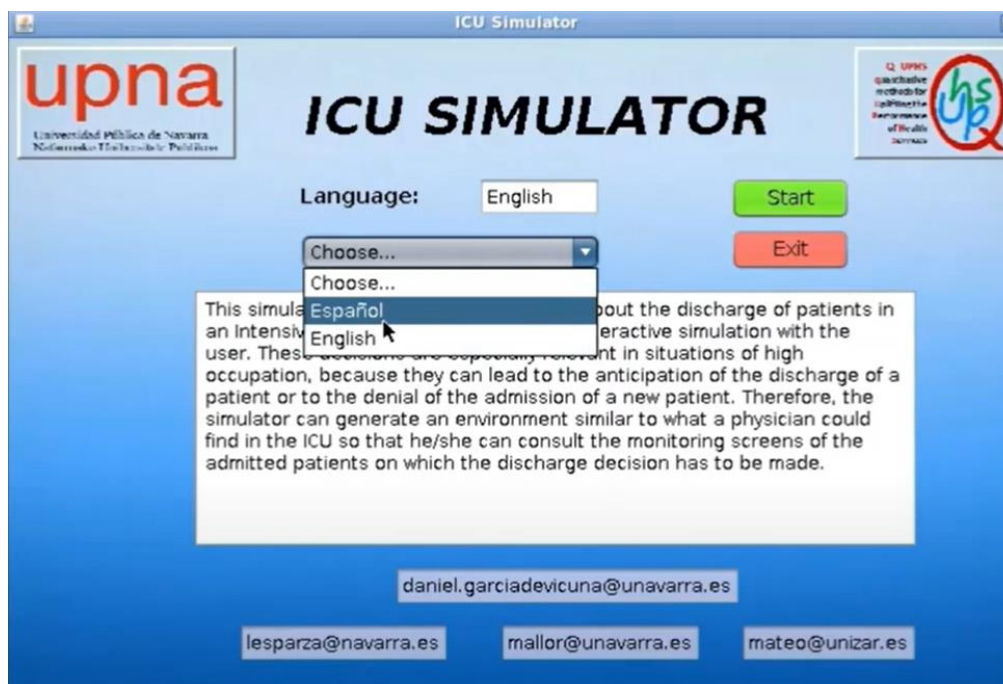


Figure D.3. Initial screen of the ICU simulator in Spanish.

This first screen gives a description of what the simulator consists of and the email addresses of the developers (Daniel García de Vicuña, Laida Esparza, Fermín Mallor, and Pedro Mateo) are shown at the bottom of the screen. The logo of the Public University of Navarre and that of the research group qUPHS, belonging to the university, are also shown. By clicking on the "Start" button, the window shown in Figure 4 opens. Initially, a personal e-mail address is required in order to register, access the simulator, and receive the simulation results. A password is sent to the user with which he/she can log in. This password can be changed later.



Figure D.4. ICU simulator registration screen.

D.2 Defining the characteristics of user and the simulation scenario

The initial screen of the ICU simulator after registration is shown in Figure D.5. In this screen, we have different options that are explained in Appendix D.7. Before starting the simulation, the characteristics of the user must be defined. By clicking on the "New simulation" button, the user can enter his or her data for the collection of results.

The user is characterized by a name, which is used to save the files generated with that name, the type of user, which can be a physician, nurse, resident, medical student..., and the years of experience in the ICU. Figure D.6 shows as an example the user Daniel, who is a physician with between 10 and 15 years of experience in ICU.

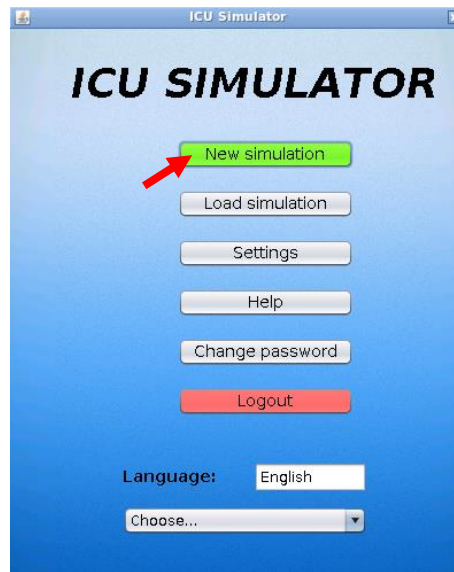


Figure D.5. ICU simulator initial screen after registration.

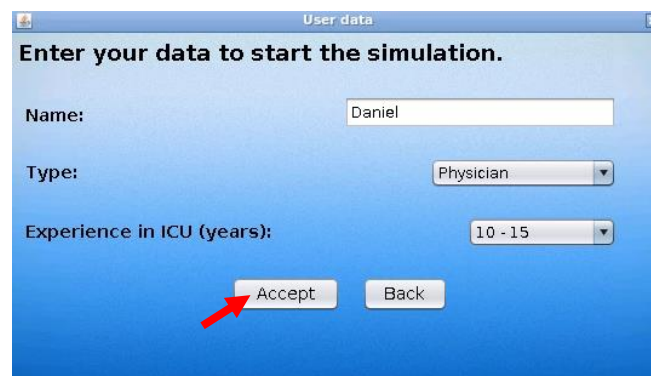


Figure D.6. User configuration screen.

By clicking the "Accept" button in Figure D.6, the window shown in Figure D.7 opens. This screen shows a summary of the conditions that the simulated scenario will have. This configuration can be modified, but what is important is that it remains the same for all user simulations, in order to compare the results correctly afterwards. In the upper left corner, we can see the mix of patients. Two types of patients are distinguished, on the one hand, the emergency admissions, those who arrive unexpectedly to the ICU (in this case 56% are considered), which in turn are divided into 6 categories. On the other hand, scheduled admissions, that is, patients arriving from surgeries that are scheduled during the week. Here again, two types of patients are distinguished, those with a standard stay and those with an extended stay.

A description of the ICU scenario is given on the right-hand side. We have a 24-bed ICU in a third-level hospital with an extreme degree of occupancy. Other aspects to note are that the simulation will start on Monday, with a duration of 21 days and that there will be no bed blocking from the hospital wards when assigning discharges. Finally, at the bottom left, the

properties of the discharge processes are defined. In this case, a clinical decision-making session is scheduled every day at 8 am. In addition, the times below indicate the times when the user can assign discharges to free up beds (from 8 a.m. to 10 p.m.), and the times when discharges can be assigned because there is saturation (all day). The bottom right options to change configuration and default settings are disabled for the collection of results to prevent users from modifying the scenarios. By clicking on the "Continue" button, the ICU simulation starts.

Figure D.7. Configuration screen of the simulation scenario.

D.3 Starting the simulation

Before starting the simulation, a window appears with information about the ICU to be simulated, so that the user can put himself in the role of the ICU physician. This window is shown in Figure D.8. A window with a summary guide to the simulation and its main parts is also shown (see Figure D.9), which will be detailed later.

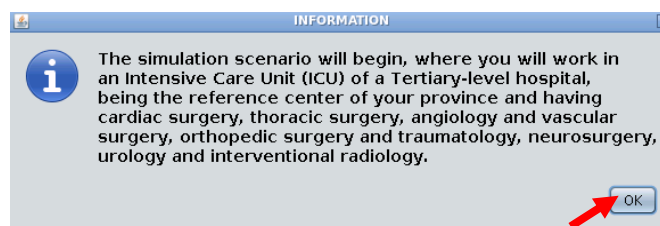


Figure D.8. Information window of the ICU to be simulated.

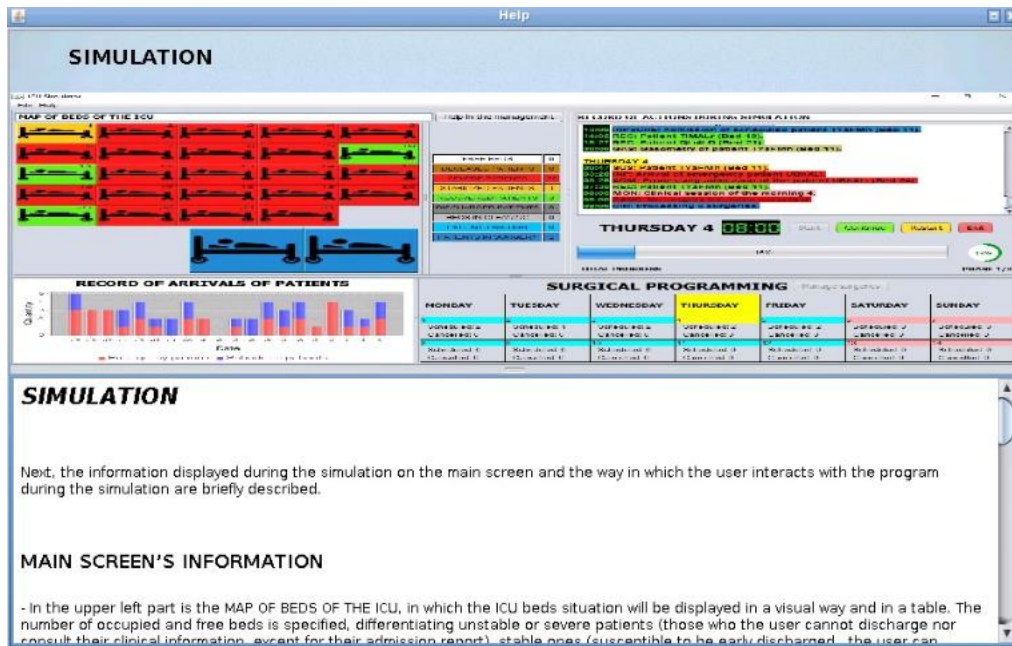


Figure D.9. Simulation help window.

To start the simulation, the user must click on the "Start" button in Figure D.10, which is the main screen of the ICU simulator, which at this point presents an empty ICU. With the initialization of the system (see Figure D.11), the software chooses which patients will be occupying the ICU beds at the beginning and in which condition. When this process finishes, the ICU beds are filled with patients (each in a different color depending on their health status) as shown in Figure D.12.

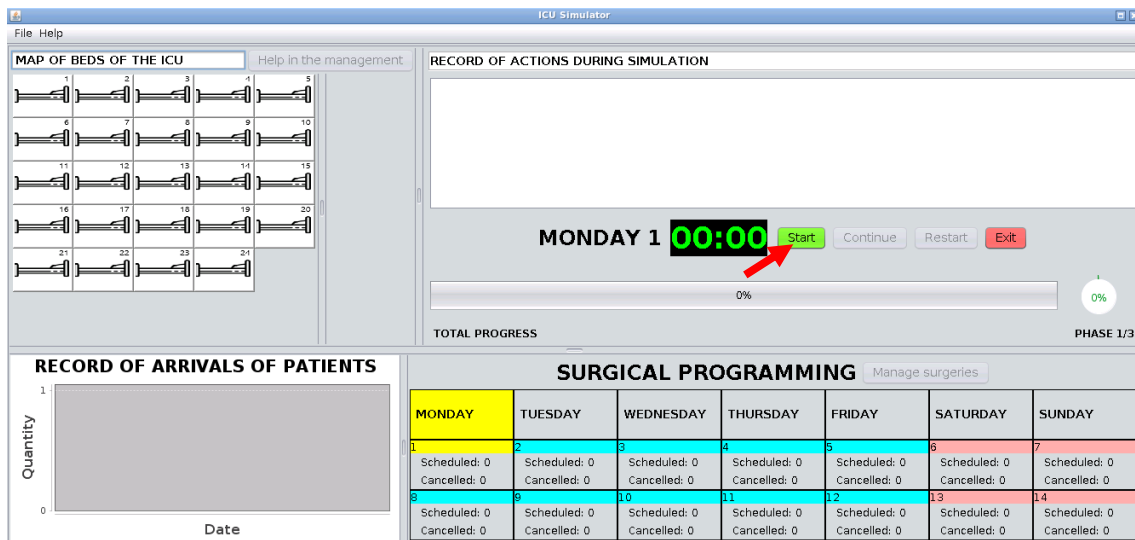


Figure D.10. Main screen of the simulator before starting the simulation.

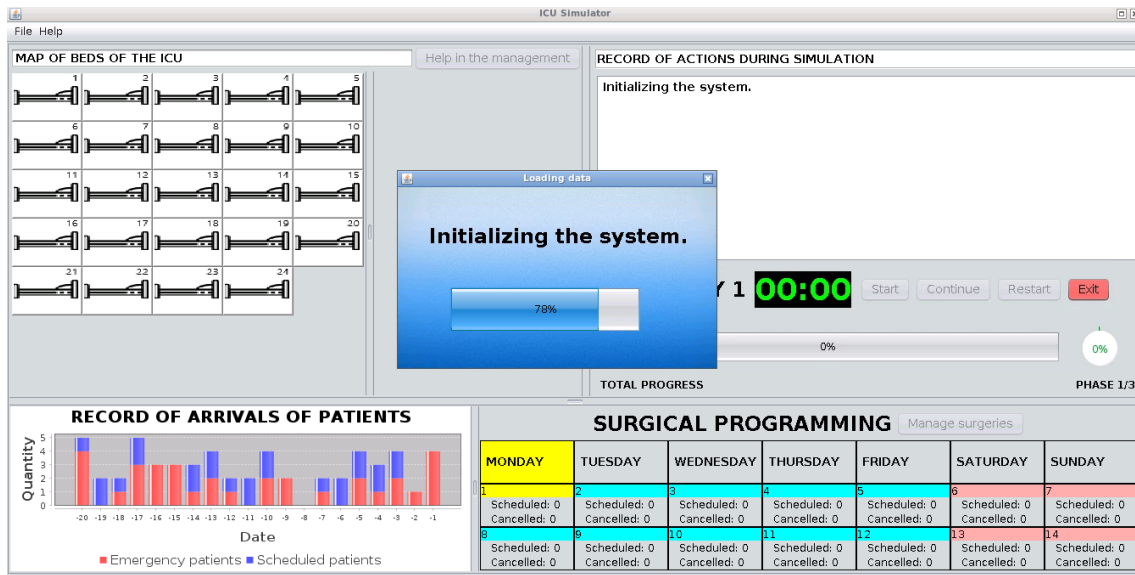


Figure D.11. Window indicating the initialization of the ICU.

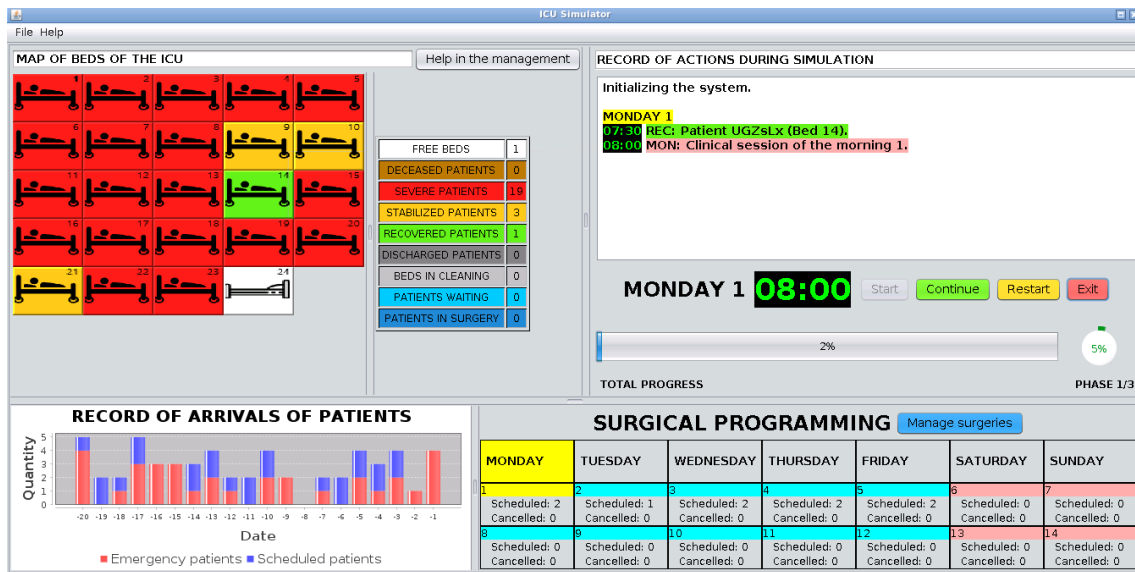


Figure D.12. Main screen of the ICU simulator at the beginning of the simulation.

On the main screen of the ICU simulator, we can distinguish four parts. In the lower part, there is a history of the number of emergency patient arrivals for the last days (left) and a panel with the scheduled surgeries of the following days (right). In this surgery dashboard, the user can access patient information and view their clinical reports. The surgeries of the next week are updated and displayed on Friday. In the upper-right part, events related to the change of health of patients appear, as well as information about admissions and discharges. On the top left side, the occupancy of the ICU is shown in a panel that represents the beds with a color code. We can see a panel indicating the number of patients in each state.

The flow diagram in Figure D.13 shows the admission and the discharge processes as they are considered in the simulator. On the left side, the emergency and scheduled patients' arrivals are represented. Medical staff must decide whether to reject or admit them to the ICU. Scheduled patients first occupy a bed in the operating theater area (dark blue icon). Admitted patients occupy a free bed (white icon) in the ICU, when they are available, when not, the patient is placed in a bed in a special room where he or she can temporarily be treated (light blue icon). The right side represents the ICU where the beds can be in 7 different occupancy states: an occupied bed by a patient that is in the process of being discharged (dark grey icon); a bed occupied by a deceased patient (brown icon); bed under cleaning process (light grey icon); available bed (white icon); and occupied beds by patients in severe, stabilized and recovered health status (red, orange and green icons, respectively).

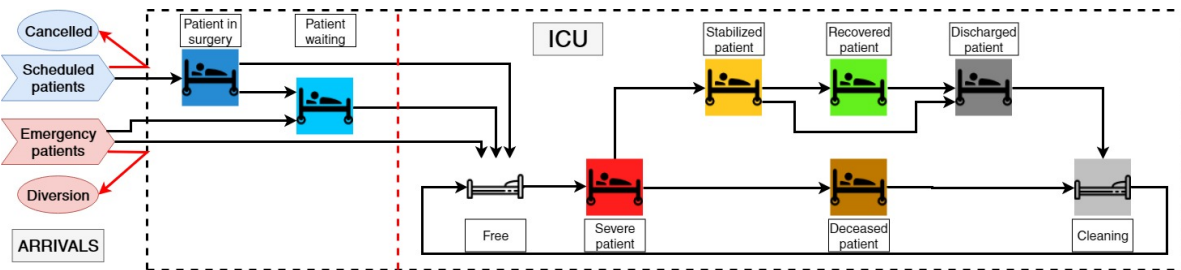


Figure D.13. Representation of the dynamics of an ICU through the change of the bed's state. The two types of patients are distinguished (scheduled and emergency ones) and also the direct entry to the ICU from a delayed one.

D.4 Bed management in the ICU

The simulator is interactively managed by the user. At the decision times, the simulator shows the user which patients are occupying the ICU. The decisions to be made by the user consist of discharging admitted patients, confirming or cancelling scheduled surgeries, and admitting or diverting unscheduled emergency patients. To support the decisions made, the user can consult the patient's clinical information, as shown in Figure D.14, with the window that opens when clicking on bed number 14 in this case. The user can consult the patient's medical history in Spanish (see Figure D.15) as well as the patient's clinical data (see Figure D.16).

So patient data are accessible, and these data are exactly the same as physicians see in the real ICU. We model the health status of a patient by using 275 health indicators (medical and nursing reports included), all recorded by the Metavision® software. These variables give an extended and realistic description of the evolution of the patient health status, showing all parameters a physician needs to discharge a patient. Users are able to access the values of these variables in the case of all stabilized and recovered patients. The volume of information provided is simplified by preventing the consultation of the data of those patients who finally

die and those who remain in serious conditions since the data of the patients that clearly cannot be discharged is meaningless.

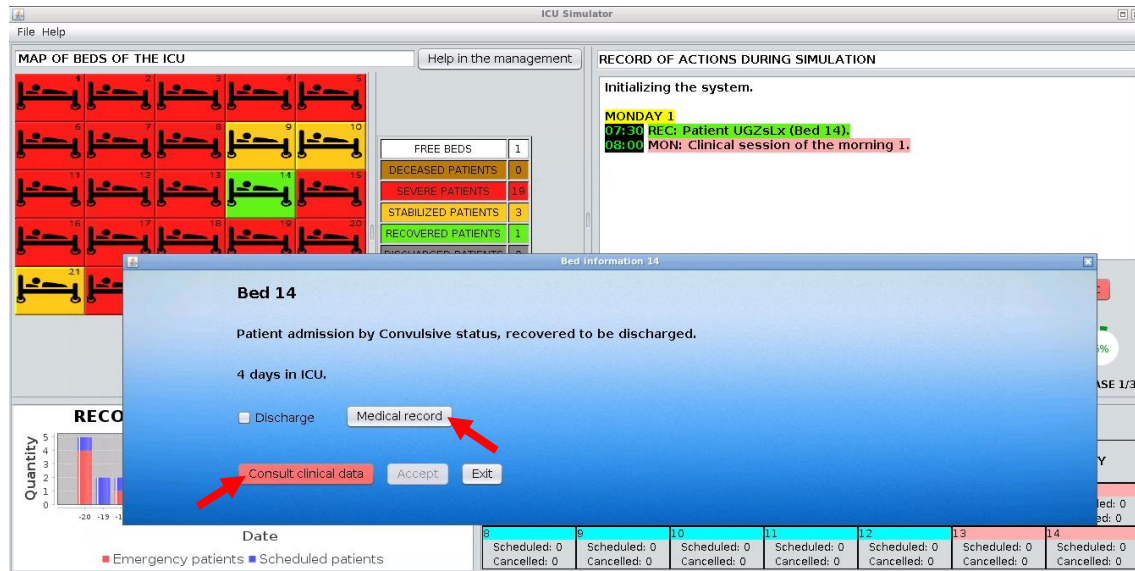


Figure D.14. Window with information about the patient that is on bed 14 and buttons to access the patient's medical history and patient data.

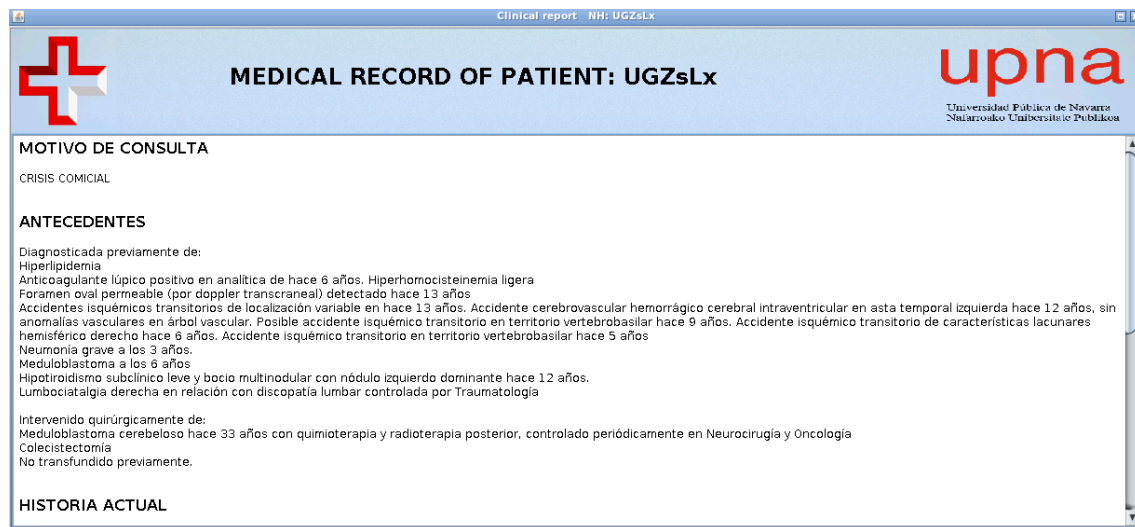


Figure D.15. Medical history of the patient that is on bed 14.

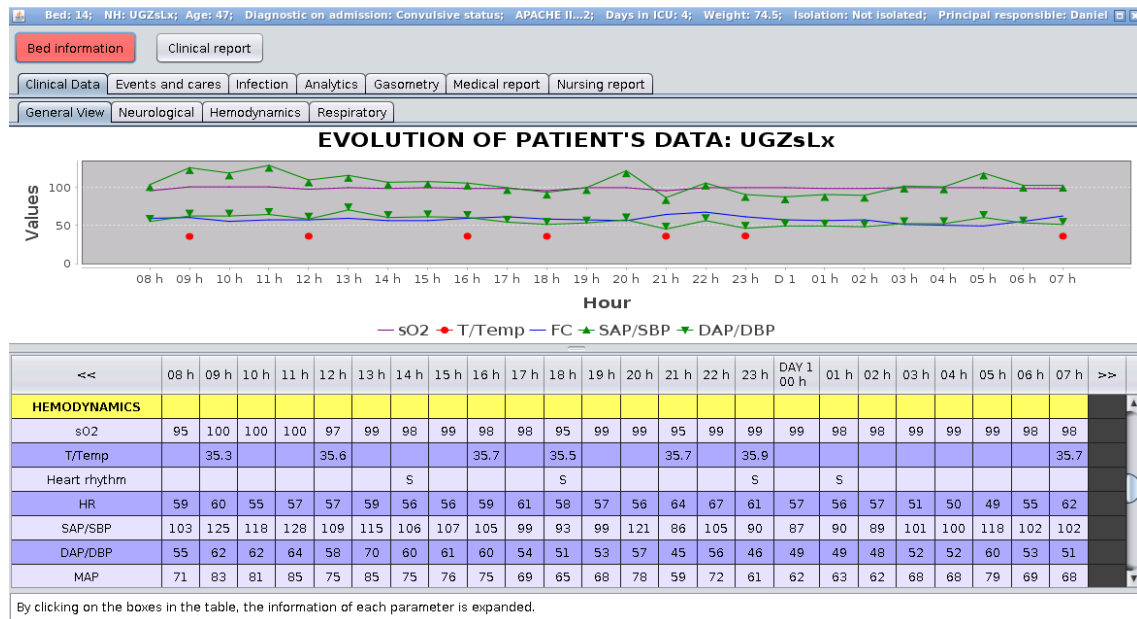


Figure D.16. Information of clinical data of the patient that is on bed 14, mimicking real screens of Metavision®.

We have collected variables of 200 real patients of an ICU. The objective of the simulator is to collect information on how each user manages an ICU in which the congestion level is *extreme*. It is not intended to assess the user's medical knowledge. Consequently, some ICU physicians collaborating in the development of the simulator, to shorten the time to assess the clinical status of all inpatients, analysed the medical records of all patients to define three states along their stay, which help the user to make decisions. On the one hand, we consider in severe conditions to be discharge a patient who has just been admitted in the ICU (red color in Figure D.13). On the other hand, patients who has finished their LoS are considered totally recovered and they should be discharged (green color in Figure D.13). Finally, an intermediate state is established for each patient (orange color in Figure D.13), which indicates the moment from which the patient is sufficiently stabilized to be discharged, although risks to his/her health are assumed.

To discharge patients, the user has to click on the corresponding patient's bed and click on the "Discharge" box as shown in Figure D.17. Whenever the user discharges a patient, the simulator asks for confirmation. To confirm or cancel the scheduled surgeries of each day, the user must click on the "Manage surgeries" button colored in blue in Figure D.12. Figure D.18 shows the window that opens to manage the 2 surgeries we can observe. The user can confirm both, one or none. Those surgeries that are cancelled must be indicated with the option "Cancel surgeries". But in this case, both surgeries are confirmed.

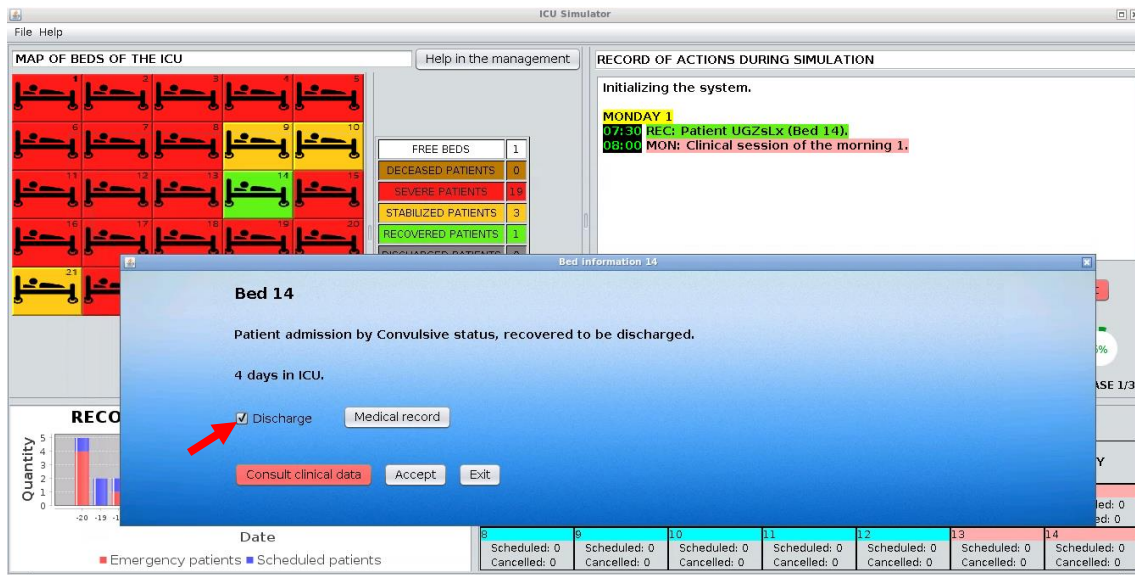


Figure D.17. The window for discharging the patient that is on bed 14.

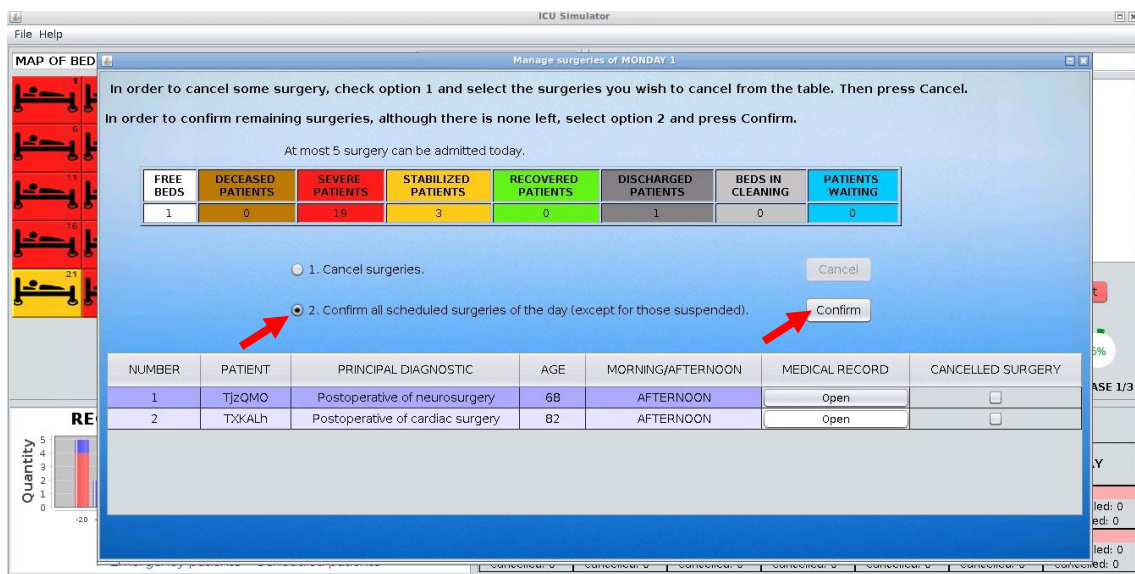


Figure D.18. The window for managing the surgeries.

Finally, with the arrival of urgent patients, windows like the one shown in Figure D.19 appear. The management options consist of admitting the patient, diverting the patient to another facility, or admitting but discharging a patient (the latter option is only enabled when there are no free beds). Figure D.19 shows that the user decides to admit the new patient.



Figure D.19. The window for admitting or diverting emergency patients.

D.5 Conflictive situations during the simulation

During the simulation, situations may arise where there are not enough free beds to care for all patients. These situations are called conflictive situations because not all patients can be treated at the same time and discrepancies appear between decision-makers. Two examples of possible conflictive situations that the user may face during the simulation are given below.

In the first situation, we have the ICU with all beds occupied, and only two of them are stabilized, the rest are in severe condition. In this situation, an emergency patient has arrived, but there is no free bed. Figure D.20 shows the moment when the emergency patient arrives. Here, the user has two options: to divert the emergency patient to another facility or to admit the patient assigning an early discharge to one of the two stabilized patients. As the admission and discharge processes are not instantaneous, if the user chooses the second option, the admitted emergency patient must wait some time for the bed to be released and cleaned before being able to occupy it. Figure D.21 shows how the admitted patient is waiting while the patient in bed 1 has been already discharged.

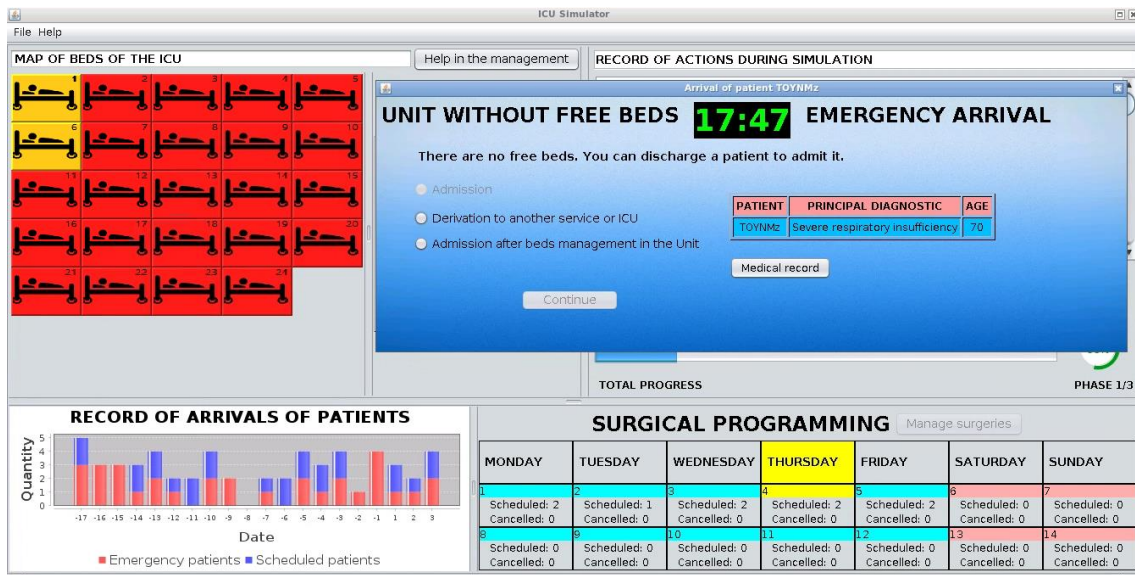


Figure D.20. The situation when an emergency patient arrives at the ICU with all beds occupied. Only two patients are stabilized while the rest are in severe condition.

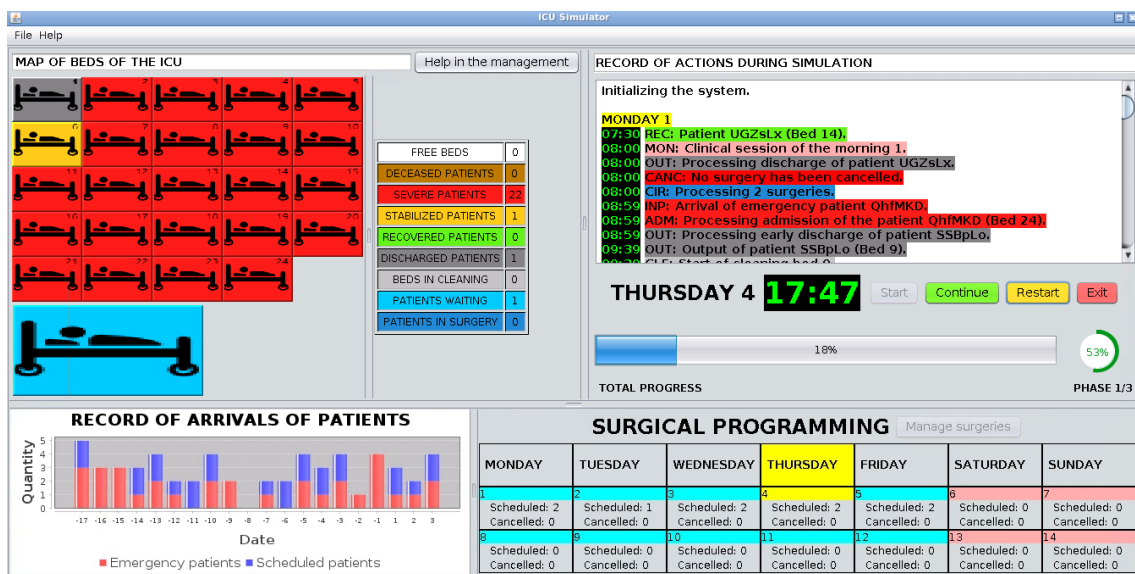


Figure D.21. The situation in which the admitted emergency patient has to wait for the bed of the discharged patient to be freed up.

The second conflict situation we present takes place on Friday at 8 am, during the morning clinical session. In this session, the two surgeries scheduled for that day have to be managed. But, the situation in the ICU is as follows: all ICU beds are occupied with critically ill patients except one, who is stabilized. Therefore, at least one surgery has to be cancelled as there is no possibility to treat both of them (see Figure D.22). The second surgery could be confirmed if the stabilized patient is early discharged. Figure D.23 shows that the second pending surgery has been confirmed, so the patient in bed 6 needs to be early discharged. The calendar at the bottom right of Figure D.23 indicates that of the two surgeries that were scheduled for Friday,

one has been cancelled. In addition, the scheduled surgeries for the following week are known at this morning clinic session, as the surgery calendar is updated on Fridays.

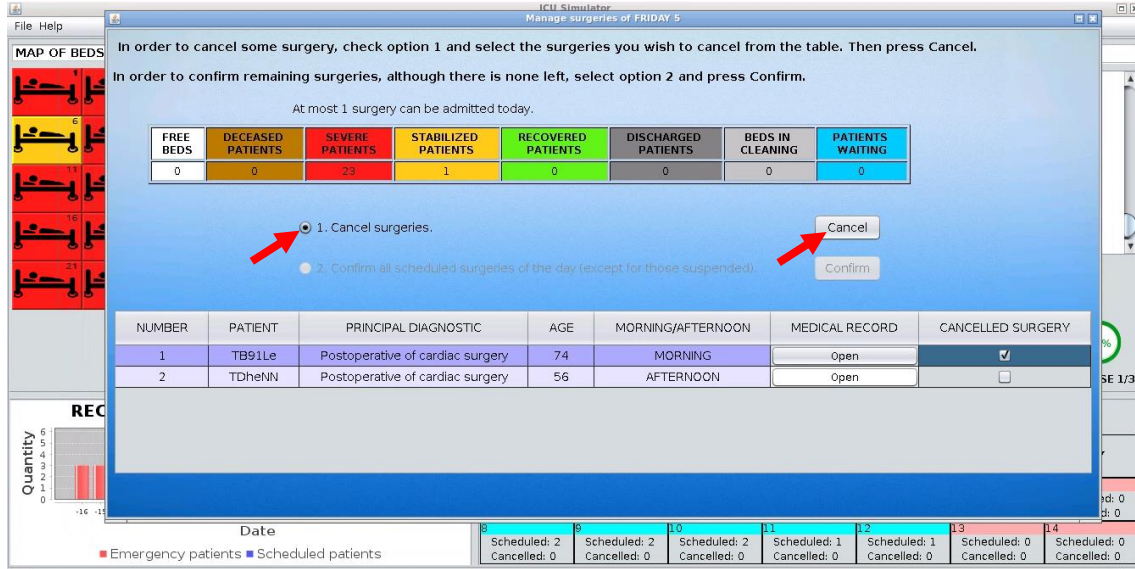


Figure D.22. The situation when two surgeries have to be managed but only one can be confirmed due to lack of ICU beds.

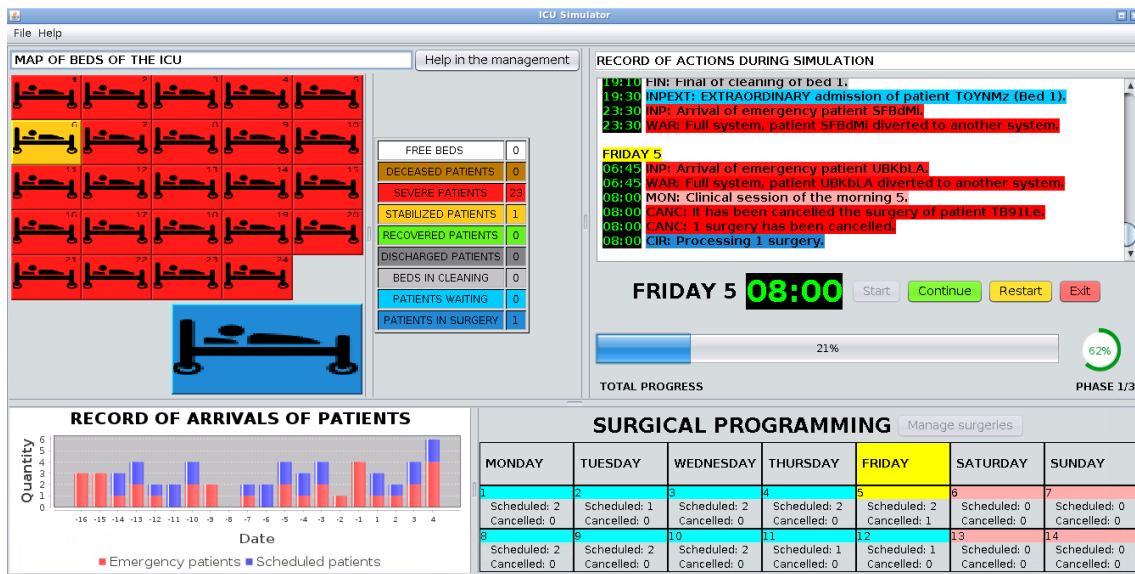


Figure D.23. The situation where the only stabilised patient in the ICU has to be discharged because one of the two surgeries scheduled for that day has been confirmed.

D.6 Saving and loading simulations

The ICU simulator allows the simulation to be saved at any time during the execution of the software. To do that, it is necessary to click on the tab "File" and on the option "Save

simulation" (see Figure D.24). To save the simulation correctly, the name of the file to be saved that the user writes must end with ".properties" as shown in Figure D.25. The simulator reminds the user to save the simulation at the end of each week and also generates an auto-saved file each day of the simulation.

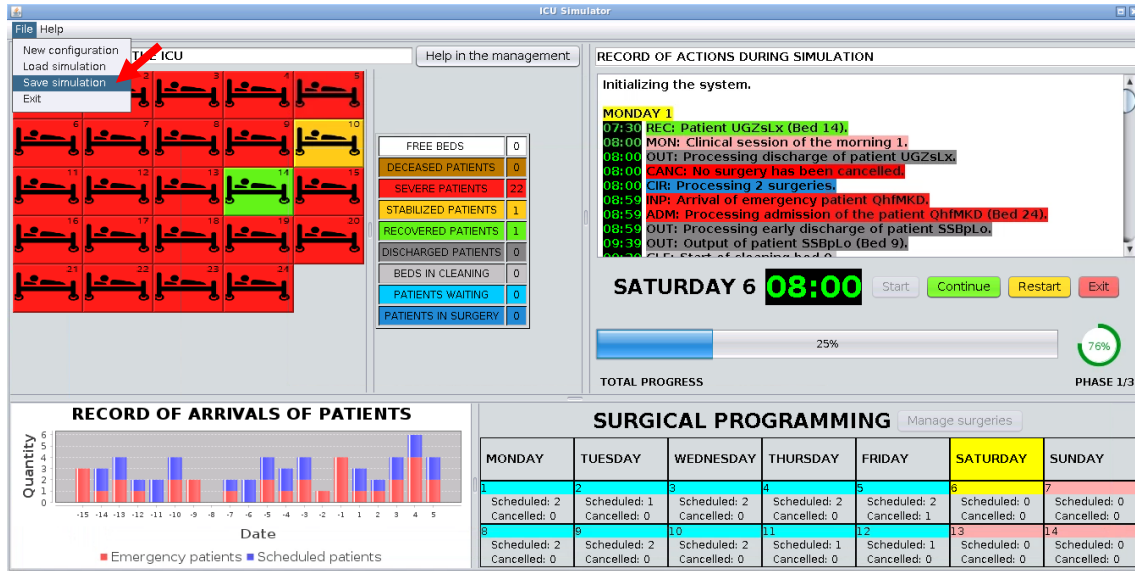


Figure D.24. Option to save the simulation with the simulator.

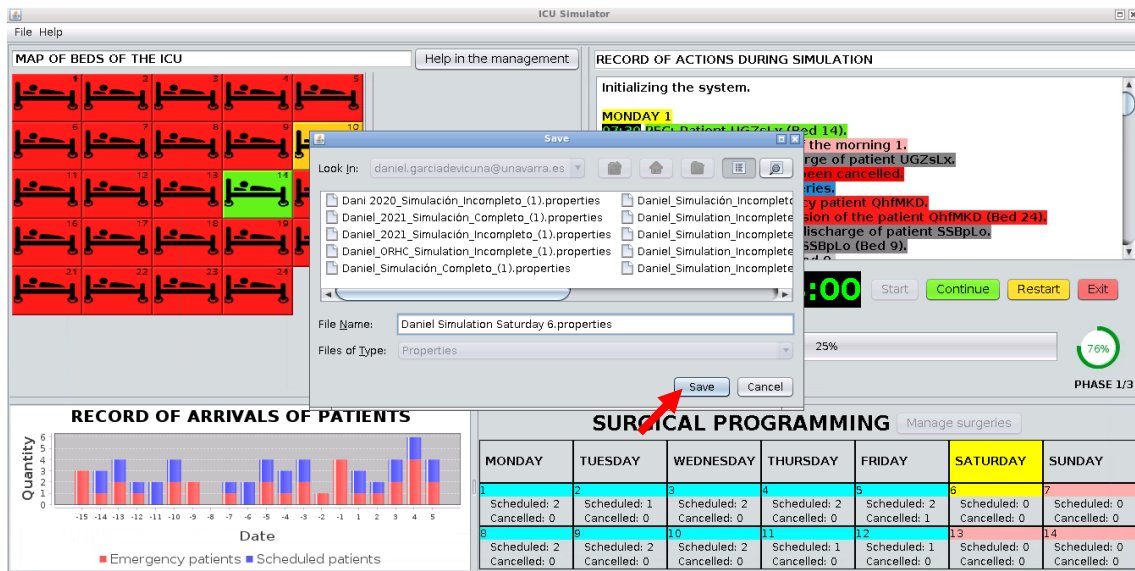


Figure D.25. Saving the simulation with the ending ".properties".

Once the simulation has been saved, the user could exit and enter again to resume the simulation at a later time. To load the simulation, the user has to click on the "Load simulation" button on the simulator start screen after registration, which has been shown earlier in Figure D.5. A window is opened with all the saved files, as shown in Figure D.26, and the user chooses which one he or she wants to load. When loading a file, the simulator automatically reproduces

all the simulation that the user had run up to the point at which he or she had saved. The simulation continues from exactly the same moment it was saved and with the same decisions made. Also, the simulation can be restarted from the beginning at any time. Figure D.27 shows the "Restart" button that allows the simulation to be restarted, and the message warning the user that restarting will result in the loss of unsaved simulation progress. When the simulation is restarted, all events are repeated in exactly the same way.

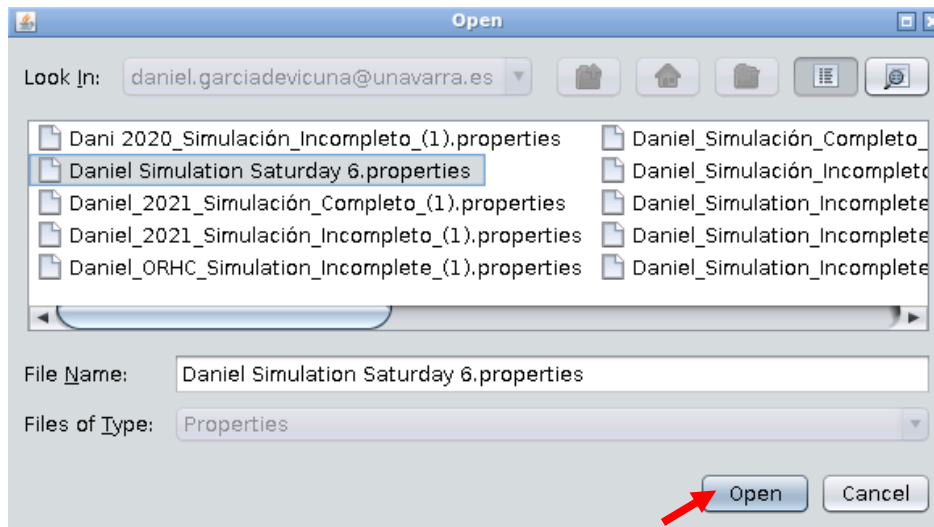


Figure D.26. Window for loading saved simulations.

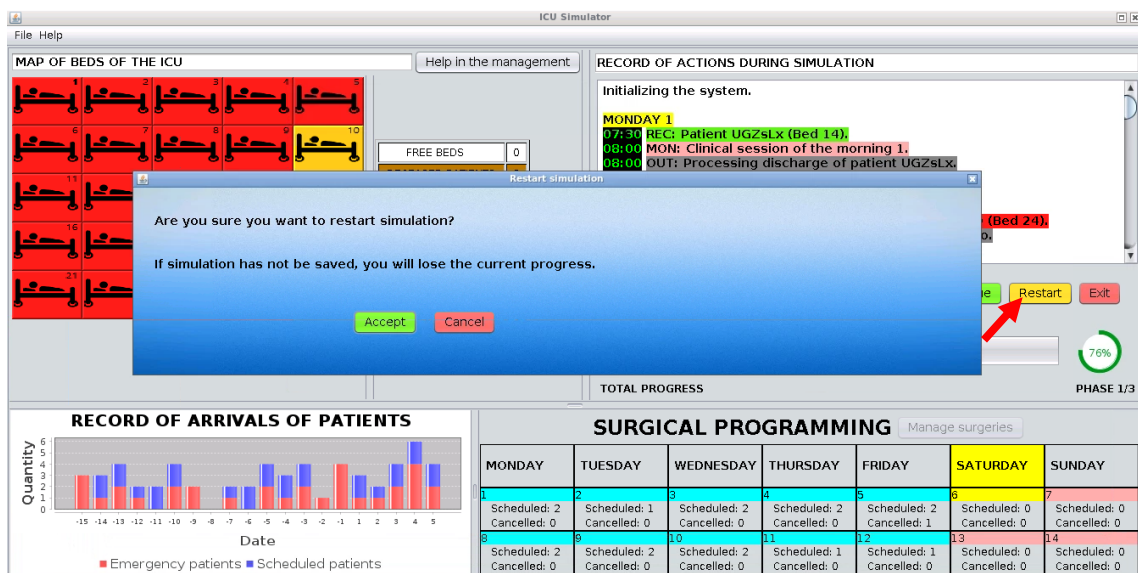


Figure D.27. The window to restart the simulation from the beginning. Unsaved progress is lost.

D.7 Help menu and exit the simulator

The ICU simulator contains different windows with information to help the user understand

the different parts of the software. With the "Help" button in Figure D.5, we can access different explanatory texts about the ICU simulator (description, users, and simulation, see Figure D.28), scenarios (mix of patients, general parameters, types of discharge, and save/load, see Figure D.29), types of simulation (new simulation, simulation saved, simulation finished, and save/load, see Figure D.30), and information collected (results of simulation and bed occupancy, see Figure D.31). In addition, during the simulation, there is a "Help" tab that provides indications and clarifications about the different aspects of the simulation that appear in Figure D.32, including the simulation control buttons, surgeries management, and the emergency patient admission, among others.

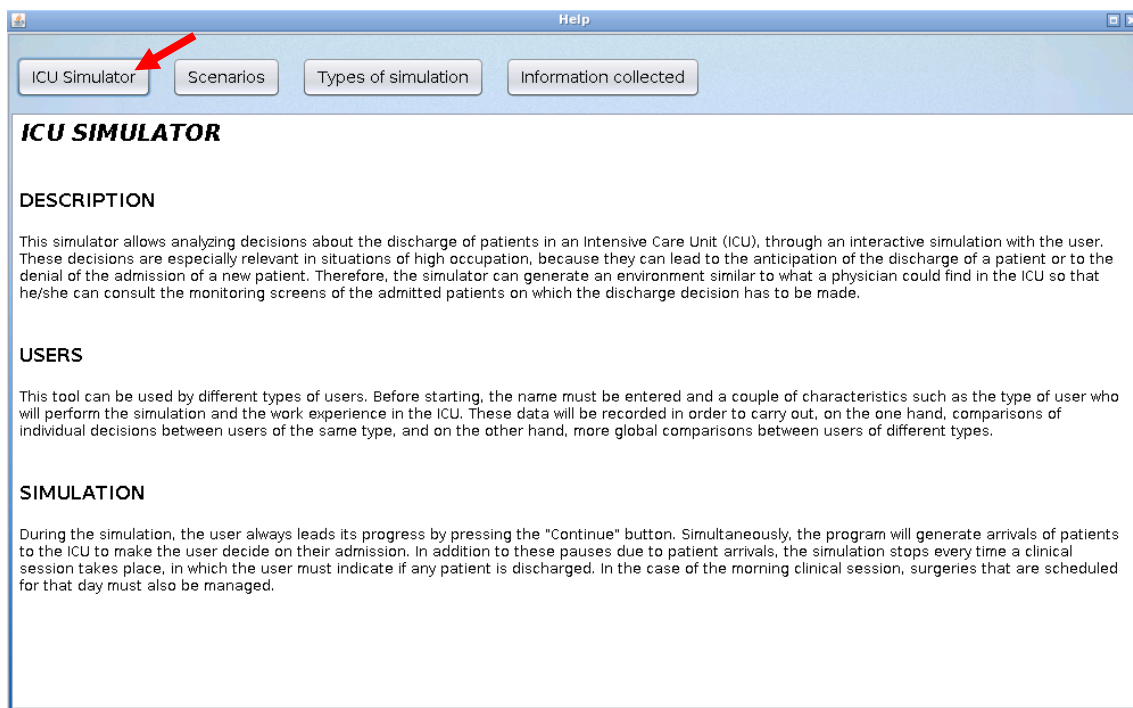


Figure D.28. Help menu with information about the ICU simulator.

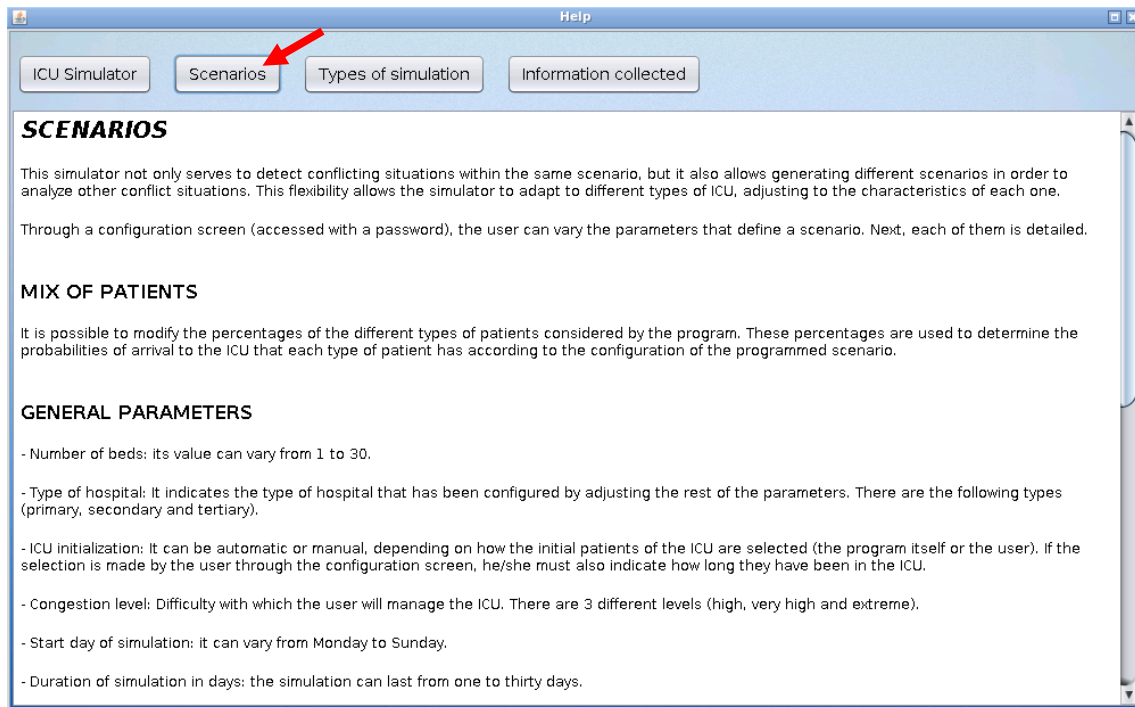


Figure D.29. Help menu with information about the scenarios that can be created with the simulator.

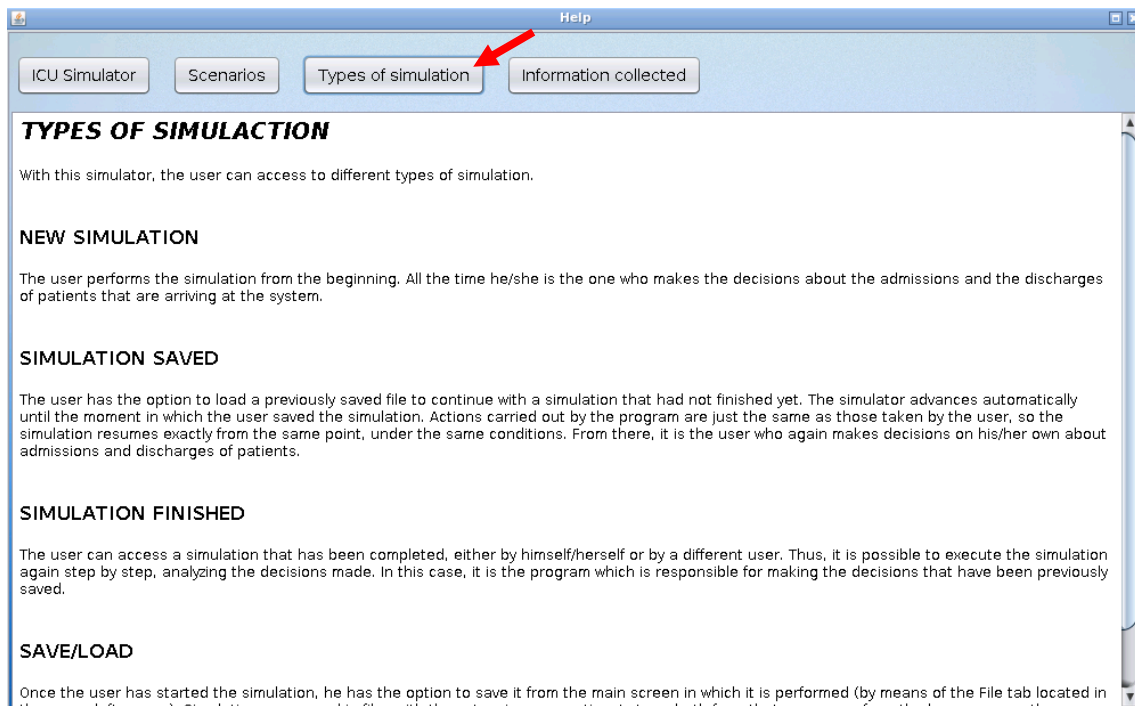


Figure D.30. Help menu with information about the types of simulation the user can access to.

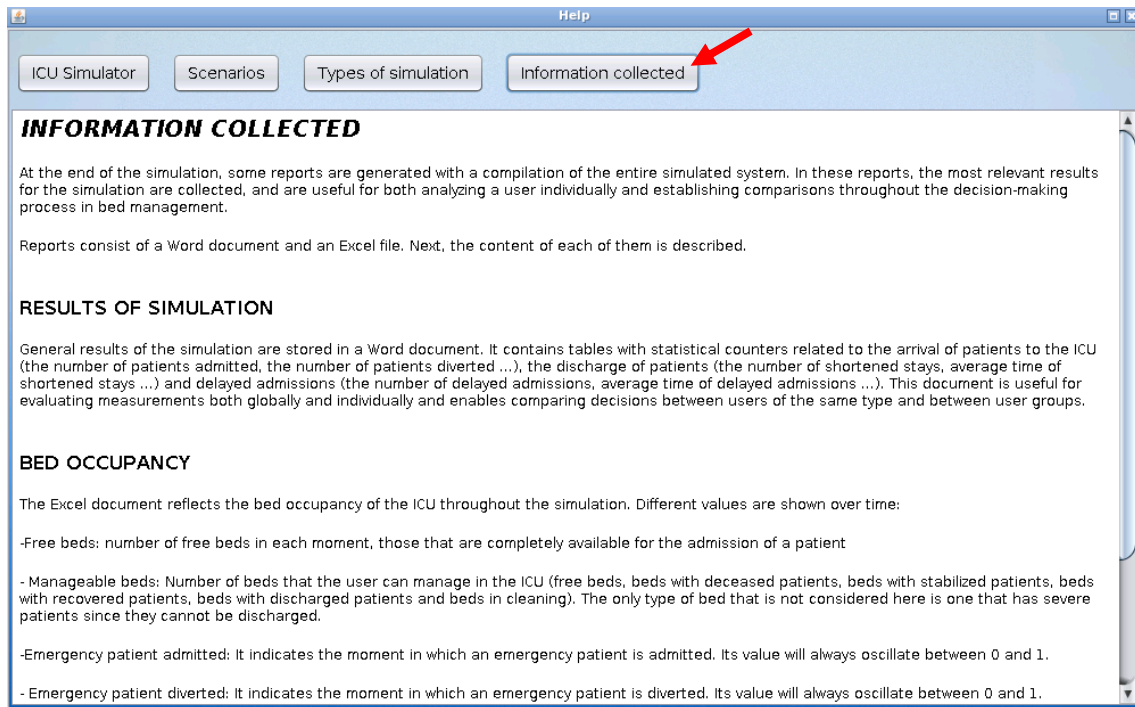


Figure D.31. Help menu with information about the information collected with the simulator.

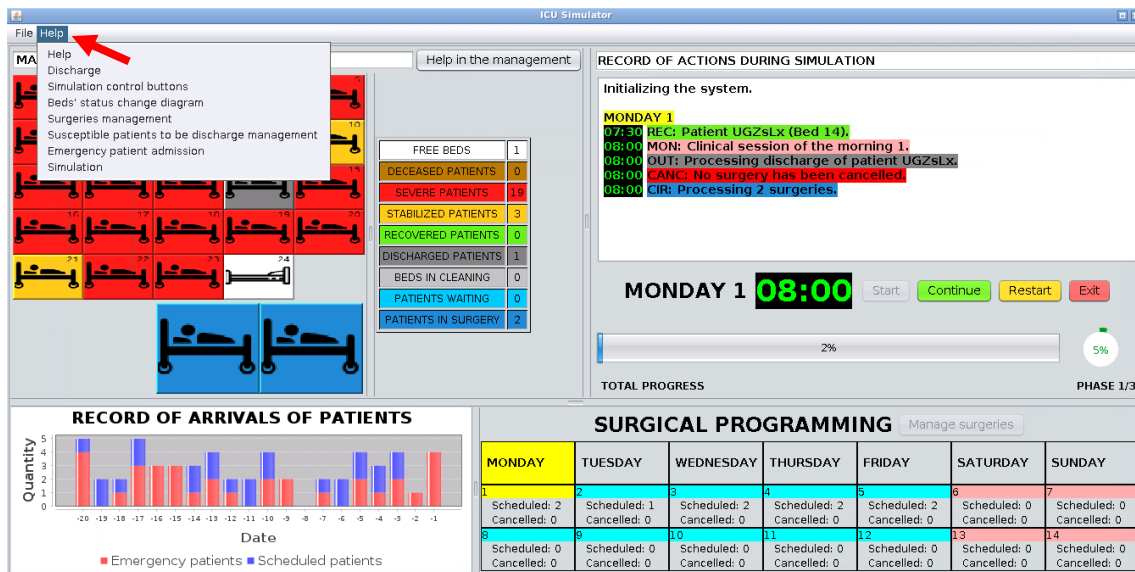


Figure D.32. Help tab about different aspects of the simulation.

Finally, this guide concludes by explaining how to correctly exit the ICU simulator. During the simulation, the user can exit the simulator at any time by pressing the "Exit" button (see Figure D.33). The simulator displays a warning window that unsaved progress will be lost upon exit. At this point, the user must press the "Logout" button in Figure D.5, and lastly, by pressing the "Exit" button in Figure D.2, the "Cerrar Sesión" button in Figure D.34 must be pressed.

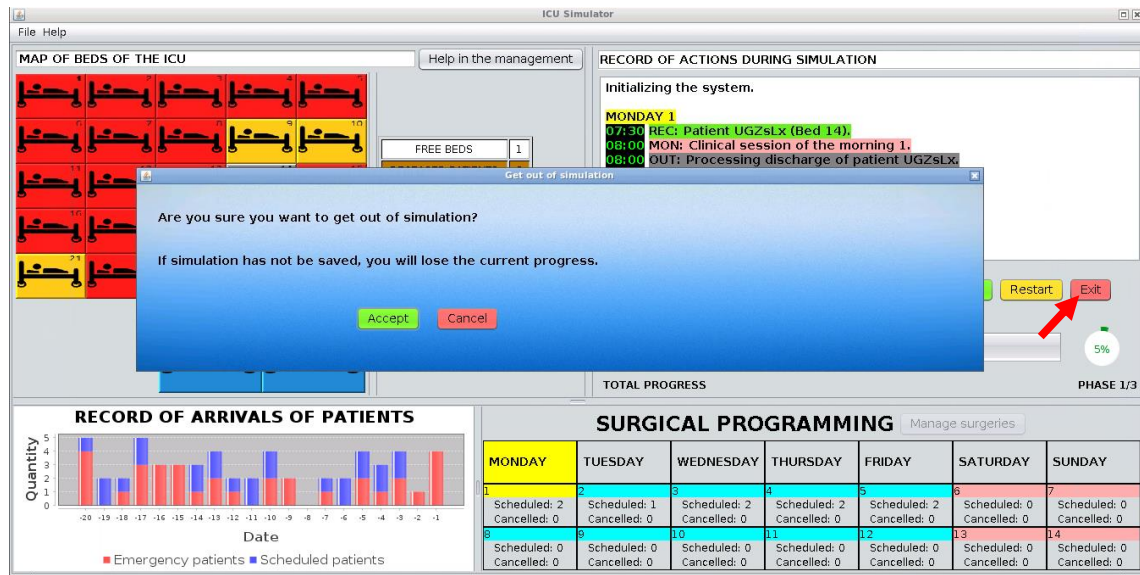


Figure D.33. The window to exit the simulation. Unsaved progress is lost.

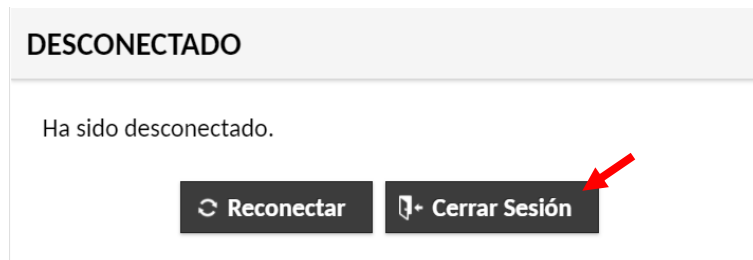


Figure D.34. The window for logging out and disconnecting from the ICU simulator.

E ICU management flight simulator results

E.1 Reviews about the ICU simulator

The following are some reviews about the ICU simulator:

- “You get into the role of the doctor very well and it feels like you are assessing the patients. It feels real. Sometimes it is difficult to decide on patient preference without having ICU experience.”
- “I liked the simulation, it is quite realistic.”
- “Congratulations, great job! I really liked the idea and how the format was developed. The same questions arise as in actual practice.”
- “I think it is a great idea to use this tool so that both healthcare professionals and people outside of healthcare know how difficult it is to carry out this task. Congratulations!”
- “I found it easier and friendlier than I thought.”
- “I found it a very useful tool.”
- “It is quite real.”
- “Congratulations on the tool!”
- “Magnificent work, a pleasure to collaborate in the simulation. Congratulations to the whole team!”
- “I loved it! Let's see if you can implement it in the ICU!”
- “I find it a very useful tool to be able to study the decision making of a hospital when it is collapsed and to understand that it is not easy to make the most appropriate decisions.”
- “Very interesting, keep up the good work!”
- “In my lack of knowledge of ICU bed management, the software seems intuitive and guides me very well through the necessary steps. However, precisely because of this lack of knowledge on my part, it is difficult for me to apply a more critical view with the aim of proposing improvements to the software that could have an impact on the actual management of an ICU.”
- “It is a pleasure to collaborate in this type of initiative.”
- “I found the simulator very interesting and a good tool for learning.”
- “Very good work!”

- “Tremendous simulator that helps to better understand the functioning of an intensive care unit and its management logic.”
- “Great simulator, which can have a very practical use in the professional field.”

E.2 Global performance results

The global results are shown below for the different types of users who, in addition to *Physicians* (see Table 5.1), have carried out the simulation: *Nurses* (see Table E.1), *Nurse technicians* (see Table E.2), *Residents* (see Table E.3), *Medical students* (see Table E.4), *OM-OR researchers* (see Table E.5), *Engineers* (see Table E.6), and *Others* (see Table E.7). Bold values represent the highest (red) and lowest (green) values.

Table E.1. Simulation global results recorded by 14 ICU nurses.

Nurse	e_{Di}	$P_i(D)$	s_{Ci}	$P_i(C)$	d_{Si} (d_{Ti})	$P_i(S)$	\bar{m}_i	$P_i(M)$
Nur_1	10	0.2941	2	0.0870	3 (38)	0.0789	4.64	0.1933
Nur_2	11	0.3235	4	0.1739	13 (33)	0.3939	3.69	0.1539
Nur_3	11	0.3235	1	0.0435	6 (35)	0.1714	4.07	0.1695
Nur_4	7	0.2059	4	0.1739	14 (34)	0.4118	2.92	0.1217
Nur_5	6	0.1765	8	0.3478	25 (34)	0.7353	3.27	0.1361
Nur_6	12	0.3529	1	0.0435	4 (37)	0.1081	5.07	0.2112
Nur_7	2	0.0588	12	0.5217	16 (31)	0.5161	3.98	0.1658
Nur_8	7	0.2059	3	0.1304	14 (35)	0.4000	2.61	0.1087
Nur_9	5	0.1471	6	0.2609	15 (35)	0.4286	3.43	0.1430
Nur_10	25	0.7353	0	0.0000	0 (32)	0.0000	6.91	0.2878
Nur_11	18	0.5294	0	0.0000	6 (33)	0.1818	5.88	0.2451
Nur_12	18	0.5294	0	0.0000	9 (34)	0.2647	5.75	0.2397
Nur_13	8	0.2353	3	0.1304	12 (35)	0.3429	2.96	0.1235
Nur_14	9	0.2647	5	0.2174	8 (34)	0.2353	4.35	0.1812

Table E.2. Simulation global results recorded by 4 ICU nurse technicians.

Nurse tech	e_{Di}	$P_i(D)$	s_{Ci}	$P_i(C)$	d_{Si} (d_{Ti})	$P_i(S)$	\bar{m}_i	$P_i(M)$
Nte_1	4	0.1176	3	0.1304	27 (40)	0.6750	2.54	0.1058
Nte_2	19	0.5588	0	0.0000	3 (35)	0.0857	6.28	0.2615
Nte_3	15	0.4412	2	0.0870	10 (35)	0.2857	4.93	0.2054
Nte_4	17	0.5000	0	0.0000	3 (34)	0.0882	5.05	0.2104

Table E.3. Simulation global results recorded by 6 residents.

Resident	e_{Di}	$P_i(D)$	s_{Ci}	$P_i(C)$	d_{Si} (d_{Ti})	$P_i(S)$	\bar{m}_i	$P_i(M)$
Res_1	5	0.1471	7	0.3043	18 (33)	0.5455	2.49	0.1038
Res_2	5	0.1471	4	0.1739	14 (36)	0.3889	3.03	0.1264
Res_3	2	0.0588	4	0.1739	27 (41)	0.6585	2.82	0.1177
Res_4	7	0.2059	3	0.1304	27 (38)	0.7105	2.56	0.1065
Res_5	6	0.1765	8	0.3478	10 (32)	0.3125	3.13	0.1305
Res_6	8	0.2353	5	0.2174	14 (33)	0.4242	3.88	0.1615

Table E.4. Simulation global results recorded by 6 medical students.

Medical student	e_{Di}	$P_i(D)$	s_{Ci}	$P_i(C)$	$d_{Si} (d_{Ti})$	$P_i(S)$	\bar{m}_i	$P_i(M)$
Mst_1	6	0.1765	4	0.1739	9 (37)	0.2432	3.46	0.1442
Mst_2	5	0.1471	5	0.2174	10 (37)	0.2703	4.26	0.1776
Mst_3	3	0.0882	9	0.3913	6 (35)	0.1714	5.22	0.2174
Mst_4	6	0.1765	5	0.2174	19 (34)	0.5588	2.53	0.1054
Mst_5	4	0.1176	3	0.1304	19 (37)	0.5135	2.94	0.1225
Mst_6	4	0.1176	5	0.2174	27 (38)	0.7105	3.11	0.1294

Table E.5. Simulation global results recorded by 11 OM-OR researchers.

OM-OR researcher	e_{Di}	$P_i(D)$	s_{Ci}	$P_i(C)$	$d_{Si} (d_{Ti})$	$P_i(S)$	\bar{m}_i	$P_i(M)$
OMr_1	10	0.2941	2	0.0870	15 (35)	0.4286	3.20	0.1333
OMr_2	5	0.1471	5	0.2174	20 (37)	0.5405	2.22	0.0925
OMr_3	4	0.1176	4	0.1739	22 (37)	0.5946	2.44	0.1017
OMr_4	11	0.3235	1	0.0435	17 (34)	0.5000	2.68	0.1115
OMr_5	8	0.2353	2	0.0870	15 (35)	0.4286	2.68	0.1117
OMr_6	7	0.2059	11	0.4783	17 (29)	0.5862	4.08	0.1701
OMr_7	8	0.2353	1	0.0435	34 (43)	0.7907	3.73	0.1555
OMr_8	6	0.1765	4	0.1739	18 (35)	0.5143	2.15	0.0898
OMr_9	4	0.1176	3	0.1304	18 (38)	0.4737	2.27	0.0944
OMr_10	4	0.1176	5	0.2174	16 (36)	0.4444	2.51	0.1046
OMr_11	6	0.1765	6	0.2609	17 (32)	0.5313	2.88	0.1199

Table E.6. Simulation global results recorded by 11 engineers.

Engineer	e_{Di}	$P_i(D)$	s_{Ci}	$P_i(C)$	$d_{Si} (d_{Ti})$	$P_i(S)$	\bar{m}_i	$P_i(M)$
Eng_1	3	0.0882	5	0.2174	14 (37)	0.3784	3.05	0.1271
Eng_2	2	0.0588	4	0.1739	16 (38)	0.4211	3.45	0.1438
Eng_3	10	0.2941	2	0.0870	13 (35)	0.3714	2.82	0.1174
Eng_4	5	0.1471	4	0.1739	25 (36)	0.6944	2.49	0.1036
Eng_5	8	0.2353	2	0.0870	21 (38)	0.5526	3.03	0.1263
Eng_6	8	0.2353	5	0.2174	8 (32)	0.2500	3.06	0.1276
Eng_7	3	0.0882	4	0.1739	26 (39)	0.6667	2.64	0.1100
Eng_8	7	0.2059	2	0.0870	16 (36)	0.4444	2.53	0.1053
Eng_9	9	0.2647	5	0.2174	5 (33)	0.1515	3.94	0.1643
Eng_10	6	0.1765	3	0.1304	23 (40)	0.5750	3.53	0.1470
Eng_11	2	0.0588	6	0.2609	23 (39)	0.5897	3.09	0.1289

Table E.7. Simulation global results recorded by 12 other users not included in former groups.

Other	e_{Di}	$P_i(D)$	s_{Ci}	$P_i(C)$	$d_{Si} (d_{Ti})$	$P_i(S)$	\bar{m}_i	$P_i(M)$
Oth_1	5	0.1471	5	0.2174	8 (35)	0.2286	3.22	0.1341
Oth_2	5	0.1471	3	0.1304	17 (37)	0.4595	2.77	0.1152
Oth_3	10	0.2941	8	0.3478	0 (36)	0.0000	7.91	0.3295
Oth_4	6	0.1765	5	0.2174	16 (32)	0.5000	2.54	0.1057
Oth_5	5	0.1471	3	0.1304	17 (37)	0.4595	2.41	0.1002
Oth_6	8	0.2353	3	0.1304	13 (37)	0.3514	3.43	0.1427

Oth_7	7	0.2059	4	0.1739	19 (37)	0.5135	2.83	0.1177
Oth_8	5	0.1471	2	0.0870	21 (40)	0.5250	2.58	0.1076
Oth_9	4	0.1176	5	0.2174	17 (35)	0.4857	2.19	0.0913
Oth_10	21	0.6176	0	0.0000	0 (36)	0.0000	7.72	0.3216
Oth_11	7	0.2059	2	0.0870	19 (37)	0.5135	2.31	0.0960
Oth_12	15	0.4412	0	0.0000	3 (36)	0.0833	4.88	0.2033

E.3 Global results considering the ICU pressure level

Below are all the tables for each type of user of the results when the pressure level is considered (except for the one of physicians which has already been shown in Chapter 5). Also included here are graphs of the conditional probabilities for each user type and the probability of each user type observing each pressure level. Table E.8 summarises information about which tables and figures contain this information for each type of user.

Table E.8. Information about the specific tables and figures for each group.

Group	Table of conditional probabilities	Figure of conditional probabilities
Physicians	Table 5.10	Figure E.1
Nurses	Table E.9	Figure E.2
Nurse techs	Table E.10	Figure E.3
Residents	Table E.11	Figure E.4
Medical students	Table E.12	Figure E.5
OM-OR researchers	Table E.13	Figure E.6
Engineers	Table E.14	Figure E.7
Others	Table E.15	Figure E.8

Table E.9. Simulation global results recorded by 14 ICU nurses considering the ICU pressure level.

Nurse	$P_i(D)$					$P_i(C)$					$P_i(S)$				
	L_1	L_2	L_3	L_4	L_5	L_1	L_2	L_3	L_4	L_5	L_1	L_2	L_3	L_4	L_5
Nur_1	0.200	0.000	0.462	0.600	-	0.000	0.000	0.200	0.500	-	0.000	0.105	0.000	0.500	-
Nur_2	0.000	0.286	0.308	0.444	0.500	0.000	0.000	0.167	0.500	-	0.000	0.500	0.333	0.400	1.000
Nur_3	0.000	0.500	0.250	0.667	0.000	0.000	0.000	0.000	0.500	-	0.000	0.125	0.250	0.667	1.000
Nur_4	0.000	0.000	0.118	0.375	0.400	0.000	0.000	0.077	0.333	1.000	0.000	0.000	0.421	0.600	1.000
Nur_5	0.000	0.000	0.182	0.286	-	0.000	0.000	1.000	0.750	-	0.400	0.842	0.667	0.750	-
Nur_6	0.167	0.167	0.615	0.333	-	0.000	0.143	0.000	-	-	0.056	0.167	0.143	-	-
Nur_7	0.000	0.000	0.063	0.250	-	0.000	0.333	0.778	1.000	-	0.000	0.500	0.643	0.500	-
Nur_8	-	0.000	0.071	0.167	1.000	0.000	0.000	0.000	0.500	-	0.000	0.143	0.471	0.714	-
Nur_9	-	0.100	0.214	0.100	-	0.000	0.000	0.143	0.833	-	0.000	0.556	0.444	0.333	-
Nur_10	0.769	0.643	0.833	1.000	-	0.000	0.000	0.000	-	-	0.000	0.000	0.000	-	-
Nur_11	0.273	0.636	0.636	1.000	-	0.000	0.000	0.000	-	-	0.208	0.125	0.000	-	-
Nur_12	0.375	0.500	0.667	1.000	-	0.000	0.000	0.000	-	-	0.208	0.444	0.000	-	-
Nur_13	-	0.000	0.200	0.273	1.000	0.000	0.000	0.000	0.429	-	0.000	0.091	0.417	0.750	-
Nur_14	0.333	0.000	0.333	0.600	1.000	0.000	0.273	0.125	0.500	-	0.000	0.267	0.429	0.500	-

Table E.10. Simulation global results recorded by 4 ICU nurse technicians considering the ICU pressure level.

Nurse tech	$P_i(D)$					$P_i(C)$					$P_i(S)$				
	L_1	L_2	L_3	L_4	L_5	L_1	L_2	L_3	L_4	L_5	L_1	L_2	L_3	L_4	L_5
Nte_1	-	0.000	0.000	0.091	0.500	0.000	0.000	0.000	0.125	1.000	0.400	0.667	0.700	0.714	1.000
Nte_2	0.364	0.588	0.800	1.000	-	0.000	0.000	0.000	-	-	0.040	0.286	0.000	-	-
Nte_3	0.400	0.400	0.500	0.500	-	0.000	0.000	0.167	0.500	-	0.263	0.400	0.000	0.333	-
Nte_4	0.000	0.385	0.667	1.000	-	0.000	0.000	0.000	-	-	0.059	0.167	0.000	-	-

Table E.11. Simulation global results recorded by 6 residents considering the ICU pressure level.

Resident	$P_i(D)$					$P_i(C)$					$P_i(S)$				
	L_1	L_2	L_3	L_4	L_5	L_1	L_2	L_3	L_4	L_5	L_1	L_2	L_3	L_4	L_5
Res_1	-	0.000	0.077	0.133	1.000	0.000	0.000	0.000	0.700	-	0.000	0.500	0.571	0.778	-
Res_2	-	0.000	0.158	0.250	0.000	0.000	0.000	0.143	-	1.000	0.000	0.250	0.400	1.000	1.000
Res_3	-	0.000	0.063	0.000	0.333	0.000	0.000	0.000	0.500	1.000	0.000	0.800	0.650	0.857	-
Res_4	-	0.000	0.091	0.167	0.667	0.000	0.000	0.000	0.167	1.000	0.000	0.571	0.824	0.778	1.000
Res_5	-	0.000	0.125	0.273	1.000	0.000	0.000	0.364	1.000	-	0.000	0.000	0.375	0.800	-
Res_6	0.000	0.111	0.235	0.429	-	0.000	0.111	0.273	0.500	-	0.400	0.389	0.500	0.500	-

Table E.12. Simulation global results recorded by 6 medical students considering the ICU pressure level.

Medical student	$P_i(D)$					$P_i(C)$					$P_i(S)$				
	L_1	L_2	L_3	L_4	L_5	L_1	L_2	L_3	L_4	L_5	L_1	L_2	L_3	L_4	L_5
Mst_1	-	0.000	0.188	0.250	0.500	0.000	0.091	0.000	0.500	1.000	0.000	0.125	0.250	0.750	1.000
Mst_2	0.000	0.000	0.188	0.400	-	0.000	0.000	0.500	0.500	-	0.125	0.350	0.167	0.333	-
Mst_3	0.000	0.071	0.167	0.000	-	0.000	0.429	0.667	1.000	-	0.000	0.250	0.375	0.500	-
Mst_4	-	0.000	0.000	0.250	1.000	0.000	0.000	0.000	0.556	-	0.000	0.250	0.667	0.667	-
Mst_5	-	0.000	0.059	0.200	1.000	0.000	0.000	0.154	0.333	-	0.000	0.333	0.609	0.750	-
Mst_6	-	0.000	0.063	0.000	1.000	0.000	0.125	0.250	0.333	-	0.000	0.846	0.667	0.857	-

Table E.13. Simulation global results recorded by 11 OM-OR researchers considering the ICU pressure level.

OM-OR researcher	$P_i(D)$					$P_i(C)$					$P_i(S)$				
	L_1	L_2	L_3	L_4	L_5	L_1	L_2	L_3	L_4	L_5	L_1	L_2	L_3	L_4	L_5
OMr_1	-	0.000	0.188	0.444	1.000	0.000	0.000	0.000	0.400	-	0.000	0.214	0.600	0.750	-
OMr_2	-	0.000	0.000	0.118	0.750	0.000	0.000	0.000	0.500	1.000	0.000	0.200	0.615	0.714	1.000
OMr_3	-	0.000	0.000	0.083	0.500	0.000	0.000	0.000	0.250	1.000	0.000	0.429	0.625	0.778	1.000
OMr_4	-	0.000	0.231	0.533	0.000	0.000	0.000	0.000	0.250	-	0.000	0.286	0.600	0.750	-
OMr_5	-	0.000	0.133	0.333	0.600	0.000	0.000	0.000	0.000	1.000	0.000	0.143	0.467	0.714	1.000
OMr_6	0.000	0.143	0.200	0.375	-	0.200	0.375	0.750	0.667	-	0.111	0.857	0.500	0.750	-
OMr_7	0.000	0.000	0.333	0.222	1.000	0.000	0.000	0.000	0.200	-	0.429	0.714	0.941	1.000	-
OMr_8	-	0.000	0.077	0.077	0.667	0.000	0.000	0.000	0.250	1.000	0.000	0.250	0.615	0.583	1.000
OMr_9	-	0.000	0.000	0.083	0.500	0.000	0.000	0.000	0.125	1.000	0.000	0.400	0.471	0.600	1.000
OMr_10	-	0.000	0.000	0.176	0.500	0.000	0.000	0.000	0.500	-	0.000	0.250	0.533	0.538	-
OMr_11	-	0.000	0.188	0.000	1.000	0.000	0.000	0.111	0.714	-	0.000	0.615	0.636	0.500	-

Table E.14. Simulation global results recorded by 11 engineers considering the ICU pressure level.

Engineer	$P_i(D)$					$P_i(C)$					$P_i(S)$				
	L_1	L_2	L_3	L_4	L_5	L_1	L_2	L_3	L_4	L_5	L_1	L_2	L_3	L_4	L_5
Eng_1	0.000	0.000	0.000	0.125	0.500	0.000	0.250	0.000	0.250	1.000	0.000	0.333	0.250	0.857	1.000
Eng_2	0.000	0.000	0.048	0.167	-	0.000	0.167	0.143	0.500	-	0.000	0.286	0.545	0.667	-
Eng_3	-	0.000	0.000	0.643	1.000	0.000	0.000	0.000	0.500	-	0.000	0.000	0.600	0.200	-
Eng_4	-	0.000	0.083	0.000	0.800	0.000	0.000	0.000	0.333	1.000	0.000	0.667	0.769	0.857	1.000

Eng_5	-	0.000	0.182	0.182	1.000	0.000	0.000	0.000	0.333	-	0.000	0.385	0.667	0.800	-
Eng_6	-	0.000	0.067	0.583	-	0.000	0.000	0.167	0.750	-	0.000	0.222	0.231	0.500	-
Eng_7	-	0.000	0.133	0.083	0.000	0.000	0.000	0.000	0.333	1.000	0.000	0.778	0.563	0.909	-
Eng_8	-	0.000	0.067	0.091	0.833	0.000	0.000	0.000	0.250	-	0.000	0.000	0.412	0.727	1.000
Eng_9	0.000	0.250	0.188	0.500	-	0.000	0.083	0.333	0.500	-	0.000	0.100	0.222	0.400	-
Eng_10	0.000	0.111	0.182	0.100	1.000	0.000	0.091	0.000	0.400	-	0.250	0.556	0.750	0.833	-
Eng_11	-	0.000	0.059	0.100	-	0.000	0.000	0.273	0.750	-	0.000	0.813	0.385	0.833	-

Table E.15. Simulation global results recorded by 12 other users not included in former groups considering the ICU pressure level.

Other	$P_i(D)$					$P_i(C)$					$P_i(S)$				
	L_1	L_2	L_3	L_4	L_5	L_1	L_2	L_3	L_4	L_5	L_1	L_2	L_3	L_4	L_5
Oth_1	0.000	0.000	0.176	0.182	-	0.000	0.000	0.111	0.667	-	0.000	0.222	0.083	0.625	-
Oth_2	-	0.000	0.059	0.250	0.500	0.000	0.000	0.000	0.250	1.000	0.000	0.429	0.526	0.400	1.000
Oth_3	0.192	0.571	1.000	-	-	0.316	0.500	-	-	-	0.000	0.000	-	-	-
Oth_4	-	0.000	0.000	0.286	1.000	0.000	0.000	0.100	0.500	-	0.000	0.375	0.636	0.600	-
Oth_5	-	0.000	0.000	0.091	0.667	0.000	0.000	0.000	0.167	1.000	0.000	0.200	0.444	0.667	1.000
Oth_6	0.000	0.111	0.091	0.364	1.000	0.000	0.000	0.000	0.375	-	0.000	0.200	0.500	0.700	-
Oth_7	-	0.000	0.143	0.267	1.000	0.000	0.000	0.000	0.571	-	0.000	0.615	0.538	0.500	-
Oth_8	-	0.000	0.000	0.167	0.750	0.000	0.000	0.000	0.000	1.000	0.000	0.200	0.545	0.778	1.000
Oth_9	-	0.000	0.000	0.000	0.667	0.000	0.000	0.000	0.375	1.000	0.000	0.250	0.467	0.700	1.000
Oth_10	0.550	0.667	0.800	-	-	0.000	0.000	-	-	-	0.000	0.000	-	-	-
Oth_11	-	0.000	0.077	0.154	0.667	0.000	0.000	0.000	0.000	1.000	0.000	0.000	0.563	0.667	1.000
Oth_12	0.000	0.385	0.667	0.500	-	0.000	0.000	0.000	0.000	-	0.000	0.111	0.250	0.500	-

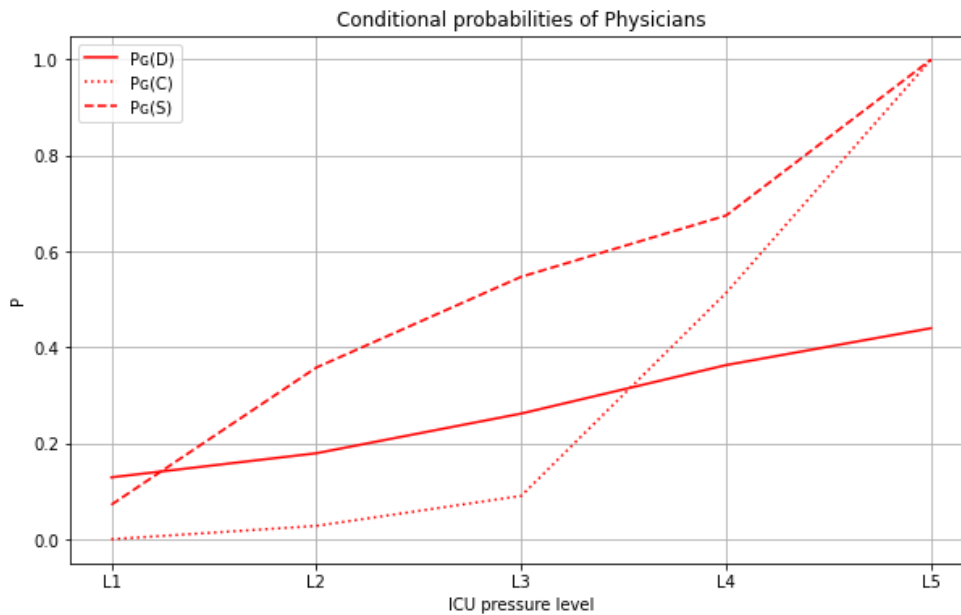


Figure E.1. Conditional probabilities recorded by 18 ICU physicians.

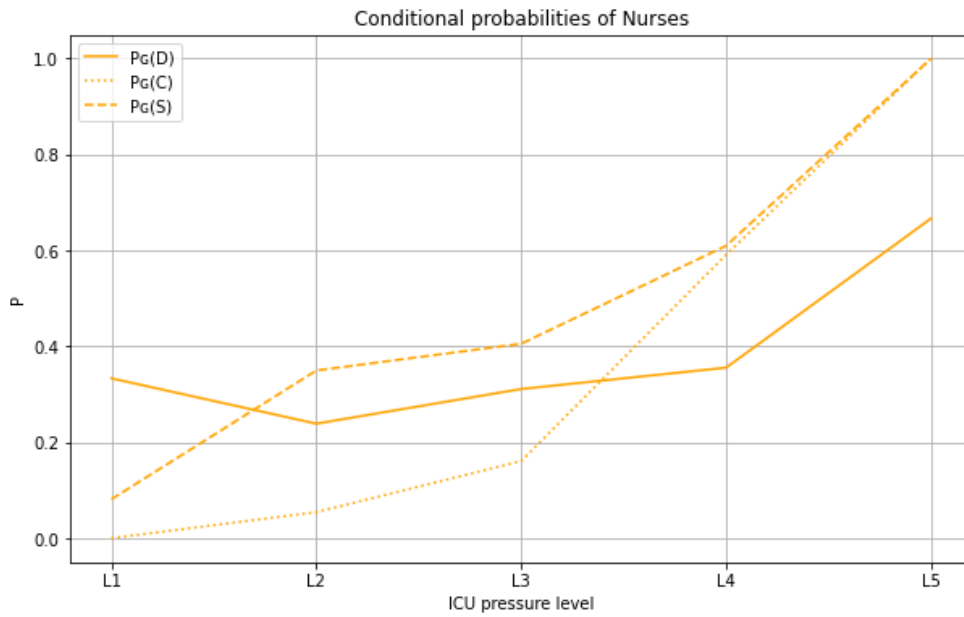


Figure E.2. Conditional probabilities recorded by 14 ICU nurses.

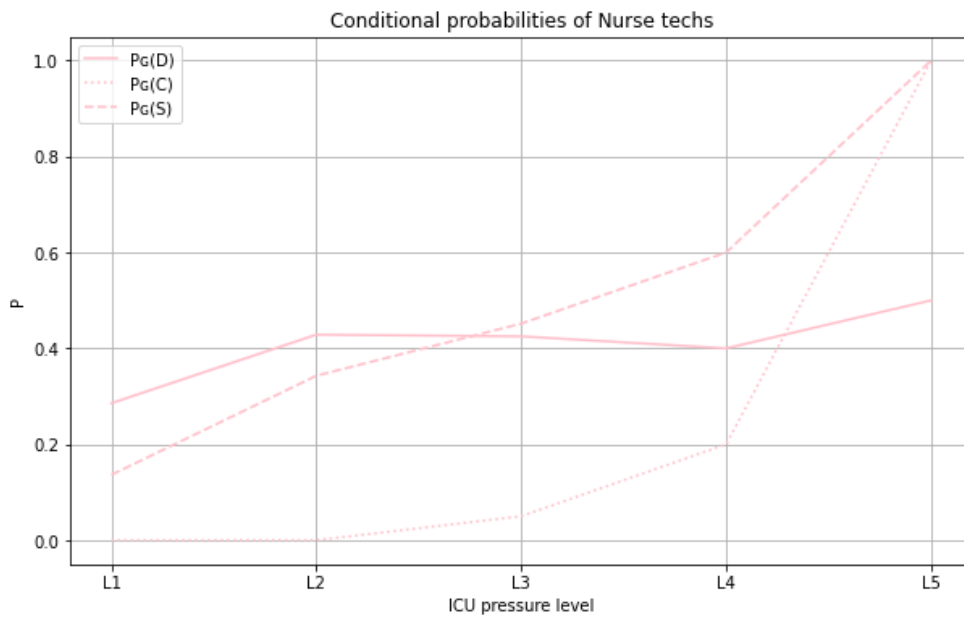


Figure E.3. Conditional probabilities recorded by 4 ICU nurse technicians.

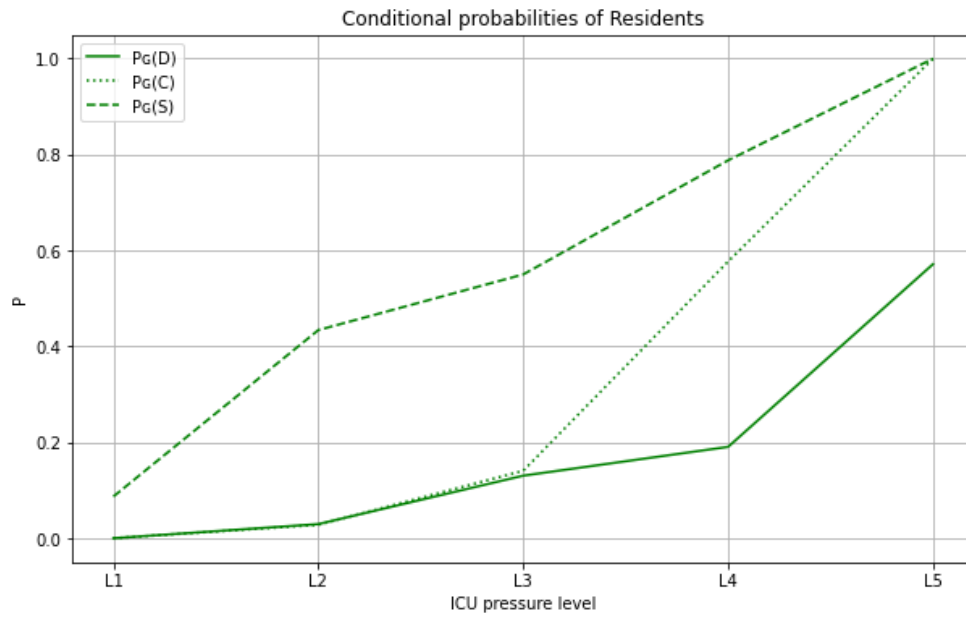


Figure E.4. Conditional probabilities recorded by 6 residents.

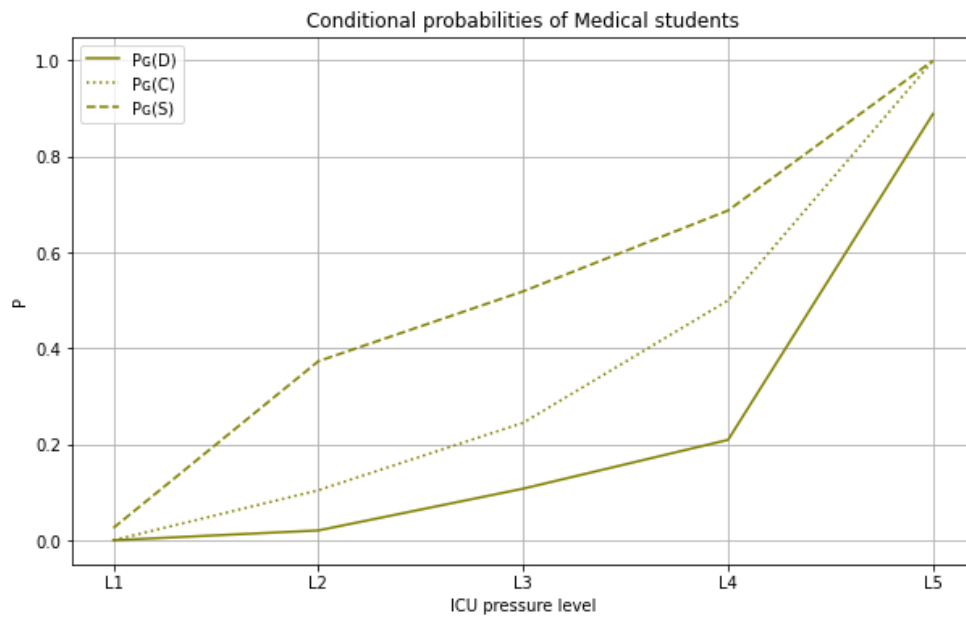


Figure E.5. Conditional probabilities recorded by 6 medical students.

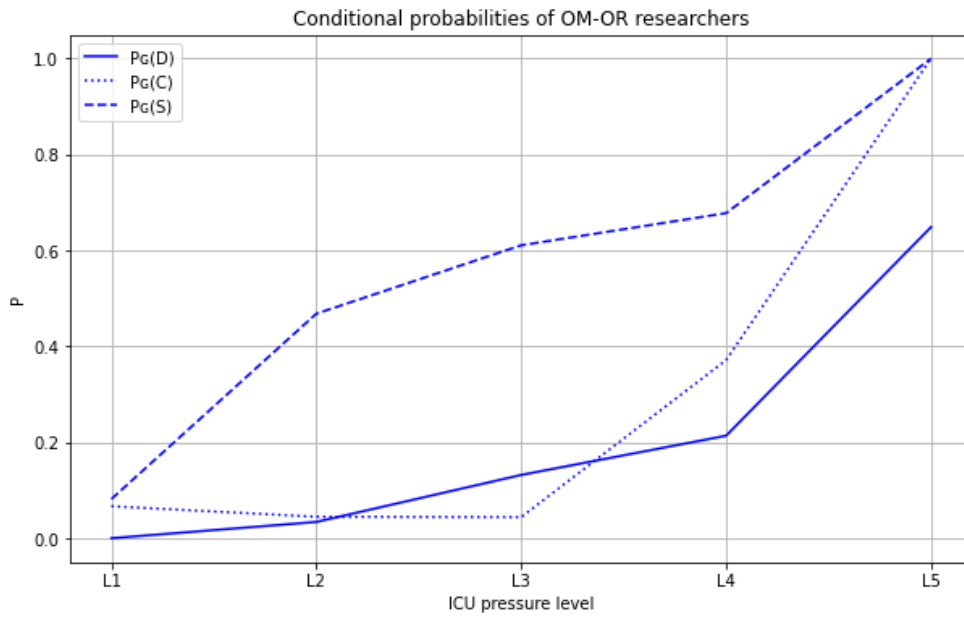


Figure E.6. Conditional probabilities recorded by 11 OM-OR researchers.

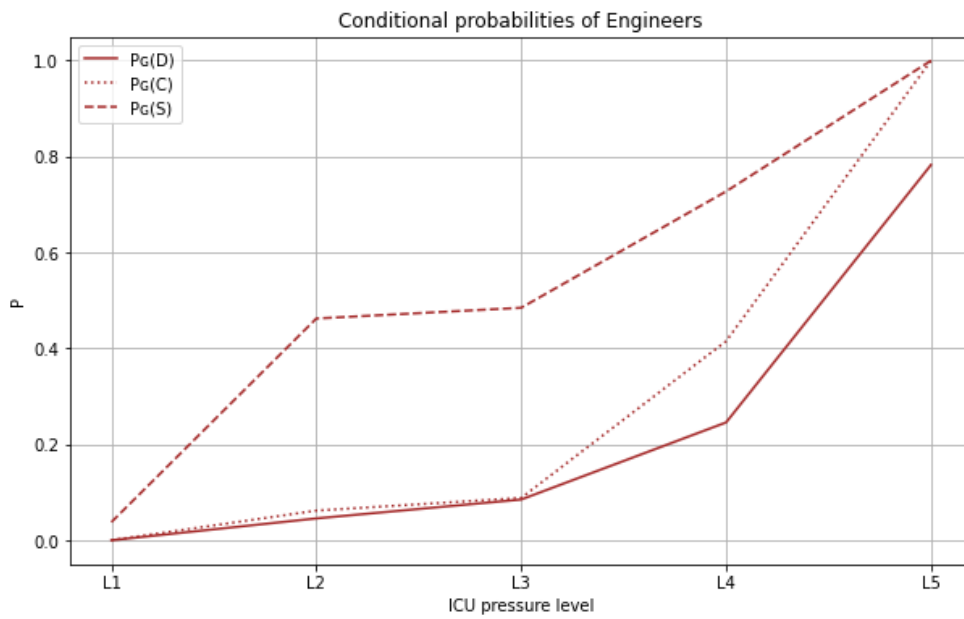


Figure E.7. Conditional probabilities recorded by 11 engineers.

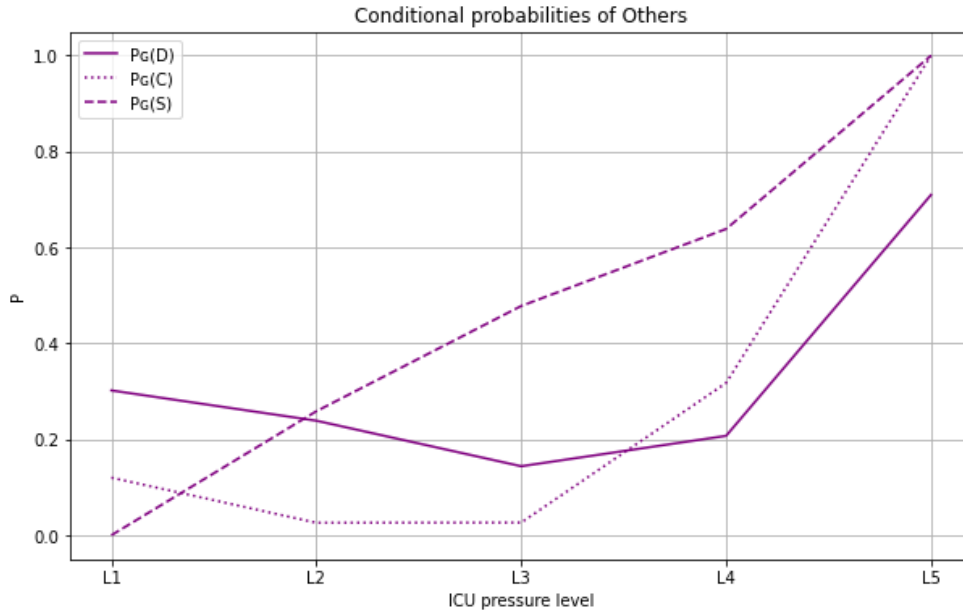


Figure E.8. Conditional probabilities recorded by 12 other users not included in former groups.

E.4 Temporal evolution of the number of manageable beds

In this section, the number of *manageable beds* in the ICU over time is shown for the different types of users: *Physicians* (see Figure E.9), *Nurses* (see Figure E.10), *Nurse technicians* (see Figure E.11), *Residents* (see Figure E.12), *Medical students* (see Figure E.13), *OM-OR researchers* (see Figure E.14), *Engineers* (see Figure E.15), and *Others* (see Figure E.16).

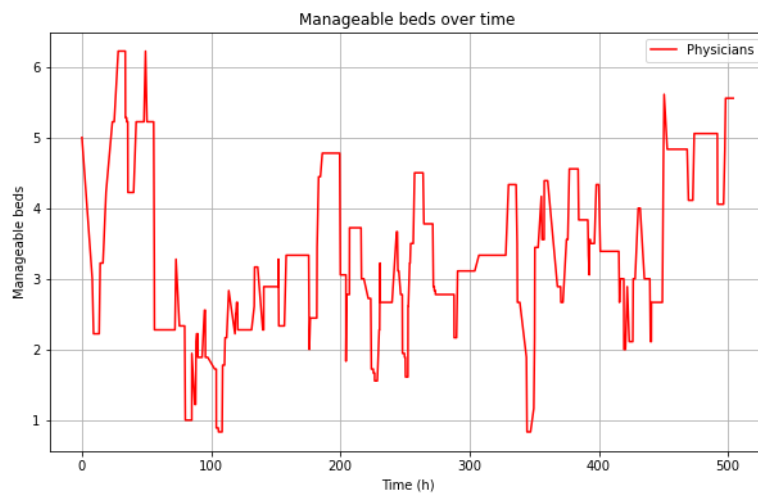


Figure E.9. Graph showing the trajectory of the mean number of manageable beds of 18 ICU physicians.

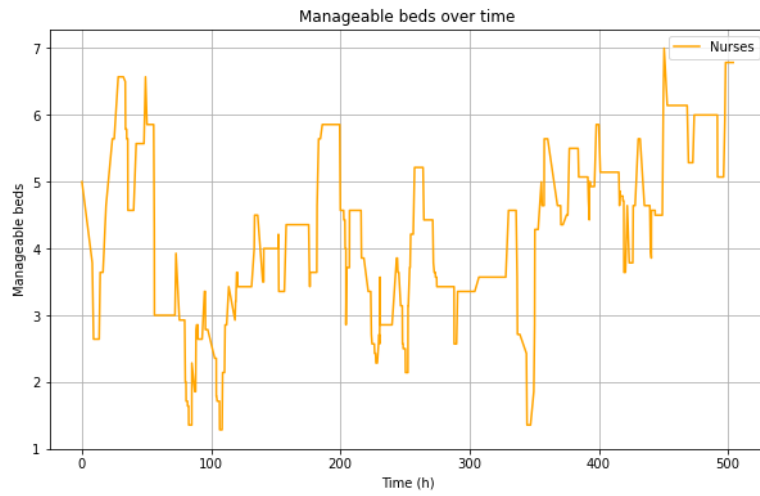


Figure E.10. Graph showing the trajectory of the mean number of manageable beds of 14 ICU nurses.

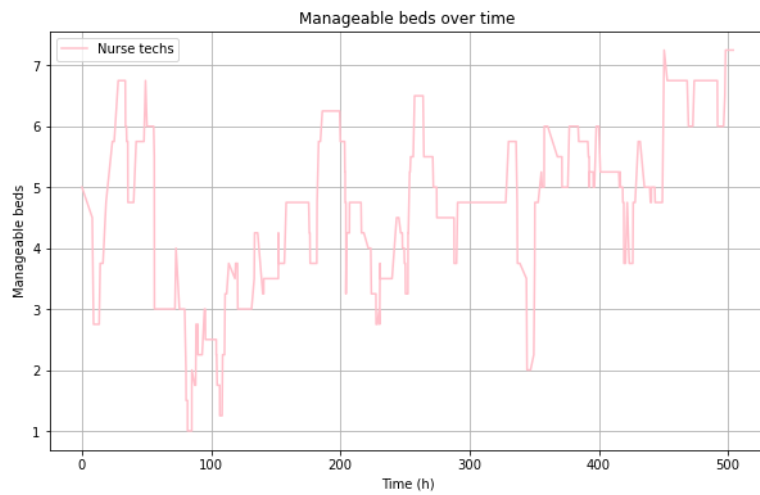


Figure E.11. Graph showing the trajectory of the mean number of manageable beds of 4 ICU nurse technicians.

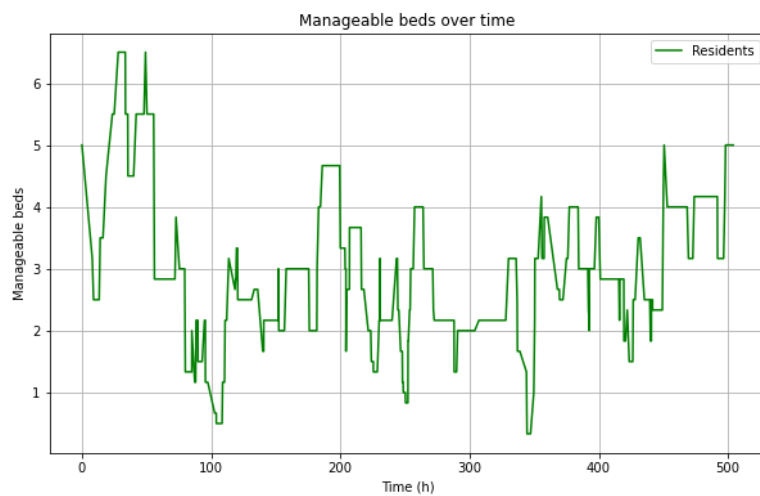


Figure E.12. Graph showing the trajectory of the mean number of manageable beds of 6 residents.

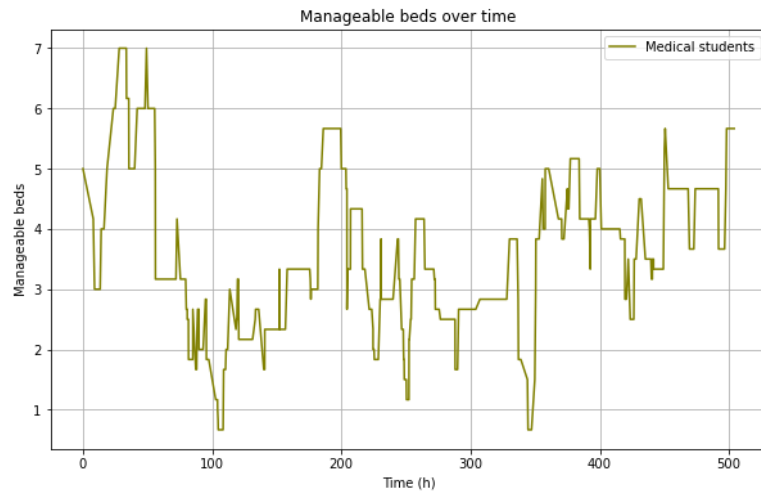


Figure E.13. Graph showing the trajectory of the mean number of manageable beds of 6 medical students.

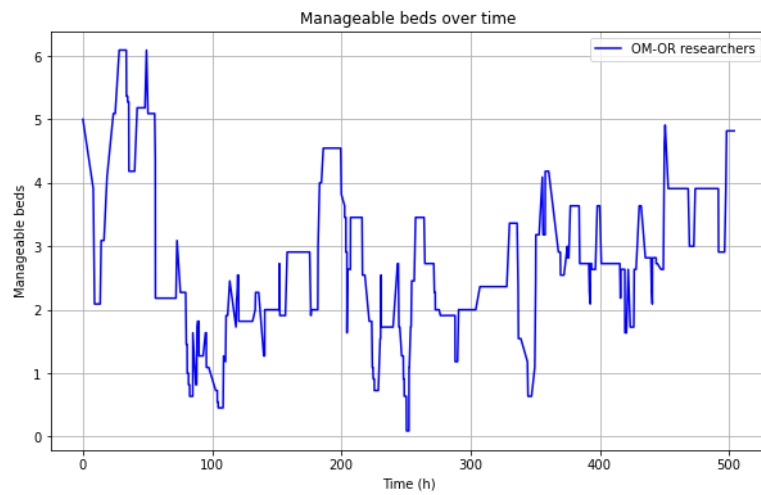


Figure E.14. Graph showing the trajectory of the mean number of manageable beds of 11 OM-OR researchers.

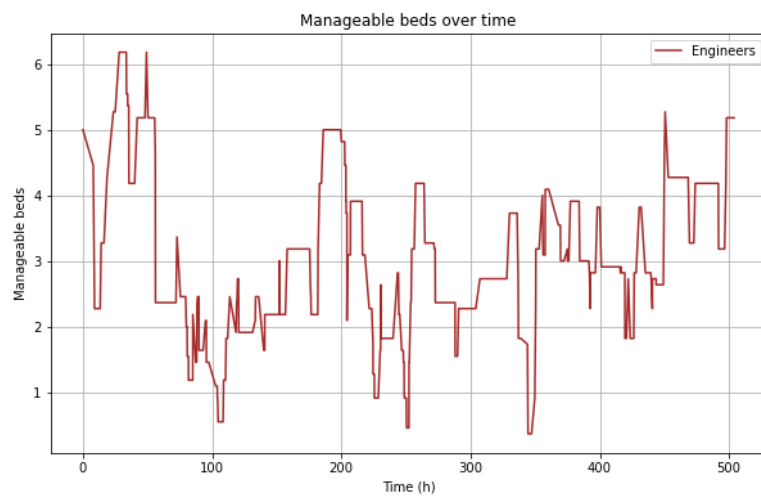


Figure E.15. Graph showing the trajectory of the mean number of manageable beds of 11 engineers.

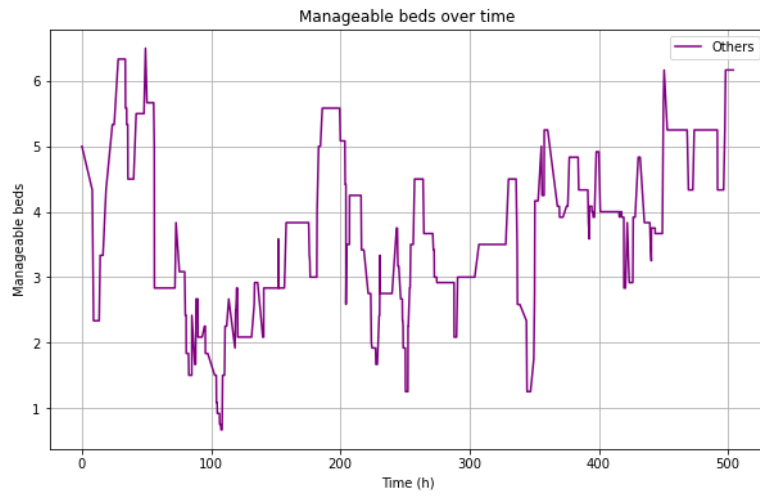


Figure E.16. Graph showing the trajectory of the mean number of manageable beds of by12 other users not included in former groups.

F Aggregation of neighbouring components in distance calculation

F.1 Analysis of the Euclidean-Aggregate distance expression

The Euclidean-Aggregate distance has two main parts in its expression in equation (5.12), which we denote as S_1 and S_2 for notation simplicity. Thus, $\delta_{EA}^2(i, j) = S_1 + S_2$. The main part of the definition of δ_{EA}^2 is included in S_1 . For each size s between 1 and Q , all possible aggregated neighbouring components of the two observations are formed and the Euclidean distance between each of them is calculated. Given an observation of Q components, the aggregated neighbouring components of size s consist of summing s neighbouring components.

Thus, with $s = 1$ we have Q aggregations (each of the components), with $s = 2$ we have $Q - 1$ aggregations (the sum of each component and its next), and so on up to $s = Q$ where only one aggregation is possible, which is the sum of all the components. As s increases, fewer aggregations can be formed. At this point it should be clarified that, for example, aggregations of size 5 contain: 2 aggregations of size 4, 3 aggregations of size 3, 4 aggregations of size 2, and 5 aggregations of size 1, which are taken into account again. Figure F.1 shows a diagram of how neighbouring components are aggregated for each iteration k of S_1 (representing the size s). The variable l indicates each of the aggregations formed at each iteration k .

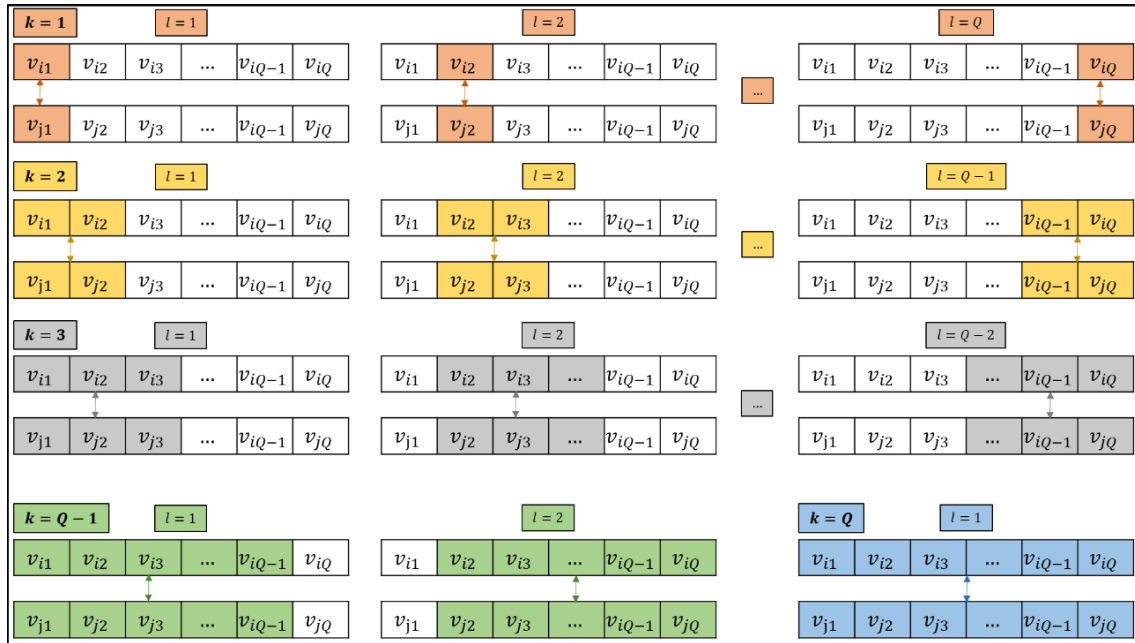


Figure F.1. Diagram of the aggregations included in term S_1 of the Euclidean-Aggregate distance between two observations. For each iteration k , all possible aggregations of size $s = k$ are formed and the Euclidean distance between them is calculated.

With the first part of the expression of the Euclidean-Aggregate distance (S_1), the weakness of the Euclidean distance in terms of the permutation of the components is solved. We can note this if we calculate δ_{EA} between those observations proposed in Section 5.3.3 (\vec{e}_{D1} , \vec{e}_{D2} , and \vec{e}_{D3}) considering only S_1 . Assigning the weights as $\alpha_k = \omega_s = 1/Q$, where $Q = 5$, the following distances between the observations are obtained: $\delta_{EA}(1,2) = 0.200 < \delta_{EA}(2,3) = 0.253 < \delta_{EA}(1,3) = 0.268$. However, by introducing a new observation $\vec{e}_{D4} = [1, 1, 1, 1, 1]$, so that $\delta_{EA}(1,4) = \delta_{EA}(2,4) = \delta_{EA}(3,4)$, what is obtained by applying S_1 is: $\delta_{EA}(3,4) = 0.200 < \delta_{EA}(1,4) = 0.253 < \delta_{EA}(2,4) = 0.268$. This occurs because when grouping the neighbouring components from the beginning to the end of the vector of observations, the central components are taken into account more often than those at the edges. Therefore, the differences observed in the aggregations of the central components are larger with respect to those observed for the components of the edges. This is the reason why $\delta_{EA}(2,4)$ is the largest distance obtained since the difference between observations is located in the central component, $e_{D2}(L_3)$.

Consequently, with S_2 the decompensation of the components of the edges is corrected. The aim is that aggregations of the same size s are taken into account in the distance calculation the same number of times. In this part of δ_{EA} , aggregations of neighbouring components are added, starting at the edges of the observations, for each size s from 1 to $Q - 2$ (note that in S_2 when $k = Q - 1$ the summand is 0). Figure F.2 shows how, for each size s , aggregations of neighbouring components are compensated from the edges. The number of times each aggregation needs to be added depends on its size s . For example, for $s = Q$ and $s = Q - 1$

there is no need to add terms since in S_1 they are already compensated. For $s = Q - 2$, however, the aggregations from the edges are included 3 times in S_1 while the aggregation from component 2 to component $Q - 1$ is taken into account 4 times. Therefore, 1 aggregation from each edge must be added in S_2 to compensate. Table F.1 shows the final amount of each aggregation of size s included in the expressions S_1 and S_2 (further information on the number of aggregations considered according to their size is given in Appendix F.2).

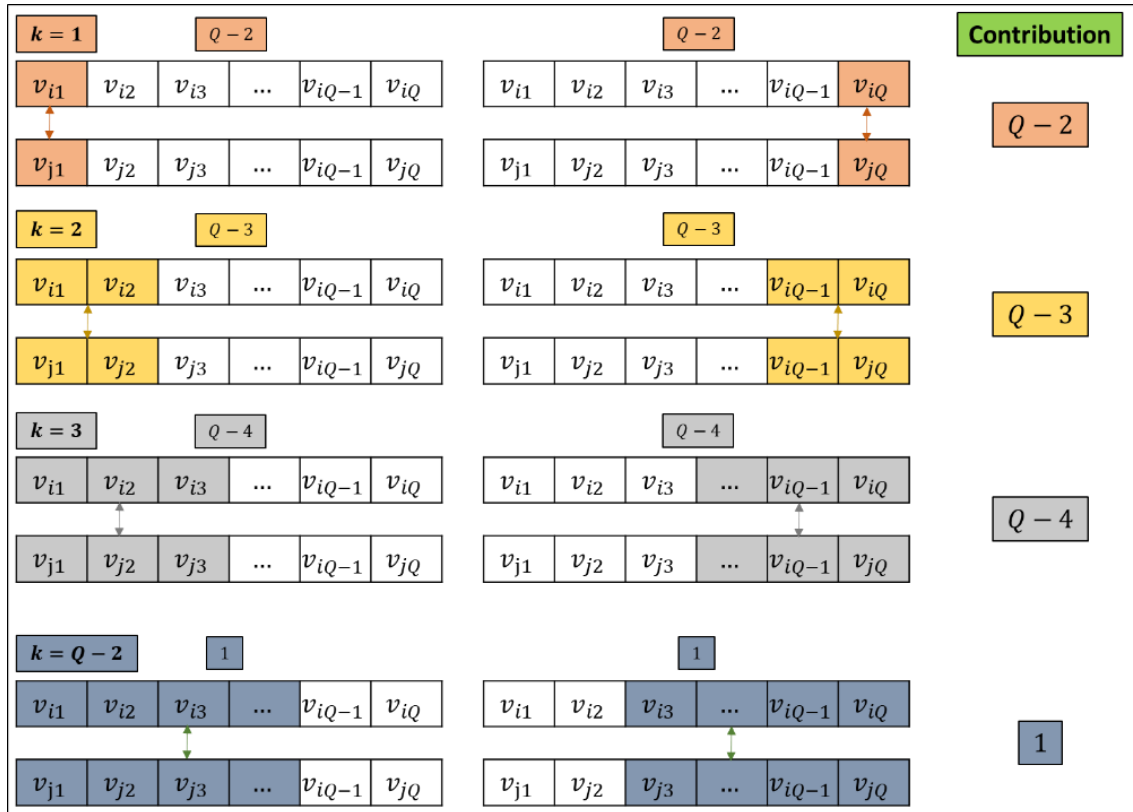


Figure F.2. Diagram of the aggregations included in term S_2 of the Euclidean-Aggregate distance between two observations. For each iteration k , the aggregations of size $s = k$ at the edges are included and the Euclidean distance between them is calculated.

By recalculating the distances between the vectors \vec{e}_{D1} , \vec{e}_{D2} , \vec{e}_{D3} , and \vec{e}_{D4} , and applying the two parts of the Euclidean-Aggregate distance (S_1 and S_2), the following results are obtained. On the one hand, since the aggregations of the central components and those of the edges have been compensated, the distances between the vector \vec{e}_{D4} and the rest are the same: $\delta_{EA}(1,4) = 0.297 = \delta_{EA}(2,4) = 0.297 = \delta_{EA}(3,4) = 0.297$. On the other hand, the property of the permutation of the components is preserved, that is, the position of each component is still taken into account: $\delta_{EA}(1,2) = 0.253 < \delta_{EA}(2,3) = 0.335 < \delta_{EA}(1,3) = 0.379$. Thus, the results are consistent when applying this methodology to compare decisions that depend on the ICU pressure level.

Table F.1. Final amount of each aggregation of size s included in the expressions S_1 and S_2 .

Size	Final amount of each aggregation
1	$1 + \frac{Q(Q-1)}{2}$
2	$1 + \frac{(Q-1)(Q-2)}{2}$
3	$1 + \frac{(Q-2)(Q-3)}{2}$
s	$1 + \frac{(Q-s+1)(Q-s)}{2}$
$Q-4$	11
$Q-3$	7
$Q-2$	4
$Q-1$	2
Q	1

F.2 Number of aggregations considered according to their size

The number of aggregations of neighbouring components included in the calculation of the Euclidean-Aggregate distance is different depending on the size s of these aggregations (see Table F.1) In this appendix, we prove that for the same size s , the number of times each aggregation is considered is constant when adding the contributions of S_1 and S_2 (remember that the Euclidean-Aggregate distance has been expressed as $\delta_{EA}^2(i, j) = S_1 + S_2$ in Appendix F.1) and corresponds to what is shown in Table F.1. Before the demonstrations, the notation of some of the elements used in the rest of the appendix are defined below.

First, let us define $v_{iA,B}$ as the aggregation of neighbouring components of user i from position A to position B , both included (see equation (F.1)). Thus, aggregations of size $s = 1$ would have the notation $v_{iA,A}$, of size $s = 2$ $v_{iA,A+1}$, and so on. As an example, $v_{i3,7}$ indicates the aggregation of components 3, 4, 5, 6, and 7, that is, $v_{i3,7} = v_{i3} + v_{i4} + v_{i5} + v_{i6} + v_{i7}$.

$$v_{iA,B} = \sum_{m=A}^B v_{im} \quad (\text{F.1})$$

Also, we define a function $f(x, y)$ that indicates, for a vector of size y , the number of positions between position x and the nearest edge of the vector (position x is also counted). For example, considering a vector of size $y = 7$, the resulting function would be as follows: $f(x, y): \{(1,7), (2,7), (3,7), (4,7), (5,7), (6,7), (7,7)\} \mapsto \{1,2,3,4,3,2,1\}$. This function is similar to the function of taking the minimum between two numbers N_1 and N_2 ($\min\{N_1, N_2\}$), which is defined in equation (F.2), where N_1 would be x and N_2 would be $y + 1 - x$. With this consideration, the function $f(x, y)$ is defined in equation (F.3). This definition of $f(x, y)$ has been introduced to simplify the notation in the rest of the appendix. Note that $f(x, y) = \min\{x, y + 1 - x\}$.

$$\min\{N_1, N_2\} = \frac{N_1 + N_2}{2} - \left| \frac{N_1 - N_2}{2} \right| = \begin{cases} N_1 & \text{if } N_1 < N_2 \\ N_2 & \text{if } N_1 \geq N_2 \end{cases} \quad (\text{F.2})$$

$$f(x, y) = \frac{y + 1}{2} - \left| x - \frac{y + 1}{2} \right|, \quad \forall x, y \in \mathbb{N} | x \leq y \quad (\text{F.3})$$

The following 5 figures illustrate the number of times each aggregation is considered for each size s , and in both S_1 and S_2 . Each figure shows the aggregation size s considered, the final quantity of all aggregations of that size s (same expressions as shown in Table F.1), and two tables with the quantities of each of the aggregations of size s that are taken into account in each iteration of S_1 and S_2 . The information for $s = 1$, $s = 2$, and $s = 3$ can be seen in Figure F.3, Figure F.4, and Figure F.5 respectively.

		$s = 1$				$1 + \frac{Q(Q-1)}{2}$		
S_1	Iteration	$v_{i1,1}$	$v_{i2,2}$	$v_{i3,3}$	$v_{i,m,m}$	$v_{iQ-2,Q-2}$	$v_{iQ-1,Q-1}$	$v_{iQ,Q}$
	1	1	1	1	1	1	1	1
	2	1	2	2	2	2	2	1
	3	1	2	3	3	3	2	1
	k	1	2	3	$\min\{f(k, Q), f(m, Q)\}$	3	2	1
	$Q-2$	1	2	3	3	3	2	1
	$Q-1$	1	2	2	2	2	2	1
	Q	1	1	1	1	1	1	1
	Total	Q	$2(Q-1)$	$3(Q-2)$	$m(Q-m+1)$	$3(Q-2)$	$2(Q-1)$	Q
S_2	Iteration	$v_{i1,1}$	$v_{i2,2}$	$v_{i3,3}$	$v_{i,m,m}$	$v_{iQ-2,Q-2}$	$v_{iQ-1,Q-1}$	$v_{iQ,Q}$
	1	$Q-2$	0	0	0	0	0	$Q-2$
	2	$Q-3$	$Q-3$	0	0	0	$Q-3$	$Q-3$
	3	$Q-4$	$Q-4$	$Q-4$	0	$Q-4$	$Q-4$	$Q-4$
	k	$Q-k-1$	$Q-k-1$	$Q-k-1$	$\begin{cases} 0 & \text{if } k \leq f(m, Q) - 1 \\ Q-k-1 & \text{if } f(m, Q) - 1 < k \leq Q - f(m, Q) \\ 2(Q-k-1) & \text{if } Q - f(m, Q) < k \leq Q-2 \\ 0 & \text{if } k > Q-2 \end{cases}$	$Q-k-1$	$Q-k-1$	$Q-k-1$
	$Q-2$	1	1	2	2	2	1	1
	Total	$\frac{(Q-2)(Q-1)}{2}$	$\frac{(Q-3)(Q-2)}{2}$	$\frac{(Q-4)(Q-3)}{2} + 1$	$\frac{(Q-m-1)(Q-m)}{2} + \frac{(m-2)(m-1)}{2}$	$1 + \frac{(Q-4)(Q-3)}{2}$	$\frac{(Q-3)(Q-2)}{2}$	$\frac{(Q-2)(Q-1)}{2}$

Figure F.3. Number of times each aggregation of $s = 1$ is considered in both S_1 and S_2 .

$s = 2$		$1 + \frac{(Q-1)(Q-2)}{2}$						
S_1	Iteration	$v_{i1,2}$	$v_{i2,3}$	$v_{i3,4}$	$v_{im,m+1}$	$v_{iQ-3,Q-2}$	$v_{iQ-2,Q-1}$	$v_{iQ-1,Q}$
	1	0	0	0	0	0	0	0
	2	1	1	1	1	1	1	1
	3	1	2	2	2	2	2	1
	k	1	2	3	$\min\{f(k-1, Q-1), f(m, Q-1)\}$	3	2	1
	$Q-2$	1	2	3	3	3	2	1
	$Q-1$	1	2	2	2	2	2	1
	Q	1	1	1	1	1	1	1
S_2	Total	$Q-1$	$2(Q-2)$	$3(Q-3)$	$m(Q-m)$	$3(Q-3)$	$2(Q-2)$	$Q-1$
	Iteration	$v_{i1,2}$	$v_{i2,3}$	$v_{i3,4}$	$v_{im,m+1}$	$v_{iQ-3,Q-2}$	$v_{iQ-2,Q-1}$	$v_{iQ-1,Q}$
	1	0	0	0	0	0	0	0
	2	$Q-3$	0	0	0	0	0	$Q-3$
	3	$Q-4$	$Q-4$	0	0	0	$Q-4$	$Q-4$
	k	$Q-k-1$	$Q-k-1$	$Q-k-1$	$\begin{cases} 0 & \text{if } k \leq f(m, Q-1) - 1 \\ Q-k-1 & \text{if } f(m, Q-1) - 1 < k \leq Q - f(m, Q-1) \\ 2(Q-k-1) & \text{if } Q - f(m, Q-1) < k \leq Q-2 \\ 0 & \text{if } k > Q-2 \end{cases}$	$Q-k-1$	$Q-k-1$	$Q-k-1$
	$Q-2$	1	1	2	2	2	1	1
	Total	$\frac{(Q-3)(Q-2)}{2}$	$\frac{(Q-4)(Q-3)}{2}$	$\frac{(Q-5)(Q-4)}{2} + 1$	$\frac{(Q-m-2)(Q-m-1)}{2} + \frac{(m-2)(m-1)}{2}$	$1 + \frac{(Q-5)(Q-4)}{2}$	$\frac{(Q-4)(Q-3)}{2}$	$\frac{(Q-3)(Q-2)}{2}$

Figure F.4. Number of times each aggregation of $s = 2$ is considered in both S_1 and S_2 .

$s = 3$		$1 + \frac{(Q-2)(Q-3)}{2}$						
S_1	Iteration	$v_{i1,3}$	$v_{i2,4}$	$v_{i3,5}$	$v_{im,m+2}$	$v_{iQ-4,Q-2}$	$v_{iQ-3,Q-1}$	$v_{iQ-2,Q}$
	1	0	0	0	0	0	0	0
	2	0	0	0	0	0	0	0
	3	1	1	1	1	1	1	1
	k	1	2	$\begin{cases} 2 & \text{if } k=4 \\ 3 & \text{if } k>4 \end{cases}$	$\min\{f(k-2, Q-2), f(m, Q-2)\}$	$\begin{cases} 2 & \text{if } k=4 \\ 3 & \text{if } k>4 \end{cases}$	2	1
	$Q-2$	1	2	3	3	3	2	1
	$Q-1$	1	2	2	2	2	2	1
	Q	1	1	1	1	1	1	1
S_2	Total	$Q-2$	$2(Q-3)$	$3(Q-4)$	$m(Q-m-1)$	$3(Q-4)$	$2(Q-3)$	$Q-2$
	Iteration	$v_{i1,3}$	$v_{i2,4}$	$v_{i3,5}$	$v_{im,m+2}$	$v_{iQ-4,Q-2}$	$v_{iQ-3,Q-1}$	$v_{iQ-2,Q}$
	1	0	0	0	0	0	0	0
	2	0	0	0	0	0	0	0
	3	$Q-4$	0	0	0	0	0	$Q-4$
	k	$Q-k-1$	$Q-k-1$	$\begin{cases} 0 & \text{if } k=4 \\ Q-k-1 & \text{if } k>4 \end{cases}$	$\begin{cases} 0 & \text{if } k \leq f(m, Q-2) - 1 \\ Q-k-1 & \text{if } f(m, Q-2) - 1 < k \leq Q - f(m, Q-2) \\ 2(Q-k-1) & \text{if } Q - f(m, Q-2) < k \leq Q-2 \\ 0 & \text{if } k > Q-2 \end{cases}$	$\begin{cases} 0 & \text{if } k=4 \\ Q-k-1 & \text{if } k>4 \end{cases}$	$Q-k-1$	$Q-k-1$
	$Q-2$	1	1	2	2	2	1	1
	Total	$\frac{(Q-4)(Q-3)}{2}$	$\frac{(Q-5)(Q-4)}{2}$	$\frac{(Q-6)(Q-5)}{2} + 1$	$\frac{(Q-m-3)(Q-m-2)}{2} + \frac{(m-2)(m-1)}{2}$	$1 + \frac{(Q-6)(Q-5)}{2}$	$\frac{(Q-5)(Q-4)}{2}$	$\frac{(Q-4)(Q-3)}{2}$

Figure F.5. Number of times each aggregation of $s = 3$ is considered in both S_1 and S_2 .

Figure F.6, shows the information of general size s . From these general expressions as a function of s , tables with the information for any size s can be obtained. Finally, the information for $s = Q - 2$, $s = Q - 1$, and $s = Q$ is shown in Figure F.7. By adding the expressions of the last rows (*Total*) for each aggregation at each size s , the expressions of Table F.1 are obtained (for the same size s the same expression is always obtained). Equation (F.4) shows the development of the general case of size s for the central aggregations of $v_{im,m+s-1}$. Adding the expressions in row *Total* we obtain the expression shown in Table F.1 for the

general case s . Therefore, as the remaining expressions are derived from the general case, the contributions of the remaining aggregations are proved.

S_1

s

$1 + \frac{(Q-s+1)(Q-s)}{2}$

Iteration	$V_{1,s}$	$V_{2,s+1}$	$V_{3,s+2}$	$V_{m,s+1}$	$V_{Q-s-1,Q-2}$	$V_{Q-s-1,Q-1}$	$V_{Q-s+1,Q}$
1	0	0	0	0	0	0	0
2	0	0	0	0	0	0	0
3	0	0	0	0	0	0	0
k	$\begin{cases} 0 & \text{if } k < s \\ 1 & \text{if } k = s \\ 2 & \text{if } k > s \end{cases}$	$\begin{cases} 0 & \text{if } k < s \\ 1 & \text{if } k = s \\ 2 & \text{if } k > s+1 \end{cases}$	$\begin{cases} 0 & \text{if } k < s \\ 1 & \text{if } k = s \\ 2 & \text{if } k = s+1 \\ 3 & \text{if } k > s+1 \end{cases}$	$\begin{cases} 0 & \text{if } k < s \\ \min(f(k-s+1, Q-s+1), f(m, Q-s+1)) & \text{if } k = s \\ 0 & \text{if } k > s \end{cases}$	$\begin{cases} 0 & \text{if } k < s \\ 1 & \text{if } k = s \\ 2 & \text{if } k = s+1 \\ 3 & \text{if } k > s+1 \end{cases}$	$\begin{cases} 0 & \text{if } k < s \\ 1 & \text{if } k = s \\ 2 & \text{if } k > s \end{cases}$	$\begin{cases} 0 & \text{if } k < s \\ 1 & \text{if } k = s \\ 1 & \text{if } k > s \end{cases}$
$Q-2$	1	2	3	3	3	2	1
$Q-1$	1	2	2	2	2	2	1
Q	1	1	1	1	1	1	1
Total	$Q-s+1$	$2(Q-s)$	$3(Q-s-1)$	$m(Q-s-m+2)$	$3(Q-s-1)$	$2(Q-s)$	$Q-s+1$

Iteration	$V_{1,s}$	$V_{2,s+1}$	$V_{3,s+2}$	$V_{m,s+1}$	$V_{Q-s-1,Q-2}$	$V_{Q-s-1,Q-1}$	$V_{Q-s+1,Q}$
1	0	0	0	0	0	0	0
2	0	0	0	0	0	0	0
3	0	0	0	0	0	0	0
k	$\begin{cases} 0 & \text{if } k \leq s-1 \\ Q-k-1 & \text{if } k = s \\ 0 & \text{if } k > s \end{cases}$	$\begin{cases} 0 & \text{if } k \leq s+1 \\ Q-k-1 & \text{if } k > s+1 \end{cases}$	$\begin{cases} 0 & \text{if } k \leq (m, Q-s+1)-1 \\ 2(Q-k-1) & \text{if } f(m, Q-s+1)-1 < k \leq Q-f(m, Q-s+1) \\ 0 & \text{if } Q-f(m, Q-s+1) < k \leq Q-2 \\ 0 & \text{if } k > Q-2 \end{cases}$	$\begin{cases} 0 & \text{if } k \leq (m, Q-s+1) \\ (Q-s-m)(Q-s-m+1) & \text{if } (m-2)(m-1) < k \leq Q-2 \\ 0 & \text{if } k > Q-2 \end{cases}$	$\begin{cases} 0 & \text{if } k \leq s+1 \\ Q-k-1 & \text{if } k > s+1 \end{cases}$	$\begin{cases} 0 & \text{if } k \leq s \\ Q-k-1 & \text{if } k > s \end{cases}$	$\begin{cases} 0 & \text{if } k \leq s-1 \\ Q-k-1 & \text{if } k > s-1 \end{cases}$
$Q-2$	1	2	2	2	2	1	1
Total	$\frac{(Q-s-1)(Q-s)}{2}$	$\frac{(Q-s-3)(Q-s-2)}{2} + 1$	$\frac{(Q-s-m)(Q-s-m+1)}{2} + \frac{(m-2)(m-1)}{2}$	$\frac{(Q-s-1)(Q-s)}{2}$	$\frac{(Q-s-2)(Q-s-1)}{2}$	$\frac{(Q-s-1)(Q-s)}{2}$	$\frac{(Q-s-1)(Q-s)}{2}$

S_2

Figure F.6. Number of times each aggregation of size s is considered in both S_1 and S_2 .

$s = Q - 2$				$s = Q - 1$			$s = Q$	
4				2			1	
S_1				S_1			S_1	
Iteration	$v_{i1,Q-2}$	$v_{i2,Q-1}$	$v_{i3,Q}$	Iteration	$v_{i1,Q-1}$	$v_{i2,Q}$	Iteration	$v_{i1,Q}$
1	0	0	0	1	0	0	1	0
2	0	0	0	2	0	0	2	0
3	0	0	0	3	0	0	3	0
k	0	0	0	k	0	0	k	0
Q-2	1	1	1	Q-2	0	0	Q-2	0
Q-1	1	2	1	Q-1	1	1	Q-1	0
Q	1	1	1	Q	1	1	Q	1
Total	3	4	3	Total	2	2	Total	1
S_2				S_2			S_2	
Iteration	$v_{i1,Q-2}$	$v_{i2,Q-1}$	$v_{i3,Q}$	Iteration	$v_{i1,Q-1}$	$v_{i2,Q}$	Iteration	$v_{i1,Q}$
1	0	0	0	1	0	0	1	0
2	0	0	0	2	0	0	2	0
3	0	0	0	3	0	0	3	0
k	0	0	0	k	0	0	k	0
Q-2	1	0	1	Q-2	0	0	Q-2	0
Total	1	0	1	Total	0	0	Total	0

Figure F.7. Number of times each aggregation of $s = Q - 2$, $s = Q - 1$, and $s = Q$ is considered in both S_1 and S_2 .

$$\begin{aligned}
& m(Q - s - m + 2) + \frac{(Q - s - m)(Q - s - m + 1)}{2} + \frac{(m - 2)(m - 1)}{2} \\
&= Qm - sm - m^2 + 2m \\
&+ \frac{Q^2 - 2Qs - 2Qm + Q + 2sm + s^2 - s + m^2 - m}{2} \\
&+ \frac{m^2 - 3m + 2}{2} = \frac{Q^2 - 2Qs + Q + s^2 - s + 2}{2} \tag{F.4} \\
&= 1 + \frac{Q^2 - 2Qs + s^2 + Q - s}{2} \\
&= 1 + \frac{(Q - s + 1)(Q - s)}{2}
\end{aligned}$$

G Using PG models to represent the evolution of the COVID-19 pandemic

G.1 Statistical analysis to elucidate the suitability of PG models

The parameter estimation of the PG models is done by minimizing the sum of squared errors. There are functions implemented in free software that perform this estimation of parameters, for instance, the *curve_fit()* function in the *optimize* module of SciPy in [Python](#) or the [growthrates package in R](#). The fit quality is measured by the Mean Absolute Errors (MAE). Table G.1 includes all MAE values calculated for each country and model. The best fits are marked in bold (differences less than 0.1% are not distinguished). Additional information in this table is the total population of each country and the total number of positive cases on June 15, 2020.

Table G.2 lists the figures in which, for each country, the fits of the four PG models are shown. In every figure, the Logistic function is shown in red, the Gompertz function in green, the Richards function in blue, and the Stannard function in purple.

Table G.1. The 20 most-affected countries by COVID-19 until June 15, 2020. The last four columns show the MAE calculated for the fit with each of the applied models.

#	Country	Population	Total positive cases (2020-06-15)	Logistic	Gompertz	Richards	Stannard
1	USA	330,922,877	2,094,069	47,128.9	21,461.2	21,464.4	21,466.7
2	Brazil	212,496,348	867,624	3,182.3	3,245.1	2,754.7	2,754.7
3	Russia	145,932,063	528,964	5,667.4	1,688.7	1,689.0	1,689.2
4	India	1,379,418,901	332,424	1,392.9	537.9	538.0	538.2
5	UK	67,871,466	295,889	4,758.0	1,046.6	1,046.9	1,047.2
6	Spain	46,754,084	245,194	5,676.2	2,261.7	2,262.1	2,262.6
7	Italy	60,465,149	236,989	4,928.0	1,061.2	1,061.6	1,061.7
8	Peru	32,951,046	229,736	2,399.4	1,255.3	1,256.6	1,257.6
9	Iran	83,944,885	187,427	8,105.8	6,176.3	6,176.6	6,176.9
10	Germany	83,773,297	186,461	4,091.4	1,519.2	1,519.5	1,519.7
11	Turkey	84,299,464	178,239	5,335.7	2,418.3	2,418.8	2,419.1
12	Chile	19,109,226	174,293	1,132.5	1,601.2	1,068.5	1,068.5
13	France	65,267,844	157,220	3,396.4	1,547.0	1,547.2	1,547.3
14	Mexico	128,873,820	153,507	1,418.9	1,641.0	1,535.5	1,535.5
15	Pakistan	220,685,460	144,478	1,631.5	1,324.5	1,301.0	1,321.6
16	Saudi Arabia	34,788,836	127,541	1,709.0	814.9	814.9	814.9
17	Canada	37,728,057	98,776	1,494.6	331.0	331.1	331.1
18	Bangladesh	164,618,467	87,520	655.6	315.5	315.6	315.7
19	China	1,439,323,776	84,335	1,166.6	1,133.0	1,097.6	1,097.7
20	Qatar	2,807,805	79,602	417.7	369.2	263.6	263.6

Bold values represent the best scores.

Table G.2. List of figures with graphs of cumulative positive cases in each country, fitted with each of the four PG models.

#	Country	Figure of fits obtained from the four PG models
1	USA	Figure G.1
2	Brazil	Figure G.2
3	Russia	Figure G.3
4	India	Figure G.4
5	UK	Figure G.5
6	Spain	Figure G.6
7	Italy	Figure G.7
8	Peru	Figure G.8
9	Iran	Figure G.9
10	Germany	Figure G.10
11	Turkey	Figure G.11
12	Chile	Figure G.12
13	France	Figure G.13
14	Mexico	Figure G.14
15	Pakistan	Figure G.15
16	Saudi Arabia	Figure G.16
17	Canada	Figure G.17
18	Bangladesh	Figure G.18
19	China	Figure G.19
20	Qatar	Figure G.20

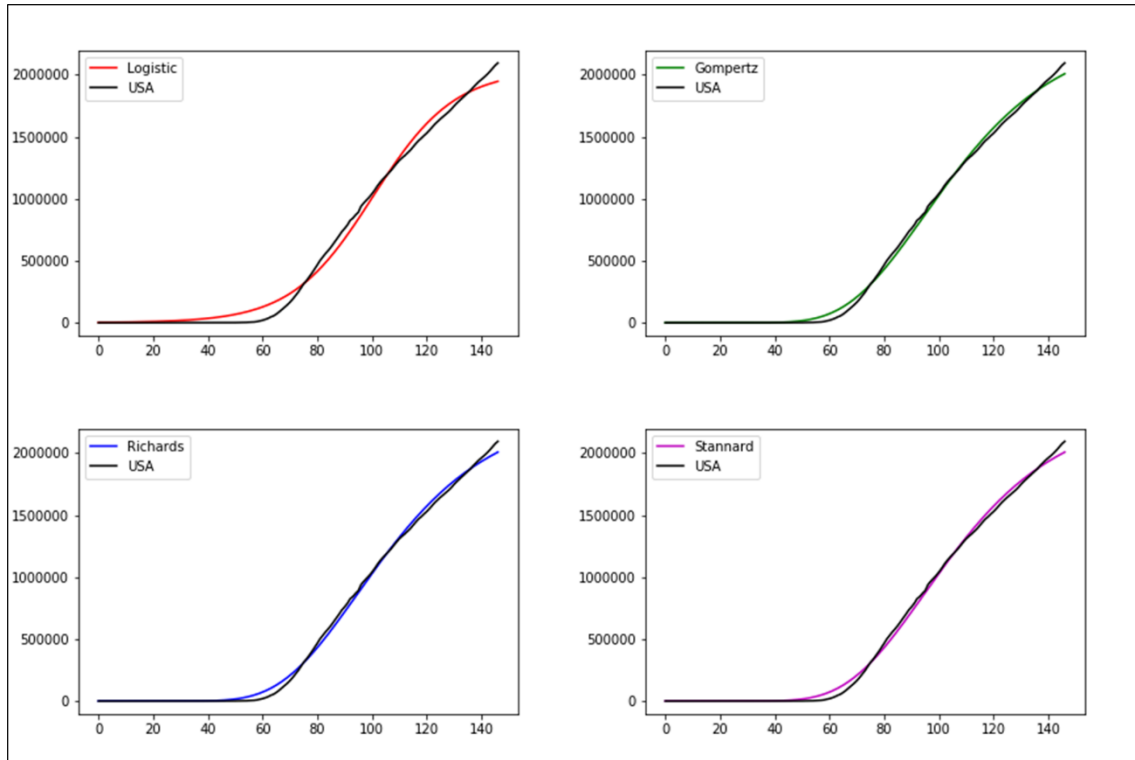


Figure G.1. Cumulative positive cases in USA and fits obtained from the four PG models.

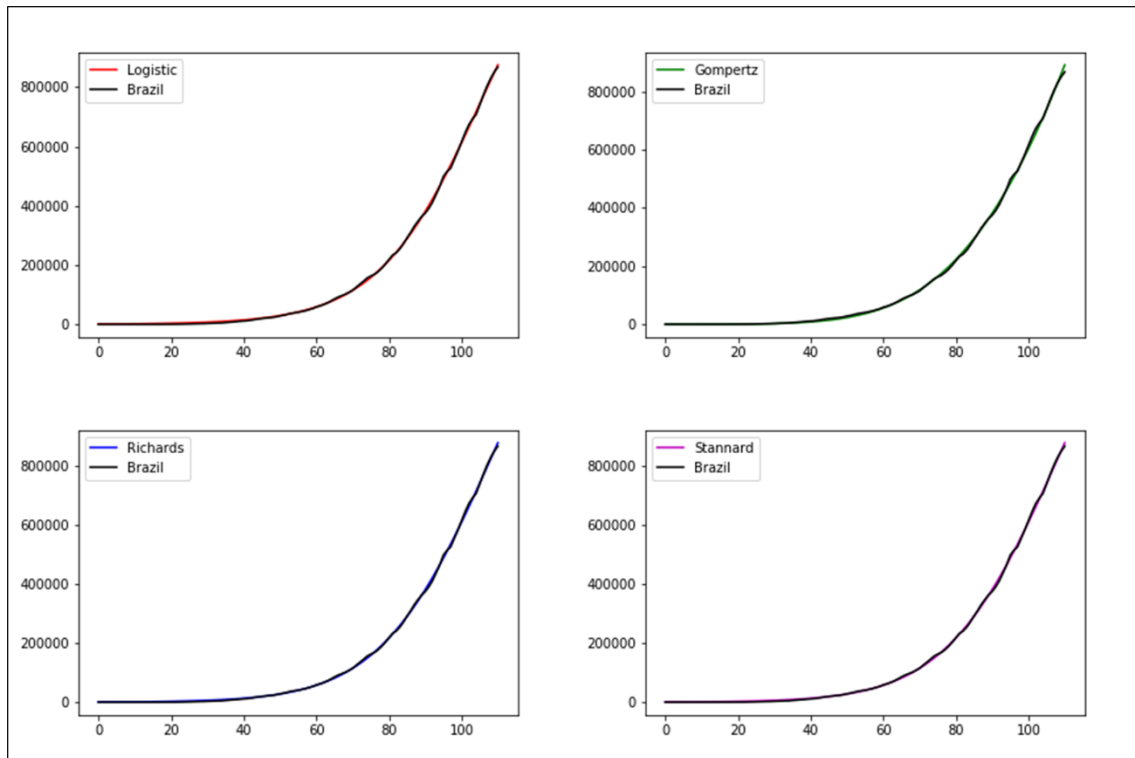


Figure G.2. Cumulative positive cases in Brazil and fits obtained from the four PG models.

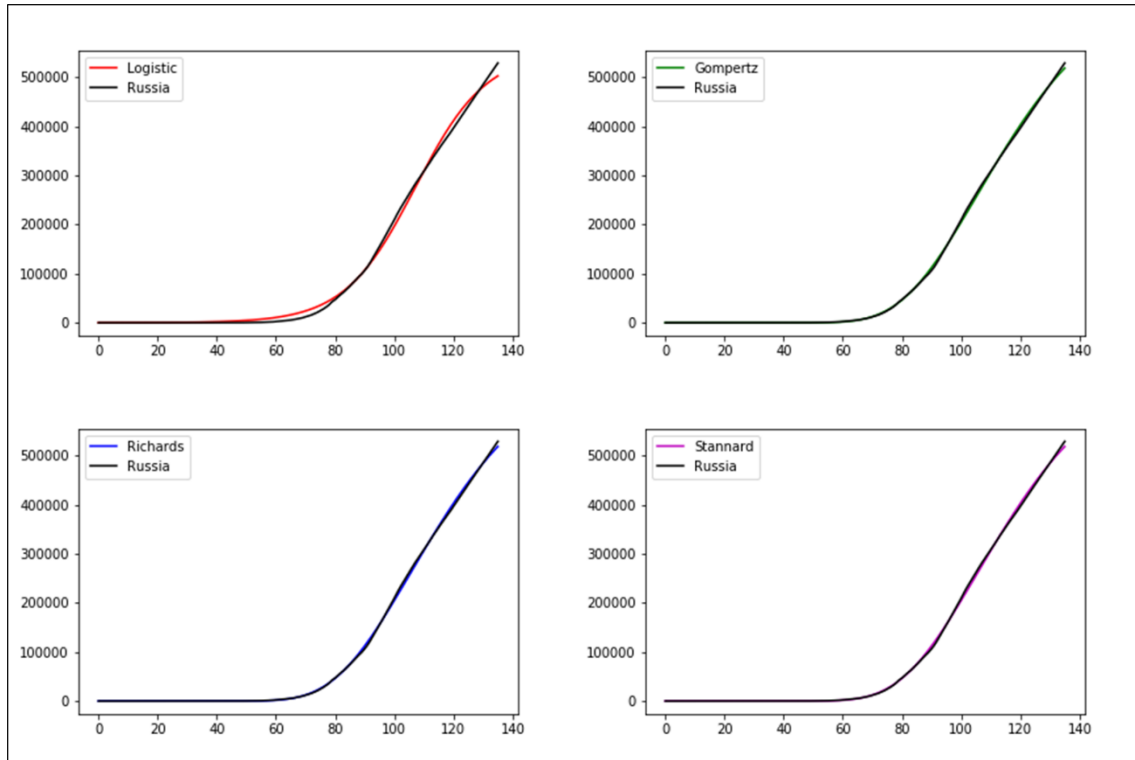


Figure G.3. Cumulative positive cases in Russia and fits obtained from the four PG models.

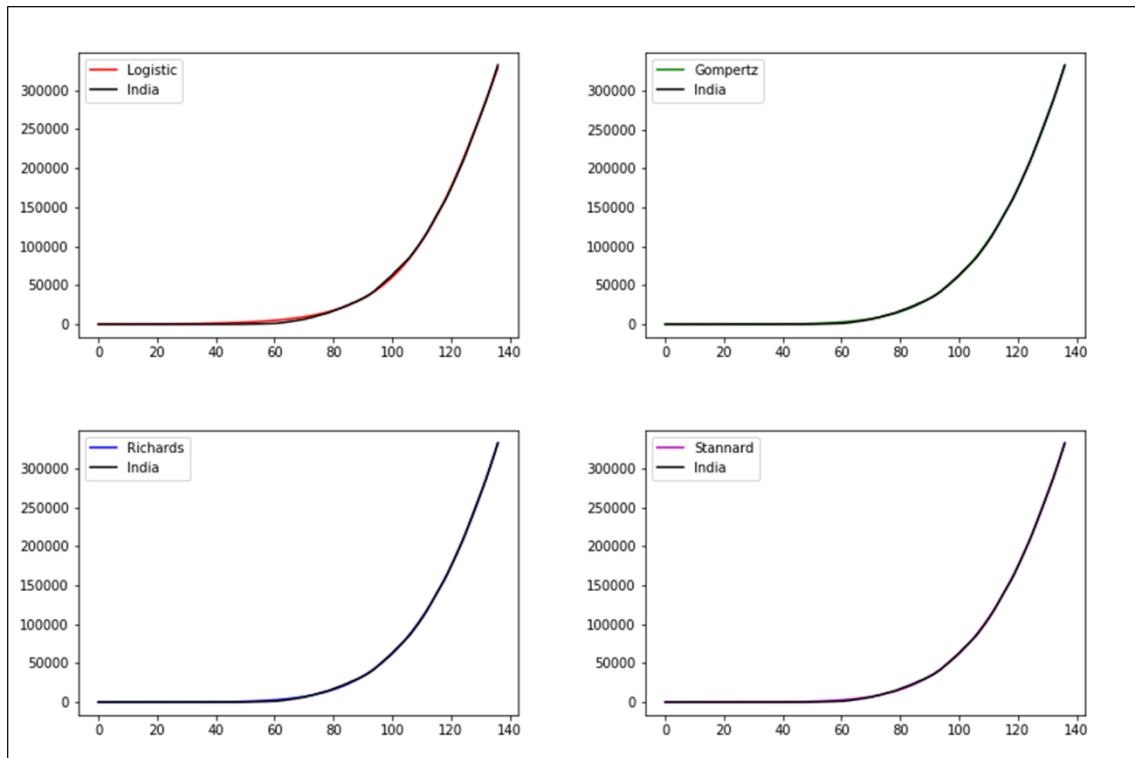


Figure G.4. Cumulative positive cases in India and fits obtained from the four PG models.

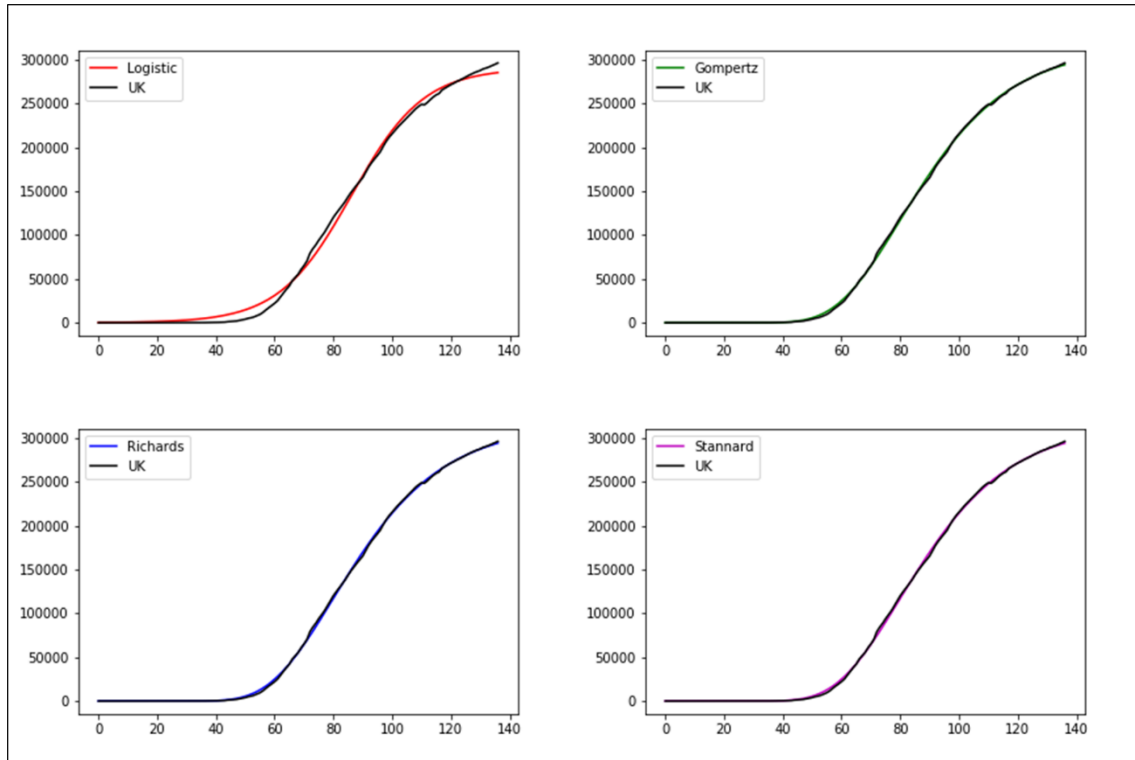


Figure G.5. Cumulative positive cases in UK and fits obtained from the four PG models.

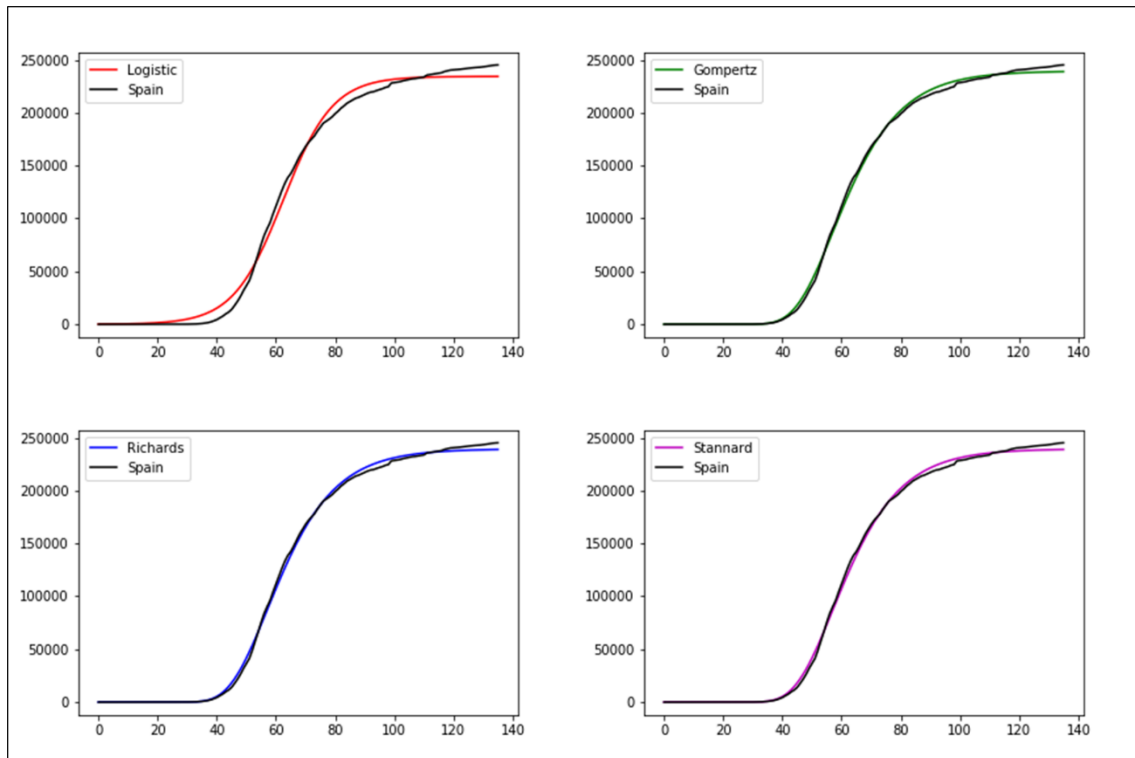


Figure G.6. Cumulative positive cases in Spain and fits obtained from the four PG models.

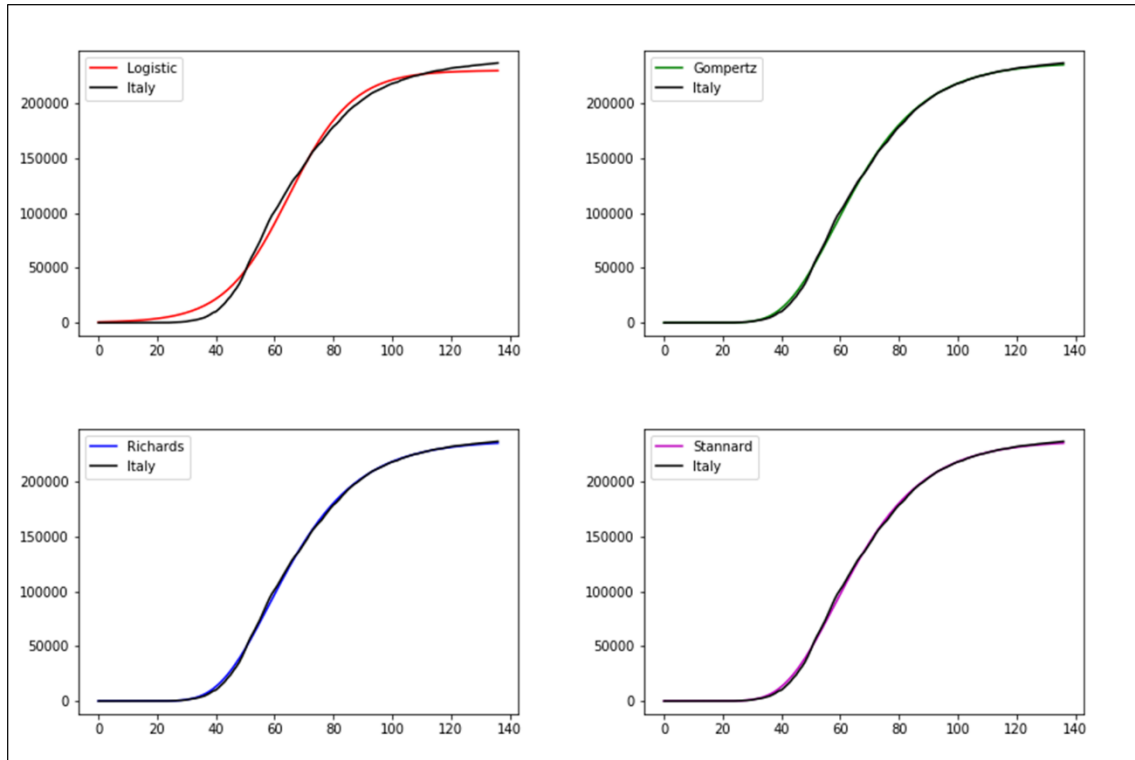


Figure G.7. Cumulative positive cases in Italy and fits obtained from the four PG models.

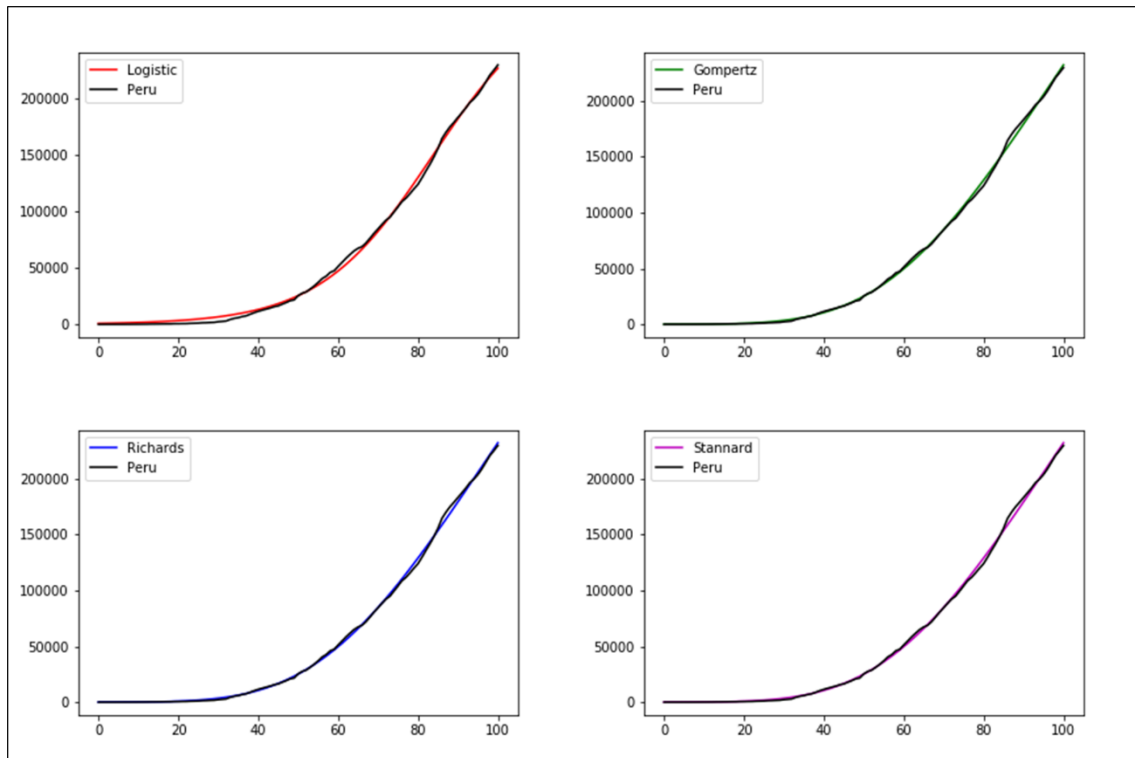


Figure G.8. Cumulative positive cases in Peru and fits obtained from the four PG models.

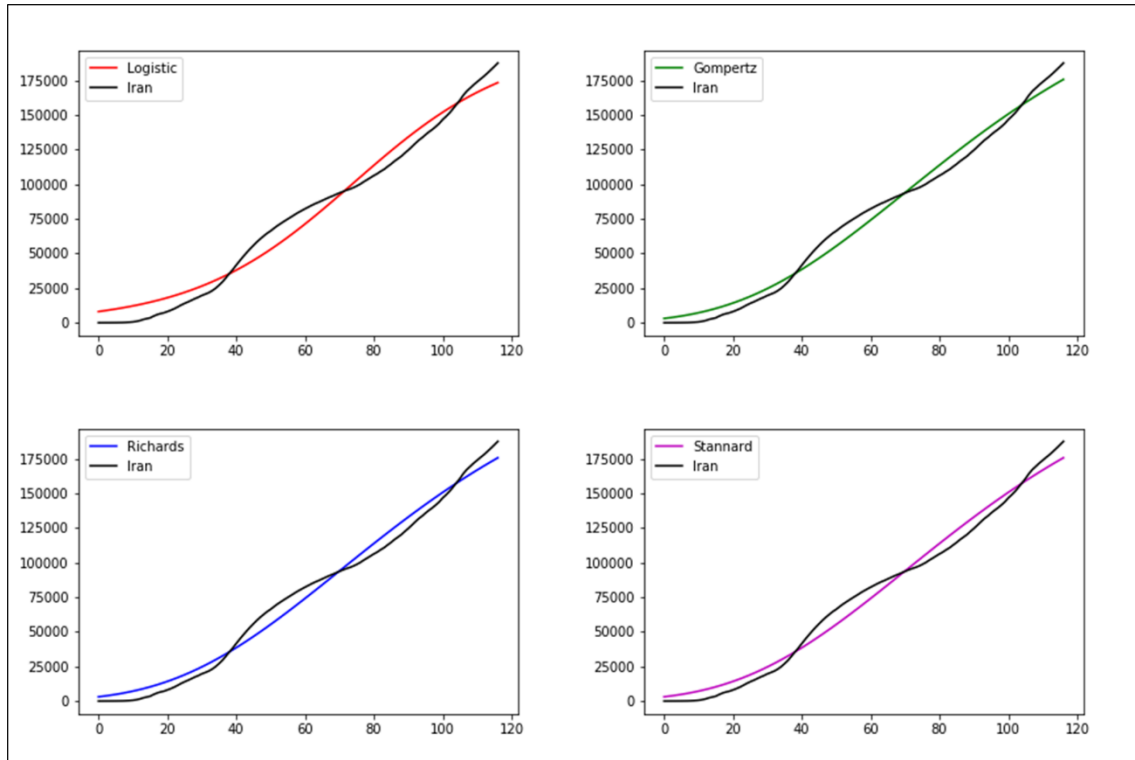


Figure G.9. Cumulative positive cases in Iran and fits obtained from the four PG models.

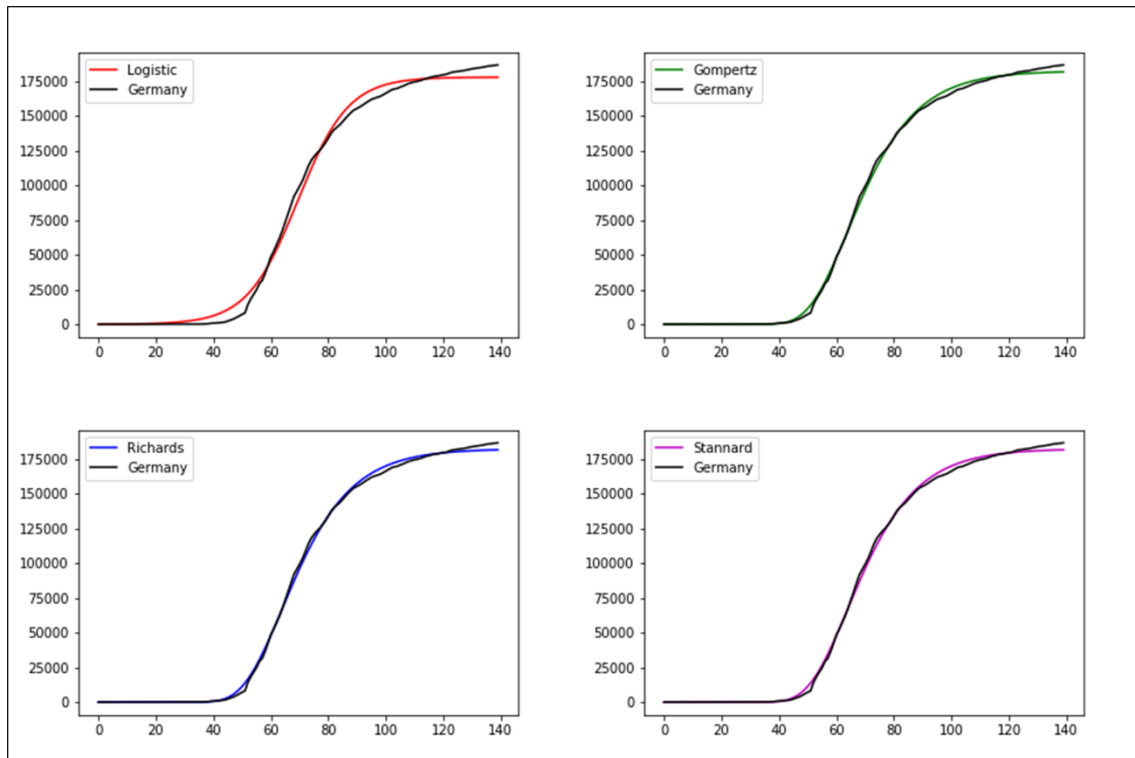


Figure G.10. Cumulative positive cases in Germany and fits obtained from the four PG models.

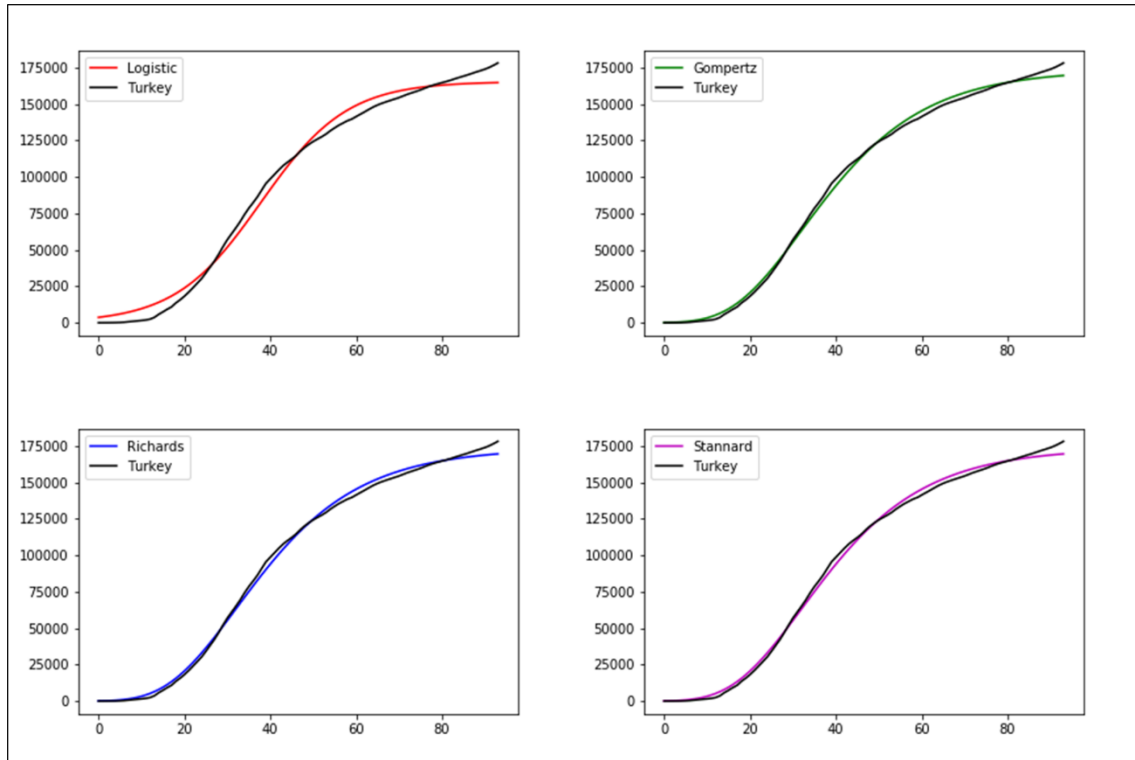


Figure G.11. Cumulative positive cases in Turkey and fits obtained from the four PG models.

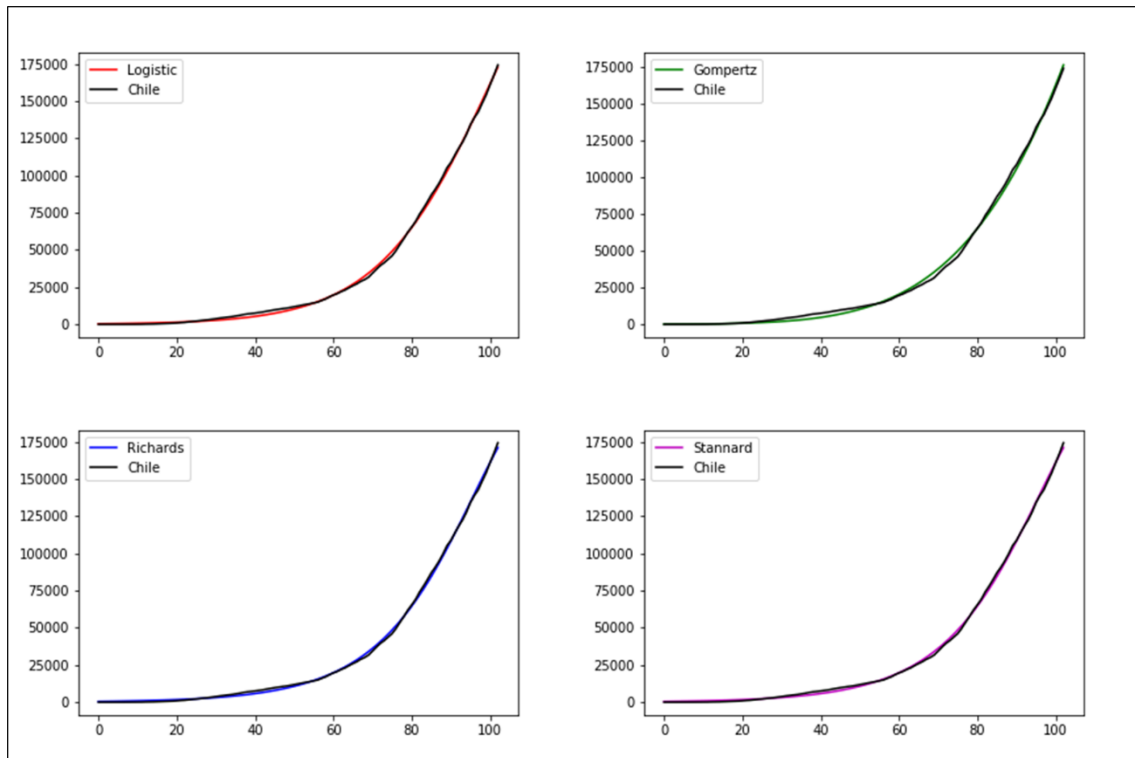


Figure G.12. Cumulative positive cases in Chile and fits obtained from the four PG models.

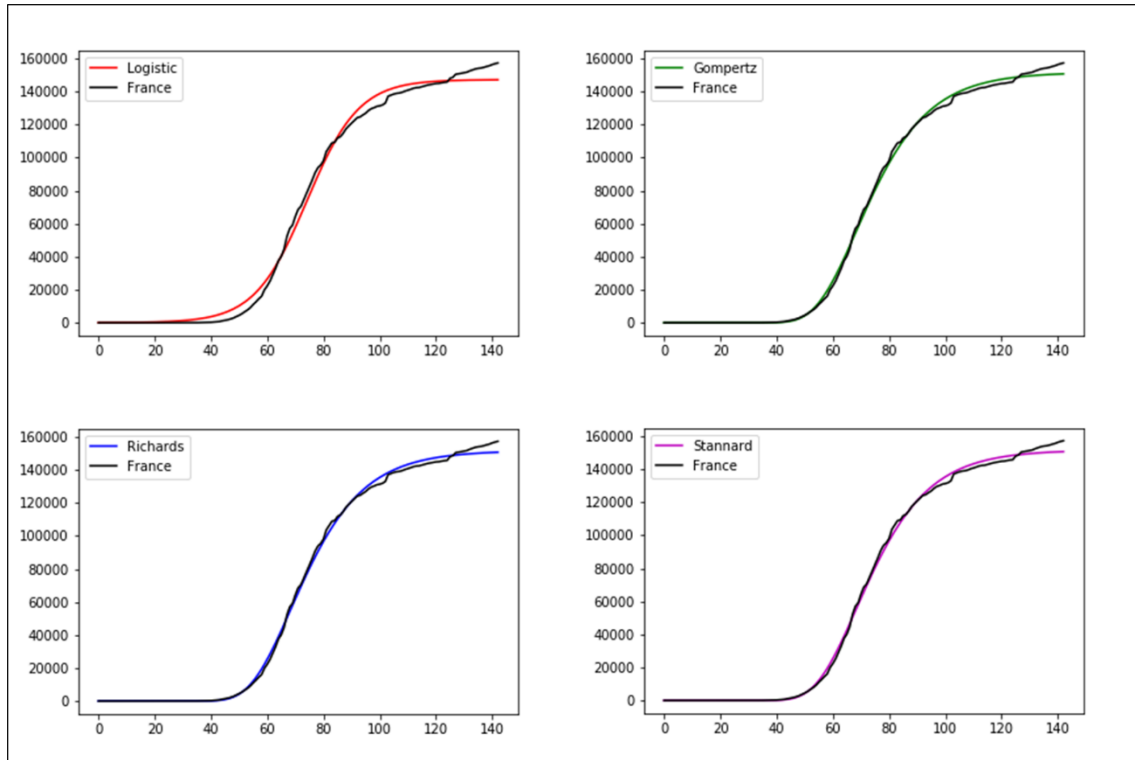


Figure G.13. Cumulative positive cases in France and fits obtained from the four PG models.

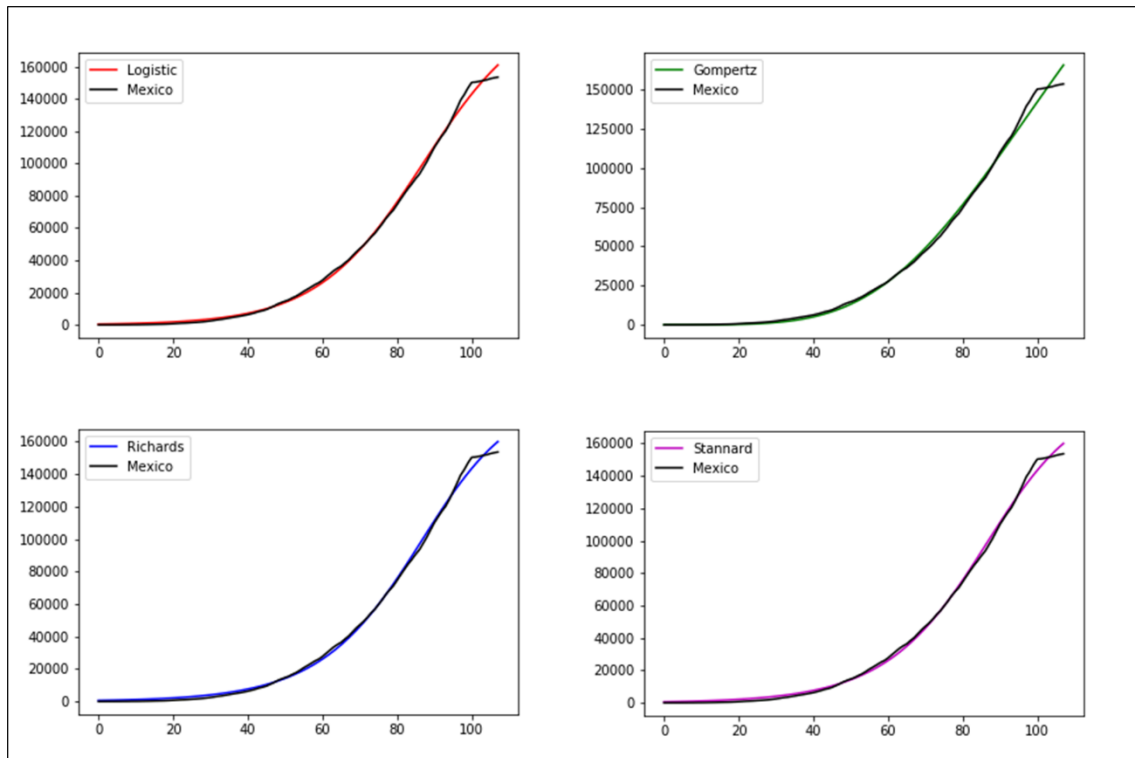


Figure G.14. Cumulative positive cases in Mexico and fits obtained from the four PG models.

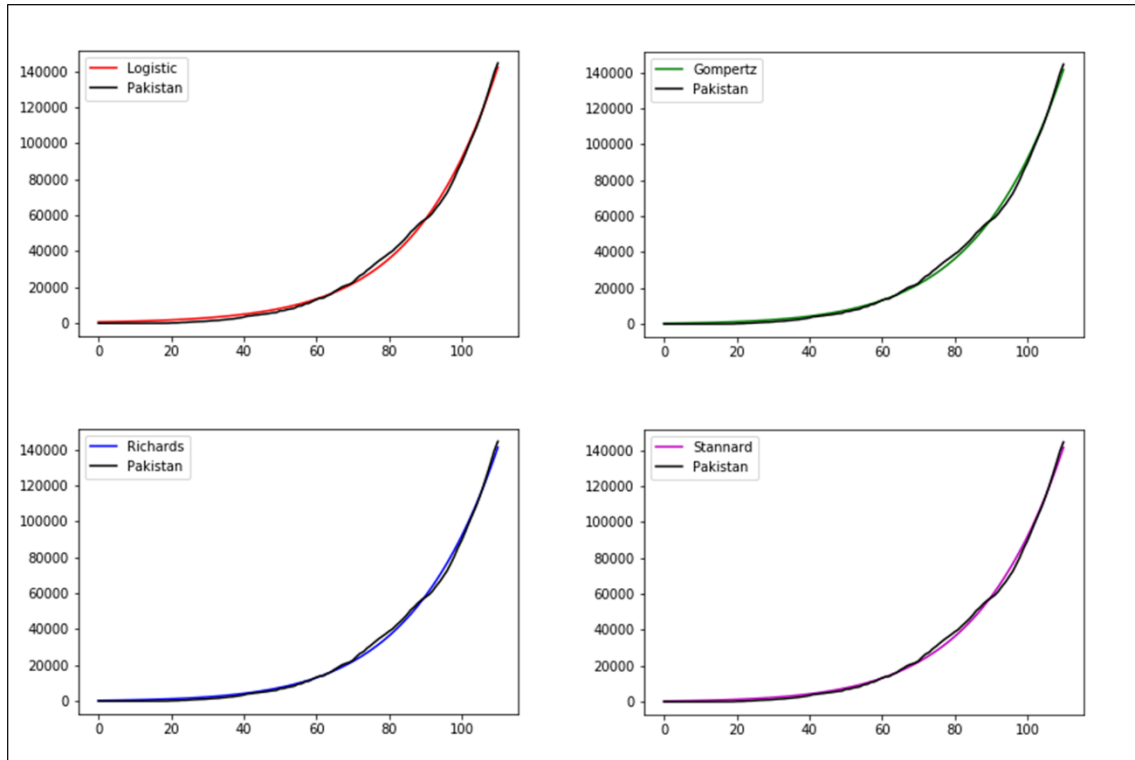


Figure G.15. Cumulative positive cases in Pakistan and fits obtained from the four PG models.

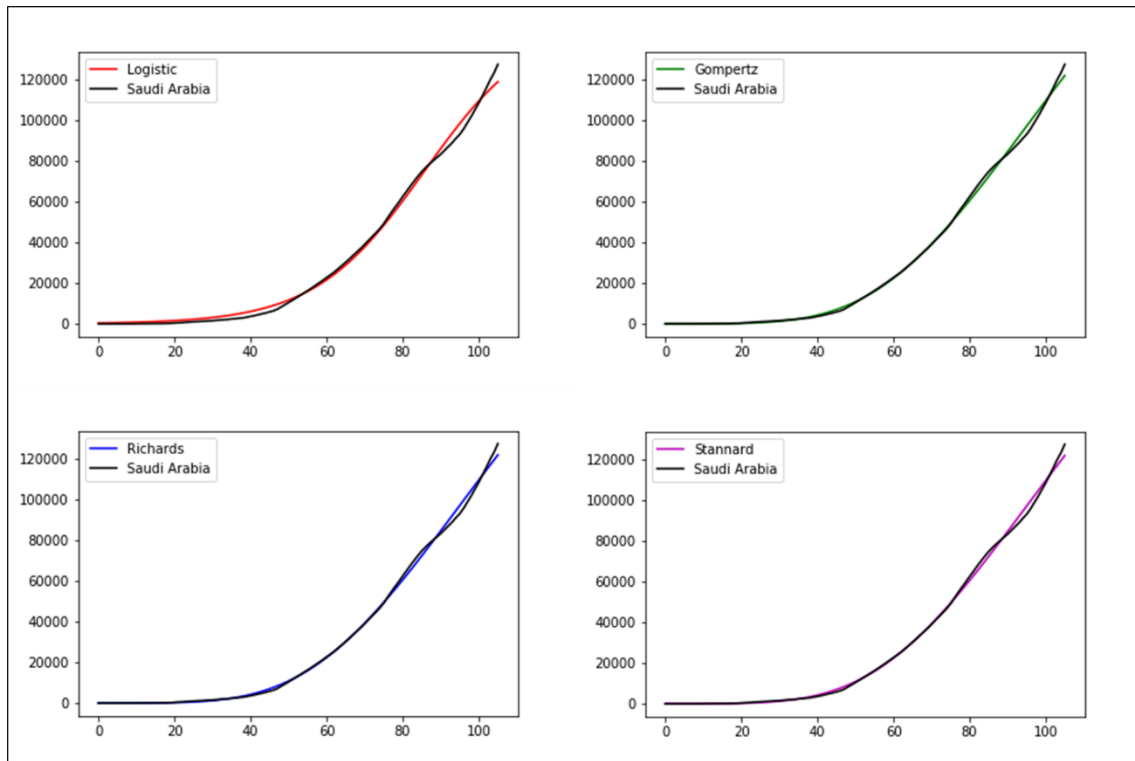


Figure G.16. Cumulative positive cases in Saudi Arabia and fits obtained from the four PG models.

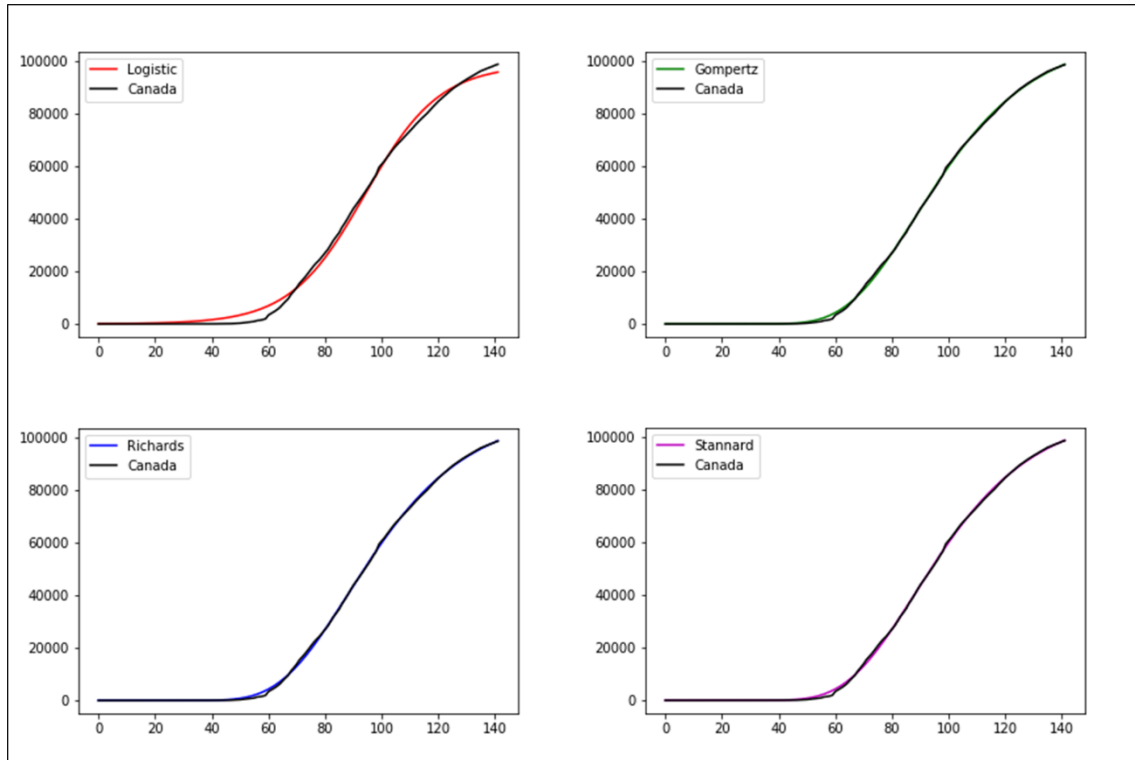


Figure G.17. Cumulative positive cases in Canada and fits obtained from the four PG models.

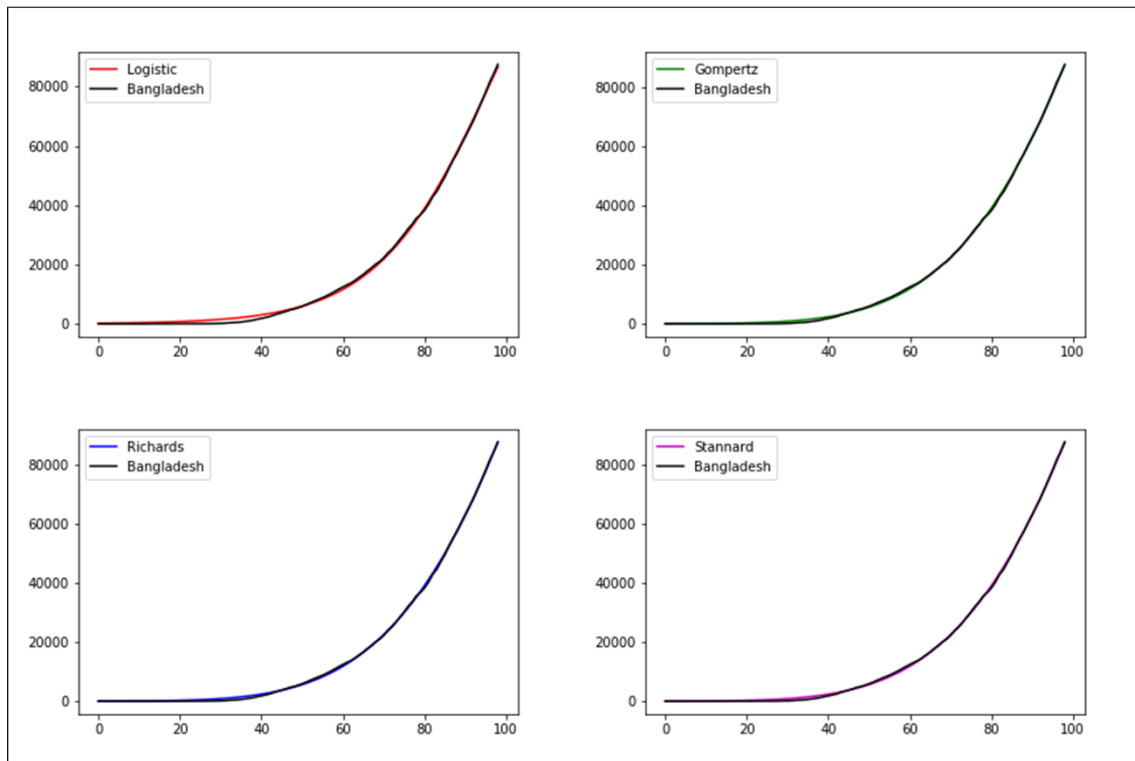


Figure G.18. Cumulative positive cases in Bangladesh and fits obtained from the four PG models.

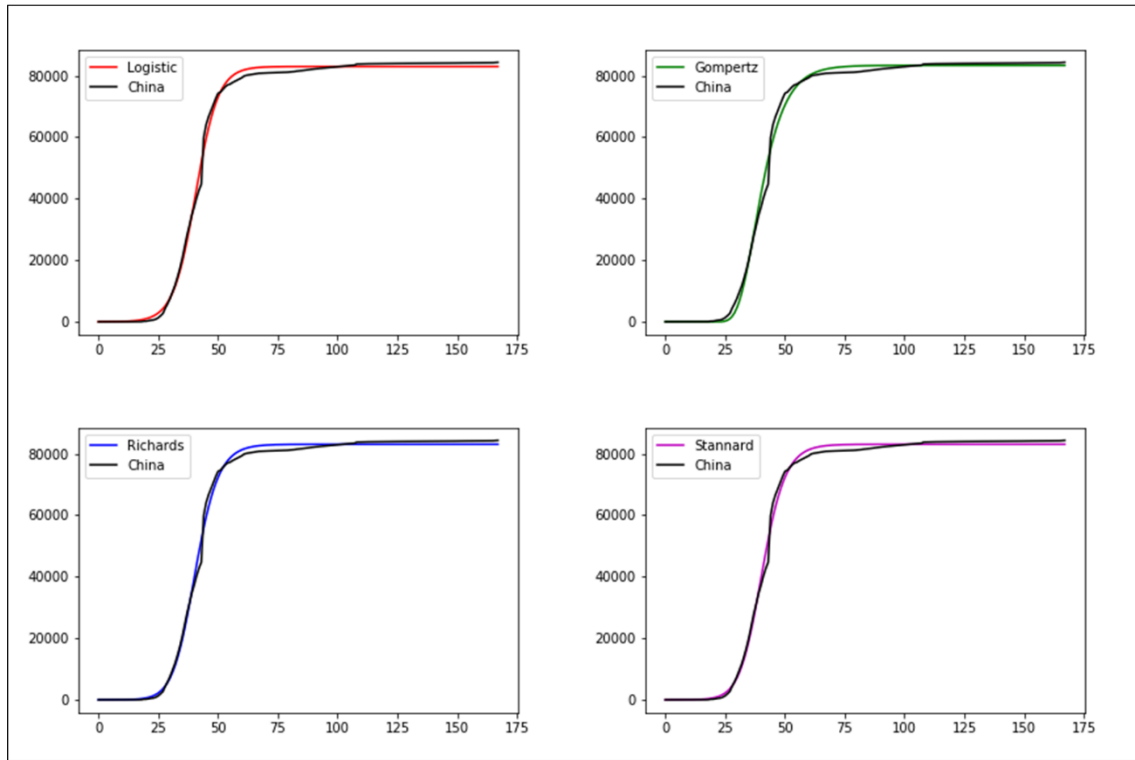


Figure G.19. Cumulative positive cases in China and fits obtained from the four PG models.

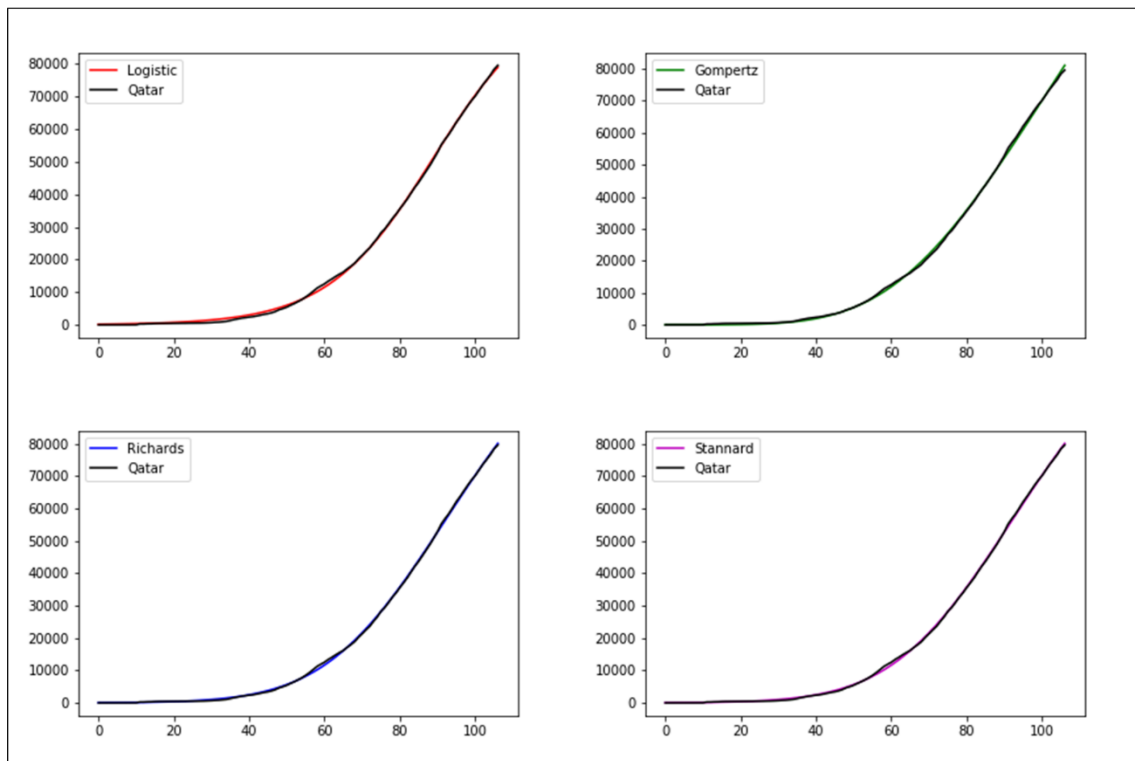


Figure G.20. Cumulative positive cases in Qatar and fits obtained from the four PG models.

G.2 Positive cases predictions for the following 5, 10, and 15 days, at 25%, 40%, and 65% of total cases detected

The prediction of the fitted curves for the next 5, 10, and 15 days is assessed by calculating the MAE. These time horizons are considered as sufficient for the hospital managers to adapt extra resources for new needs. As new positive case data is added every day, and predictions are refreshed also every day, the long-term predictive capacity of the model will not be analysed. Table G.3 summarizes the relevant information from all the tables shown on the following pages. It indicates the number of countries in which each model is the best in terms of predictive capacity (as before, differences smaller than 0.1% have been considered equal). It is observed that the Gompertz model is the one that more accurately predicts future values, specifically in all time horizons analysed. For this reason, the Gompertz model is recommended for the prediction of new cases of COVID-19.

Table G.3. The number of countries in which each model is equal or better than the others in terms of predicting new positive cases for the next 5, 10, and 15 days.

Model	25%			40%			65%		
	5 days	10 days	15 days	5 days	10 days	15 days	5 days	10 days	15 days
Logistic	4	5	5	4	4	3	2	1	2*
Gompertz	11	12	13	13	14	14	15	15	13*
Richards	11	9	7	13	9	10	15	15	11*
Stannard	11	8	7	13	9	10	15	15	11*

Bold values represent the best scores.

*These values are of 18 countries because 2 of them (Pakistan and Bangladesh) have no data for that period.

The rest of the section of this appendix is organized as follows. On the one hand, we present fits to the curves until the selected days, obtaining an MAE for each model and country (see Table G.4, Table G.6, and Table G.8). On the other hand, the tables of the MAEs made in the predictions are shown. To facilitate the comparison of results, MAEs are normalized by the total number of positive cases on the selected days (see Table G.5, Table G.7, and Table G.9). From these results, we can conclude that the Gompertz model outperforms in predictive capacity the other PG models and it is recommended to predict new cases of COVID-19.

To abbreviate the headings in the following tables, we use L for the Logistic model, G for the Gompertz model, R for the Richard model, and S for the Stannard model.

Table G.4. MAE calculated for the fit of each model at 25% of total cases detected in each country.

#	Country	Date	Total positive cases	Logistic	Gompertz	Richards	Stannard
1	USA	2020-04-12	529,951	2,233.0	554.9	553.7	553.7
2	Brazil	2020-05-16	218,223	1,497.5	1,099.9	1,098.4	1,100.4
3	Russia	2020-05-04	134,687	564.2	381.8	357.2	357.2
4	India	2020-05-16	85,940	601.4	350.0	350.0	350.1
5	UK	2020-04-12	78,991	320.6	249.7	209.7	209.7
6	Spain	2020-03-26	66,460	297.1	147.8	147.8	147.9
7	Italy	2020-03-24	63,927	269.7	150.8	156.7	156.7
8	Peru	2020-05-08	58,526	608.4	385.0	385.1	385.1
9	Iran	2020-04-02	47,593	1,192.5	969.6	969.6	969.7
10	Germany	2020-03-28	48,582	269.9	315.8	287.4	287.4
11	Turkey	2020-04-11	47,029	639.9	272.4	272.5	272.6
12	Chile	2020-05-18	43,781	741.7	732.2	735.8	735.8
13	France	2020-03-30	40,174	163.2	92.6	93.0	94.6
14	Mexico	2020-05-06	40,186	207.8	130.5	128.3	128.3
15	Pakistan	2020-05-15	37,218	304.3	223.5	223.1	223.5
16	Saudi Arabia	2020-05-07	31,938	194.3	281.4	195.2	195.2
17	Canada	2020-04-14	25,663	97.0	83.7	57.3	57.3
18	Bangladesh	2020-05-18	22,268	270.9	134.5	134.5	134.5
19	China	2020-02-05	24,320	164.3	114.1	114.1	114.1
20	Qatar	2020-05-09	20,201	147.6	206.0	139.2	139.2

Bold values represent the best scores.

Table G.5. Normalized MAEs obtained for each prediction and model at 25% of total cases detected in each country.

#	Country	5 days				10 days				15 days			
		L (%)	G (%)	R (%)	S (%)	L (%)	G (%)	R (%)	S (%)	L (%)	G (%)	R (%)	S (%)
1	USA	6.840	2.234	2.090	2.091	15.771	1.732	1.558	1.559	26.066	2.473	2.646	2.645
2	Brazil	5.154	1.565	1.596	1.567	12.003	3.820	3.899	3.827	20.594	4.942	5.080	4.956
3	Russia	14.866	7.418	8.145	8.145	27.301	12.043	13.585	13.585	40.983	15.807	18.525	18.525
4	India	6.100	2.053	2.055	2.056	13.805	5.244	5.247	5.248	24.003	8.760	8.765	8.768
5	UK	8.099	1.903	1.089	1.089	16.215	3.978	1.343	1.343	26.289	6.670	2.387	2.387
6	Spain	3.502	10.295	10.283	10.284	9.853	31.939	31.899	31.898	19.188	65.792	65.700	65.691
7	Italy	1.865	10.643	7.881	7.881	5.990	24.930	17.171	17.171	13.465	44.691	28.294	28.295
8	Peru	1.806	3.482	3.480	3.480	5.851	5.624	5.619	5.618	12.624	8.101	8.092	8.089
9	Iran	2.635	1.778	1.777	1.777	2.157	7.030	7.027	7.028	3.204	16.013	16.006	16.007
10	Germany	10.915	3.847	2.470	2.470	30.272	3.495	12.258	12.258	50.039	4.967	23.066	23.066
11	Turkey	15.075	4.756	4.761	4.764	29.363	6.250	6.261	6.268	45.514	7.633	7.652	7.666
12	Chile	5.868	8.082	5.183	5.183	10.310	13.948	8.985	9.253	12.393	18.030	9.969	20.650
13	France	9.720	4.424	4.396	4.302	15.968	17.090	16.910	16.324	26.496	37.173	36.735	35.309
14	Mexico	6.396	0.895	2.187	2.187	13.397	2.498	5.044	5.044	23.518	5.093	9.494	9.494
15	Pakistan	0.886	4.092	4.063	4.089	1.968	5.827	5.779	5.823	3.048	10.311	10.236	10.303
16	Saudi Arabia	5.616	2.142	6.813	6.814	12.669	2.608	14.917	14.917	24.360	2.470	27.770	27.770
17	Canada	11.915	3.656	6.871	6.871	24.599	10.482	16.277	16.277	38.866	19.003	27.603	27.603
18	Bangladesh	13.722	8.747	8.748	8.750	25.468	15.608	15.610	15.613	40.500	24.279	24.283	24.288
19	China	13.144	5.681	5.669	5.663	44.477	12.518	12.528	12.534	75.439	11.828	11.796	11.775
20	Qatar	8.920	1.879	11.294	11.294	19.084	5.653	23.360	23.360	31.546	9.641	37.870	37.870

Bold values represent the best scores.

G.2 Positive cases predictions for the following 5, 10, and 15 days, at 25%, 40%, and 65% of total cases detected

Table G.6. MAE calculated for the fit of each model at 40% of total cases detected in each country.

#	Country	Date	Total positive cases	Logistic	Gompertz	Richards	Stannard
1	USA	2020-04-23	842,629	6,372.8	1,421.9	1,422.8	1,433.3
2	Brazil	2020-05-24	347,398	2,085.6	1,422.1	1,413.6	1,422.7
3	Russia	2020-05-12	221,344	1,316.9	521.2	521.3	521.5
4	India	2020-05-25	138,845	882.2	480.3	480.4	480.5
5	UK	2020-04-20	120,067	617.4	320.3	257.3	257.3
6	Spain	2020-03-31	104,267	351.9	438.7	343.9	343.9
7	Italy	2020-03-30	97,689	374.7	343.5	205.8	205.8
8	Peru	2020-05-18	92,273	759.3	483.2	482.1	482.1
9	Iran	2020-04-16	76,389	1,071.3	1,201.7	1,043.0	1,043.0
10	Germany	2020-04-03	79,696	486.0	339.2	338.2	338.2
11	Turkey	2020-04-17	74,193	795.4	345.4	345.5	345.7
12	Chile	2020-05-26	73,997	854.4	858.2	854.4	854.4
13	France	2020-04-04	64,338	260.8	200.4	219.2	219.2
14	Mexico	2020-05-15	62,527	438.7	151.8	151.8	151.9
15	Pakistan	2020-05-27	59,151	335.9	276.6	285.4	285.4
16	Saudi Arabia	2020-05-17	52,016	360.6	273.4	256.6	256.6
17	Canada	2020-04-23	40,179	405.1	175.7	175.7	175.7
18	Bangladesh	2020-05-26	35,585	434.7	270.4	270.4	270.5
19	China	2020-02-08	34,625	185.9	130.2	126.6	126.6
20	Qatar	2020-05-18	32,604	274.1	216.8	216.8	216.8

Bold values represent the best scores.

Table G.7. Normalized MAEs obtained for each prediction and model at 40% of total cases detected in each country.

#	Country	5 days				10 days				15 days			
		L (%)	G (%)	R (%)	S (%)	L (%)	G (%)	R (%)	S (%)	L (%)	G (%)	R (%)	S (%)
1	USA	9.702	3.501	3.503	3.525	15.921	6.527	6.531	6.567	22.590	10.112	10.117	10.167
2	Brazil	1.165	3.163	2.984	3.161	2.858	3.924	3.617	3.919	6.209	6.041	5.547	6.032
3	Russia	3.420	2.303	2.301	2.299	5.698	6.093	6.090	6.085	9.245	10.728	10.721	10.714
4	India	4.669	1.331	1.334	1.333	9.212	2.274	2.278	2.277	16.059	3.695	3.701	3.700
5	UK	6.330	1.005	0.710	0.711	11.831	0.913	2.210	2.210	19.098	1.746	5.344	5.344
6	Spain	6.632	5.630	5.905	5.906	13.015	11.927	11.725	11.725	20.529	18.121	18.794	18.795
7	Italy	3.211	6.294	1.096	1.096	8.347	9.938	1.571	1.571	14.945	13.137	4.334	4.334
8	Peru	6.317	0.817	1.035	1.035	11.975	1.669	2.145	2.146	22.254	6.073	6.872	6.873
9	Iran	0.582	6.097	1.628	1.628	1.757	8.452	3.338	3.337	3.372	10.640	5.413	5.413
10	Germany	11.428	2.083	2.224	2.220	19.849	2.095	2.390	2.381	27.383	1.755	1.802	1.801
11	Turkey	7.319	1.436	1.432	1.429	13.559	3.472	3.463	3.457	19.637	6.500	6.486	6.476
12	Chile	1.645	1.636	1.645	1.645	5.823	5.639	5.823	5.817	14.435	14.059	14.432	7.991
13	France	2.158	12.580	6.941	6.940	3.202	22.970	9.453	9.451	7.545	35.881	10.903	10.900
14	Mexico	7.023	2.499	2.501	2.503	12.126	3.558	3.563	3.566	19.255	5.141	5.149	5.154
15	Pakistan	3.195	1.697	1.489	1.489	11.675	4.830	7.837	7.837	23.909	11.558	17.595	17.595
16	Saudi Arabia	9.921	4.418	5.822	5.822	15.880	5.955	8.499	8.499	20.963	5.429	9.512	9.512
17	Canada	12.339	6.475	6.477	6.478	19.244	9.745	9.749	9.751	27.788	14.521	14.526	14.529
18	Bangladesh	4.289	1.024	1.025	1.025	11.261	3.951	3.955	3.954	20.791	7.544	7.550	7.550
19	China	11.511	10.730	10.225	10.225	37.831	12.943	16.756	16.756	52.069	10.778	15.505	15.506
20	Qatar	5.565	1.188	1.204	1.211	9.960	1.348	1.379	1.392	16.349	1.774	1.827	1.849

Bold values represent the best scores.

Table G.8. MAE calculated for the fit of each model at 65% of total cases detected in each country.

#	Country	Date	Total positive cases	Logistic	Gompertz	Richards	Stannard
1	USA	2020-05-13	1,369,964	20,036.0	7,343.8	7,345.7	7,346.8
2	Brazil	2020-06-04	584,016	2,654.8	1,857.5	1,908.6	1,908.4
3	Russia	2020-05-25	344,481	1,469.0	1,097.0	846.3	846.3
4	India	2020-06-04	216,919	1,113.0	511.4	511.6	511.7
5	UK	2020-05-06	194,990	2,136.8	593.2	593.2	593.3
6	Spain	2020-04-10	163,472	917.7	639.9	382.2	382.2
7	Italy	2020-04-13	156,363	1,420.8	585.3	526.1	526.1
8	Peru	2020-05-31	155,671	1,757.1	792.6	792.9	793.1
9	Iran	2020-05-19	122,492	3,124.1	1,912.6	1,912.7	1,912.8
10	Germany	2020-04-13	123,016	907.9	419.2	400.3	400.3
11	Turkey	2020-04-30	117,589	1,222.6	528.2	463.3	463.3
12	Chile	2020-06-04	113,628	1,011.6	1,038.2	844.2	844.2
13	France	2020-04-15	103,573	495.0	525.4	350.4	350.4
14	Mexico	2020-05-27	101,238	746.9	237.1	237.2	237.3
15	Pakistan	2020-06-06	93,983	918.8	565.8	565.8	566.0
16	Saudi Arabia	2020-05-31	83,384	683.4	453.3	430.7	430.7
17	Canada	2020-05-08	64,922	836.0	346.9	346.9	347.0
18	Bangladesh	2020-06-05	57,563	534.4	310.3	310.4	310.4
19	China	2020-02-13	59,865	841.5	556.6	556.6	556.7
20	Qatar	2020-05-30	52,907	352.0	199.7	199.6	199.6

Bold values represent the best scores.

Table G.9. Normalized MAEs obtained for each prediction and model at 65% of total cases detected in each country.

#	Country	5 days				10 days				15 days			
		L (%)	G (%)	R (%)	S (%)	L (%)	G (%)	R (%)	S (%)	L (%)	G (%)	R (%)	S (%)
1	USA	7.840	3.355	3.356	3.356	10.822	4.910	4.911	4.911	13.993	6.696	6.698	6.698
2	Brazil*	2.720	1.445	1.396	1.397	3.898	3.799	3.153	3.156	4.007	4.631	3.863	3.867
3	Russia	4.285	1.705	0.901	0.902	7.670	1.598	2.524	2.524	11.790	1.254	4.822	4.822
4	India*	4.293	0.859	0.861	0.861	7.276	0.607	0.609	0.610	8.062	0.575	0.577	0.578
5	UK	9.641	4.441	4.443	4.444	12.914	5.616	5.618	5.620	16.050	6.681	6.684	6.687
6	Spain	6.365	0.354	2.477	2.477	9.902	0.485	4.430	4.430	13.199	1.001	6.451	6.451
7	Italy	7.789	2.131	3.037	3.037	11.523	3.678	4.993	4.993	15.241	5.390	7.116	7.116
8	Peru	10.445	6.119	6.121	6.122	12.525	5.208	5.210	5.212	15.847	4.811	4.815	4.818
9	Iran	14.856	10.700	10.702	10.702	18.765	13.960	13.962	13.963	23.212	17.807	17.809	17.810
10	Germany	4.053	2.415	1.864	1.864	7.360	2.354	1.473	1.473	10.611	2.080	1.118	1.118
11	Turkey	4.858	1.079	0.484	0.484	7.419	0.972	1.333	1.333	10.097	0.817	2.504	2.504
12	Chile*	6.750	9.179	7.516	7.517	11.535	16.538	17.398	17.400	12.420	18.133	19.826	19.827
13	France	5.234	1.690	1.813	1.813	7.530	2.840	2.534	2.534	9.905	3.784	3.530	3.530
14	Mexico	5.207	1.082	1.084	1.085	8.908	1.584	1.587	1.588	11.785	2.536	2.537	2.538
15	Pakistan*	11.997	9.348	9.351	9.351	18.651	14.243	14.246	14.247	-	-	-	-
16	Saudi Arabia	0.598	4.724	3.395	3.395	4.029	4.289	2.612	2.612	10.167	3.939	4.547	4.547
17	Canada	5.661	0.861	0.862	0.863	7.801	0.674	0.676	0.677	10.379	0.791	0.793	0.794
18	Bangladesh*	5.516	2.097	2.099	2.099	9.975	3.061	3.064	3.065	-	-	-	-
19	China	14.044	5.492	5.495	5.495	14.165	8.987	8.976	8.973	14.158	16.806	16.781	16.776
20	Qatar	4.045	0.780	0.777	0.775	5.683	2.302	2.293	2.286	7.766	4.616	4.600	4.589

Bold values represent the best scores.

The symbol (*) indicates insufficient data in the comparison with the prediction of the next 15 days.

G.2 Positive cases predictions for the following 5, 10, and 15 days, at 25%, 40%, and 65% of total cases detected 227

Table G.10 lists the figures in which, for each country, the cumulative positive cases predictions for the following days at 25%, 40%, and 65% of total cases detected using the four PG models. In every figure, the Logistic function is shown in red, the Gompertz function in green, the Richards function in blue, and the Stannard function in purple.

Table G.10. List of figures with predictions for the following days at 25%, 40%, and 65% of total cases detected in each country using each of the four PG models.

#	Country	Figure of predictions obtained using the four PG models
1	USA	Figure G.21
2	Brazil	Figure G.22
3	Russia	Figure G.23
4	India	Figure G.24
5	UK	Figure G.25
6	Spain	Figure G.26
7	Italy	Figure G.27
8	Peru	Figure G.28
9	Iran	Figure G.29
10	Germany	Figure G.30
11	Turkey	Figure G.31
12	Chile	Figure G.32
13	France	Figure G.33
14	Mexico	Figure G.34
15	Pakistan	Figure G.35
16	Saudi Arabia	Figure G.36
17	Canada	Figure G.37
18	Bangladesh	Figure G.38
19	China	Figure G.39
20	Qatar	Figure G.40

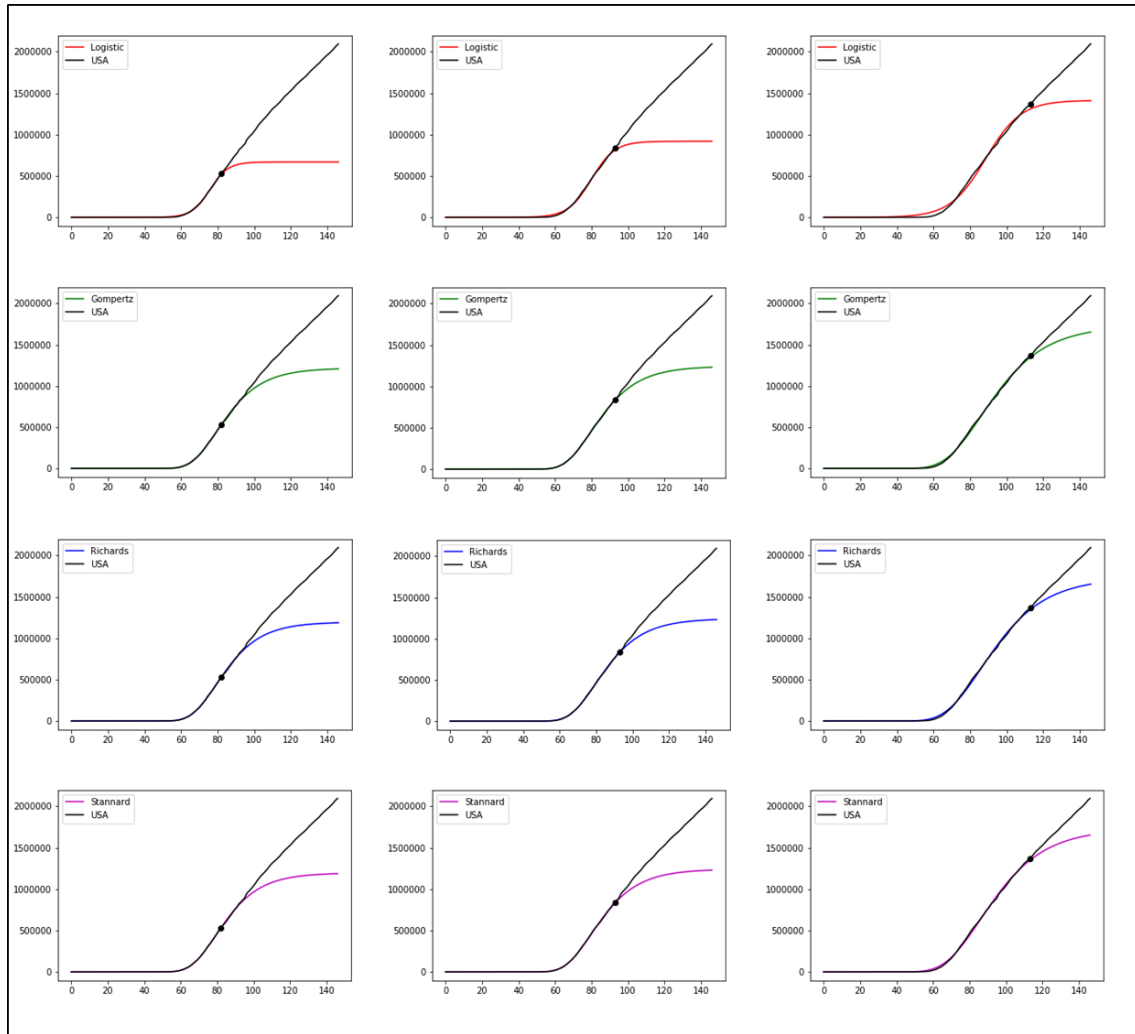


Figure G.21. Cumulative positive cases predictions for the following days at 25% (left), 40% (centre), and 65% (right) of total cases detected in USA using the four PG models.

G.2 Positive cases predictions for the following 5, 10, and 15 days, at 25%, 40%, and 229 65% of total cases detected

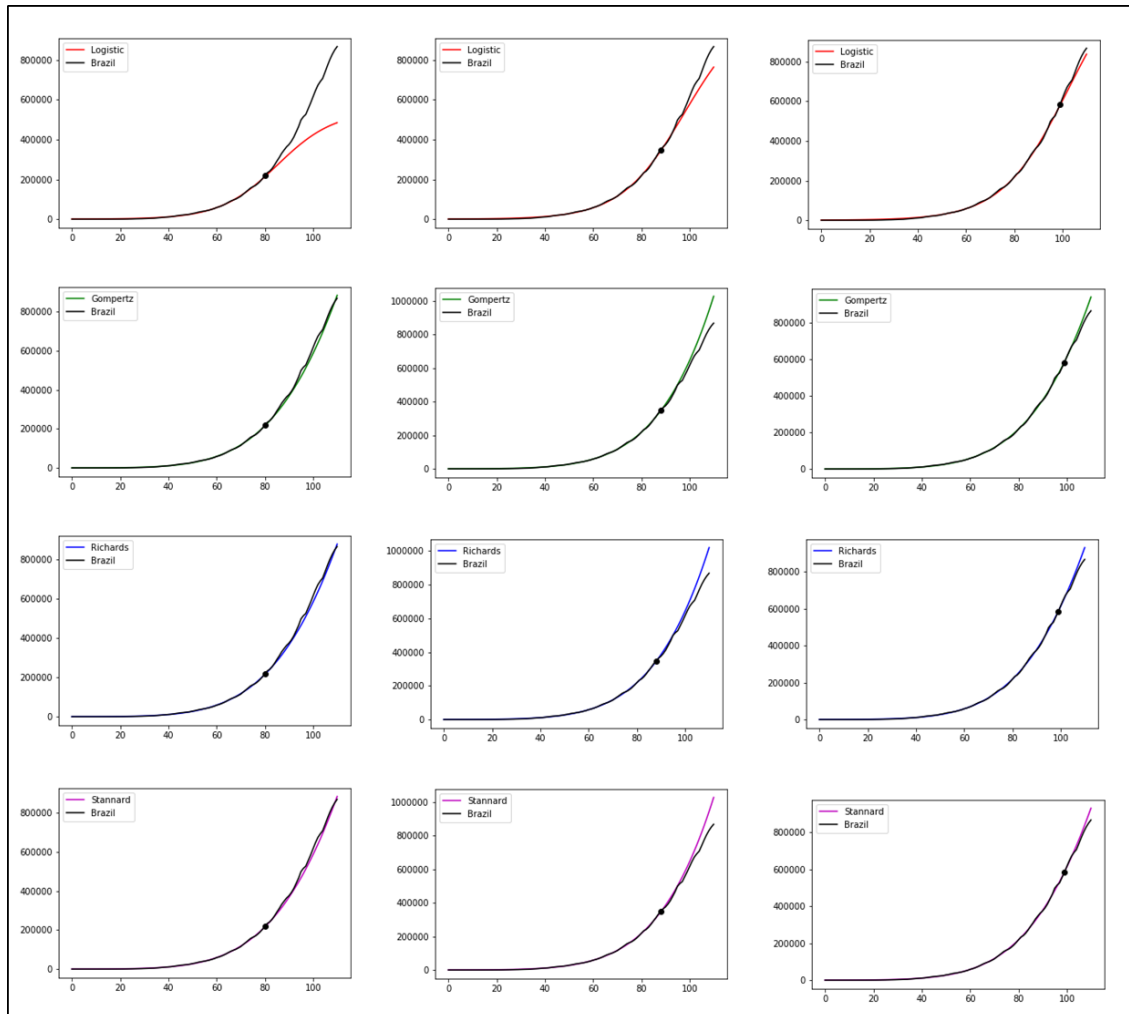


Figure G.22. Cumulative positive cases predictions for the following days at 25% (left), 40% (centre), and 65% (right) of total cases detected in Brazil using the four PG models.

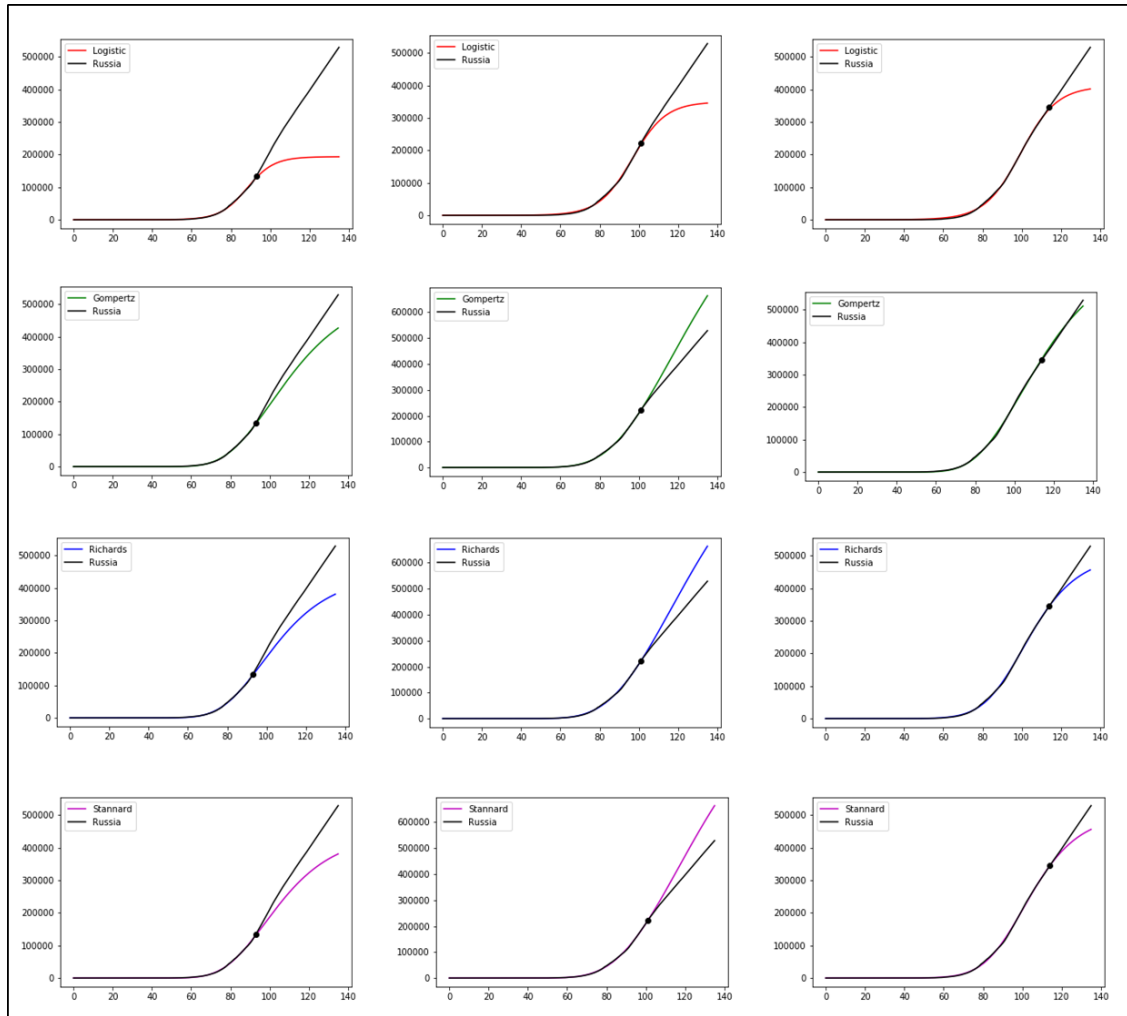


Figure G.23. Cumulative positive cases predictions for the following days at 25% (left), 40% (centre), and 65% (right) of total cases detected in Russia using the four PG models.

G.2 Positive cases predictions for the following 5, 10, and 15 days, at 25%, 40%, and 231 65% of total cases detected

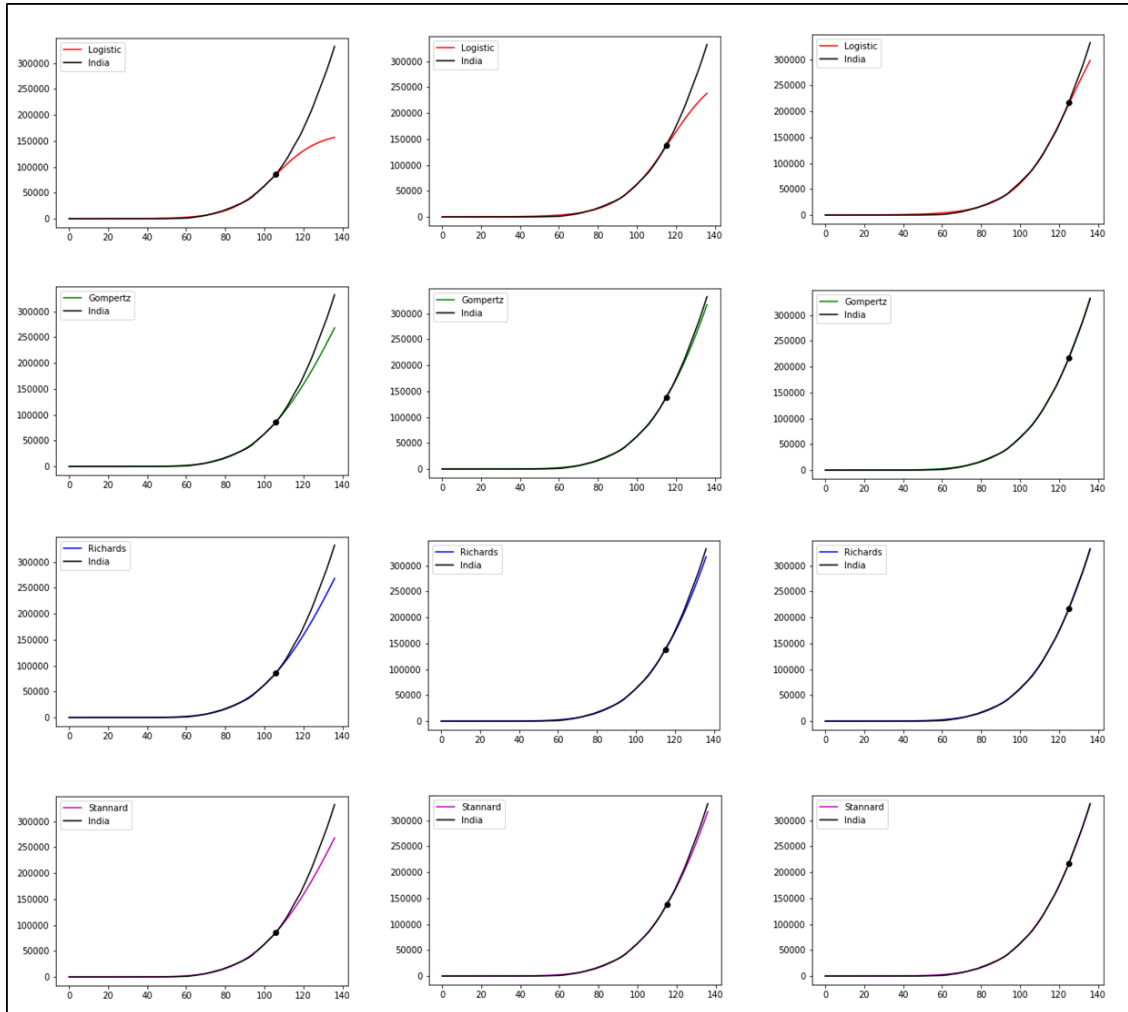


Figure G.24. Cumulative positive cases predictions for the following days at 25% (left), 40% (centre), and 65% (right) of total cases detected in India using the four PG models.

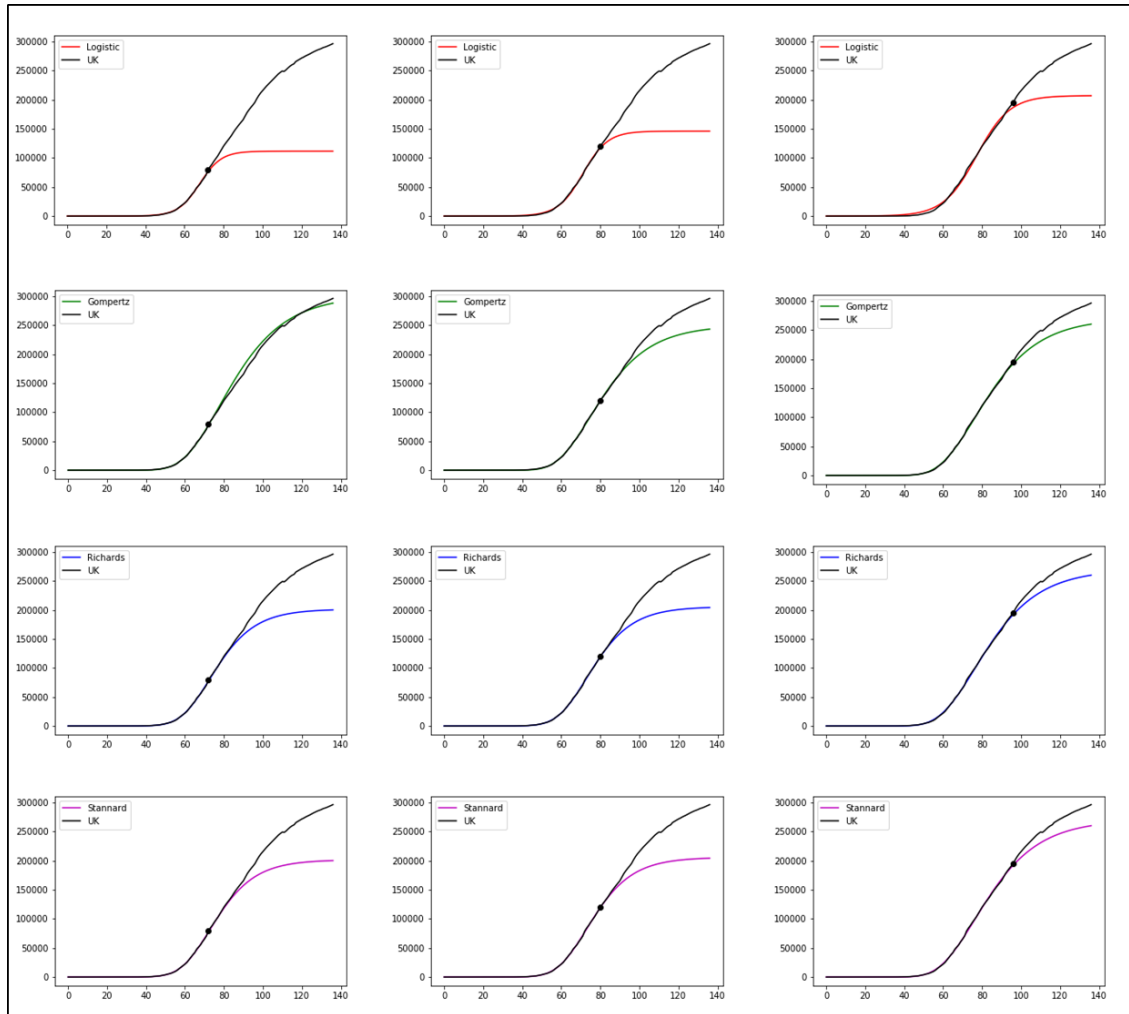


Figure G.25. Cumulative positive cases predictions for the following days at 25% (left), 40% (centre), and 65% (right) of total cases detected in UK using the four PG models.

G.2 Positive cases predictions for the following 5, 10, and 15 days, at 25%, 40%, and 65% of total cases detected

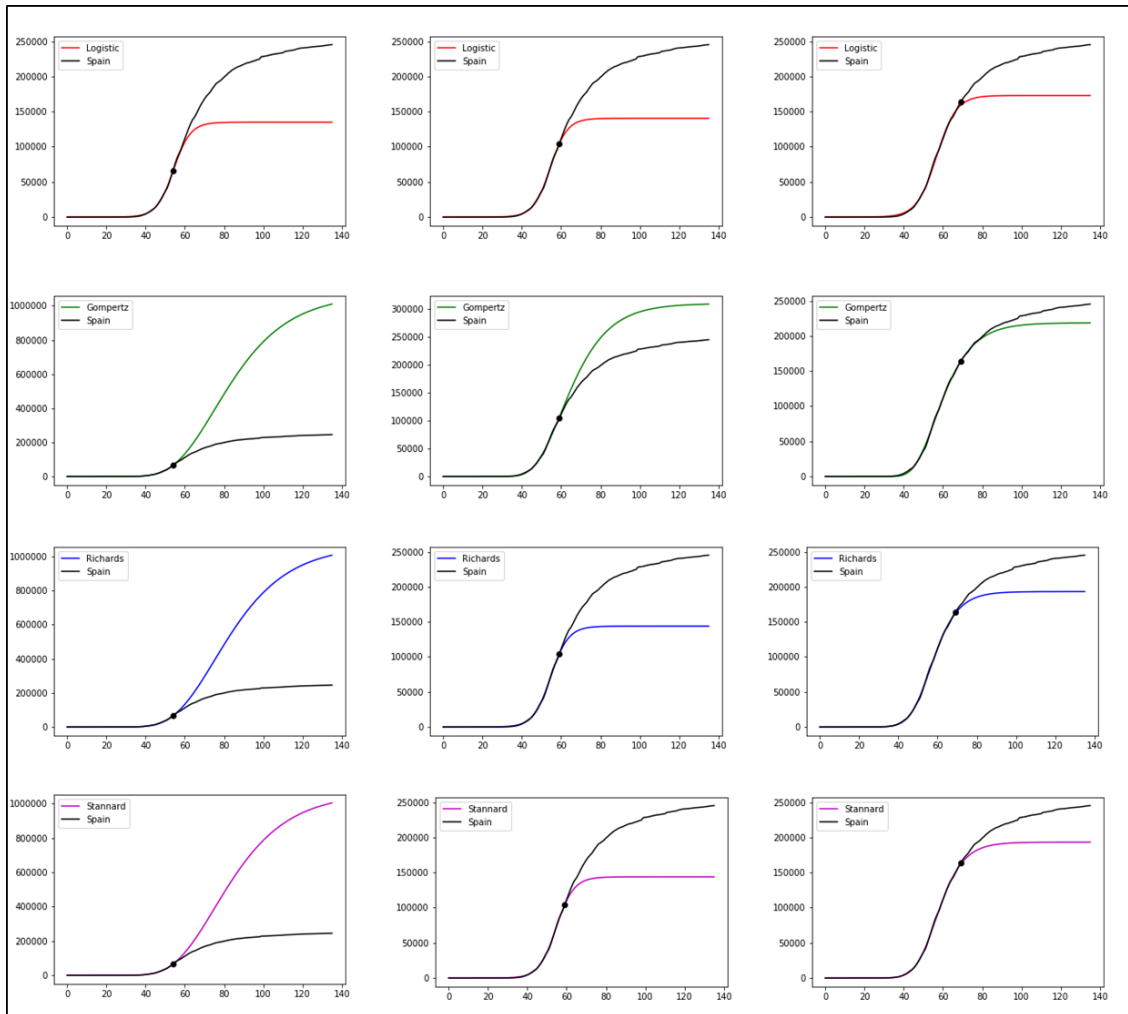


Figure G.26. Cumulative positive cases predictions for the following days at 25% (left), 40% (centre), and 65% (right) of total cases detected in Spain using the four PG models.

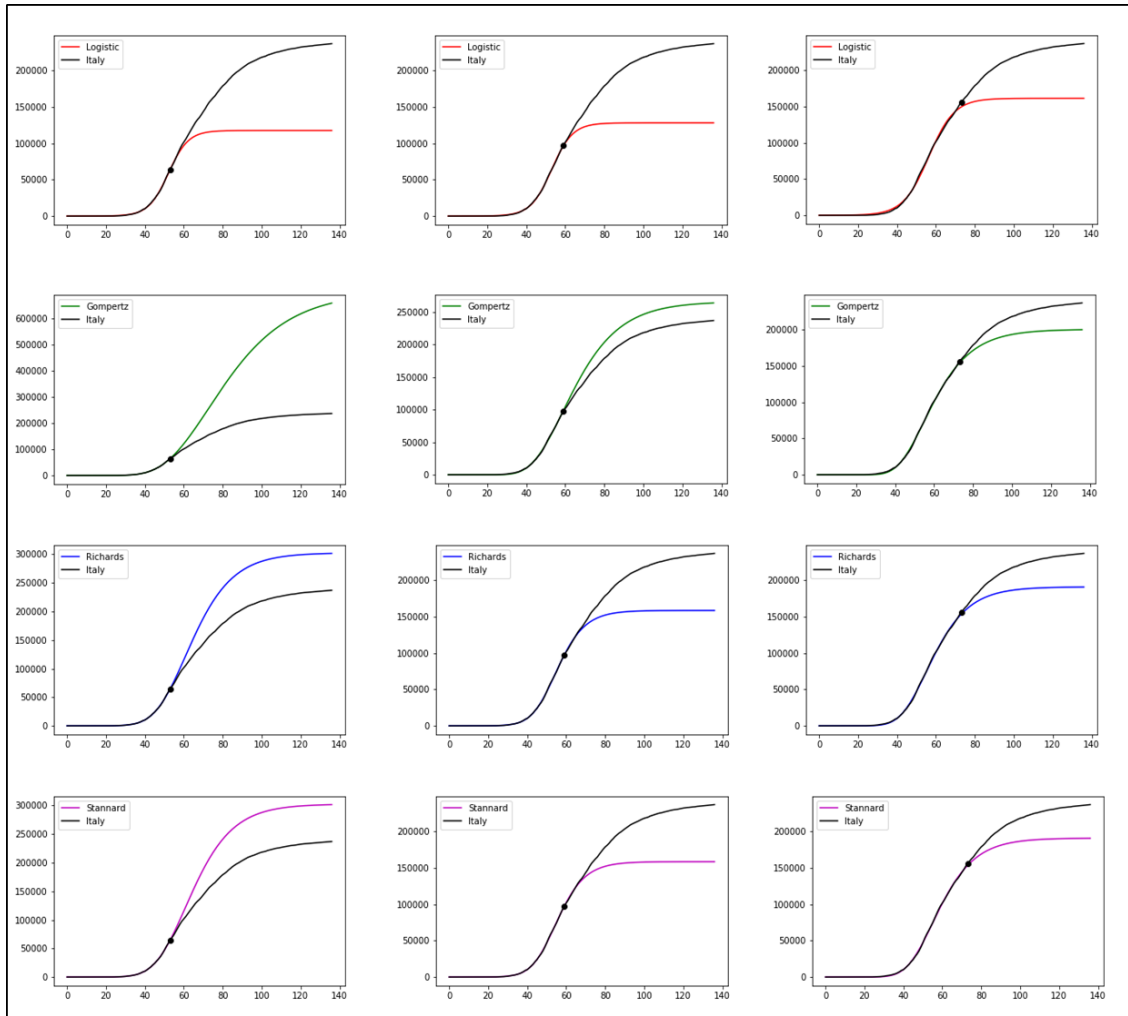


Figure G.27. Cumulative positive cases predictions for the following days at 25% (left), 40% (centre), and 65% (right) of total cases detected in Italy using the four PG models.

G.2 Positive cases predictions for the following 5, 10, and 15 days, at 25%, 40%, and 235 65% of total cases detected

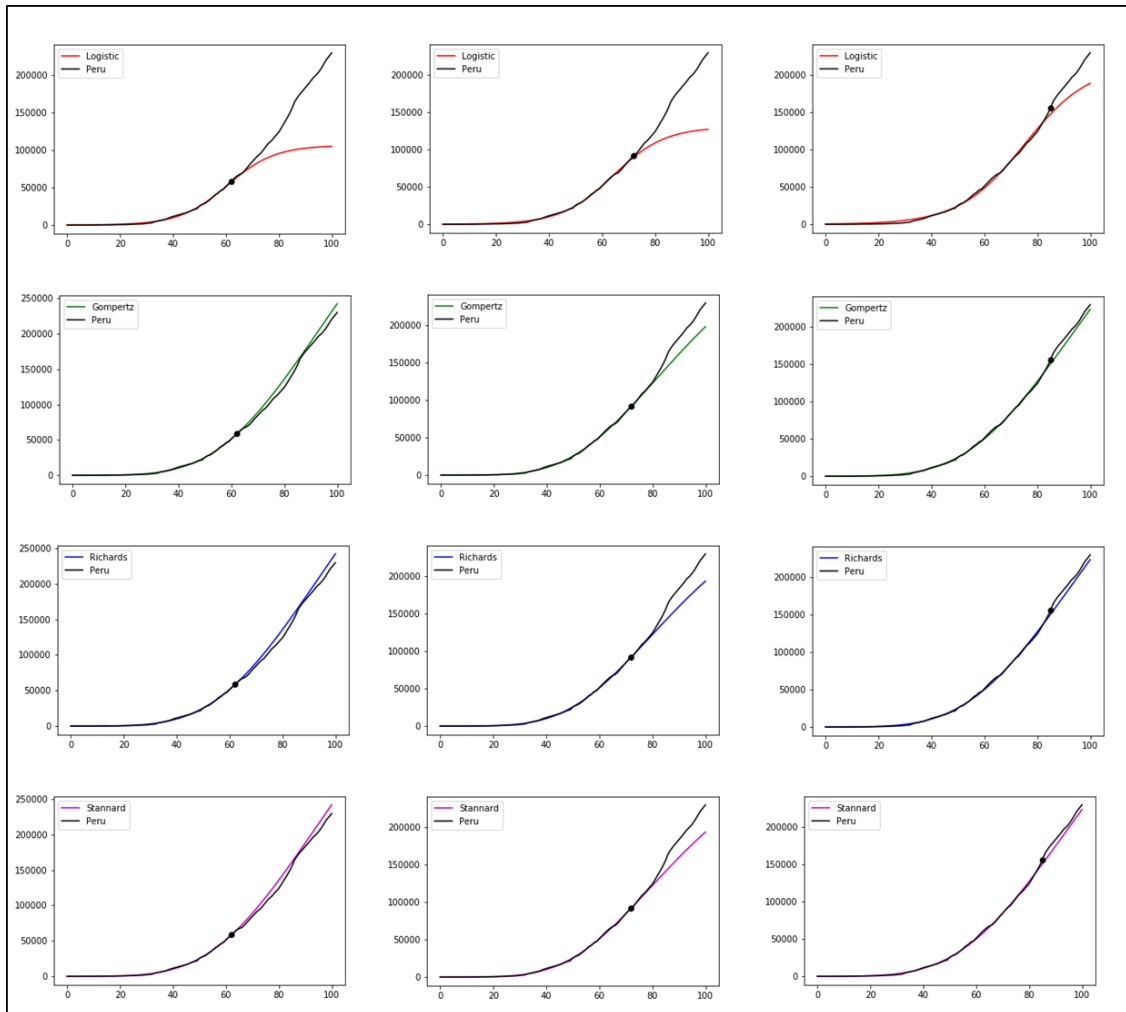


Figure G.28. Cumulative positive cases predictions for the following days at 25% (left), 40% (centre), and 65% (right) of total cases detected in Peru using four PG models.

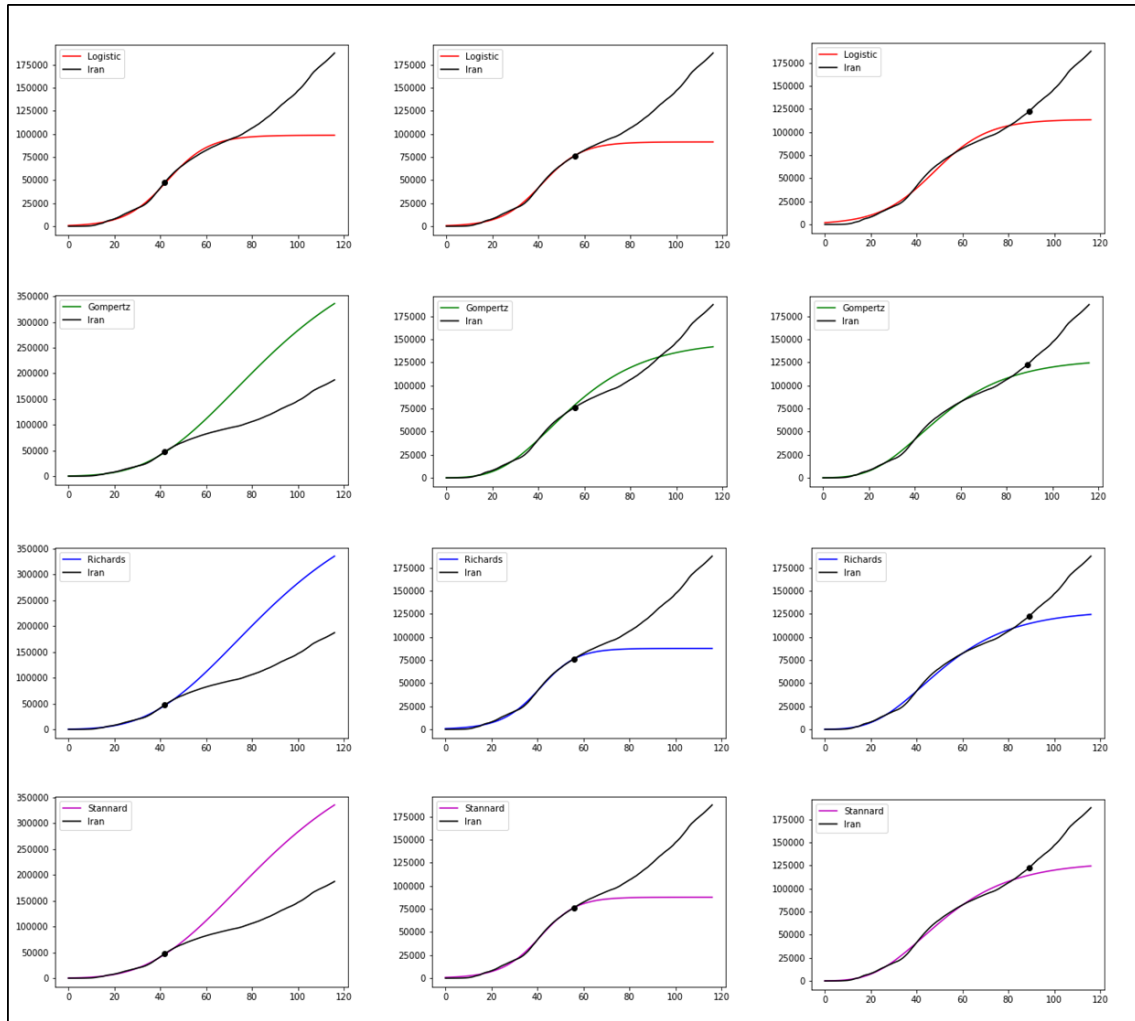


Figure G.29. Cumulative positive cases predictions for the following days at 25% (left), 40% (centre), and 65% (right) of total cases detected in Iran using the four PG models.

G.2 Positive cases predictions for the following 5, 10, and 15 days, at 25%, 40%, and 237 65% of total cases detected

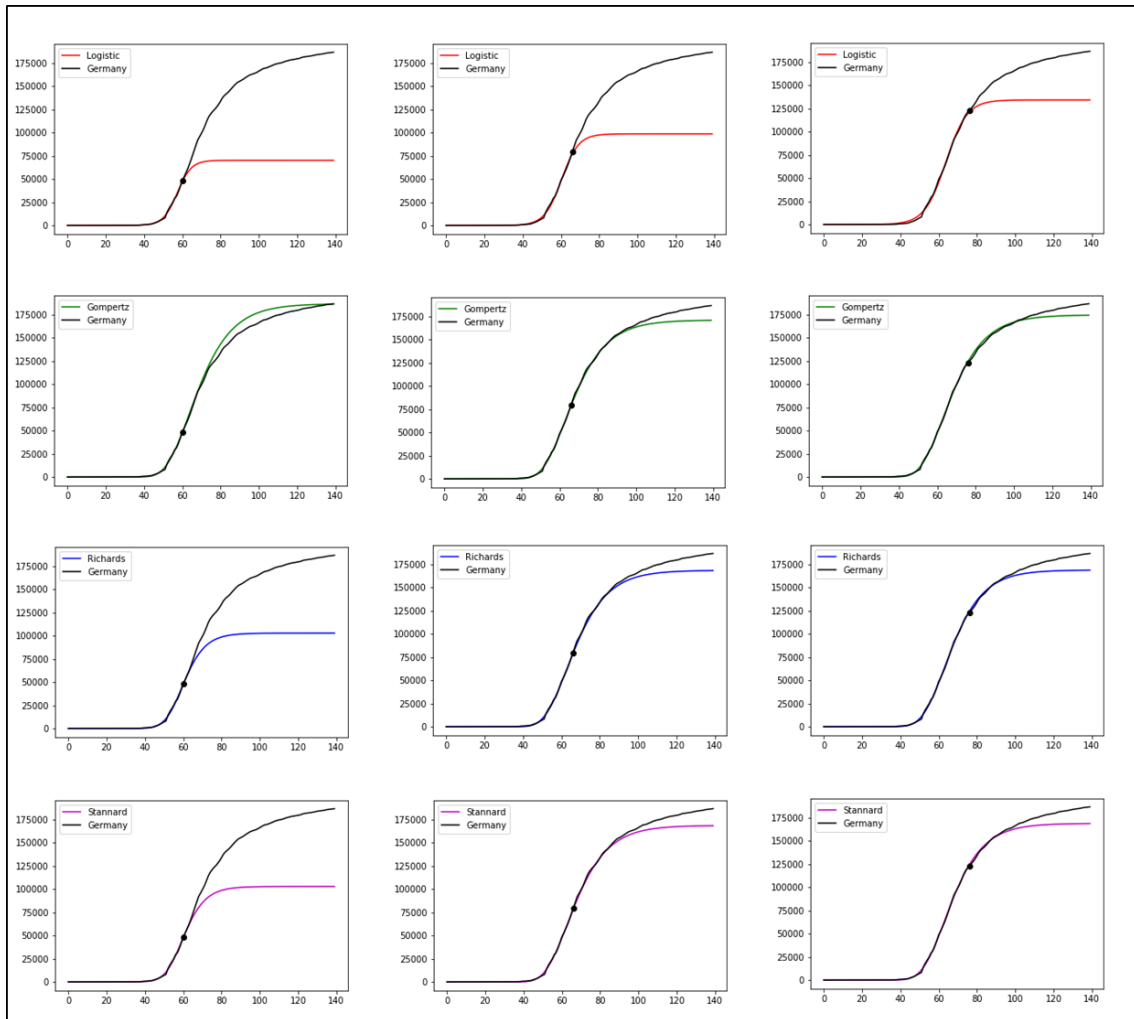


Figure G.30. Cumulative positive cases predictions for the following days at 25% (left), 40% (centre), and 65% (right) of total cases detected in Germany using the four PG models.

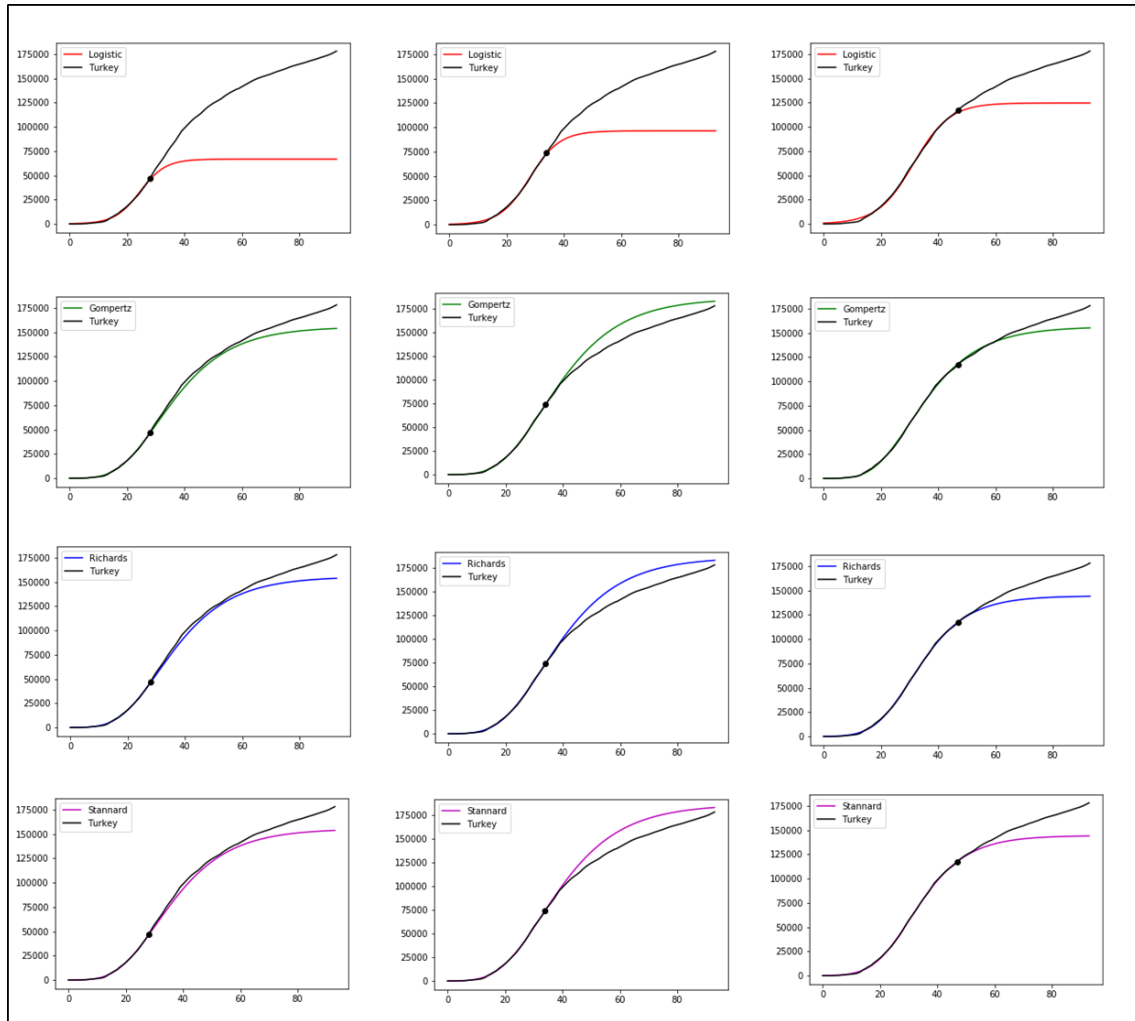


Figure G.31. Cumulative positive cases predictions for the following days at 25% (left), 40% (centre), and 65% (right) of total cases detected in Turkey using the four PG models.

G.2 Positive cases predictions for the following 5, 10, and 15 days, at 25%, 40%, and 239 65% of total cases detected

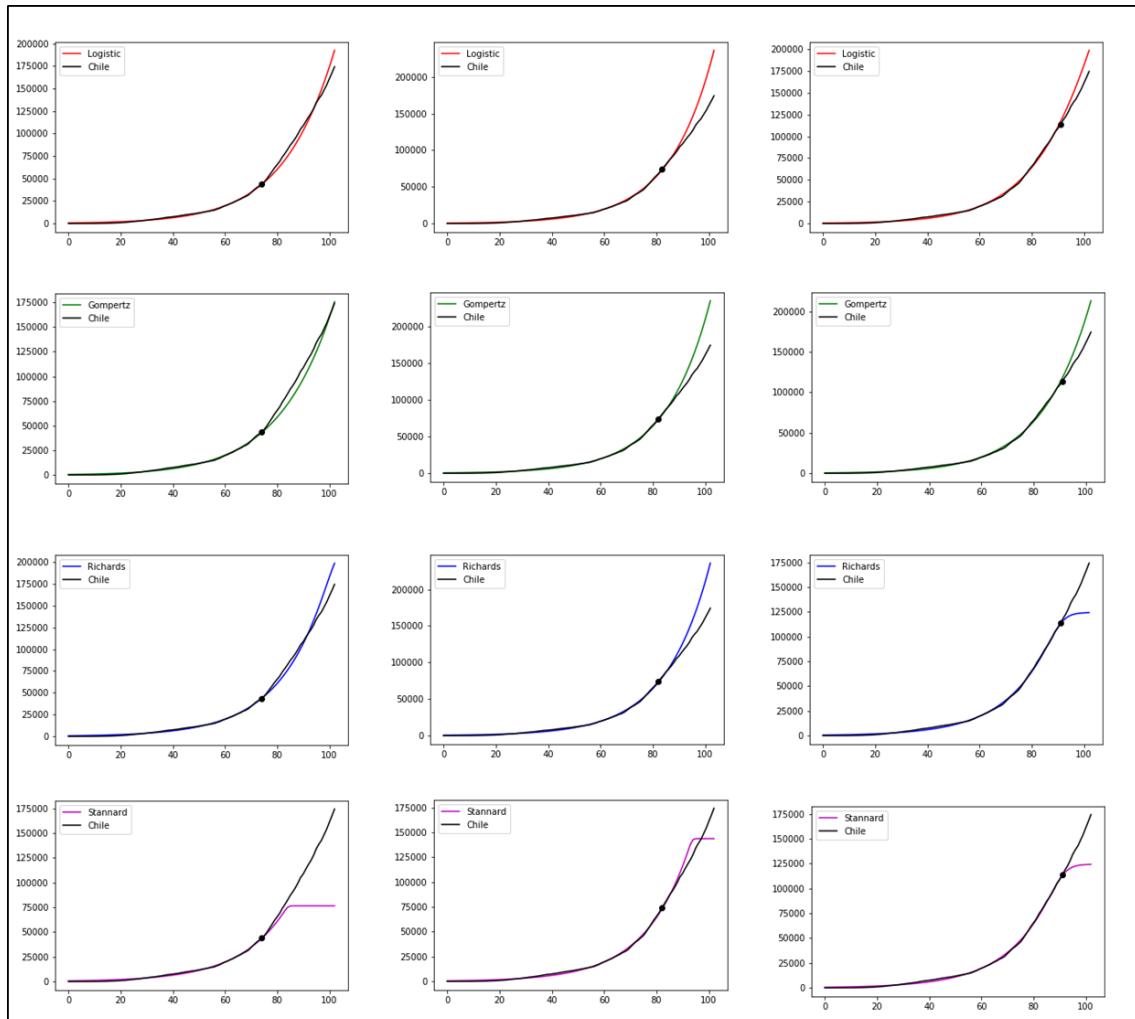


Figure G.32. Cumulative positive cases predictions for the following days at 25% (left), 40% (centre), and 65% (right) of total cases detected in Chile using the four PG models.

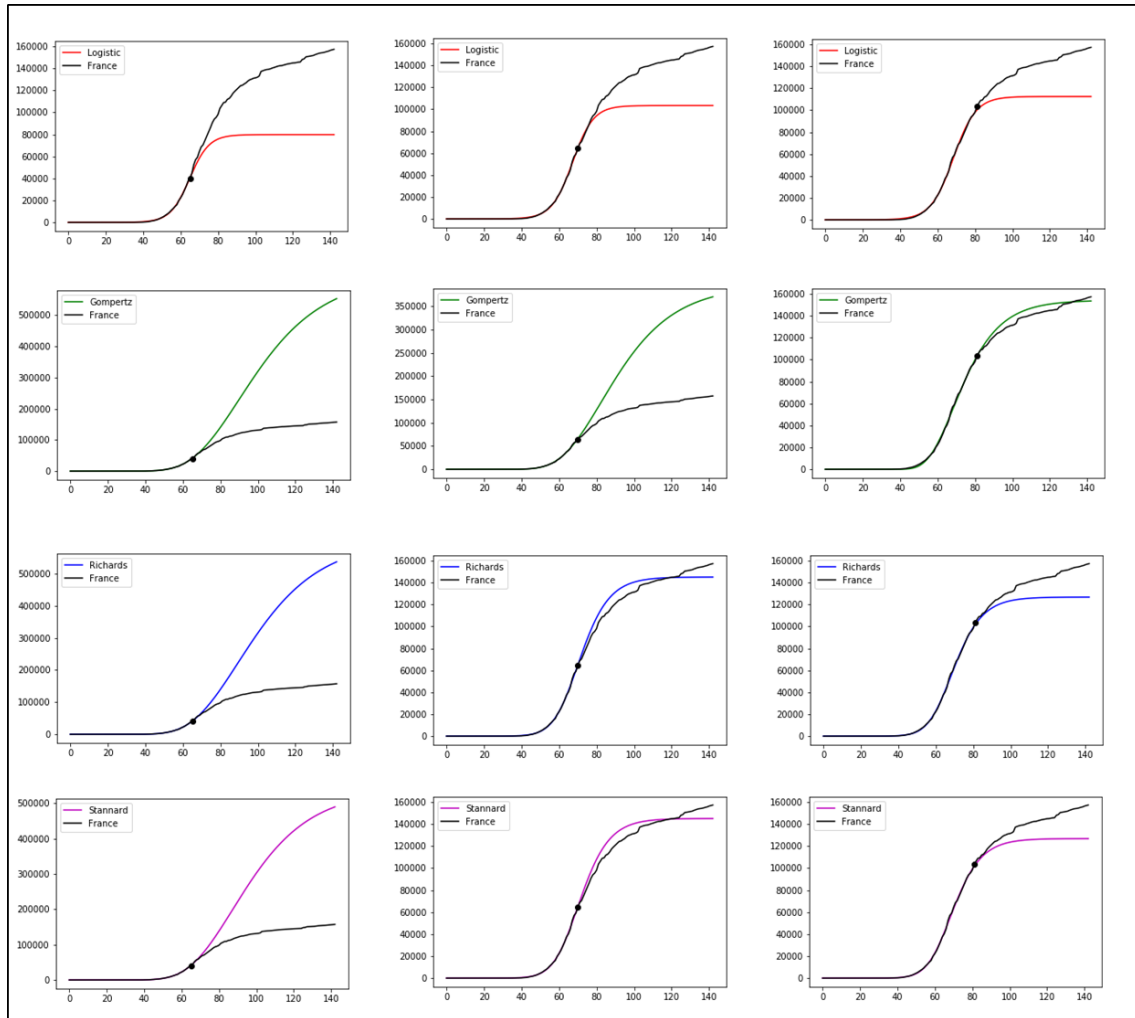


Figure G.33. Cumulative positive cases predictions for the following days at 25% (left), 40% (centre), and 65% (right) of total cases detected in France using the four PG models.

G.2 Positive cases predictions for the following 5, 10, and 15 days, at 25%, 40%, and 241 65% of total cases detected

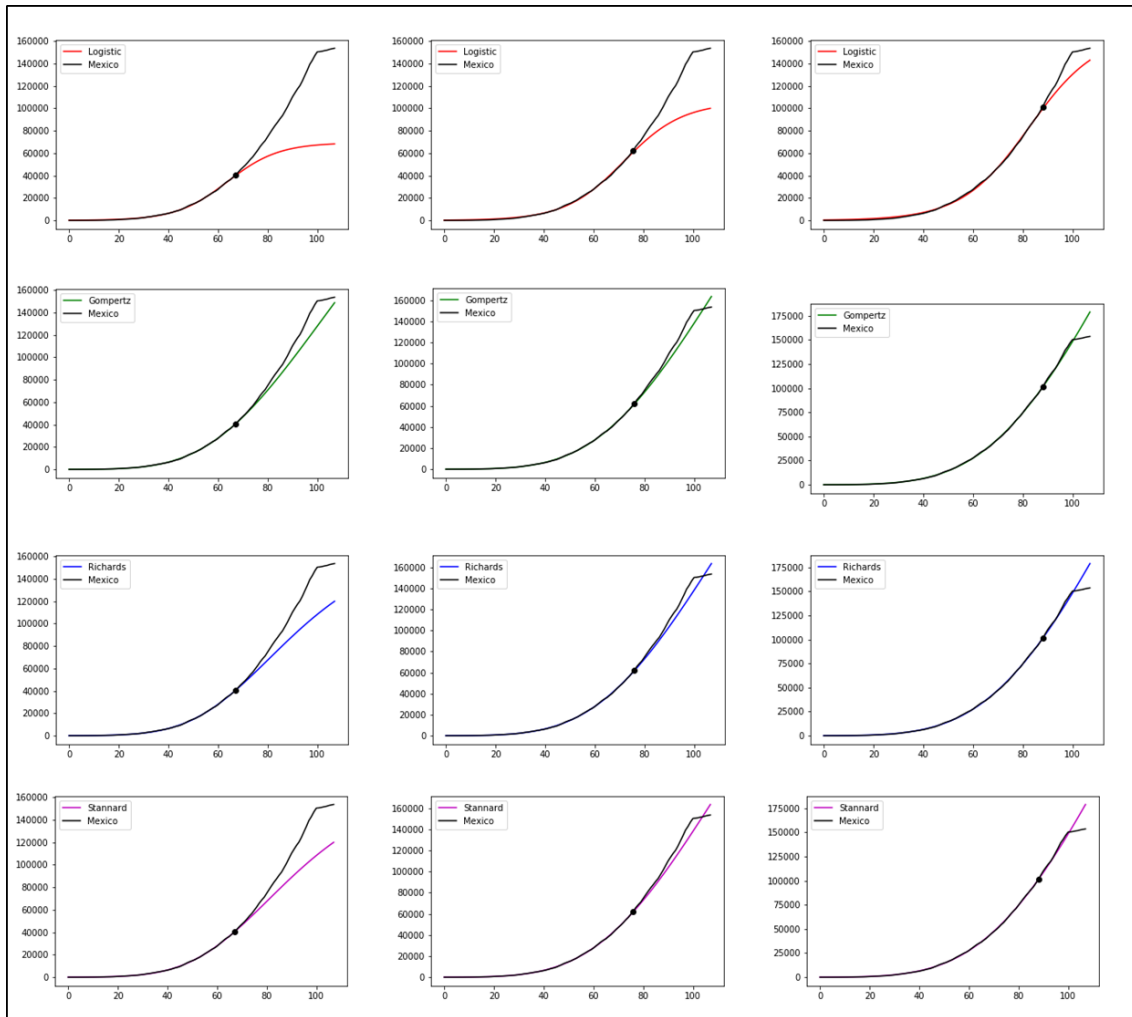


Figure G.34. Cumulative positive cases predictions for the following days at 25% (left), 40% (centre), and 65% (right) of total cases detected in Mexico using four PG models.

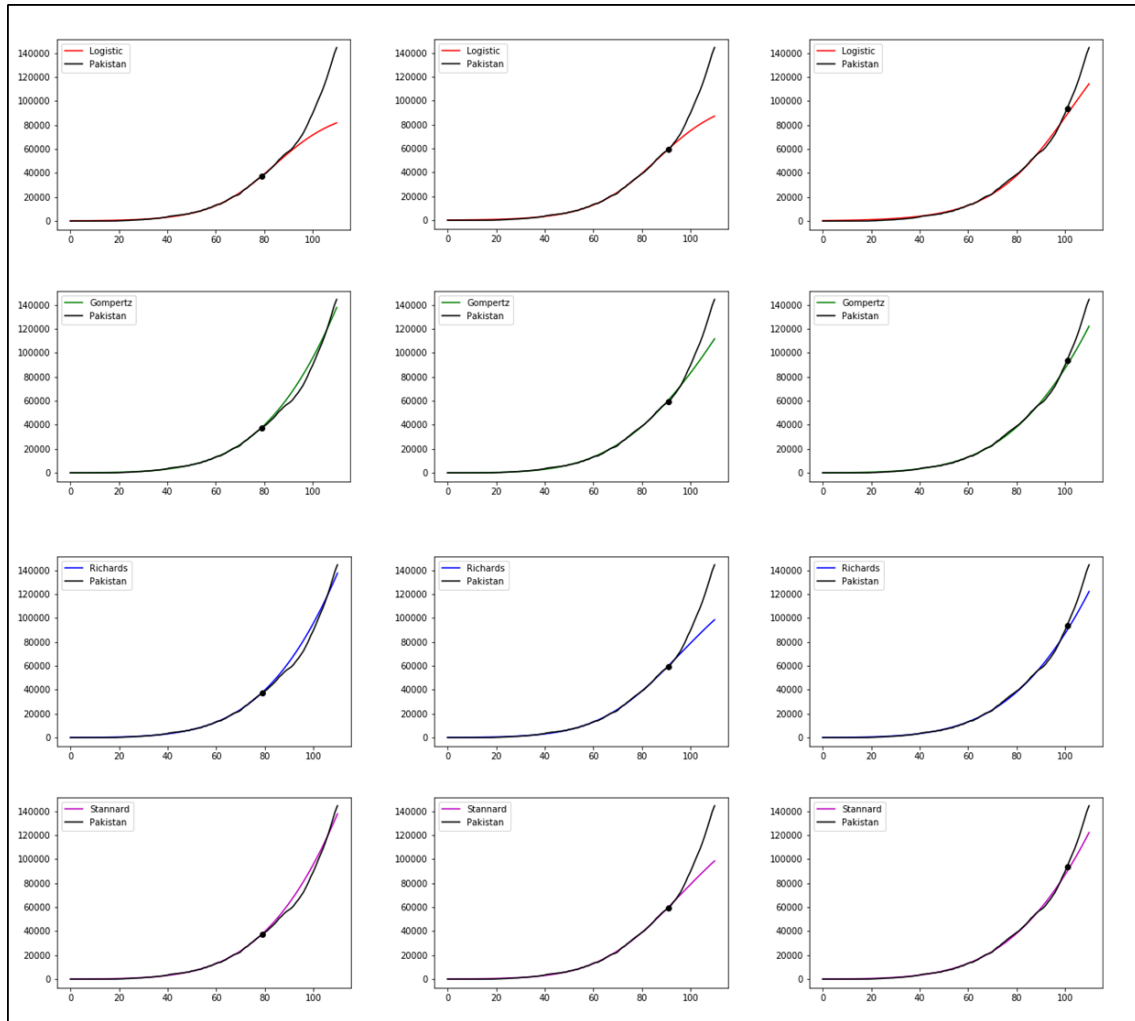


Figure G.35. Cumulative positive cases predictions for the following days at 25% (left), 40% (centre), and 65% (right) of total cases detected in Pakistan using the four PG models.

G.2 Positive cases predictions for the following 5, 10, and 15 days, at 25%, 40%, and 65% of total cases detected

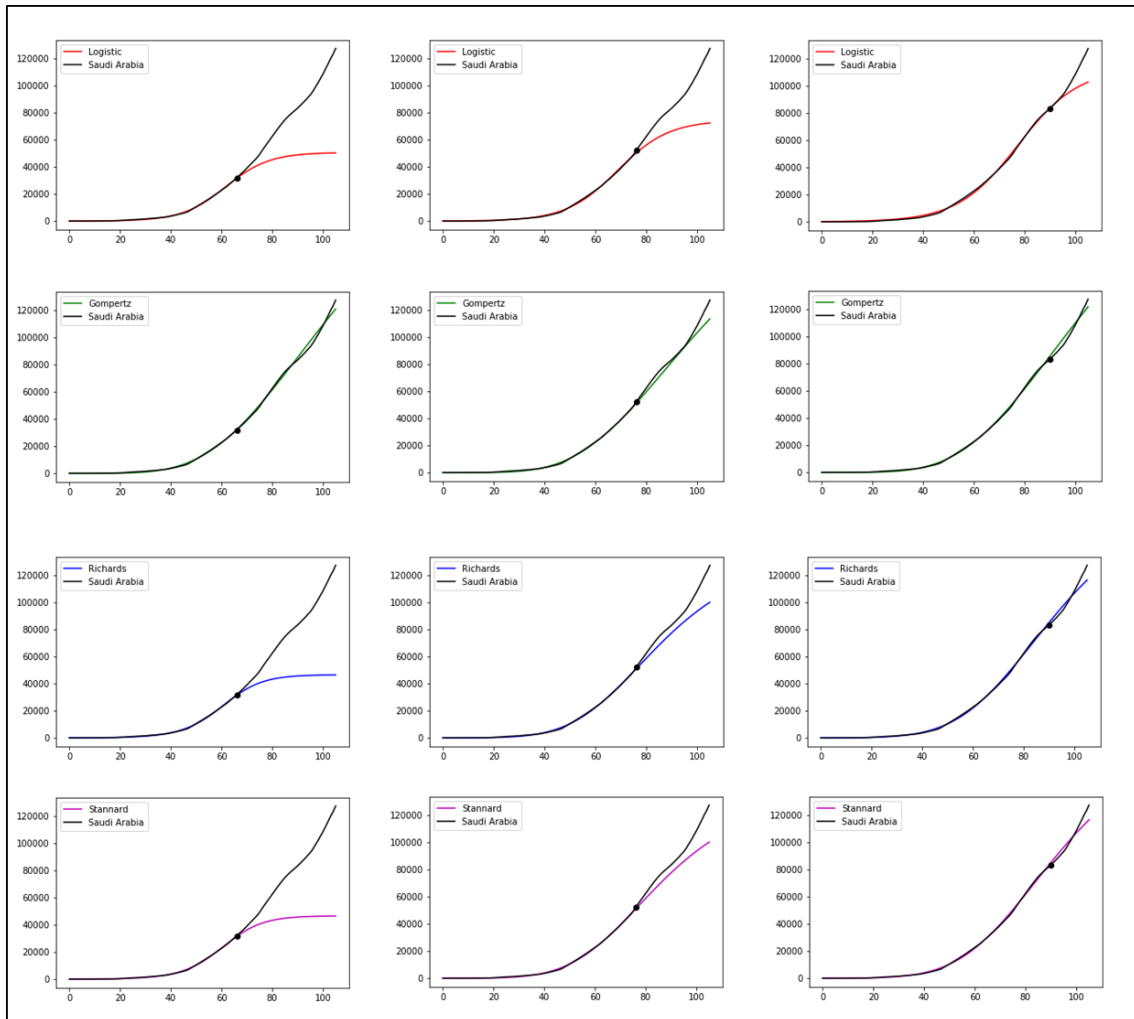


Figure G.36. Cumulative positive cases predictions for the following days at 25% (left), 40% (centre), and 65% (right) of total cases detected in Saudi Arabia using the four PG models.

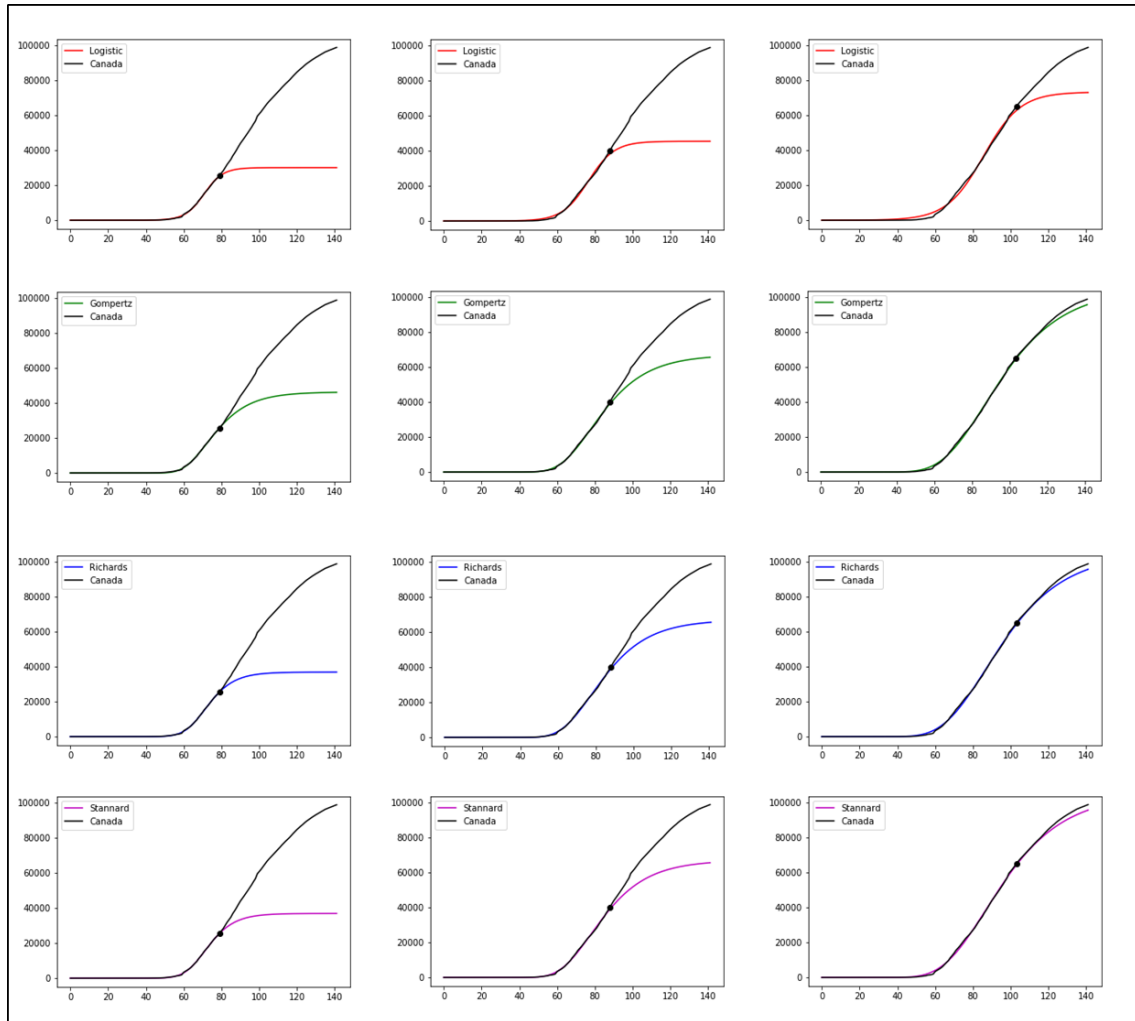


Figure G.37. Cumulative positive cases predictions for the following days at 25% (left), 40% (centre), and 65% (right) of total cases detected in Canada using the four PG models.

G.2 Positive cases predictions for the following 5, 10, and 15 days, at 25%, 40%, and 245 65% of total cases detected

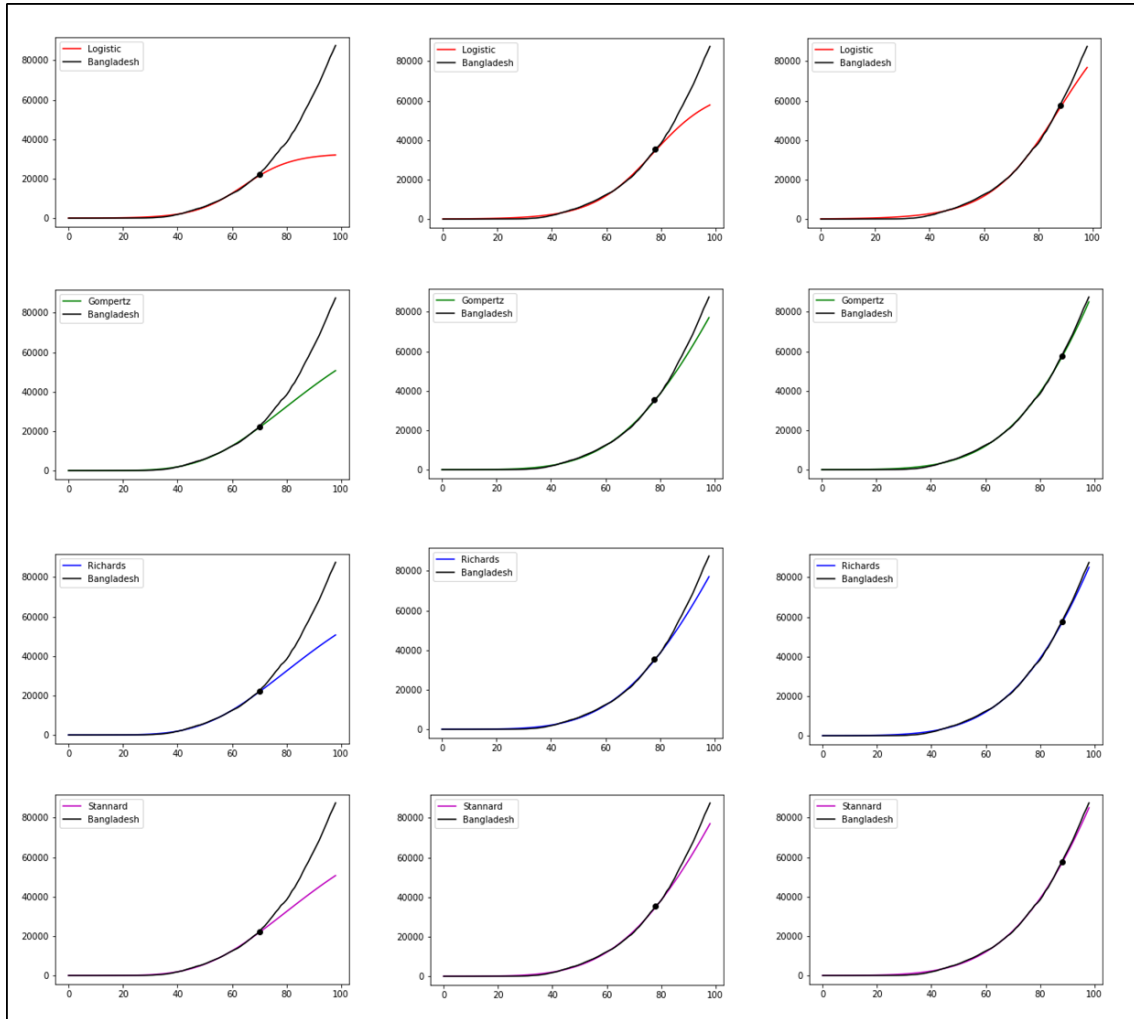


Figure G.38. Cumulative positive cases predictions for the following days at 25% (left), 40% (centre), and 65% (right) of total cases detected in Bangladesh using the four PG models.

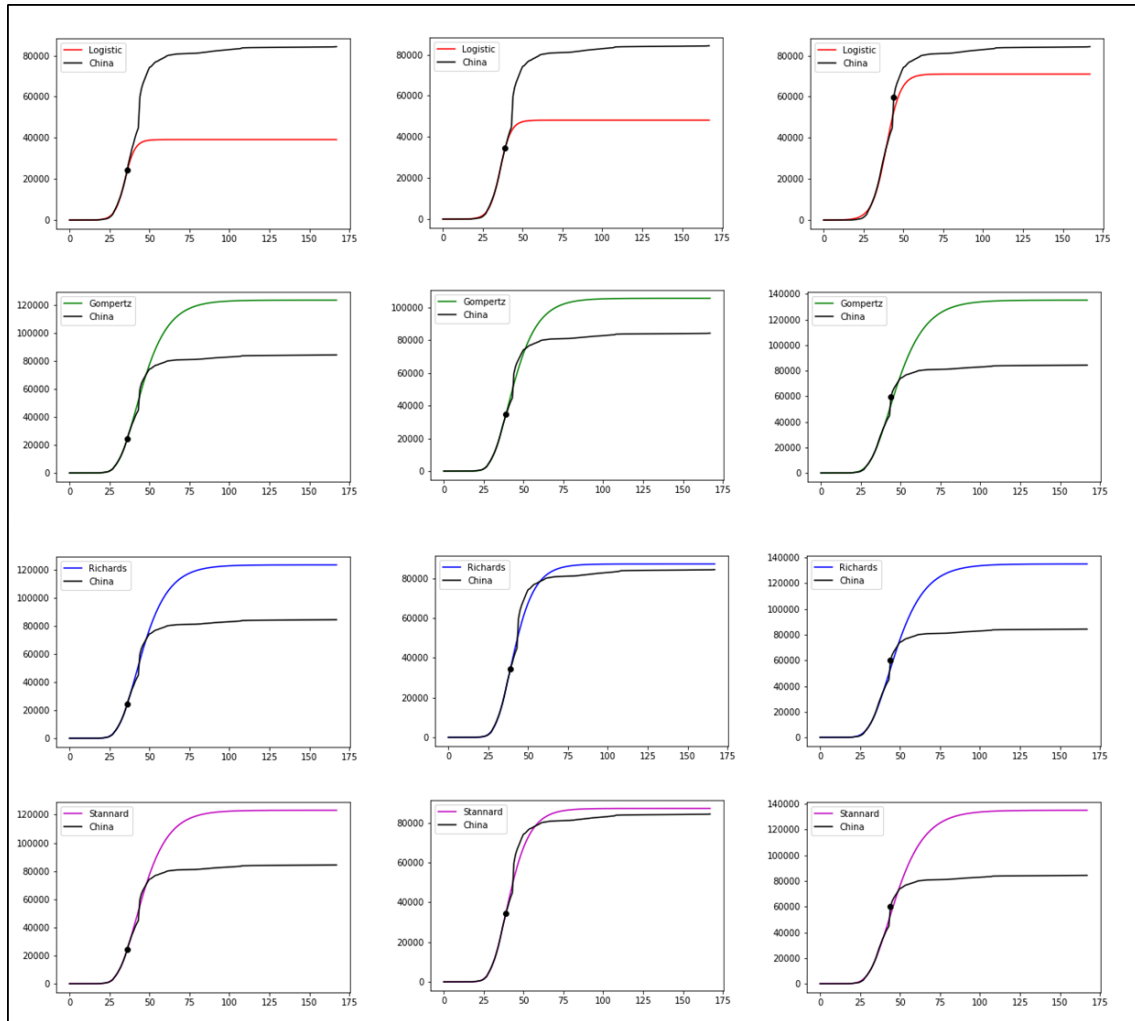


Figure G.39. Cumulative positive cases predictions for the following days at 25% (left), 40% (centre), and 65% (right) of total cases detected in China using the four PG models.

G.2 Positive cases predictions for the following 5, 10, and 15 days, at 25%, 40%, and 247 65% of total cases detected

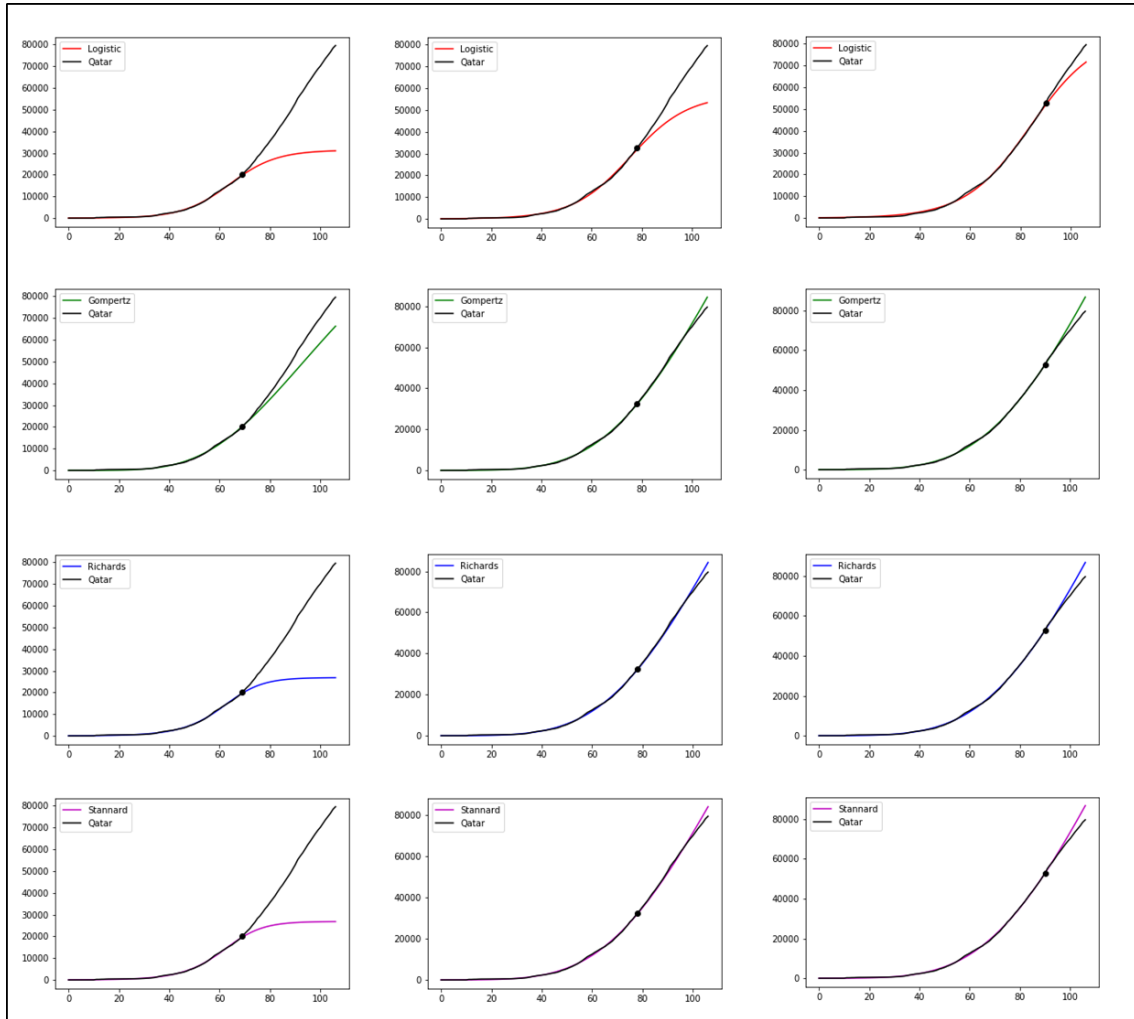


Figure G.40. Cumulative positive cases predictions for the following days at 25% (left), 40% (centre), and 65% (right) of total cases detected in Qatar using the four PG models.

H COVIDSIM software user guide

This is a user guide to the COVIDSIM software, a pandemic hospital resource simulator. It explains all the parts and steps necessary for its use, as well as showing the different possibilities offered by the software. The data used in this guide have been provided by the main hospital of La Rioja.

H.1 Starting the software

The COVIDSIM software is a Python file (extension .py). This file can be opened with different integrated development environments (IDE), such as Spyder, which is the one used for programming. Before running the software, it is important to check that the following files also appear in the folder where the software is saved:

- logo_Rioja salud.jpg.
- logo_qUPHS.png.
- qUPHS.ico
- Patient flow.png
- White background.png

These files are read to be loaded into different parts of the software. Once this check is done, you can proceed to run the software. When running the software, a new window will be opened as shown in Figure H.1.

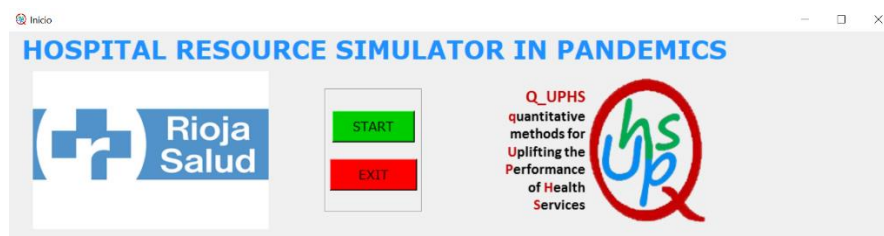


Figure H.1. Start window of the COVIDSIM software.

This window will always remain open while the software is running in the background. The "EXIT" button closes the program. The "START" button opens a new window with different tabs, which must be configured to perform the simulation. Each of these tabs is described in detail in the following sections.

H.2 Modelling pandemic spread

The first tab you see in the new window after starting the software corresponds to the pandemic expansion modelling. This tab is shown in Figure H.2.

Figure H.2. Modelling pandemic spread.

As can be seen in Figure H.2, two parts can be distinguished. On the one hand, on the left-hand side there is the estimation of the parameters of the Gompertz curve, and on the right-hand side, fields concerning the visualization of the growth curve fit. The fields that appear in each section and the way in which they can be selected or filled in are explained below.

Parameter estimation of the Gompertz curve

Gompertz-type curves are used in population growth models and have been found to fit well the growth of cumulative (positive or hospitalized) cases in both the first and second waves of the COVID-19 pandemic. In total, the Gompertz function has 3 parameters that define the shape of this curve. Each of these parameters is related to a physical interpretation, which is as follows:

- The total number of cases (positive or hospitalized, depending on the series to be represented) at the end of the pandemic.
- Time in days, in which the central 90% of the population (infected or hospitalized) is infected. That is the time between the moment when 5% and 95% of the total number of cases are registered.
- The number of cumulative cases that are known on a particular day of the pandemic.

These fields allow a personalized growth curve to be generated by entering the parameters manually. However, the software also allows for partial or full fit of the curve using a data file, as shown in Figure H.3.

Parameter estimation of the Gompertz curve

Manual introduction	Estimation mode
· Number of total cases at the end of the pandemic: 1000	Data file
· Time of infection of central 90% of the population (days): 21	Data file
· Number of cases on the date: 300 2020-09-19	Data file
-> Select data file: Open	Manual Data file
Route: ...tos/INGRESOS POR COVID-19 ANOM 15_10 800.xlsx	
Parameters for indirect estimation of hospitalisations	
· Geographic factor: 100 %	
· Hospitalization factor: 100 %	

Figure H.3. Estimation of the parameters of the Gompertz curve, both manually and using a data file.

To select the file, first, click on the "Open" button shown in Figure H.3 and then browse to the location of the file on the computer, as shown in Figure H.4. The file can contain the records of positive cases or patients admitted to the hospital. This information is specified later in this section.

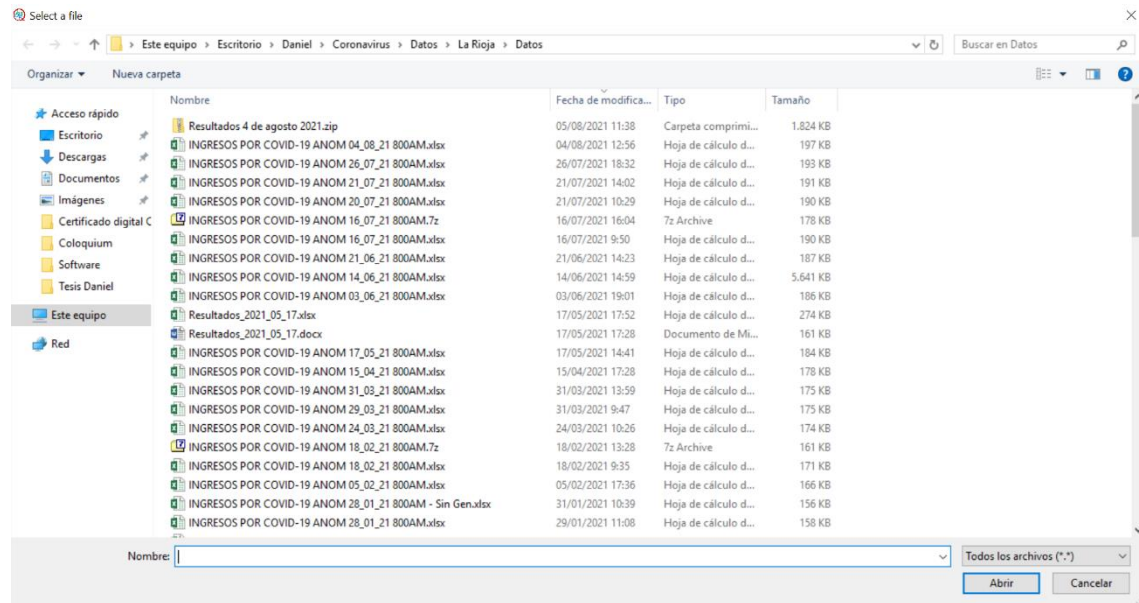


Figure H.4. Window to search the data file.

Finally, at the bottom of Figure H.3, there are two fields for entering percentages. These percentages serve to rescale the curve, in case the inpatient series is not being used. On the one hand, the geographical factor scales the number of cases from an area larger than the study area. On the other hand, the hospitalization factor, which indicates the percentage of patients admitted to the hospital with respect to the accumulated series (if the series coincides with that of hospitalized patients, these percentages are 100%). It may be the case that the series of hospitalized patients are not sufficiently extensive to be able to estimate it correctly and these intermediate calculations are necessary.

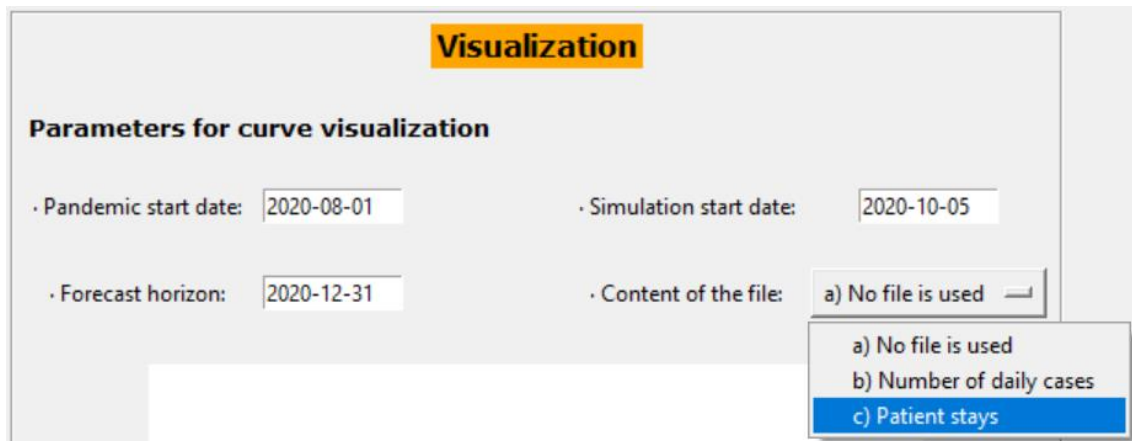
Curve display

In order to visualize the Gompertz growth curve, it is necessary to fill in three fields with the key dates of the situation under analysis.

- **Pandemic start date (yyyy-mm-dd):** This date indicates the time at which the pandemic is considered to start. It is therefore the date from which the curve is fitted to the data. If there are records in the data file prior to this start date, they will not be considered for curve fitting.
- **Simulation start date (yyyy-mm-dd):** This date indicates the time from which the predictions are to be made, which corresponds to the start of the simulation. If a data file is used to perform the curve fitting, there must at least be records up to this start date. Otherwise, the program will fail.
- **Forecast horizon (yyyy-mm-dd):** This date indicates the time up to which the curve being fitted is to be displayed. This date is independent of the simulation horizon, which is specified in Appendix H.4.

- Content of the file: With the drop-down menu, the user chooses the form in which he or she wants to obtain the curve. There are three alternatives. The first consists of generating the curve without using a file, so that all the parameters of the curve must be entered manually as explained before in *Parameter estimation of the Gompertz curve*. The second way is to use the file on the number of daily cases (positive or hospitalized) that have been recorded (Appendix H.6 describes how the data should be organized in this file). The third way consists of selecting a file with the data on patient stays (Appendix H.6 also explains what the contents of the file should be).

Figure H.5 shows all these fields filled in, and the drop-down menu with the three options for the file content.



The screenshot shows a web interface titled "Visualization" with a sub-section "Parameters for curve visualization". It contains four input fields: "Pandemic start date" (2020-08-01), "Simulation start date" (2020-10-05), "Forecast horizon" (2020-12-31), and "Content of the file". The "Content of the file" field is a dropdown menu with three options: "a) No file is used", "b) Number of daily cases", and "c) Patient stays". Option "c" is currently selected and highlighted in blue.

Figure H.5. Fields to be filled in for the display of the fitting curve.

Once the way in which the curve is to be fitted has been decided, establishing all the necessary dates, the curve is generated. To do this, the user must click on the "Refresh chart" button shown in Figure H.6. In this example, it is being selected that all the parameters of the curve are going to be fitted according to the data file, the start of the pandemic occurs on the date 2020-08-01, the start of the simulation is set on the date 2020-10-05 and the forecast horizon is set to 2020-12-31. Figure H.7 shows the result of the fitted curve.

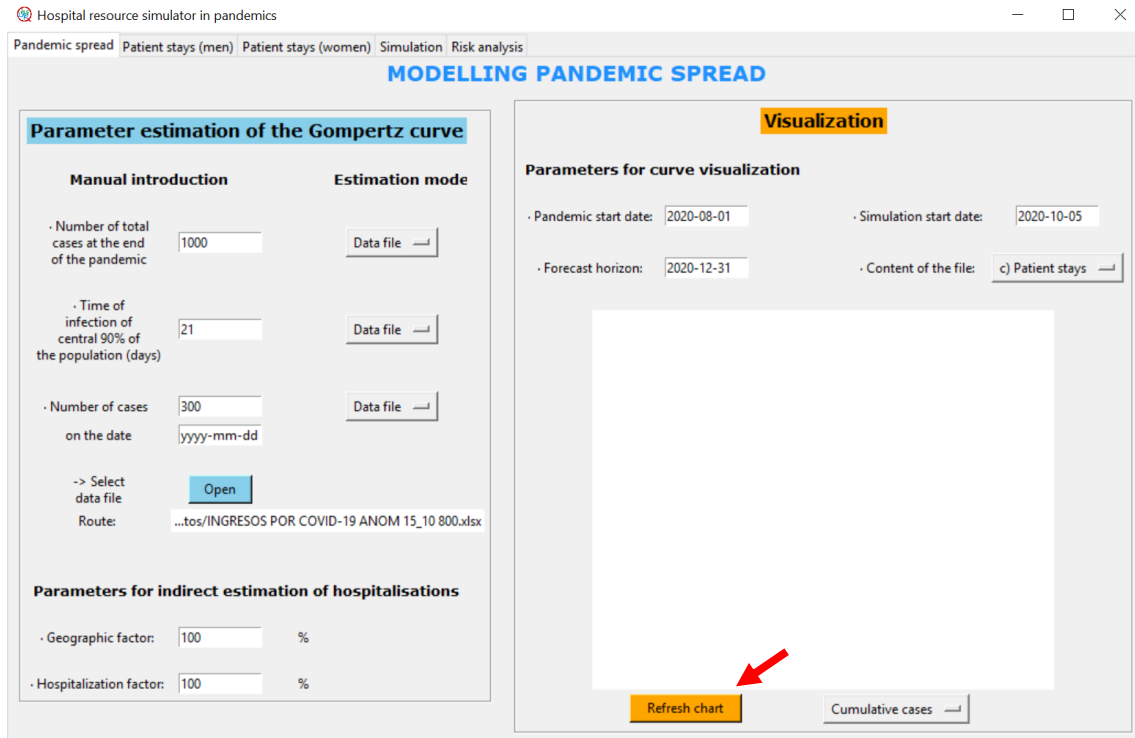


Figure H.6. Fields needed to obtain the fit of the Gompertz curve to the historical data.

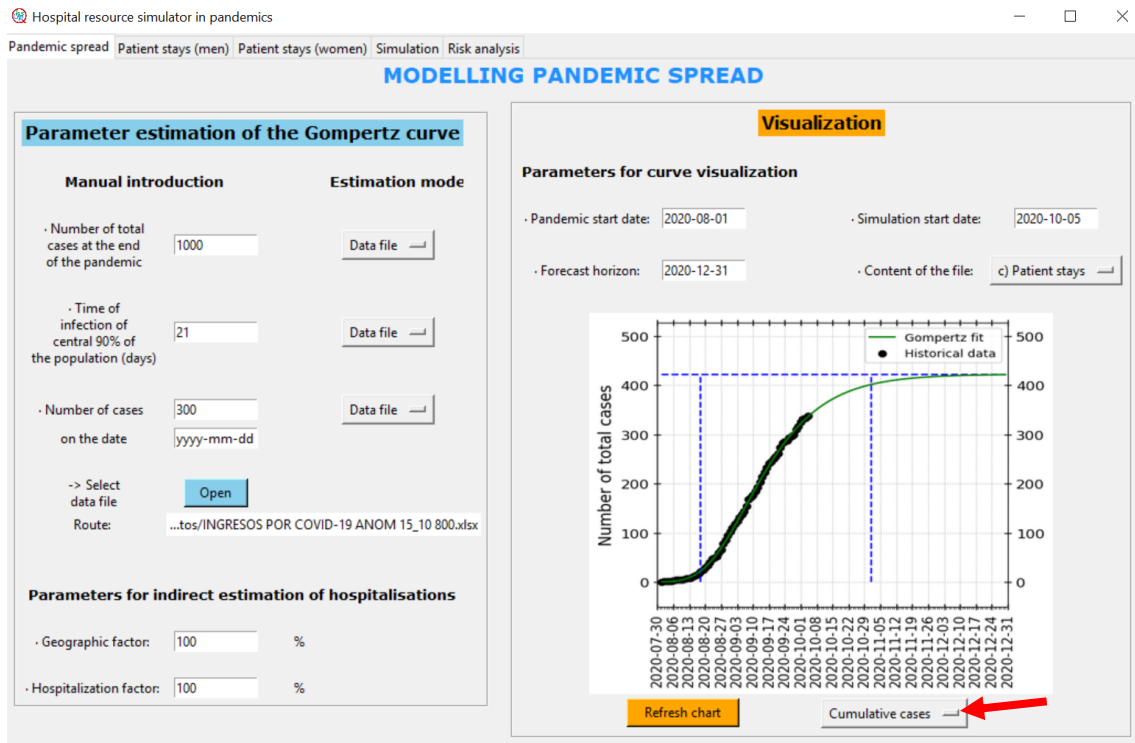


Figure H.7. Gompertz curve fit to historical data, represented by the black dots from 2020-08-01 to 2020-10-05.

Using the drop-down menu below the graph, in addition to the display of the cumulative cases fit, it is possible to display the daily cases and a linearization of the curve (the latter is useful to easily detect if the fit is good). Figure H.8 and Figure H.9 show these two graphs respectively.

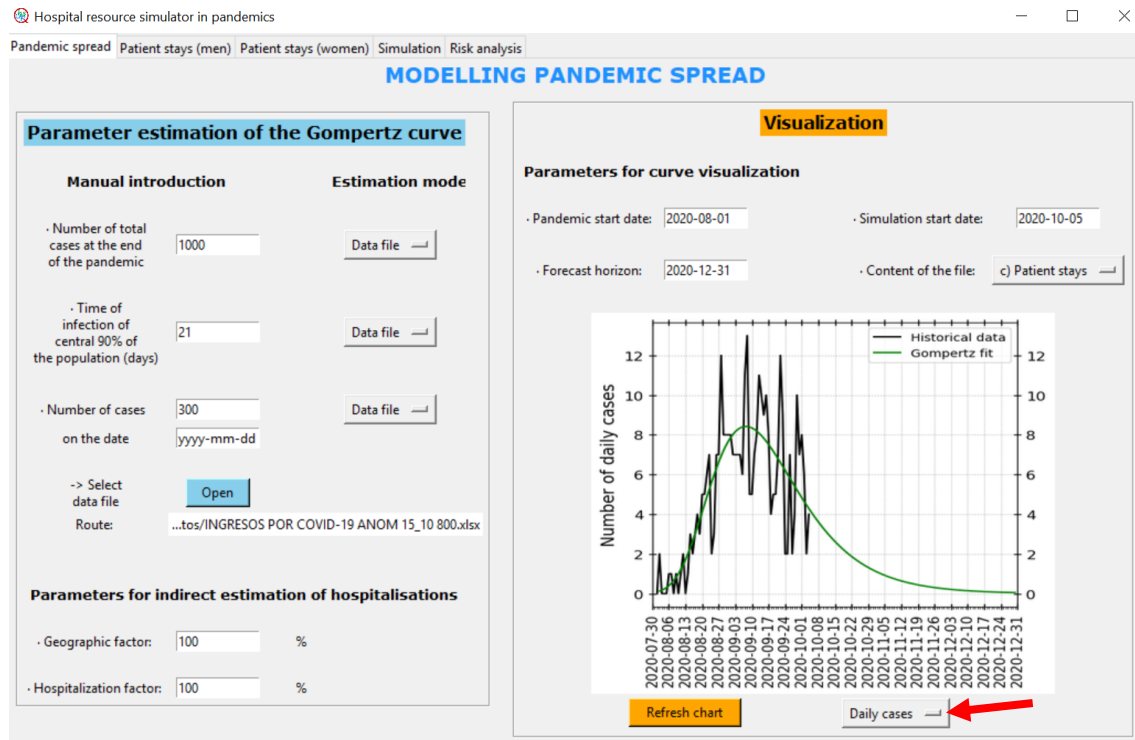


Figure H.8. Fitting of the Gompertz curve to daily data.

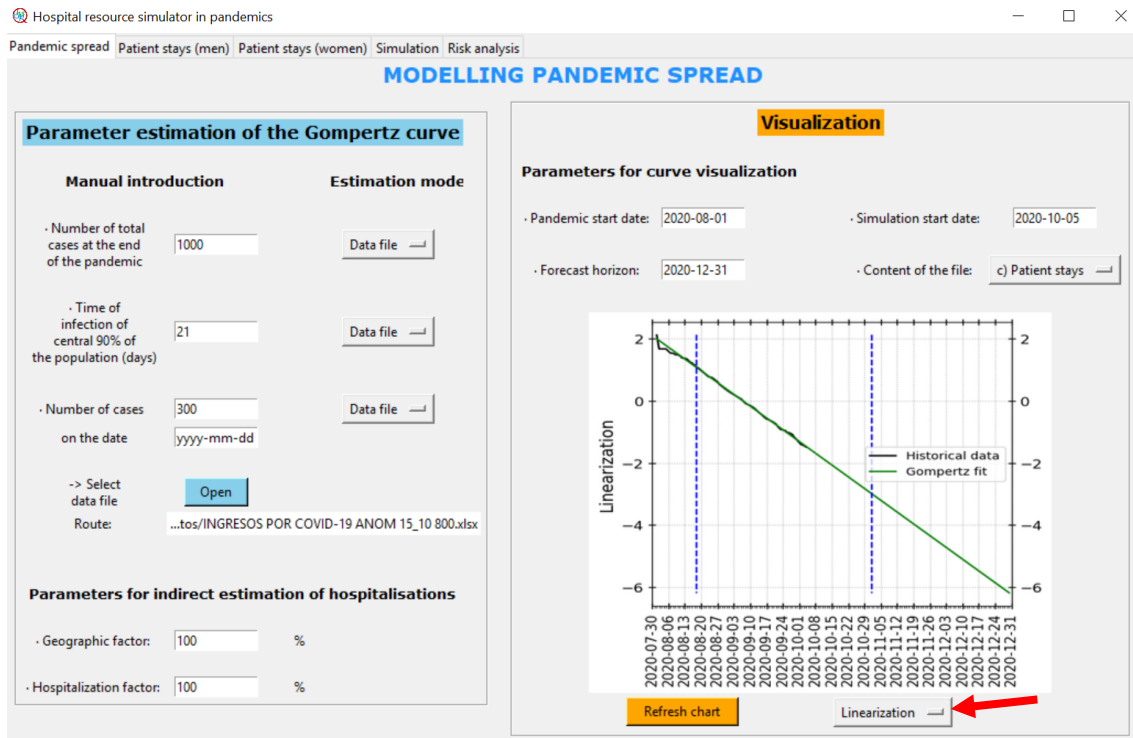


Figure H.9. Linearization of the fitted Gompertz curve.

As explained before in *Parameter estimation of the Gompertz curve*, the parameters of the curve can be chosen manually, and the software offers the possibility of a mixed fit, in which it fits the data but with some of the parameters fixed. For example, if it is considered that the total number of cases (patients admitted in this example) at the end of the pandemic will be higher than the fit to the data, a higher number can be selected, such as 700. Figure H.10 shows the result after setting the total number of admissions at 700.

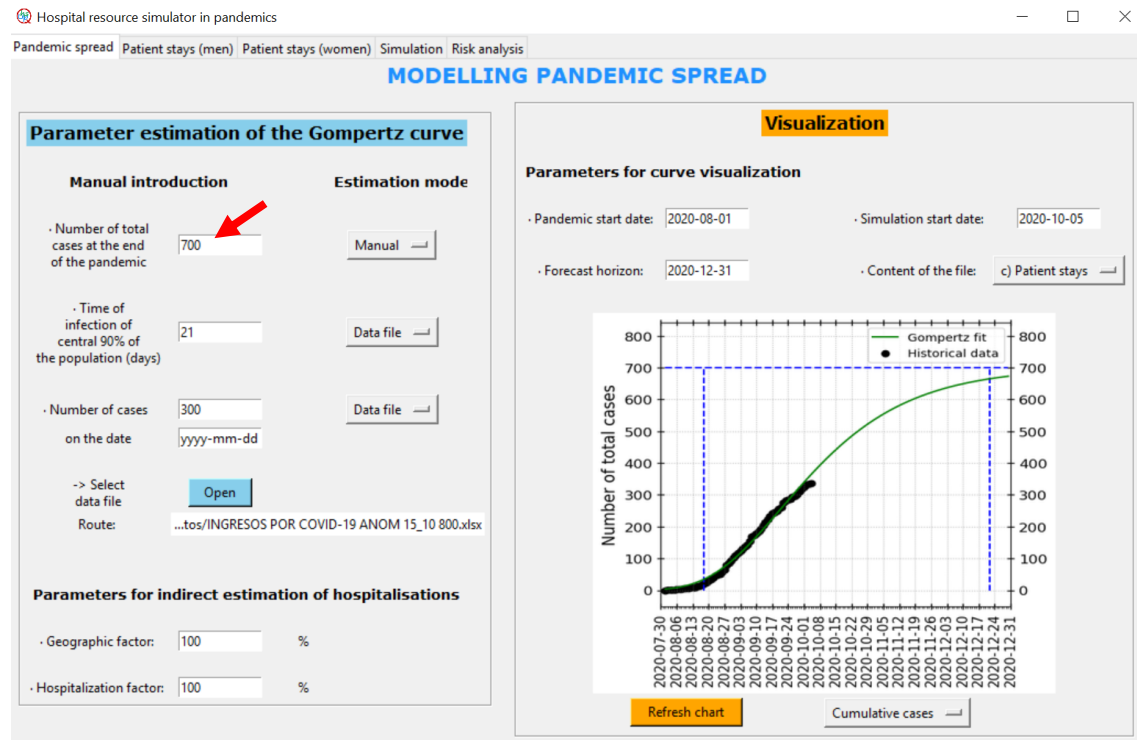


Figure H.10. Fit obtained by manually modifying the total number of cases at the end of the pandemic (700).

Customized curve

With the software, it is also possible to generate customized growth curves, that is, without fitting to the data. This is not a combination of manual input of some of the parameters and data fitting (see Figure H.10), but the whole curve is obtained by the user's selection of the parameters.

The three parameters that the user must define in order to fully customize the curve are described before in *Parameter estimation of the Gompertz curve*. As an example, Figure H.11 shows a curve generated in which the total number of patients admitted to the hospital at the end of the pandemic is 1,000, the time in which 90% of the core population is infected is 90 days, and it is assumed that 300 patients had already been admitted by 2020-10-01. The graph generated no longer shows the series of black dots, as it does not follow the trend of the historical data recorded. Only two dots are marked. The blue one indicates the data entered manually, in this case, the 300 patients who were admitted on October 1. The black one indicates the present time, i.e. the starting date of the simulation. This option can be relevant to evaluate different scenarios and represent different levels of infection. It is also possible to create new pandemic curves for further analysis.

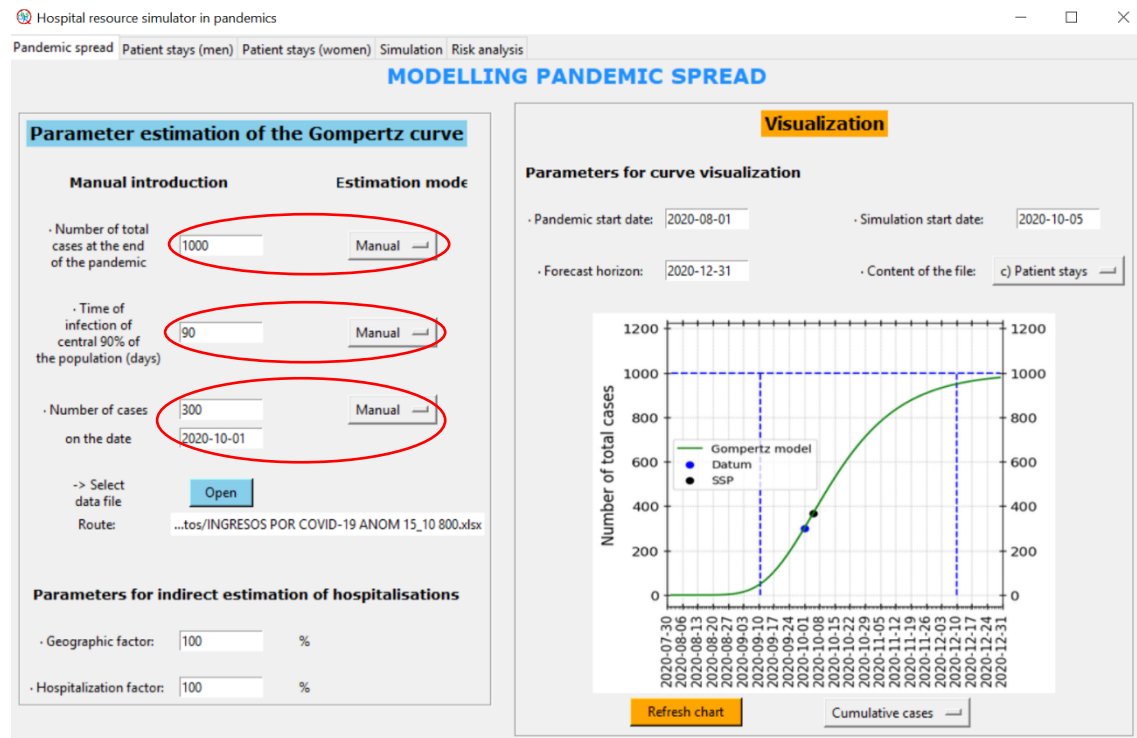


Figure H.11. Customized pandemic curve obtained after fitting the total number of admissions (1,000), the duration of the pandemic (90 days), and the number of cases on a selected day (300 on 2020-10-01).

H.3 Modelling of patient stays in hospital

The second tab to be configured before starting the simulation is the one concerning the modelling of patient stays in the hospital. Figure 12 shows an overview of this tab, which appears twice in the software it is distinguished by the gender of the patient (the first data analysed show that there are significant differences in the mean stays of men and women).

In order to model patient stays in the hospital, it is first necessary to create a flow diagram that represents the different paths a patient may take in the hospital. This patient flow diagram is shown in Figure H.13 and appears in the programme at the top right of Figure H.12. The following paths are considered in this diagram:

- The patient is admitted to the hospital ward, and after his or her stay he or she is discharged.
- The patient is admitted to the hospital ward, after a few days he or she is admitted to the ICU, and at the end of his or her stay in the ICU he or she leaves the hospital (due to transfer or death).
- The patient is admitted to the hospital ward, after a few days he or she is admitted to the ICU, and at the end of his or her stay in the ICU he or she is transferred to the hospital ward where his or her stay ends.

- The patient is admitted directly to the ICU, and at the end of the ICU stay leaves the hospital (due to transfer or death).
- The patient is admitted directly to the ICU, and at the end of his or her stay in the ICU is transferred to the hospital ward where his or her stay ends.

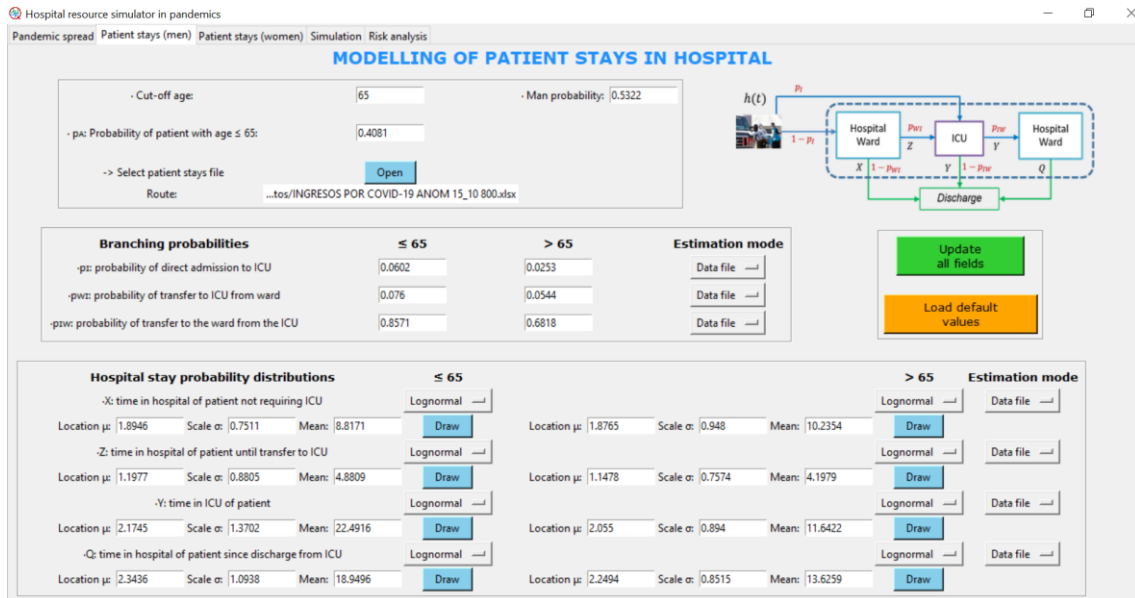


Figure H.12. Modelling of patient stays in the hospital.

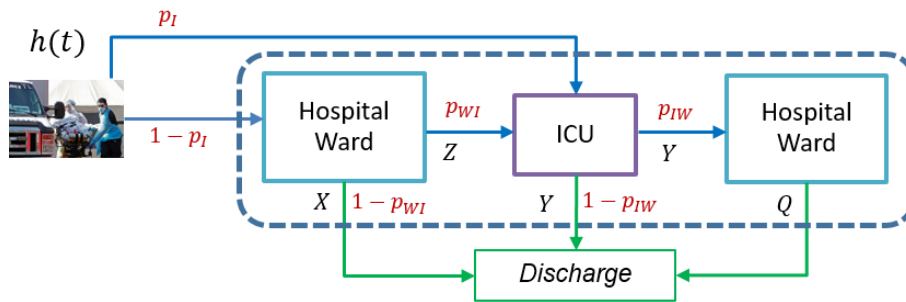


Figure H.13. Patient flow diagram through the hospital.

Figure H.13 shows a number of parameters related to the branching probabilities of the paths (p_I , p_{WI} , and p_{IW}) and the probability distributions of the stays on each path (X , Z , Y , and Q), which are defined and explained later in *Branching probabilities* and in *Probability distributions of hospital stays*.

Input data (age of cut-off and stay file)

In the upper part of Figure H.12, there are the fields concerning the cut-off age of the patients, probabilities related to the cut-off age and gender of the patients, and the historical stays file used for the analysis. Figure H.14 shows this part of the tab.

The screenshot shows a software interface with the following fields and values:

- Cut-off age: 65
- Man probability: 0.5322
- p_A : Probability of patient with age ≤ 65 : 0.4081
- Route: ...tos/INGRESOS POR COVID-19 ANOM 15_10 800.xlsx

There is a blue "Open" button and a label "-> Select patient stays file".

Figure H.14. Fields related to the cut-off age of patients and the stays file.

Firstly, the cut-off age of the patients. This age is entered manually and is used to divide the patients into two populations according to this cut-off age. By default, the cut-off age of 65 years is selected. This age can be chosen independently for men and women. Related to this age, we have the field of the probability of being a patient with age less than or equal to the cut-off age (p_A). This value can be calculated through the data file or entered manually.

On the right-hand side of Figure H.15 is a field with the probability that the patient is male. This value, like p_A , can be obtained from the data or entered manually. In the tab with the female data, this field is greyish (see Figure H.15), as its value depends on the percentage of males.

The screenshot shows a software interface with the following fields and values:

- Cut-off age: 65
- Woman probability: 0.4678 (highlighted with a red arrow)
- p_A : Probability of patient with age ≤ 65 : 0.3986
- Route: ...tos/INGRESOS POR COVID-19 ANOM 15_10 800.xlsx

There is a blue "Open" button and a label "-> Select patient stays file".

Figure H.15. Female patients tab for the fields related to the cut-off age and the stays file.

Finally, concerning the patient stays file, it can be opened in exactly the same way as explained in Figure H.3 and Figure H.4. However, this step would not be necessary if the patient's stays file has been entered in the first tab of the software when the Gompertz curve is fitted. So the file would be loaded automatically.

Branching probabilities

In the central part of Figure H.12, there are fields of branching probabilities. Each of them can be entered manually or using a data file, as shown in Figure H.16. Within the same gender, each probability is distinguished according to the age of the patient, based on the cut-off age.

The screenshot shows a software interface with the following fields and values:

Branching probabilities	≤ 65	> 65	Estimation mode
p_i : probability of direct admission to ICU	0.0086	0.0114	Manual
p_w : probability of transfer to ICU from ward	0.0391	0.026	Manual
p_{iw} : probability of transfer to the ward from the ICU	0.6364	0.3077	Manual Data file (highlighted with a red arrow)

Figure H.16. Branching probabilities.

These probabilities define the trajectory of patients through the flow diagram in Figure H.13, and are defined as follows:

- p_I : the probability that a patient arriving at the hospital is admitted directly to the ICU. Therefore, patients arriving at the hospital are admitted to the ward with probability $(1 - p_I)$.
- p_{WI} : the probability that a patient who is admitted to the hospital ward is transferred to the ICU. Then, a patient is discharged from the hospital (by recovery, transfer, death...) with probability $(1 - p_{WI})$.
- p_{IW} : the probability that a patient who is admitted to the ICU is transferred to the hospital ward. Thus, a patient is discharged from the ICU directly (usually by death or transfer) with probability $(1 - p_{IW})$.

Probability distributions of hospital stays

In the lower part of Figure H.12, the probability distributions of hospital stays are defined. As with the branching probabilities, the parameters which describe each probability distribution can either be automatically fitted according to the patient stay data (data file) or set by the user (manual), distinguishing patients by gender and cut-off age, as shown in Figure H.17.

Parameter	Location μ	Scale σ	Mean	Estimation mode
X: time in hospital of patient not requiring ICU	1.8946	0.7511	8.8171	Lognormal
Z: time in hospital of patient until transfer to ICU	1.1977	0.8805	4.8809	Lognormal
Y: time in ICU of patient	2.1745	1.3702	22.4916	Lognormal
Q: time in hospital of patient since discharge from ICU	2.3436	1.0938	18.9496	Lognormal
X: time in hospital of patient not requiring ICU	1.8765	0.948	10.2354	Lognormal
Z: time in hospital of patient until transfer to ICU	1.1478	0.7574	4.1979	Lognormal
Y: time in ICU of patient	2.055	0.894	11.6422	Lognormal
Q: time in hospital of patient since discharge from ICU	2.2494	0.8515	13.6259	Lognormal

Figure H.17. Probability distributions of hospital stays.

These probability distributions describe the length of stay (LoS) of each patient in each phase of the process. In total 4 probability distributions are distinguished, which are shown in the flow chart in Figure H.13. They are as follows:

- X : LoS in hospital of a patient not requiring ICU. This time is determined by the difference between the date of discharge and the date of admission of a patient to the hospital.
- Z : LoS in hospital of a patient until transfer to the ICU. It is determined by the difference between the date of admission to the ICU and the date of admission to the hospital. When these two dates are the same, it means that the patient has been admitted directly to the ICU and this stay is not considered.

- Y : LoS in the ICU of a patient. This time is determined by the difference between the date of discharge from the ICU and the date of admission to the ICU.
- Q : LoS in hospital of a patient discharged from the ICU. This time is obtained from the difference between the hospital discharge date and the ICU discharge date. It is obviously only defined for patients who have been in the ICU. When the ICU discharge date coincides with the hospital discharge date, it implies that the patient has been discharged directly from the ICU, usually due to death or transfer, without being transferred to the hospital ward.

Default values and updating of values

The software assigns default values to all the probability values and parameters of the distributions of the stays defined before in *Input data (age of cut-off and stay file)*, *Branching probabilities*, and *Probability distributions of hospital stays*. These default values correspond to the scenario that was observed in the first wave of the pandemic (between March and June 2020) and can be used if not enough data have yet been observed from the new wave. Therefore, they are referenced values that can be modified either by fitting the values through the data file or by entering new data manually. In any case, it is always possible to return to the default values, by clicking on the orange button "Load default values", which can be seen in Figure H.12.

Parameter fitting using data file

To fit the parameters using a data file, the estimation mode "Data file" must be selected, and by clicking on the green button "Update all fields", only those fields with this option will be modified. Figure H.18 shows an update of the values in all parameters except for the distribution of the LoS in the hospital of patients discharged from ICU (Q), as the "Manual" option has been maintained.

For the probability distributions of hospital stays, it is possible to select the distribution to be used for the fit and to check the quality of the fit by clicking on the "Draw" button. Figure H.19 shows the fit made for the LoS in the hospital of non-ICU patients (X) over 65 years old. The distribution selected for the fit of this LoS is the Weibull distribution. This graphical output is used to compare two fits with different probability distributions. For example, in Figure H.20, the same fit is shown, modifying the distribution to Lognormal. It can be seen that the fit with the Weibull distribution is better in this case.

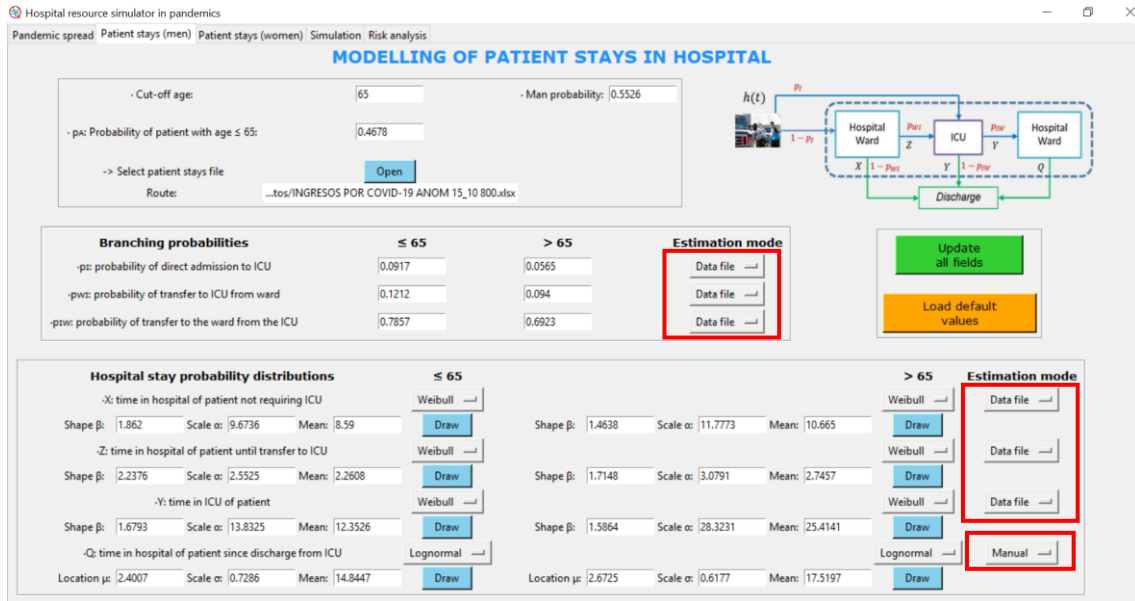


Figure H.18. Parameter fitting using the data file.

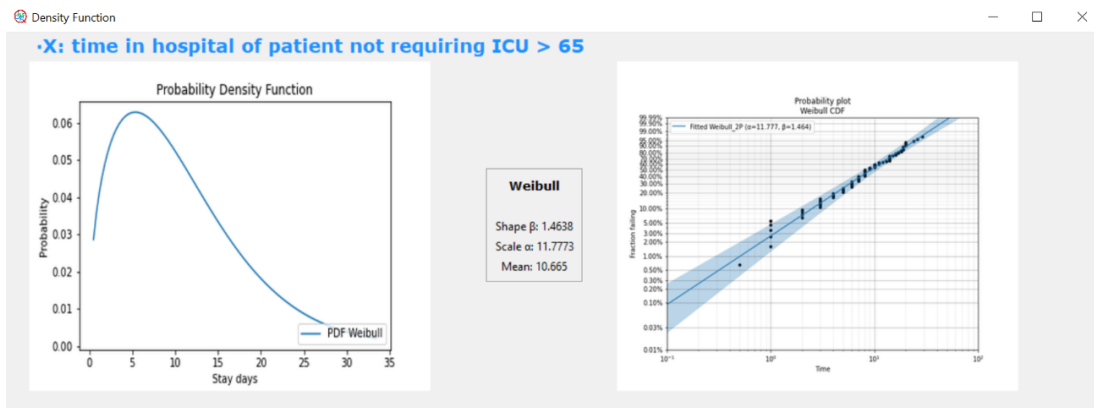


Figure H.19. Density function and quality of fit to a Weibull distribution for LoS in hospital for patients over 65 years old who do not require ICU.

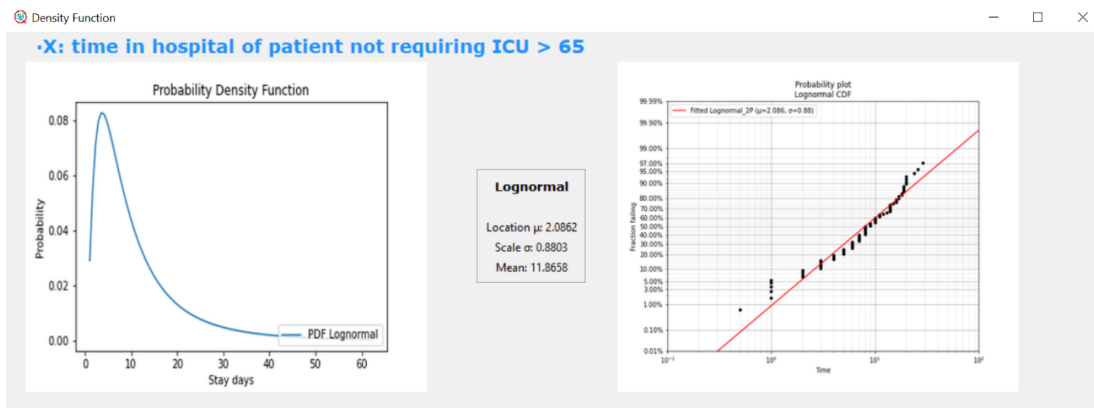


Figure H.20. Density function and quality of fit to a Lognormal distribution for LoS in hospital for patients over 65 years old who do not require ICU.

A detail to be taken into account is that the fits of the distributions through the data file can be made as long as there are at least 10 observations of the corresponding LoS. In cases where there are not enough observations, three zeros will appear in the distribution parameter boxes. Figure H.21 shows an example of the LoS in hospital for patients discharged from ICU over 65 years old. On the one hand, it is possible to keep the default values of the parameters, which are those corresponding to the first wave of the pandemic (between March and June 2020). On the other hand, it is possible to enter values manually according to medical criteria or based on expert opinion. In any case, these boxes should not be left with a value of 0 before starting the simulation, as this would cause an error when assigning the stay of that group of patients.

The screenshot shows the 'MODELLING OF PATIENT STAYS IN HOSPITAL' interface. It features a flowchart on the right with states: Hospital Ward (X), ICU (Y), and Hospital Ward (Q). Transitions are labeled with probabilities: P_{wi} , P_{wi} , P_{wi} , $1 - P_{wi}$, $1 - P_{wi}$, and Q . The main interface is divided into sections: 'Cut-off age' (65), 'Man probability' (0.5526), 'Branching probabilities' (with values for p_{pi} , p_{pw} , and p_{pw} for ≤ 65 and > 65), and 'Hospital stay probability distributions'. The distributions section includes Weibull and Lognormal distributions for various time intervals. A red box highlights the 'Location μ : 0' field for the distribution of time in hospital since discharge from ICU for patients over 65 years old.

Figure H.21. Parameter fitting using a data file in which there is insufficient data for the LoS in the hospital of patients over 65 years old discharged from the ICU.

Manual setting of parameters

All the parameters described above in *Input data (age of cut-off and stay file)*, *Branching probabilities*, and *Probability distributions of hospital stays* can be entered manually by the user for the simulation. Therefore, the cut-off age of the patients and the probability that a patient is younger than that age, as well as the probability that a patient is male or female can be varied by the user. The branching probabilities of the flowchart can also be modified directly. In Figure H.22, an example is shown with some changes introduced.

The screenshot displays the 'Modelling of Patient Stays in Hospital' software interface. It features several input fields and a flowchart. The flowchart shows transitions between 'Hospital Ward', 'ICU', and 'Hospital Ward' with probabilities p_w , p_{wz} , p_{wy} , p_{yz} , and p_{yw} . A 'Discharge' box is also shown. The interface includes a table for branching probabilities and an estimation mode dropdown menu.

Branching probabilities	≤ 70	> 70
-pa: probability of direct admission to ICU	0.002	0.03
-pwz: probability of transfer to ICU from ward	0.02	0.1
-pzw: probability of transfer to the ward from the ICU	0.6	0.4

Estimation mode: Manual

Figure H.22. Manually entered modifications with respect to the default values.

The parameters of the probability distributions can also be varied. But unlike the fields shown in Figure H.22, there is also the possibility to update them if two of the three parameters are chosen for a probability distribution. Below, we explain how the values of the distributions can be entered and updated depending on which one is selected, and by selecting the "Manual" estimation mode:

- Weibull distribution: In this probability distribution it is always mandatory to enter the shape parameter (β). Then, you can enter both the scale (α) and the mean manually, leaving the other empty. By pressing the "Update all fields" button, the software recalculates the parameter that has not been defined.
- Lognormal distribution: In this case, the parameter that must always be entered manually is the scale parameter (α). Then you can choose whether to enter the location (μ) or the mean. As with the Weibull distribution, the parameter not entered is recalculated.
- Triangular distribution: This distribution has three parameters, minimum (a), mode (b), and maximum (c). The one that must always be entered is the minimum, and then, depending on which of the other two is entered, the software recalculates the third so that the mode is at the same distance from the minimum and maximum.

If for the same probability distribution the user enters all three field values and then presses the "Update all fields" button, the software checks whether the combination of parameters is correct. For both a Weibull and a Lognormal distribution, the value of the mean can be obtained from the two parameters of the distribution. If this value does not match the value entered by the user, the software recalculates the scale parameter (α) for the Weibull distribution, and the location parameter (μ) for the Lognormal distribution, using the set mean. This is important to ensure that the combination of parameters entered provides the mean required by the user. On the other hand, for the case of the Triangular distribution, the software recalculates the value of the mode (b) so that it is at the same distance from the minimum and the maximum. This

variation is not a correction, since the Triangular distribution does not have to be symmetrical, but it has been programmed in this way to control the cases in which the mode is outside the limits marked by the minimum (a) and the maximum (c).

Figure H.23 and Figure H.24 show the parameter values of the distributions before and after clicking the "Update all fields" button respectively. This is a manual calculation of the four types of stays that are considered and in which all the possibilities mentioned in this section are included.



Figure H.23. Manually entered parameters of LoS distributions, before recalculating missing values.

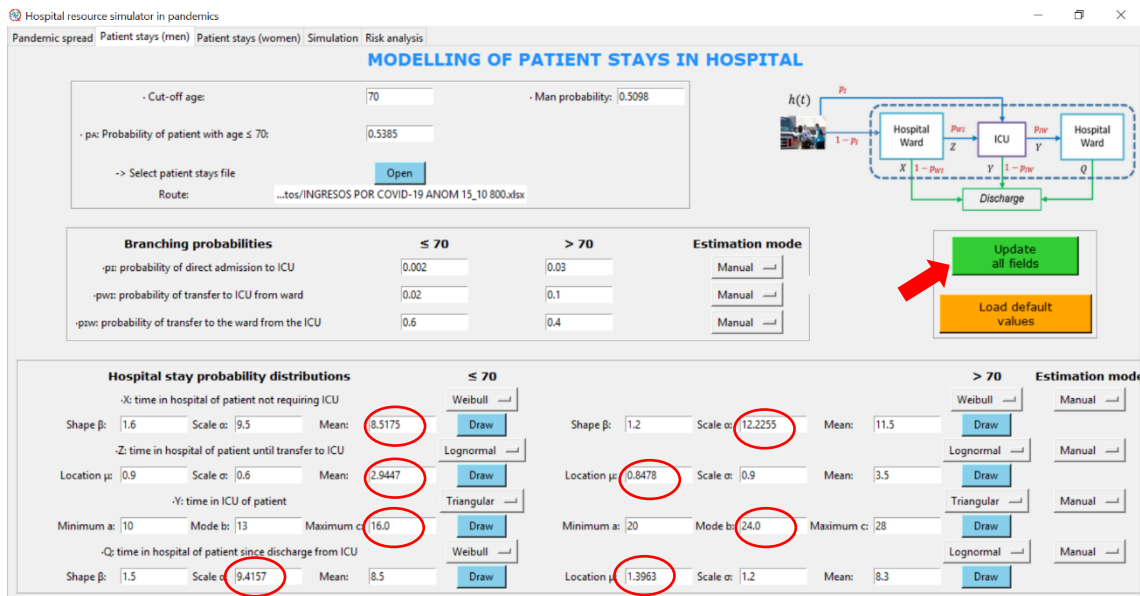


Figure H.24. Manually entered LoS distributions parameters recalculated for missing or incorrect ones.

H.4 Pandemic simulation

The fourth tab of the software is where the user enters the values needed to run the pandemic simulation. It is essential to complete the previous tabs in order to run the simulation correctly. Figure H.25 shows the parts of this tab.

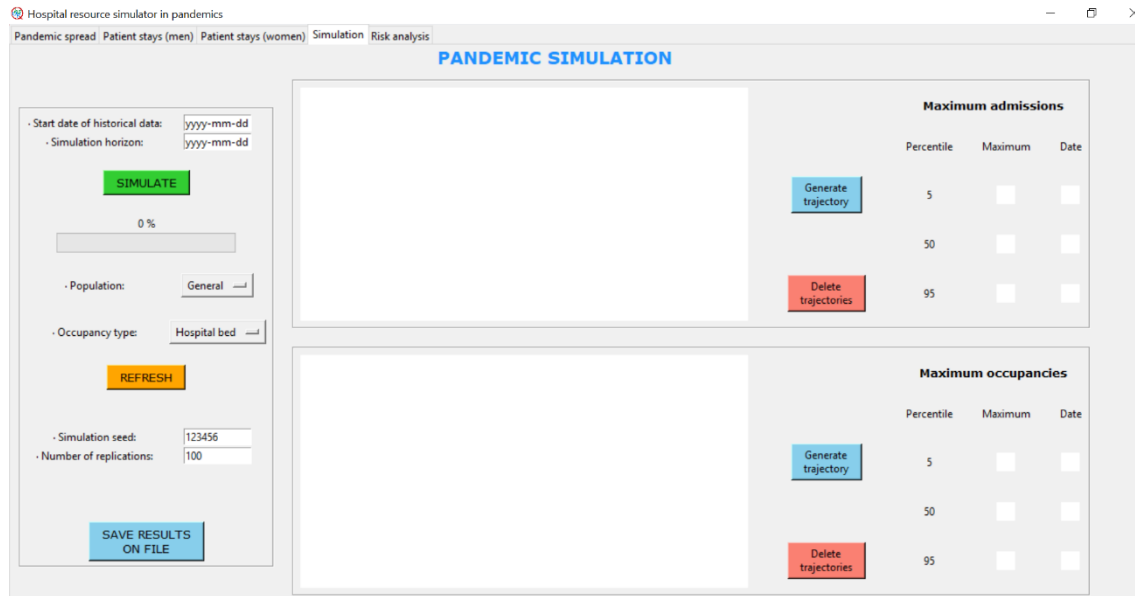


Figure H.25. Pandemic simulation.

First, at the top on the left hand side, two dates must be entered:

- Start date of the historical data (yyyy-mm-dd): This corresponds to the date from which the user wants to record the actual admissions and discharges of patients in order to represent them over time. This date may be prior to the date considered as the start of the pandemic, in order to see a greater evolution over time.
- Simulation horizon (yyyy-mm-dd): This is the date up to which the user wants to visualize the simulation.

Also, the software allows the user to select the population to be displayed in the graphs, whether all patients simultaneously (General) or separated by gender and age cut-off. Similarly, the user can choose to display the occupancy type in hospital beds, ICU beds, or both aggregated. To finish with the input parameters of this tab, at the bottom right the user must enter a seed for the simulation (to control the randomness of the simulation, the user can use the default one) and the number of replications (number of times the simulation will be repeated to observe different trajectories).

Figure H.26 shows the configuration set as an example, where the historical data date is 2020-08-01, the simulation horizon is 2020-12-31, the simulation seed is 123,456 and the number of replications is 1,000. When the user presses the green button "SIMULATE", the simulation starts, and the user can see the progress of the simulation by means of a bar with a percentage.

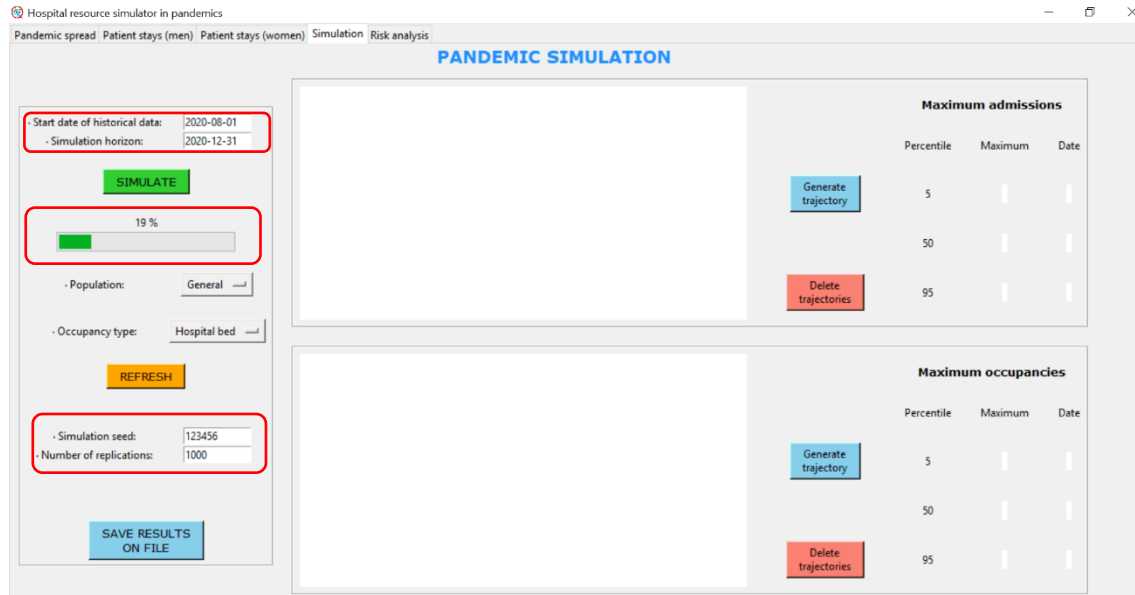


Figure H.26. Pandemic simulation progress with historical data date from 2020-08-01, simulation horizon to 2020-12-31, simulation seed of 123,456, and 1,000 replications.

When the established replications are finished, the user can visualize two graphs that appear in the central part of the tab. The first one reflects the daily number of admissions and the second one refers to bed occupancy. Depending on the type of occupancy selected, these graphs will correspond to the situation of hospital beds, ICU beds, or both aggregated. With the orange button "REFRESH", the results of each type can be loaded instantly. Figure H.27 and Figure H.28 show the results obtained in this example for hospital and ICU beds respectively. In both types of graphs (daily admissions and occupancy), the green line represents the real evolution of the historical data up to the moment of the start of the simulation, which is marked with a black dot. From this point onwards, 3 lines appear, two in blue marking the 5th and 95th percentiles, and the orange one representing the median.

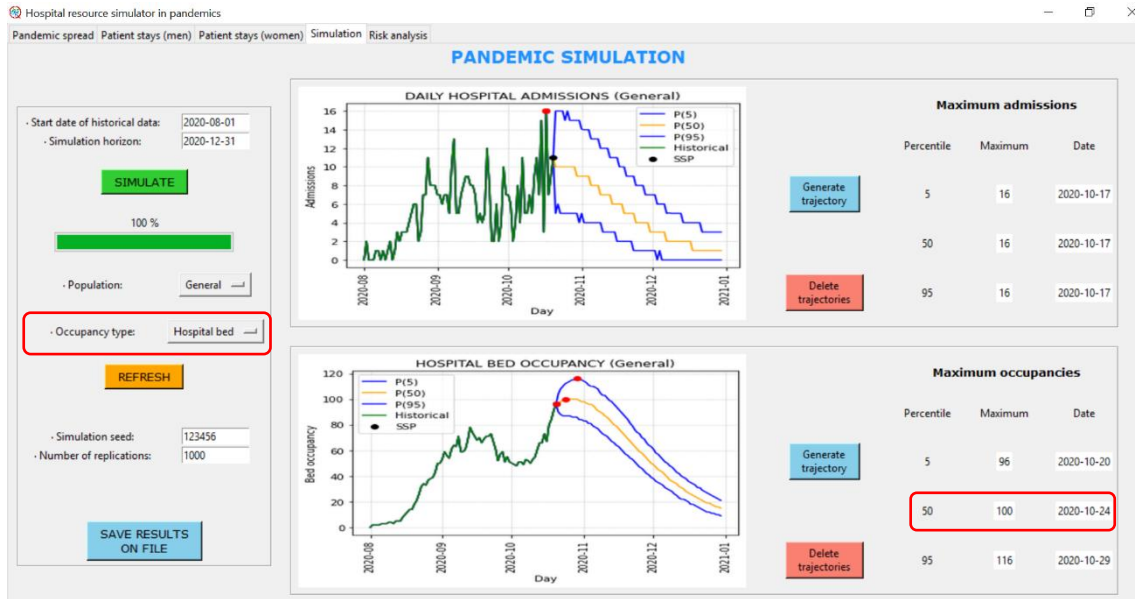


Figure H.27. Simulation results for hospital beds.

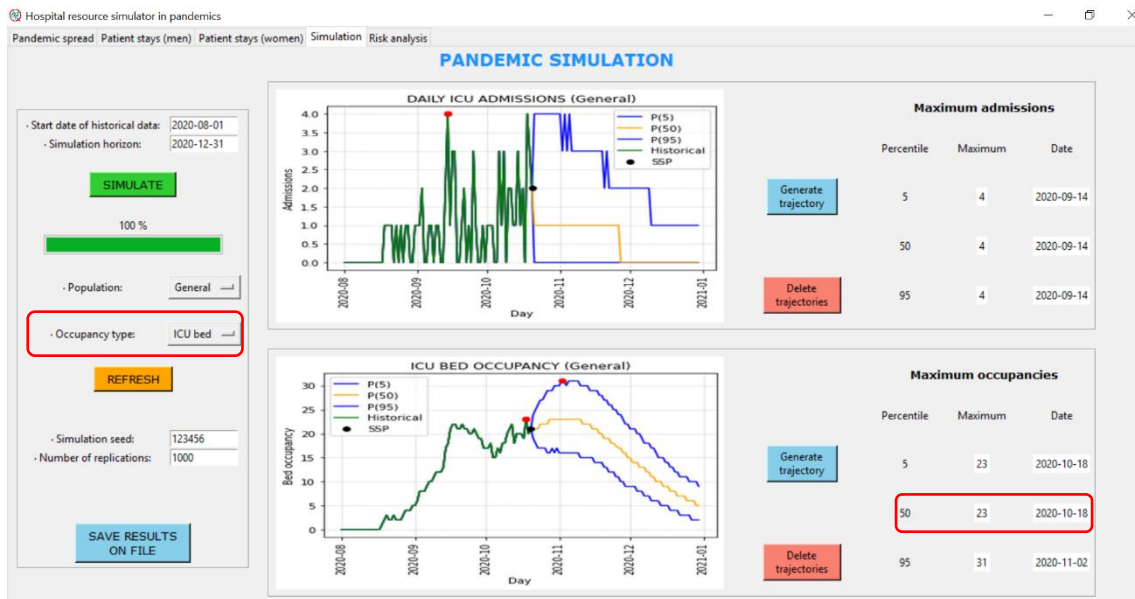


Figure H.28. Simulation results for ICU beds.

In addition, on the right-hand side of the tab, there are fields that record both the date with the maximum admissions and the date with the maximum occupancy, for each of the percentiles represented in the graphs. For example, the results obtained show that the maximum occupancy at the 50th percentile for hospital beds will be 100 on 2020-10-24, while for ICU it was 23 on 2020-10-18. Furthermore, by means of the blue button "Generate trajectory", it is possible to represent different simulated situations on the graph (in this case, each of the 1,000 replications can be represented). With the red button "Delete trajectories", trajectories can be

removed from the graph so that new ones can be displayed more clearly. Figure H.29 shows 3 trajectories generated with different colors for the ICU curves.

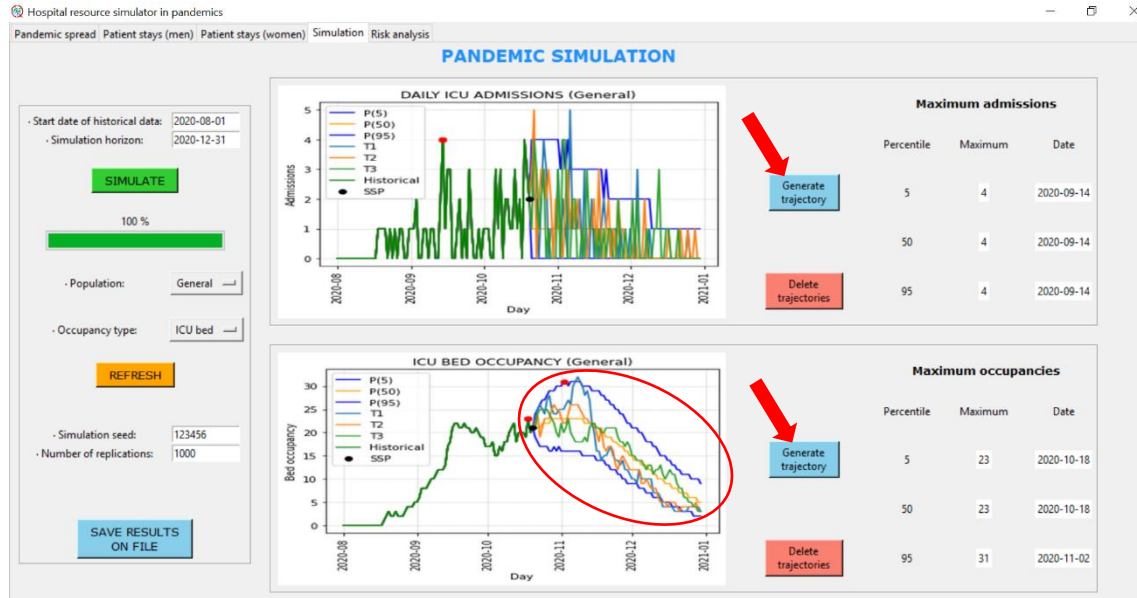


Figure H.29. Generated trajectories in the ICU, from among the 1000 simulations run by the software.

Finally, using the button at the bottom on the left "SAVE RESULTS ON FILE", it is possible, as the name suggests, to save the results obtained in data files. Specifically, it is possible to generate an Excel file with the numerical results of all the graphs that have been shown, and a Word file with the graphs of admissions and bed occupancy for the hospital and the ICU. When this button is clicked, a window similar to the one shown in Figure H.4 appears, with which these files can be saved in any location on the computer and with any name the user wants. Figure H.30 shows the window for saving the files.

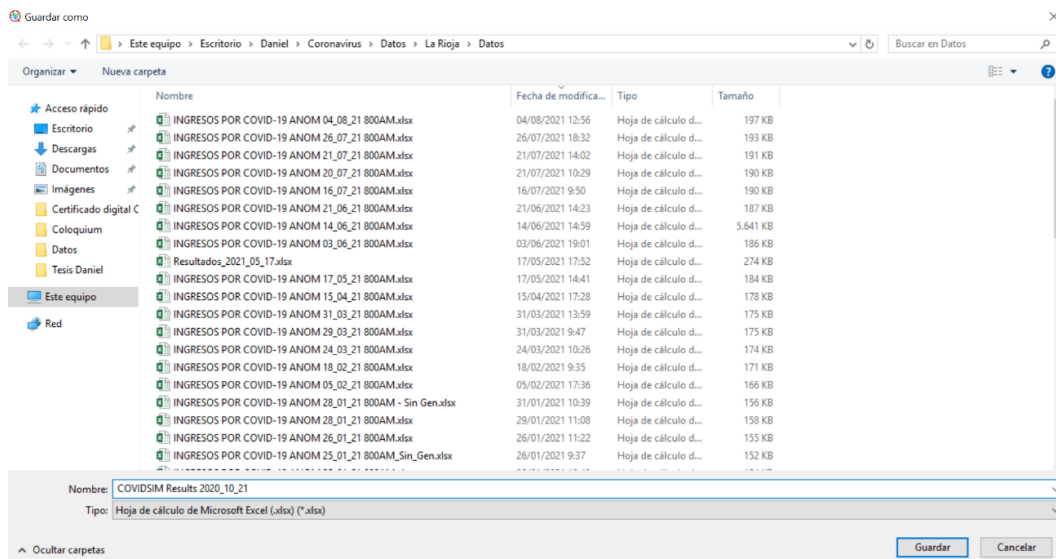


Figure H.30. Window used to save the simulation results in files.

H.5 Analysis of the system saturation risk

The fifth and last tab of the software offers the possibility to analyse the system saturation risk, distinguishing between hospital capacity and ICU capacity. These analyses can only be performed once the simulation has been completed, as the calculations are made based on these simulations. Figure H.31 shows the visualization of this tab.

Area	Current capacity	Maximum capacity
Hospital	500	800
ICU	50	80

Figure H.31. Analysis of the system saturation risk.

In this tab, the user can enter values in different fields to calculate the different saturation risks. On the one hand, the horizon of the analysis (yyyy-mm-dd) must be indicated, which would be limited to the simulation horizon. On the other hand, the user must enter the current capacity and the maximum capacity of both the hospital and the ICU. With these data, the software calculates the saturation risk for both areas until the indicated date. In addition, to explore the intermediate occupancy values, between the current and the maximum set by the user, nine intermediate occupancies are added, for which the saturation risk is also calculated.

The calculation of the saturation risk consists of analyzing all the simulations run by the software, and for each day calculating the percentage of times that the occupancy has exceeded the current capacity, for example. By clicking on the orange button "CALCULATE", a time series of the percentage of saturation is obtained for each occupancy value, which is represented in a separate graph for each area. Figure H.32 shows the analysis up to 2020-11-15 for occupancies between 100 and 120 in the hospital, and 20 and 30 in the ICU.

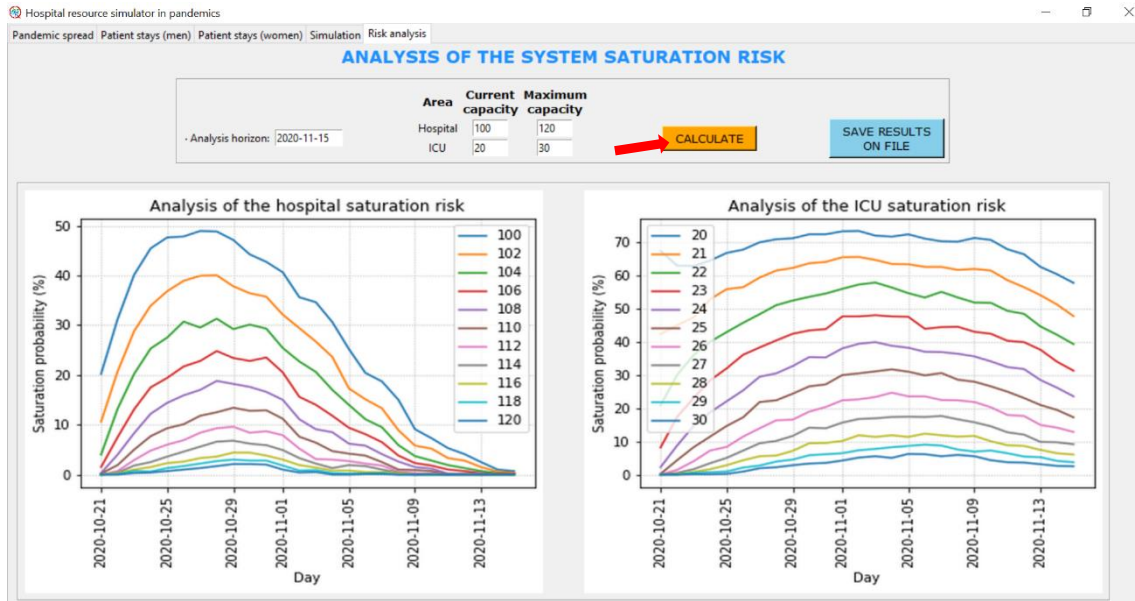


Figure H.32. Results obtained of system saturation risk for the hospital and ICU analysed up to 2020-11-15.

Like the simulation results, these analyses can be saved in files using the "SAVE RESULTS ON FILE" button. An Excel file is generated with the numerical results, as well as a Word file with the graphs obtained in Figure H.32. As for saving the simulation results, the window that appears to save these files is similar to the one in Figure H.4, with which the user can select both the name of the files to be generated and their location on the computer. Figure H.33 shows this window.

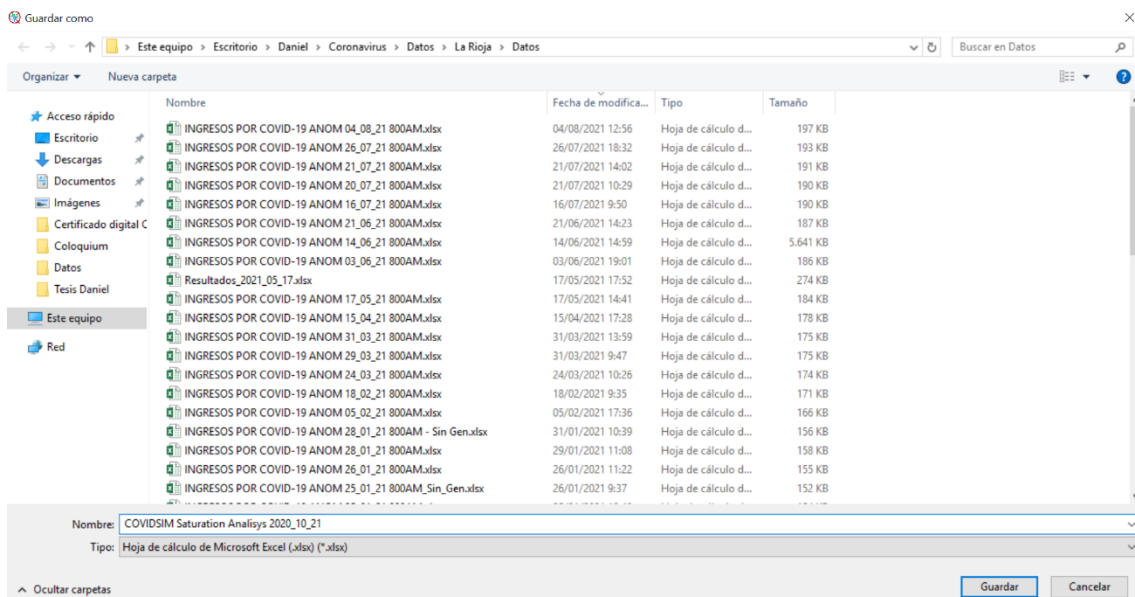


Figure H.33. Window used to save the results of the saturation risk in the files.

H.6 Extension to flu

The COVIDSIM software is used to simulate and forecast bed occupancy due to COVID-19 disease. However, this same approach can be extended and adapted to other diseases with similar patterns, such as the flu. A second tab has been extended in the software to perform simulations on the flu, independent of those on COVID-19, with the possibility of obtaining combined results for both diseases in the hospital.

The mathematical modelling of flu patients is the same as those of COVID-19 patients, as well as the tabs that the user has to use to fit the pattern of arrivals and the stay of patients in the hospital. However, there are certain aspects to be taken into account that differentiate the flu from COVID-19, and this is what is going to be discussed in this section.

Observed data

Flu patient data from the 2017-18 and 2018-19 seasons have been used. With these data, we have verified that the evolution of the pandemic can be represented with a Gompertz-type curve, and we have also been able to analyse patient stays in order to introduce default distributions in the software.

Figure H.34 and Figure H.35 show both cumulative and daily historical data for patients admitted with flu to the hospital of the 2017-18 and 2018-19 seasons, respectively, in La Rioja. From these plots, it can be seen that the data are highly variable between consecutive days, which shows the difficulty of the fit. However, the fit to the Gompertz curve is reasonably good (green curve in the plots), making it possible to use this model in the simulation.

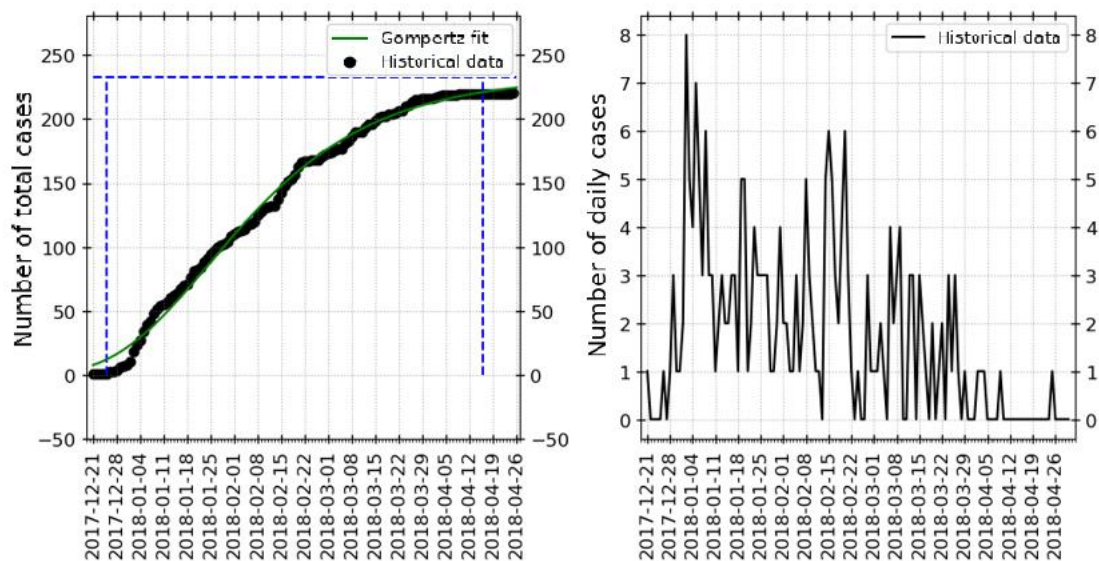


Figure H.34. Cumulative and daily data for patients admitted to the hospital with flu in the 2017-18 season in La Rioja.

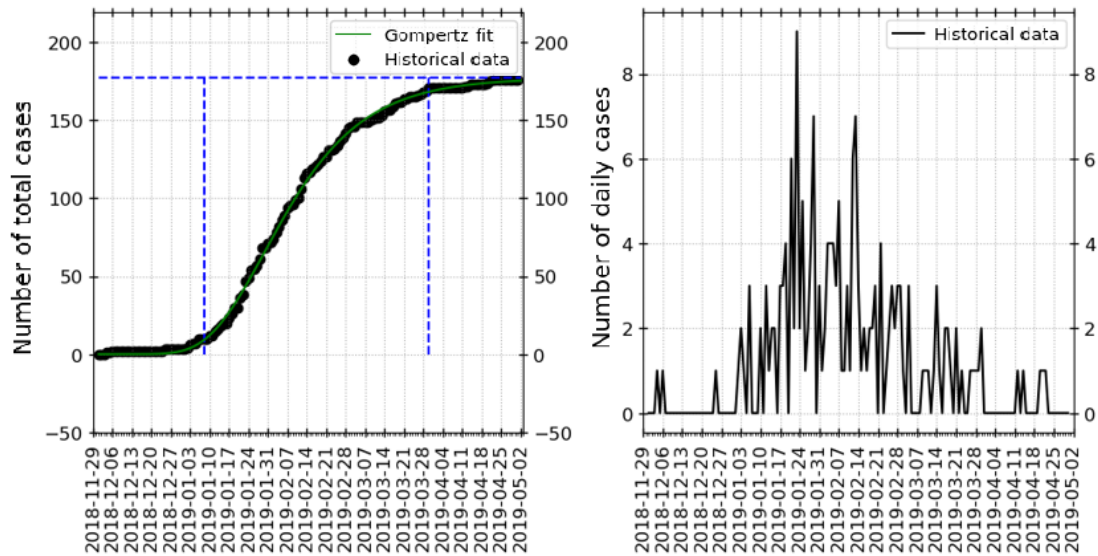
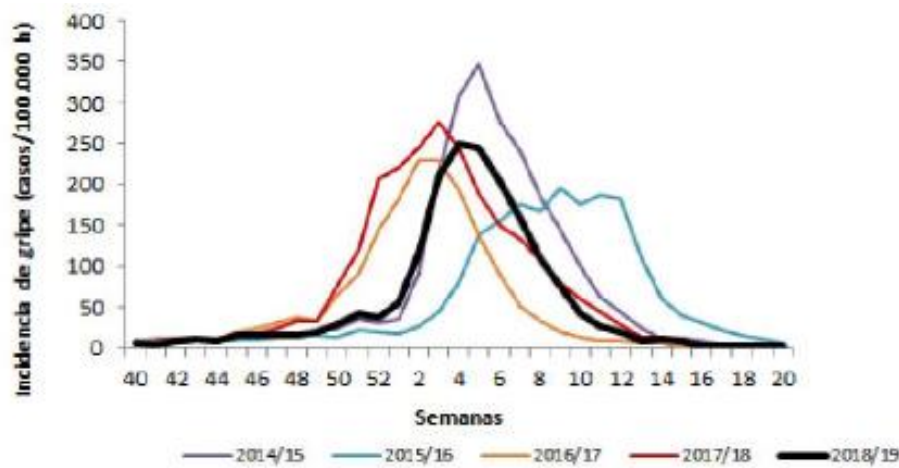


Figure H.35. Cumulative and daily data for patients admitted to the hospital with flu in the 2018-19 season in La Rioja.

Figure H.36 shows a graph of the weekly incidence of the flu in Spain between the 2014-15 and 2018-19 seasons. Although it has not always occurred on the same dates, it can be seen that the shape is similar in the different seasons.



Fuente: CNE. ISCIII. Sistema centinela de Vigilancia de Gripe en España

Figure H.36. Weekly incidence of the flu. Sentinel Flu Surveillance System in Spain. Seasons 2014-15 to 2018-19, Spain.

Tips for simulations

One of the problems involved in carrying out daily follow-up of patients admitted with flu is the scarcity of data available, especially in the early stages of this disease. The lack of data negatively affects both the fit of the hospital admission curve and the fit of hospital stays.

However, from the data observed before in *Observed data*, it can be concluded that the flu is a "repetitive" pandemic whose duration can be estimated at around 90 days. This fact, together with the total number of admissions, which was 225 and 175 in both periods analysed, facilitates the estimation of the Gompertz curve at the beginning of the outbreak, according to the following steps detailed below:

1. During the first 5 days in which daily admissions are observed, the parameters of the curve are manually set with a total number of admissions of 250 and a duration of 90 days. Also, the number of accumulated admissions known up to a date before the start of the simulation is entered (for example, it can be the accumulated admissions up to the previous day).
2. From the fifth day on, the total number of admissions remains fixed at 250 and the duration is maintained at 90 days. However, the third parameter is fitted through the data file. This can be done until day 10 of the start of the pandemic.
3. Between day 10 and day 60, only the duration parameter is entered manually and remains at 90. The other two parameters are fitted by file. The values obtained must be monitored. If the value of the number of total admissions is outside the range between 150 and 400, it is advisable to enter it manually so as not to exceed too much with what has been observed in past flu episodes.
4. From day 60 until the end, there will already be enough data for the curve to be fully fitted by file. It should also be checked that the shape of the curve is reasonable.

These four steps described are a previous recommendation that is established. Both the time intervals and the values to be entered are flexible and may vary as data are observed on a daily basis. Regarding the fit of the stay distributions, it is advisable to use the default values until a total of at least 30 complete hospital stays and 20 ICU stays have been observed. Fitting with too few values may lead to unreliable results.

COVID-19 and flu results

The software includes two tabs to perform independent simulations for each disease ("COVID" and "Flu"). In addition, a third tab called "Altogether" has been included to obtain the aggregated results. In this tab, it is possible to obtain, on the one hand, the graphs of admissions and bed occupancy both in the hospital and in the ICU for the two diseases separately or together (see Figure H.37), and on the other hand, the analyses of the hospital and ICU saturation risk taking into account the two diseases (see Figure H.38).

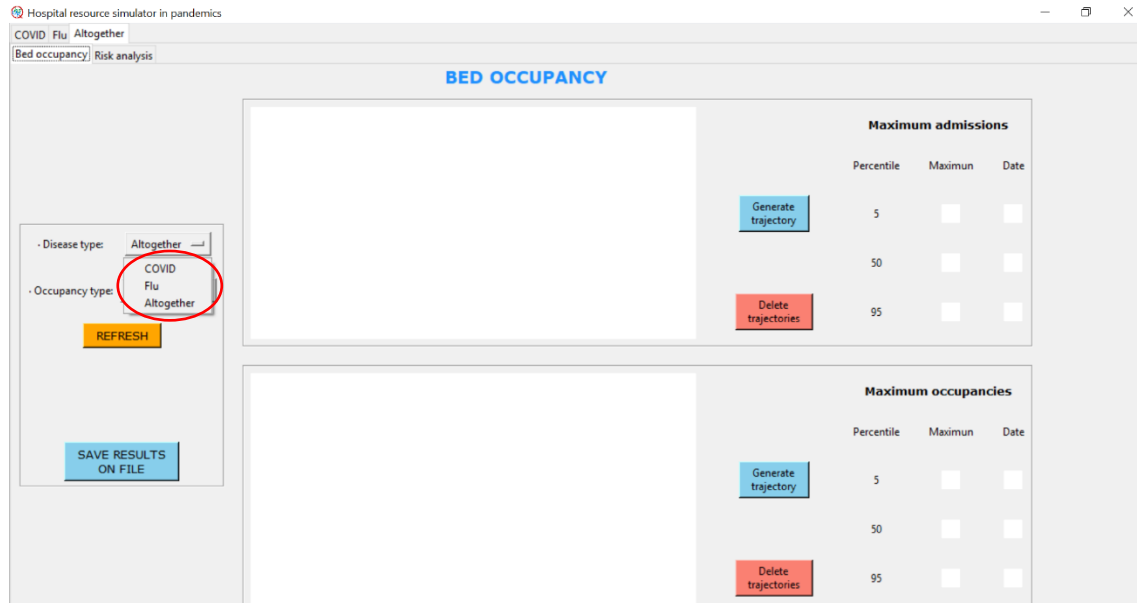


Figure H.37. Tab where the graphs of admissions and bed occupancy are obtained for the two diseases aggregated and individually.

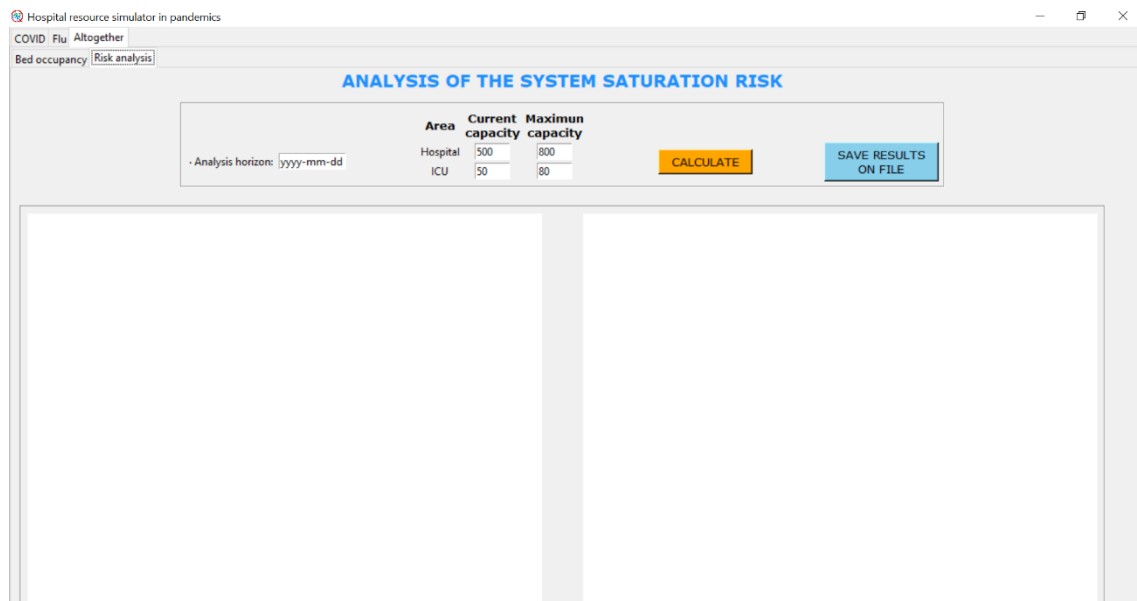


Figure H.38. Tab showing the hospital and ICU saturation risk analysis taking into account both diseases.

H.7 Input data file

This section describes the content of the software input files. Two types of file are distinguished: on the one hand, an Excel file with the data of patient stays in the hospital (both on the ward and in the ICU if required) and their characteristics (sex and age), and on the other hand, the file with the data of daily cases (which can be positive cases or hospital admissions).

If the first file is available, it would not be necessary to prepare the second file for the operation of the software.

The file of hospital stays should be an Excel file with individualized data of patients admitted to the hospital (which are anonymized). It is essential that it always has the same column structure and the format of the data must also be maintained, such as the age, the label of male (H) and female (M), and the format of the dates of admission and discharge (date format and without the time). Figure H.39 shows visually how the information is organized in this file. The columns marked in red are the ones that are read in the software.

	A	B	C	D	E	F	G	H	I	J	K	L	M	N	O	P	Q	
1	ORISEN	MEDICALRECORD	ID UNIVERSAL	MEDICALCARD	MEDICALCARD2	DATEOFBIRTH	NHK	EDAD	SEXO	TIPO	ESTADO	ID_ACTO	MOTIVO_ALTA	FECI	INGRESO	FECHA_ALTA	FECI_INGRESO_UMI	FECI_ALTA_UMI
2	HSP	333370						37	M	HOSPITALIZACION					03/03/2020	16/03/2020		
3	HSP	30949						57	F	HOSPITALIZACION					03/03/2020	05/04/2020	11/03/2020	05/04/2020
4	HSP	271707						61	M	HOSPITALIZACION					04/03/2020	18/03/2020		
5	HSP	115485						55	M	HOSPITALIZACION					05/03/2020	16/03/2020	06/03/2020	09/03/2020
6	HSP	332988						71	M	HOSPITALIZACION					05/03/2020	16/03/2020		
7	HSP	136551						54	M	HOSPITALIZACION					05/03/2020	27/03/2020		
8	HSP	373604						47	M	HOSPITALIZACION					07/03/2020	16/03/2020		
9	HSP	56552						74	M	HOSPITALIZACION					07/03/2020	09/03/2020		
10	HSP	102897						83	F	HOSPITALIZACION					07/03/2020	16/03/2020		
11	HSP	344971						25	F	HOSPITALIZACION					08/03/2020	16/03/2020		
12	HSP	371130						51	F	HOSPITALIZACION					08/03/2020	20/03/2020	14/03/2020	20/03/2020
13	HSP	161598						58	M	HOSPITALIZACION					09/03/2020	20/03/2020		
14	HSP	6044						68	F	HOSPITALIZACION					09/03/2020	25/03/2020	12/03/2020	25/03/2020
15	HSP	58812						76	M	HOSPITALIZACION					09/03/2020	19/03/2020		
16	HSP	349135						50	M	HOSPITALIZACION					10/03/2020	29/03/2020		
17	HSP	130798						53	M	HOSPITALIZACION					10/03/2020	27/03/2020		
18	HSP	131592						61	M	HOSPITALIZACION					10/03/2020	09/07/2020	19/03/2020	18/05/2020
19	HSP	439125						70	M	HOSPITALIZACION					10/03/2020	19/03/2020	15/03/2020	19/03/2020
20	HSP	586623						48	M	HOSPITALIZACION					11/03/2020	24/03/2020		
21	HSP	148388						54	M	HOSPITALIZACION					11/03/2020	19/03/2020		
22	HSP	213972						69	F	HOSPITALIZACION					11/03/2020	20/03/2020	15/03/2020	20/03/2020
23	HSP	307591						88	F	HOSPITALIZACION					11/03/2020	14/03/2020		
24	HSP	414603						48	M	HOSPITALIZACION					11/03/2020	20/03/2020		
25	HSP	62457						48	M	HOSPITALIZACION					12/03/2020	20/03/2020		
26	HSP	453817						51	F	HOSPITALIZACION					12/03/2020	11/03/2020	15/03/2020	21/03/2020
27	HSP	356788						64	M	HOSPITALIZACION					12/03/2020	20/04/2020	04/04/2020	10/04/2020
28	HSP	65965						68	M	HOSPITALIZACION					12/03/2020	16/03/2020	12/03/2020	16/03/2020
29	HSP	256386						75	F	HOSPITALIZACION					12/03/2020	27/03/2020		
30	HSP	194715						78	M	HOSPITALIZACION					12/03/2020	21/03/2020		
31	HSP	571483						82	M	HOSPITALIZACION					12/03/2020	26/03/2020		
32	HSP	435096						86	F	HOSPITALIZACION					12/03/2020	18/03/2020		
33	HSP	6038						87	F	HOSPITALIZACION					12/03/2020	20/03/2020		
34	HSP	197361						87	F	HOSPITALIZACION					12/03/2020	12/03/2020		
35	HSP	212171						92	F	HOSPITALIZACION					12/03/2020	21/03/2020		
36	HSP	100594						51	F	HOSPITALIZACION					12/03/2020	21/03/2020		

Figure H.39. Excel file format of patient stay data.

On the other hand, when the file of patient stays is not available, it is possible to fit the curve of hospital admissions using the historical series of admissions. Figure H.40 shows the format that this Excel file should have, which contains the date column, the column of daily cases and the column of cumulative cases.

	A	B	C
1	Date	Daily cases	Cumulative cases
2	01/08/2020	0	0
3	02/08/2020	2	2
4	03/08/2020	0	2
5	04/08/2020	0	2
6	05/08/2020	0	2
7	06/08/2020	1	3
8	07/08/2020	1	4
9	08/08/2020	0	4
10	09/08/2020	1	5
11	10/08/2020	0	5
12	11/08/2020	1	6
13	12/08/2020	2	8
14	13/08/2020	0	8
15	14/08/2020	1	9
16	15/08/2020	3	12
17	16/08/2020	2	14
18	17/08/2020	3	17
19	18/08/2020	4	21
20	19/08/2020	3	24
21	20/08/2020	5	29

Figure H.40. Excel file format of daily case data.